Biochemical characterisation of UMAD1 and functional implications for ESCRT mediated cytokinetic abscission

Scourfield, Edward

Awarding institution:
King's College London

Biochemical characterisation of UMAD1 and functional implications for ESCRT mediated cytokinetic abscission

Edward James Scourfield

This thesis is submitted to King's College London for the degree of Doctor of Philosophy

Department of Infectious Diseases

King's College London

School of Immunology & Microbial Sciences

- July 2020 -

Declaration

I, Edward James Scourfield, confirm that the work presented in this thesis is my own. Where information has been derived from other sources, I confirm that this has been indicated.

11th July 2020

Abstract

The Endosomal Sorting Complex Required for Transport (ESCRT) machinery facilitates topologically equivalent membrane remodelling and scission events in an ever-growing number of cellular processes, notably MVB biogenesis and endosomal sorting, enveloped viral budding and cytokinetic abscission. ESCRTs are recruited in a modular fashion to target membranes by site specific adaptor proteins, where they assemble within cytosol-filled membranous stalks to mediate bending and scission away from the cytoplasm.

Cytokinesis is the process of separation of the cell cytosol into two daughter cells during cell division. During cytokinesis, the inward constriction of cell membrane eventually results in the formation of a thin protein rich stalk-like structure termed the midbody. Cytokinetic abscission is the final stage of cytokinesis during which the midbody is severed leading to the final resolution of daughter cells. The ESCRT machinery is central to cytokinetic abscission, during which it is recruited by the adaptor protein CEP55 to the midbody where it mediates the final severing event.

ESCRT-I is a heterotetramer comprised of TSG101, VPS28, VPS37A, B, C or D and MVB12A, MVB12 B or UBAP1. In this thesis, I identify UMAD1 by mass spectrometry and coprecipitation assays as another novel alternative MVB12 subunit of ESCRT-I, that is able to form a functional ESCRT-I complex and is involved in cytokinetic abscission. A direct interaction between the midbody adaptor protein CEP55 with TSG101 has been described, and coprecipitation assays have shown that TSG101 binds less well to CEP55 in the absence of UMAD1. Use of microscopy to more directly examine cytokinetic defects and differences in the time taken for abscission to occur have also provided evidence for both a generalised role for UMAD1 in mediating successful cytokinesis and also contribution specifically at the stage of abscission. We hypothesise that UMAD1 forms part of an ESCRT-I complex that contributes to abscission in one of two parallel partially redundant pathways, the other pathway being mediated by the ESCRT associated protein ALIX, which also interacts with CEP55. Consistent with this hypothesis are synergistic effects on abscission and cytokinetic defects upon co-depletion of UMAD1 with ALIX.

Table of Contents

Acknowledgements

First and foremost, I would like to give a huge thank you to my primary supervisor Professor Juan Martin-Serrano and co-supervisor Dr Monica Agromayor. In all my education so far, I can safely say without a doubt that the past four years have been the most fulfilling and enjoyable learning experience, and I feel so grateful for being given the opportunity to do a PhD with you, in such a wonderful lab. Thank you for such superb mentoring and support, for your encouragement, for motivating me to do good science, and above all for always having faith in me. It has been a privilege to work with such distinguished scientists and to work in such a varied and fascinating area of cell biology. Your management style has worked so well for me, and I am very grateful. Thank you also for your hospitality at the Christmas and new year parties at your apartment, with such delicious food, and your generosity in and outside the lab.

I would like to extend my thanks to all other members of my thesis committee: Professor Stuart Neil, Dr Jason Mercer, Dr Mark Dodding and Dr Roger Williams. External support from all of you has been invaluable at every stage of my PhD process and has helped things run so smoothly. You have all provided lots of food for thought along the way and very helpful discussions. Thank you also for your time and travelling to London Bridge for our meetings.

In any working environment, the people are what makes it such a great place to work and this is true for both current and previous lab colleagues. Thank you, Jessica, for being such a good teacher, and for the emotional support at times. You provided a feminine touch that acted as the glue that kept the lab together! All the best with motherhood! Leandro, the lab would never be the same without your great sense of humour and friendly personality, and thanks always for your encouragement and help with microscopy! A big thanks to Yan for always being so approachable and for our meaningful discussions about mass spec. The peanut butter cookies were great, by the way! Sam and Desi, it's been lovely having you as fellow PhD students in the lab. Your baking skills have also been much appreciated in lab meetings, and I will miss your late evening company in the lab. Thanks for inviting me to such a lovely wedding, Sam, it was a beautiful day in Cornwall. All the best to you and Ruby! Desi, when I look at all your

clonogenic assay plates I think you are a model of stoicism as a scientist and will no doubt end up with a great PhD at the end of it!

I am also very grateful to previous lab members, Anna, Miguel Angel, and Marc for their help at the start of my PhD, helping me to settle into the lab and showing me the ropes. Thank you also to everyone from Monica's lab: Carmen, Evita, Mara, Nawal and Andrea. It's been a pleasure getting to know you all and your cheerful personalities. We make a great team together! Thank you to all other labs in the Department of Infectious Diseases. You've all been lovely people to work with and to get to know, and have all been very sociable. I also extend my thanks to the Faculty of Life Sciences and Medicine and the MRC for funding and supporting my studentship.

I would never have come this far in life without such unconditional support from my wonderful family, and all they have done for me in life. Thank you so much, mum and dad, for always being at the end of the phone for me to offload any angst, and for such good advice. The home cooked food and all the help with DIY in London is always much appreciated. You really do always go the extra mile to help me out and I really can't thank you enough! A huge thanks also to my sister, Sally, and her partner, Charlie, for equally being so understanding and helpful when it came to having someone to talk to about the 'roller-coaster' life of doing a PhD, and, together with Jessica, for introducing me to bouldering – a great way to deal with stress. I love you all very much!

I have really enjoyed meeting so many people at Tomobu – the London Japanese-English language exchange meetup and would like to say a special thanks to Hiroki, Yusuke, Kiyo, Daisuke. I am also extremely grateful to Sorami, who I've known since I was an undergraduate and has been such a great friend with such a positive outlook on life that many people should learn from. A big thank you also to Sumiko, for keeping in touch with me over all these years. I always look forward to hearing your news, and learn so much new vocabulary from such a well-read person. We've had some lovely times together, both in London and Japan, and I wish you all the best for the future in the UK and abroad. 皆さんにお会いできて本当に嬉しいです。一緒にいると話が弾んでいて楽しいですね。いつも応援してくれていると同様、こちらもみんな応援しているので頑張ってください！

Last but not least, I'd like to thank my current and former flatmates Visaly, Jamie, Sean and Ming for being such lovely people to live with. I have really enjoyed out chats, going out for drinks and cooking together in the kitchen. Ming, thanks so much for moving in. It's been wonderful to be able to live with such a great friend again after living together previously in Cambridge. Your American optimism and encouragement have done me so much good, and you've been such a great influence on me, in terms of being more adventurous with cooking and life in general. I wish all of you the best for the future!

Edward J. Scourfield

Abbreviations

ADP – Adenosine diphosphate
ALG-2 - Apoptosis-linked gene-2
ALIX - ALG-2-interacting protein X
AMSH - Associated molecule with the SH3 domain of STAM
ANCHR - Abscission/NoCut Checkpoint Regulator
APC/C - anaphase promoting complex or cyclosome
APS - Ammonium Persulfate
ARMM - Arrestin domain containing 1 (ARRDC1)-mediated microvesicle
ARRDC1 - Arrestin domain containing 1
ART - Arrestin-related trafficking
ATCC - American Type Culture Collection
ATM - Ataxia Telangiectasia Mutated
ATP – Adenosine triphosphate
ATR - Ataxia Telangiectasia and Rad3-related
BAPTA-AM – 1,2-Bis(2-aminophenoxy)ethane-N,N,N′,N′-tetraacetic acid tetrakis(acetoxymethyl ester)
bp – base pair
BRCT – BRCA1 C-terminal domain
BRUCE – BIR repeat containing ubiquitin-conjugating enzyme, isoform B
BSA – Bovine Serum Albumin
CA - Capsid
CA-SP1 - CA-spacer peptide 1
CAK - CDK activating kinase
Cas9 - CRISPR-associated protein 9
CBB - clathrin binding box
Cbl - Casitas B-lineage lymphoma proto-oncogene ligase
CC2D1B - Coiled-coil and C2 domain-containing protein B
CD2AP – CD2 Associated Protein
CDK - Cyclin dependent kinase
cDNA – complementary DNA
CEP55 - Centrosomal Protein 55
CFBP - CIN85/CD2AP family binding protein
CFP – Cyan Fluorescent Protein
CHMP - Charged multivesicular body protein/Chromatin-modifying protein
CID - Collision-Induced Dissociation
Cin85 – Cbl-interacting protein of 85 kDa
CKI - CDK inhibitor
CORVET - Class C core vacuole/endosome tethering complex
CPC - Chromosomal passenger complex
CPS - Carboxypeptidase S
CPY - Carboxypeptidase Y
CRISPRCas9 - clustered regularly interspaced short palindromic repeats
crRNA - CRISPR RNA
CYK-4 – CYtoKinesis defect 4

dATP - Deoxyadenosine triphosphate
dCTP - Deoxycytidine triphosphate
ddH_2O - Double-distilled water
DEEM - deep-etch electron microscopy
dGTP - Deoxyguanosine triphosphate
Did2 – DOA4-independent degradation protein 2
DMEM - Dulbecco's Modified Eagle Medium
DMSO - Dimethyl sulfoxide
DNA - Deoxyribonucleic acid
DNA-PKcs - DNA-dependent protein kinase, catalytic subunit
dNTP - Deoxynucleoside triphosphate
Doa4 – Ubiquitin carboxyl-terminal hydrolase 4
dsDNA – double-stranded DNA
dTTP - Deoxythymidine triphosphate
DUB – Deubiquitinase
EABR - ESCRT and ALIX binding region
EAP - ELL-associated protein
EBB - ESCRT-I binding box
EBOV – Ebola virus
ECL - Enhanced chemiluminescence
ECT2 - Epithelial cell-transforming sequence 2 oncogene
EDTA - Ethylenediaminetetraacetic acid
EE - Early endosome
EEA1 - Early Endosome Antigen 1
EGFR – Epidermal Growth Factor Receptor
EGTA - ethylene glycol-bis(β-aminoethyl ether)-N,N,N’,N’-tetraacetic acid
EIAV - Equine infectious anaemia virus
ER – Endoplasmic reticulum
ESCRT – Endosomal Sorting Complex Required for Transport
FACS - Fluorescence-activated cell sorting
FCCP - Fluoromethoxy carbonyl cyanide phenylhydrazone
FCS – Foetal calf serum
FYVE - Fab1p/ YOTB/Vac1p/EEA1
FYVE-CENT – FYVE domain-containing centrosomal protein
g - gravity
GAP – GTPase-activating protein
GAT - GGAs and Tom domain
GEF - Guanine nucleotide exchange factor
GFP – Green Fluorescent Protein
GLUE - Gram-like, ubiquitin binding in EAP45
Grb2 - Growth factor receptor-bound protein 2
GST - Glutathione S-transferase
GUV - Giant unilamellar vesicles
HA- Human influenza hemagglutinin tag
HCD - Higher-energy Collisional Dissociation
HD-PTP – His Domain-containing Protein Tyrosine Phosphatase
HEK293T - Human embryonic kidney 293T cells

hIST1 – human Increased Sodium Tolerance 1
HIV-1 - Human immunodeficiency virus 1
HOPS - Homotypic fusion and protein sorting complex
HRP – Horseradish peroxidase
HRS - Hepatocyte growth factor-regulated tyrosine kinase substrate
HSP90 - heat shock protein 90
HTLV – Human T-lymphotropic virus,
ILV – Intralumenal vesicle
INCENP - Inner centromere protein
INM - Inner nuclear membrane
IP-TMT – Immunoprecipitation – Tandem Mass Tag
IQGAP1 – IQ Motif Containing GTPase Activating Protein 1
KIF4A – Kinesin Family Member 4A
L-domain - Late budding domain
LB - Lysogeny/Luria broth
LBPA – Lysobisphosphatidic acid
LC-MS/MS - Liquid Chromatography with tandem mass spectrometry
LE - Late endosome
LEM – LAP2, emerin, MAN1 domain
LIM - Lin-11, Isl-1 and Mec3 domain
LIP5 – LYST-interacting protein 5
LLOMe - L-leucyl-L-leucine O-methyl ester
LTR - Long terminal repeats
MA - Matrix
MABP - MVB12 associated β-prism domain
MCh - mCherry
mg – milligram
MHC – Major histocompatibility complex
MICAL – Molecule interacting with CasL
MIM - MIT-interacting motif
MIT - Microtubule Interaction and Transport
MITD1 – Microtubule Interacting And Trafficking Domain Containing 1
MKLP – Mitotic kinesin-like protein 1
mL – millilitre
MLV - Murine leukaemia virus
Mod(r) - Modifier of rudimentary domain
MTOC - microtubule organising centre
MVB – Multivesicular body
MYPT – Myosin phosphatase targeting protein
NC – Nucleocapsid
NE – Nuclear envelope
NEB - New England Biolabs
ng – nanogram
NPC - Nuclear pore complex
NTH - N-terminal helix
Nup – nucleoporin
NUP153 – Nucleoporin 153

OCRL – Oculocerebrorenal syndrome protein/Inositol polyphosphate 5-phosphatase OCRL
OD – Optical density
Oligo – Oligonucleotide
ONM - Outer nuclear membrane
OSHA - One-Strep tag haemagglutinin
PALM - Photo-activated localisation microscopy
PAM - Protospacer adjacent motif
PAR1 – Protease-activated receptor 1
PBS - Phosphate-buffered saline
PCNA – Proliferating cell nuclear antigen
PCR – Polymerase chain reaction
PDGFR-β - Platelet-derived growth factor receptor-β
PEI - Polyethylenimine
PFA - Paraformaldehyde
$PI(3,5)P_2$ – Phosphatidylinositol 3,5-bisphosphate
PI3P - phosphatidylinositol 3-phosphate
PIPES - Piperazine-N,N'-bis(2-ethanesulfonic acid)
PKCε - Protein kinase Cε
PLD - Phospholipase D
PLK-1 – Polo-like kinase-1
PM – Plasma membrane
POM152 – pore membrane protein of 152 kD
pRb - product of the retinoblastoma tumour suppressor gene
PRC1 - Protein regulator of cytokinesis 1
PRD – Proline Rich Domain
PRR – Proline Rich Region
PS – Phosphatidylserine
PSM - Peptide-spectrum match
PTP - Protein Tyrosine Phosphatase
RNA – Ribonucleic acid
ROCK - Rho-associated kinase
RPA3 - Replication Protein A3
RPM - Revolutions per minute
rRNA – Ribosomal RNA
RSV - Rous sarcoma virus
SCAMP3 –Secretory carrier-associated membrane protein 3
SDS - Sodium dodecyl sulfate
SDS-PAGE - Sodium Dodecyl Sulfate Polyacrylamide Gel Electrophoresis
SEPT – Septin
sgRNA - single guide RNA
SH3 – Src homology 3
SIM - Structured illumination microscopy
SINC - storage of improperly assembled nuclear pore complexex
SMC - Structural maintenance of chromosomes family
SNARE - Soluble NSF adaptor protein receptor
Snf – Sucrose nonfermenting protein 7

SOLCAR - Solute carrier
SOUBA – Solenoid of Overlapping UBA domains
SP – Spacer peptide
ssDNA - single-stranded DNA
STAM1/2 - signal transducing adaptor molecule1/2
STIV - *Sulfolobus* turreted icosahedral virus
SV40 - simian vacuolating virus 40
Tal – Tsg101-associated ligase
TEMED - Tetramethylethylenediamine
TGFβ - Transforming growth factor β
TGN - Trans-Golgi network
TIRF – Total internal reflection fluorescence microscopy
TMT – Tandem Mass Tag
tracrRNA - trans-activating crRNA
Tris - tris(hydroxymethyl)aminomethane
tRNA – Transfer RNA
TSG101 - Tumour susceptibility gene 101 protein
TTC19 – Tetratricopeptide Repeat Domain 19
Ub – Ubiquitin
UBA – Ubiquitin associated domain
UBAP1 - Ubiquitin-associated protein 1
UBD – Ubiquitin binding domain
UBPY - Ubiquitin isopeptidase Y
UEV - Ubiquitin Enzyme Variant domain
UFD1 - Ubiquitin fusion and degradation 1
UIM - Ubiquitin Interacting Motif
ULK3 – Unc-51 Like Kinase 3
UMA – UBAP1-MVB12 associated
UMAD1 – UMA domain containing 1
VAMP8 – Vesicle Associated Membrane Protein 8
VHS - Vps27/HRS/STAM
Vps - vacuolar protein sorting
VSV-G - Vesicular stomatitis virus G
VTA - Vta1–SBP1–LIP5
YFP- Yellow Fluorescent Protein
μg – microgram
μl – microlitre

Index of figures

Index of tables

Chapter 1 – Introduction

1.1. Discovery of the ESCRT machinery

The ESCRT machinery was first identified in budding yeast (Saccharomyces cerevisiae) through a series of light, electron and immunofluorescence microscopy experiments aimed at characterising 41 vacuolar protein sorting (vps) mutant genes that showed defective sorting of proteins to the vacuole – the equivalent of the mammalian lysosome[1–5]. Vps mutants were classified into six classes, termed A-F, according to the distinct vacuole morphologies they displayed. Class E vps mutants had vacuoles of normal morphology but displayed the presence of a malformed pre-vacuolar endosomal compartment termed the class E compartment[1,4]. In class E mutants, biosynthetic and endocytic cargo destined for transport to the vacuole for degradation, such as carboxypeptidase Y, vacuole membrane V-ATPase, vacuolar proteinases and the pheromone receptor Ste3 did not reach the vacuole and instead accumulated at the class E compartment[1,3,4,6]. 13 class E vps genes were initially identified. Further work focussing on sorting of carboxypeptidase S (CPS) and the G protein–coupled pheromone receptor Ste2p showed that class E vps genes were required for sorting of such proteins into the multivesicular body (MVB) pathway: in addition to localisation to the class E compartment, some GFP-CPS localised to the limiting membrane of the vacuole in class E vps mutants, rather than localisation to the lumen, as is mediated by the MVB pathway[7,8].

The products of the class E vps genes were later shown to assemble into four endosomal sorting complexes required for transport (ESCRT): ESCRT-0, ESCRT-I, ESCRT-II and ESCRT-III together with the ATPase Vps4[8–11]. The composition and functions of each of these complexes is discussed in detail in the following sections. Around the same time, it was also shown that ubiquitination of cargo provided a signal for sorting into the MVB pathway, and that the ESCRT complexes interact with ubiquitin, thus providing a link between the requirements for ubiquitination and class E gene products in MVB sorting[8–10]. The ESCRT complexes and Vps4 were found to be sequentially recruited to the limiting membrane of late endosomes, to facilitate sorting of ubiquitinated cargo into

Intralumenal vesicles (ILVs). The resulting MVBs would later fuse with the vacuole, allowing degradation of ILV membrane bound cargo.

1.2. Expansion of ESCRT mediated processes in mammals

The ESCRT machinery shows strong conservation across eukaryotes, and mammalian homologues of all of the yeast class E vps proteins have been identified (Table 1). A gene expansion in the number of ESCRT proteins can also be seen, to adapt to an ever-growing number of discovered ESCRT mediated processes.

In addition to a role in endosomal sorting to the mammalian lysosome and MVB biogenesis, the ESCRT machinery was subsequently established to be essential for other topologically equivalent membrane remodelling processes, notably budding of enveloped viruses[12–15] and cytokinetic abscission[16,17]. The number of discovered ESCRT mediated processes in mammals has continued to grow, extending to processes such as nuclear membrane reformation[18,19], plasma membrane repair[20,21], exosome release[22] and others (Figure 1A). In all of these cases, the ESCRT machinery must assembly within cytosol-filled membranous stalks to stabilise negative membrane curvature and subsequently mediate membrane bending and scission in 'reverse' topology, away from the cytoplasm. This contrasts with 'normal' topology membrane remodelling towards the cytoplasm as seen, for example, in clathrin mediated endocytosis. During clathrin and coated vesicle mediated processes of vesicle biogenesis, the scission machinery, such as BAR/dynamin family proteins must assemble around the outside of the neck of budding vesicles to constrict membrane and mediate severing[23–26].

ESCRT-III represents the macromolecular machine that forms filaments that constrict and sever membrane (Section 1.3.4.). As such, it is essential for all ESCRT mediated processes. The characterisation of numerous ESCRT mediated processes in mammals has shown, however, that in contrast to the classical ESCRT-0 – ESCRT-I – ESCRT-II – ESCRT-III pathway of recruitment necessary for MVB formation in yeast, process specific pathways for ESCRT-III recruitment exist, mediated by site specific adaptors, that recruit ESCRT-III to target membranes in a modular fashion[27] (Figure 1B).

	Yeast subunits	Mammalian subunits
ESCRT-0	Vps27	HRS
	Hse1	STAM1, STAM2
ESCRT-I	Vps23	TSG101
	Vps28	VPS28
	Vps37	VPS37A, B, C, D
	Mvb12	MVB12A, MVB12B, UBAP1
ESCRT-II	Vps36	EAP45/VPS36
	Vps22/Snf8	EAP30/VPS22
	Vps25	EAP20
ESCRT-III	Vps20	CHMP6
	Snf7/Vps32	CHMP4A, B, C
	Vps24	CHMP3
	Vps2	CHMP2A, B
	Did2/Vps46	CHMP1A, B
	Vps60	CHMP5
	Ist1	hIST1
	Chm7	CHMP7
ESCRT associated proteins	Vps4	VPS4A, B
	Vta1	LIP5
	Bro1	ALIX, HD-PTP, Brox
	Doa4	UBPY, AMSH

Table 1. ESCRT machinery components
The subunits of each ESCRT complex are shown for yeast together with their mammalian orthologues. As shown, there has been an expansion in the number of paralogues for many ESCRT proteins in mammals.

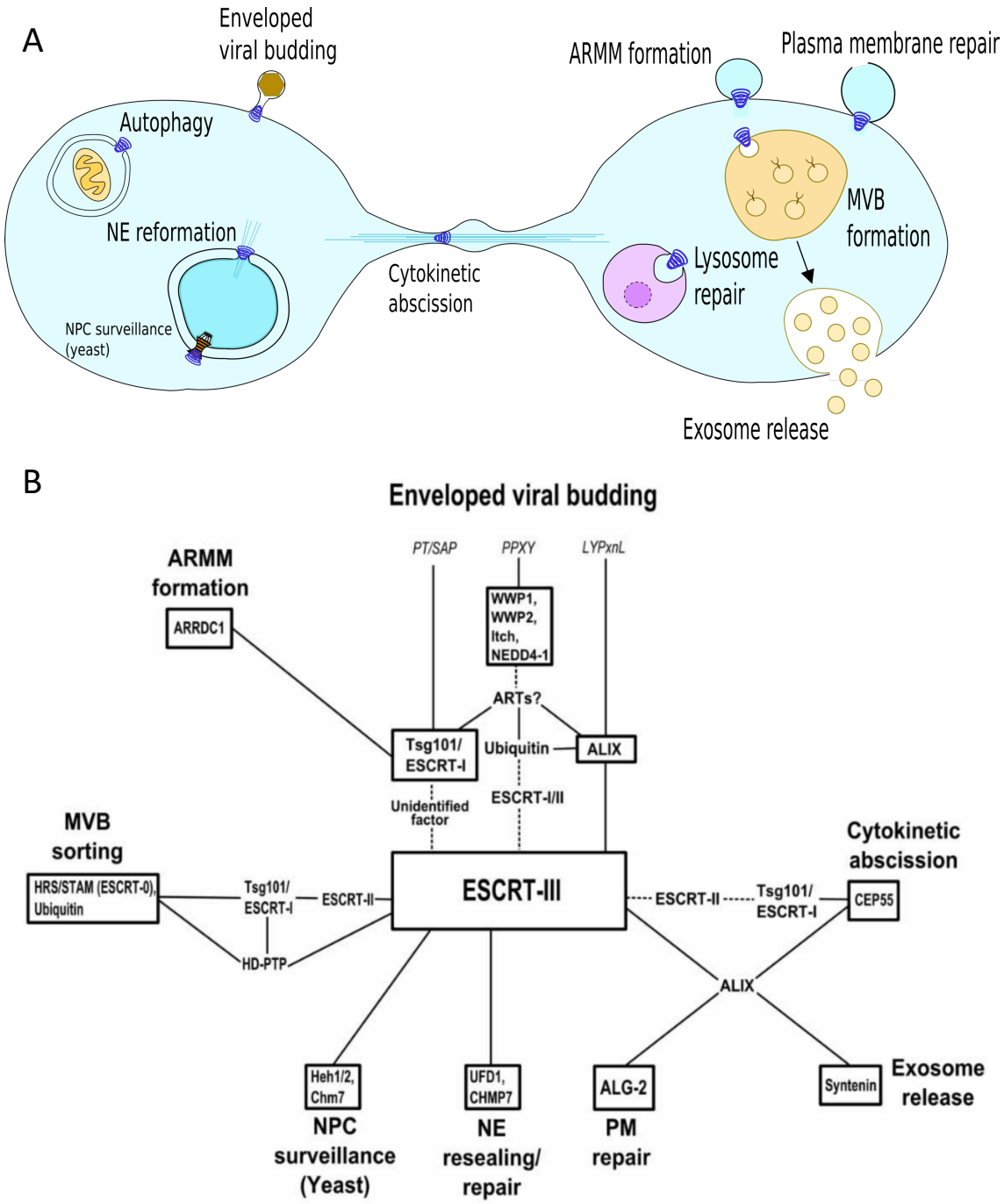

Figure 1. ESCRT mediated processes

A. Whilst the ESCRT machinery was initially discovered to play a role in MVB formation and vacuolar sorting in yeast, an expansion in ESCRT mediated processes is seen in mammals to include an ever-growing number of processes. The ESCRT machinery is represented by dark blue spirals at each of its sites of action. **B.** Modular system of ESCRT-III recruitment by site specific adaptors and pathways. Characterisation of the expanded number of ESCRT mediated processes in mammals has led to a modular model for ESCRT-III recruitment to target membranes. Site specific adaptors recruit ESCRT-III to target membranes to play a role in membrane remodelling and scission in a growing number of discovered ESCRT mediated processes. Site specific adaptors for each process are boxed. Confirmed interactions are represented by solid lines. Interactions that require further validation or that are speculative are represented by dashed lines. NPC = Nuclear pore complex, NE = Nuclear envelope, PM = Plasma membrane, ARMM = Arrestin domain containing 1 (ARRDC1)-mediated microvesicles, MVB = Multivesicular body, ART = arrestin-related trafficking.

1.3. Components of the ESCRT machinery

1.3.1. ESCRT-0

Although conventionally called ESCRT-0, this complex consisting of hepatocyte growth factor-regulated tyrosine kinase substrate (HRS) (Vps27 in yeast) and signal transducing adaptor molecule1/2 (STAM1/2) (Hse1 in yeast) has so far been shown only to play a role in endosomal sorting of ubiquitinated cargo for lysosomal degradation and MVB biogenesis[28]. It is highly adapted for this function by possession of multiple ubiquitin binding motifs and would better be described as an endosomal sorting adaptor protein[29]. HRS and STAM1/2 associate via central coiled-coil GGAs and Tom (GAT) domains[30,31] (Figure 2).

HRS contains a Fab1p/ YOTB/Vac1p/EEA1 (FYVE) zinc finger domain that specifically binds the early endosome associated lipid phosphatidylinositol 3-phosphate (PI3P)[32]. This provides both membrane interaction and endosome specificity[33]. The N-terminus of HRS upstream of the FYVE domain contains a Vps27/HRS/STAM (VHS) domain that binds ubiquitin, as do two tandem ubiquitin interacting motifs (UIMs) downstream of the FYVE domain, forming a double-sided ubiquitin-interacting motif (DUIM)[34–38]. In addition to these domains, HRS contains a C-terminal clathrin binding box (CBB) for interaction with clathrin lattices. This interaction with clathrin has been shown to be important for clustering of HRS bound ubiquitinated cargo into endosomal microdomains, preventing their recycling to the cell surface, thus committing proteins to lysosomal degradation[39–41]. Recent studies have also shown that the HRS-clathrin interaction is important for ILV morphology[42]. As discussed in the following section, a PSAP motif in between the DUIM and the GAT domain is essential for interaction with ESCRT-I via interaction with the UEV domain of TSG101[43–47].

Like HRS, STAM1/2 also contains an N-terminal VHS domain and a UIM just downstream of this. Together with the ubiquitin binding motifs of HRS, this gives a total of five ubiquitin binding motifs in ESCRT-0, providing strong binding to ubiquitin moieties and clustering of ubiquitinated cargo at endosomal membranes. STAM1/2 also contains an SH3 domain just upstream of its central GAT domain, which recruits the deubiquitinases AMSH and UBPY to remove ubiquitin from cargo prior to sorting into ILVs[48–50].

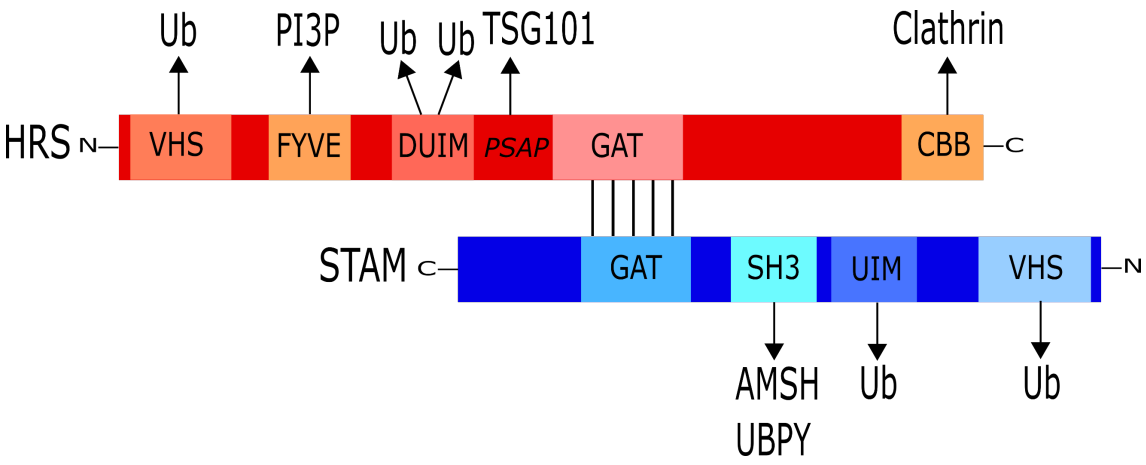

Figure 2. Domain organisation of ESCRT-0
ESCRT-0 consists of HRS and STAM, which form a complex capable of strong binding and clustering of ubiquitin moieties, through binding up to 5 ubiquitin moieties, through VHS and UIM/DUIM domains. HRS additionally contains a clathrin binding box and a central PSAP motif mediates interaction with ESCRT-I through interaction with the UEV domain of TSG101. HRS = hepatocyte growth factor-regulated tyrosine kinase substrate, STAM1/2 = signal transducing adaptor molecule1/2 VHS = Vps27/HRS/STAM domain, FYVE = Fab1p/ YOTB/Vac1p/EEA1 zinc finger domain, UIM = ubiquitin-interacting motif, DUIM = double-sided ubiquitin-interacting motif, GAT = GGAs and Tom domain, CBB = clathrin binding box, SH3 = SRC homology 3 domain.

1.3.2. Focus on ESCRT-I

ESCRT-I is involved in the majority of ESCRT mediated processes described so far, including endosomal sorting[8,51–53], viral budding[12–14,54], cytokinetic abscission[17,55], arrestin domain-containing protein 1-mediated microvesicles (ARMMs) formation[56,57], autophagy[58–61] and endolysosomal repair[62,63]. Whilst a complete mammalian ESCRT-I structure has not yet been solved, inter-subunit interactions are largely consistent with those elucidated in yeast ESCRT-I, suggesting that mammalian ESCRT-I structure is likely to be reasonably well conserved with the structure solved for yeast ESCRT-I. Whilst this section focuses on yeast ESCRT-I, mammalian ESCRT-I composition is discussed in detail in section 3.1.

In yeast, ESCRT-I is specifically involved in the process of MVB biogenesis and vacuolar sorting of ubiquitinated cargo (section 1.4.). It specifically forms a link between ESCRT-0 and ESCRT-II, coupling endosomal membrane recognition and binding to ubiquitinated cargo with the downstream ESCRT machinery.

Yeast ESCRT-I is a heterotetramer containing Vps23, Vps28, Vps37 and Mvb12 subunits[8,64–67]. The yeast ESCRT-I structure supports a “body and appendages” arrangement (Figure 3A), consisting of a central core containing regions of all four

subunits, from which terminal regions of subunits project by connections to the core via flexible linkers. These regions include the N-terminal ubiquitin enzyme variant (UEV) domain of Vps23 that binds to ubiquitinated endosomal cargo and to the Vps27 subunit of ESCRT-0, the N-terminus of Vps37, and, at the other side of ESCRT-I, the C-terminus of Vps28 that interacts with the GLUE domain of the Vps36 (EAP45) subunit of ESCRT-II and Vps20 (CHMP6) of ESCRT-III[8,35,44,46,64,68,69].

The yeast ESCRT-I core can be further divided into an elongated stalk and globular headpiece (Figure 3A). Whilst the headpiece contains regions of all four subunits, the core contains regions of Vps23, Vps28 and Mvb12[64]. Prior to the discovery of Mvb12 as a fourth ESCRT-I subunit, the structure of the headpiece alone was initially solved[68,70]. The headpiece was shown to contain three structurally similar antiparallel helical hairpins, each consisting of two α-helices from each of Vps23, Vps28 and Vps37 arranged at 30° angles from each other like blades of a fan. Vps23 formed the central hairpin in between those of the other two subunits. Whilst no contact was seen between Vps28 and Vps37, extensive contacts between each of these subunits with Vps23 were seen, and stable Vps23-Vps28 and Vps23-Vps37 subcomplexes could be formed. The discrepancy between the molecular weight of yeast ESCRT-I, at 350 kDa, and that of the full-length recombinant ESCRT-I trimer purified from *E. Coli*, at 200 kDa, in gel filtration experiments suggested the presence of additional subunits in the ESCRT-I complex. This led to the discovery of Mvb12 (ORF YGR206w) as the fourth ESCRT-I subunit, as a protein that when mutated showed defective Sna3 and carboxypeptidase Y (CPY) sorting[64–67]. Mvb12 showed pairing with Vps23 and Vps37 in yeast proteome-wide screens, and gel filtration and co-immunoprecipitation experiments confirmed its incorporation into ESCRT-I, further demonstrating that both Vps23 and Vps37 are necessary for its incorporation and stability.

The structure of the entire ESCRT-I core, including the stalk, was subsequently solved (Figure 3B)[64]. The headpiece in this structure matched well with that previously characterised for the trimer. Mvb12 was found to contribute both an N-terminal α-helix and one strand of an antiparallel β-sheet to the headpiece, the other strand provided by Vps28. This β-sheet links the headpiece to the stalk.

The stalk contains a hybrid region proximal to the headpiece, a triple coiled-coil region and a base[64]. Helices from each of Vps23, Vps37 and Mvb12 come together at the central triple coiled-coil region, whilst in the hybrid region Mvb12 contributes to stabilisation of a groove between the same two helices of Vps23 and Vps37 as a series of unstructured hydrophobic residues. Mutational analysis has shown that the triple coiled coil and hybrid regions represent the most important regions necessary for ESCRT-I assembly in yeast, and that correct assembly of all subunits is important for optimal sorting function. Disruption of binding between Vps23 and Vps28 or Vps37 led to clear class E phenotypes, indicating that an intact complex is required for sorting[64,70]. The base of the stalk consists of a four-helix bundle containing the more C-terminal region of the same Mvb12 helix within the triple coiled coil, and two other N-terminal helical regions from Vps23 and Vps37[64].

The N-terminal UEV domain of Vps23 binds to the ubiquitinated moieties of endosomal cargo and to the Vps27/HRS subunit of ESCRT-0[8,35,46]. UEV domains show homology with E2 ubiquitin ligases but lack an active site cysteine residue necessary for catalytic activity[71,72]. They generally consist of a 4-stranded anti-parallel β-sheet against which four α-helices are packed, and lack an additional two C-terminal helices found in E2 ubiquitin ligases. The structure of the UEV in complex with ubiquitin has been solved and has revealed a “pincer” like binding mechanism whereby loops within a unique β-hairpin “tongue” between β-strands 1 and 2, and a “lip” region, closer to the vestigial active site within helix 3, come together to grasp a single ubiquitin moiety (Figure 3C)[73,74]. Although a structure has not been solved for the same UEV in complex with the Vps27 subunit of ESCRT-0, binding sites on Vps27 have been shown to comprise at least a ^{581}PTVP^{584} and ^{524}PSDP^{527} motif and possibly a third ^{447}PSDP^{450} [35,46]. These PXXP motifs are analogous to similar PT/SAP motifs in mammalian ESCRT-0 and viral structural proteins that bind TSG101 (Sections 1.7. and 3.1.1.). Interaction with ESCRT-0 is essential for membrane localisation of yeast ESCRT-I and sorting, and binding of the Vps23 UEV to ubiquitin and Vps27 can occur simultaneously[73,74]. By analogy to the human TSG101 UEV structure (Section 3.1.1.), this is most likely due to separate binding sites for ubiquitin and PXXP motifs at grooves on opposite sides of the vestigial active site, allowing simultaneous binding[13,75,76].

The C-terminus of Vps28 is another well conserved appendage that is not required for ESCRT-I assembly but is crucial for interaction with ESCRT-II and also shows interaction with ESCRT-III[68,69]. The Vps28 C-terminus interacts with the N-terminus of the ESCRT-II subunit Vps36 (EAP45) at its Gram-like, ubiquitin binding in EAP45 (GLUE) domain, at one of a pair of zinc fingers (NZF-N), the other being NZF-C, which binds ubiquitin[68,77,78]. The Vps28 C-terminus forms a 4-helix bundle, containing a hydrophobic pocket between helices 2 and 3 which binds two hairpin loops of NZF-N[79]. In contrast, helices 1 and 4 form the interaction surface for the ESCRT-III subunit Vps20 (CHMP6), with the solvent exposed side chain of a conserved phenylalanine residue at position 228 being particularly important here[69].

In yeast, the VPS37 N-terminal basic region of 34 residues also represents a helical appendage (N-terminal helix (NTH)) that has been suggested to provide some membrane binding activity. These residues showed binding to acidic phospholipids *in vitro* but not *in vivo*[64]. The C-terminus of Mvb12 from approximately residues 74-84 have additionally been shown to bind ubiquitin, representing another UBD. Mutations that abolish ubiquitin binding here, however, did not display a strong sorting defect, suggesting that this is not essential for lysosomal sorting[80].

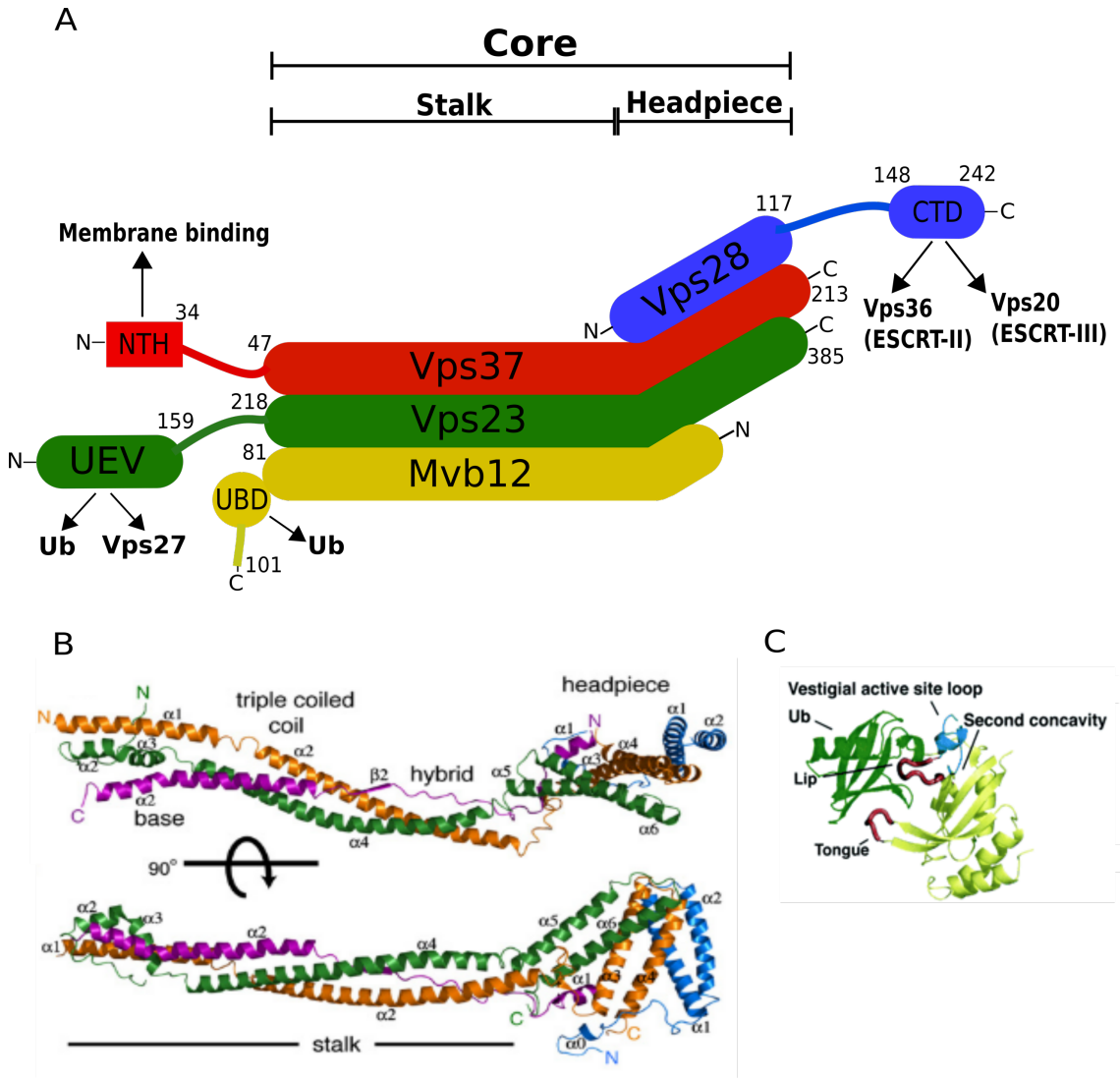

Figure 3. Structure of yeast ESCRT-I

A. 'Body and appendages' structure of yeast ESCRT-I. ESCRT-I contains a core, which represents a body containing regions of all four subunits. The core can be further divided into a stalk, containing regions of Vps23, Vps37 and Mvb12, and a headpiece containing regions of all four subunits. Terminal regions of subunits project from the core via flexible linkers. These include the Vps28 UEV, the membrane binding N-terminal helix of Vps37, the C-terminal UBD of Mvb12 and the C-terminal domain of Vps28 which interacts with ESCRT-II and ESCRT-III. NTH = N-terminal helix, UEV = Ubiquitin enzyme variant, UBD = Ubiquitin binding domain, CTD = C-terminal domain, Ub = Ubiquitin. **B.** Complete structure of yeast ESCRT-I core by *Kostelansky et al 2007*, as described in the text, showing the stalk and headpiece and the hybrid, triple coiled-coil and hybrid regions within the stalk. Orange = Vps23, Green = Vps37, Purple = Mvb12, Blue = Vps28. **C.** Vps23 UEV structure by *Teo et al 2004*. Ubiquitin (shown in green) binds the UEV via a 'pincer' like mechanism whereby loops (shown in red) within a β-hairpin 'tongue' and helical 'lip' region form contacts with ubiquitin. The vestigial active site loop is shown in blue. A second concavity on the opposite side of this most likely represents the site of binding to Vps27 (ESCRT-0), by analogy to the structure for the UEV of the human homologue TSG101 in complex with a PTAP motif.

1.3.3. ESCRT-II

ESCRT-II is a Y shaped heterotetramer consisting of single copies of each of ELL-associated protein of 45kDa (EAP45, also called VPS36/Vps36) and EAP30 (Also called VPS22/Vps22 or Snf8 in yeast), which form the stalk whilst two EAP20 subunits form the arms (Figure 4). All subunits have winged helix (WH) motifs, and PPXY motifs within the first winged helix of EAP20 contact pockets within the WH domains of EAP45 and EAP30 mediating interaction between the subunits[81–83]. ESCRT-II forms a curvature sensing supercomplex with ESCRT-I, that recruits and activates ESCRT-III[79,84]. The stalk is required for interaction with ESCRT-I, as described above, which in yeast is mediated through a Vps36/EAP45 GRAM-like ubiquitin-binding in EAP45 (GLUE) domain Npl4-type zinc-finger 1 (NZF1) zinc finger interaction with Vps28 of ESCRT-I, whilst NZF2 binds ubiquitin[77,79]. The structure of the GLUE domain in humans is not conserved with yeast and does not contain these zinc fingers. Instead, interaction with VPS28 is mediated in part by an alpha helix just downstream of the GLUE domain of EAP45, although this is not sufficient for binding and other interaction sites are likely to be involved[83]. Ubiquitin binding also occurs via another non-conserved site within the GLUE domain[85–87].

In addition to mediating connection to ESCRT-I and binding ubiquitin, the GLUE domain also mediates binding to PI3P[68,85]. Together with a basic helix at the N-terminus of EAP30 which binds acidic lipids, this mediates membrane recruitment[68,83]. Both EAP20/Vps25 subunits are able to interact with CHMP6/Vps20 via their WH motifs, which bind the N-terminus of CHMP6[82,88,89].

Whilst the role of ESCRT-II in MVB biogenesis and vacuolar sorting has been well characterised in yeast, its role in mammals is less clear[10,90–92]. As discussed more in relevant later sections (section 1.4.3. and 1.7.1.), initial studies showed endosomal sorting and viral budding to remain relatively refractory to ESCRT-II depletion. Despite this, some involvement in these processes has later been described, as has a recent role in cytokinetic abscission (sections 1.4.3. 1.7.1 and 4.1.), where it forms a parallel pathway for recruitment of ESCRT-III together with the ESCRT associated Bro1 domain containing protein ALIX[93].

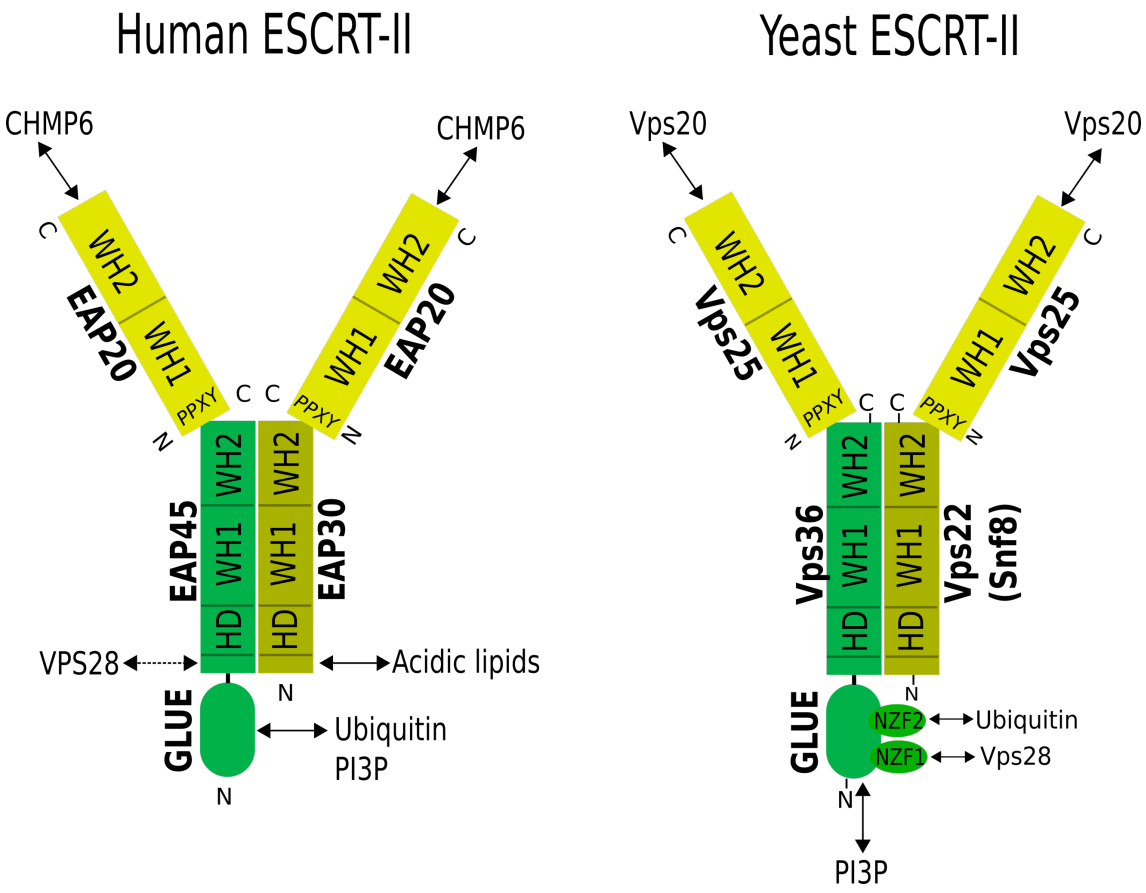

Figure 4. Domain organisation and interaction partners of human and yeast ESCRT-II
ESCRT-II is a Y-shaped heterotetramer in both human and yeast, consisting of WH domain containing subunits. The stalk is composed of EAP45/Vps36 and EAP30/Vps22 (Snf8), whilst the arms are formed by two EAP20/Vps25 subunits which interact with the C-terminal WH domains of EAP45/Vps36 and EAP30/Vps22. The N-terminal GLUE domain of yeast Vps36 contains two NZF zinc fingers, the first of which mediates interaction with Vps28 (ESCRT-I) whilst the second interacts with ubiquitin. The GLUE domain also interacts with PI3P. The human GLUE domain does not contain these zinc fingers and instead binds directly to ubiquitin and PI3P. Interaction with VPS28 is instead partially mediated by an alpha helix just downstream of the GLUE domain, within a helical domain upstream of WH1 and WH2. The equivalent region of EAP30 has been shown to be important for binding to acidic lipids. Each EAP20/Vps25 subunit is able to interact with CHMP6/Vps20, potentially nucleating pairs of ESCRT-III filaments. GLUE = GRAM-like ubiquitin-binding in EAP45, NZF = Npl4-type zinc-finger

1.3.4. Focus on ESCRT-III

1.3.4.1. ESCRT-III structure

Whilst ESCRT-0, -I and -II represent complexes that stably assemble in the cytoplasm prior to membrane recruitment, ESCRT-III represents a more transient complex that assembles directly on membranes. ESCRT-III forms the core macromolecular machine that drives membrane bending and scission through polymerisation of subunits

involving a complex network of homo and heteromeric interactions. ESCRT-III is composed of structurally similar charged multivesicular body proteins (CHMPs) that exist in a 'closed' autoinhibited soluble form in the cytoplasm prior to nucleation mediated transition to an 'open' polymerisation competent form on membranes[9,94–97]. Yeast expresses five main ESCRT-III subunits: Vps20, Snf7, Vps24, Vps2 and Chm7 and three accessory proteins: Did2, Vps60 and Ist1. There has been an expansion in the number of CHMP proteins in mammals to include 12 homologues: CHMP6 (Vps20), CHMP4A-C (Snf7), CHMP3 (Vps24), CHMP2A, B (Vps2), CHMP1A, B (Did2), CHMP5 (Vps60), hIST1 (Ist1) and CHMP7 (Chm7) (Figure 5A). CHMPs are highly charged helical proteins with a basic, positively charged N-terminus and an acidic, negatively charged C-terminus[95,96]. Structures for CHMP1B, CHMP3, CHMP4, hIST1 and yeast Snf7 have been solved and point to a commonly shared architecture, consisting of five α-helices[95,98–102]. Secondary structure predictions also predict a sixth C-terminal helix, which due to instability has so far only been seen in the crystal structure for hIST1[103]. This α6 helix is responsible for MIM-MIT domain interactions and/or interactions with Bro1 domain containing proteins (Sections 1.3.4.5. and 1.3.5.). In their 'closed' conformation, the first four helices form a structured asymmetric 4-helix bundle, in which the two acidic α3 and α4 helices pack asymmetrically against the basic α1 and α2 helices which form a 7 nm hairpin[95,96,98,99,101]. The C-terminal α5 helix folds back on this bundle via multiple contacts to maintain a polymerisation incompetent state (Figure 5B)[95,96,98,99,104,105]. Consistent with an autoinhibitory role for α5 is the finding that various CHMPs form filaments when this region in truncated[96,102,106]. In their 'open' conformation, α2 and α3 together form a single helix which extends the hairpin with α1, to form an elongated structure which forms multiple hydrophobic and electrostatic interactions with neighbouring subunits and membrane acidic phospholipids during polymerisation[98–101]. Polymerisation occurs concomitantly with membrane binding.

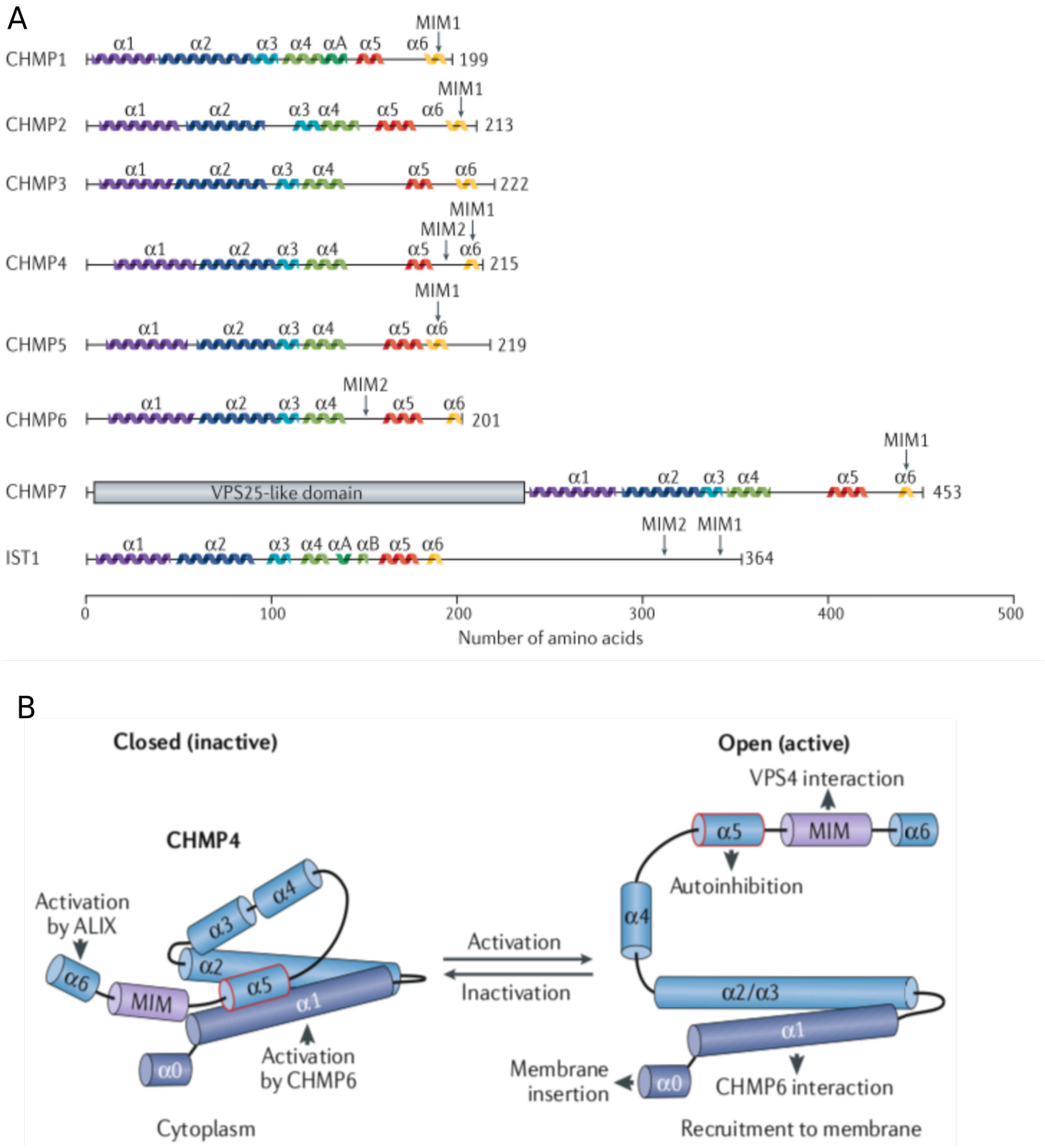

Figure 5. Structural organisation of CHMP proteins

A. Structural organisation of the human CHMP proteins. Each of the 12 human CHMP proteins contain 6 α-helices. The first four helices play a structural role, whilst α5 plays an autoinhibitory role in the 'closed' state. α6 is responsible for MIM-MIT interactions (Section 1.3.4.5.) and interactions with Bro1 domain containing proteins, such as ALIX, Brox and HD-PTP (Section 1.3.5.). CHMP7 displays a hybrid structure with an EAP20/Vps25-like N-terminus and CHMP6-like C-terminus. *Schöneberg et al 2016* **B.** Conformational change upon transition from 'closed' to 'open' conformations. CHMPs exist in an inactivated, 'closed', soluble form in the cytoplasm in which the first four helices form an asymmetric bundle against which the α5 helix folds back to maintain a polymerisation incompetent state. Activation of CHMPs can occur through interaction with CHMP6, CHMP7 or Bro1 domain containing proteins and is promoted by negative membrane curvature. CHMPs transition to an 'open' polymerisation competent form, capable of membrane binding and lateral interactions with other CHMP proteins. Structural reorganisation involves formation of a single helix from α2 and α3 which forms a hairpin with α1. *Adapted from Vietri et al. 2019*

1.3.4.2. ESCRT-III filaments

The relative simplicity of the ESCRT system and the smaller number of ESCRT-III proteins in yeast has facilitated the elucidation of a defined order of assembly of CHMP subunits, through genetic and mutant analysis. ESCRT-III subunits are recruited in the order: Vps20, Snf7, Vps24 and Vps2. Vps2 then recruits the AAA ATPase Vps4 for disassembly and recycling of ESCRT-III subunits[9,107]. All ESCRT-III proteins were shown to co-localise and form a transient 450kDa complex on endosomes. These proteins were proposed to form two subcomplexes being Vps20-Snf7 and Vps24-Vps2 which showed separate phenotypes upon depletion. Whilst depletion of Vps20 or Snf7 lead to redistribution of Vps2 from class E compartments to the cytoplasm in Vps4Δ cells, depletion of Vps2 or Vps24 showed an increase in class E compartment associated Vps20 and Snf7[9]. The main constituent of this complex was Snf7, comprising around half of the complex, and predicted to contribute around 10-15 subunits to the complex. Overexpression of Snf7 led to increased polymerisation of Snf7 to form a >600kDa structure with a concomitant increase in the diameter of ILVs[108]. Vps24-GFP was seen to decorate larger Snf7 structures and a similar increase in polymerisation of Snf7 was seen in Vps24Δ cells[89]. In a separate study, Snf7 also formed filaments at the plasma membrane when overexpressed[97]. It has also been observed *in vitro* that when Vps24 is mixed with Snf7, polymerisation is attenuated[89]. These studied led to a model whereby the role of Vps20 is to nucleate polymerisation of Snf7 to form filaments. The Vps24-Vps2 subcomplex then caps filaments to prevent further growth, and recruits Vps4 for filament disassembly and recycling. Importantly, this sequence of events has been observed using fluorescently tagged proteins and also *in vitro* using purified proteins[9,89,107,108].

Myristoylation of Vps20, probably coupled with electrostatic interactions at its N-terminus, has been shown to be necessary for membrane binding[9]. In the case of the human homologue, CHMP6, myristoylation has also been shown to favour an open conformation, consistent with its role as an upstream nucleating subunit, which promotes polymerisation of CHMP4 by causing a conformational change that displaces the inhibitory α5 helix from the core[109]. Negative membrane curvature has also been shown to contribute to nucleation, and interaction between ESCRT-I - ESCRT-II - CHMP6

has been proposed to form a curvature sensing supercomplex that initiates polymerisation[88,110,111].

The function of the main ESCRT-III subunits described above is believed to be largely conserved from yeast to humans. However, one prominent difference is the existence of additional proteins with potential nucleation ability besides the ESCRT-II-CHMP6 subcomplex, notably the Bro1 domain containing proteins ALIX, Brox and HD-PTP, and also CHMP7 (Section 1.3.5.). Bro1 domain containing proteins bind to the most C-terminal α6 helix of CHMP4, which also harbours a MIM1 domain (Figure 5A). This has been suggested to weaken autoinhibitory interactions and/or promote clustering and scaffolding of CHMP4 subunits, thus promoting nucleation[112]. Whilst CHMP7 displays a hybrid structure with an EAP20-like N-terminus and CHMP6-like C-terminus (Figure 5A), nucleation capability has not yet been shown[113]. ALIX can dimerise via its V domain and in this way bind two CHMP4 subunits, just as each EAP20 subunit of ESCRT-II can nucleate filament polymerisation[102,104,108,114–117]. 6nm spiral filaments form when CHMP4B is overexpressed in COS-7 cells, and this filament width is likely to be due to bundling of pairs of 3nm filaments, as seen mediated by ALIX *in vitro*[97,114]. Nucleator mediated bundling is likely to account for some of the variation seen in filament width both *in vitro* and *in vivo*[97,102,118–120]. Variation in filament width is required to accommodate the observed severing of membrane necks of varying diameter by the ESCRT machinery. For example, the necks of nascent ILVs are generally 20-40nm in diameter, whilst during cytokinetic abscission, the midbody connecting nascent daughter cells is around 1μm wide[118,121].

1.3.4.3. Membrane deformation by ESCRT-III

Both *in vitro* and *in vivo* electron microscopy studies have shown formation of ESCRT-III polymers of varied morphologies and dimensions, involving both homo and heteropolymerisation of CHMPs. Spirals, tubes, coils and cone structures have been observed, and this diversity in structure has made it difficult to define a unifying mechanism for ESCRT-III action[102,104,106,119,120,122]. It also strongly suggests that ESCRT-III can assume a variety of different structures to accommodate scission at different sites of ESCRT action. CHMP4 has been shown to form spirals of approximately 4nm diameter

filaments both *in vitro* and *in vivo,* at the plasma membrane of COS-7 cells (Figure 6A)[97,104,119,123]. Analysis of yeast Snf7/CHMP4 showed that whilst the inner ring of similar spirals is overbent, the outer rings are underbent, and the resulting stiffness of the filaments is predicted to be sufficient for the spirals to behave as mechanical springs. When these spirals covered the entire membrane, they showed buckling activity due to release of elastic energy and protruded from the plasma membrane into tubes[123]. Similarly, in the case of human CHMP4A, overexpression in a VPS4 mutant background resulted in tubular evaginations from the plasma membrane, consistent with the characteristic ESCRT mediated deformation of membrane away from the cytoplasm (Figure 6C)[97]. CHMP2B showed similar formation of tubes when overexpressed[124]. Earlier studies showed Snf7 to form sheets, rings and filamentous structures when activated by truncating the C-terminus[105,114,123]. CHMP2A and CHMP3 have been found *in vitro* to form approximately 50nm membrane associated heteropolymeric tubes, the inner surface of which recruits VPS4[97,106,125]. Interestingly, these two subunits also form cones and domes closing the tubes, potentially consistent with the role for these CHMPs in capping filaments to prevent further growth (Figure 6B). A further interesting observation from another study was that the addition of Vps24 and Vps2 to recombinant Snf7 caused formation of filaments of a greater diameter to be formed, showing an increase from 9nm to around 65nm[104].

A high resolution cryo-EM structure was recently solved for a double-stranded helical filament of approximately 7nm consisting of N-terminal domains of hIST1 and CHMP1B subunits[102]. Intriguingly, this structure showed hIST1 to form the outer strand of the helix in a 'closed' conformation whilst CHMP1B formed the inner strand in an 'open' conformation (Figure 6D). The resulting tubule had a negatively charged exterior and positively charged interior that was capable of membrane binding with normal topology: the structure assembled around rather than inside membrane. This structure is interesting in that it opens up the possibility that 'closed' CHMP conformations may not always represent polymerisation incompetent conformations, and that CHMPs could be capable of directing membrane scission of normal rather than 'inside-out' topology in some instances.

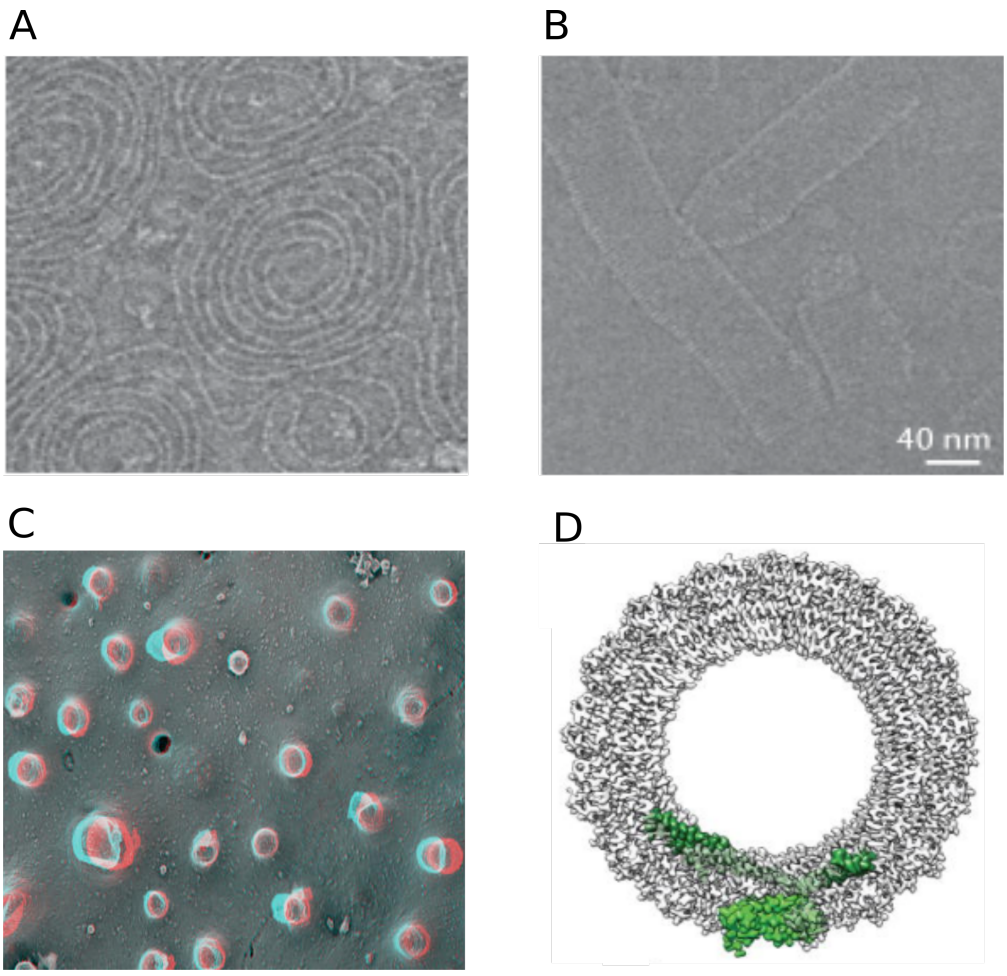

Figure 6. Cryo-EM ESCRT-III polymer structures
A. *C. elegans* CHMP4 spirals *Shen et al 2014* **B.** Cone capped tubules of CHMP2A-CHMP3 *Effantin et al. 2013* **C.** Buds and tubules of CHMP4A protruding from membranes in a VPS4 mutant background *Hanson et al 2008.* **D.** Cryo-EM reconstructed hIST1$_{NTD}$-CHMP1B tube. IST1 = light green outer strand, CHMP1B = dark green inner strand. *McCullough et al 2015*

1.3.4.4. Models for ESCRT-III mediated membrane scission

A consensus model for the mechanism of ESCRT-III mediated scission does not exist yet. Reasons for this include the difficulty in proposing a model that unifies all of the above described structures, and it is likely, given the variety of structures seen, that more than one mechanism exists. It is also unclear whether or not some of the above described structures genuinely exist under physiological conditions, due to the overexpressed nature of the CHMPs in these studies. Furthermore, as particularly evident from studying ESCRT-III in mitosis/cytokinesis, CHMPs do not show redundant functions, so

lack of the entire complement of CHMP proteins used in the above studies is also not representative of physiological conditions.

Earlier more simple models proposed for membrane constriction and severing included a filament mediated model based on the observed ability of Snf7/CHMP4 to polymerise into tight spirals, thus providing the force necessary to constrict membranes (Figure 7A)[97,114]. This model, however, does not take the capping role of CHMP2 and CHMP3 into account. A VPS4 mediated remodelling model has also been proposed, suggesting that VPS4 actively mediates constriction of assembled tubular structures within membrane tubes by sequential removal of ESCRT-III subunits (Figure 7B)[89,97,105,126]. This would lead to constriction and thinning until opposing membranes are close enough for scission to be energetically favourable. Although VPS4 is essential for ESCRT-III disassembly and recycling, whether it plays a role in filament constriction, remodelling and/or severing remains an open question. Going against a role in constriction would be the observation in yeast that ILV formation was not perturbed by the absence of Vps4 or Vps2, however Vps4 was required for subsequent budding events[127]. This is more supportive for a role in recycling.

A 'whorl' model was originally put forward to account for ILV formation in yeast and takes into account the abovementioned upstream ability of ESCRT-I – ESCRT-II – CHMP6 to sense negative membrane curvature and nucleate polymerisation of pairs of CHMP4 filaments (Figure 7C)[84]. These pairs of filaments are stabilised by their interaction with ESCRT-I and -II, and form spokes that extent into a whorl, meeting at the point of scission, at which VPS4 is involved in clustering the ends of the spokes. Membrane-filament interaction would naturally cause membrane to constrict towards the site of scission. Consistent with this model is the finding that deletion of one Vps25/EAP20 subunit of ESCRT-II in yeast disrupts ILV formation[108].

A dome model has been put forward to account for the abovementioned ability for CHMP2 and CHMP3 to form dome shaped caps at the ends of tubes, and represents the best supported model so far (Figure 7D)[106,128]. In this model, membrane is scaffolded by tubules which taper to the point of scission at the dome shaped caps. Membrane interaction with the progressively narrowing polymers at the cap would constrict membrane, pulling opposing membranes together until a diameter narrow enough to favour spontaneous fission (approximately 3nm) is reached[106,128–130]. Whether VPS4 is

required for fission in this model is still unclear[102,130]. This model is more consistent with the observation that the ESCRT machinery can mediate scission of tubes of varied diameter ranging from 50nm-1μm.

An inverse buckling model has additionally been proposed based on the overbent inner filaments and underbent outer filaments seen in Snf7/CHMP4 conical structures (Figure 7E)[123,131,132]. In this model, polymerisation would occur outwards from the centre of the spiral. VPS4 mediated severing of the overbent inner ring would then release the spiral from upstream ESCRTs such as ESCRT-I, -II and/or viral Gag proteins, and cause relaxation of the cone back into a flattened disk[129]. The concomitant release of energy has been proposed to drive scission.

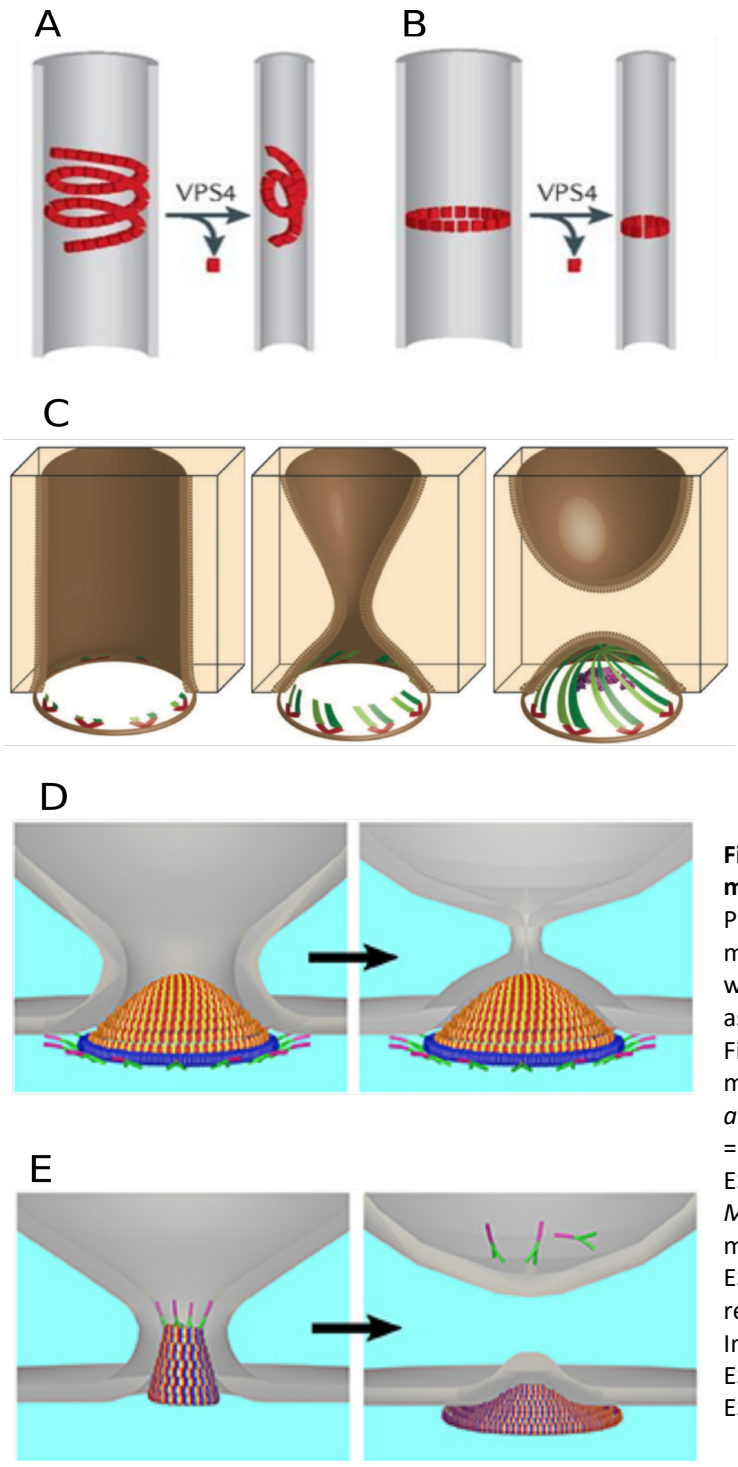

Figure 7. ESCRT-III polymerisation models
Proposed models for ESCRT-III mediated membrane scission from within narrow membranous stalks, as described in the text include **A.** Filament mediated model. **B.** VPS4 mediated model. *Martin-Serrano and Neil 2011*. **C.** Whorl model. Red = ESCRT-I – ESCRT-II, Green = ESCRT-III filaments, Purple = VPS4. *McCullough et al. 2013* **D.** Dome model. Green = ESCRT-I, Purple = ESCRT-II, Blue = CHMP4, red/yellow = CHMP2/CHMP3 **E.** Inverse buckling model. Green = ESCRT-I, Purple = ESCRT-II, Red = ESCRT-III. *Caspi and Dekker 2018*

1.3.4.5. MIM-MIT domain interactions

With the exception of CHMP3, all CHMP proteins contain C-terminal MIT-interacting motifs (MIMs)[96,101,133]. In CHMP 'open' conformations, these interact with varying affinities to microtubule interaction and transport (MIT) domains found in a variety of important ESCRT-III associated proteins, particularly those involved in cytokinetic

abscission (discussed in more detail in sections 1.5.5. – 1.5.7.) and notably VPS4 and its activator LIP5[134,135]. MIT domains consist of asymmetric three-helix bundles. Two classes of MIM motifs have been described according to their structure and interaction surface with MIT domains. MIM1 domains were initially characterised as single helices containing the consensus sequence (D/E)XXLXXRLXXL(K/R), and with the exception of hIST1 are represented by the single α6 helix of CHMPs 1, 2, 4, 5 and 7[103,136]. A MIM1 motif in hIST1 is located downstream of α6 towards the C-terminus[101]. MIM2 domains are found in CHMPs 4 and 6, upstream of α6 and α5 respectively[126]. hIST1 contains a MIM2 motif upstream of its MIM1[126]. The single amphipathic helix of MIM1 domains interacts through conserved leucine residues with the groove in between helices 2 and 3 of MIT domains[136,137]. MIM2 domains, conversely, form extended structures with the consensus (L/V)Px(V/L)P (where x denotes a hydrophilic residue) that bind in the groove between MIT domain helices 1 and 3[126]. As discussed in the context of cytokinesis in sections 1.5.5. – 1.5.7., preferences in binding are seen for the MIT domains of certain ESCRT accessory proteins for certain CHMPs.

1.3.4.6. VPS4 AAA ATPase

VPS4 is the AAA ATPase required for ESCRT-III filament disassembly and recycling by harnessing the energy from ATP hydrolysis to mechanically disassemble polymers. VPS4 exists as monomers or dimers in the cytoplasm and depends on binding to both ATP and ESCRT-III filaments for assembly and activation[138–141]. Cryo-EM structures have shown that VPS4 assembles to form two asymmetric hexameric rings that combine to form a membrane-bound dodecameric structure[139–143]. Each monomer consists of an N-terminal MIT domain and an ATPase cassette that can be further divided into a large and small ATPase domain[144]. The large domain is responsible for catalytic activity, containing a Walker A motif responsible for ATP binding and a Walker B motif responsible for hydrolysis. An arginine finger also facilitates coordination of ATP at subunit interfaces. Loops within the large ATPase domain also mediate interaction with ESCRT-III filaments. The small domain contains a β-domain within an internal loop structure that binds to the VPS4 activator, LIP5[145–149].

Binding to ESCRT-III filaments is mediated at the exposed C-termini of CHMP proteins via MIM-MIT domain interactions, and binding activates VPS4 by relieving autoinhibitory interactions previously mediated by its MIT domain[138,150,151]. Cryo-EM structures point to a 'conveyor-belt' model of action whereby VPS4 translocates along ESCRT-III filaments which pass through the central pore of the hexamers one dipeptide at a time (Figure 8). Cycles of ATP hydrolysis lead to the movement of the loops, which force conformational changes in CHMP subunits causing them to unfold and disassemble[139,141]. According to this model, when the subunits of the VPS4 hexamer are labelled A-F, the subunit in position F of the hexamer detaches from that in position E and re-joins the hexamer at position A, binding the next ESCRT-III dipeptide motif. Hydrolysis of ATP is proposed to occur at the interface between subunits C and D whilst ADP and ESCRT-III subunits are released at the E to F transition[139,141].

LIP5 binds to the VPS4 β-domain through a Vta1–SBP1–LIP5 (VTA) domain and is believed to activate VPS4 in two ways. Firstly, from a structural point of view it links the β-domain to the ATPase domain of adjacent subunits, around the ring exterior[140,141]. Secondly, it contains two tandem MIT domains that bind to the MIM domains of CHMPs, thus facilitating their interaction with VPS4. Since the MIMs of CHMP4 and CHMP3 do not bind as strongly to the VPS4 MIT domains as those of CHMPs 1, 2, 5, 6 and hIST1, prior interaction of CHMPs 4 and 3 with LIP5 has been suggested to facilitate their disassembly. Alternatively, it has been proposed that these CHMPs simply disassemble more readily following disassembly of the CHMPs that bind more strongly to VPS4[135,148,149].

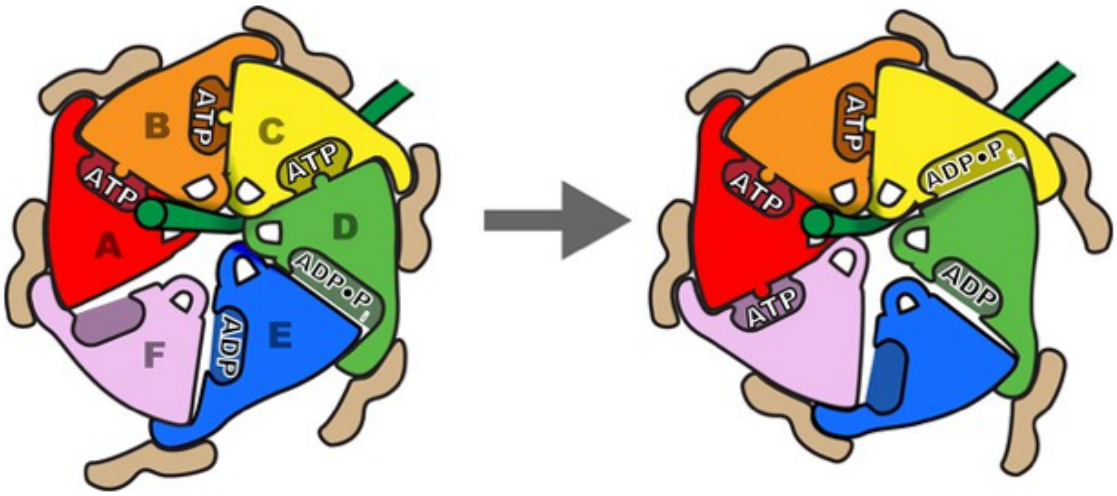

Figure 8. 'Conveyor-belt' model of VPS4 translocation along ESCRT-III filaments
Hydrolysis of ATP occurs betweensubunits C and D of the VPS4 hexamer, providing the energy to disassemble ESCRT-III filaments as VPS4 translocates along a filament one dipeptide at a time. the subunit in position F of the hexamer detaches from the subunit in position E and re-joins the hexamer at position A, binding the next ESCRT-III dipeptide motif. LIP5 adaptor protein, required for VPS4 activation, is shown in light brown around the VPS4 ring exterior. *Monroe et al. 2017*

1.3.5. Bro1 domain containing ESCRT associated proteins

Although often referred to as accessory proteins of the ESCRT machinery, Bro1 domain containing proteins Bro1 in yeast, and ALIX, HD-PTP and Brox in mammals are essential in a wide variety of ESCRT mediated processes. These ESCRT associated proteins represent important scaffolding platforms that form numerous interactions with upstream ESCRT proteins, ESCRT-III, membranes and a variety of other proteins outside the ESCRT family. Bro1 domains generally consist of 14 α-helices and 3 β-sheets that form a banana-shaped structure, the convex surface of which has been proposed to potentially sense negative membrane curvature[152–154]. Six helices towards the centre form three tetratricopeptide repeat-like helical hairpins, organised in a right-handed superhelix. This is flanked by a more N-terminal helical bundle and the β-sheets.

1.3.5.1. Bro1

Yeast Bro1 consists of a Bro1 domain at its N-terminus followed by a central coiled coil region, called the V-domain, and a proline-rich C-terminal domain[155,156]. Bro1 is essential for endosomal sorting in yeast, as evidenced by localisation of GFP-tagged CPS to the vacuole membrane rather than to the lumen in Bro1 mutants[155]. Furthermore,

overexpression of Bro1 has been shown to inhibit Vps4 mediated ESCRT-III disassembly *in vitro* and *in vivo* and this leads to a reduction in the efficiency of ILV detachment from late endosome membranes[157].

Bro1 binds Snf7/CHMP4 via a conserved hydrophobic surface in the middle of the concave side of its banana shaped Bro1 domain, and this interaction is required for endosomal localisation and function[153,155]. Some endosomal localisation is still observed, however, when the Snf7/CHMP4 binding site is mutated, suggesting that other mechanisms for membrane recruitment are present[153]. Bro1 binds a motif in Snf7/CHMP4 that is similar to a MIM1 motif and analogous to the site in mammalian CHMP4 homologues that binds ALIX (see below)[157]. Bro1 has also been shown to play a seemingly separate role in recruitment of the ubiquitin hydrolase Doa4/UBPY to endosomes[158]. This interaction is mediated by its proline rich domain, which binds to the catalytic domain of Doa4 and stimulates its activity[159]. Doa4 localisation to endosomes and deubiquitination is impaired upon deletion of Bro1[160]. This role appears to be separate from the above-mentioned role in inhibiting ESCRT-III disassembly, as overexpression of Bro1 has no effect on deubiquitination of CPS, and ILV formation is reduced upon deletion of Bro1 but not Doa4[157,159].

The V-domain of Bro1 binds ubiquitin and has also been found to bind Rfu1 – a regulator of ubiquitin homeostasis, that inhibits the activity of Doa4[161,162]. Bro1 binds a YPEL motif in Rfu1, analogous to the YPXnL motifs of cellular and viral structural proteins that bind ALIX (see below), and is necessary for endosomal localisation of Rfu1[162]. In addition to Rfu1, the proline rich domain of Bro1 binds the ubiquitin ligase Rsp5, which has been implicated in the degradation of Rfu1[163]. A more precise relationship between these proteins and Bro1 in ubiquitin regulation remains to be investigated, but it would appear from the above findings that Bro1 plays an important role in bringing together important regulators of ubiquitin homeostasis in yeast.

1.3.5.2. ALIX

ALG-2-interacting protein X (ALIX, also called AIP-1), together with HD-PTP (see below) is one of two mammalian homologues of yeast Bro1, that shows 22% sequence identity with Bro1[164]. ALIX was initially discovered as an interaction partner for the calcium binding protein ALG-2, which is involved in apoptotic signalling[165,166]. It is an essential

ESCRT associated protein involved in a wide variety of ESCRT mediated processes including viral budding, cytokinetic abscission, endosomal sorting, exosome biogenesis and plasma membrane repair, as discussed in the relevant sections.

Like yeast Bro1, ALIX consists of a Bro1 domain, a central V domain and a C-terminal proline rich domain (Figure 9). As in the case of Bro1, the banana shaped Bro1 domain of ALIX binds to CHMP4 proteins at its concave surface via an interaction through the same hydrophobic patch as in yeast Bro1 with the most C-terminal amphipathic helices of CHMP4 paralogues[167]. A distinct pattern of hydrophobic residues in these CHMP4 helices with the consensus M/L/IxxLxxW, differs from that seen in CHMPs 1-3, which display the consensus L/I/MxxxLxxL, and thus confers binding specificity to Bro1 domain containing proteins rather than MIT domain containing proteins (Section 1.3.4.5)[167]. In addition to binding CHMP4 paralogues, the Bro1 domain has been implicated in binding the nucleocapsid (NC) of HIV-1, in addition to the interaction between the V domain with HIV-1 p6 (section 1.7.1.)[168–170]. A unique loop within the Bro1 domain also mediates binding to the late endosome associated phospholipid LBPA and an additional conserved hydrophobic patch at the tip of the Bro1 domain has also been found to bind the SH2 domain of Src kinase, implicating ALIX in endosomal sorting as discussed further below[171,172].

The V-domain in ALIX consists of two extended 3-helix bundles, forming two helical arms that form a V shape, at approximately 30° to each other, hence the name for this region[152,173,174]. This contrasts with the single coiled-coil in the V-domain of yeast Bro1, although this also forms a similar V shape, with two arms connected by a flexible hinge[161,162]. Dimerisation of ALIX is essential for its function and this is mediated via the V-domain[114,161,175,176]. The second of these V domain helical arms also binds polyubiquitin chains and the YPxnL motifs found in cellular and viral structural proteins (sections 1.7.1 and 1.8.)[152,173,175,177]. A conserved phenylalanine residue at position 676, within a conserved FYX_2L sequence is particularly important in mediating interaction with YPXnL motifs[173].

A number of binding partners have been identified for the C-terminal proline rich region of ALIX including CEP55 and TSG101 (sections 1.5.4 and 4.1), ALG-2 (sections 1.8.2. and 4.1.), endophillins, the SH3 domain of Src kinase, and Cin85 (also known as SETA or Ruk), as discussed below[172,178,179]. In addition to the unique loop in the Bro1 domain that binds

LBPA and the necessity for dimerization, a further unique feature of ALIX is autoinhibition in its cytosolic form, which is again mediated by the proline rich region. The PRR folds back, interacting with the Bro1 domain and renders the Bro1 and V domains inaccessible to binding partners[180]. Activation of ALIX has been proposed to occur by a number of mechanisms including dimerization, interaction with the abovementioned binding partners and phosphorylation in the PRR[114,180–182].

Depletion of ALIX has not conclusively been shown to block degradation of EGFR, and ALIX has not been shown to play as prominent a role in endosomal sorting as HD-PTP, or function in classical ubiquitin mediated receptor internalisation into ILVs[90,183–185]. Nonetheless, involvement in negative regulation of EGFR sorting at the plasma membrane has been implied through its interactions with Cin85, endophilin and Src kinase. ALIX binds to the SH3 domain of Cin85 – an adaptor protein for Cbl E3 ubiquitin ligase, which ubiquitinates the cytoplasmic domain of membrane bound EGFR leading to its endocytosis[186–188]. It also binds the SH3 domains of endophilins, which facilitate endocytosis[189,190]. This is believed to prevent association of endophilins and Cin85 with Cbl, thus preventing ubiquitination and endocytosis of EGFR[188]. Conversely, stimulation of EGFR activates Src kinase which via its SH2 domain first binds the Bro1 domain of ALIX. Its SH3 domain also binds to the PRD of ALIX. Hyperphosphorylation of ALIX by Src kinase prevents interaction of ALIX with Cin85, thus allowing Cin85 to interact with EGFR bound Cbl[172,188]. A further example of involvement of ALIX in a non-classical ESCRT mediated sorting process is in the ubiquitin independent sorting of PAR1 – the G protein coupled receptor for thrombin. Sorting of PAR1 into ILVs does not require recognition of ubiquitin moieties by ESCRT-0, -I and -II and instead interacts directly with the V-domain of ALIX via a YPX_3L motif[177,191].

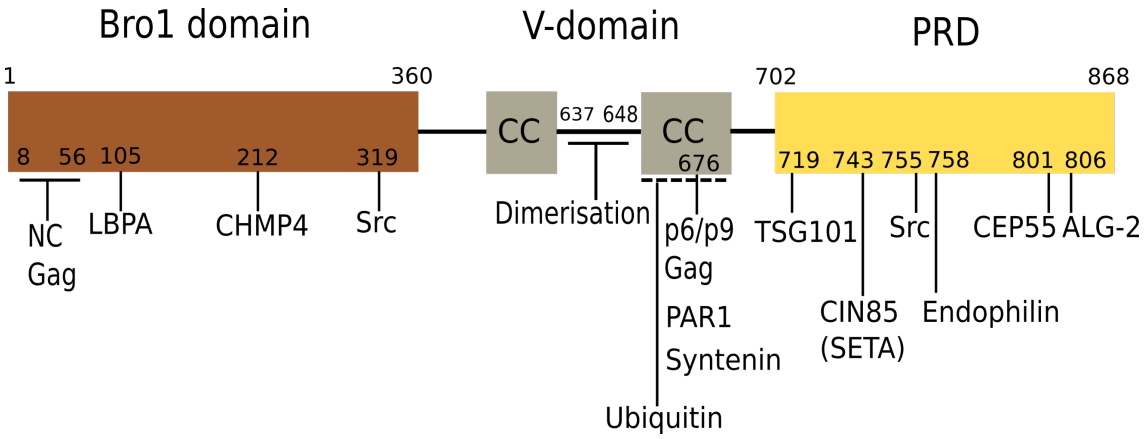

Figure 9. Domain organisation and interaction partners of ALIX
ALIX consists of an N-terminal Bro1 domain, a central coiled-coil region known as the V-domain and a C-terminal proline rich domain (PRD). ALIX mediates interaction with multiple ESCRT and ESCRT associated proteins, notably CHMP4, thus ESCRT-III, CEP55, TSG101, and YPXnL containing viral structural proteins such as HIV-1 p6 Gag and EIAV p9 Gag (Section 1.7.1.). Approximate central binding residue positions, or regions are shown for each interaction partner. Dotted line represents a generalised region through which binding occurs, although more precise mapping of shorter regions/residues involved have yet to be elucidated. PRD = Proline rich domain, NC = nucleocapsid, LBPA = Lysobisphosphatidic acid, PAR1 = Protease-activated receptor-1, CIN85 = Cbl-interacting protein of 85 kDa, ALG-2 = Asparagine-linked glycosylation protein 2 homolog, TSG101 = Tumor susceptibility gene 101, Centrosomal Protein of 55 kDa

1.3.5.3. HD-PTP

Like the other ESCRT associated Bro1 domain containing proteins, His Domain Protein Tyrosine Phosphatase (HD-PTP, also called PTPN23) consists of a Bro1 domain followed by a V-domain and PRD. However, it contains an additional C-terminal protein tyrosine phosphatase (PTP) domain and PEST domain (Figure 10)[192]. Unlike ALIX which plays a role in the numerous ESCRT mediated processes listed above, HD-PTP has so far been shown to play a role specifically in endosomal sorting and MVB biogenesis[184,193–197]. It is highly adapted to this role, as evidenced by interactions with ESCRT-0, ESCRT-I and ESCRT-III. HD-PTP has been shown to be essential for the sorting of EGFR, MHC class I, PDGFR-β and α5β1 integrin, and its depletion disrupts EGFR sorting and leads to accumulation of ubiquitin-conjugated proteins in malformed endosomal compartments[184].

In contrast to ALIX, HD-PTP does not dimerise or show autoinhibition, and adopts a more rigid extended conformation[198,199]. The V-domain is considerably different from that in Bro1 or ALIX and forms a continuous extended backbone. Like the V-domains of ALIX and Bro1, this region also interacts with ubiquitin. Importantly, however, it also directly

interacts with UBAP1 – an MVB12-like subunit of mammalian ESCRT-I that is highly adapted for recognition of ubiquitin and endosomal sorting (Sections 1.4.3 and 3.1.4.)[184,199]. Interaction with UBAP1 occurs via the same conserved FYX_2L motif that in ALIX binds the YPX_nL motifs of viral structural/cellular proteins, and in this case binds to an FPXL motif within the centre of UBAP1 between its UMA and SOUBA domains (section 3.1.4.)[199]. The Bro1 domain of HD-PTP binds the ESCRT-0 subunit STAM, via its GAT domain, at the same hydrophobic pocket that interacts with CHMP4 proteins[197,200]. CHMP4 proteins and STAM therefore compete for binding to HD-PTP at this site. Likewise, the proteins SARA and endofin, which are involved in TGFβ receptor signalling, also compete with CHMP4 for binding to this site[201]. STAM also interacts with the PRD via its SH3 domain, by recognising a PPRPTAPKP binding motif, that also interacts with TSG101[197,200]. An interaction between the EGFR adaptor Grb2 with the PRD has also been described, further highlighting how highly adapted HD-PTP is to its sorting function[202]. The PTP domain of HD-PTP has largely been shown to be catalytically inactive, due to divergence of residues that are normally conserved within the phosphatase domain[203]. It does appear to show phosphatase activity towards FYN kinase, however[204]. This suppresses FYN activity and has been suggested to account for the identity of HD-PTP as a tumour suppressor. The C-terminal PEST domain corresponds to a known proteolytic signal that likely accounts for the short half-life of HD-PTP[192]. The relevance of the PTP and PEST regions have not yet been studied in detail. Interactions with the abovementioned subunits of ESCRT-0, -I and -III together with their competition for binding to identical sites on HD-PTP has led to proposal of a shuffling model for ILV sorting of ubiquitinated cargo[205]. According to this model, HD-PTP would support the sequential recruitment of ESCRT-0, -I and -III, by first binding STAM (ESCRT-0) at the two interaction surfaces described above. Binding of ESCRT-I via TSG101 and UBAP1 subunits would then compete with ESCRT-0 for binding to HD-PTP at the PRD, partially displacing ESCRT-0 whilst maintaining the STAM GAT domain interaction with the Bro1 domain. ESCRT-III CHMP4 interaction with the Bro1 domain would further displace STAM, leaving ESCRT-0 bound to HD-PTP only via any potential interaction with EGFR, via Grb2. According to this model, the ubiquitin binding domains of ESCRT-0 and ESCRT-I would be located close to the EGFR binding site on HD-PTP, at the opposite side of the protein from where ESCRT-III binds, at the Bro1 domain and via the VPS28 (ESCRT-

I) – CHMP6 interaction. This both supports a model for sequential recruitment of ESCRTs and further extends this model to potentially explain how ESCRT-III could be positioned at the necks of nascent ILVs, juxtaposed with the ubiquitinated cargo 20-30nm away to be sorted into the ILVs[205].

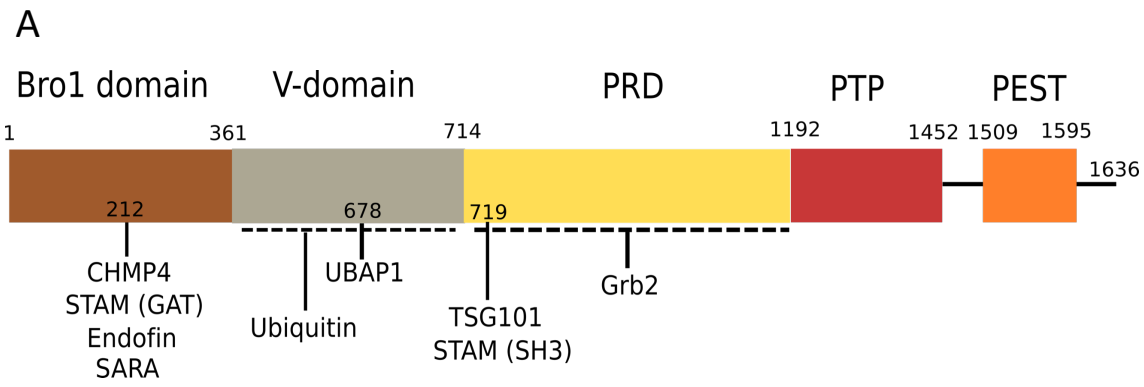

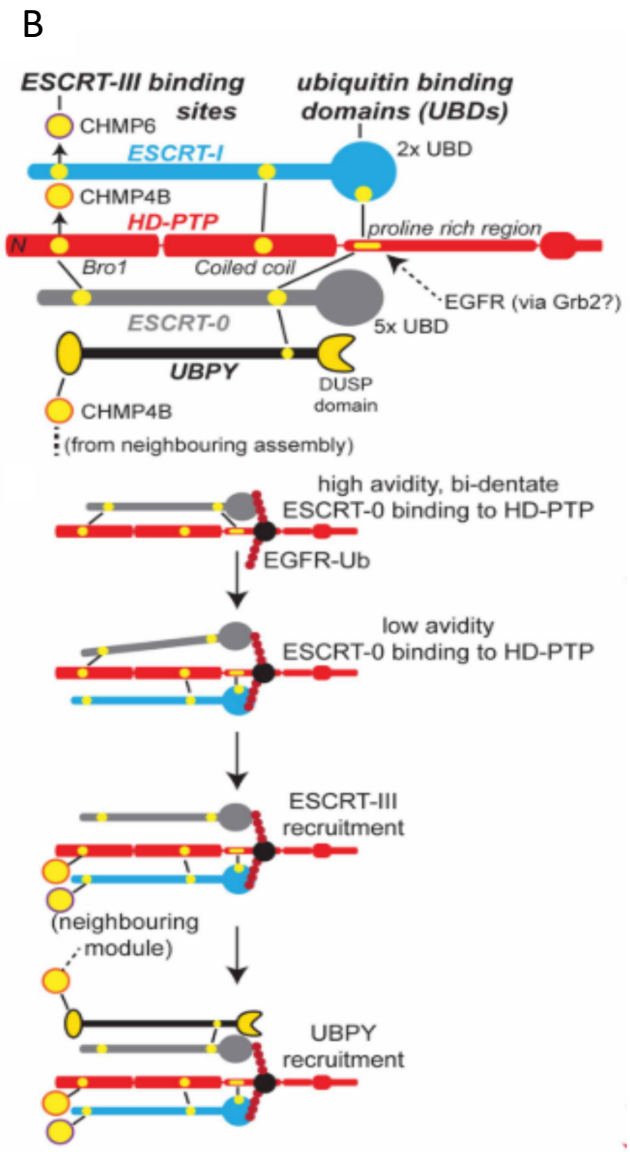

Figure 10. Domain organisation of HD-PTP and model for action in endosomal sorting
A. Domain structure and interaction partners for HD-PTP. HD-PTP contains an N-terminal Bro1 domain, a V-domain and a PRD like ALIX, however it also contains a largely catalytically inactive PTP domain and a PEST domain, suggested to be involved in protein degradation. Approximate central binding residue positions, or regions are shown for each interaction partner. Dotted lines represent a generalised region through which binding occurs, although more precise mapping of shorter regions/residues involved have yet to be elucidated. PRD = Proline rich domain, PTP = protein tyrosine phosphatase, SARA = Smad anchor for receptor activation, Grb2 = Growth factor receptor-bound protein 2. **B.** Model for sequential shuffling of ESCRT complexes by competitive binding to HD-PTP. HD-PTP first interacts with ESCRT-0 at endosome membranes by binding to STAM1/2 at both its binding sites. Binding of TSG101 and UBAP1 would then displace STAM1/2 from its binding site within the PRD, but leaving it still able to bind via its GAT domain at the Bro1 domain. Subsequent binding of CHMP4 to the Bro1 domain would fully displace STAM1/2 leaving ESCRT-0 only able to interact with HD-PTP via interaction with EGFR via Grb. Later recruitment of the deubiquitinase UBPY (Section 1.4.3.) via STAM1/2 can also be accounted for by this model. *Tabernero and Woodman 2018*

1.3.5.4. Brox

Although at an early stage of investigation at present, Brox represents another ESCRT associated Bro1 domain containing protein that encodes a short CAAX farnesylation motif downstream of its Bro1 domain, in place of the V domain and PRD[206]. Like ALIX and HD-PTP, Brox binds to CHMP4 paralogues but also to CHMP5[207]. Structural characterisation of these interactions has shown that whilst both CHMP4 proteins and CHMP5 interact with the same concave hydrophobic surface of the Bro1 domain, The C-terminal regions of these CHMPs that interact with Brox are completely different. Whilst the C-terminus of CHMP4 proteins forms an amphipathic α-helix, as described above, that of CHMP5 forms a tandem β-hairpin structure consisting of three short β-strands. The second of these strands forms important contacts with the Bro1 domain[207].

1.4. ESCRTs in endosomal sorting

1.4.1. Overview of the endosomal system

The endocytic pathway in mammals comprises a transport system of heterogeneous membrane bound compartments that through various morphological changes and fusion events serves to sort incoming intracellular cargo back to the extracellular environment or to the lysosomes/vacuole for degradation. The system can be divided into a recycling system consisting of the plasma membrane, early endosomes (EEs) and recycling endosomes; a degradative system consisting of endolysosomes and lysosomes; a feeder system connecting the recycling and degradative systems consisting of late endosomes (LEs); and a biosynthetic system linked to both the recycling and degradative systems represented primarily by the trans-Golgi network (TGN) (Figure 11)[208].

Cells are constantly sampling their extracellular environment, taking up solutes, macromolecules, receptor-ligand complexes, lipids and nutrients. The majority of this internalised cargo is returned to the extracellular environment via the recycling pathway. Cargo is internalised into primary endocytic vesicles such as those formed by clathrin mediated endocytosis. EEs are believed to form from fusion of these primary endocytic vesicles, and function to further sort cargo into recycling endosomes and return them to the extracellular environment, or to sort them into LEs for entry into the degradative system[208].

EEs contain both tubular and vacuolar domains and localise close to the plasma membrane. Rab and Arf GTPases are important markers of vesicle identity and act to control homotypic fusion events through recruitment of appropriate effector proteins and provision of the energy required for fusion[209–212]. Rab5 is associated with early endosomes and associates with its effectors, notably VPS34/p150, early endosome antigen 1 (EEA1) and class C core vacuole/endosome tethering (CORVET)[209,213–219]. VPS34 is a phosphatidylinositol 3-kinase complex that catalyses the formation of the lipid PI3P - another marker of EE identity[213,220]. Rab5 and PI3P together recruit EEA1, which is yet another marker specific to EEs that is involved in ensuring homotypic fusion with other EEs or incoming endocytic vesicles[215–218]. Likewise, the CORVET complex

interacts with Rab5 and soluble NSF adaptor protein receptors (SNARE) proteins appropriate for catalysing homotypic fusion of EEs[221,222].

Cargo destined for degradation must be fed into the degradative system via LEs, involving fusion of EEs with LEs and accompanying morphological changes. Endosomes become larger and more spherical with an increased number of ILVs. They also acidify, as mediated by V-ATPases[223–226]. Importantly, there is a Rab5 to Rab7 switch, and a PI3P to PI(3,5)P_2 conversion, conferring LE identity (Figure 11)[208,227,228]. The Rab5 to Rab7 switch is mediated primarily by the SAND (SAND endocytosis family)1/MON-CCZ1 (Vacuolar fusion protein CCZ1 homolog) complex[229,230]. PI3P to PI(3,5)P_2 conversion is mediated by the PI3P 5-kinase PIKfyve/Fab1p[231,232]. Just as Rab5 interacts with the CORVET complex, Rab7 interacts with the homotypic fusion and protein sorting (HOPS) complex – a similar hexameric complex containing two alternative subunits, Vps39 and Vps41, in place of Vps3 and Vps8 from CORVET[233]. This confers specific binding to Rab7. Like CORVET, HOPS mediates interaction with SNAREs appropriate for homotypic LE fusion events and LE to lysosome fusion events to form endolysosomes, in which the majority of cargo degradation takes place. Lysosomes represent more of a storage vesicle for degradative enzymes such as acid hydrolases[219,233,234].

Bidirectional vesicle exchange with the TGN ensures delivery of lysosomal components to the lysosomes, via LEs, and the delivery and removal of the abovementioned endosomal components associated with the progression from a recycling to a degradative identity.

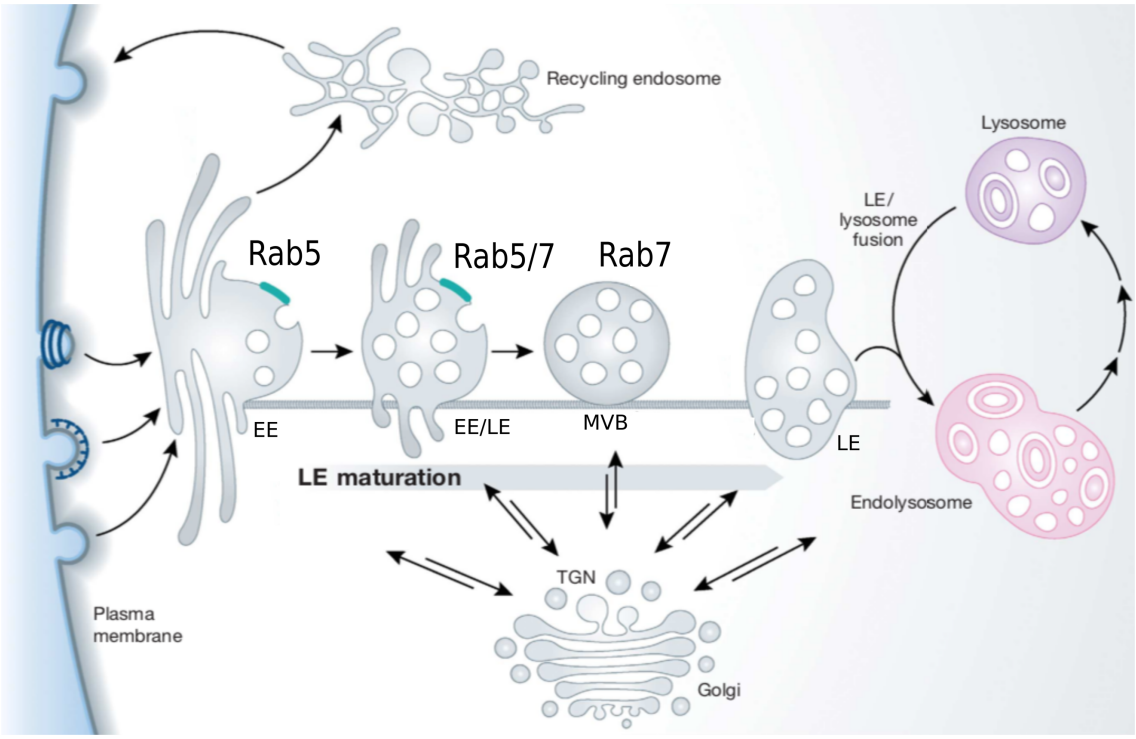

Figure 11. Overview of endosomal sorting
Endosomal sorting serves to either recycle internalised cargo back to the extracellular environment or sort cargo to the vacuole/lysosome for degradation. It can be divided into a recycling system consisting of the plasma membrane, early endosomes (EEs) and recycling endosomes; a degradative system consisting of endolysosomes and lysosomes; a feeder system connecting the recycling and degradative systems consisting of late endosomes (LEs); and a biosynthetic system linked to both the recycling and degradative systems represented by the trans-Golgi network (TGN). Whilst the majority of cargo is recycled via the recycling system, cargo destined for degradation passes from EEs to LEs and then to vacuoles/lysosomes via fusion events as described in detail in the text. Degradation takes place in the resulting endolysosomes by enzymes such as acid hydrolases. Vesicle transition from EEs to LEs and vacuoles/lysosomes involves various morphological changes including a switch in surface Rab5 to Rab7 GTPase and PI3P to PI(3,5)P2, acidification of the lumen and an increase in size. Vesicles also become more spherical and an increase in multivesicular bodies (MVBs) are seen. Vesicle exchange with the TGN ensures the delivery of the necessary components to each vesicle to ensure progression from a recycling to a degradative identity. Adapted from *Huotari and Helenius 2011*

1.4.2. Ubiquitination

Ubiquitin is a protein of 76 amino acids that acts as a molecular signal most commonly associated with proteasomal degradation and MVB sorting when covalently attached to proteins. Ubiquitin is attached to lysine residues in the form of either monoubiquitination, diubiquitination or polyubiquitination. Ubiquitin chains are formed mainly through attachment of ubiquitin to lysine 48 or lysine 63 residues of ubiquitin, although a total of seven lysine residues capable of ubiquitination are present[235]. Whilst Lys48-linked chains serve as a signal for proteasomal degradation, Lys63-linked chains

are associated with sorting into MVBs via the ESCRT machinery, and lysosomal degradation. Despite this, it is not clear at the molecular level whether early ESCRTs topologically favour binding to polyubiquitin chains or whether polyubiquitin chains simply increase avidity by bringing the ubiquitin binding ESCRT subunits together. Monoubiquitination is sufficient for MVB sorting, and most structural determination of ubiquitin binding motifs of ESCRT proteins has been performed using monoubiquitin[236–238].

Ubiquitination is mediated by three enzymes: an E1 ubiquitin activating enzyme, an E2 ubiquitin conjugating enzyme and an E3 ubiquitin ligase[235]. The E1 ubiquitin activating enzyme activates ubiquitin using ATP and transfers it to the E2 ubiquitin conjugating enzyme. E3 ubiquitin ligases act as a scaffold binding to both the ubiquitin bound E2 enzyme and a specific substrate, thus facilitating transfer of ubiquitin to the substrate protein. The first mammalian E3 ubiquitin ligase to be discovered in MVB targeting of proteins was c-Cbl (as previously mentioned in section 1.3.5.2.) which has been shown to function in EGFR sorting[239,240]. Nedd4-like E3 ligases represent another type of E3 ligase that interacts with the ESCRT machinery and is involved in MVB sorting, such as in that of β2-adrenergic receptor[241]. Arrestin related trafficking adaptors (ARTs) have also been implicated in viral budding (Section 1.7.2.)[242].

1.4.3. Sorting of ubiquitinated cargo into MVBs

According to a model whereby the ESCRT complexes are sequentially recruited to the limiting membrane of LEs to facilitate sorting of ubiquitinated proteins into ILVs, initial recruitment is thought to occur through recognition of the lipid PI3P by the FYVE domain of HRS/Vps27 (ESCRT-0) (Figure 12)[8,44,46,243]. The multiple ubiquitin binding domains of ESCRT-0 generate a high avidity interaction with ubiquitinated cargo, which localise to distinct microdomains on the surface of LEs of specific lipid composition. In addition to PI3P, these sites are particularly rich in cholesterol and LBPA, and also contain ceramides and sphingomyelin[244–247]. Such a composition is likely to play a role in generating membrane curvature and budding. The interaction between HRS and clathrin, which enables association of ESCRT-0 with flat clathrin lattices is also thought to help define microdomains at which ILV formation occurs where ubiquitinated cargo is captured and

clustered favouring sorting and MVB formation. Deletion of the clathrin binding box of HRS leads to a more equal distribution of ESCRT-0 on endosome membranes[39,40].

ESCRT-0 then recruits ESCRT-I via the TSG101/Vps23 UEV domain, which also binds ubiquitinated cargo once at the endosome membrane[45,46]. ESCRT-II is recruited to the membrane via the interaction of the ESCRT-I VPS28/Vps28 C-terminus with EAP45/Vps36 (Figure 12)[68,248]. ESCRT-II is further able to bind ubiquitin and PI3P via its EAP45/Vps36 GLUE domain[77,86]. Although these early acting ESCRTs bind ubiquitin relatively weakly, cargo sorting into MVBs is still impaired when these ESCRTs are mutated[38,77,80,249,250]. ESCRT-II is essential for sorting in yeast, and its overexpression can partially suppress the class E phenotype observed upon depletion of ESCRT-I[10,251]. Furthermore, its non-competitive interactions with ESCRT-I, endosome membrane and ubiquitin has been shown, in yeast, to be necessary for sorting of cargo into MVBs[10,68,79,85]. In mammals, however, the role of ESCRT-II in endosomal sorting is less clear: whilst initial studies showed cargo degradation to be largely refractory to ESCRT-II depletion, later studies reported some perturbation[90,92,194]. It is highly likely that ESCRT accessory proteins such as HD-PTP can bypass the need for ESCRT-II by interacting with ESCRT-0, ESCRT-I and ESCRT-III (Section 1.3.5.3.). HD-PTP has been shown to play roles in the sorting of EGFR, MHC class I, PDGFR-β and $\alpha5\beta1$ integrin and displays endosomal recruitment kinetics similar to ESCRT-0 (Section 1.3.5.3.)[42]. A study examining ESCRTs required for sorting of MHC class I importantly showed that whilst ESCRT-II and CHMP6 were not required for sorting, components of all other ESCRT complexes and HD-PTP were required[194]. This is consistent with a role for HD-PTP in bridging ESCRT-0 and ESCRT-I with CHMP4 proteins.

ESCRT-I and ESCRT-II are believed to form a transiently recruited ubiquitin sensing supercomplex on the endosome membrane[84]. Support for sequential transfer of ubiquitinated cargo from ESCRT-0 to ESCRT-I and -II comes from the fact that all known ubiquitin binding motifs bind the same hydrophobic patch on the surface of ubiquitin within a β-sheet, centered around Ile44. Simultaneous binding of multiple ESCRT ubiquitin binding motifs to ubiquitin would therefore not be possible. Furthermore, depletion of ESCRT-0 prevents recruitment and function of ESCRT-I, consistent with a role upstream of ESCRT-I/-II[44,46]. The finding that ESCRT-I and -II contain fewer ubiquitin binding sites than ESCRT-0, however argues against sequential transfer of cargo. It has

therefore been suggested that perhaps ESCRT-I/-II alternatively act to inhibit diffusion of cargo once captured into sites of MVB formation[252]. Alternatively, as detailed in section 1.3.5.3, proteins such as HD-PTP may act as a platform to direct sequential shuffling of ESCRT complexes, or the monoubiquitination of HRS may promote transition to an inactive state favouring transfer of cargo to ESCRTs I and II.

In addition to functioning as a ubiquitin binding supercomplex, ESCRT-I and -II have been proposed to represent a curvature sensing complex that not only recruits ESCRT-III to regions of curvature, but also potentially drives membrane deformation[84]. This was shown *in vitro* using giant unilamellar vesicles (GUVs), however, which showed production of vesicles of varying size, much larger than ILVs formed *in vivo*[253]. This system was also not able to sort cargo into vesicles. Lipid composition of the membrane has gained much plausibility to account for membrane invagination and MVB formation from both *in vitro* and *in vivo* studies[254]. LBPA containing liposomes have been shown to form ILVs simply by applying a pH gradient across the membrane, suggesting that protein composition is not a hugely important factor in mediating bending[255]. This has been proposed to again account for part of the reason why endosomal sorting in mammalian cells remain refractory to depletion of some ESCRT proteins. One study, by Stuffers et al. 2009 even observed that although cargo sorting was impaired by simultaneous depletion of subunits from ESCRT-0, -I, -II and -III, some MVB formation still occurred, despite showing an increase in size and containing no cargo[256]. This suggests that the early ESCRTs are more responsible for directing and sequestering cargo into MVBs and stabilising the necks of budding ILVs. This would leave a role for ESCRT-III strictly in severing of the necks of budding vesicles, despite the previously described observation that several ESCRT-III proteins can form tubular evaginations when overexpressed (Section 1.3.4.3.) and even form ILVs in GUVs[127].

In the case of the classical pathway for ESCRT recruitment, as essential in yeast, ESCRT-III is recruited via interaction of the EAP20/Vps25 subunits of ESCRT-II with CHMP6/Vps20 (Figure 12). ESCRT-III and VPS4 show rapid recruitment to sites of ILV scission upon maximal attainment of early ESCRTs, which are more gradually recruited to the membrane[42,257,258]. ESCRT-III does not contain any ubiquitin binding domains but importantly is responsible for recruiting the deubiquitinases (DUBs) associated molecule with the SH3 domain of STAM (AMSH) and ubiquitin isopeptidase Y (UBPY)[259–263]. The

equivalent deubiquitinase in yeast is Doa4, and is recruited not by ESCRT-III but by Bro1[158,159] (section 1.3.5.1.). Interaction with Vps20/CHMP6, however, has been shown to be necessary for Doa4 function in MVB formation[160]. Such DUBs function to remove ubiquitin moieties from cargo prior to scission of ILVs, ensuring that ubiquitin is recycled back to the cytosol, thus maintaining ubiquitin homeostasis. Whilst AMSH interacts preferentially with CHMP3, via a MIT-MIM interaction, it also interacts with CHMP1A, CHMP1B, CHMP2A, clathrin and STAM (ESCRT-0) at its SH3 domain[48,259–262,264]. UBPY also interacts with STAM and ESCRT-III and appears to rely more on its interaction with ESCRT-0 for its activity[263]. Another important difference between these DUBs is that whilst AMSH removes Lys63-linked polyubiquitin chains, UBPY removes both Lys63 and Lys48-linked chains[48,49]. Depletion of AMSH leads to increased EGFR degradation, consistent with prolonged signalling for lysosomal degradation due to the loss of removal of ubiquitin[261]. Likewise, loss of Doa4 leads to a reduction in cytosolic ubiquitin levels coupled with an increase in vacuolar levels[159,265]. Studies on UBPY depletion, however have shown both increased and decreased EGFR degradation[49,90,266–269]. This has been suggested to be due to a potential role of UBPY in the deubiquitination of ESCRT proteins such as TSG101 and HRS[270]. UBPY has also been shown to be involved in HD-PTP mediated sorting of EGFR where in addition to deubiquitination it helps facilitate the transfer of cargo from early ESCRTs to ESCRT-III[197,205] (section 1.3.5.3.).

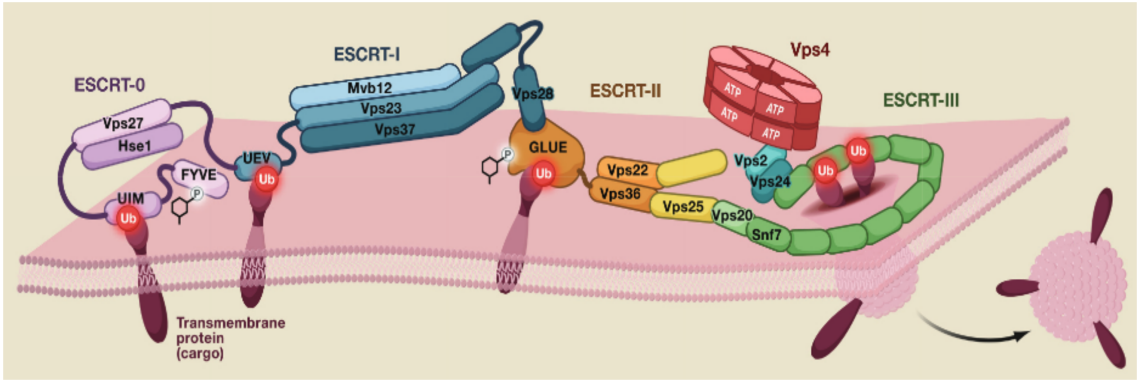

Figure 12. Classical recruitment of the ESCRT machinery to endosomal membranes in yeast
The ESCRT complexes are sequentially recruited in the order ESCRT-0, -I, -II and -III to the limiting membranes of endosomes through a pathway that is largely conserved from yeast to mammals. ESCRT-0 is initially recruited to membrane associated PI3P via the FYVE domain of HRS/Vps27. ESCRT-0 also binds strongly to ubiquitin moieties of cargo to be sorted, through its multiple ubiquitin binding domains (UBDs). ESCRT-0 then recruits ESCRT-I via the TSG101/Vps23 UEV domain, which also binds ubiquitinated cargo. ESCRT-II is recruited via interaction of EAP45/Vps36 with the ESCRT-I VPS28/Vps28 C-terminus. ESCRT-II binds ubiquitin and PI3P via its EAP45/Vps36 GLUE domain. ESCRT-I and -II have been proposed to form a curvature sensing super complex that drives membrane deformation in addition to recruitment of ESCRT-III. ESCRT-III is recruited via interaction of the two EAP20/Vps25 subunits of ESCRT-II with CHMP6/Vps20. Whether ESCRT-III directly contributes to membrane invagination to form intralumenal vesicles (ILV)s, or whether it simply severs the necks of nascent ILVs is unclear at present. Myristoylation of CHMP6/Vps20 facilitates interaction with the membrane. Scission is mediated by formation of filaments consisting mainly of CHMP4/Snf7 and CHMP3/Vps24. CHMP2/Vps2 and CHMP1/Did2 mediate capping of filaments and recruit VPS4/Vps4 ATPase to disassemble and recycle filaments. Prior to sorting into ILVs, ubiquitin moieties are removed from cargo by the deubiquitinases AMSH/Doa4 or UBPY, which are recruited by ESCRT-0 and ESCRT-III. *Teis et al. 2009*

1.5. ESCRTs in cytokinesis

1.5.1. Overview of the cell cycle

There is huge variation according to how often a eukaryotic cell divides according to cell type[271]. The cell cycle serves to allow time for cell growth and duplication of organelles, genetic material and all other components prior to cell division to produce two genetically identical daughter cells. The cell cycle can be divided into two main stages, being interphase and mitosis. Interphase is the stage during which cell growth and duplication of DNA occurs and can be further divided into three phases being Gap1 (G1), synthesis (S) and Gap2 (G2) phases (Figure 13). Mitosis is the process whereby replicated DNA is partitioned into forming daughter cells and cytokinesis occurs concomitantly with the end of this process to separate daughter cells (Figure 13). Mitosis can be divided into prophase, prometaphase, metaphase, anaphase and telophase[272,273]. Cytokinesis occurs concomitantly with anaphase and telophase, and the final abscission event to separate daughter cells typically occurs during G1 phase, but can occur as late as in early to mid G2 phase[274,275]. Since mitosis and cytokinesis generally last only for about one hour, cells spend the majority of their time in interphase[276].

1.5.1.1. Phases of the cell cycle

During the G1 phase of interphase, cells are metabolically active and grow, doubling their mass and organelles, and importantly prepare for DNA replication. Cells also monitor the environment to ensure that conditions are favourable for DNA replication to occur. The majority of cells do not constantly divide and enter a resting phase from G1 called G0, during which proliferation ceases but cells remain metabolically active. G0 can be temporary (quiescence) and last for days to years, or be permanent, in the case of senescence caused by permanent DNA damage or attainment of a terminally differentiated state such as nerve cells[277].

The synthesis (S) phase typically lasts between 8-12 hours, occupying around half of the cell cycle time. During S phase, each pair of chromosomes in the diploid cell (2n) is replicated so that each consists of two sister chromatids (4n), held together by the protein cohesin – a member of the structural maintenance of chromosomes (SMC)

family. Replication of the centrosome, or microtubule organising centre (MTOC) also occurs during S phase to form two pairs of replicated centrioles.

S phase is followed by G2 phase, during which cells continue to grow and importantly prepare for mitosis.

Mitosis begins with prophase, during which condensation of chromosomes occurs, making them appear visible in their characteristic X-shaped structure. Condensation is largely mediated by the protein condensin, which like cohesin is another SMC family protein. Condensin binds chromatids at multiple locations, mediating looping and compaction of chromosomes[278]. Cohesin is removed from the arms of chromosomes in preparation for chromatid separation but retained at the centromere[279]. The centromere is a specialised region at the centre of each chromosome that serves to link sister chromatids and represents the site of kinetochore assembly. Its identity is determined at an epigenetic level, but often contains repetitive DNA sequence and is rich in heterochromatin. The mitotic spindle also starts to form during prophase following localisation of the duplicated centrosomes to opposite poles of the cell, and initiation of microtubule polymerisation[271,276].

Prometaphase begins with breakdown of the nuclear envelope, in eukaryotic cells, to allow spindle microtubules access to the condensed chromosomes. Further growth of microtubules occurs and attachment of microtubules from each pole to each sister chromatid of each chromosome occurs. Attachment occurs at kinetochores, which are disc-shaped macromolecular complexes that attach to the centromeres of each chromosome. Crucially, the kinetochores of sister chromatids are oriented in opposite directions to ensure that each chromatid is captured by microtubules at opposite poles of the cell. This is known as bi-orientation, or amphitelic attachment[280,281]. Whilst microtubules that attach to kinetochores are known as kinetochore microtubules, other non-kinetochore microtubules from both poles interact to form the mitotic spindle framework.

By metaphase, chromosomes are fully condensed and lined up at the equator of the mitotic spindle, equidistant from both poles at the metaphase plate. This is caused by pulling of kinetochore microtubules at both poles of the cell, in both directions until forces from each pole are balanced. Despite this force, sister chromatids do not separate yet, due to their attachment to each other by cohesin.

Sister chromatids separate during anaphase, following degradation of cohesin by the protease separase[282,283]. Sister chromatids move towards each pole due to shortening of kinetochore microtubules. The later sliding of non-kinetochore microtubules past each other, as catalysed by motor proteins, is also an important feature of anaphase and serves to separate the spindle poles.

Upon reaching the poles, sister chromatids begin to decondense during telophase. Nuclear envelope reformation also occurs at this stage.

1.5.1.2. Regulation of the cell cycle by Cyclin/CDK complexes

The cell cycle is an extremely tightly regulated process, ensuring that cells do not progress from one stage to the next until both internal and external conditions are favourable[284]. Central to regulation of the cell cycle are cyclin dependent kinases (CDKs) (Figure 13). These serine/threonine kinases are activated at specific points during the cell cycle, following which they phosphorylate effectors necessary for cell cycle progression. Whilst expression levels of CDKs remain constant throughout the cell cycle, they are activated by cyclins whose levels rise and fall thereby activating them at specific times[285,286]. Cyclin D, which activates CDK4 and CDK6, is an exception in that its levels remain constant as long as there is continued growth factor stimulation. Levels of cyclin H also do not vary greatly over the course of the cell cycle (see below)[287]. Upon binding cyclins, CDKs are not only activated but move into the nucleus due to the nuclear localisation signal provided by the cyclins. Phosphorylation of transcription factors necessary for cell cycle progression can then take place. The most studied substrate of CDK4 and CDK6, in complex with cyclin D, for example is the product of the retinoblastoma tumour suppressor gene (pRb)[288–290]. Phosphorylation of this protein leads to release of the transcription factor E2F which is responsible for the activation of genes necessary for S phase entry, such as cyclins E and A.

Whilst cyclins D1, D2 and D3 bind CDK4 and CDK6 and mediate entry into G1, cyclin E binds CDK2 to mediate entry into S phase[291,292]. Cyclin A also binds CDK2, as required during S phase. The G2 to M phase transition further requires cyclin A, but now in complex with CDK1. During mitosis, cyclin B in complex with CDK1 is required[293,294]. CDK7 (also known as CDK activating kinase (CAK)) is activated by cyclin H, which is expressed throughout the whole cell cycle, and mediates phosphorylation of CDK1,

CDK2 and CDK4 at specific sites[285,295,296]. Together with binding to their respective cyclins, these phosphorylations are also necessary for activation. In addition to phosphorylations that activate CDKs, other phosphorylations inactivate CDKs. For example, phosphorylation of CDK1 within its active site at tyrosine 15 and threonine 14 by Wee1 and Myt1 kinases inactivates CDK1 upon its entry into the nucleus until mitosis, upon which the phosphatase Cdc25 removes these inhibitory phosphorylations[297]. CDK inhibitors (CKIs) also exist. These can be divided into the INK4 family, which targets CDKs alone by competing for binding with cyclins, and the Cip/Kip family which targets CDK-Cyclin complexes[298–301]. Both of these families target CDK4 and CDK6, during G1, however the Cip/Kip family also targets CDK1-cyclin B complexes. In this way, control of cell cycle progression at the level of CDK activity is regulated by both activating and inhibitory phosphorylations, CKIs, and specific cyclin pairing.

1.5.1.3. Checkpoint control of the cell cycle

Another essential feature of the cell cycle necessary for tight regulation is the presence of checkpoint mechanisms to ensure that each step is monitored, and errors in DNA replication or damage are repaired before progression to the next step. There are three main checkpoints in eukaryotic cell division: the G1-S checkpoint, the G2-M checkpoint and the spindle checkpoint[284]. The restriction point is another checkpoint during G1 phase, that represents the point at which cells are committed to entering the cell cycle and do not revert to G0, even if growth factor is removed[302].

The G1-S checkpoint is induced by DNA damage and is dependent on the transcription factor p53. DNA damage of a varied nature is recognised by p53, including base pair mismatch, single stranded DNA and free DNA ends[303]. All are recognised by the presence of single-stranded DNA, or double-strand breaks. More specifically, damaged DNA legions are recognised by the proteins Ataxia Telangiectasia and Rad3-related (ATR), Ataxia Telangiectasia Mutated (ATM) and DNA-dependent protein kinase, catalytic subunit (DNA-PKcs)[304,305]. These are kinases which phosphorylate and activate p53. p53 substrates are numerous. However, an important gene activated by p53 is that encoding the Cip/Kip family CKI p21, which leads to CDK inhibition and cell cycle arrest until DNA damage is repaired. p21 also inhibits DNA synthesis by inhibiting the DNA clamp protein PCNA, which is required for DNA polymerase activity[306].

The G2-M DNA damage checkpoint appears to be largely p53 independent and relies more on an alternative pathway, known as the Chk1 pathway[307,308]. This pathway again relies upon recognition of single-stranded DNA by ATR and its associated DNA-binding proteins. ATR then phosphorylates BRCT-domain mediator proteins which recruit Chk1. Chk1 is phosphorylated, thus activated, by ATR, following which it is able to phosphorylate the previously mentioned Wee1 kinase and Cdc25 phosphatase, leading to activation and deactivation respectively, so that CDK1 is maintained in an inactive form, preventing transition to M phase[309–311].

The spindle checkpoint serves to ensure that all sister chromatids are correctly attached to the mitotic spindle at both poles, in bi-orientation, and are under tension before transition to anaphase. The target of the spindle checkpoint is the anaphase promoting complex or cyclosome (APC/C). The main targets for degradation by this macromolecular E3 ubiquitin ligase are securin, and mitotic cyclins (cyclins A and B)[312,313]. Securin inhibits the enzyme separase, which is necessary for degradation of cohesin, allowing sister chromatids to separate[314,315]. Degradation of mitotic cyclins inactivates corresponding CDKs, promoting anaphase and cytokinesis, and ultimately mitotic exit. Mad2 inhibits the activity of the APC regulator Cdc20 under conditions of absent or incorrect spindle-kinetochore attachment, preventing transition to anaphase[316].

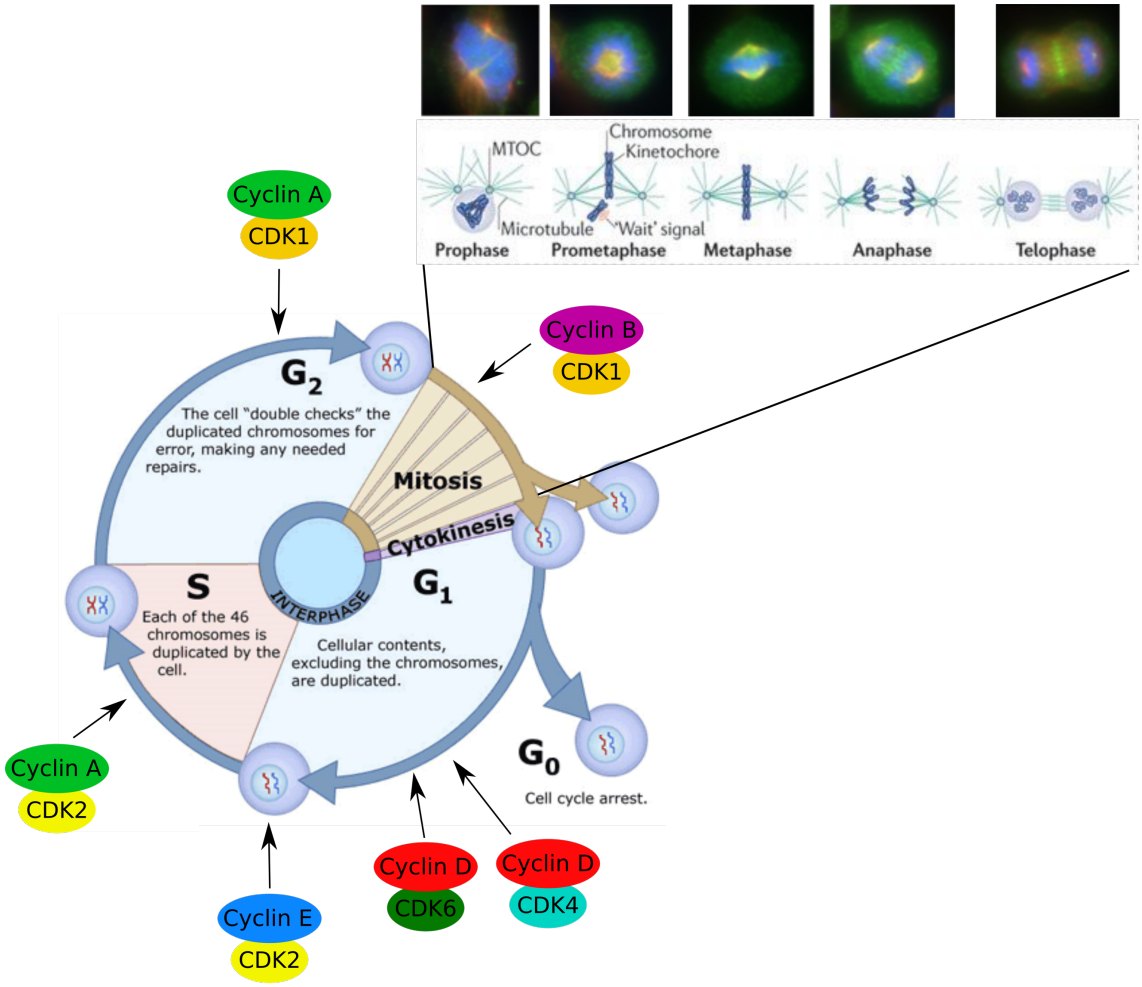

Figure 13. The cell cycle
The cell cycle can be divided into interphase and mitosis. Interphase can be further divided into G_1, S and G_2 phases, and mitosis into prophase, prometaphase, metaphase, anaphase and telophase, as described in detail in the text. The relevant phases of the cell cycle at which activity of each of the relevant Cyclin/CDK complexes are involved are shown. Adapted from © *Clinical tools, Inc.* and *Pines 2011* using images from *Zhao et al 2006*

1.5.2. Early events in cytokinesis

Cytokinesis and mitosis represent the process of cell division to produce two genetically identical daughter cells. It is the process whereby nuclei, cytoplasm organelles and cell membrane are partitioned into the two newly forming daughter cells and their later separation. Cytokinesis requires tight spacial and temporal regulation involving many interconnected factors which play overlapping and non-redundant roles. It occurs concomitantly with anaphase and telophase, and begins with the process of furrow ingression, mediated by contraction of an actomyosin ring. This actomyosin ring forms at the cell cortex around the cell equator, midway between the poles of the anaphase spindle to ensure equal separation of genetic material and organelles into daughter cells.

1.5.2.1. Central spindle formation

Central to polymerisation and contraction of the actomyosin ring is the GTPase RhoA, which accumulates at the equatorial cell cortex in response to signals from the central spindle, also known as the spindle midzone[317]. This is a specialised structure acting as a signalling hub, which forms at the start of cytokinesis at the centre of the mitotic spindle where microtubules overlap at their plus ends in antiparallel arrays[318]. The central spindle is derived partly from the metaphase spindle and partly by augmin mediated *de novo* nucleation of microtubules[319–321]. Its formation depends on removal of prior CDK1 mediated inhibitory phosphorylations of various components, coupled with other phosphorylation events mediated by Aurora B kinase, which relocates to the central spindle from chromosomes at anaphase onset as part of the chromosomal passenger complex (CPC)[322,323]. Three essential components of the central spindle are PRC1, the centralspindlin complex and the CPC (Figure 14).

Protein regulator of cytokinesis 1 (PRC1) is a microtubule bundling protein that binds at the interface between anti-parallel microtubules as a homodimer. Prior to cytokinesis, its dimerization is inhibited by CDK1[324–330]. The centralspindlin complex is a heterotetramer consisting of two kinesin-6 motor protein MKLP1 subunits and two Rho-family GTPase-activating CYK-4 subunits (also termed MgcRacGAP or RacGAP1)[331,332]. Centralspindlin stabilises the central spindle by binding to it as higher order clusters[333,334]. Removal of CDK1 phosphorylation of MKLP1 subunits promotes

interaction with microtubules, whilst Aurora B phosphorylation of MKLP1 triggers release from its inhibitor 14-3-3, thus promoting cluster formation. Aurora B itself is a component of the CPC complex, which also contains the inner centromere protein (INCENP), borealin and survivin[335]. At metaphase the CPC localises to the centromeres, where it facilitates correct kinetochore-mitotic spindle attachment and chromosome structure[336]. At anaphase it re-localises to the central spindle in response to removal of CDK1 phosphorylation of INCENP, allowing INCENP to bind MKLP2, which together with MKLP1 mediates re-localisation of the CPC to the central spindle[337]. The CPC has been proposed to promote microtubule bundling and actomyosin ring formation in addition to phosphorylation of other central spindle components through Aurora B[338–340]. The kinesin KIF4A is directed to microtubule plus ends by PRC1 and other kinesins. KIF4A is activated by Aurora B here, where it inhibits microtubule growth, thus stabilising the central spindle (Figure 14)[324,329]. Aurora B phosphorylation also inhibits activity of the microtubule depolymerase KIF2A[341].

1.5.2.2. Cleavage plane positioning

A detailed understanding of how the cell division plane is specified at right angles to the central spindle remains somewhat lacking, in terms of the role played not just by the central spindle but also by astral microtubules. The mechanism by which central spindle derived signalling molecules localise to the to the cell cortex to specify the division plane is also not so well understood, and has been suggested to be mediated through diffusion, actin cables or microtubule transport. However, activation of RhoA GTPase at the equatorial cell cortex is known to be critical for cleavage plane determination and is regulated by the guanine nucleotide exchange factor (GEF) ECT2 and the GTPase activating activity of the CYK-4 subunit of centralspindlin[317].

RhoA is activated by ECT2, which localises to the central spindle through an interaction with PLK-1 kinase phosphorylated CYK-4[342–345]. Prior to this, the interaction between CYK-4 and ECT-2 is inhibited by CDK1 phosphorylation at metaphase[345]. Upon interaction with CYK-4, ECT-2 it is activated and travels to the cell cortex where it causes localised activation of RhoA (Figure 14)[343]. ECT-2 activation also depends on dephosphorylation of its previously CDK1 phosphorylated C-terminal basic cluster of amino acid residues and this enables binding to the cell membrane[346]. Whilst the GAP

activity of CYK-4 has been shown to be necessary for RhoA activation and potentially its cycling between GDP and GTP bound states, its mechanism of action appears to be more indirect[347,348]. Whilst CYK-4 has been shown to regulate ECT-2, there is also support for a role in the regulation of the GTPase Rac1, which appears to be a preferred substrate[349,350]. Inactivation of Rac1 has been proposed to inhibit formation of a branched actomyosin web at the cell cortex, and also reduce cell adhesion, thus facilitating furrow ingression[349,351,352]. Although less well understood, it has been shown through laser ablation and genetic studies that in addition to the action of RhoA and the central spindle, the more dynamic spindle asters are also involved in cleavage plane positioning, in part through inhibition of RhoA at cortical regions[353–355]. The exact nature of the inhibitory signal mediated by the asters in conjunction with the central spindle remains to be fully elucidated.

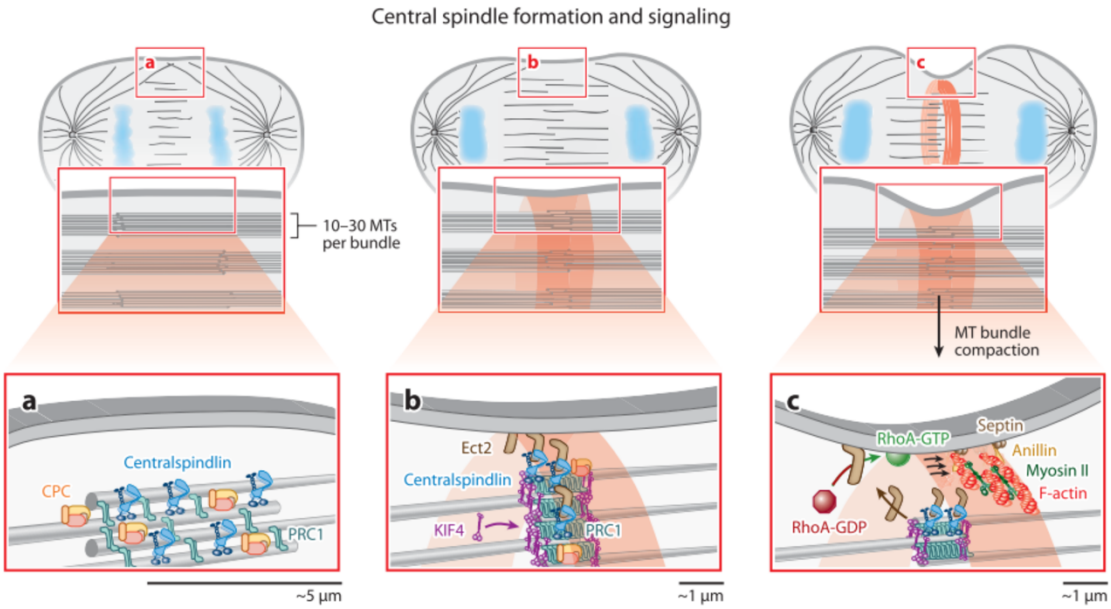

Figure 14. Early events in cytokinesis – central spindle formation and cleavage plane positioning
The central spindle is a specialised structure that forms at the centre of the metaphase spindle at anaphase, where microtubules overlap. It acts as a signalling hub, specifying cleavage plane positioning. As shown in **a**, PRC1, CPC and Centralspindlin are important components of the central spindle. PRC1 bundles microtubules where they overlap at their plus ends. Centralspindlin, consisting of two MKLP1 subunits and two CYK-4 subunits, also helps stabilise the central spindle, as does the CPC, which contains INCENP, borealin, survivin and importantly Aurora B kinase. Aurora B mediated phosphorylation of various components, such as MKLP1, is essential for central spindle formation. As shown in **b**, the kinesin KIF4 is recruited to the central spindle by PRC1, where it further restricts microtubule growth upon activation by Aurora B. The guanine nucleotide exchange factor (GEF) ECT-2 is recruited to the central spindle by interaction with CYK-4, where it is activated and travels to the cell cortex to specify cleavage plane positioning through localised activation of RhoA GTPase, as shown in **c**. RhoA GTPase stimulates actin polymerisation and activation of myosin II to form a contractile actomyosin ring. Anillin, Citron kinase and Septins represent important scaffolding proteins of the actomyosin ring which facilitate attachment of the actomyosin ring to the cell membrane and central spindle. PRC1 = Protein regulator of cytokinesis 1, CPC = Chromosomal passenger complex, MKLP1 = Mitotic kinesin-like protein 1, INCENP = inner centromere protein, ECT-2 = Epithelial cell-transforming sequence 2 oncogene *Green et al. 2012*

1.5.2.3. Furrow ingression

Mediation of actomyosin ring assembly and constriction by RhoA is so far believed to be the most prominent mechanism of furrow ingression. Upon activation, RhoA further activates Diaphanous-related formins which stimulate actin polymerisation[356–358]. RhoA also stimulates the activity of Rho-associated kinase (ROCK), which phosphorylates myosin light chain, thus activating myosin II (Figure 14)[359]. In addition to this, ROCK mediates phosphorylation of the counteracting MYPT myosin phosphatase leading to its inactivation[360]. Anillin and citron kinase are involved in attachment of the actomyosin ring to the cell membrane and central spindle. Anillin is a scaffolding protein which not

only links actin and myosin to the cell membrane, but also binds RhoA, CYK-4, ECT-2, Septins and PtdIns(4,5)P2, facilitating interaction with the central spindle[361–364]. Citron kinase binds to actin, myosin and RhoA and has been shown to be necessary for stability of the actomyosin ring and correct localisation of RhoA[365]. Both Anillin and citron kinase are additionally involved in midbody maturation and stability (Section 1.5.3.).

The mechanism by which the actomyosin ring contracts and generates the force necessary to partition the newly forming daughter cells is not well understood, and potentially varies across species. Whilst a 'purse-string' mechanism has been suggested, whereby aligned myosin II and actin filaments slide across each other, as in muscle contraction, this would necessitate alignment of actin and myosin filaments, which although observed at the equatorial ring is accompanied by many unaligned filaments[366–371]. Unaligned filaments have also been proposed to generate contraction, by potentially forming a network of filaments that contract, mediated by motor activity or cooperation of actin depolymerases with filament end-tracking crosslinkers[372]. The extent to which remodelling of filaments contributes to contraction is also unclear. Whilst dynamic turnover of actin and myosin to maintain a constant unit length of filaments has been observed in urchins and *C. elegans*, stable pools have also been observed, and filament disassembly does not appear to be required for budding in fission yeast[366,373–376]. Despite being well studied in yeast, the role of Septins is less clear in mammals, but these GTP-binding proteins are also likely to be involved in mediating furrow ingression and formation of membrane bound filaments as another component of the actomyosin ring, to which they are recruited by anillin[362]. Whilst depletion of SEPT2, SEPT7 and SEPT11 causes multinucleation, indicative of early stage cytokinetic defects, depletion of SEPT9 causes an increase in midbody connected daughter cells, indicative of a role at a later stage, nearer abscission[377,378].

During furrow ingression, the increase in cell surface area necessitates additional deposition of membrane at the cleavage furrow. This is brought about by targeted fusion of membrane derived from vesicles of both the endocytic and secretory pathways. In addition to membrane, these vesicles also serve to deliver further factors necessary for actomyosin ring assembly, ingression, and abscission (Section 1.5.3.). Experiments in *Drosophila* have shown that several Golgi associated proteins such as syntaxin 5, Cog5 and Cog7 and COPI are required for cytokinesis[379–386]. Proteins of the endocytic pathway

such as clathrin and dynamin have been shown to be necessary for cytokinesis in mammalian cells[387–389]. Although the GTPases Rab11, Arf6 and Rab35 have been better studied for their role in midbody maturation and stabilisation (Section 1.5.3.), Rab11 has also been shown to localise to the cleavage furrow and has been suggested to be necessary for furrow ingression in both Drosophila and mammalian cells[390–392]. Specific lipids, particularly those of the phosphatidylinositol (PI) family are also necessary at both early and later, midbody, stages of cytokinesis as discussed later. Specialised lipid domains containing long chain fatty acids at the cleavage furrow are necessary for membrane remodelling during furrow ingression, and PI(4,5)P2 in particular is enriched at the furrow where it is believed to be necessary for stability and structure of the actomyosin ring, and to promote actin remodelling via its interaction with the actin binding proteins Profilin and Cofilin[393–400].

1.5.3. Midbody formation and maturation

Contraction of the actomyosin ring progresses until a diameter of 1-2μm has been reached. PLK-1 mediated reorganisation of central spindle components, clearance of the cytoskeleton, further vesicle trafficking and membrane fusion events and maturation of the contractile ring then mediate formation of another distinct structure known as the midbody, or intercellular bridge. Daughter cells remain connected by the midbody for between 80 minutes to several hours into G1, before the final abscission event occurs. Why the midbody persists for so long and what events take place during this time period, together with what eventually triggers abscission remains largely unknown. The midbody is a protein rich structure containing more than 100 different proteins, whose main role is to act as an assembly platform for subsequent recruitment of the abscission machinery. The central electron dense region where the compacted interdigitating microtubules of the central spindle overlap at their plus ends is known as the Flemming body[401]. Due to antibody excluding characteristics in immunofluorescence microscopy, this region is also known as the dark zone. Midbody microtubules are highly acetylated, forming stable bundles[402]. Both continuous microtubules, that pass straight through the midbody, and polar microtubules, which overlap at the Flemming body, are found within the midbody[403]. Cryo-electron tomography and fluorescence microscopy have shown

that whilst polar microtubules disappear from the spindle midzone towards the end of cytokinesis, continuous microtubules remain next to abscission sites, demonstrating that microtubules are an important structural component of the midbody, present throughout most of its existence until abscission, and that the midbody is a dynamic structure[403].

During midbody formation, KIF4 and PRC1 remain associated with microtubules where they overlap at the Flemming body. Centralspindlin, ECT2, RhoA, anillin, citron kinase ARF6 and septins re-localise to a ring surrounding the Flemming body known as the midbody ring, and MKLP2 and AuroraB kinase re-localise to microtubules flanking the Flemming body[404–408]. These relocalisation events and maintenance of the midbody structure are dependent on the activity of PLK-1. PLK-1 has been shown to display differing localisation patterns during cytokinesis, localising with KIF4 at the central spindle at the start of cytokinesis, with a gradual dissociation from KIF4 during furrow ingression. PLK-1 reappears, however, at the Flemming body following midbody formation[405].

The lipid composition of the plasma membrane of the midbody is also important for midbody stability and successful abscission (Figure 15). $PI(4,5)P_2$ localisation at the equatorial cortex is initially important for midbody stability and the relocalisation of anillin, septins, RhoA and CYK-4, around the Flemming body by interaction with $PI(4,5)P_2$ through polybasic or Pleckstrin Homology (PH) domains[395–397,409–413]. Phosphatidylethanolamine (PE) accumulates within the outer leaflet of the midbody plasma membrane at telophase and is important for inactivation of RhoA and actomyosin ring disassembly (see below)[395,410,414]. Its depletion prevents abscission, as does cell surface immobilisation by PE-binding peptides[410,414]. This suggests that precise spaciotemporal control of PE composition is necessary for successful completion of abscission. PI3P is another phosphoinositide that has been found to be required for successful completion of cytokinesis, as evidenced by the observed cytokinesis failure upon depletion of the VPS34 or Beclin-1 subunits of the class III PI-3-kinase, which also localises to the midbody[415–417]. Transport of PI3P positive endosomes to the midbody has been shown to be necessary for the localisation of the PI3P interacting protein FYVE-CENT and its binding partner TTC19 to the midbody, which also requires kinesin KIF13A for transport[415,417]. FYVE-CENT together with its binding partner TTC19 appears to be

necessary for cytokinesis, with depletion leading to multinucleation and delayed abscission (Figure 15)[415]. Interestingly, an interaction between TTC19 and the ESCRT-III protein CHMP4B has also been described[415,416]. This potentially represents an interesting link between ESCRT mediated cytokinetic abscission (Section 1.5.4.) with membrane lipid composition, although this requires further validation.

Following furrow ingression, the contractile actomyosin ring must disassemble whilst other components must be retained through a maturation process to form the midbody ring. The inactivation of RhoA by PKCε and 14-3-3 protein leads to disassembly of actin[118,418]. This is also facilitated by Rab35, which recruits its effector PtdIns(4,5)P2 phosphatase OCRL to the intercellular bridge where it reduces PtdIns(4,5)P2 levels, in contrast to the earlier midbody requirement for increased PtdIns(4,5)P2 levels (Figure 15)[394]. Since PtdIns(4,5)P2 promotes actin polymerisation and inhibition of the actin severing enzyme Cofilin, its decrease leads to a reduction in actin filaments[419]. OCRL depletion has been shown to cause a strong increase in cortical actin, which delays or inhibits abscission. Depletion of Rab35 leads to an identical phenotype[394].

Following disassembly of the actomyosin ring, maturation of the midbody ring ensures tight anchorage of the cell cortex to the midbody to prevent furrow regression. Anillin appears to play a much more important role at this later stage of cytokinesis, where it is involved in anchorage of the midbody ring to the plasma membrane, through binding to septins[408,420–422]. RhoA is required for the correct localisation of anillin to the midbody ring and citron kinase is required for the retention of both RhoA and anillin[407]. Citron kinase also interacts with the centralspindlin subunit MKLP1 and KIF14 which interact with PRC1 at the Flemming body[334,407,408,423,424]. An interaction between MKLP1 with Arf6 has also been described, and Arf6 is able to bind membrane through its N-terminal myristoylated helix[425]. Furthermore, Arf6 competes with centralspindlin inhibitor 14-3-3 protein for binding to centralspindlin, thus ensuring that centralspindlin remains clustered and stabilises the midbody[426]. The CYK-4 subunit of centralspindlin also contains a membrane binding domain which contributes to membrane anchorage[427].

In addition to delivery of abovementioned components to the midbody, Golgi and recycling endosome derived vesicle trafficking plays other essential roles at the midbody, such as mediation of further events leading to actin depolymerisation, formation of the secondary ingression sites at which abscission occurs, and has also been suggested to

mediate abscission itself (below and section 1.5.4). Vesicle trafficking is central to all aspects of cytokinesis and has shed light on the overlapping roles of many factors demonstrating a great deal of functional interconnectivity[392].

In addition to the previously described function of Rab35 and OCRL in controlling PI(4,5)P2 levels necessary for abscission, recycling endosome associated Rab 11 represents the other most well studied Rab GTPase in cytokinesis, and is transported to the midbody via its effector FIP3[428]. Fusion of Rab11-FIP3 vesicles has been shown to contribute to narrowing of the midbody at sites adjacent to the Flemming body where abscission takes place, known as the secondary ingression sites, and depletion of Rab11 or FIP3 leads to abscission delay and furrow regression[428,429]. Rab11-FIP3 vesicles also contribute to actin depolymerisation by transport of the RhoA GAP p50RhoGAP to the midbody, to inactivate RhoA (Figure 15)[429]. Since FIP3 is also an effector for Arf6, and both FIP3 and Arf6 bind the centralspindlin components CYK-4 and MKLP1 respectively, this represents a link between Rab11-FIP3 vesicle trafficking and the abovementioned roles of Arf6 and centralspindlin in membrane anchorage[425,430]. FIP3, Rab11 and Arf6 have further been shown to interact with the exocyst complex through interactions with its Exo70, Sec15 and Sec10 subunits respectively[431–433]. The exocyst complex is an octameric vesicle tethering complex required for cytokinesis, together with v-SNAREs, such as VAMP8, and t-SNAREs such as syntaxin2. The exocyst complex depends on the centrosomal protein Centriolin for localisation to the midbody ring, as do SNARE components Snapin and Endobrevin[434].

Syntaxin 16 appears to be another important t-SNARE in cytokinesis, which is required for accumulation of both the exocyst complex and Rab11-FIP3 vesicles at the midbody[435]. It is also necessary for CEP55 and ALIX accumulation at the midbody representing another link between upstream trafficking events with recruitment of the ESCRT machinery to mediate abscission (Section 1.5.4.)[435]. Along the same lines, the post-Golgi secretory carrier membrane protein SCAMP3 has been shown to interact with TSG101 and like SCAMP2 also localises with FIP3 at midbodies[429,436]. SCAMP2 and SCAMP3 have been shown to be necessary for the FIP3 mediated formation of secondary ingression sites and recruitment of ESCRT-III[429].

Lastly, the multifunctional ubiquitin ligase BRUCE has been implicated in cytokinesis through its interactions with MKLP1, Rab8, Rab11 and exocyst components Sec6 and

Sec8[437]. Its interaction with MKLP1 is necessary for midbody ring localisation, and its other interactions further facilitate targeting of Rab11 containing vesicles to the midbody. Furthermore, the ubiquitin ligase activity of BRUCE appears to be necessary for successful cytokinesis: BRUCE depletion leads to the disruption of an observed re-localisation of ubiquitin from the tips of microtubules at their plus-ends to the midbody ring during midbody constriction[437]. The role of ubiquitination during cytokinesis is unclear as yet but is likely to mediate structural or regulatory functions rather than proteasomal degradation, as mono-ubiquitination is mainly seen at the midbody[437]. Another possibility is that ubiquitination generates binding sites for ESCRT machinery as in lysosomal sorting.

There is conflicting data regarding whether vesicle targeting occurs at one or both sides of the midbody, or shows initial targeting to both sides followed by targeting to only one side nearer abscission. Fluorescently tagged FIP3 and VAMP8 have been visualised at the secondary ingression at the side at which abscission occurs and another study visualised asymmetric targeting of GFP-tagged secretory vesicles from only one nascent daughter cell to a region adjacent to the Flemming body at one side only[434,438]. Abscission later occurred at this side. Another study employed TIRF imaging to show that trafficking occurred at both sides of the midbody from both nascent daughter cells[439]. Whatever the case, the observed vesicle fusion within the midbody, and the potentially asymmetric nature of trafficking and fusion has led to one hypothesis that abscission occurs through SNARE mediated fusion of vesicles with the plasma membrane. In disagreement with this model, however, is the observation from other studies that vesicles disappear from the midbody before abscission[118]. Another study reported no effect on abscission when Golgi derived secretion was disrupted[118].

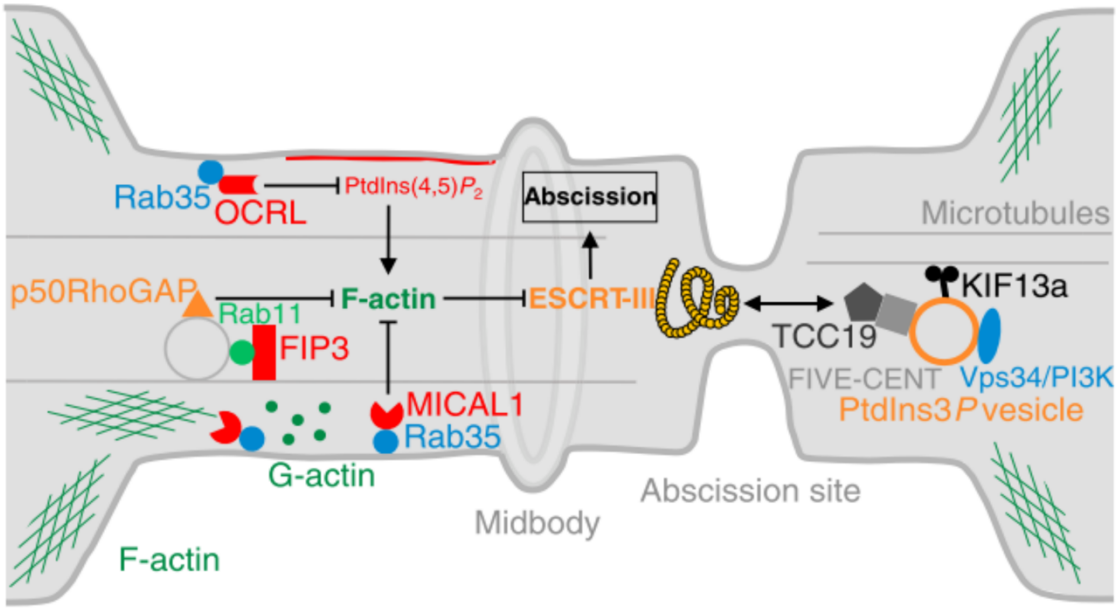

Figure 15. Vesicle trafficking and contribution of phosphoinositides to midbody maturation and ESCRT recruitment

Whilst PI(4,5)P_2 is initially required for midbody stability and reorganisation of its components, its levels must later decrease to allow actin removal, recruitment of the ESCRT machinery and cytokinetic abscission. This is brought about, in part, by PI(4,5)P_2 phosphatase OCRL, which is recruited to the midbody by Rab35. Rab35 also recruits and activates MICAL1, which plays a role in actin clearance prior to abscission (Section 1.5.5.). Rab11-FIP3 vesicles contribute to actin depolymerisation by transport of the RhoA GAP p50RhoGAP to the midbody, to inactivate RhoA kinase. Rab11-FIP3 vesicles also contribute to narrowing of the midbody at the site of abscission. PI3P positive endosomes are transported to the midbody by KIF13A. FYVE-CENT and its binding partner TTC19 interact with PI3P positive vesicles, and are required for successful cytokinesis. An interaction between TTC19 and the CHMP4B has been shown, potentially linking such trafficking events with ESCRT recruitment. *Frémont and Echard 2018*

1.5.4. Cytokinetic abscission

Cytokinetic abscission is the final membrane cleavage event that separates daughter cells following midbody maturation and narrowing. Earlier models put forward for a mechanism for this process included the above-mentioned SNARE mediated fusion of endocytic and Golgi derived vesicles with the plasma membrane of the midbody, or mechanical rupture of the membrane. A mechanical rupture model was largely based on the similarity in requirements for cellular wound healing with cytokinesis, including formation of an actomyosin ring[440]. The later discovery of requirement for the ESCRT machinery in abscission, together with examples of its adaptability to this process and links to upstream factors in mitosis and cytokinesis has led to ESCRT mediated models of abscission gaining the most plausibility.

1.5.4.1. ESCRT recruitment to the abscission site

Initial suggestions for involvement of the ESCRT machinery in abscission came from studies showing that TSG101 localisation was cell cycle dependent and localised to centrosomes and midbodies during mitosis[441]. Inactivation of expression or mutation of TSG101 led to mitotic abnormalities and an increase in multinucleation. Support for the role of the ESCRT machinery in abscission ultimately came from the identification by yeast two-hybrid and mass spectrometry of an interaction between TSG101 and ALIX with the centrosome and midbody protein CEP55[17,442]. During interphase, CEP55 shows centrosome localisation. At anaphase, CEP55 moves to the central spindle where it is phosphorylated by PLK-1[443]. This prevents it associating with the centralspindlin component MKLP1 at the midbody. At mitotic exit, PLK-1 is degraded by the APC/C allowing re-localisation of CEP55 from the mitotic spindle to the midbody. CEP55 was shown to be essential for cytokinesis, causing abscission failure and furrow regression upon depletion, as did depletion of TSG101 and ALIX[17,442,444–446]. Co-localisation of both TSG101 and ALIX with CEP55 at both the centrosome and later the Flemming body was observed, and localisation of both proteins was shown to be dependent on CEP55[17,442]. By analogy to the similar dependence on viral Gag proteins for recruitment of the ESCRT machinery during viral budding (Section1.7.), CEP55 was identified as the ESCRT adaptor protein for cytokinetic abscission. Importantly, neither CEP55 depletion nor mutation of TSG101 at its CEP55 binding site had an effect on TSG101 or ALIX mediated viral budding, demonstrating functional/site specific adaptation[17,55,442].

ESCRT-III proteins including CHMP2A, CHMP4A and CHMP5 were subsequently identified at the midbody forming two concentric rings adjacent to the Flemming body[17]. Midbody localisation of VPS4A also showed a similar localisation at a later stage closer to abscission following further midbody thinning, consistent with its more downstream role[17]. ALIX mutants unable to bind CHMP4 proteins failed to rescue cytokinetic defects caused by endogenous ALIX depletion, and overexpression of all YFP-CHMP4 isoforms, a dominant negative CHMP3 1-179-GFP protein and VPS4 (in both ATP binding (K173Q) and ATP hydrolysis defective (E228Q) dominant negative mutants and as wild type protein) inhibited cytokinesis[17,55,442,447]. Interestingly, CHMP4 and VPS4 homologues have been identified in Archaea of the genus *Sulfolobus* and have been shown to play a role in cell division[448–450]. Since these organisms lack an endosomal system, cytokinesis

has been suggested to represent the original, anscestral role of the ESCRT proteins. This discovery also refutes the possibility that the ESCRT machinery contributes to cytokinesis via an endosomal sorting function, rather than directly in abscission.

CEP55 consists of two coiled-coil 'arm' regions from residues 19-156 and 237-402 separated by an unstructured 'hinge' region from residues 156-237 (Figure 16)[445,446]. The N-terminal 'arm' mediates homodimerization whilst the C-terminal 'arm' mediates interaction with MKLP-1[444–446,451]. Part of the 'hinge' region from residues 160-217, termed the ESCRT and ALIX binding region (EABR) was found to be necessary for binding to both TSG101 and ALIX, and both proteins were found to interact with CEP55 via a GPP motif[451]. The binding of TSG101 to CEP55 was mapped to residues $_{157}$GPPNTSY$_{163}$ of TSG101, within an unstructured linker in its proline rich region between the UEV and the core[17,442,451]. Binding to ALIX was mapped to residues $_{800}$GPP$_{802}$ of ALIX within its C-terminal proline rich region. Residues $_{805}$TY$_{806}$ were also found to be equally important for mediating interaction[17,442]. Mutation of these binding sites in both TSG101 and ALIX suggested specificity of these sites for involvement in cytokinesis: TSG101 δ158-162 still interacted with its other main binding partners such as other ESCRT-I subunits, viral Gag proteins and endosomal proteins, and could still support viral budding[17,442]. Similarly, mutation of residues in ALIX known to mediate binding to other known partners, or expression of fragments lacking such regions were still able to function in cytokinesis[17,55,442].

Dimerisation of CEP55 was shown to be necessary for binding to TSG101/ALIX, and competition binding assays showed that TSG101 and ALIX compete for binding to CEP55 at the same site within the EABR[451]. The EABR becomes structured upon binding to TSG101/ALIX forming a non-canonical coiled coil, which cannot bind simultaneously to both TSG101 and ALIX. This led to a model suggesting multiple CEP55 dimers are required in cytokinesis to recruit both TSG101 and ALIX to the midbody for efficient abscission, since TSG101 and ALIX show at least some non-redundancy[451].

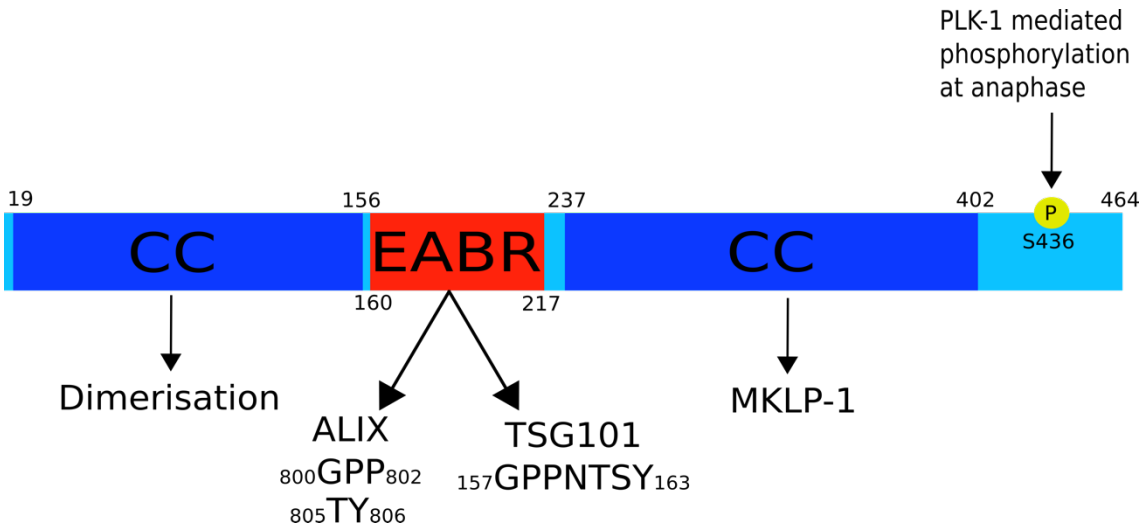

Figure 16. Domain structure of CEP55
CEP55 represents the adaptor protein that recruits the ESCRT machinery to the midbody to function in cytokinetic abscission, via interaction with TSG101 and ALIX. Both TSG101 and ALIX bind the same site within the central unstructured hinge region of CEP55 called the ESCRT and ALIX binding region (EABR). The hinge region is flanked on either side by coiled-coil regions the N-terminal of which mediates dimerization, whilst the C-terminal of which binds MKLP-1. PLK-1 kinase mediated phosphorylation of S436 at anaphase prevents midbody localisation until mitotic exit.

In addition to their role in abscission, ESCRTs appear to be important for maintenance of the midbody, centrosomes and mitotic spindle. Depletion of CEP55 or ALIX, or expression of ALIX mutants that are unable to bind ESCRT-III leads to an abnormal midbody staining pattern in which α-tubulin staining can be seen at the Flemming body[55,442,446,452,453]. Since protein density at the Flemming body normally masks tubulin epitopes, hence appearing as a 'dark zone', this suggests ALIX and ESCRT-III represent important midbody components. Localisation of both TSG101 and ALIX with CEP55 at centrosomes during interphase has been observed, and TSG101 depletion led to the appearance of multiple mitotic spindles and centrosomes, in addition to multinucleation[441,454]. A study in 2010 in which each of the 11 human CHMP proteins and VPS4A/B were individually depleted showed that each protein displayed non-redundant, differing effects on abscission, centrosome number and nuclear morphology[454]. Whilst CHMP3 depletion displayed a phenotype in cytokinesis similar to that seen upon depletion of ALIX/CEP55 without any striking mitotic effects, other CHMPs such as CHMP1A, CHMP2B, CHMP4B, CHMP4C and VPS4B displayed less severe cytokinetic defects but very prominent rapid increases in centrosome number and multipolar spindles. It is still unclear how ESCRTs may regulate centrosome duplication.

However, CC2D1A has been shown to control centrosome duplication, and an interaction with CHMP4 proteins has been uncovered[264,455]. Defective chromosome alignment or perturbed nuclear morphology was also observed in the case of CHMP1A, CHMP1B, CHMP2B, CHMP4B, CHMP4C, CHMP7, VPS4A and VPS4B. In contrast, CHMP2A and CHMP5 displayed an increase in cells with a single centrosome, hence a monopolar spindle. In both cases, this led to failed chromosome segregation, failed abscission, and aberrant nuclei[454]. In addition to these increases or decreases in centrosome number, cells depleted of VPS4A/B displayed smaller centrosomes whilst those depleted of CHMP2A displayed larger centrosomes and pericentriolar material. Localisation of endogenous VPS4 proteins to centrosomes and spindle poles from interphase to metaphase was also observed in this study[454].

More recent studies have built on this, showing dynamic association of VPS4 with both mother and daughter centrioles, within the pericentriolar material, in the absence of other ESCRT-III components. Decreased centrosomal γ-tubulin levels were seen upon expression of the catalytically inactive dominant negative VPS4 E228Q mutant. This led to a reduction in microtubule polymerisation, altered centrosome positioning, hence spindle orientation, and defective ciliogenesis due to the abolishment of centriolar satellites[456]. Similarly, another recent study using Drosophila and human stem and epithelial cells showed ALIX localisation to the pericentriolar material where it was required for correct mitotic spindle orientation, accumulation of γ-tubulin, and nucleation of astral microtubules necessary for anchorage of the spindle to the cell cortex[457]. VPS28 has also been suggested to be involved in aster microtubule organisation via interaction with the heterodimer Gβγ, and formation of a complex with the microtubule associated proteins Eg5 and TPX2, which help maintain spindle bipolarity and balance of pole to pole forces[458]. A role for CHMP4C, again in the absence of other ESCRT proteins, has been suggested in the spindle checkpoint (section 1.5.1.3.), by maintaining stable kinetochore-microtubule attachments by recruiting the Rod–ZW10–Zwilch (RZZ) complex to unattached kinetochores[459]. The RZZ is required at kinetochores, in metazoans, together with Mad1-Mad2 for a functional spindle checkpoint.

The striking phenotypes seen in the above studies strongly suggest a role for the ESCRT machinery in control of mitosis and centrosome/spindle maintenance and function, in

addition to cytokinetic abscission. Involvement in the spaciotemporal control of progression from mitosis to cytokinesis is also implied. Despite this, a unifying model for ESCRT activity at the centrosomes and mitotic spindle is lacking at present, and the above studies likely suggest roles for individual ESCRT proteins in processes such as centrosome clustering, independent of their canonical function in reverse topology membrane remodelling.

Whilst the effect of ALIX depletion has consistently been shown to be more detrimental to cytokinesis than that of TSG101, binding of each protein to CEP55 and subsequent recruitment of ESCRT-III has been suggested by Christ et al. 2016 to represent two partially redundant parallel arms of ESCRT-III recruitment: CEP55-ALIX-ESCRT-III and CEP55-TSG101 (ESCRT-I)-ESCRT-II-CHMP6-ESCRT-III[93]. The same study also described the interaction between VPS28 and CHMP6 (thereby bypassing ESCRT-II) as contributing to CHMP4B recruitment during cytokinesis. This study is discussed in more detail in section 4.1.

1.5.4.2. Models of abscission

Although initial confocal microscopy studies showed localisation of TSG101 and ALIX to single bands at the centre of the Flemming body, more detailed structured illumination microscopy (SIM) and high-resolution temporal imaging showed localisation of TSG101 as two distinct hollow rings either side of the Flemming body about 0.25µm apart[121]. The Flemming body, or 'dark zone', was shown to be around 0.6µm wide with a diameter of around 1µm. The TSG101 rings were around 0.28µm wide and likely contacted the membrane, judging from the diameters of the inner and outer rings, being around 1µm and 1.7µm respectively. CEP55 and MKLP1, in contrast, were shown to concentrate at the Flemming body as a solid disk around 0.75µm wide, penetrated by microtubules, which electron microscopy showed to form a dense bundle. CHMP4B also showed similar localisation to two membrane associated concentric rings, as previously observed in earlier studies by confocal microscopy (section 1.5.4.1.). These rings were located slightly further away from the centre of the Flemming body, around 0.45µm apart, but still showed 50% overlap with the TSG101 rings. Whilst CEP55 and MKLP-1 were present from midbody formation, TSG101 and CHMP4B showed localisation at midstage midbodies[121].

Due to the density of the overlapping microtubules at the Flemming body, the actual abscission event to sever the midbody membrane cannot occur here and instead takes place at a separate site at one side of the Flemming body approximately 1µm adjacent to it. This site is known as the secondary ingression and forms approximately 10-20 minutes before abscission[118,429,452]. Midbody thinning occurs to create the secondary ingression, narrowing the membrane from approximately 1-2µm to 50-100nm. In addition to localisation at the Flemming body, ESCRT-III and VPS4 have been observed at this site in late stage midbodies closer to the time of abscission (Figure 17)[118,121]. Electron microscopy has revealed that membrane at the secondary ingression appears rippled due to 17nm membrane associated filaments, which although unproven are likely to be those of ESCRT-III since these disappear upon depletion of CHMP2A[118]. Electron tomography revealed these cortical filaments to be regularly spaced around 35.3nm apart, as single or intertwined helices, perpendicular to the microtubules passing through the midbody. Depletion of the ESCRT associated microtubule severing enzyme spastin (section 1.5.5.) delayed abscission but did not prevent formation of these filaments[118].

A model put forward by Guizetti et al. 2011 suggests that ESCRT-III is responsible for thinning to create the secondary ingression, by continuous polymerisation and constriction away from the Flemming body towards the secondary ingression where further constriction mediates abscission[118]. In agreement with this model, CHMP4B, CHMP2A, CHMP2B and CHMP6 appeared to extend from the Flemming body to the secondary ingression in a continuous band, and depletion of CHMP2A prevented constriction to form the secondary ingression[118]. Furthermore, Sherman et al 2016 also observed continuous polymerisation of nested spirals between the Flemming body and secondary ingression by soft-X-ray cryo-tomography[460].

Elia et al 2011, meanwhile, observed that continuous fluorescence of CHMP4B-mCherry was not so obvious between the Flemming body and secondary ingression, and instead was seen to localise to separate pools, either side of the Flemming body and at the secondary ingression[121]. Closer examination of the dynamics of CHMP4B-mCherry showed that prior to abscission, CHMP4B shows an increase in intensity at one of its rings near the Flemming body, overlapping with TSG101. This is promptly followed by appearance at the secondary ingression around 20 minutes prior to abscission. VPS4B-

GFP similarly appeared to re-localise from the Flemming body to the secondary ingression even closer to the time of abscission, around 10 minutes beforehand, consistent with its downstream role in ESCRT disassembly/recycling. This study led to proposal of another 'cut and slide' model for abscission, whereby VPS4 mediates breakage of part of the initial ESCRT-III polymer ring overlapping that of TSG101/ALIX at one side of the Flemming body[461]. This is followed by constriction of the polymer to its spontaneous diameter of around 50 nm, and since the polymer is membrane-bound, membrane constriction with an associated increase in elastic energy occurs. This increase in elastic energy leads to sliding of the ESCRT-III polymer away from the Flemming body until the equilibrium position is reached at the secondary ingression (Figure 17)[461]. VPS4 activity then catalyses membrane scission. In addition to the observed co-localisation of VPS4 with both ESCRT-III pools, at the Flemming body and secondary ingression, inhibition of VPS4 activity by ATP depletion was seen to induce spreading of CHMP4B from the Flemming body to the secondary ingression as one continuous band. This suggests disruption of spaciotemporal localisation and supports this 'cut and slide' model. Also in favour of this model was the observation that further constriction of this ESCRT-III pool did not lead to further sliding, suggesting the equilibrium position had been reached, around 0.7µm away from the initial pool adjacent to the Flemming body[461].

In contrast to this model and potentially more consistent with the continuous polymerisation model proposed by Guizetti et al. 2011 is a recent study by Mierzwa et al. 2017[117]. This study used FRAP to examine the dynamics of ESCRT-III subunit turnover with a focus on cytokinesis. It appeared to show high dynamic turnover of midbody membrane bound ESCRT-III subunits with the cytoplasmic pool of ESCRT-III subunits, during ESCRT-III polymerisation. VPS4 was suggested to be continuously necessary for this turnover, required for continuous ESCRT-III polymerisation, remodelling and constriction. Contrary to the specific appearance of VPS4 following that of CHMP4B, shown by Elia et al. 2011[121], VPS4 was seen to localise at the midbody together with CHMP4B at early stages. Also, potentially in agreement with the model of ESCRT-III mediated formation of the secondary ingression was the observation in this study that neither 17nm filaments nor secondary ingressions formed upon VPS4 depletion[117].

Another recent more detailed higher resolution study of ESCRT localisation by Goliand et al. 2018 used 3D stochastic optical reconstruction microscopy (STORM) to principally examine the localisation of the CHMP-like protein hIST1, required in abscission (section 1.5.6.)[462]. Whilst consistent with earlier studies that examined localisation mainly of CHMP4B, this study provided a more in-depth picture of hIST1 localisation, identifying five different localisation patterns at the midbody. Examination of antibody stained endogenous hIST1 revealed localisation similar to that of other ESCRT-III proteins as 179nm wide, 1.11 diameter rings at both sides of the Flemming body. A second localisation pattern as thicker 390nm wide rings of slightly smaller diameter were also observed at the rims of the Flemming body. A series of between 3-5 parallel rings of successively smaller diameter ranging from 1.08µm to 0.62µm diameters, likely forming a continuous spiral of around 846nm was seen as a third localisation pattern. An even more extended fourth localisation pattern was observed as another continuous deformed spiral extending to the secondary ingression. These spirals consisted of rings of irregular diameters and pitch angles but generally decreased in diameter from 0.82µm – 0.28µm at the abscission site. In agreement with previous studies, the fifth localisation pattern consisted of two pools of hIST1: one of large diameter rings at the rims of the Flemming body and another as two small diameter rings at the secondary ingression[462]. Midbody narrowing was used as a measure of abscission progression, and began to occur during the third localisation pattern for hIST1. Calculations taking into account spiral length and the radius and pitch of each turn revealed that whilst early constriction of the midbody, represented by the third type of hIST1 localisation, involved polymerisation, later constriction, represented by localisations 4 and 5, represented filament depolymerisation.

These observations and calculations led to a model whereby initial polymerisation and elongation of ESCRT-III filaments, represented by hIST1 localisations 1-3, is followed by more acute constriction of the midbody membrane in stage 4. At this stage, ESCRT-III filaments form the distorted spiral due to mechanical stress caused by continued constriction to their preferred diameter, at the abscission site, whilst remaining anchored to the Flemming body. This stress leads to VPS4 mediated filament breakage and depolymerisation leading to the Flemming body and abscission site localised bands seen in localisation 5. Further polymerisation and capping of the filament at the

abscission site then mediates midbody severing. This model is more consistent with that suggested by Guizetti et al. 2011, involving continuous polymerisation from the Flemming body to the secondary ingression[118].

In addition to proposing this model, this study using 3D STORM provided a more detailed study of the effects of depletion of Spastin and various ESCRT-III proteins on filament morphology during abscission. Spiral formation was largely unperturbed in spastin knockout cells. However, midbody constriction was perturbed, likely due to lack of microtubule clearance. VPS4A/B depletion led to the appearance of large diameter hIST1 filaments at the centre of the midbody that did not elongate or constrict the midbody. This is consistent with a model for VPS4 in continuous remodelling of filaments to drive constriction, as described by Mierzwa et al 2017[117]. CHMP2B depletion led to the formation of elongated hIST1 spirals, but of constant small diameter, of around 210nm. These spirals also appeared to be internal and not membrane associated. This suggests a role for CHMP2B in maintaining correct spiral morphology or membrane binding of ESCRT-III filaments. CHMP4B depletion led to disordered partially circular hIST1 structures, unaligned with the rims of the Flemming body. Only the hIST1 localisation pattern seen upon CHMP2B depletion was also observed for CHMP4B localisation, implying that these phenotypes are generally specific to hIST1. Nonetheless, such studies highlight differential contribution of individual CHMPs to filament composition and their lack of redundancy in cytokinesis[462].

Another model proposed by Schiel et al 2012 involves initial formation of the secondary ingression in an ESCRT independent manner by fusion of FIP3 positive endosomes with the membrane[429]. The secondary ingression is later stabilised by ESCRT-III filaments, which mediate abscission. This model was primarily based on the observation that CHMP4B depletion did not perturb secondary ingression formation and arrived at the secondary ingression following its formation. Possible continuous polymerisation of ESCRT-III from the Flemming body to the secondary ingression was observed in this study in 27% of cases whilst in the remaining 73% of cases, distinct CHMP4B puncta at the secondary ingression were seen. This together with the well-established importance of both vesicle trafficking and the ESCRT machinery in cytokinesis suggests that in reality, features of all three models could be involved in abscission.

On a related note, the observance of vesicles exterior to the midbody and vesicles budding from it in a process analogous to viral budding suggests that the ESCRT machinery contributes directly to midbody thinning by expulsion of vesicles[463].

Finally, another recent study related to spaciotemporal control of the ESCRT proteins at the midbody showed that septins may play a role here[464]. Septins 9, 2, 7 and 6 were shown to form membrane bound double rings either side of the Flemming body, similar to those of ESCRT proteins. It was reported that these rings appeared at the same time as those of TSG101 and partially overlapped with the rings of ESCRTs I, II and III subunits. The septin rings were shown to demarcate the sites of ESCRT-III recruitment and showed an inverse temporal recruitment pattern with ESCRT-III, with disassembly prior to the spreading of ESCRT-III to the site of abscission[464]. Co-precipitation experiments suggested a potential interaction between SEPT9 and TSG101 via two N-terminal PTAP motifs, and whilst its depletion did not prevent recruitment of TSG101, recruitment of EAP20 (ESCRT-II) and CHMP6 were prevented. This was proposed to be dependent on the interaction between the TSG101 UEV domain and SEPT9 PTAP motifs. Although depletion of SEPT9 did not prevent recruitment of CHMP4B/CHMP2B, an increase in failure to form cones towards the secondary ingression was seen, as were abnormal distorted accumulations as single bands at the Flemming body, as opposed to concentric rings. An increase in the time between furrow ingression and abscission was also reported. Involvement of the septins in ESCRT-III organisation and remodelling, was therefore proposed via the ESCRT-I – ESCRT-II – CHMP6 axis of recruitment. This study may provide some insight into why ESCRT-I and ESCRT-III form spatially separate rings adjacent to the Flemming body[464].

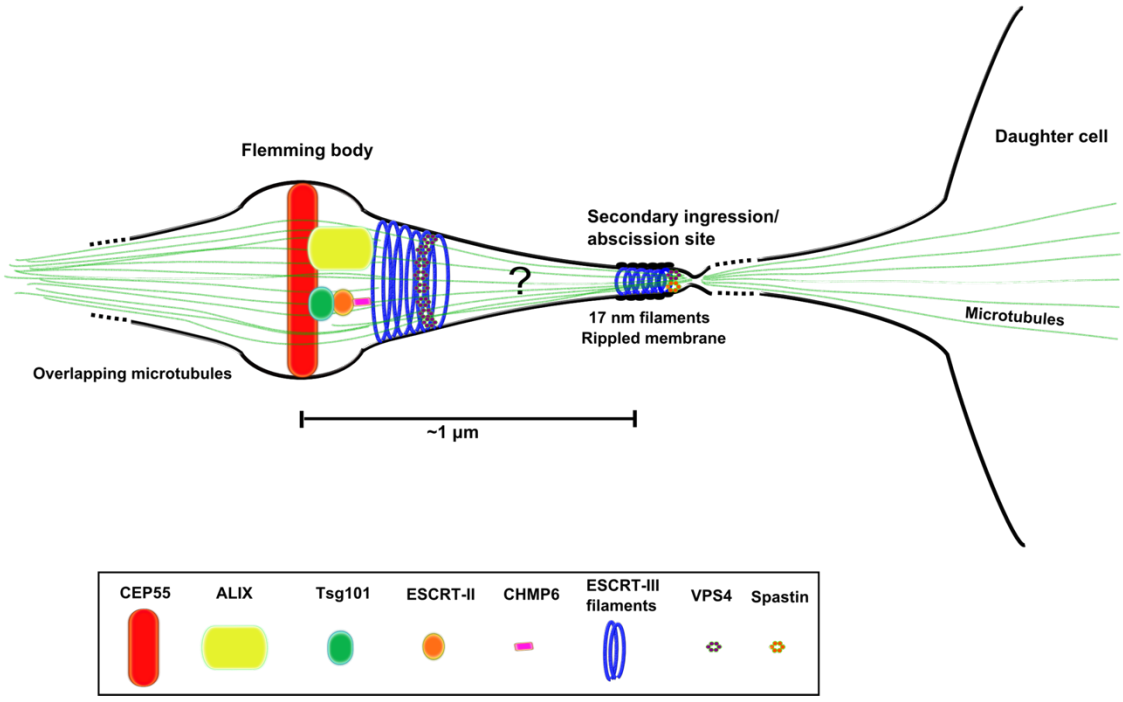

Figure 17. Midbody localisation and action of ESCRT proteins in cytokinetic abscission
ALIX and TSG101, hence ESCRT-I, are recruited to the Flemming body via direct interaction with the adaptor protein CEP55. The Flemming body is a protein rich structure at the centre of the midbody, derived from the central spindle where microtubules overlap. Recruitment of ESCRT-III has been proposed to occur via two partially redundant arms of recruitment involving a CEP55-ALIX-CHMP4B branch and a TSG101 (ESCRT-I)-ESCRT-II-CHMP6-CHMP4B branch. ESCRT-III proteins appear as two concentric rings immediately adjacent to the Flemming body. However closer to the time of abscission, they are also observed at sites approximately 1µm away from the Flemming body known as secondary ingressions, at which the diameter of the membrane tube is thinned from 1.5-2µm to around 100 nm. One of these ingressions represents the site at which abscission occurs. The membrane at these sites appears rippled due to 17nm filaments beneath the membrane, which are likely to be those of ESCRT-III. A 'cut and slide' model for abscission has proposed breakage of Flemming body adjacent ESCRT-III filaments by VPS4. These filaments are then propelled away from the Flemming body by constriction of the filaments, constricting the membrane as they move until they reach the secondary ingressions, representing their equilibrium positions at which their spontaneous diameter of around 50-100nm is reached. Further polymerisation at the secondary ingression would then mediate membrane scission. Continuous polymerisation and constriction of ESCRT-III filaments from the Flemming body to the secondary ingressions has also been proposed, as has an ESCRT independent mechanism of secondary ingression formation, followed by independent nucleation and scission by ESCRT-III. Membrane thinning to form the secondary ingression in the latter case is proposed to be mediated by fusion of FIP3 positive vesicles with the membrane. Microtubule severing is a rate-limiting step of abscission and has been proposed to be mediated by the enzyme AAA ATPase Spastin, which interacts with CHMP1B and hIST1 via MIT-MIM interactions.

1.5.4.3. CEP55 in human disease and animal models

Three genetics studies to date have shown disruption of CEP55 to result in lethal foetal disorders in humans, displaying perturbed brain and kidney development resembling a Meckel-like syndrome[465–467]. Meckel-Gruber syndrome (MKS) is a ciliopathy

characterised by renal cystic dysplasia, perturbed formation of the central nervous system and polydactyly. Stillborn foetuses from these three studies were homozygous for nonsense mutations in CEP55 that removed the EABR (R86X)[465], disrupted midbody localisation (S425X)[466] or were homozygous for an Amish founder frameshift variant (I172Nfs*17) that also resulted in a premature stop codon within the EABR[467]. Although there were differences in phenotype, even between the two foetuses homozygous for the same R86X mutation, all showed features such as hydranencephaly and occipital encephalocele, indicating perturbed brain development, and dysplastic, cystic or degraded kidneys, indicating perturbed kidney development. In keeping with *in vitro* studies, multinucleated neurons and hepatocytes were also observed in the case of the S425X cases[465].

Studies in zebrafish models of CEP55 knockout have shown that, as seen in humans, heterozygous knockouts are still viable and fertile but display reduced brain size, craniofacial abnormalities and renal dysplasia or atrophy. Apoptosis and cell cycle dysregulation were also observed[466,468,469].

A recent publication described the first mouse knockout model for CEP55 and provided a more detailed study of its relationship with the ESCRT machinery *in vivo*[470]. Interestingly in this case, mice that were homozygous for the knockout were born live but died postnatally. Such mice presented with microcephaly, due to apoptosis in the brain cortex, and kidney dysmaturity. Multinucleated cells were observed in the brain cortex, however no increase in midbody connected cells was observed, in contrast to the previously described *in vitro* work (section 1.5.4.1.). Established cultures of knockout mouse neural progenitor cells also displayed an increase in multinucleation, which was not seen to the same extent in cultured primary tail tip fibroblasts. This was consistent with the observation that knockout mice did not show obvious anatomical defects and changes in cell proliferation and apoptosis in tissues other than that of the brain. In keeping with these observations, CEP55 was shown to be necessary for both mChmp2B and mChmp4B to the midbodies of mouse neural progenitor cells and fibroblasts. However, only around 30% fibroblasts showed localisation of CEP55, mChmp2B and mChmp4B compared to over 60% of neural progenitor cells. Furthermore, CEP55 knockout mouse fibroblasts were still able to complete abscission, in the absence of the ESCRT machinery, in contrast to neural progenitor cells, over 60% of which failed

abscission upon depletion of Chmp4B[470]. A similar observation was made in *C. elegans*: abscission is delayed but not prevented when the ESCRT machinery is disrupted[471]. Taken together these animal models suggest that the CEP55 and the ESCRT machinery are essential for cell division in neural progenitor and kidney cells during development, but that CEP55 and ESCRT independent pathways for abscission exist in other cell types. In contrast to CEP55, MKLP1 depletion in mouse fibroblasts led to a significant increase in multinucleated cells, and Drosophila, which do not express a CEP55 homologue, have been shown instead to recruit ALIX and TSG101 via direct interaction with the MKLP1 homologue, Pavarotti[275,470,472,473]. Studies performed using cultured embryonic cells or female germline stem cells in Drosophila showed both ALIX and TSG101 to be individually required for ESCRT-III recruitment, rather than the partial redundancy seen in mammals[472]. This highlights a further difference compared to the most commonly studied context, of cancer cell lines in culture. The requirement for the ESCRT machinery in *Drosophila* somatic cells is unclear, as is the case for *C. elegans*, embryonic cells of which show retarded but successful abscission upon ESCRT depletion[471].

1.5.5. Cytoskeleton remodelling at the site of abscission

In order for abscission to occur, both F-actin and microtubules must be removed from the midbody. These have been proposed to act as a physical barrier, blocking access of ESCRTs and vesicle trafficking to the secondary ingression. Alternatively, excess actin has been proposed to alter membrane tension, hence the ability of ESCRT-III to translocate to the secondary ingression via the 'cut and slide' model detailed above.

In addition to the more indirect roles of OCRL and p50RhoGAP in preventing actin polymerisation, as previously described in section 1.5.3., a more direct role in actin depolymerisation mediated by the MICAL family of oxidoreductases has been uncovered[474]. Mammals express three of these enzymes, being MICAL1, MICAL2 and MICAL3, together with the MICAL-like proteins MICAL-L1 and MICAL-L2[475–482]. MICAL1, -2 and -3 possess an N-terminal flavoprotein monooxygenase domain followed by a calponin homology domain and a (Lin-11, Isl-1 and Mec3) LIM domain. MICAL1 and -3 also possess C-terminal Rab binding domains[483–487]. MICALs have previously been implicated in several processes where they mediate actin cytoskeleton remodelling[474].

Actin depolymerisation has been suggested to occur via oxidation of methionine residues in actin, upon binding to it. This has been suggested to weaken longitudinal interactions between actin subunits, thus increasing fragility of actin filaments, leading to a high rate of depolymerisation from both ends of the filament[474,488,489]. Alternatively, the production of reactive oxygen species by MICALs, such as hydrogen peroxide, have been suggested to modify amino acid residues within actin, leading to depolymerisation[484,490,491].

A role for MICAL1 has been shown in clearance of actin from the secondary ingression prior to cytokinetic abscission. Like ESCRT-III, MICAL1 has been shown to initially localise to the Flemming body prior to the secondary ingression, prior to abscission. Depletion of MICAL1 abrogates CHMP4B recruitment to the secondary ingression, but not initial recruitment to the Flemming body. Its depletion also delays or inhibits abscission[492–494]. Just as Rab35 controls localisation of OCRL to the midbody, Rab35-GTP also interacts with MICAL1 and mediates its Flemming body and secondary ingression localisation[492,495,496]. Binding of Rab35 to MICAL1 has also been shown to relieve its autoinhibition. MICAL1 exists in an autoinhibited state in the cytoplasm, in which its C-terminus folds back, interacting with its N-terminus. Binding of Rab35 to its binding site at the C-terminus prevents this interaction[492].

Roles for MICAL3 and MICAL-L1 in cytokinesis have also been described, although these proteins seemingly play redox independent roles, in contrast to MICAL1. MICAL3 has been suggested to act as a midbody associated scaffold for vesicle targeting that interacts with MKLP1 and tethers Rab8 positive vesicles at the midbody[497,498]. MICAL-L1 also appears to be involved in membrane trafficking[498]. MICAL-L1 is another Rab35 effector that also interacts with Rab8 and Arf6[499]. Importantly, it directs Rab11-FIP3 endosome targeting, hence delivery of p50RhoGAP, to the midbody. This prevents excess accumulation of actin[500,501].

In order for abscission to occur, central spindle microtubules must be removed from the midbody. Microtubule severing at the secondary ingression coincides closely with abscission and has been shown to be a rate-limiting step of abscission, like recruitment of ESCRT-III[118]. The mammalian microtubule severing AAA ATPase Spastin plays an important role in this process, and mutations in this protein are the most common cause of hereditary spastic paraplegia – a disease caused by length-dependent degeneration

of the distal ends of long axons[502]. Spastin, like VPS4, forms a hexameric ring structure with a central pore through which microtubules are pulled and broken by the force generated. Depletion of Spastin leads to an increased number of cells connected by long tubular structures, although no increase in multinucleation is seen, indicating a role during late stages of cytokinesis[503,504]. Spastin was found to possess an N-terminal MIT domain upstream of its microtubule binding and ATPase domains, that forms a non-canonical high affinity interaction specifically with the MIM domain of CHMP1B (Figure 18)[504–506]. This MIM-MIT interaction surface is twice that of other MIT-MIM domain interactions of ESCRT-III proteins, and Spastin localises to the midbody in a MIT domain and CHMP1B dependent manner[505]. Whilst Spastin has been proposed to mediate microtubule severing at secondary ingressions prior to abscission, another model proposed by Schiel et al. 2011 proposed a non-essential role for Spastin in microtubule severing[438]. This study suggested that Spastin contributes to microtubule release from centrosomes and their appropriate bundling within the midbody, which they suggested was required for appropriate trafficking of FIP3 positive vesicles to the midbody. This study suggested that microtubule buckling and breaking, as occurs during interphase, was necessary for abscission, rather than spastin mediated severing.

1.5.6. Adaptation of the ESCRT machinery to cytokinesis and associated accessory proteins

In contrast to their role in viral budding (Section 1.7.3.), which appears to require only a small subset of ESCRT-III proteins, cytokinetic abscission and/or mitosis appears to require all 12 ESCRT-III proteins, with CHMP1A, CHMP2A, CHMP3 and hIST1 showing the most obvious cytokinetic defects upon depletion[454,507]. In addition to interaction with various accessory proteins, as outlined in this section, another possibility for requirement of a larger complement of ESCRT-III proteins could be to drive formation of intermediary structures, such as filaments at the midbody of a diameter much larger than the 50-100nm diameter filaments required for MVB formation. The cytokinesis specific CHMP-like protein hIST1, for example, has been shown to spontaneously polymerise into approximately 700nm diameter tubular structures, suggesting it may be a subunit necessary for generation of the larger diameter filaments that form rings

adjacent to the Flemming body[98]. Another example of adaptation to cytokinesis is the CHMP1B-Spastin interaction described above.

hIST1 is an ESCRT-III associated regulatory protein that is essential for cytokinetic abscission, as indicated by the strong increase in multinucleated cells and midbody connected cells upon its depletion[507]. Closer examination of this phenotype by time-lapse microscopy showed that furrow regression leading to multinucleation always occurs following an extended period of midbody connection of the nascent daughter cells[507,508]. This indicates that midbodies are very stable and that hIST1 depletion causes a late cytokinesis defect consistent with a role specifically in abscission. hIST1 shows functional specificity in cytokinesis and nuclear envelope resealing (Section 1.6.1.) but not lysosomal sorting or viral budding[507]. hIST1 is a CHMP-like protein, that shows similar localisation to the midbody in two concentric rings, like other ESCRT-III proteins[507]. Structurally it contains a conserved N-terminal ELYC domain (named after this conserved sequence of residues) which like other CHMP proteins forms a 4-helix bundle and another 3 helical regions involved in autoinhibition[509]. Downstream of the ELYC domain is a central proline rich linker, predicted to be largely unstructured, and tandem C-terminal MIM2 and MIM1 domains, that mediate interactions with MIT domain containing proteins such as VPS4, LIP5, UBPY, AMSH, MITD1, ULK3 (Section 1.3.4.5.), Spartin and Spastin (Figure 18)[507,509,510]. Unlike other CHMP proteins, these MIM domains are both located downstream of the α6 helix, presumably ensuring that both MIM domains are available for MIT domain binding regardless of whether hIST1 is in an open or closed, autoinhibited conformation. MIM domains of other CHMPs are occluded when these CHMPs are in an autoinhibitory conformation. Perhaps this, together with its binding to nearly all MIT domain containing proteins identified so far, explains why hIST1 plays such a prominent role in cytokinesis.

hIST1 interacts with CHMP1A and CHMP1B through its N-terminal ELYC domain at surface exposed residues within both the α2 helix of its characteristic 4-helix bundle, and the autoinhibitory helix α5[98,507,508]. The binding surface for hIST1 on CHMP1B has been mapped by yeast two-hybrid to approximately residues 61-156, encompassing the majority of helices α2 - α5 (Figure 18)[507]. Like hIST1, depletion of CHMP1 proteins leads to an increase in both multinucleation and midbody connected cells, and the hIST1-

CHMP1 interaction is necessary for successful abscission, as shown by experiments using hIST1 mutants that are defective for CHMP1 binding: the ability of hIST1 mutants to rescue abscission (midbody arrest) correlated with how well they bound CHMP1[507,508]. Along the same lines, both hIST1 and CHMP1 are required for efficient recruitment of VPS4 to the midbody, and hIST1 and CHMP1 proteins are less stable upon VPS4 depletion, indicative of formation of a complex between hIST1, CHMP1 proteins, VPS4 and probably other MIT domain containing proteins[509]. Interestingly, both MIM1 and MIM2 domains in hIST1 have been shown to be necessary for optimal binding of VPS4, and the MIM1 domains of hIST1 and CHMP1 proteins bind overlapping but non identical regions of the VPS4 MIT domain[508]. It is therefore conceivable that the MIM domains of CHMP1 proteins, hIST1 and other ESCRT-III proteins act together to form a network of MIM domains to recruit VPS4 and its effector LIP5 with high affinity to function during cytokinesis. Binding of the MIM-MIT interaction mediates strong activation of VPS4 ATPase activity (Section 1.3.4.6.). This network of MIM domains also likely functions to recruit the other, abovementioned MIT domain containing proteins to function at the end stages of cytokinesis, tethering them to the ESCRT-III polymers and bringing them into close proximity to act together in abscission. Spartin is another MIT domain containing protein that depends on its interaction with hIST1 for midbody recruitment. Its function is unknown, but depletion leads to abscission failure, manifested by increased multinucleation and midbody connected cells, and increased abscission time[510].

MIT domain containing 1 (MITD1) is another MIT domain containing protein that is specifically involved in cytokinesis and binds the MIMs of CHMP1A, CHMP1B, CHMP2A and hIST1[511,512]. Only CHMP2A, however, appears to be essential for its midbody recruitment[511]. In contrast to hIST1, which so far appears to function specifically at a late stage close to abscission, MITD1 appears to act at an early stage in midbody stability in addition to abscission[511]. It thereby represents an important example of ESCRT adaptability to cytokinesis and spaciotemporal coordination with more upstream events. MITD1 contains an N-terminal MIT domain and a C-terminal phospholipase D (PLD)-like fold. Characterisation of its structure revealed a homodimer[511].

In contrast to depletion of hIST1, depletion of MITD1 causes an increase in multinucleation but no concomitant increase in midbody connected cells, consistent

with a role at an early stage of cytokinesis. This was further characterised as a role in midbody stability, by time-lapse experiments using cells depleted of MITD1, which showed furrow regression within time frames shorter than the average time taken for abscission in wild type cells. Since an additional small population of cells remained connected by midbodies for an extended period of time prior to abscission, like hIST1, an additional function in abscission was implied[511]. Consistent with a function in midbody stability, depletion of MITD1 also caused increased plasma membrane blebbing, and in cells that successfully divided, abscission was on average 10 minutes faster, possibly due to a reduction in midbody tension caused by blebbing at the midbody. Blebbing also suggests MITD1 could be playing a role in actin clearance at the midbody[511].

An exposed basic patch on the surface of the MITD1 dimer was found to mediate interaction with membranes by binding to phosphoinositides, and this interaction was also found to be important for localisation to the midbody. Taken together these observations have led to a model whereby MITD1 binds ESCRT-III and midbody membrane simultaneously to facilitate cortical stability at the midbody and anchorage, whilst coordinating this with ESCRT-III recruitment and stability. By competing with VPS4 for binding to hIST1, but not with Spastin due to the particularly strong hIST1-Spastin MIT-MIM interaction, it has also been proposed that MITD1 could act to inhibit ESCRT-III disassembly until necessary[511].

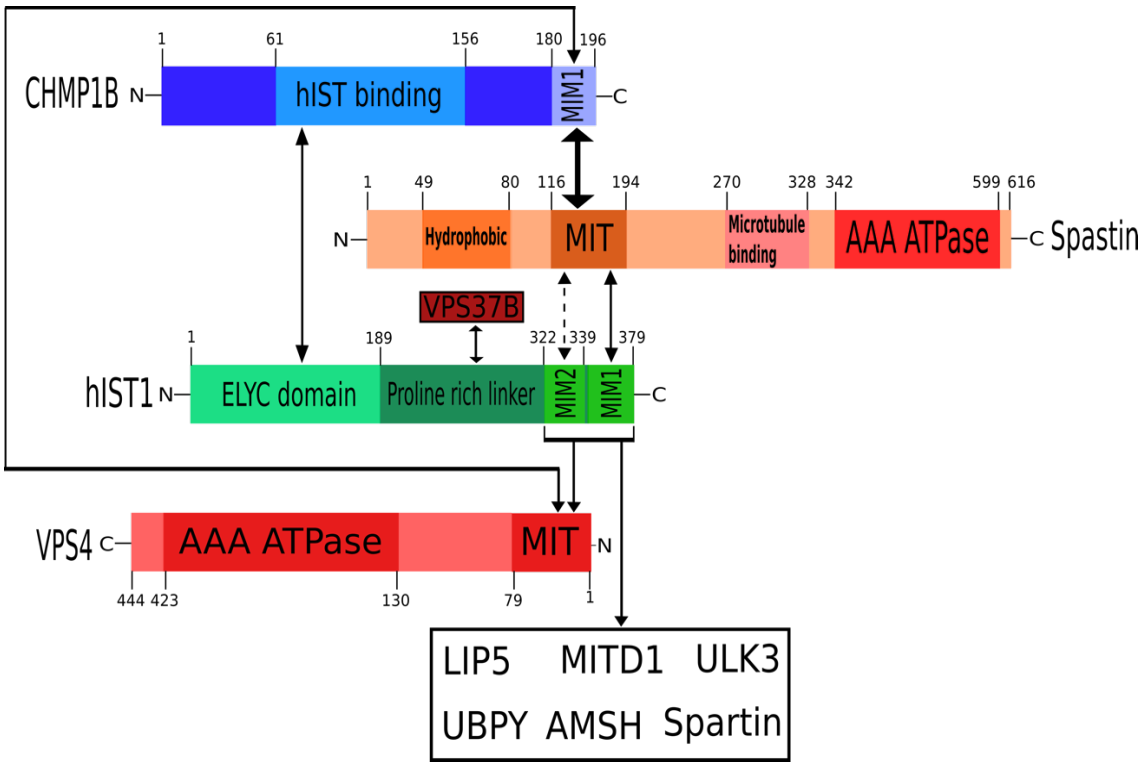

Figure 18. MIT-MIM interactions of the ESCRT machinery in cytokinetic abscission
The microtubule severing AAA ATPase Spastin interacts with CHMP1B through an especially strong non-canonical MIT-MIM interaction. Spastin localises to the midbody in a MIT domain and CHMP1B dependent manner. hIST1 interacts with CHMP1A and CHMP1B through its N-terminal ELYC domain (named after this conserved sequence) at surface exposed residues within helices α2 - α5. Both MIT1 and MIT2 domains of hIST1 have been shown to be necessary for optimal binding to the MIT domain on VPS4, and most likely its other MIT domain containing interaction partners such as Spastin, LIP5, MITD1, ULK3, UBPY, AMSH and Spartin. hIST1 is essential for cytokinetic abscission and interacts with nearly all MIT domain containing proteins identified so far.

Aside the above described interactions mediated by MIT-MIM motifs, and the potential interaction between CHMP4B with midbody membrane via an interaction with TTC19/FYVE-CENT, which binds PI3P, BRCA2 has also been suggested to facilitate the interaction between CEP55 with TSG101 and ALIX. BRCA2 has been proposed to show interaction with all three proteins and contribute to abscission[513]. Tsg101 has also been shown to interact with several proteins that show midbody localisation and are involved in upstream cytokinetic events. Such proteins include CD2AP, which is involved in endocytic protein trafficking, ROCK1 and IQGAP1, which are both involved in cytoskeletal remodelling and actomyosin ring assembly and contraction, and SCAMP3, as previously mentioned in Section 1.5.3.[17]. Perhaps this partly explains why Tsg101 and ALIX do not show complete redundancy in cytokinetic abscission: each could be

specifically involved in binding to other factors required for coordination of abscission with more upstream events.

1.5.7. ESCRTs in the abscission checkpoint

In contrast to the various phosphorylations mediated by CDK1, AuroraB and PLK-1 in temporal control of cytokinesis during mitotic exit and early stages of cytokinesis, the involvement of the ESCRT machinery in the AuroraB dependent abscission checkpoint, (also known as NoCut) represents a role for the ESCRT machinery in control of cytokinesis at a later stage, closer to abscission. The discovery of ESCRT proteins as part of the abscission checkpoint pathway represents another important example of adaptability of the ESCRT machinery to cytokinetic abscission and the importance of MIT-MIM interactions.

NoCut was originally identified in yeast as a surveillance mechanism to ensure that abscission does not take place until chromatin from unsegregated chromosomes has been cleared from the intercellular bridge[514–516]. This prevents cutting through chromatin, causing DNA damage. This phenomenon was later identified in eukaryotes, where it prevents genomic instability arising from furrow regression and tetraploidisation, in addition to DNA damage[335,516]. Anaphase chromatin bridges that persist through the midbody arise from defects in chromosome architecture leading to incomplete separation of sister chromatids. The NoCut pathway in yeast is different from that in mammals, involving inhibition of septin mediated abscission by localisation of the bud-neck proteins Boi1 and Boi2 to the cleavage site, in response to chromatin mediated activation of Lpl1 kinase activity[515,517]. Despite this, the key kinase in this process in mammals, AuroraB, is the homologue of Lpl1, demonstrating evolutionary conservation of this checkpoint. The abscission checkpoint is also activated in mammalian cells in response to defective nuclear pore complex assembly and high levels of midbody tension, resulting from cell growth at low densities[518–520].

AuroraB activity at the midbody is sustained specifically by chromatin[515,516,521]. Although the mechanism for this has not been elucidated, AuroraB mediated phosphorylation of MKLP1 stabilises the cleavage furrow until later inactivation of AuroraB, required for abscission[335,516].

In terms of the ESCRT machinery, CHMP4C has been identified as an important regulatory protein in the abscission checkpoint, and AuroraB specifically phosphorylates CHMP4C at residue 210, within a unique insertion (INS) from residues 201-217 that is not present in CHMP4A or CHMP4B (Figure 19)[521,522]. This phosphorylation is facilitated by interaction of CHMP4C with Borealin (a subunit of the CPC, which contains AuroraB, INCENP, borealin and survivin) and is necessary for localisation of CHMP4C to the Flemming body rather than the midbody arms during late cytokinesis[521]. Interestingly, dephosphorylation at residues 214 and 215 also accompanies CHMP4C Flemming body localisation suggesting control of the checkpoint by unknown phosphatase activity in addition to kinase activity[523]. Involvement of CHMP4C in the abscission checkpoint was first demonstrated by the inability of depletion of the nuclear pore protein NUP153 to trigger the abscission checkpoint, manifested by an increase in midbody connected cells, upon codepletion with CHMP4C[521]. Mutation of residue 210 or the unique insertion from 201-217 produced a similar phenotype[521]. CHMP4C was thus identified as a negative regulator of abscission, even though it did not appear to be essential for abscission, likely due to redundancy with CHMP4A and CHMP4B. Interaction of CHMP4C with ALIX was later also shown to be necessary for a functional checkpoint, even though ALIX was not necessarily required for midbody localisation of CHMP4C. This was demonstrated in a recent publication, by a polymorphism in CHMP4C represented by a mutation that confers susceptibility to various cancers. This mutation reduces binding of ALIX to CHMP4C and does not support the abscission checkpoint[524].

CHMP4C interacts with VPS4 via a MIT-MIM interaction as does Abscission/NoCut Checkpoint Regulator (ANCHR) - another ESCRT associated protein involved in the abscission checkpoint (Figure 19)[525]. In an Aurora B dependent manner, ANCHR has been proposed to form a complex with VPS4 and CHMP4C, retaining VPS4 in an inactive form at the Flemming body, and preventing its localisation to the secondary ingression to mediate abscission[525].

ULK3 kinase represents another important signalling node of the abscission checkpoint that acts downstream of AuroraB in a CHMP4C dependent manner[520]. ULK3 also phosphorylates CHMP4C, but at different sites from those phosphorylated by AuroraB. Its preferred substrate, however, is believed to be hIST1, through which it interacts via an especially strong MIT-MIM interaction (Figure 18)[520]. Like CHMP4C depletion,

checkpoint activation also fails upon ULK3 depletion or mutation of hIST1 at its phosphorylation sites.

Whilst retention of VPS4, its effector LIP5, ANCHR and ESCRT-III proteins such as hIST1 at the Flemming body could explain one mechanism by which the abscission checkpoint delays abscission, the various phosphorylations could also prevent transition of CHMPs from their closed states to open polymerisation competent states as another means of inhibiting abscission (Figure 19). CHMP4C has also been proposed to delay abscission by competing with CHMP4B for binding to ALIX, thus preventing polymerisation of CHMP4B filaments[167]. Further details of the pathway and mechanisms involved in maintenance of the checkpoint remain to be characterised for a more complete understanding. It would also appear that there are differences in the pathway depending on how the checkpoint is triggered. For example, when the ULK3 phosphorylated residues of hIST1 are mutated, the checkpoint is still activated in response to midbody tension, even though it can no longer be activated by NUP153 depletion or lagging chromosomes[520].

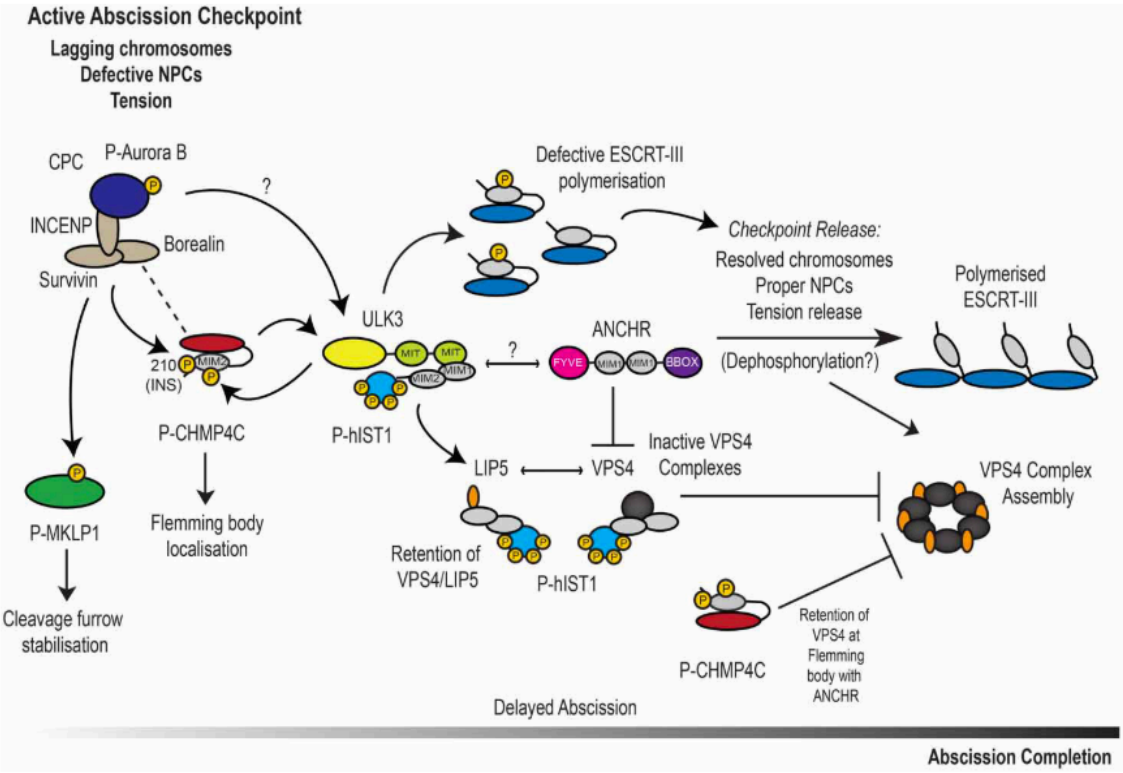

Figure 19. The ESCRT machinery in the NoCut Aurora B-dependent abscission checkpoint.
Activated aurora B kinase, as part of the chromosomal passenger complex (CPC), stabilises the cleavage furrow, by phosphorylation of MKLP1. Aurora B also phosphorylates the ESCRT regulatory protein CHMP4C at residue 210 within a unique insertion (INS) not present in CHMP4A or CHMP4B, located between its MIM and ALIX binding regions. This leads to retention of CHMP4C at the Flemming body during late cytokinesis. ULK3 kinase also phosphorylates CHMP4C and other ESCRT-III subunits, but its preferred binding partner and substrate is hIST1, with which it interacts through an especially strong MIT-MIM interaction. Such phosphorylations have been proposed to render CHMP proteins in their inactive 'closed' forms, thus inhibiting polymerisation and abscission. Alternatively, such phosphorylations have been proposed to sequester VPS4, its effector Lip5 and and other ESCRT-III proteins at the Flemming body, thus preventing their polymerisation and activity at the secondary ingression. In line with this, ANCHR has been proposed to act in concert with CHMP4C to bind and sequester VPS4 at the Flemming body in an aurora B dependent manner. Question marks represent speculative interactions that have not yet been validated.

1.6. ESCRTs at the nuclear envelope

1.6.1. ESCRTs in nuclear envelope reformation

The nuclear envelope mediates nucleo-cytoplasmic compartmentalisation and is continuous with the ER, forming a double membrane structure consisting of an inner nuclear membrane (INM) and outer nuclear membrane (ONM)[526]. In contrast to budding yeast which undergoes a 'closed' mitosis, mammalian cells undergo 'open' mitosis in which the nuclear envelope (NE) and lamina must be broken down at prophase and incorporated into the ER to allow chromosomes access to the mitotic spindle[526–529]. NE breakdown is mediated by a dynein mediated microtubule tearing process under the control of CDK1, Aurora B kinase and PLK-1[528]. Aurora B associates with chromosomes to prevent decondensation and NE reformation until anaphase, when chromosomes have segregated[530]. The NE is reformed from ER membrane at anaphase by recruitment of ER membrane to the rims of decondensing chromatin disks[531]. Membrane then flattens and encapsulates chromatin; however, gaps still exist in the double membrane where ER tubules have not fused together, particularly where spindle attachment persists[531–534]. Spindle severing and annular fusion of membrane must therefore take place to seal such holes, and this has been shown to involve the ESCRT machinery.

Involvement of ESCRTs in annular fusion was initially demonstrated in studies by Olmos et al. 2015 and Vietri et al 2015, who showed recruitment of CHMP2A and CHMP4B to nucleo-cytoplasmic channels in the reforming nuclear envelope[18,19]. Both studies also made use of correlative light electron microscopy to strengthen their findings. Localisation of other ESCRT-III proteins, such as CHMP3, CHMP1A, CHMP1B, VPS4 and hIST1 was additionally observed, and knockdown of these subunits led to reduced nuclear integrity and DNA damage caused by loss of compartmentalisation, hence protection from cytoplasmic nucleases. Vietri et al. 2015 showed that as in cytokinesis (Section 1.5.5.), the microtubule severing AAA ATPase Spastin was recruited in a hIST1 dependent manner, via a MIT-MIM domain interaction, to disassemble microtubules, and that microtubule severing is a rate-limiting step of NE resealing: expression of dominant negative Spastin led to retention of CHMP4B-GFP at open fenestrations in the NE[19]. In contrast to cytokinesis, however, CHMP1B knockdown did not perturb Spastin recruitment, suggesting an alternative mechanism of recruitment.

Ubiquitin fusion and degradation 1 (UFD1) and CHMP7 have been suggested as adaptor proteins that recruit ESCRT-III to the nuclear envelope. UFD1 is an adaptor protein that associates with the p97 AAA ATPase, which has been shown to play a role in directing fusion of Golgi and ER membrane, removal of ubiquitinated Aurora B from chromosomes, ER membrane recruitment to the NE and NE resealing[18,535,536]. An interaction between UFD1 with CHMP2A was seen by yeast two hybrid and UFD1 was shown to be necessary for ESCRT-III recruitment to the reforming NE[18].

CHMP7 shows features of a hybrid ESCRT protein with a C-terminus similar to CHMP6 showing typical CHMP structure, consisting of 6 helical regions, and an N-terminus that resembles the tandem winged helix domains of ESCRT-II subunit EAP20[537,538]. Knockdown of CHMP7 led to abolishment of ESCRT-III and VPS4 to the NE, and interaction with CHMP4B has been shown[19,539]. The first of the two winged helix domains at the N-terminus contains an extended loop of hydrophobic amino acids that anchor CHMP7 to the ER membrane[538]. Given the continuity of the ER membrane with the NE, this suggests a possible mechanism of recruitment for ESCRTs to NE fenestrations, and membrane binding is necessary for further ESCRT-III assembly[113]. Assembly of ESCRT-III at the NE, with potential specificity for sites at which annular fusion occurs, however, has been shown to depend on interaction between CHMP7 with the LEM domain containing protein LEMD2[540–543]. This INM protein binds CHMP7 via its C-terminal MSC (MAN1/Src1-C-terminal homology) domain, and bridges chromatin with the nuclear envelope. CHMP7 also contains a nuclear export signal at its C-terminus that ensures localisation to the cytosolic side of the NE, thus preventing ESCRT-III polymerisation until required, perhaps by interaction with LEMD2[540,541]. This together with coincidence detection of ER derived membrane, LEMD2 and possibly spindle microtubules has been suggested to specify assembly of ESCRT-III at sites where the INM meets the ONM and direct annular fusion.

Fission yeast undergoes a ‘semi-open’ mitosis, in which the MTOC enters the nucleus through a fenestration in the NE during mitosis. Whilst it is unclear whether the ESCRTs are involved in resealing such fenestrations, studies have shown that, loss of function mutations in *Cmp7* or *Lem2* in fission yeast suppresses defects in NE resealing seen upon depletion of Vps4[542]. This suggests that as in mammalian cells, the aforementioned CHMP7 and LEMD2 homologues are important for nuclear integrity, even if they play

slightly different roles in yeast. A recent publication studying the fission yeast *S. japonicus* probed further, showing that the ESCRT machinery remodels INM localised Lem2-Nur1 complex attachment with heterochromatin, mediating its release from heterochromatin, as required during mitosis, and for proper nucleocytoplasmic compartmentalisation following mitosis[540].

A recent study by Ventimiglia et al. 2018 shed light on the role of coiled-coil and C2 domain-containing protein B (CC2D1B) as a regulator of NE reformation, by preventing premature recruitment of ESCRTs to the NE. CC2D1B must later be removed prior to ESCRT recruitment[544]. CC2D1B is a member of the Lgd/CC2D1 family that also includes CC2D1A and the *Drosophila* homologue Lgd. These proteins have been shown to bind CHMP4 paralogues, and CC2D1A has been shown to inhibit polymerisation of CHMP4B[545–547]. An interaction of CC2D1B with CHMP7 and CHMP2A, in addition to CHMP4, was discovered, and CC2D1B was shown to localise to the NE in a CHMP7 dependent manner, where it also binds the lipid PI(4,5)P2. Depletion of CC2D1B led to premature recruitment of ESCRT-III to the NE, around 5 minutes earlier than usual, at a time closer to furrow ingression, before more complete coverage of NE around the nuclear perimeter. It also led to reduced accumulation of CHMPs and disruption of coordination of their recruitment at the NE, as demonstrated by an approximate two-minute lag between recruitment of CHMP7 and CHMP4B[544]. Observations were extended to spastin in this study, and both premature recruitment and a reduction in spastin was observed at the NE upon CC2D1B depletion, potentially due to the asynchronous recruitment of CHMPs. Persistence of microtubules and delayed disassembly was observed as a result of this, accounting for aberrant NE morphology[544].

Aside the role of ESCRTs in NE reformation during mitosis, increased hydrostatic pressure causes NE rupture to occur in interphase during the migration of cells of the immune system and cancer cells through confined spaces[548,549]. Studies have shown that the ESCRTs play a similar role here in NE repair, to lessen DNA damage[548,549]. In these cases, rupture occurs at localised regions of NE extrusion where excess pressure causes loss of lamins and NPCs. As expected, depletion of ESCRT-III subunits leads to disrupted repair and cell death.

A role upstream of ESCRT-III for barrier to autoantigen factor (BAF) in membrane recruitment to NE ruptures has recently been described. BAF interacts with cytosol

exposed chromatin, through nuclear ruptures, and recruits membrane to the exposed chromatin[550]. Recruitment of membrane occurs via interaction of phosphorylated BAF with LEM domain proteins, which bind the INM. Recruitment of LEMD2 in this way recruits CHMP7 and the ESCRT machinery to the rupture to direct sealing[550].

1.6.2. ESCRT function in yeast nuclear pore complex surveillance

Budding yeast undergoes a closed mitosis in which the NE is not broken down, and the mitotic spindle instead forms within the nucleus. Nuclear pore complexes control entry and exit of proteins and RNA, thus maintaining nucleocytoplasmic compartmentalisation. The ESCRTs have been implicated in removal or sequestration of defectively formed nuclear pore complexes (NPCs) in yeast as a quality control mechanism, since the NE is not broken down and reassembled as in mammalian cells[551–554].

NPCs are macromolecular structures that consist of around 600-700 subunits called nucleoporins (Nups)[555–557]. Epistasis screens initially uncovered genetic interactions between Vps4, Snf7 (CHMP4), Vps24 (CHMP3) and Vps2 (CHMP2) with nucleoporin POM152 and Nup170[551]. Nup170 interacts with the inner nuclear membrane LEM domain proteins Heh1 (LEMD2 homologue) and Heh2, and further interactions between Snf7 and Chm7 (CHMP7) with Heh1 and Heh2 were subsequently uncovered[558,559]. In addition to this observed interaction with Chm7, the identity of Heh1 and Heh2 as putative adaptors for ESCRT-III recruitment to defective NPCs was suggested by the observed necessity of the Chm7-Heh1/2 interaction for recruitment of Chm7 to defective NPCs[551]. Furthermore, defective NPCs accumulated in a structure at a single site at the NE, within INM invaginations in the perinuclear space, known as the storage of improperly assembled nuclear pore complexes (SINC) upon deletion of Heh2, ESCRT-III or Vps4. Deletion of Chm7 prevented this[551,558]. This demonstrated a role for Chm7 in SINC formation. The SINC is formed to ensure that only one daughter cell inherits the defective NPCs rather than both, thus representing a further feature of NE quality control[551,552].

The exact mechanism by which defective NPCs are dealt with by the ESCRT machinery is not clear. Models put forward include direct disassembly by Vps4, or indirectly via

disassembly of NPC bound ESCRT-III[551,552,558]. In a similar parallel with the role of CHMP7 in mammalian NE reformation, yeast Chm7 has also been shown to seal the NE above defective NPCs to prevent unfavourable nucleo-cytoplasmic mixing[558].

1.7. ESCRTs in viral budding

1.7.1. Late domain mediated viral budding

CHMP4 and VPS4 homologues are required for replication and budding of *Sulfolobus* turreted icosahedral virus (STIV) in Archaea of the genus *Sulfolobus*. This suggests that whilst cytokinesis may represent the ancestral function of the ESCRT machinery, viral budding is also a well conserved ESCRT mediated process[448–450].

A study by Gottlinger et al. 1991 demonstrated that removal of HIV-1 p6 led to the tethering of nascent virions to the plasma membrane by membranous stalks, representing a defect at the late stages of the virus lifecycle[560]. Follow up experiments by Huang et al. 1995 showed that this phenotype was largely due to a p6 ^{7}PTAP^{10} motif[54]. Additional conserved tetrapeptide late budding domains (L-domains) were subsequently discovered in other viruses, most importantly an LYPxnL motif in Equine infectious anaemia virus (EIAV) p9(Gag) and a PPxY motif in Rous sarcoma virus (RSV) p2b(Gag) (Figure 20)[561,562]. Prior to further elucidation of the mechanism by which these L-domains mediated viral budding, it was found that despite variation in budding efficiencies from wild type levels, such L-domains from EIAV, RSV and Murine leukaemia virus (MLV), which also contains a PPXY motif, were able to function in exchangeable and position independent manners[561,563,564]. Whilst PT/SAP motifs were later shown to recruit TSG101 (ESCRT-I) via its UEV domain, mimicking the interaction with HRS (ESCRT-0)[12–15,75,565], LYPX$_n$L motifs were found to recruit ALIX, via the second arm of its V domain[152,566–568], and PPXY motifs were found to recruit Nedd4-like HECT domain E3 ubiquitin ligases notably WWP1, WWP2 and Itch via their WW domains[569,570]. Since these initial studies, L-domains have been discovered in a wide range of other enveloped viruses[571].

The discovery of ESCRT usurpation for viral budding represented an important step in understanding how the ESCRT machinery functions. The conserved requirement for ESCRT-III in budding regardless of the L-domains employed helped give rise to the

concept of the ESCRT machinery as a modular system, that uses site-specific adaptor proteins to recruit ESCRT-III to various sites/viral structural proteins to mediate membrane remodelling[13,565,572–574]. Together with this conserved requirement for ESCRT-III, viral budding was the second ESCRT mediated process to be discovered, following endosomal sorting, and the shared membrane remodelling topology helped reinforce its membrane remodelling function.

Viruses often encode more than one L-domain. In such cases the activity of one L-domain displays dominance whilst the others display more of an auxiliary role. Whilst the ^{7}PTAP^{10} motif in HIV-1, for example, is primarily responsible for mediating budding, an ALIX binding ^{35}LYPLTSL^{41} within p6 also shows L-domain activity, as evidenced by the ability of ALIX overexpression to rescue budding of a PTAP mutant HIV-1 virus (Figure 20)[566,568,575]. In addition to this, the ability of HIV-1 Gag to recruit Nedd4-2 in a PPXY independent manner has been elucidated, via the naturally truncated C2 domain of Nedd4-2[576,577]. This has been proposed to explain why overexpression of Nedd4-2 can rescue L-domain mutant HIV-1[578]. Both Ebola VP40 and MLV Gag encode all three classical PPXY, PTAP and LYPX$_n$L motifs[14,569,579–581]. In the case of MLV, the PPXY motif shows dominance[579], whereas in Ebola the PTAP and PPXY motifs which overlap in a ^{7}PTAPPEY^{13} sequence are both required for optimal budding (Figure 20)[14,569,580]. A more downstream IYPX$_n$L motif was later identified in Ebola VP40, and shown to display some L-domain activity: ALIX overexpression showed some rescue of a budding deficient Ebola virus, containing a mutated PTAPPEY motif, as previously shown for HIV-1[581]. There is some evidence that the activity of different L-domains is employed in different cell types, such as potentially a more prominent role for the ^{35}LYPLTSL^{41} motif of HIV-1 in T cells[582]. In this way, multiple L-domains would broaden viral tropism. However, another possibility would be to confer an evolutionary advantage to viruses, such that propagation can still occur, albeit to a more limited extent, if the dominant L-domain acquires loss of function mutations.

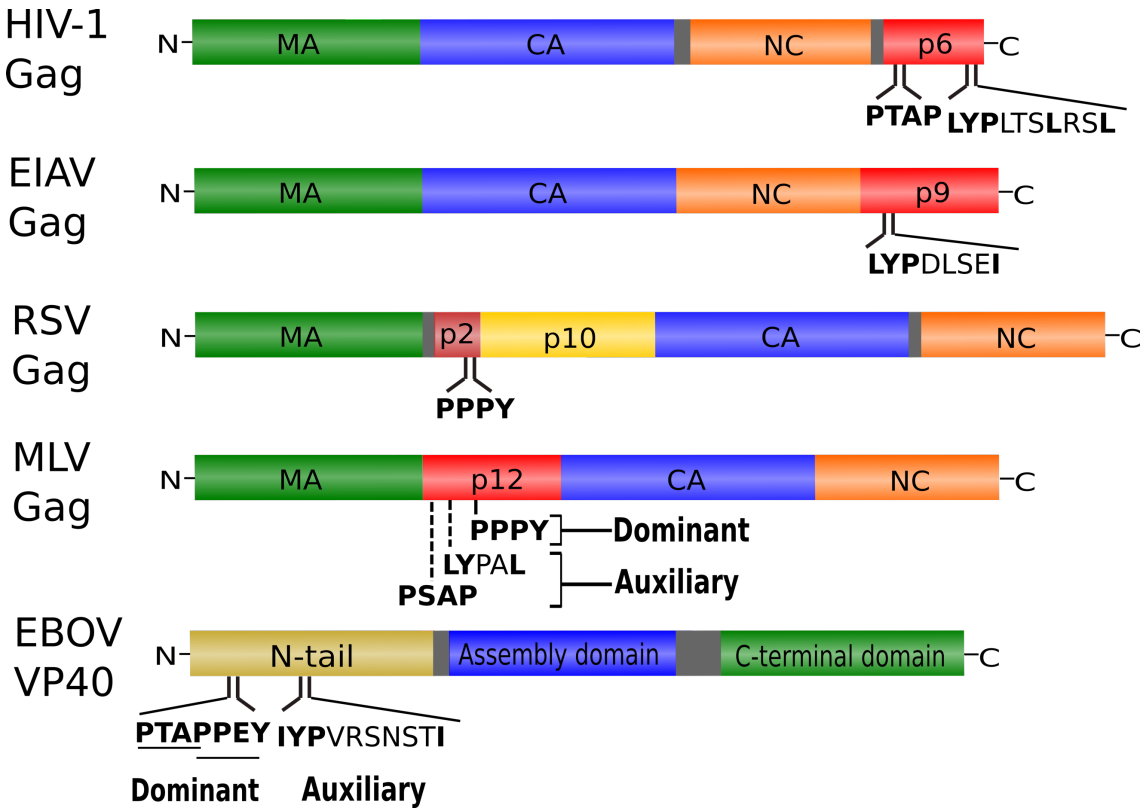

Figure 20. Late domain motifs in viral structural proteins recruit the ESCRT machinery to sites of budding

Late domains (L-domains) are short peptide sequences in structural proteins of enveloped viruses, so called because they function during the late stages of enveloped virus assembly to mediate envelopment at the plasma membrane and budding from the cell by usurping the ESCRT machinery. PT/SAP motifs directly recruit TSG101 (ESCRT-I), $LYPX_nL$ motifs recruit ALIX and PPXY motifs recruit Nedd4-like HECT domain E3 ubiquitin ligases notably WWP1, WWP2 and Itch. HIV-1 budding is mediated predominantly by a PTAP motif, however an auxiliary $LYPX_nL$ motif also shows some L-domain activity. EIAV depends on a $LYPX_nL$ motif for budding whilst RSV depends on a PPXY motif for budding. MLV and EBOV are further examples of viruses that encode all three of these classical L-domains. In the case of MLV, the overall picture so far is that its PPXY motif shows dominance, whilst in the case of EBOV, overlapping PTAP and PPXY motifs (PTAPPEY) are both required for optimal budding, whilst a later discovered auxiliary $IYPX_nL$ motif was shown to mediate some activity. HIV-1 = Human immunodeficiency virus 1, EIAV = Equine infectious anaemia virus, RSV = Rous sarcoma virus, MLV = Murine leukaemia virus, EBOV = Ebola virus, MA = Matrix protein, CA = Capsid protein, NC = Nucleocapsid protein.

Whilst ALIX is able to directly bridge viral YPX_nL motifs with CHMP4 proteins, hence ESCRT-III, pathways for ESCRT-III recruitment are less clear in the case of PT/SAP and PPXY L-domain mediated budding. One reason for this is the observation that budding in these cases appears relatively refractory to ESCRT-II depletion, suggesting that other unidentified bridging factors are present[91,583]. Although ESCRT-II is essential for recruitment of ESCRT-III to HIV-1 Gag by ESCRT-I using purified ESCRT proteins and a giant unilamellar system (GUV)[584], ESCRT-II was originally shown to be dispensable for

HIV-1 and MLV budding in siRNA knockdown experiments[91,583]. Later studies suggested, however, that although not essential for budding, ESCRT-II shows signs of contributing to overall HIV-1 budding levels[585,586]. Such studies used shRNA knockdown, CRISPR/Cas9 knockout HAP1 cells and dominant negative protein expression together with siRNA knockdown to come to such conclusions. ESCRT-II has also been suggested to be necessary for RNA trafficking in HIV-1[587].

1.7.2. Ubiquitination in viral budding

Although the catalytic activity of Nedd4-like E3 ubiquitin ligases is required for PPXY motif mediated budding, this process is also not so well understood. The role of ubiquitination in viral budding is complicated, and whilst it would seem logical to assume that ubiquitination of viral structural proteins generates sites for attachment of ESCRT-0, -I and -II, studies in varied viral contexts have implied requirements for ubiquitination of viral structural proteins and/or trans-acting factors. The importance of ubiquitination of viral structural proteins is perhaps most obviously implied by studies showing that mutation of ubiquitin acceptor sites in HIV-1 and RSV Gag abolishes budding[588,589]. In contrast, however, is the observation that increased ubiquitination of HIV-1 Gag by introduction of a PPXY motif does not enhance budding[590]. Fusion of ubiquitin to L-domain deficient EIAV and HTLV has also been shown to rescue budding, and viruses that exhibit PPXY dependent budding display increased budding efficiency upon Gag ubiquitination[590–592].

Several lines of evidence have demonstrated the importance of ubiquitination of trans-acting factors. Two studies made used of an engineered prototypic foamy virus Gag protein devoid of its single lysine residue, hence ubiquitination site[593,594]. This did not disrupt budding mediated by the single PSAP motif present. When the PSAP motif was mutated but the PPPY motif and surrounding sequence from MLV was C-terminally fused to the Gag protein, budding was still able to proceed. Furthermore, overexpression of a catalytically active YFP-WWP1 enhanced budding[593,594]. This clearly demonstrates the substrate for ubiquitination to be a trans-acting factor. A further finding implicating trans-acting factors as ubiquitination substrates includes the observation that hydrophobic surface mutations of ubiquitin rather than mutation of

residues that disrupt the TSG101 UEV interaction display a more potent disruption of HIV-1 budding[591,594].

The arrestin-related trafficking (ART) proteins are highly likely to represent ubiquitinated trans-acting factors involved in ESCRT mediated viral budding. These proteins have been shown to interact with TSG101, ALIX and ubiquitin in addition to Nedd4-like ubiquitin ligases, including WWP1, WWP2, Itch and Nedd4[569,595]. Furthermore, recruitment to sites of viral budding is observed, as is ability to perturb MLV budding when overexpressed[595]. It has been difficult to convincingly prove involvement in PPXY motif mediated budding, however, due to lack of specific knockdown phenotypes[595]. This suggests that functional redundancy amongst these proteins, and additional binding partner requirements are likely to be seen.

1.7.3. ESCRT-III requirements in viral budding

In contrast to mitosis and cytokinesis (Section 1.5.6.), which have been shown to require the full complement of ESCRT-III proteins, the smaller number of CHMPs identified as necessary for viral budding represents yet another example of how studying the role of the ESCRT machinery in viral budding has facilitated general understanding of ESCRTs – in this case the core ESCRT-III subunits necessary for all ESCRT mediated processes. A prominent role for CHMP2A and CHMP4B is apparent, as evidenced by preferential recruitment of these subunits for MLV and EIAV budding[573,574,586]. Requirement of these two proteins in HIV-1 budding appears less specific: as long as both a CHMP2 (2A or 2B) and a CHMP4 (4A, 4B or 4C) are expressed, viral budding is not drastically reduced[573,586]. Depletion of other ESCRT-III proteins generally has been shown to result in weaker perturbation of viral budding[573,574,583,586]. Taken together, these studies demonstrate an essential role for CHMP4 and CHMP2, whilst that of the other CHMPs appears to vary depending on the virus.

1.7.4. Models for ESCRT mediated viral budding

Variations of the dome model for ESCRT-III assembly and membrane remodelling (Section 1.3.4.4.) have been proposed to account for structures observed at the necks of budding virions by deep-etch electron microscopy (DEEM), and the capture of ESCRTs

inside released virions[129]. The attractiveness of the original dome model as described in section 1.3.4.4. in viral budding lies in its ability to explain the presence of ESCRTs inside budded virions, as observed by photo-activated localisation microscopy (PALM)[596]. In this model, ESCRT-III filaments would polymerise away from Gag, tapering to a point towards the cytosol. In this way, the polymerisation of ESCRT-III filaments away from the virion would mean that following disassembly by VPS4 and scission, ESCRTs would become trapped within the virions (Figure 21). This original dome model, however, would not support the observation that VPS4 is steadily observed in bud necks[597,598]. The observation of VPS4 inside bud necks suggests a more active role for VPS4 in membrane remodelling, in more than just the disassembly and recycling of filaments. The dome model also does not explain the tapering of the dome/cone towards the virion, rather than the cytosol, as seen by DEEM[122]. Other models have therefore been put forward such as the reverse dome model and the inverse buckling model (section 1.3.4.4.)[129]. In a reverse dome model, filaments would still nucleate on the virion side of the membrane and form successively narrower rings, tapering to a point (Figure 21). However, in order to account for tapering towards the virion, inversion of the direction of growth would have to occur soon after polymerisation is initiated. This has been suggested to potentially be mediated by VPS4[129]. The reverse dome model would not account for the observed entrapment of ESCRTs inside budded virions but would be more consistent with the classical view that ESCRTs are released back into the cytoplasm. The inverse buckling model would also be consistent with tapering of the dome/cone towards the virion (Figure 21). Unlike the reverse dome model, a buckling model would not require the direction of filament growth to change, as filaments are predicted to form successively wider rings away from the virion[123,599]. The severing of the overbent inner ring would then cause relaxation and flattening of the polymer, together with detachment from upstream ESCRTs. This would also drive scission and release of most of the ESCRTs back into the cytoplasm.

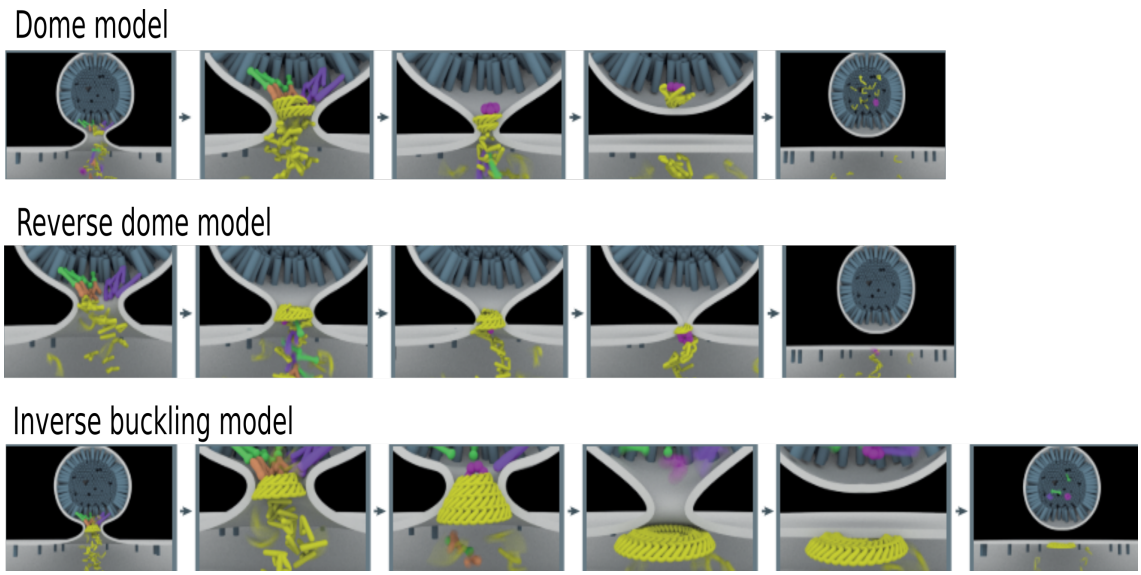

Figure 21. Models for ESCRT-III polymerisation in viral budding
Models for ESCRT-III polymerisation and severing of budding virions have been put forward to account for the presence or absence of ESCRTs inside released virions, the direction of tapering of ESCRT-III cones and the presence or absence of VPS4 in bud necks. The dome model would involve tapering of ESCRT-III filaments towards the cytosol, contrary to tapering towards the virion, as seen by Deep-etch electron microscopy (DEEM). However, it would explain the capture of ESCRT-III and VPS4 inside released virions. The inverse dome model is more consistent with filament tapering towards the virion and the classical view that ESCRTs are released back into the cytosol following severing. Reversal of the direction of filament tapering following nucleation at the virion side, has been proposed to explain this. VPS4 has been proposed to be involved in mediating this change in direction of tapering. This is potentially consistent with the more persistent localisation of VPS4 in bud necks. An inverse buckling model (Section 1.3.4.4.) would also be consistent with the observed tapering of filaments towards the virion and would not require change in the direction of filament tapering. In this model, the majority of ESCRTs would be recycled to the cytoplasm, however a few, notably upstream ESCRTs, would become entrapped in the virion. Yellow = ESCRT-III, Green = ESCRT-I, Orange = ESCRT-II, Purple = ALIX, Pink = VPS4, Grey = Viral Gag. *Adapted from Schöneberg et al. 2016*

1.8. Additional ESCRT mediated processes

1.8.1. ESCRTs in autophagy

Autophagy refers to any of the recycling processes that employ lysosomal degradation to remove damaged or excess cellular components under basal conditions or upon induction by stress stimuli. Autophagy is important in protection against cancer, neurodegenerative diseases, pathogen infection and ageing[600,601]. Broadly speaking, there are three types of autophagy being microautophagy, macroautophagy and chaperone mediated autophagy. Endosomal microautophagy represents an additional form of microautophagy.

Microautophagy refers to the process whereby organelles such as mitochondria and peroxisomes are directly engulfed by lysosomes through invagination of the lysosome membrane. Endosomal microautophagy meanwhile refers to the process whereby cellular components are first internalised into MVBs prior to the fusion of MVBs with lysosomes. Given the role of ESCRTs in MVB formation, it comes as no surprise that ESCRTs have been implicated in this process[61]. Macroautophagy is the process by which organelles are sequestered by a double membrane structure known as a phagophore to form an autophagosome, which subsequently fuses with the lysosome, leading to degradation. ESCRTs have also been implicated in this process[58,59]. Chaperone mediated autophagy is the process whereby proteins interact directly with the chaperone protein hsc70 and are directly transported into the lysosome via the lysosomal transporter LAMP2-A.

During microautophagy, ESCRTs have been implicated in the sorting of KFERQ motif containing proteins into ILVs, following endosomal targeting of such proteins by interaction of this motif with hsc70[61].

Involvement of the ESCRT machinery in macroautophagy has been implied by the observed increase in autophagosomes upon depletion of various ESCRT proteins including subunits of ESCRT-I, -II and -III and VPS4[58–60,602]. This has been observed in mammals, yeast, *C. elegans* and *Drosophila*, and is either due to inhibition of autophagic flux or promotion of autophagosome biogenesis. The role played by ESCRTs in autophagy, however, is still not entirely clear, and has until recently been hampered by the technical limitations involved in distinguishing between sealed and unsealed autophagosome membranes, when investigating whether ESCRTs are involved in sealing phagophore membranes. A role in sealing phagophore membrane would appear plausible, given the shared topology in sealing the double membrane with that of other ESCRT mediated processes. Consistent with this is the observation of numerous, enlarged unclosed phagophores in chmp1 mutant Arabidopsis[603]. However, ESCRTs have also been proposed to potentially facilitate fusion of autophagosomes with MVBs to form amphisomes, prior to fusion with lysosomes, or directly with lysosomes to form autolysosomes[58,59,604,605]. It has also been suggested that although ESCRTs appear to be playing a role in autophagy, this is simply a consequence of disrupted lysosome biogenesis or induction of cellular stress upon their depletion[606].

Although the identification of relevant site-specific adaptor proteins and specific pathways for ESCRT recruitment remain to be elucidated for macroautophagy, progress has recently been made in strengthening evidence for a potential role in phagosome closure. Novel assays have been developed for measuring phagosome closure, involving the use of protease protection assays, a HaloTag-LC3 autophagosome completion assay, and an optogenetic closure assay[607,608]. Two separate studies have shown a particularly prominent role for CHMP2A in phagosome closure. CHMP3 and CHMP7 were also identified as potentially important contributors to this process[607,608]. CHMP4B/Snf7 has been observed in both human and yeast cells at autophagosomes, by examining co-localisation with autophagosome markers LC3 and Atg17, and VPS4 depletion has consistently shown strong defects in phagosome closure[608,609]. Amphisome formation also appears to be disrupted upon VPS4 depletion[606].

1.8.2. ESCRTs in plasma membrane repair

ESCRTs have been described to play a role in calcium influx triggered repair of plasma membrane (PM) wounding[20]. PM wounding can occur in nature by bacterial pore forming toxins and mechanical stress[610–613]. ESCRT-III has been shown to rapidly accumulate at sites of wounding at the PM, induced by a variety of techniques including laser ablation and use of detergents[21,614]. Here they mediate extrusion of damaged regions followed by scission and shedding of the region[21,614]. Localisation of Tsg101, ALIX, CHMP3, CHMP2A, CHMP2B, CHMP1A and CHMP4B has been observed at sites of PM wounding, and a prominent role for ALIX has been described in this process, by interacting with its earlier described binding partner calcium sensing protein apoptosis-linked gene-2 (ALG-2)[21,614] (sections 1.3.5.2. and 4.1.). ALG-2 is therefore likely to represent the site specific ESCRT adaptor in this process. Strengthening the dependence of this process on ALIX is the finding that ESCRT-0 and ESCRT-II appear not to be required, and an increase in the nucleating factor CHMP6 at the PM is not observed. These findings support a role for ALIX as a bridging factor between ALG-2 and CHMP4, providing nucleation of ESCRT-III.

1.8.3. ESCRTs in microvesicle release

In a process analogous to the shedding of damaged PM legions, the ESCRTs have also been implicated in microvesicle shedding at the PM in *C. elegans* embryos upon loss of the P4-ATPase TAT-5[615]. TAT-5 is a lipid flippase that maintains phosphatidylethanolamine symmetry. Its depletion therefore causes phosphatidylethanolamine to accumulate on the cell surface and this causes a loss of cell adhesion, vesicle shedding and thickening of the PM. Whilst ESCRT-0 and ESCRT-I were suggested to be required for vesicle shedding, as shown by loss of membrane thickening in TAT-5 mutant cells upon their depletion, localisation of ESCRT-III to the membrane was not observed. The function of the ESCRT machinery in this process therefore remains to be established.

Arrestin domain containing 1 (ARRDC1)-mediated microvesicles (ARMMs) are a type of microvesicle of unknown function, that use the ESCRT machinery to bud from the PM with a striking similarity to viral budding[56,57]. ARRDC1 is a ubiquitin ligase adaptor for ESCRT recruitment in this process, that directly recruits TSG101 via a central PSAP motif. In addition to this motif, ARRDC1 encodes an N-terminal arrestin domain that mediates membrane localisation, and two C-terminal PPXY motifs that recruit WWP2 ubiquitin ligase. WWP2 ubiquitinates ARRDC1, which has been shown to be necessary for optimal ARMM budding[56,57]. Multimerisation of ARRDC1 at the plasma membrane has also been observed, as for HIV-1 Gag[56]. Mutation of the PSAP motif and expression of dominant negative VPS4 were shown to inhibit microvesicle release[56]. Although functional characterisation of ARMMs is lacking, the observed transfer of ARRDC1 between cells hints at a possible role in intercellular communication[56].

1.8.4. ESCRTs in exosome release

In contrast to the direct involvement of ESCRTs at the PM in microvesicle release, a more indirect role for the ESCRT machinery has been elucidated in exosome release, i.e. vesicles shed from the PM as ILVs within MVBs that fuse with the plasma membrane[22]. Exosome identity is characterised by presence of the tetraspanin CD63. ESCRTs have been implicated in formation of exosomes that contain syndecans, which are heparan sulphate presenting proteins[616]. For this they require the adaptor syntenin,

with which an interaction with ALIX via a YPXL motif has been described[616,617]. Whilst ESCRTs are responsible for the formation of the initial ILVs in this process, they are not required for fusion of the resulting MVBs with the PM and exosome release.

1.8.5. ESCRTs in axon pruning

Pruning of axons and dendrites occurs during development of the nervous system to remove previously formed synaptic connections as they are replaced with new ones. This involves scission of neurons, and ESCRTs have been implicated in this process[618,619]. Both a direct role in severing of membrane necks of neurons has been suggested, as has a more indirect role in the endosomal sorting and degradation of the cell surface receptors neuroglian (Nrg) and Patched (Ptc), which inhibit pruning[618].

In terms of a more direct role for the ESCRT machinery in neuron pruning, studies in *Drosophila* have shown localisation of Shrub/CHMP4 and Myopic/HD-PTP to sites of neuron severing, and direct interaction between the Bro1 domain of Myopic/HD-PTP with Shrub/CHMP4 was shown to be necessary for severing. This process was also shown to require ESCRT-I but not ESCRT-II, hence a role for Myopic/HD-PTP here as a bridging factor[620]. Identification of adaptor proteins for ESCRT recruitment in this process are yet to be elucidated.

1.8.6. ESCRTs in lysosome repair

In contrast to lysophagy, in which lysosomes damaged beyond repair are removed by autophagy, ESCRTs have recently been implicated in membrane repair of less severely damaged salvageable lysosomes[62,63]. Lysosome repair is essential for preventing cell death from the release of acidic contents and degradative enzymes. Two studies by Radulovic et al 2018 and Skowyra et al 2018 in excellent agreement with each other demonstrated that the ESCRT machinery is rapidly recruited to small ruptures in lysosome membranes[62,63]. These studies principally made used of the lysosomotropic compound L-leucyl-L-leucine O-methyl ester (LLOMe) to permeabilise lysosome membranes. LLOMe is small enough to traverse membranes and enter organelles. Upon entry to the lysosome, this compound is cleaved by cathepsin C and condenses into a membranolytic polymer, within the acidic environment[621].

ESCRTs appeared at damaged lysosome membranes at an early time point, associated with small membrane ruptures, before appearance of the larger ruptures that trigger lysophagy. This was demonstrated by appearance of the ESCRT machinery before Galectin-3. Galectin-3 is a cytosolic lectin that recognises the carbohydrate portions of glycoproteins found within the lysosome lumen. This triggers lysophagy. Numerous ESCRTs were observed at LLOMe generated puncta including subunits of ESCRT-I, -II -III, VPS4 and ALIX[62,63]. Whilst both studies observed no discernible decrease in CHMP4B recruitment to damaged lysosomes upon depletion of ALIX, a delay in recruitment was seen upon depletion of TSG101 and lack of recruitment was seen upon co-depletion of both TSG101 and ALIX. This indicated that these early ESCRTs function upstream of ESCRT-III in this process. Skowyra et al. also showed that in a striking parallel with plasma membrane repair, calcium efflux from the lysosome mediated rapid recruitment of the ESCRT machinery, and that ESCRTs colocalised with ALG-2[62]. Treatment of cells with the calcium chelator BAPTA-AM prevented the recruitment of ESCRTs to damaged lysosomes. ALG-2 therefore potentially represents the adaptor for ESCRT recruitment again in this case.

Involvement of ESCRTs in early repair of damaged lysosomes was demonstrated by measuring the recovery time of the fluorescent compounds Magic red and Lysotracker to the lysosome lumen[62,63]. Following depletion of TSG101 and ALIX and membrane perforation by LLOMe, recovery time was delayed demonstrating a role for the ESCRT machinery in repair. Consistent with this was also the observation that CHMP1B-GFP puncta appeared just after loss of fluorescence but before complete recovery.

1.9. ESCRTs in human disease and animal models

Mutations and dysregulation of ESCRT protein expression levels have been implicated in diverse phenotypes and pathologies, notably neurodegenerative disease and cancer. Further implications in cell migration, maintenance of cell polarity, development and mycobacterial infection have also been uncovered[622–624].

Autosomal dominant mutations in CHMP2B have been found in patients with frontotemporal dementia and amyotrophic lateral sclerosis[625,626]. Accumulation of

ubiquitinated protein inclusions in neurons is seen in both these neurodegenerative diseases. Given the role played by the ESCRT machinery in autophagy, and the accumulation of autophagosomes and ubiquitin positive inclusions in autophagy deficient mice and flies[627–630], the explanation that has gained most support for this pathology is that the accumulation of such aggregates is due to disruption of ESCRT mediated autophagy. Mouse neurons, human cell lines and *Drosophila* expressing a CHMP2B splice site mutant corresponding to that uncovered in a case of frontotemporal dementia displayed an increase in autophagosomes suggesting a direct link between the ESCRT machinery and the disease aetiology[58,59,604]. The CHMP2B mutant formed aberrant complexes with mChmp4B[59]. p62 binds ubiquitin in the observed protein aggregates, and recruits the autophagy marker LC3, providing a link to autophagic degradation. Neurons are particularly sensitive to perturbations in endocytosis and related vesicular trafficking, since endocytosis is required for reuptake of synaptic vesicles and maintenance of the correct membrane protein composition for nerve transmission. It is also necessary for membrane repair following damage by delivery of membrane. This could account for why perturbation of the ESCRT machinery is commonly associated with neurodegeneration as opposed to more generalised symptoms.

Drosophila and mammalian cell models of Huntington's disease have shown that ESCRT depletion increases neurotoxicity by preventing clearance of polyglutamine protein aggregates[58,604]. Conversely, stimulation of autophagy reduces neurodegeneration in *Drosophila*, mouse and human cell models of the disease[631,632]. A functional MVB pathway has also been shown to be necessary for clearance of the aggregates, further implicating the ESCRT machinery in preventing neurodegenerative disease[604]. In mice, a null mutation in the gene encoding the E3 ubiquitin ligase Mahogunin causes the prion-like disease spongiform neurodegeneration[633]. Mahogunin, like Tal (section 3.1.1.), is known to ubiquitinate TSG101[633]. Spartin and Spastin are mutated in spastic paraplegia – another disease characterised by length dependent axon degeneration[506,634].

TSG101, VPS37A and CHMP1A and VPS4B were initially described as tumour suppressors, in experiments using mice, *Drosophila* and expression screens for human cancer cell lines[635–639]. The picture for TSG101, however, was later complicated by the observation that its knockout caused cell death in mouse mammary epithelial cells, as opposed to

proliferation initially seen in mouse 3T3 fibroblasts and Drosophila epithelial cells[640,641]. In the case of Drosophila, cell proliferation upon TSG101 depletion has potentially been attributed to increased Notch signalling which directs interleukin-6-like secretion, leading to hyperplasia in surrounding tissue via JAK/STAT signalling, whilst the mutant cells themselves display apoptosis[636,642–644]. Loss of epithelial cell polarity is also seen as a consequence of TSG101 depletion in Drosophila, suggesting involvement in cytoskeleton rearrangement[636,642,643]. This is potentially due to a role of the ESCRT machinery in E-cadherin turnover and integrin signalling[643,645,646]. Similar phenotypes are observed upon depletion of Vps25/EAP20 (ESCRT-II)[642,643]. In contrast to a role as a tumour suppressor, TSG101 has been proposed to stimulate cell growth in mice by interacting with the ubiquitin ligase Mdm2 and stabilising this enzyme which ubiquitinates the tumour suppressor p53, thus labelling it for lysosomal degradation[647,648].

In terms of development, ESCRT deficiency is commonly associated with embryonic lethality. Mouse embryos depleted of ESCRT-0 generally do not progress past day E11, showing severe defects in the foregut, heart tubes and ventral region, with enlarged endosomes[649,650]. Drosophila also show pupal lethality and disrupted patterning due to disrupted EGF and *Torso* signalling[644]. Mice depleted of TSG101 die around day E6.5 displaying no mesoderm and reduced overall size[647]. Knockdown of Chmp1a in zebrafish causes severe brain developmental defects, and knockdown of Vps37a causes reduced mobility[651,652].

Finally, A protective function for the ESCRTs has been implicated in mycobacterial infection, using *Drosophila* and mammalian macrophages. Although not studied in detail, this is believed to occur through facilitation of phagosome-lysosome fusion, or phagosome maturation, to destroy such intracellular bacteria. This suggests a role for ESCRTs in membrane fusion in addition to budding and remodelling[653,654].

1.10. Aim of thesis

The aim of this thesis is first to identify novel interaction partners of ESCRT-I by mass spectrometry. Following identification of such partners, I aim to confirm their interaction with ESCRT-I through co-precipitation assays, and then to functionally characterise such proteins, by testing involvement in known ESCRT-I mediated processes.

Chapter 2 – Materials and Methods

2.1. Cloning and molecular biology

2.1.1. Protein expression plasmids and retroviral vectors

To facilitate sub-cloning between vectors, a previously established cloning system in the lab ensured that all protein expression plasmids were modified to contain polylinkers containing EcoRI, XhoI and NotI restriction sites upstream or downstream of the sequence encoding the specific tag/viral protein to be fused to the protein of interest. All tagged proteins used in this thesis are tagged at the N-terminus unless otherwise stated.

pCR3.1 (Invitrogen), used for overexpression of tagged proteins by transient transfection, was modified to contain an HA-, YFP-, mCh- or Myc-EcoRI-XhoI-NotI poly-linker in place of the original multiple cloning site. Likewise, pCAGGS (Martin-Serrano 2003[567])was modified to contain a GST-EcoRI-NotI-XhoI poly-linker for overexpression of GST-tagged fusion proteins.

The bi-cistronic retroviral packaging vector pCMS28, derived from pMigRI (Pear et al. 1998[655]), was kindly gifted from Professor Mike Malim (King's College London, UK). This plasmid was modified by Dr Chad Swanson (King's College London, UK) to replace the GFP gene with a puromycin resistance gene linked via an internal ribosome entry site (IRES) to a multiple cloning site containing OSHA-, mCh- or YFP-EcoRI-NotI-XhoI. In this way, puromycin resistance is coupled to mRNA expression of the gene of interest. pCMS28 was further modified to create pNG72, which contains a geneticin resistance gene in place of that for puromycin. pCMS28 and pNG72 were packaged using murine leukaemia virus (MLV) Gag-Pol and VSV-G pseudotyped pHIT plasmid, pHIT-VSV-G, as described by Soneoka et al., 1995[656]. Both these plasmids were kindly gifted from Professor Paul Bieniasz (Aaron Diamond AIDS Research Center, New York, USA).

The full-length X4 strain HIV-1 proviral plasmid pNL-HxB was kindly gifted from Professor Paul Bieniasz. The full length proviral pHxB-STOP construct used in section 3.2.2. was based on this provirus and modified by Professor Juan Martin-Serrano (King's College London, UK) to containin a termination codon upstream of p6 Gag (Martin-Serrano et al., 2003[567]). The shorter trans-complementing pHxB-ENX plasmid was also based on

pNL-HxB but was modified to contain an EcoRI-NotI-XhoI polylinker in place of the p6, pol, vif and vpr sequences as outlined by Martin-Serrano et al. 2001[14].

2.1.2. Constructs

TSG101, VPS28, VPS37B, VPS37C, MVB12A and MVB12B had already been cloned in each of their tagged forms and vectors used in this thesis by Professor Juan Martin-Serrano (Martin-Serrano et al. 2001[14], 2003[565,567,575], and 2004[590], Eastman 2005[657]). VPS37A and D constructs were cloned by Dr Bethan McDonald (formerly King's College London, UK) and UBAP1 by Dr Monica Agromayor (King's College London, UK) (Agromayor et al. 2012[658]). UMAD1 (NM_001302348.1) was initially cloned from HeLa cell cDNA into pCR3.1 as GST-, HA- and Myc-tagged forms by Magdalena Kloc (formerly King's College London), and I subcloned UMAD1 and point mutants into all other appropriate vectors.

Wild type R9, R9ΔPTAP, R9ΔYP and R9ΔPTAPΔYP full-length HIV-1_{NL4-3} retroviral constructs were kindly gifted by Professor Wesley Sundquist (Fisher et al. 2007[152], Garrus 2001[13], Strack 2003[568]). pHxB-p6 was previously cloned by Professor Juan Martin-Serrano (Martin-Serrano et al. 2001[14]).

RPA3 (NM_002947.4) was cloned from HeLa cell cDNA as pNG72-YFP-RPA3 and also without a tag, in pNG72-RPA3. CHMP4B was cloned with a GFP C-terminal tag separated by a flexible 25-nm linker as described by Kim et al., 2016[659]. CHMP4B-Linker was generated by gene synthesis (GeneArt, Thermofisher) following which this construct was cloned by Dr Leandro Ventimiglia (King's College London, UK) as the C-terminal GFP fusion in pNG72 as pNG72-CHMP4B-Linker-GFP. pCMS28-mCh-Tubulin was previously cloned by Dr Monica Agromayor (Agromayor et al., 2009[507]).

A list of all plasmids used in this thesis together with restriction sites used for cloning is presented in Appendix 1.

2.1.3. Polymerase chain reaction (PCR)

Lyophilised unmodified oligonucleotide primers were ordered from Eurofins MWG Operon using a 0.01µmol synthesis scale, and resuspended in double-distilled water (ddH_2O) to 100pmol/µl. A list of all primers used in this thesis is presented in Appendix

1. Primers for cloning were typically designed to include appropriate EcoRI, XhoI and/or NotI restriction sites for ligation into vectors using the pre-established system in the lab (Section 2.1.1). Primers were typically designed when possible to be between 20-30 base pairs in length ending with a C/G cap, with similar melting temperatures and a 40% minimum GC content.

PCR reactions were carried out in a total volume of 50µL, consisting of 10µL 5X Phusion® HF Buffer (containing 7.5 mM $MgCl_2$), 0.5µL of each of forward and reverse primers at 10pmol/µL (0.1µM final conc.), 1 µL of 10mM deoxynucleotide triphosphates (200µM final conc.) (dNTPs: dATP, dCTP, dGTP, dTTP, Roche)), 0.5µL Phusion® High-Fidelity DNA polymerase (New England Biolabs), i.e. 1 unit/50µl, and 1ng plasmid DNA/purified PCR product, 200ng genomic DNA or 1µL cDNA (Section 2.1.16) template. 10µL 1M Betaine solution was also added to reduce template DNA secondary structure thus improving reaction efficiency. Reaction volumes were made up to 50µL using double distilled water (ddH_2O). Reactions were prepared on ice. PCR reactions were performed in an Eppendorf® Mastercycler Ep Gradient Thermal Cycler or Eppendorf® Mastercycler® Nexus Thermal Cycler. Typical thermocycling included an initial denaturation step at 98°C for 2 minutes followed by 35 cycles of denaturation at 98°C for 15s, annealing at 55°C for 30s and extension at 72°C for 120s. This was followed by a final 10 minute extension step at 72°C after which completed reactions were incubated at 4°C until unloading.

2.1.4. Site directed mutagenesis

An overlap extension PCR approach was employed to generate site specific point mutations in genes of interest. Overlapping forward and reverse primers centred around the base pairs to be mutated were designed to include the desired mutation flanked on both sides by around 15 nucleotides of the gene. Each of these primers were used in separate PCR reactions together with appropriate reverse of forward primers, respectively, designed to anneal at the end or start of the gene of interest and include appropriate restriction sites for cloning. Following purification of each PCR product, 10ng of each was used as template in a second PCR reaction, again using the forward and reverse primers that anneal at the start/end of the gene of interest. The product of

this reaction is the gene sequence with the desired mutation and appropriate restriction sites for cloning, so following purification, restriction endonuclease digestion and ligation into appropriate vectors could be carried out (Sections 2.1.6 – 2.1.8.).

2.1.5. Agarose gel electrophoresis

Agarose gel electrophoresis was used to resolve DNA fragments prior to purification for downstream cloning, or to check for the presence of DNA fragments of a particular size following various steps within the cloning procedure. 1-2% gels were generally used depending on the size of the fragment in question. UltraPure™ Agarose (Invitrogen) was dissolved in TAE buffer (10X solution: Tris-Base 48.4g/L, Acetic acid 11.4mL/L, EDTA 3.7g/L) by boiling, following which the solution was cooled until hand hot. Ethidium bromide (Fisher Scientific) was then added to a final concentration of 5µg/mL and the solution was allowed to solidify in a casting tank (BioRad). The gel was then transferred to an electrophoresis tank and submerged in TAE buffer. DNA samples were mixed with DNA loading dye (10X solution: 50% glycerol, 0.1M EDTA, Bromophenol blue, ddH_2O) prior to loading, and run at 90V for between 45 – 90 mins depending on the fragment size. DNA was visualised under ultra-violet light using a Chemi-Doc imaging system (BioRad).

2.1.6. DNA purification by gel extraction

Following excision of bands from agarose gels containing desired DNA, purification of DNA was carried out using a QIAGEN QIAquick Gel Extraction Kit according to the manufacturer's instructions. Bands were weighed and a volume of QG buffer equal to 3 × mass of the band was added. Bands were then melted at 56°C, with regular vortexing, after which a volume of isopropanol equal to the mass of the original band was added and the solution vortexed. The solution was transferred to a QIAquick spin column placed in a collection tube and centrifuged for 1 minute at 13,000 rpm. Flow through was discarded and the DNA, now bound to the column, was washed by adding 750µL PE buffer and centrifuging again twice, with discard of flow-though between runs. 50µL ddH_2O was then added to the column and incubated at room temperature for 5 mins before a final centrifugation step to elute into a clean 1.8 mL Eppendorf tube.

2.1.7. Restriction endonuclease digestion of DNA

Reactions were carried out at 37°C for 2-3 hrs in a total volume of 50µL typically using 2-3µg plasmid/PCR product/mini prep DNA. 0.5µL each restriction endonuclease (1-2 units/sample), supplied by NEB, was used with the appropriate buffer, as detailed and supplied by the manufacturer. Buffers compatible with both enzymes in the case of double digests were typically available. Enzymes used in this thesis included EcoRI-HF® (NEB R3101), XhoI (NEB R0146), NotI-HF® (NEB R3189) BsmBI (NEB 0580).

2.1.8. DNA Ligation

Reactions were carried out at room temperature for at least 1 hour, or overnight at 4°C. An approximate 5:1 insert:vector DNA ratio was typically used in a 10µL total volume using 1µL 10X T4 DNA ligase buffer (NEB) and 0.5µL T4 DNA ligase. Vector only reactions (making up the volume with ddH_2O) were carried out side by side as an appropriate negative control. T4 ligase was heat inactivated at 65°C for 10 mins following ligation, and transformation of bacteria (Section 2.1.11).

2.1.9. Bacteria cells: media and maintenance

The *Escherichia Coli* strain DH10β genotype Genotype: F– mcrA Δ(mrr-hsdRMS-mcrBC) Φ80lacZΔM15 ΔlacX74 recA1 endA1 araD139 Δ(ara leu) 7697 galU galK rpsL nupG λ– was used for plasmid transformations. Autoclaved Luria Broth (LB) agar (37g/L) was used for solid phase growth medium, set in Sterilin 10cm Petri dishes. Autoclaved LB broth (25g/L) was used for liquid phase growth medium. When required, appropriate antibiotics for selection of transformed bacteria (Ampicillin (Fisher Scientific, 100µg/mL in ddH2O) or Kanamycin Sulphate (Fisher Scientific, 50µg/mL in ddH2O) were added to autoclaved media. In the case of agar, this was done prior to plating once autoclaved medium had cooled to around 50°C. A stock of DH10β cells was plated and grown on agar plates followed by storage at 4°C for no more than 2 months. Prior to competent cell preparation, bacteria were inoculated and grown in LB broth.

2.1.10. Generation of competent *E. coli* bacteria

A 10mL starter culture of DH10β cells inoculated from the stock plate was grown overnight at 37°C shaking at 200 rpm. The following day, the starter culture was diluted 1:40 in LB broth and further grown until log phase was reached (OD_{500nm} of 0.4-0.5). Cells were chilled on ice for 10 mins before pelleting by centrifugation at 300rpm, 10 mins, 4°C. Supernatant was discarded and cells were resuspended and incubated for a further 5 mins in 100mL pre-chilled filter sterilised TfB1 buffer (30mM KAc, 100mM RbCl, 10mM $CaCl_2$, 50mM $MnCl_2$ and 15% glycerol in ddH_2O). Cells were again centrifuged as previously and next resuspended and incubated in pre-chilled filter sterilised TfB2 buffer (10mM PIPES pH 6.5, 10mM RbCl, 75mM $CaCl_2$ and 15% glycerol in ddH_2O). 200µL aliquots were dispensed in 1.8mL Eppendorf tubes, snap frozen on dry ice and stored at -80°C.

2.1.11. Transformation of competent bacteria

100µL thawed competent bacteria were immediately incubated with 8µL completed DNA ligation reactions (Section 2.1.8.), or less than 100ng of other plasmid DNA for replenishment on ice for one hour. A heat shock of the bacteria at 42°C for 1 minute was then carried out, following which the bacteria were placed back on ice for 2 minutes. 250µL LB broth without antibiotic was added, and the bacteria were incubated at 37°C for 1 hour. Bacteria were then plated and spread on LB agar plates containing appropriate antibiotic using glass beads (Sigma), and grown upside-down overnight at 37°C, or 30°C in the case of retroviral constructs to minimise recombination.

2.1.12. Small scale plasmid DNA amplification and purification – Mini prep

Buffers for mini prep DNA purification were prepared and filtered in-house but based on the QIAGEN P1-P3 buffers.

Single bacterial colonies were picked and grown in 2mL LB broth + appropriate antibiotic overnight, shaking at 37/30°C. The following day, 1.5mL bacterial suspension was transferred to an Eppendorf tube, and the bacteria pelleted at 14,000rpm for 1 minute. Supernatant was discarded and the pellet resuspended in 100µL of chilled 50mM Tris-Cl

pH 8.0, 10mM EDTA and 100 µg/mL RNAse A (QIAGEN P1 resuspension buffer). An equal volume of 200mM NaOH, 1% SDS (w/v) (QIAGEN P2 lysis buffer) was added and the solution mixed by inverting the tube. The solution was incubated at room temperature for 5 mins. 100µL chilled 3M potassium acetate, pH 5.0 (QIAGEN P3 neutralisation buffer) was then added and the solution incubated for a further 10 mins on ice. The suspension was cleared of cell debris by centrifugation at 14,000rpm for 10 mins and the supernatant was transferred to a clean 1.8mL Eppendorf tube. DNA was precipitated by adding 300µL isopropanol to the solution, vortexing and incubating on ice for 10 mins followed by centrifugation at 14,000rpm 4°C for 10 mins to pellet DNA. The DNA pellet was then washed with 350µL 70% ethanol and left to air-dry for 5 mins before reconstitution in 30µL ddH_2O containing bovine ribonuclease A (1/200 dilution, Sigma). Successful cloning of constructs was confirmed by digesting mini prep DNA (Section 2.1.7.) and checking for the presence of correctly sized bands corresponding to inserts. In the case of sub-cloning previously cloned sequence between vectors, the remaining 0.5mL bacterial culture was inoculated in LB broth for further DNA amplification and midiprep purification (section 2.1.13.), whereas in the case of newly cloned constructs, DNA concentration was measured and a sample sent for sequencing (Section 2.1.15).

2.1.13. Medium scale plasmid DNA amplification and purification – Midi prep

Midi prep plasmid purification was performed using a Macherey Nagel NucleoBond® Xtra Midi Kit according to the manufacturer's instructions. This kit uses a silica-based anion-exchange resin to bind negatively charged DNA under low pH conditions. Following washing of bound DNA, to remove contaminants such as protein and RNA, the DNA is eluted under high salt, alkaline conditions to neutralise the positive charge of the resin.

100mL LB broth + appropriate antibiotic was inoculated with the remaining 0.5mL bacterial culture previously prepared for mini prep purification (Section 2.1.12), or a single bacterial colony, in the case of DNA stock replenishment, and grown at 37/30°C overnight at 200rpm. Bacteria were harvested in Nalgene 250mL bottles by centrifugation at 5000g for 10 mins and the supernatant discarded. 8mL of resuspension

buffer (buffer RES) was added and the pellet resuspended by vortexing and pipetting. Cells were lysed by adding 8mL of lysis buffer (buffer LYS) and gently inverting the tube 5 times, before incubating at room temperature for 5 mins. 8mL neutralisation buffer (buffer NEU) was added and the suspension was mixed by inverting until the blue colour disappeared. The entire suspension was then applied to a NucleoBond® Xtra Column filter that had previously been equilibrated with 12mL buffer EQU, and the column was allowed to empty by gravity flow whilst DNA bound to the resin. The filter was again washed with a further 5mL EQU buffer and then discarded from the column. The column was given one final wash with 8mL of buffer WASH before DNA was eluted by adding 5mL buffer ELU to the column and allowing solution to leave by gravity flow directly into a 50mL Falcon tub containing 3.5mL isopropanol for DNA precipitation. This solution was vortexed and then centrifuged at 15,000g for 30 mins at 4°C to pellet DNA. Supernatant was discarded and the pellet was washed in 2mL 70% ethanol before air-drying and reconstitution in typically 500µl ddH_2O. DNA yield was subsequently measured (Section 2.1.15), and was usually between 300-800ng/µL.

2.1.14. Genomic DNA extraction and purification from human cells

Genomic DNA extraction from HeLa/293T cell clones was required to obtain template DNA for PCR to confirm successful generation of homozygous CRISPR/Cas9 knockout clones (Section 3.2.5.). Extraction and purification was performed using a QIAGEN DNeasy® Blood & Tissue Kit (250) (cat. No. 69506) according to the mini Spin-Column protocol for cultured cells. Spin columns employ a similar silica-based resin that binds DNA under high salt conditions, whilst contaminants pass through. DNA is then eluted due to decreased salt concentration.

Cells were grown in wells of a 24-well plate until confluent. Medium was removed and cells were lysed in the well by addition of 200µL PBS + 200µL buffer AL + 20µL proteinase K and repeated pipetting. 200µL ethanol was added and the suspension was further resuspended by transferring to a 1.8mL Eppendorf tube and vortexing. The suspension was transferred to a spin column within a collection tube and centrifuged at 8000rpm for 1 minute. The collection tube with flow-through was discarded and the column placed in a clean collection tube. 500µL buffer AW1 was added and centrifugation and

discard of flow through was repeated as previously. The spin column was then washed with 500µL AW2 centrifuging at 14,000rpm for 3 mins. The flow-through and collection tube was discarded, and the spin column placed this time in a clean Eppendorf tube for elution. DNA was eluted by adding 200µL buffer AE to the centre of the spin column, incubating for 1 minute and centrifuging at 8000rpm for 1 minute. DNA concentration was subsequently measured (Section 2.1.15.).

2.1.15. Determination of DNA concentration and sequencing

DNA concentrations were determined using a Nanodrop ND-100 Spectrophotometer (Labtech International). Calibration was first performed using 1.5µL ddH_2O loaded onto the pedestal. The pedestal was then dried, and an equal volume of DNA solution loaded. Concentration was determined by measuring absorbance at 260nm, assuming that 1 OD_{260nm} = 50µg/µL dsDNA. Purity was gauged by the OD_{260}/OD_{280} ratio, which at around 1.8 is considered pure in the case of DNA.

Sequencing was performed by Eurofins MWG Operon or Genewiz. A minimum volume of 15µL of DNA was generally sent at 100ng/µL for plasmid DNA, 15ng/µL for PCR products <1000bp and 60ng/µL for PCR products >1000bp. 5µL for each additional reaction over 3 reactions was supplied. Primers were supplied at 10pmol/µL using 10µL/reaction, minimum volume of 15µL. Sequencing primers used are listed in Appendix 1.

2.1.16. mRNA extraction and purification from human cells

mRNA was extracted and purified from HeLa/293T cells to be used as template for the production of cDNA to be used for cloning new constructs or to check for successful production of CRISPR/Cas9 knockout clones (Section 3.2.5.). mRNA extraction was carried out using a QIAGEN RNeasy® Mini Kit (cat. No. 7410), using spin columns, according to the manufacturer's instructions. This kit again relies on the principle of binding nucleic acid under high salt conditions whilst impurities are washed away, but is optimised to bind mRNA by excluding RNA < 200 nucleotides in length (e.g. rRNA and tRNA). Furthermore, the lysis buffer contains highly denaturing guanidine-thiocyanate, which immediately inactivates RNases, ensuring reduced mRNA digestion. Given the

inherent instability of RNA, all steps were carried out in a laminar flow cabinet to ensure aseptic conditions, and reduced introduction of RNases from the environment.

Cells were grown to confluency in wells of a 24-well plate and lysed in the wells by addition of 350µL buffer RLT + 3.5µL β-mercaptoethanol and repeated pipetting. 350µL of 70% ethanol was added followed by continued pipetting. The entire suspension was transferred to an RNeasy mini spin column in a collection tube and centrifuged at 10,000g for 15s. the collection tube and flow-through was discarded, the column placed in a new collection tube and 700µL buffer RW1 was added. Centrifugation, discard of flow-through and replacement of the collection tube was repeated, and the column was washed as previously with 500µL buffer RPE first using a centrifugation time of 15s for a first wash and 2 minutes for a second wash. The column was placed in a clean collection tube and centrifuged at full speed for 1 minute to remove residual wash buffer and dry the resin. To elute RNA, the column was placed in a clean, sterile 1.8mL Eppendorf tube, 50µL RNase-free water was added and the tube was centrifuged for 1 minute at 10,000g.

RNA concentration was measured using a Nanodrop ND-100 Spectrophotometer by measuring absorbance at 260nm, assuming that 1 OD_{260nm} = 40µg/µL ssRNA. Purity was gauged by the OD_{260}/OD_{280} ratio, which at around 2.0 is considered pure in the case of ssRNA.

2.1.17. cDNA synthesis from purified RNA

cDNA synthesis was carried out using a High-Capacity cDNA Reverse Transcription Kit (Applied Biosystems™, Cat. No. 4368814) according to the manufacturer's instructions. In the case of cDNA production to use as template in PCR reactions to assess knockdown of a corresponding mRNA molecule by RNA interference, RNA sample concentrations were first adjusted to that of the sample with the lowest concentration. Reactions were prepared on ice.

10µL each RNA sample was mixed gently in a PCR tube with 10µL of 2X reverse transcription master mix, consisting of 2µL of 10X RT buffer, 0.8µL 25X dNTP mix (100mM), 10X RT random primers, 1µL MultiScribe™ reverse transcriptase and 4.2µL ddH2O. PCR tubes were placed in a thermocycler and incubated at 25°C for 10 mins,

37°C for 120 mins, 85°C for 5 mins and then held at 4°C until unloading. Completed reactions were ready for direct use in downstream PCR reactions.

2.1.18. Generation of CRISPR/Cas9 knockout cell clones

CRISPR/Cas9 knockout clones were generated by transient transfection of two lentiCRISPRv2GFP plasmids (Sanjana et al., 2014[660], Shalem et al., 2014[661], Walter et al., 2017[662]) to direct Cas9 endonuclease cleavage both upstream and downstream of the UMAD1 locus (Section 3.2.5.), thus removing the entire locus. This plasmid contains expression cassettes for a mammalian codon-optimised *Streptococcus pyogenes* Cas9 nuclease (hSpCas9) and a chimeric single guide RNA (sgRNA). The sgRNA consists of a custom-designed CRISPR RNA (crRNA), complementary to sequence at sites of cleavage, thus guiding the Cas9 endonuclease, together with sequence encoding appropriate trans-activating crRNA (tracrRNA), required for maturation of the crRNA and pairing with Cas9. Plasmids are designed for crRNA encoding DNA sequence to be ligated into the sgRNA scaffold cassette using BsmBI. A transient transfection approach rather than generation of cells that stably express the aforementioned components was adopted to prevent constitutive expression and potential off-target cleavage by Cas9.

crRNA sequences to be ligated into plasmids were designed using the Integrated DNA Technologies gRNA design tool at:

https://www.idtdna.com/site/order/designtool/index/CRISPR_CUSTOM

This tool identifies a selection of appropriate 20bp sequences to use as crRNA, upstream of *Streptococcus pyogenes* protospacer adjacent motif (PAM) sites i.e. NGG trinucleotides, together with off-target analysis. The 20bp sequences with the best off-target scores upstream and downstream of the UMAD1 locus (Section 3.2.5.) were selected and each ordered from Eurofins MWG Operon as two custom designed complementary oligonucleotides designed to anneal to each other and contain appropriate sticky ends (shown in red) for ligation into BsmBI digested lentiCRISPRv2GFP. Oligonucleotide sequences were as follows:

UMAD1 start guide:

UMAD1start forward:
CACCGTGTCGGCTGACATCTAGAGA

UMAD1start reverse:
AAACTCTCTAGATGTCAGCCGACAC

UMAD1 end guide:

UMAD1end forward:
CACCGACTGTTTAAGGTCCTCAGCA
UMAD1end reverse:
AAACTGCTGAGGACCTTAAACAGTC

Cloning was performed as suggested by Sanjana et al., 2014[660] with some modifications. 5µg lentiCRISPRv2GFP was digested and dephosphorylated in the same reaction with BsmBI (NEB) and Antarctic phosphatase (NEB), respectively, both compatible with NEB buffer 3.1. Successful digestion of plasmid was indicated by release of a 2kb stuffer fragment. Digested plasmid was gel purified. Each pair of oligos to encode crRNA were phosphorylated and annealed, using T4 Polynucleotide kinase (PNK) (NEB M0201S) and T4 ligase buffer. 1µL each oligo at 100µM was used in a 10µL total volume reaction using 0.5 µL T4 PNK. The reaction was incubated at 37°C for 30 mins, followed by 95°C for 5 mins, and then a gradually ramped down to room temperature by switching off the heat block and leaving samples to cool down. Annealed oligos were then diluted 1:200 in ddH_2O and ligated into 50ng previously digested lentiCRISPRv2GFP, as described in (Section 2.1.8.) using 1µL diluted oligos and T4 DNA ligase. A vector only negative control ligation was performed in parallel.

Following confirmation of successful cloning by mini prep and sequencing (Sections 2.1.12 and 2.1.15), and further amplification and purification of plasmids by midi prep (Section 2.1.13) HeLa/293T cells were transfected with both start and end guide plasmids in a well of a 6-well plate using Lipofectamine 3000 (Section 2.2.4.). Medium was changed 6 hours later and a further 12 hours later, the cells were trypsinised, washed in complete medium and resuspended in 500µL filtered fluorescence activated cell sorting (FACS) buffer (1X PBS + 1mM EDTA + 2% FCS). Single GFP expressing cells were in-house FACS sorted into wells of 2 × 96-well plates, and following growth, individual clones were checked for homozygous knockout, i.e. complete removal of all copies of the UMAD1 gene at genomic, mRNA and protein levels (Section 3.2.5.).

2.2. Human cell culture and nucleic acid transfection

2.2.1. Cell lines

HeLa cells, derived from human epithelial cervical adenocarcinoma cells, were obtained from the American Tissue Culture Collection (ATCC). HEK293T Human Embryonic Kidney cells (293Ts) were kindly gifted from Professor Stuart Neil (King's College London, UK), initially obtained from the ATCC. These are 293 cells, modified to express the SV40 T antigen to promote increased replication of plasmids containing the SV40 origin of replication. HeLa TZM-bl reporter cells were kindly gifted from Professor Paul Bieniasz. These are HeLa cells adapted to express the CD4+, CXCR4+, CCR5+ HIV-1 receptors together with HIV-1 LTR-Lac Z for infectious virus release readout (Derdeyn et al., 2000[663]).

2.2.2. Cell maintenance

All work involving cell culture was performed in a laminar flow cabinet, to ensure aseptic conditions, and all plastic consumables for cell culture were purchased from Corning Incorporated. Cell lines were grown in 10cm dishes at 37°C, 5% CO_2 in a humidified atmosphere in Dulbecco's Modified Eagle Medium (DMEM) +4.5g/L Glucose, +L-Glutamine, +Pyruvate (GIBCO 41966, Invitrogen) supplemented with 10% heat inactivated (56°C, 30 mins) Foetal calf serum (FCS) (GIBCO, Invitrogen) and 20µg/mL gentamycin (GIBCO, Invitrogen), i.e. complete medium. Cells were split every two days by aspiration of medium from the dish, followed by addition of 2mL pre-warmed 1x Trypsin substitute (TrypLE™ Express + Phenol red) (GIBCO 126050, Invitrogen). Following 1 – 5 minutes trypsinisation at 37°C, cells were resuspended by repeated pipetting, after which an appropriate volume of cell suspension was transferred to a new dish containing 10mL pre-warmed fresh medium.

2.2.3. Cell Freezing and thawing

At around 60 – 70% confluency, cells were trypsinised and washed in 15mL complete medium, following which cells were pelleted by centrifugation at 1000rpm for 10 mins at room temperature. Medium was aspirated, following which cells were resuspended

in 1mL of cryoprotective medium consisting of FCS + 10% DMSO (Sigma-Aldrich 276855). Cell suspension was then transferred to a 1.8mL cryovial and cooled slowly to -80°C for at least 48 hours before transfer to liquid nitrogen for long-term storage.

Cells were revived by rapid thawing at 37°C upon removal from liquid nitrogen. Cells were then washed to remove DMSO by gently transferring to 15mL complete medium followed by centrifugation at 1000rpm for 10 mins at room temperature. Medium was aspirated, and cells resuspended in 10mL fresh medium. Cell suspension was then transferred to a clean 10cm dish and were not used for any experimental work until confluency was reached.

2.2.4. Transient transfection of DNA

293T cells were transfected using Polyethylenimine (PEI) (Polysciences), whilst HeLa cells were transfected with Lipofectamine 3000 (Invitrogen) in the case of DNA only transfections. Lipofectamine 2000 (Invitrogen) was used to simultaneously transfect DNA and RNA together, in HeLa or 293T cells (Section 2.5.5.). Transfections were generally performed in wells of a 24-well plate using 1µg plasmid DNA, unless otherwise stated. Cells were seeded the evening before, to generally reach >60% confluency by the following day.

For PEI transfection, 1µg DNA was incubated with 4µg PEI in 50µL serum-free DMEM, for 10 mins before adding dropwise to the 293T cells, in fresh medium (300µl). Cells were incubated for between 6-12 hrs with the DNA+PEI after which the medium was again changed, and the cells left to grow for another 24 hrs.

For Lipofectamine 3000 transfection, 1µg DNA was incubated with 2µL p3000 reagent in 25µL optimem (GIBCO 31985, Invitrogen) for 5 minutes whilst 1.5µL Lipofectamine 3000 was incubated with optimem in a separate Eppendorf tube for 5 minutes. Both solutions were then combined and gently mixed, following which the solution was incubated at room temperature for 20 mins and then added dropwise to the HeLa cells in fresh medium. Amounts of DNA and transfection reagents were scaled-up accordingly in the case of transfecting a larger number of cells.

2.2.5. Transient transfection of siRNA

Both HeLa and 293T cells were transfected with siRNA using Dharmafect1 (Dharmacon). siRNA oligonucleotides were ordered from either Dharmacon or QIAGEN at 2nmol/tube, 5nmol/tube or 50nmol/tube and resuspended with either ddH_2O (QIAGEN) or 1X siRNA resuspension buffer (Dharmafect), to a final concentration of either 20µM or 75µM. siRNA was aliquoted into 20µL aliquots and stored at -80°C until use. A list of all siRNA oligonucleotides used in this thesis is presented in Appendix 1.

All siRNA transfections were performed in wells of a 24-well plate, using a reverse transfection procedure, according to the manufacturer's instructions, using 50pmol siRNA per well. 50pmol siRNA was incubated with 50µL optimem for 5 mins. 1µL Dharmafect was likewise incubated with 50µL optimem in a separate tube. Both solutions were then combined and incubated for a further 20 mins, following which they were mixed gently with 6×10^4 cells and added to the well in a total volume of 400µL complete medium. Medium was changed at least 12 hrs later. If a second siRNA transfection was required to ensure maximum silencing of gene expression, the cells were trypsinised 24 hrs after the first dose and an appropriate volume re-seeded and transfected as previously at least another 12 hours following re-seeding.

Lipofectamine 2000 was used to transfect plasmid DNA and siRNA simultaneously. In such cases, cells were seeded >12 hrs prior to transfection. The transfection procedure, volumes and amounts of reagents was exactly as for Dharmafect, except DNA and RNA were incubated together, and solution was added dropwise to the pre-seeded cells. Due to greater toxicity of Lipofectamine 2000, it was also necessary to change medium no later than 8 hours following transfection. 150ng DNA was co-transfected with the 50pmol siRNA.

2.2.6. Generation of stable cell lines

Stable cell lines were generated using the retroviral packaging vectors pCMS28 and pNG72 encoding the gene of interest. 293T cells were seeded in wells of a 12-well plate and PEI transfected (Section 2.2.4.) >12 hrs later with 1µg retroviral packaging construct, 700ng MLV Gag-pol and 300ng pHIT-VSV-G. Medium was changed 12 hrs later, and

HeLa/293T cells to be transduced were seeded in wells of a separate 6-well plate, using two wells/construct plus at least one well of cells to use as an non-transduced control. 48 hrs post transfection, supernatant from the 293T producer cells was harvested and filtered using 0.22µm Millex PVDF sterile filters (Millipore). 700µL supernatant was used to transduce the previously seeded HeLa/293T cells after medium was changed, replacing with fresh complete medium and Polybrene reagent (Millipore) at 1:1000 dilution, to enhance transduction efficiency. Medium was changed again 48 hrs after transduction, and appropriate antibiotic for selection of transduced cells was added, i.e. 200ng/mL of puromycin dihydrochloride (Sigma) for pCMS28 or 500 µg/mL of G418 (Geneticin, Invitrogen) for pNG72. Stocks of 5mg/mL puromycin and 50mg/mL G418 dissolved in ddH2O were stored at -20°C Once 100% cell death in the non-transduced control wells was attained, successfully transduced stable cell lines were expanded and frozen/used for experiments whilst passaged under continual antibiotic selection.

2.3. Protein-protein interaction assays

2.3.1. Glutathione-S-transferase co-precipitation assay (GST "pull-down" assay)

Initial co-precipitation assays to investigate protein-protein interactions using overexpressed tagged fusion proteins were performed using a GST pull-down approach. 293T cells in wells of a 6-well plate were PEI transfected with 2µg each pCAGGS-GST/pCR3.1 plasmid encoding alternatively tagged ESCRT proteins (Section 2.2.4.). Medium was changed ≥6 hrs later and cells were washed with 1X PBS and lysed in the well, 48 hrs post-transfection in pre-chilled lysis buffer (50 mM Tris-HCl, pH 7.4, 150mM NaCl, 5mM EDTA, 5% Glycerol, 1% Triton X100 and protease inhibitors (Roche)), using 1mL lysis buffer per well. Lysates were transferred to 1.8mL Eppendorf tubes and incubated at 4°C on a rotating wheel for 15 mins. Lysates were then clarified by centrifugation at 14,000rpm for 10 mins at 4°C and supernatants were transferred to clean Eppendorf tubes. 100µL supernatants were added to 20µL 6X protein loading buffer (Laemmli buffer) (0.5M Tris-Cl, 0.4% SDS pH 6.8, 30% glycerol, 0.11g/mL SDS, 60µl/mL 2-Mercaptoethanol, 0.12mg/mL Bromopheonol blue) to achieve a 1X final concentration of loading buffer. These samples were boiled and kept as input samples

to examine protein expression levels prior to co-precipitation. The remaining 900µL lysates were each added to 25µL Glutathione-Sepharose beads (GE Healthcare Life Sciences), that had previously been washed three times in wash buffer (50 mM Tris-HCl, pH 7.4, 150mM NaCl, 5mM EDTA, 5% Glycerol, 0.1% Triton X100) and resuspended in a final 100µL wash buffer. Samples were incubated for 3 hrs at 4°C on a rotating wheel. Beads were then washed another three times with 1mL wash buffer, and bound protein was finally eluted from beads by boiling each sample in 100µL 2X protein loading buffer for 10 mins. Input and pull-down samples were analysed by immunoblotting (Section 2.4.2.) using antibodies appropriate for each tag.

2.3.2. GFP-trap immunoprecipitation assay

To examine interactions of a tagged stably expressed exogenous protein with endogenously expressed cellular proteins, a GFP-trap based co-immunoprecipitation approach was employed. The principle is similar to GST pull-down assays but uses magnetic agarose beads coated with GFP specific nanobodies to trap and immunoprecipitate GFP (or YFP) tagged bait proteins together with binding partners. Lysis and wash buffer compositions were exactly as described for GST pull-down assays (Section 2.3.1.).

Following generation of cell lines that stably expressed each YFP-tagged bait protein (Section 2.2.6.) , each cell line was grown to confluency in a 15cm dish, following which cells were trypsinised and washed three times in 15mL Falcon tubes with 6mL of 1X PBS, centrifuging to pellet the cells between each wash at 1000rpm for 10 mins. Cells were then lysed in 3.6mL lysis buffer for 15 mins at 4°C on a rotating wheel and sonicated for 10s using a Branson Sonifier 250 (microtip). Lysates were clarified by centrifugation at maximum speed, 4°C for 15 minutes, following which lysates were transferred to clean 15mL Falcon tubes. Input samples were taken and added to protein loading buffer (exactly as for GST pull-down assay) and the remaining lysates were incubated overnight on a rotating wheel at 4°C with 35µL washed GFP-trap® Magnetic Agarose beads (Chromotek) (previously washed three times using a magnetic rack to pellet beads in between washes, rather than centrifugation). Following overnight incubation, beads

were washed three times for 10 mins at 4°C following which protein was eluted from the beads by boiling in 35µL 2X protein loading buffer.

In the case of immunoprecipitations for analysis by mass spectrometry, 2×15cm dishes of cells per bait protein were used and volumes of buffers and beads were scaled up accordingly (70µL beads and 70µL final elution volume). Input samples were not taken. All solutions were filtered prior to use and all steps of the protocol, except sonication, were performed in a laminar flow cabinet. A clean lab coat, plastic sleeves, mask and hairnet were worn. Sterile filter tips were used for pipetting and eluted protein samples were transferred to sterile screw cap 1.8mL Eppendorf tubes. All equipment was sprayed with 70% ethanol before use.

2.4. Protein detection and quantification

2.4.1. Sodium dodecyl sulphate polyacrylamide gel electrophoresis (SDS-PAGE)

Protein sample mixtures i.e. cell lysates and co-precipitation experiment eluates, were resolved according to size on 8%, 10% or 12% SDS-PAGE resolving gels, obtained by altering the 40% Acrylamide (Bis-Acrylamide 29:1, (Fisher Scientific)) : ddH_2O ratio in a polymerisation reaction containing 1.5M Tris-Cl/ 0.4% SDS pH 8.8, 3.3µL/mL 10% ammonium persulphate (APS) (Sigma) and 0.6µL/mL N,N,N'N'-tetramethylethylenediamine (TEMED) (Sigma). A 5% stacking gel made using 0.5M Tris-Cl/ 0.4% SDS pH6.8, 5µL/mL 10% APS, 1µL/mL TEMED was polymerised on top of resolving gels with appropriately sized wells for loading protein samples. Gels were immersed in running buffer (25mM Tris, 192mM Glycine, 0.1% SDS, pH 8.3) in a compatible running tank before loading protein samples.

All protein samples were boiled for 10 mins in protein loading buffer (Section 2.3.1.), and 10µL was generally loaded into wells of the stacking gel. 1X protein loading buffer was also used to directly lyse cells and release and denature proteins in cases where direct analysis of expressed protein levels was required. The negatively charged SDS in the protein lysis buffer ensures that proteins have a constant mass/charge ratio and therefore migrate according to size. Gels were run at 120V for 90 mins, or until the dye front had reached the bottom of the gel. All SDS-PAGE apparatus was supplied by Biorad.

The protean II mini gel electrophoresis kit and Precision Plus Protein™ Dual Colour Standard molecular weight protein marker was used.

2.4.2. Immunoblotting, protein detection and quantification

Following SDS-PAGE, protein was blotted onto 0.45µm nitrocellulose membrane (VWR International) using a BioRad Mini Trans-Blot® or Criterion® blotter transfer system, at 18V overnight in transfer buffer (1X Tris-HCl pH 7.4 + 20% Methanol). Following transfer, gels were discarded and blocking of the nitrocellulose membrane was carried out for 1 hour by incubating in 1% skimmed milk dissolved in wash buffer (50mM Tris-HCl pH 7.4, 150mM sodium chloride and 0.1% Tween-20 (Fisher Scientific)). Nitrocellulose membranes were then incubated with the appropriate primary antibody and dilution in 1% skimmed milk (see Appendix 1 for a list of all antibodies and dilutions used in this thesis). Membranes were next given 3×5 min washes in wash buffer, following which they were incubated for 45-60 mins in the appropriate secondary antibody diluted in 1% skimmed milk. Fluorophore conjugated secondary antibody incubations were protected from light using aluminium foil. Membranes were finally given another 3×5 min washes before imaging according to the detection method specific to the secondary antibody conjugation.

Fluorescence using an anti-rabbit Infrared IRDye®-conjugated 800nm antibody (LI-COR) was the method of choice used to detect and quantify ALIX depletion in experiments to measure cytokinetic defects/abscission time (Chapter 4), to avoid exponential amplification of signal over time, as seen with enhanced chemiluminescence (ECL). HSP90 signal could also be detected on the same membrane, to ensure better accuracy of quantification, using an anti-mouse Infrared IRDye®-conjugated 680nm secondary antibody (LI-COR). ECL using horseradish peroxidase (HRP) conjugated secondary antibodies was the method of choice for detection of proteins in all other situations, except in instances where detection of many proteins from one sample was facilitated by being able to image more than one protein on the same membrane by combining ECL with fluorescence detection. Amersham ECL™ Primer western blotting detection reagent (GE Healthcare) was used for ECL detection, by mixing equal volumes of reagent A and B and applying to the membrane, which was then sandwiched between two

transparent plastic sheets and promptly imaged, ensuring that the reagent was distributed evenly across the membrane surface. Imaging was performed using a LI-COR Odyssey® Fc Imaging system (LI-COR Biosciences).

Quantification of protein band intensities was performed using the square measuring tool in Image Studio Lite version 5.2.

2.5. Functional assays and microscopy

2.5.1. Clonogenic assays to examine cell viability

80,000 cells per condition were plated and reverse transfected in wells of a 24-well plate with 50pmol of each siRNA oligo as described in section 2.2.5. Medium was changed ≥ 12 hrs later. 48 hrs following transfection, cells in each well were trypsinised and thoroughly resuspended in 200µL trypsin and an equal volume of complete medium. 10µL of cell suspension was transferred to wells of a 6-well plate, in 3mL complete medium and again mixed thoroughly by repeated pipetting. Cells were left to grow for 10 days, following which medium was discarded and colonies were fixed and stained by adding enough crystal violet stain (0.5% w/v in methanol) to cover the base of each well and incubating for 1 hour at room temperature. Crystal violet was then washed away with tap water and plates were left to dry upside-down at room temperature. Following imaging of plates using a Chemi-Doc imaging system (BioRad), area occupied by colonies on the base of each well was scored using ImageJ. A constant area of the base of wells for each condition was selected and cropped using the square cropping tool. This area was then converted to an 8-bit greyscale image and the thresholding to remove background, i.e. the sides of the dishes that appeared in the image, was performed. A threshold value that was suitable for all wells was selected. The remaining colonies in the image were then selected and their area measured.

2.5.2. Fixation, immunostaining and imaging of cells

Following growth of cells on glass coverslips, cells were fixed to crosslink proteins using 500µL of 4% paraformaldehyde (PFA) (Sigma) in 1X PBS, for 10 mins at room temperature. Coverslips were subsequently washed three times with 1X PBS, and cells

were permeabilised with chilled 0.1% Triton X-100 in 1X PBS for 10 mins. Cells were washed three times, as previously, and then blocking was performed using 3% w/v bovine serum albumin (BSA) in 1X PBS at room temperature for 1 hour. Cells were then incubated with the appropriate primary antibody (i.e. mouse anti-Tubulin) diluted in 50µL 3% BSA for 3 hrs, by placing coverslips face down in a 50µL drop of the antibody solution on a parafilm sheet kept in a wet chamber to prevent drying. Coverslips were returned to wells of the 24-well plate and washed as previously. Coverslips were then incubated for 1 hour with appropriate fluorophore conjugated secondary antibody (594λ- anti-mouse secondary antibody) and a 1:10,000 dilution of Hoechst chromatin stain (VWR International) and then washed, in the same way as for the primary antibody. Coverslips were mounted face down on microscope slides (VWR International) using an 8µL drop of Prolong® mountant (ThermoFisher), ensuring not to introduce air bubbles into the mountant. Slides were left to dry overnight in the dark at room temperature, and the back of coverslips was cleaned with 70% ethanol prior to microscopy.

Imaging was performed with a Nikon Ti-Eclipse Widefield inverted microscope (Nikon, 60x or 100x 0.75 N.A. oil objective lens) and acquired with a CoolSnap HQ2 CCD camera (Photometrics) controlled by NIS-Elements (Nikon). Images were acquired using excitation and emission filters specific to mCherry, YFP and Hoechst as a series of 0.15µm spaced Z-stacks and deconvolved with AutoQuant X3 Deconvolution software (MediaCybernetics). ImageJ (Fiji) was used to produce maximum intensity projections of images. Images from figure 45A were obtained using an Eclipse Ti-E Inverted CSU-X1 Spinning Disk Confocal (Nikon) equipped with an Ixon3 EM-CCD camera (Andor). Images were acquired in a series of 0.1 µm-spaced Z-stacks with a 100x objective.

2.5.3. Live cell imaging

HeLa cells were plated and reverse siRNA transfected as detailed in section 2.2.5. in wells of a 24-well glass bottom imaging plate (Eppendorf), pre-treated with poly-L-Lysine (Sigma) for 20 mins at 37°C. Medium was changed 12 hrs later and cells were imaged for 24 hours every 10 mins using 12 fields of view for each condition and 3 × 0.6µm Z-stacks. Imaging was acquired using a Nikon Ti-Eclipse Widefield inverted microscope (Nikon, 40X 0.75 N.A. dry objective lens) controlled by NIS-Elements and equipped with

a perfect focus system and 37°C microscope chamber (Solent Scientific) supplied with 5% CO_2. The excitation and emission filter for mCherry was used and abscission times were scored manually by frame to frame analysis using NIS-Elements. Abscission time was taken as the time interval between midbody appearance to midbody scission.

2.5.4. Multi-nucleation/midbody scoring assay

HeLa cells were transfected with 2×50pmol siRNA doses as detailed in section 2.2.5. in the case of assays to score cytokinetic defects upon MVB12/VPS37 protein depletion. One dose using amounts of siRNA as detailed in chapter 4 was used in the case of ALIX depletion. 24 hrs post-transfection of the second dose of siRNA (or single dose in the case of ALIX depletion), cells were trypsinised and a volume appropriate for achieving around 40% confluency after 24 hrs was transferred to fresh medium in wells of a new 24-well plate with glass coverslips placed at the base of wells. Another volume of cell suspension, kept the same for all conditions, was re-seeded in wells without coverslips for later immunoblotting to check protein depletion. 24 hrs later, the cells plated on coverslips were fixed, stained with anti-Tubulin and Hoechst (as detailed in section 2.5.2.), to visualise midbodies and the cell cytoskeleton, and mounted on slides for microscopy. Cells that were not plated on coverslips were lysed in the wells with 1X protein loading buffer (Section 2.3.1.), boiled and subsequently analysed by immunoblotting.

Cells were visualised using a Nikon Ti-Eclipse Widefield inverted microscope (Nikon, 60x 0.75 N.A. oil objective lens), using excitation and emission filters specific to the 594λ-anti-mouse secondary antibody and Hoechst. Cells with more than one nucleus and intercellular bridge (midbody) connected cells were scored blind for each condition. 300 cells/condition were scored. Midbody connected cells were considered one cell, rather than two daughter cells.

2.5.5. HIV-1 infectivity assays

For viral trans-complementation assays (section 3.2.2.) 293T cells were PEI transfected in wells of a 24-well plate (Section 2.2.4.) with 300ng full-length pHxB-STOP proviral construct (section 2.1.2) and 200ng pHxB- trans-complementing plasmids (section

2.1.2/3.2.2.). Cells were immediately moved to a CL3 (Biosafety level 3) facility. Medium was changed ≥7 hrs later. 48 hrs post-transfection, viral supernatants were clarified by centrifugation at 1500 rpm for 10 minutes, and 200µL was used to infect previously seeded TZM-bl reporter cells at between 40-60% confluency in wells of a 48-well plate. In addition to overexpressing the appropriate HIV-1 receptor and co-receptors, TZM-bl cells express β-galactosidase, under the control of an HIV-1 LTR which is responsive to the HIV-1 tat protein, provided upon infection with virus. Remaining viral supernatant was transferred to screw cap 1.8 mL Eppendorf tubes and frozen at -80°C for pelleting virus later. The 293T producer cells were lysed in 200µL of 1X protein loading buffer and boiled. Immunoblotting (Section 2.4.2.) to detect cellular HIV-1 Gag levels was performed using a 12% polyacrylamide gel and anti-p24 HIV-1 Gag (183-H12-5C). TZM-bl cells were lysed 48 hrs post-infection in 100µL Applied Systems Tropix GalactoStar kit lysis buffer. Lysates were clarified by centrifugation at 12,000rpm for 10 mins and 200µL of lysates were added to wells of a white 98-well imaging plate (PerkinElmer). Infectious virus release readout using a Wallac Victor 1420 workstation counter to measure chemiluminescence was employed, following addition of 50µL substrate mix to each well (1µL Galacton-Star® substrate + 49µL provided reaction buffer diluent). Measurements were taken 2 mins, 5 mins and 10 mins following addition of substrate, choosing the time which gave values of between 10^5 – 10^6. 300µL of remaining viral supernatant, frozen earlier, was pipetted on top of a cushion of filtered 20% sucrose in PBS, in a screw cap Eppendorf tube. The tube was marked, to facilitate location of the invisible viral pellet following centrifugation, and centrifuged at maximum speed for 3 hrs at 4°C. The sucrose cushion was aspirated away at the side of the tube opposite the viral pellet, leaving around 10-15µL at the base of the tube, with the pellet. Virions were vortexed and lysed thoroughly in 75µL of 2X protein loading buffer and transferred to regular 1.8mL Eppendorf tubes, before leaving the CL3 facility, to facilitate boiling prior to SDS-PAGE and immunoblotting. As for lysates, budded virion samples were resolved on a 12% gel and detection using the same anti-p24 HIV-1 Gag (183-H12-5C) primary antibody was carried out.

For experiments to investigate the effect of UMAD1 knockout on HIV-1 budding, using CRISPR/Cas9 UMAD1 knockout cells (Chapter 5), 293T cells were given two 50pmol siRNA doses (siNT or siTSG101 controls), the first using Dharmafect and the second using

Lipofectamine 2000 to transfect siRNA simultaneously with 150ng proviral constructs (pNL-HxB, R9, and R9ΔYPXnL) . Since two 50pmol doses of siTSG101 is toxic to HeLa cells, experiments using HeLa cells were later performed with one 50pmol siRNA dose co-transfected with 150ng pNL-HxB (Section 5.2.2.). All other steps for performing a TZM-bl assay and immunoblotting were as described above, except TZM-bl cells were infected with 10µl viral supernatant from 293T producer cells, or 50µL supernatant from HeLa producer cells.

2.5.6. Immunoprecipitation – Tandem Mass Tag (IP-TMT) based Mass Spectrometry

Eluates from GFP-trap immunoprecipitation experiments were taken to the King's College London proteomics facility, Centre of Excellence for Mass Spectrometry at the James Black Centre, Denmark Hill, where samples were prepared for multiplex TMT analysis and analysed by Dr Xiaoping Yang and Dr Steven Lynham.

30µL of each sample, corresponding to approximately 57µg protein, was run around 1cm into a commercially available 10% polyacrylamide gel, following which staining with Imperial protein stain (Thermo Fisher Scientific) was performed. Background was removed by destaining, and gel slices containing all the protein in each sample were excised. The proteomics facility in-gel trypsin digestion and isobaric tag labelling protocol was then followed, to generate tryptic signature peptides to be used for protein identification. This involved reduction of cysteine residues with dithiothreitol and alkylation with iodoacetamide to form stable carbamidomethyl derivatives. Trypsin digestion was then carried out overnight, followed by isobaric mass tag labelling of each sample with a different TMT tag (Thermo Fisher Scientific). TMT tags all have the same structure and molecular weight, consisting of a mass reporter and mass normaliser region, separated by a cleavable linker, and an amine reactive group which reacts with the N-termini and lysine residues within peptides thus labelling them. Alternative positioning of ^{13}C and ^{15}N atoms within the mass reporter and mass normaliser regions, however, ensures that the mass reporter ions released during fragmentation of peptides at the MS2 stage each have different masses. Sample specific information regarding differences in protein abundancies between samples can be inferred from these

different reporter ion masses. Labelled samples were pooled and desalted using C18 reversed-phase Zip-Tips (Millipore), before being subjected to LC-MS/MS tandem mass spectrometry.

Peptides were resolved by reversed phase chromatography on a C18 column using an Ultimate 3000 NanoLC system (Thermo Fisher Scientific). Eluate was then ionised by electrospray ionisation using an Orbitrap Fusion Lumos (Thermo Fisher Scientific) operating under Xcalibur v4.1. acquisition using a "Synchronous Precursor Selection with MultinotchMS3" method (SPS) was employed. Synchronous Precursor Selection is a process of selecting multiple MS2 precursors using a single fill and single waveform in a CID or HCD cell, while MultinotchMS3 is to reduce co-isolated interference from MS2 in an ion-trap cell. This method allows for accurate and sensitive quantitation based on isobaric TMT tags.

Raw mass spectrometry data were processed into peak list files using Proteome Discoverer v2.2 (Thermo Fisher Scientific) (PD 2.2) Processed data was then searched using Mascot search algorithm and Sequest search engine embedded in PD 2.2, against the current version of the reviewed Swissprot Homo Sapiens (Human) database downloaded from Uniprot. Data analysis and generation of figures was performed using Perseus (Tyanova et al. 2016[664])

Chapter 3 – Biochemical characterisation of UMAD1

3.1. Introduction

Although a structure for the core of human ESCRT-I has not been solved, mammalian ESCRT-I, as in yeast, is approximately 350 kDa and shows strong conservation with yeast ESCRT-I in terms of its subunit organisation and function. In mammals there has been an expansion in the number of available subunits to form the heterotetramer, to include alternative VPS37 and MVB12 paralogues, and two isoforms of VPS28. The mammalian homologue of yeast Vps23 is TSG101, and the two mammalian isoforms of VPS28 are termed VPS28 I and II. Mammals have so far been shown to express four VPS37 paralogues, being VPS37A-D, and three MVB12-like proteins, being MVB12A, MVB12B and UBAP1.

TSG101, like yeast Vps23, represents the central lynchpin-like subunit of ESCRT-I which interacts with all of the other subunits. As in yeast ESCRT-I, TSG101 shows independent interaction with VPS28, at its C-terminal helical headpiece region[51,53,565,665], and VPS37 subunits, at a more upstream predicted coiled-coil/leucine zipper region (Figure 22)[657,665–667]. Also consistent with the structure of yeast ESCRT-I is the finding that TSG101-VPS37 dimers provide the minimal binding surface required for MVB12-like subunits[657,665–667]. Like Vps23, human TSG101 also contains a UEV domain at its N-terminus, which in addition to binding ubiquitin[13,76] and ESCRT-0[44,45,47] binds to PT(S)AP L-domain motifs of retroviral Gag proteins, ALIX, HD-PTP and a double PTAP-PSAP motif in TSG101-associated ligase (Tal) – a RING E3 ubiquitin ligase involved in control of cellular TSG101 levels (Figure 22)[17,442,566,668,669].

3.1.1. TSG101

TSG101 was originally identified in a screen for genes for which homozygous depletion led to metastatic cell growth, hence the name tumour susceptibility gene 101[635]. Whilst knockout led to tumorigenesis, its overexpression also led to transformation and perturbed cell cycling in mouse NIH3T3 fibroblasts, suggesting that precise control of its

expression is required for a normal cell cycle and growth. In addition to its sequence conservation with yeast Vps23 (52% sequence similarity), TSG101 was later characterised as the mammalian homologue of Vps23 based on its requirement for efficient lysosomal sorting[51,670,671], its association with dominant negative VPS4 induced endosomal vacuoles[53] and its ability to rescue L-domain defective viral budding when fused to HIV-1 Gag[14,565]. Specifically, a region from 250-390, encompassing the majority of the stalk and headpiece, was largely sufficient to mediate budding, indicating that binding to all other ESCRT-I subunits is important for function[14].

Consistent with potentially tight levels of control of TSG101 expression was the finding that the level of TSG101 expression is tightly controlled at a post-translational level by an intrinsic 'steadiness box', mapped to its C-terminal 43 amino acids (Figure 22)[669,672]. Increased expression of exogenous TSG101 causes decreased expression of the endogenous protein in an attempt to maintain steady state levels of expression[672]. Further work by McDonald and Martin-Serrano 2008 showed that Tal ligase is recruited to the UEV domain of TSG101 but specifically ubiquitinates lysine residues within and around the steadiness box, thus targeting excess uncomplexed TSG101 for proteasomal degradation[669]. Since the VPS28 binding site overlaps the steadiness box, these lysine residues are occluded when TSG101 is in complex with VPS28, thus preventing ubiquitination and degradation of TSG101. In this way, VPS28 is a limiting factor for cellular levels of TSG101, hence ESCRT-I. In addition to regulation of TSG101 levels by this mechanism, ESCRT-I subunits show mutual dependence on each other for stability: a decrease in the levels of VPS28 and VPS37 paralogues is seen upon depletion of TSG101[666].

In addition to the other ESCRT-I subunits, TSG101 has been shown to bind a number of other proteins, notably CEP55 and other proteins involved in cytokinesis (Section 1.5.6.). The structure of the N-terminal UEV domain of TSG101 has been solved both in isolation and in complex with the PTAP motif of HIV-1 p6[75,76,673]. Like yeast Vps23 (Section 1.3.2.), a characteristic β-hairpin "tongue" consisting of two β-strands represents the most important site for mediating interaction with ubiquitin. Residues closer to the vestigial active site within a hydrophobic sheet are also involved in interaction with ubiquitin, as in yeast[73,76]. PT/SAP motif binding occurs independently at a different site within a groove at the other side of the vestigial active site loop, and binding causes the UEV

domain to wrap around the peptide involving more pronounced conformational changes[75]. One potentially significant difference with the yeast Vps23 UEV domain is the presence of a six-residue insertion within the N-terminal side of the vestigial active site loop. This has been suggested to explain the difference in binding of the yeast protein to PXXP motifs and that of mammals to related but similar PT/SAP motifs[73]. TSG101 contains an internal PTAP motif within a loop upstream of its coiled-coil/leucine zipper motif (Figure 22)[76]. Interaction between this motif with the UEV domain has been suggested to possibly form an "auto-inhibited" conformation of TSG101, preventing interaction with other PTAP motif containing proteins such as HRS until required[76]. In addition to interactions with the PT/SAP motifs of ESCRT-0, Tal ligase and viral structural proteins, TSG101 has been shown interact with ALIX via both a ^{717}PSAP^{720} and ^{852}PSYP^{855} motif in ALIX[55]. This ALIX-TSG101 interaction has been suggested to be necessary in cytokinetic abscission (Section 4.1.). Interaction with ALIX has also been shown to occur via ALG-2 – a calcium binding dimeric protein, each monomer of which interacts with TSG101 or ALIX (sections 1.8.2. and 4.1.)[674–676]. Likewise, HD-PTP interacts with TSG101 via a ^{720}PTAP^{723} motif, during the proposed shuttling between ESCRT-0, ESCRT-I and ESCRT-III (Section 1.3.5.3.)[668].

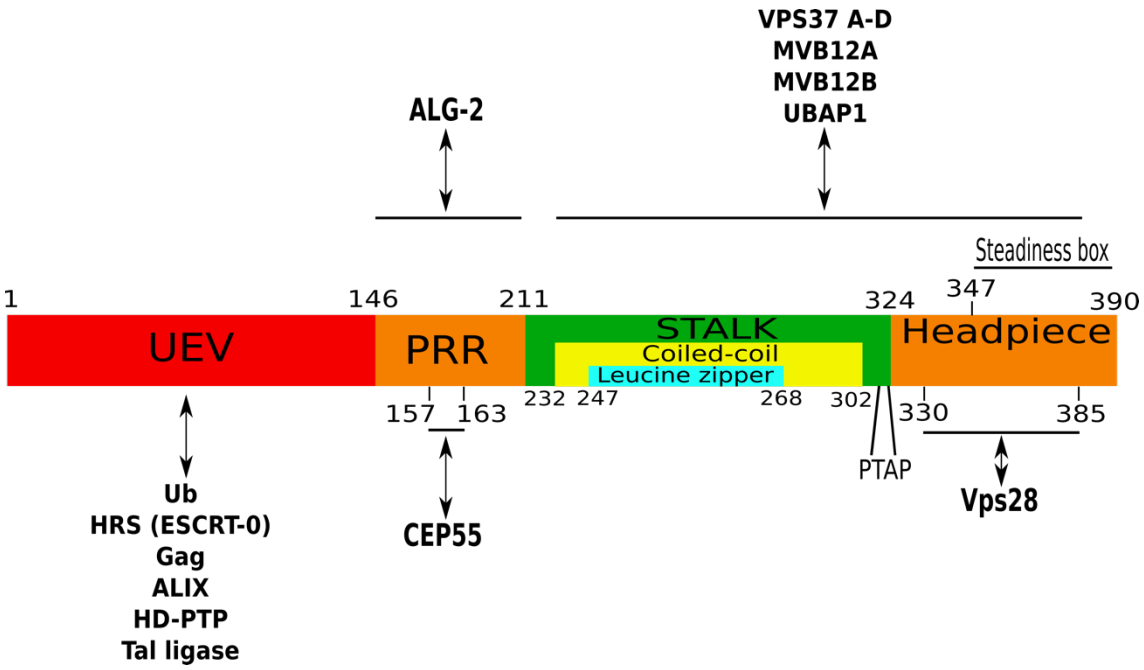

Figure 22. Domain structure of TSG101 and main binding partner interaction sites
The overall structure of TSG101 is well conserved with that of yeast orthologue Vps23. An N-terminal UEV domain is primarily responsible for mediating interaction with ubiquitin and PT/SAP motif containing proteins, such as HRS and viral Gag proteins, as shown. A downstream PRR mediates interaction with CEP55, the adaptor protein for cytokinetic abscission. As in yeast Vps23, the stalk and headpiece regions mediate interaction with the other ESCRT-I subunits. As described in the text, the steadiness box represents an intrinsic mechanism for control of cellular TSG101 levels. An internal PTAP motif upstream of the coiled-coil/leucine zipper region of the stalk has been suggested to mediate auto-inhibition of TSG101, by interacting with the UEV domain, until binding to other PT/SAP motif containing proteins is required. UEV = Ubiquitin enzyme variant, PRR = Proline rich repeat.

3.1.2. VPS28

Human VPS28 shows 66% similarity with yeast Vps28, and like TSG101 also showed localisation to dominant negative VPS4 induced endosomal vacuoles[53]. Taken together, mapping from two studies has shown the binding site for VPS28 to optimally exist between residues 330-385 of TSG101, with residues 368-371 representing the minimal region required for binding[565,665]. Virus work also demonstrated the importance of the interaction between VPS28 and TSG101, in that a VPS28 binding mutant of TSG101 (TSG101 δ368-371) was unable to rescue L-domain defective HIV-1 budding when fused to Gag. HIV-1 budding was also disrupted when C-terminal regions of TSG101 that corresponded to the VPS28 binding site were removed[565]. Binding to TSG101 was also shown to be necessary for cytokinesis, as again evidenced by the inability of a VPS28 binding site mutant TSG101 to rescue the increase in multinucleation seen upon depletion of TSG101[565].

3.1.3. VPS37 subunits

Human VPS37 orthologues VPS37A-D were identified based on homology to yeast Vps37 and previously uncharacterised *Drosophila* TSG101 interaction partners[657,665,666]. A Modifier of rudimentary (Mod(r)) domain of approximately 150 residues represents the most conserved region amongst the VPS37 paralogues and with yeast Vps37 (Figure 23)[677]. The Mod(r) is predicted to contain at least one helical region in each paralogue and forms the primary interaction surface with the core of TSG101, which through yeast two-hybrid studies has been shown to bind at least part of each Mod(r) domain[665]. Mod(r)-TSG101 core dimers also form the binding site for the various MVB12 subunits (see below), as shown by both yeast two-hybrid and immunoprecipitation studies[667].

Whilst VPS37B, C and D contain ~30% proline rich regions downstream of their Mod(r) domains, VPS37A lacks this and instead contains an N-terminal UEV domain (Figure 23)[657,665,666]. VPS37A shows preferential pairing with UBAP1 to form an ESCRT-I complex that is specifically involved in endosomal sorting (see below). Depletion of VPS37A shows decreased lysosomal sorting and degradation of EGFR, hence a marked accumulation in its cellular levels[666]. Given the specific role for VPS37A in endosomal sorting, it would seem reasonable to assume that the UEV domain of VPS37A represents a specialisation for ubiquitin binding, like the UEV of TSG101. Despite this, the residues that bind ubiquitin and PT/SAP motifs in the TSG101 UEV are not conserved in the VPS37A UEV, and binding to ubiquitin has not been observed, leaving an open question surrounding the function of this region[637,665,666]. An N-terminal region of VPS37A encompassing the UEV, however, did show some weak interaction with TSG101, even though binding was stronger using a C-terminal fragment encompassing the Mod(r) domain (Figure 23)[666]. Functions for the proline rich regions of VPS37B-D also remain to be elucidated.

Aside the well-defined role for VPS37A in endosomal sorting (see below), function specific roles for VPS37B-D have not been described in detail. However, their identity as ESCRT proteins and requirement for ESCRT function has been demonstrated by their observed clustering on catalytically inactive dominant negative VPS4 induced aberrant endosomes, and their ability to rescue budding of L-domain defective HIV-1 virus when fused to Gag[657,665]. Contribution of VPS37B and C to viral budding is discussed in chapter 5.

Notable differences between the VPS37 proteins also include the presence of a ^{185}PTAP^{188} motif in VPS37B which provides another site of interaction with TSG101 by binding to its UEV domain (Figure 23)[665]. This is not found in any of the other VPS37 proteins. VPS37A also appears to show some potential direct interaction with VPS28, as shown by both yeast two-hybrid and co-precipitation studies in which an interaction between GST-VPS28 with *in vitro* translated VPS37A was seen[666]. The same was not seen for VPS37B or C. Yeast two-hybrid and co-precipitation studies have also shown VPS37A, B and C to bind HRS, although to varying extents for each protein, with binding to VPS37C perhaps being more apparent due to the observed co-localisation of YFP-VPS37C with CFP-HRS[657,665,666]. This was not observed in the case of YFP-VPS37B. An

interaction between VPS37C with ALIX was also observed by yeast two-hybrid, however no such binding has been reported for the other VPS37 paralogues[657].

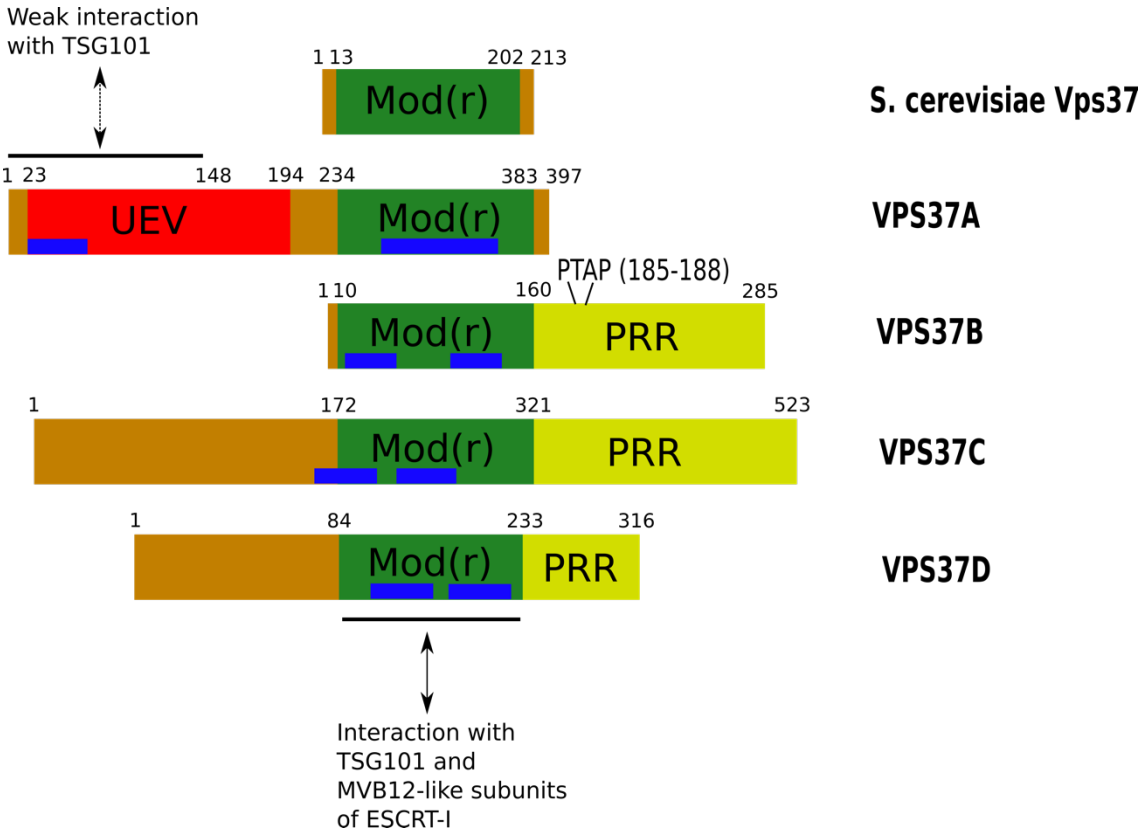

Figure 23. Domain structure of VPS37 paralogues
As described in the text, all mammalian VPS37 paralogues contain a Mod(r) region responsible for interaction with TSG101 and MVB12-like subunits, hence the rest of ESCRT-I. Each of these Mod(r) regions contain at least one predicted helical region shown in blue. Whilst VPS37B, C and D contain C-terminal PRRs, VPS37A does not contain a PRR and instead contains an N-terminal UEV, which has not definitively been shown to bind ubiquitin, but potentially shows some weak binding to TSG101. The $_{185}$PTAP$_{188}$ motif shown in VPS37B provides another site of interaction with TSG101, at the TSG101 UEV domain.

3.1.4. MVB12 subunits

Three mammalian MVB12-like subunits have so far been described: MVB12A, MVB12B and UBAP1 (Figure 24A)[196,658,667,678]. Mammalian MVB12A and MVB12B were identified by mass spectrometry as proteins sharing around 30% sequence identity that co-precipitated with One-STrEP FLAG (OSF)-tagged TSG101, VPS28 and VPS37A-D co-expressed in 293T cells. Although no discernible sequence conservation between yeast Mvb12 and the mammalian isoforms MVB12A and MVB12B is apparent, a TSG101-

VPS37 dimer was found to provide the binding site for incorporation of MVB12A and MVB12B into ESCRT-I[667]. Further mapping studies narrowed down the binding site to the regions of TSG101 and VPS37 subunits that corresponded to the ESCRT-I core, i.e. the stalk and head forming regions of TSG101 and the Mod(r) regions of VPS37 proteins. Mapping studies using recombinantly expressed MVB12 fragments to define the regions of MVB12A and MVB12B necessary for incorporation into ESCRT-I identified two non-overlapping C-terminal fragments from residues 192-233 and 234-273 (Figure 24B) that both independently bound ESCRT-I. These were termed ESCRT binding boxes (EBB1 and EBB2)[667].

The N-terminus of both MVB12A and MVB12B, upstream of EBB1 and EBB2 forms a relatively unique type of β-prism fold known as an MVB12 associated β-prism (MABP)[679,680]. The structure of this fold in MVB12B has been crystallised and shown to consists of three antiparallel β-sheets arranged about a pseudo threefold axis[679]. These domains have been implicated in membrane binding, *in vitro* and *in vivo*, showing non-specific binding to anionic lipids via an exposed surface loop and adjacent electropositive surface patch. Although binding is weak, such an interaction in combination with those of other membrane binding domains of the ESCRT machinery has been proposed to facilitate targeting to anionic lipids at late endosomes and the plasma membrane[679].

UBAP1 was identified as a fourth alternative mammalian MVB12 subunit by Stefani et al. 2011[196], as an HD-PTP interacting protein accounting for approximately 10% of ESCRT-I complexes, and by Agromayor et al. 2012[658] as a protein that shared sequence similarity with both vertebrate and invertebrate MVB12 sequences. Its identification in a bioinformatics screen in 2010 also defined a more specific region of homology of approximately 50 residues shared with MVB12A and MVB12B at its N-terminus, that was termed the UBAP1-MVB12-associated (UMA) domain[680]. UMA domains were identified in metazoan proteins only and were characterised by a highly conserved N-terminal proline residue followed by a hydrophobic residue, and an even more highly conserved C-terminal glutamate residue (Figure 24B). The UMA domain corresponds to a region of MVB12A and MVB12B encompassing parts of both EBB1 and EBB2 (Figure 24B) and in human MVB12 proteins, the conserved N-terminal proline residue corresponds to the central residue of a shared VPF motif[667,680]. EBB1 contains this VPF

motif whilst EBB2 contains the conserved glutamate residue, consistent with a role for these residues in binding ESCRT-I, as shown for UBAP1[196,658,681] (Figure 24B). Secondary structure predictions for the UMA domains of MVB12A, MVB12B and UBAP1 are consistent with that of UMA domains in general, showing an α+β fold[680]. Both JPRED 4 and NetSurfP-2.0 predict human MVB12A, MVB12B and UBAP1 to possess a short beta strand immediately following or overlapping the VPF motif. Two helical regions are predicted to exist downstream of this, the second of which contains the conserved glutamate residue (Figure 24B).

The C-terminus of UBAP1, downstream of the UMA domain forms a solenoid of overlapping ubiquitin associated (UBA) domains (SOUBA), which binds to both monoubiquitin and K48 and K63-linked diubiquitin chains with equal affinity, around 10 times stronger than the UEV domain of TSG101 (Figure 24A)[658]. This confers a process specific function to UBAP1 in the ESCRT mediated process of endosomal sorting of ubiquitinated receptor proteins. UBA domains consist of small 3-helix bundles with a conserved hydrophobic surface that binds ubiquitin moieties via a GF/Y motif[682–684]. The SOUBA consists of three overlapping UBA domains in which the third helices of UBAs 1 and 2 form the first helices of UBAs 2 and 3 respectively, to form a ridged right-handed solenoid structure consisting of seven overlapping helices. Each overlapping UBA domain can bind ubiquitin, however simultaneous binding to more than one ubiquitin moiety has not been shown[658].

UBAP1 represents a mammalian MVB12 subunit with a clear direct function in sorting, as shown by its ability to form an ESCRT-I complex that binds HD-PTP and ubiquitin with high affinity to specifically function in MVB formation and lysosomal sorting. Depletion of UBAP1 leads to endosomal clustering and accumulation of ubiquitinated proteins and EGF on endosomal membranes showing co-localisation with HRS[196]. Depletion also leads to defective lysosomal sorting of tetherin and MHC class I[658].

Functions specific to yeast Mvb12 have been described in sorting and recycling of the ESCRT-I complex from membranes, based on analysis of mutants that do not express Mvb12 or express of Mvb12 point mutants that disrupt interaction with ESCRT-I. Mutation of Mvb12 disrupted sorting of biosynthetic cargo such as CPS and Sna3 and endocytic cargo such as Ste2 and Ste3[64]. There is conflicting evidence regarding whether Mvb12 plays a cargo selective role, favouring the sorting of one type of cargo over

another[67]. Curtiss et al 2007 also proposed a function for Mvb12 in recycling of ESCRT-I from membranes, which is dependent upon ubiquitin binding[66]. Chu et al. 2006 proposed a role for Mvb12 in preventing the premature interaction between ESCRT-I and ESCRT-II until both complexes are membrane bound[65]. In any case, sorting defects are less severe upon deletion/mutation of Mvb12 than any of the other yeast ESCRT-I subunits, and do not lead to a classic class E phenotype[67]. Cargo still reaches the vacuole limiting membrane, even if not reaching the lumen. Furthermore, deletion of Mvb12 does not disrupt recruitment of ESCRT-I to membranes and the resulting trimer still shows some sorting activity despite being less stable and extended[66]. Mvb12 is the least stable of all yeast ESCRT-I subunits and has the highest turnover[79]. Whilst a unique role for Mvb12 in the fine tuning of sorting cannot be ruled out, all these findings point to a less important role for Mvb12 than the other yeast ESCRT-I subunits in ESCRT-I function, and suggest its main role to be maintenance of stability and structure, as further evidenced by prevention of aggregation and proteolysis upon its co-expression with the other recombinant ESCRT-I subunits[79].

In contrast to UBAP1, human MVB12A and MVB12B are similar to yeast Mvb12 in that their depletion does not appear to have such a detrimental effect on EGFR sorting, and function specific roles remain to be elucidated in detail[681]. ESCRT identity was again shown by localisation of MVB12A to aberrant endosomes caused by dominant negative VPS4 expression, and a minor role for MVB12A and B in viral budding is discussed in section 5.1.2.[667].Both MVB12A and MVB12B show serine, threonine and tyrosine phosphorylation patterns[667,685,686]. Mutation of these phosphorylation sites in MVB12A did not disrupt incorporation into ESCRT-I but reduced the ability of the overexpressed protein to disrupt HIV-1 budding[667]. It is also often overlooked that MVB12A was originally identified not as an ESCRT-I component but as a protein named CIN85/CD2AP family binding protein (CFBP), identified in a screen for proteins that are tyrosine-phosphorylated upon EGF stimulation[686]. Phorphorylation was proposed to increase binding affinity of CIN85/CD2AP to MVB12A and promote EGF receptor downregulation through recruitment of Cbl ubiquitin ligase to the CD2AP/CIN85 complex[686]. Tyrosine phosphorylation at the equivalent positions in MVB12B was also later observed, in response to EGF stimulation[667,685]. These observations potentially suggest a role in endosomal sorting, albeit a more minor one compared to UBAP1.

Selective subunit pairing between VPS37A and UBAP1 has been well defined[196,658,681]. Like MVB12A and MVB12B, a TSG101-VPS37A Mod(r) dimer has been shown to provide the binding interface for UBAP1 incorporation into ESCRT-I, and preferred pairing with VPS37A has been shown both *in vivo* and *in vitro*. Co-precipitation of VPS37A but not VPS37B or VPS37C using UBAP1-strep, and co-precipitation of UBAP1 using Myc-VPS37A but not using Myc-VPS37B or VPS37C has been shown[681]. The same publication also showed this selective pairing *in vitro*, in the absence of any possible bridging factors, using tagged proteins expressed at physiological levels in rabbit reticulocyte lysates. A predicted neighbouring helical region downstream of the UMA domain in UBAP1 has been shown to confer selective binding to VPS37A, specifically by preventing binding of VPS37C, and most likely VPS37B. In contrast it was shown that the bare UMA domain of MVB12A alone was able to selectively pair with VPS37C, and probably VPS37B, but not VPS37A[681]. These co-precipitations demonstrate that selective pairing is conferred by differences both within and flanking the UMA domains of MVB12 subunits.

Aside the selective subunit pairing between VPS37A and UBAP1, preferred pairing between VPS37B and VPS37C with MVB12A and MVB12B has so far not been described, and pairing has been suggested to be stochastic, particularly since these paralogues are more similar to each other at the level of their primary sequences. In this chapter I present a further example of selective pairing between VPS37 and MVB12 subunits for UMAD1 – a newly identified alternative MVB12 subunit that pairs with both VPS37B and VPS37C but shows preferential binding to VPS37C.

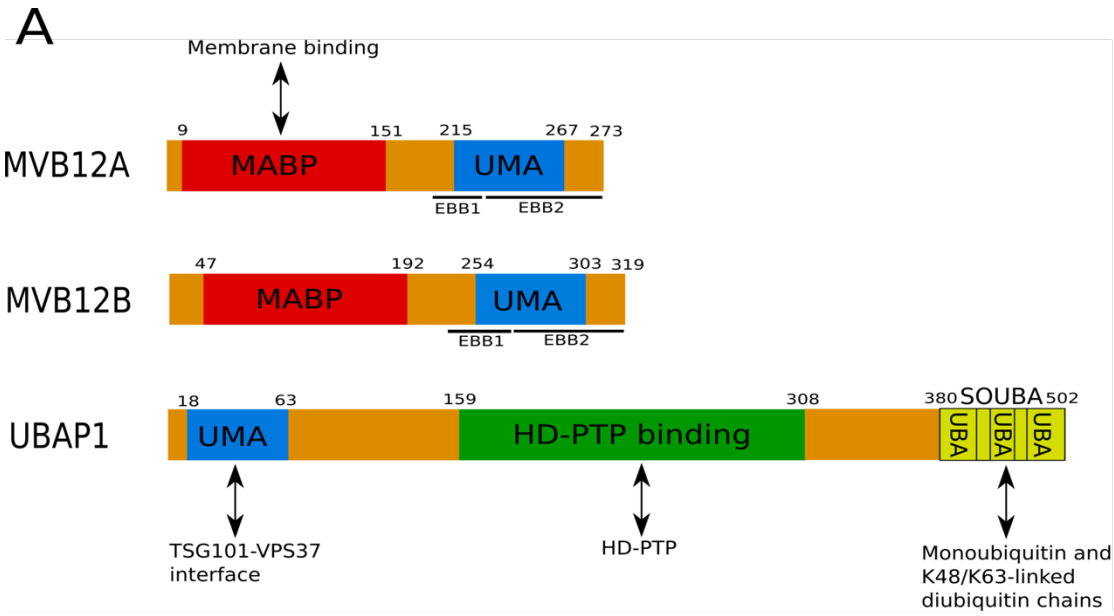
A
Membrane binding
MVB12A
9
151
215
267
273
MABP
UMA
EBB1
EBB2
MVB12B
47
192
254
303
319
MABP
UMA
EBB1
EBB2
UBAP1
18
63
159
308
380
SOUBA
502
UMA
HD-PTP binding
UBA
UBA
UBA
TSG101-VPS37 interface
HD-PTP
Monoubiquitin and K48/K63-linked diubiquitin chains

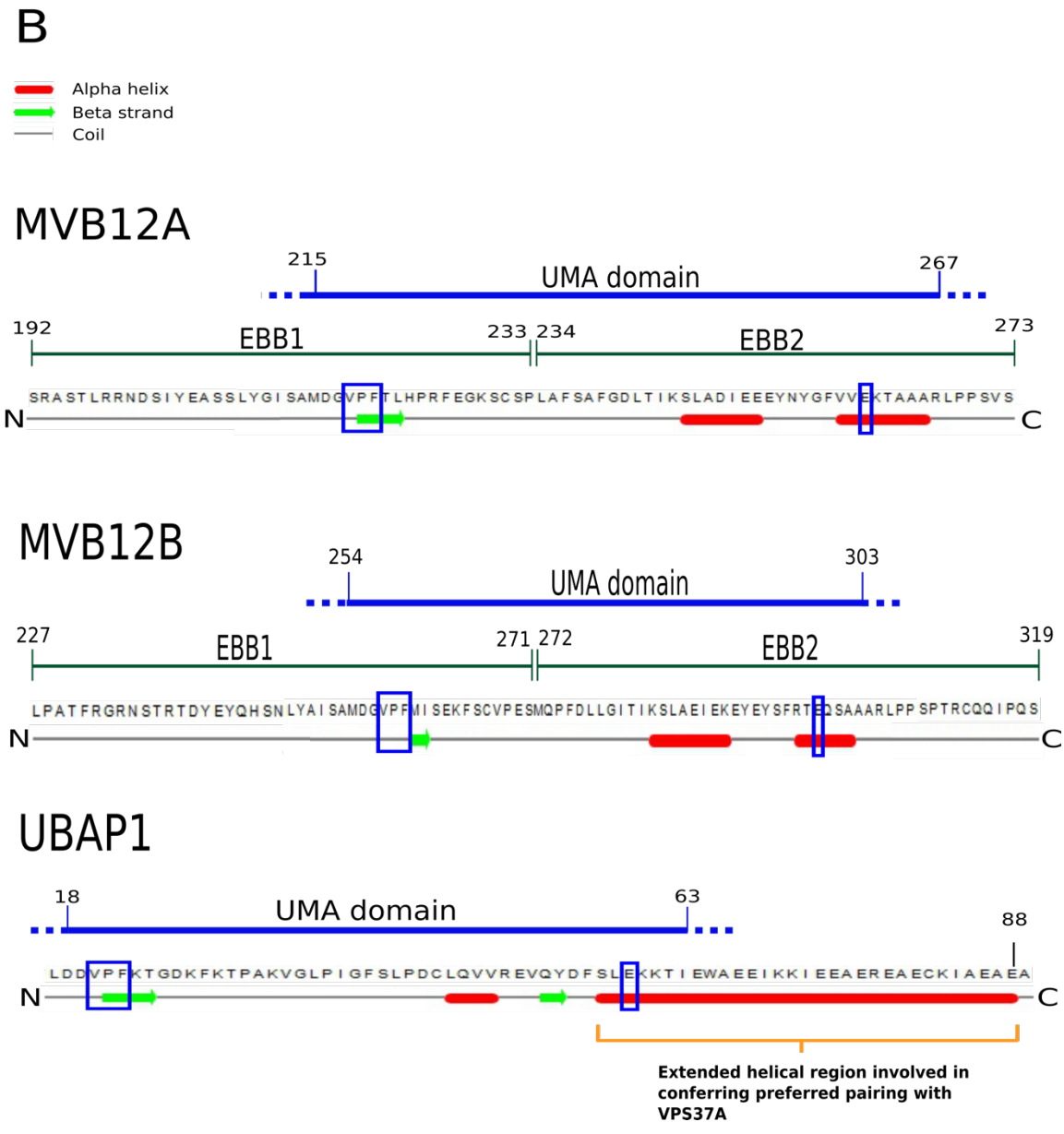
B
Alpha helix
Beta strand
Coil
MVB12A
215
UMA domain
267
192
EBB1
233
234
EBB2
273
SRASTLRRNDSIYEASSLYGISAMDGVPFTLHPRFEGKSCSPLAFSAFGDLTIKSLADIEEEYNYGFVVEKTAAARLPPSVS
N
C
MVB12B
254
UMA domain
303
227
EBB1
271
272
EBB2
319
LPATFRGRNSTRTDYEYQHSNLYAISAMDGVPFMISEKFSCVPESMQPFDLLGITIKSLAEIEKEYEYSFRTEQSAAARLPPSPTRCQQIPQS
N
C
UBAP1
18
UMA domain
63
88
LDDVPFKTGDKFKTPAKVGLPIGFSLPDCLQVVREVQYDFSLEKKTIEWAEEIKKIEEAEREAECKIAEAEA
N
C
Extended helical region involved in conferring preferred pairing with VPS37A

Figure 24. Domain structure of human MVB12-like proteins and UMA domains

A. As described in the text, human MVB12A and MVB12B proteins contain N-terminal MABP domains involved in membrane binding. Their C-termini contain UMA domains involved in interaction with ESCRT-I, specifically TSG101-VPS37 dimer interfaces. UBAP1 is an MVB12-like protein that is highly adapted for endosomal sorting of ubiquitinated cargo. It contains an N-terminal UMA domain, a central region that interacts with HD-PTP and importantly a C-terminal SOUBA capable of binding ubiquitin moieties of cargo with high affinity. EBB1 and EBB2 regions represent frements of MVB12A and MVB12B that were each originally shown to bind ESCRT-I prior to subsequent characterisation of UMA domains. MABP = Matric associated β-prism, UMA = UBAP1-MVB12-associated domain, UBA = Ubiquitin associated domain, SOUBA = Solenoid of overlapping UBA domains, EBB1 = ESCRT-I-binding box 1, EBB2 = ESCRT-I-binding box 2. **B.** Location of UMA domains with surrounding sequence and predicted secondary structures in human MVB12-like subunits. Positions of the UMA domains within MVB12A, MVB12B and UBAP1 are shown, based on protein primary structure, together with surrounding regions of relevance. Signature UMA domain N-terminal VPF motifs and C-terminal conserved glutamate residues are boxed in blue. Secondary structure predictions using JPred 4 are shown. These predictions also matched well with those generated using NetSurfP-2.0.

3.2. Results

3.2.1. Identification of UMAD1 as an ESCRT-I subunit

As part of an attempt to identify novel ESCRT-I interaction partners, a GFP trap co-immunoprecipitation assay was performed using lysates from HeLa cells that stably expressed the bait proteins YFP-TSG101, YFP-VPS37C or YFP alone, as a negative control. Following binding of protein to trapping beads, eluted proteins were digested with trypsin and prepared for multiplex tandem mass tag (TMT) based LC-MS/MS mass spectrometry, using a different isobaric TMT tag to label the tryptic peptides generated for each sample, as detailed in section 2.5.6. of materials and methods.

To determine binding partners specific to TSG101 or VPS37C, a criterion based on the TMT tag reporter ion ratio for YFP-TSG101 or YFP-VPS37C to the YFP negative control was introduced. A protein was defined as a specific binding partner if this ratio was ≥3. A complete list of identified interaction partners is presented in Appendix 1. Upon applying this cut-off, ESCRT-I proteins showed the highest ratios (Table 2) and all known ESCRT-I subunits except for VPS37D and MVB12B were identified. This suggests that VPS37D and MVB12B do not bind, or more likely are either not expressed or show negligible expression levels in HeLa cells, consistent with data from the Human Protein Atlas version 18.1 and other publications[667,681]. Despite being less enriched, CEP55 was also identified as a binding partner for at least YFP-TSG101. Reassuringly in the case of YFP-VPS37C, values for VPS37A and VPS37B were very close to or at zero (Table 2), as would be expected, due to their being outcompeted by YFP-VPS37C. Lack of enrichment for UBAP1 can be explained by the preferred pairing between VPS37A with UBAP1, rather than VPS37C.

Besides all previously identified ESCRT-I components, UMAD1 was identified as a binding partner for both YFP-TSG101 and YFP-VPS37C (Table 2). UMAD1 was previously identified as another UMA domain containing protein, based on homology with human MVB12A and MVB12B in the same bioinformatics screen from 2010[680] (Section 3.1.4.). This strongly suggested that UMAD1 could be a novel unconfirmed ESCRT-I interaction partner. Detection of only one peptide could be due to the relatively small size of UMAD1 (137 amino acid residues), hence a lower number of tryptic peptides (4

theoretically expected) and simpler fragmentation pattern compared to other ESCRT proteins.

Like MVB12A, MVB12B and UBAP1, the C-terminal UMA domain of UMAD1 contains the same canonical VPF and glutamate residues, however secondary structure prediction using both the full-length protein and a shorter region mainly encompassing the UMA domain (Figure 25) predicts a more helical structure (Figure 25). The beta strand at the site of the VPF motif appears to be replaced with two helical regions, the second of which either overlaps or is positioned just downstream of the VPF motif. The UMA domain of UMAD1 encompasses approximately the most C-terminal 50-60 residues, whilst the N-terminal 75-85 residues are predicted to be largely unstructured, apart from a beta strand from approximately residues 22-29. The primary sequence of this predicted strand and that around the conserved UMA domain VPF and glutamate residues correspond to the most highly conserved regions of the protein across species. According to the Ensembl genome browser, UMAD1 appears in general to be very well conserved across vertebrate species, found in mammals, birds, reptiles and even the Coelacanth – one of the oldest species of fish to date. UMAD1 also appears to be quite ubiquitously expressed, present at substantial levels in all cell lines listed in the Human Protein Atlas version 18.1. This thesis provides the first characterisation of UMAD1 as a novel MVB12 subunit and exploration of its function.

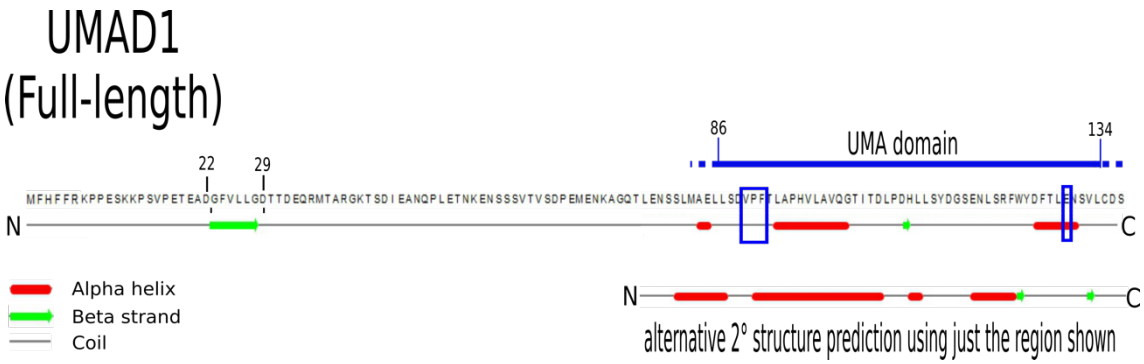

Figure 25. Primary sequence and secondary structure prediction for UMAD1
Positions of the predicted UMA domain (approximately residues 86-134) and N-terminus (approximately 1-86) of UMAD1 are shown, based on the protein primary structure. Signature UMA domain N-terminal VPF motifs and C-terminal conserved glutamate residues are boxed in blue. Secondary structure predictions using JPred 4 are shown. These predictions also matched well with those generated using NetSurfP-2.0.

Protein identity	HeLa YFP-TSG101/YFP control	HeLa YFP-VPS37C/YFP control
VPS37C	13.50332642	156.4856277
UMAD1	3	3.579606866
CEP55	3.817730904	2.779191864
VPS37A	9.110055923	0.404141535
TSG101	11.63141537	27.47899204
VPS37B	16.80769157	0
VPS28	17.70149231	12.81665716
UBAP1	25.3847065	0.522414828
MVB12A	7.418165684	23.14501004

Table 2. ESCRT-I subunit enrichment when co-precipitated by YFP-TSG101 or YFP-VPS37C as determined by IP-TMT based mass spectrometry
GFP trap immunoprecipitations using YFP-TSG101 and YFP-VPS37C, in a HeLa cell background, together with an appropriate YFP negative control were performed. Eluates were analysed by multiplex IP-TMT based mass spectrometry following digestion with trypsin and isobaric TMT tag labelling, using a different tag per sample. Following total normalisation of signal values across samples to eliminate variation in signal at the level of sample preparation and data acquisition, signal values for YFP-TSG101/YFP control and YFP-VPS37C/YFP control were calculated.

3.2.2. UMAD1 rescues L-domain defective HIV-1 budding

An HIV-1 viral trans-complementation assay was performed to test UMAD1's ability to form a functional ESCRT-I complex. This assay exploits the ability of the ESCRT machinery to mediate HIV-1 budding. Briefly, ESCRT proteins are fused to a defective HIV-1 Gag lacking the L-domains (GagΔp6), which is unable to release viral particles. This leads to artificial recruitment of the ESCRT machinery to sites of viral budding, thus rescuing budding to varying extents[14,565,567,575].

In terms of experimental setup, this assay involves co-transfection of 293T cells with two plasmids (Figure 26A). The first plasmid encodes a full-length L-domain defective provirus in which a stop codon is placed just upstream of p6 (pHxB-STOP). The second plasmid encodes a more truncated proviral construct, which encodes Gag as a fusion to various ESCRT proteins. When expressed, Gag proteins encoded by both plasmids are processed and multimerise to form a virus with improved budding competency. Infectious virus release was quantified in this assay using TZM-bl reporter cells. Upon infection, TZM-bl reporter cells express β-galactosidase, which is under the control of an

HIV-1 tat protein responsive HIV-1 LTR promoter. β-galactosidase readout is therefore measured to quantify infectious virus release.

UMAD1 was tested in parallel with TSG101 and UBAP1, since these proteins have previously been shown to rescue budding in this assay[14,658]. Gag with p6 re-introduced (pHxB-p6) or with no fusion present (pHxB-ENX) were used as positive and negative controls respectively (Figure 26B). UMAD1 was found to rescue infectious release, showing over 4-fold rescue compared to pHxB-ENX (Figure 26B). 293T producer cell lysates show reasonably constant cellular Gag expression across all conditions. The characteristic p25 (CA-SP1) to p24 (CA) processing defect characteristic of disrupted L-domain activity is also seen, as manifested by the p25/p24 doublet seen for all conditions[560]. Whilst theoretically the band intensities for Gag for pelleted virion samples should mirror the infectious virus release levels seen in the TZM-bl assays, the artificial nature of this assay has previously shown this to not always be the case[658], as seen here. Trans-complementation with pHxB-TSG101, for example, appears to show more budded virions than when using pHxB-UMAD1 or pHxB-UBAP1, despite observing a better rescue using the latter two constructs than pHxB-TSG101 in the TZM-bl assay. A possible explanation for this discrepancy could be that not all the budded virions are infection competent using this artificial system due to interference by the bulky Gag fusions to varying degrees.

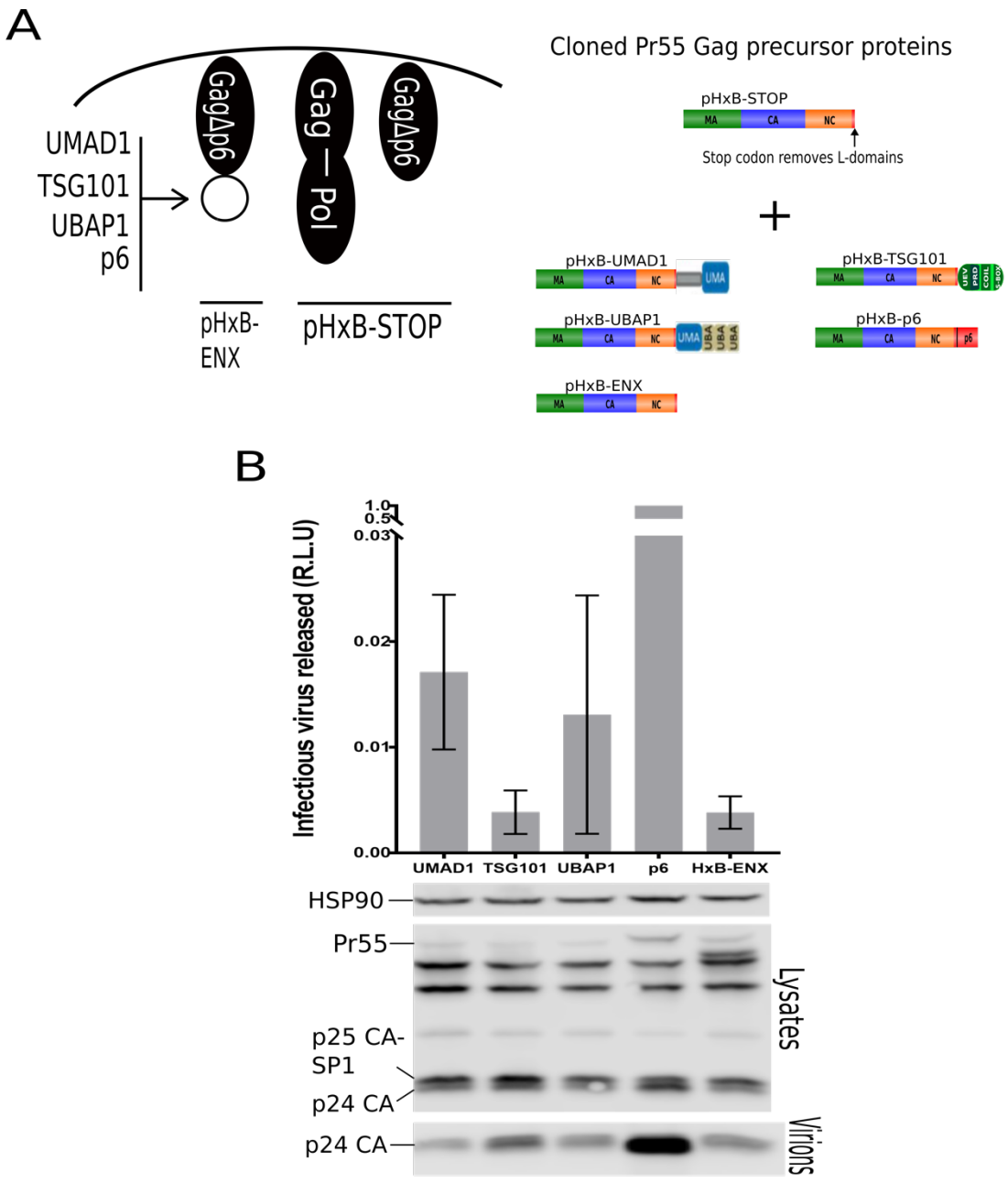

Figure 26. UMAD1 rescues L-domain defective HIV-1 budding when fused to HIV-1 Gag.
A. Schematic representation of modified trans-complementing HIV-1 proviral Pr55 Gag precursor proteins. The stop codon in the pHxB-STOP full length proviral construct is designed to disrupt L-domain activity but not expression of Pr160 Gag-Pol precursor protein, as generated in 5% of cases by frameshifting. **B.** 293T cells were transfected with L-domain defective pHxB-STOP full-length proviral plasmids together with pHxB-UMAD, -TSG101, -UBAP1, -p6 or HxB-ENX trans-complementing plasmids. Viral supernatant was harvested 48 hrs later and used to infect TZM-bl reporter cells. TZM-bl cell lysates were harvested another 48 hrs later and infectious virus release was determined by HIV-1 Tat dependent β-galactosidase induction measured by quantification of chemiluminescence. Results show the mean numbers obtained for four independent experimental repeats, and error bars represent the standard deviation from the mean. Immunoblotting of producer cell lysates and 20% sucrose cushion pelleted virions was performed with α-Gag. Blotting with α-HSP90 was also performed for lysates, as a loading control.

3.2.3. UMAD1 is incorporated into ESCRT-I complexes

The above viral trans-complementation assay and mass spectrometry results strongly suggest that UMAD1 is a novel ESCRT interacting protein and specifically could be an ESCRT-I binding partner, given its co-precipitation by both TSG101 and VPS37C and its possession of a UMA domain shared with MVB12A, MVB12B and UBAP1[680] (Figure 24). We therefore decided to test whether UMAD1 could specifically be incorporated into ESCRT-I. To this end, a GST co-precipitation assay was initially performed using lysates from 293T cells that were transiently transfected with plasmids overexpressing GST-TSG101, Myc-VPS28, HA-tagged VPS37A, VPS37B, VPS37C or VPS37D and HA-UMAD1 (Figure 27A), similar to that used previously by Agromayor et al. 2012[658] to test UBAP1 incorporation into ESCRT-I. In this way, both incorporation of UMAD1 into ESCRT-I complexes and any potential VPS37 subunit pairing specificity could be examined.

Three independent experimental repeats consistently showed the absence of a band for HA-UMAD1 in pull-down conditions using HA-VPS37A, whilst the presence in the cases of HA-VPS37B, HA-VPS37C and less so to HA-VPS37D. This suggested VPS37 subunit pairing specificity with VPS37B, C and D (Figure 27A). This result was reassuring in that UMAD1 was indeed co-precipitated and that specific VPS37 subunit pairing appeared to be seen. Co-precipitation using HA-VPS37C generally showed a more intense band for HA-UMAD1 compared to when using HA-VPS37B and even less in the case of VPS37D, as quantified in Figure 27B, suggesting a further preference for incorporation into ESCRT-I complexes containing VPS37C over VPS37B or VPS37D.

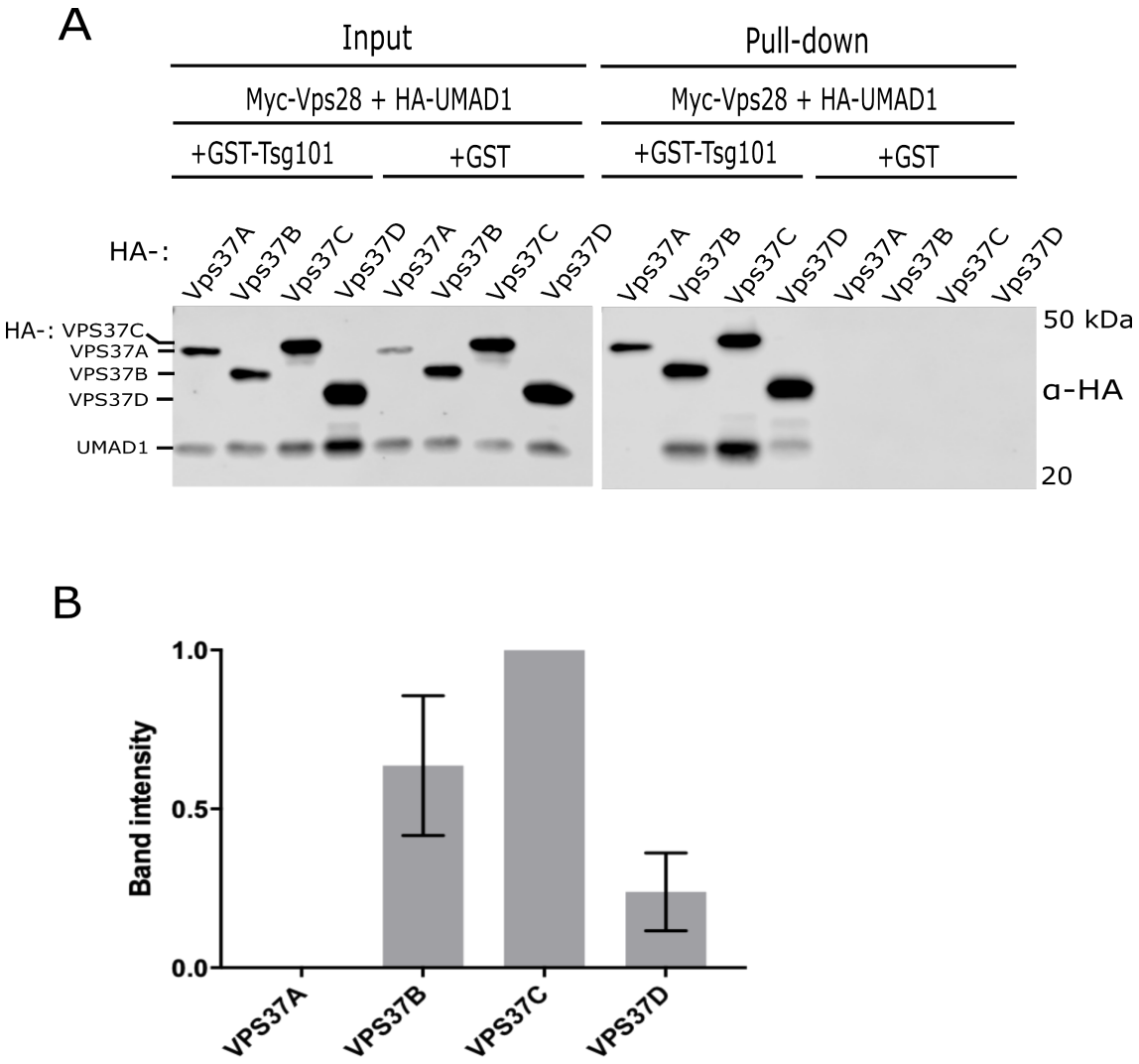

Figure 27. UMAD1 is incorporated into ESCRT-I complexes containing VPS37B, C or D
A. GST pull-down co-precipitation assay using transiently overexpressed, tagged ESCRT-I proteins in 293T cells. 293T cells were transfected with plasmids expressing GST-TSG101, Myc-Vps28, HA tagged VPS37A, VPS37B, VPS37C or VPS37D and HA-UMAD1. 48 hrs post-transfection cell lysates were incubated with glutathione-sepharose beads and proteins were co-precipitated. 1% cell lysate (input) and 10% bead eluate volumes (pull-down) were resolved by SDS-PAGE and analysed by immunoblotting with α-HA antibody. **B.** Quantification of the mean UMAD1 band intensities for three independent experimental repeats. Band intensities were measured using Image Studio Lite software, and normalised to those for VPS37C, which consistently showed the highest intensity. Error bars represent the standard deviation from the mean.

This pulldown system used so far has the caveat that it is somewhat artificial in that proteins are exogenously overexpressed at non-physiological levels. In order to address the issue of potential formation of aberrant subunit pairings due to protein overexpression in Figure 27A, a GFP trap co-immunoprecipitation assay using lysates from HeLa cells that stably express YFP-UMAD1 was performed to test co-precipitation

of endogenous VPS37 proteins (Figure 28). Results to this assay matched well with those shown in figure 27, showing co-precipitation of VPS37B and C but not A using YFP-UMAD1. A preference for VPS37C over VPS37B was also observed much more clearly than in figure 27, with the level of VPS37C co-precipitated by YFP-UMAD1 matching that using YFP-TSG101. Since VPS37D was not identified in the mass spectrometry screen (Table 2) and is not expressed in HeLa cells, according to the Human Protein Atlas version 18.1, immunoblotting against this protein was not performed.

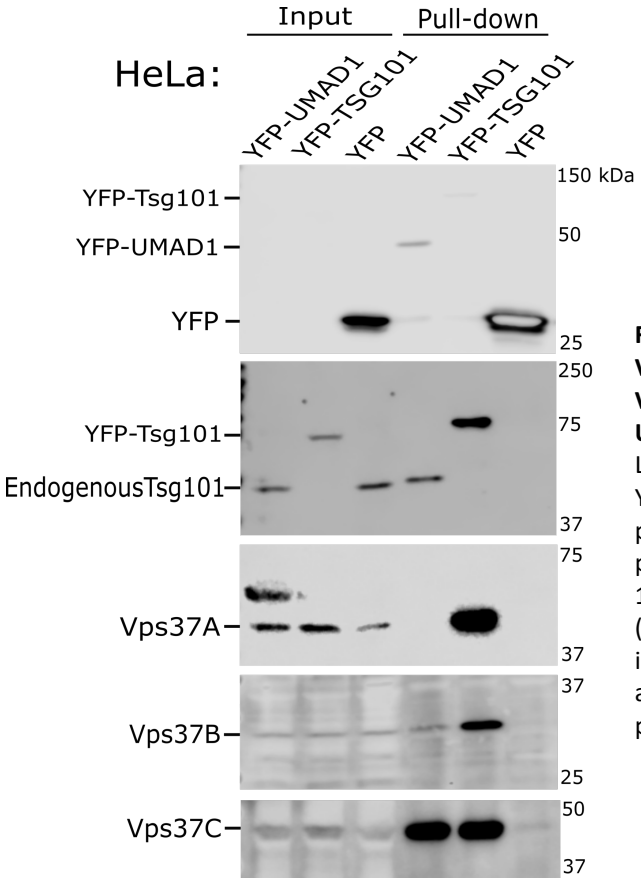

Figure 28. Co-precipitation of endogenous VPS37B and VPS37C with a preference for VPS37C is seen using stably expressed YFP-UMAD1 in HeLa cells.
Lysates from HeLa cells that stably express YFP-UMAD1 or YFP-TSG101/YFP alone as positive/negative controls respectively, were purified by incubation with GFP trap beads. 1% cell lysates (input) and 10% bead eluates (pull-down) were resolved by SDS-PAGE and immunoblotting using α-GFP and antibodies against each of the proteins shown was performed.

Altogether, these experiments confirm that UMAD1 binds ESCRT-I specifically when it contains VPS37B or VPS37C, with a particular preference for VPS37C.

3.2.4. UMAD1 binds ESCRT-I through its UMA domain

Given the role of the UMA domains of MVB12 proteins in ESCRT-I binding[196,658,667,680,681], alignment of the UMA domains of MVB12A, MVB12B, UBAP1 and UMAD1, using Clustal Omega[687,688], was used to identify evolutionarily conserved amino acid residues that might be necessary for binding to ESCRT-I (Figure 29A). Alignment revealed four

conserved point residues (M3-M6), including the UMA domain signature C-terminal glutamate residue (M6), and the conserved UMA domain signature VPF triplicate motif at the start of MVB12 protein UMA domains, which in UMAD1 spans residues 89-91 ($V_{89}P_{90}F_{91}$ (M2)). This same motif was found to abolish binding of UBAP1 to ESCRT-I when mutated, as did mutation of the three less well conserved residues prior to this[658]. We therefore decided to test this additional mutation in UMAD1 ($L_{86}S_{87}D_{88}$/AAA (M1)) despite lack of conservation.

The results for three independent repeats of GST co-precipitation results showed only mutation of the N-terminal UMA domain signature VPF motif (M2) to completely abolish binding to ESCRT-I (Figure 29B). Binding to ESCRT-I containing VPS37B and VPS37C appeared to be undisturbed in the case of all other mutants, including the non-conserved M1 mutant. A trace of a band representing binding to VPS37D was sometimes seen, although as previously observed in figure 27, binding to VPS37D containing ESCRT-I complexes is generally weak even for wild type UMAD1.

Mutant M6, representing the C-terminal conserved UMA domain signature glutamate residue appears to show reduced binding to ESCRT-I, compared to all other mutants and wild type UMAD1. Interestingly, the same mutation has been shown to abolish binding in the case of UBAP1[196,658] and most likely MVB12A, as separate fragments that encompassed either the VPF motif (EBB1) or this glutamate residue (EBB2) respectively were each able to bind ESCRT-I[667].

In conclusion, these GST co-precipitation experiments show that UMAD1 behaves as a novel alternative MVB12 type subunit of ESCRT-I that, like the other three MVB12 subunits so far characterised, shows binding to ESCRT-I through its UMA domain. Its conserved UMA domain N-terminal signature VPF motif and C-terminal glutamate residue are necessary for incorporation of UMAD1 into ESCRT-I, as also previously implied for the other three characterised MVB12-like subunits[196,658,667].

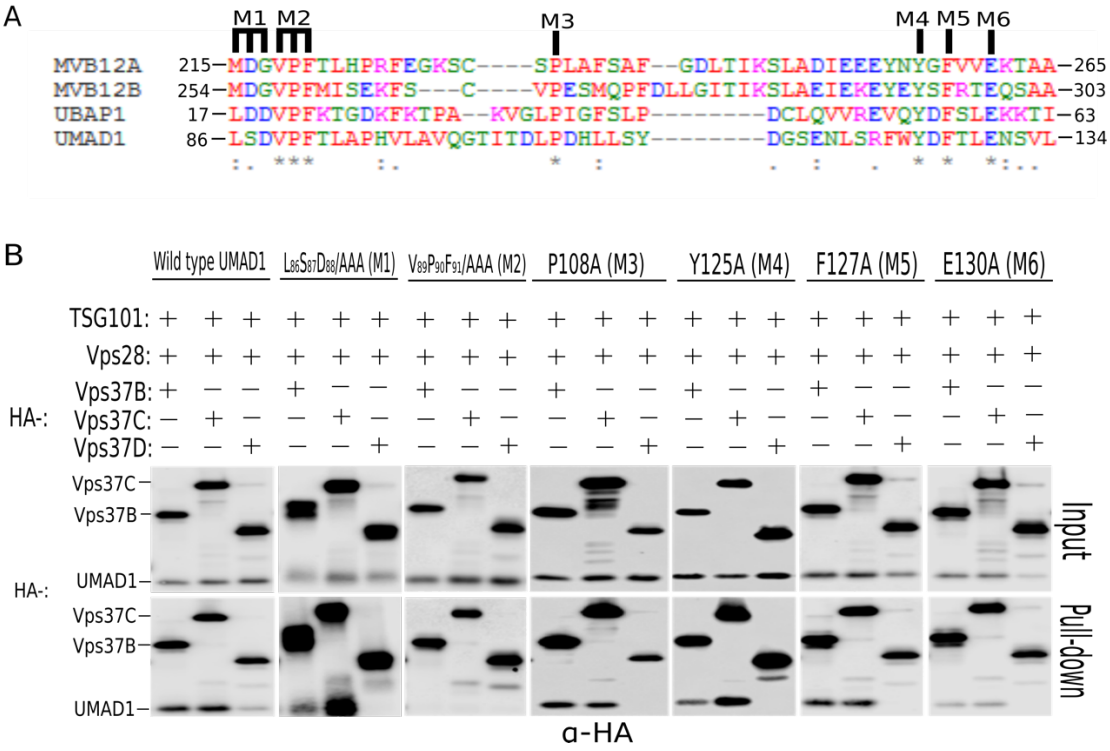

Figure 29. UMAD1 is incorporated into ESCRT-I complexes containing VPS37B, C or D through its UMA domain

A. Clustal Omega protein sequence alignment of the UMA domains of MVB12A, MVB12B, UBAP1 and UMAD1 shows the location of conserved residues tested for ESCRT-I binding ability when mutated to alanine in UMAD1. M1 represents a triplicate motif which when mutated in UBAP1 displayed loss of binding to ESCRT-I, despite not being fully conserved (Agromayor et al. 2012) **B.** GST pull-down assay performed using transiently overexpressed, tagged ESCRT-I proteins in 293T cells to test ESCRT-I binding ability of UMAD1 UMA domain mutants. 293T cells were transfected with plasmids expressing GST-TSG101, Myc-Vps28, HA-VPS37A, B, C or D and HA tagged wild type UMAD1 or each of the UMAD1 mutants shown in A. 48 hrs post-transfection cell lysates were incubated with Glutathione-Sepharose beads and proteins were co-precipitated. 1% cell lysate (input) and 10% bead eluate volumes (pull-down) were resolved by SDS-PAGE and analysed by immunoblotting with α-HA antibody.

3.2.5. Generation of *UMAD1* CRISPR/Cas9 knockout cells

UMAD1 knockout cells were generated using CRISPR/Cas9 in preparation for loss-of-function phenotypic studies, and further immunoprecipitation assays with removal of potential interference from endogenous UMAD1. Knockout cell lines were produced for HeLa and 293T cells, as outlined for HeLa cells in figure 30, by transfecting cells with LentiCRISPRv2GFP plasmids encoding appropriate guide RNA (crRNA), followed by FACS single cell sorting to obtain single GFP expressing clones. The location of cleavage sites together with the guide RNA (crRNA) annealing sites, to direct cleavage, are shown (Figure 30B).

Initial screening of clones for *UMAD1* knockout was performed at the level of transcription, by extracting mRNA from clones followed by reverse transcription, to generate cDNA. A PCR using cDNA template was then performed to screen for the absence of a band corresponding to UMAD1 cDNA (Figure 30A). Two separate HeLa cell clones were obtained (clone 20 and clone 28).

UMAD1 is located on human chromosome 7, and HeLa cells show an average copy no. of 3.87 for this chromosome, according to CanSAR[689], whilst 293Ts show a copy no. of between 2 and 3, according to the American Type Culture Collection (ATCC). To ensure that complete removal of all copies of the gene had been successful, a diagnostic PCR using genomic DNA template was further performed to check for removal of the *UMAD1* locus (Figure 30C). Primer annealing sites to check not only for the absence but also the presence of any undesired remaining copies of the gene following transfection of the LentiCRISPRv2GFP plasmids are shown. This PCR revealed complete removal of all copies of UMAD1 in both HeLa clones (Figure 30D) and was further performed at regular intervals to ensure that the clones were still knockout and suitable for experiments. On a side note, although other clones that appeared negative for UMAD1 mRNA expression were identified by the above described RT-PCR, clones 20 and 28 were the only two clones that gave the desired genomic PCR result, i.e. no products using primer combinations 1+2 or 3+4 but a product using 1+4. In order to further check that the Cas9 cleavage was specific to the sites specified by the guide RNAs, without off-target cleavage, the PCR products obtained using primers 1 and 4 were sequenced (Figure 30C). Results revealed specific cleavage at both cut sites. As later shown in section 3.2.6., further confirmation of abolishment of UMAD1 protein expression in these clones was performed using an anti-UMAD1 antibody.

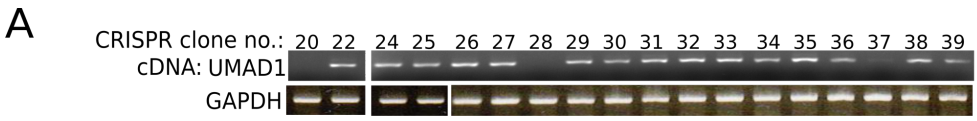
A
CRISPR clone no.: 20 22 24 25 26 27 28 29 30 31 32 33 34 35 36 37 38 39
cDNA: UMAD1
GAPDH

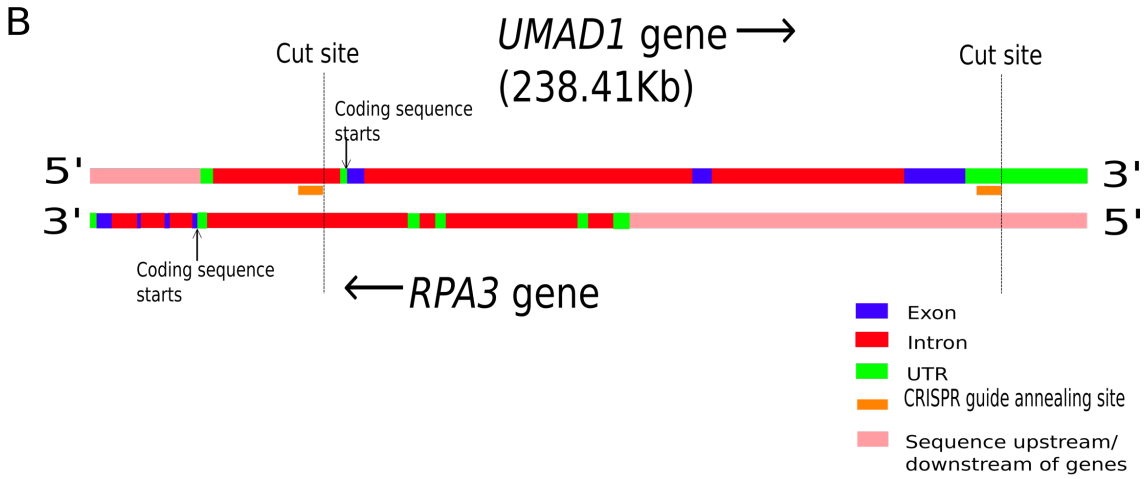
B
Cut site
UMAD1 gene
(238.41Kb)
Cut site
Coding sequence starts
5'
3'
3'
5'
Coding sequence starts
RPA3 gene
Exon
Intron
UTR
CRISPR guide annealing site
Sequence upstream/ downstream of genes

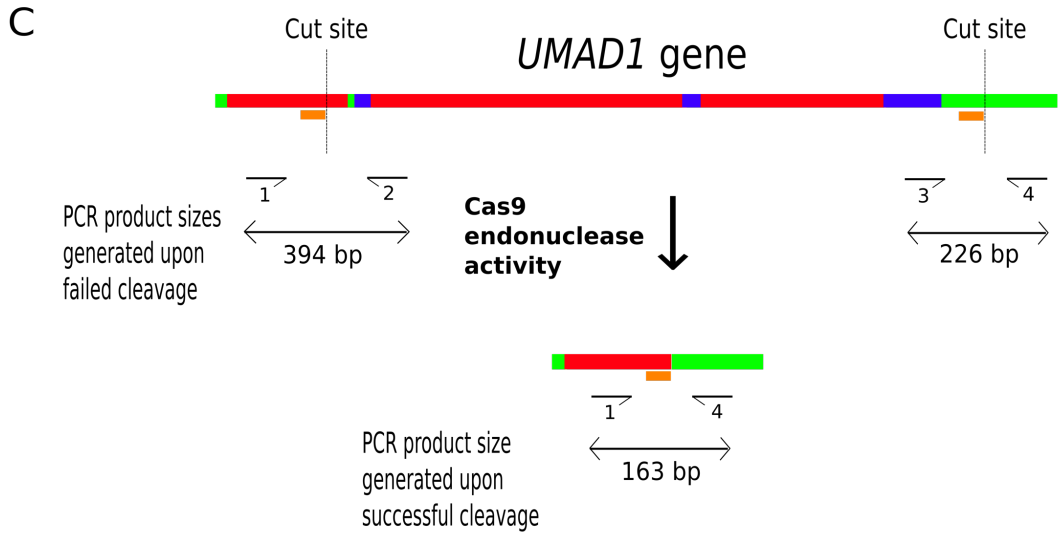
C
Cut site
UMAD1 gene
Cut site
1
2
3
4
PCR product sizes generated upon failed cleavage
394 bp
Cas9 endonuclease activity
226 bp
1
4
PCR product size generated upon successful cleavage
163 bp

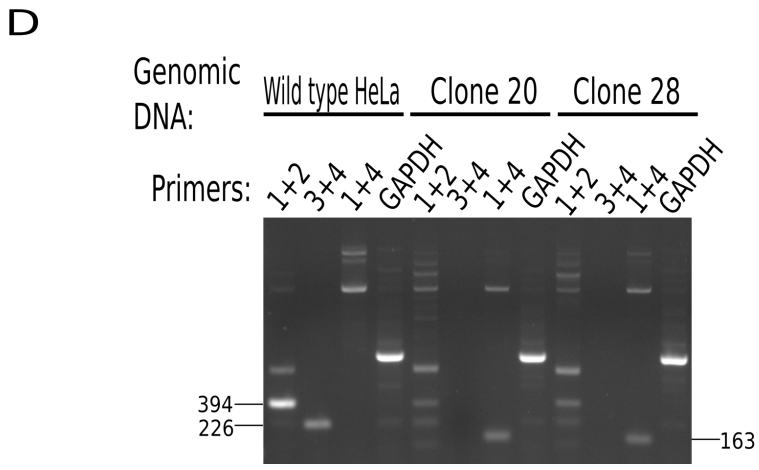
D
Genomic DNA:
Wild type HeLa
Clone 20
Clone 28
Primers:
1+2
3+4
1+4
GAPDH
394
226
163

Figure 30. Generation of UMAD1 CRISPR/Cas9 knockout HeLa cells.
A. PCR to detect amplified UMAD1 cDNA sequence from cDNA template generated by reverse transcription from mRNA extracted from individual HeLa cell CRISPR clones. Clones were obtained by FACS single cell sorting of GFP expressing cells following transfection of two lentiCRISPRv2GFP plasmids encoding start and end guide crRNA to direct Cas9 endonuclease cleavage and removal of the *UMAD1* locus. Clones 1-10 were positive for UMAD1 mRNA expression and therefore not shown. **B.** Schematic representation of the *UMAD1* gene locus and its overlap with *RPA3*. Sites of CRISPR guide annealing and cleavage are shown. **C.** Diagnostic PCR strategy to check for complete removal of all copies of *UMAD1*. Sites of PCR primer annealing and expected PCR product sizes obtained following successful/unsuccessful removal of the gene are shown. In the case of unsuccessful removal of one or more copies of *UMAD1*, primer combinations 1+2 and 3+4 generate the products of sizes shown, whilst PCR using primers 1+4 fails due to inability to amplify such a large region. In the case of successful removal of *UMAD1*, annealing sites for primers 2 and 3 are removed, so no PCR product is observed using primers 1+2 and 3+4, but primers 1+4 now generate a product of 163 bp. **D.** Agarose gel electrophoresis to show PCR products generated using genomic DNA template extracted from clones 20 and 28 using the primer combinations shown in C.

Closer examination of the *UMAD1* locus revealed overlap with that of *RPA3*, which is transcribed in the opposite direction on the complementary strand (Figure 30B). RPA3 is a protein involved in DNA replication and DNA damage response and repair[690–692]. Generation of UMAD1 CRISPR knockout cells was found to have disrupted the sequence for part of this gene, specifically a large part of the 5' UTR, but none of the actual protein coding sequence (Figure 30B). Critically, a side by side comparison of HeLaΔUMAD1 clone 28 cell lysate with that of wild type HeLa cells resolved by SDS-PAGE and immunoblotted with antibody against RPA3, revealed no obvious disturbance of RPA3 protein expression (Figure 31). As further controls to check the α-RPA3 antibody specificity to RPA3, and ensure that the bands observed corresponded to RPA3, lysate from 293T cells stably expressing YFP-RPA3 or untagged RPA3 were resolved and blotted with the antibody. As expected, bands of the expected size corresponding to YFP-RPA3 and endogenous RPA3 were seen using lysate from the 293T YFP-RPA3 cells. A band of slightly higher intensity than in the previous lanes representing combined exogenous untagged RPA3 and endogenously expressed RPA3 was observed using lysate from the 293T RPA3 cells.

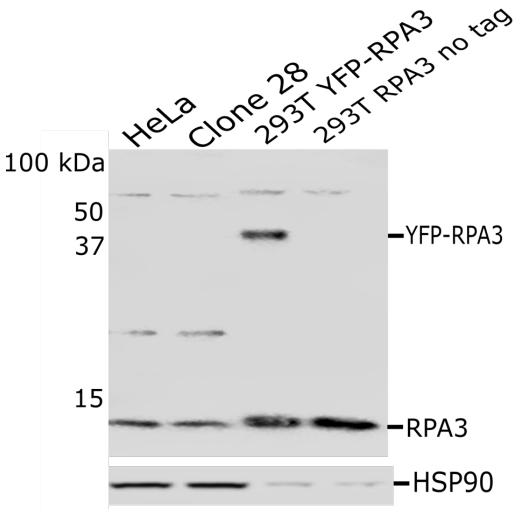

Figure 31. Confirmation of undisrupted RPA3 protein expression in HeLaΔUMAD1 clone28
Lysates from wild type HeLa cells, HeLaΔUMAD1 clone28 and 293T cells that stably express YFP-RPA3 or untagged RPA3 were resolved by SDS-PAGE and subjected to immunoblotting using α-RPA3 and α-HSP90.

Having already checked at the level of mRNA transcription for absence of all copies of the *UMAD1* locus, we next decided to confirm UMAD1 knockout at the level of protein expression. A rabbit polyclonal antibody against UMAD1 was custom-made and purified for us by Lampire Biologicals with the aim of being able to detect endogenous UMAD1.

Immunoblotting of both HeLa and 293T cell lysates using this antibody did not detect a band corresponding to the size of UMAD1 (15.2 kDa) (Figure 32). However, when cells were transfected with pCR3.1 HA-UMAD1 to transiently overexpress HA-UMAD1, a clear band was observed, indicating that the antibody is functional, but unable to detect endogenous levels of UMAD1 expression. We could therefore not use the antibody for confirming UMAD1 protein knockout. Further affinity purification of the rabbit serum was performed by Lampire Biologicals in an attempt to concentrate and improve efficiency of the antibody, however the purified antibody was still unable to detect endogenous UMAD1.

Whilst inability of the antibody to recognise endogenous levels of UMAD1 could simply be due to low antibody sensitivity, it could also be due to possible low levels of endogenous UMAD1 expression. This could perhaps be another reason for its lower enrichment compared to other ESCRT-I proteins in the previous IP-TMT based mass spectrometry experiment (Table 2).

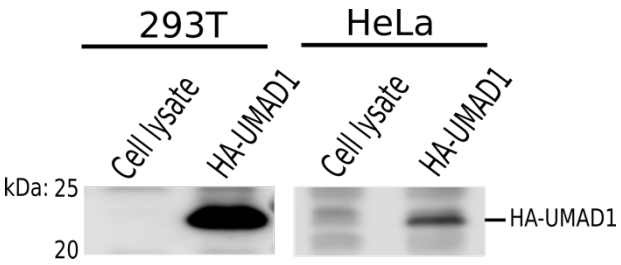

Figure 32. Rabbit polyclonal α-UMAD1 antibody recognises overexpressed UMAD1

Immunoblotting of lysates from both 293T and HeLa cells was performed side by side with lysates harvested 48 hours post-transfection with pCR3.1 HA-UMAD1, to overexpress HA-UMAD1. Blotting was performed using a custom-made rabbit polyclonal α-UMAD1 antibody from Lampire Biologicals.

3.2.6. Endogenous UMAD1 is co-precipitated using ESCRT-I subunits

To confirm that UMAD1 is a genuinely expressed protein and confirm its incorporation into ESCRT-I, we decided to proceed with a GFP-trap co-precipitation of endogenous UMAD1 using lysate from HeLa cells that stably express YFP-TSG101 to co-precipitate, thus enriching endogenous UMAD1 (Figure 33). As a negative control, we made HeLa UMAD1 knockout cells stably expressing YFP-TSG101, which should not precipitate UMAD1.

Immunoblotting using the rabbit α-UMAD1 antibody showed a clear intense band representing co-precipitated endogenous UMAD1 from wild type HeLa cells stably expressing YFP-TSG101 (Figure 33). No trace of a band the same size was observed using either of the two HeLa UMAD1 knockout cell lines.

This experiment represents an important finding, demonstrating that UMAD1 is a genuinely expressed protein, and that it is incorporated into ESCRT-I. It also removed any remaining doubt surrounding the integrity of the knockout cells, proving that no endogenous UMAD1 protein is expressed. Although for completeness, the sensitivity of a quantitative RT-PCR would further ensure no residual mRNA, hence protein expression, the above result shows that UMAD1 expression is abolished or at least reduced to an extremely low level in the two CRISPR/Cas9 knockout clones.

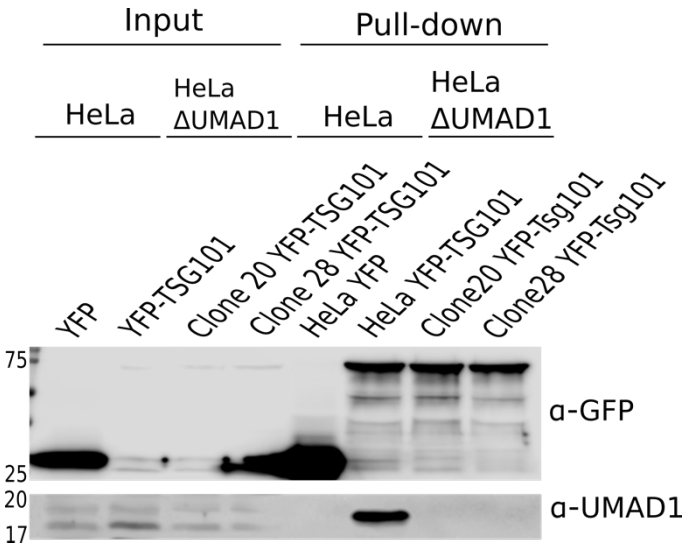

Figure 33. Endogenous UMAD1 is co-precipitated using YFP-TSG101
Cell lysates from wild type HeLa cells or Clone20/Clone28 CRISPR/Cas9 knockout clones stably expressing YFP-TSG101 bait were incubated with GFP-trap beads to immunoprecipitate YFP-TSG101 and associated proteins. 1% cell lysates (input) and 10% beads eluates (pull-down) were resolved by SDS-PAGE, and immunoblotting using α-GFP and α-UMAD1 was performed.

Having obtained an α-UMAD1 antibody, a further GFP-trap immunoprecipitation experiment was performed to examine the co-precipitation assays in figures 27 and 28 in reverse, i.e. co-precipitation of endogenous UMAD1 by YFP-VPS37 baits (Figure 34). In this experiment, lysates from wild type HeLa cells stably expressing YFP-tagged VPS37A, VPS37B, VPS37C, TSG101 or YFP alone, were subjected to GFP-trap immunoprecipitation, and immunoblotting using antibodies against each of the proteins indicated in figure 34.

Results from previous co-precipitation assays (Figure 27 and 28) to examine UMAD1 subunit pairing specificity and preference were very nicely recapitulated here. For seemingly equal levels of YFP-VPS37B and YFP-VPS37C immunoprecipitation, a band of much higher intensity for endogenous UMAD1 co-precipitated by YFP-VPS37C was observed, compared to YFP-VPS37B, for which only trace levels were seen. This result also clearly demonstrates genuine preferred pairing for VPS37C over VPS37B, rather than tissue specific differences in expression levels of VPS37B and VPS37C. No trace of a band was seen using YFP-VPS37A. The intense bands seen when blotting with α-UMAD1 using input samples are the same non-specific bands seen above and below the

expected size of UMAD1 for input samples in figure 33. They simply appear more intense here since this blot was performed following the previously mentioned additional affinity purification of the antibody by Lampire Biologicals in an attempt to increase its efficiency and potential ability to recognise endogenous UMAD1. UBAP1 was only co-precipitated by YFP-TSG101 and YFP-VPS37A, as expected. This result confirms and strengthens the finding that UMAD1 pairs preferentially with VPS37C. It eliminates any doubt previously caused by differences in α-VPS37B and α-VPS37C antibody sensitivity, when using these antibodies to detect their respective proteins co-precipitated by YFP-UMAD1 (Figure 28).

The intrinsic TSG101 steadiness box mechanism to control protein levels[669,672], can be clearly seen for blotting using α-TSG101: in the case of the input sample for YFP-TSG101 expressing cells, YFP-TSG101 expression without any endogenous expression is seen. In other words, the overexpression of YFP-TSG101 causes ESCRT-I uncomplexed endogenous TSG101 to be degraded, thus maintaining a constant level of cellular TSG101, hence ESCRT-I expression.

A similar striking observation can be made when examining levels of endogenous VPS37A, B and C proteins in the starting cell lysates (Figure 34. Lanes 2,3 and 4 from the left). It appears that expression of the YFP tagged form of each of these proteins causes a decrease not only in the level of the corresponding endogenous protein, but also in the levels of the other VPS37 paralogues. This suggests that a steadiness box type of mechanism similar to that seen for TSG101 is operating to maintain a constant total cellular level of VPS37 proteins. Given what is known about the steadiness box of TSG101, this is most likely to ensure that any ESCRT-I uncomplexed VPS37 proteins are rapidly degraded. Whilst it could be argued that the decrease in endogenous levels of VPS37 proteins in this experiment could simply be due to less protein in the starting cell lysates, this is highly unlikely given that levels of TSG101 in these input samples are not less than that seen for YFP alone. Since TSG101 levels are finely controlled by its steadiness box, TSG101 levels effectively serve as a loading control.

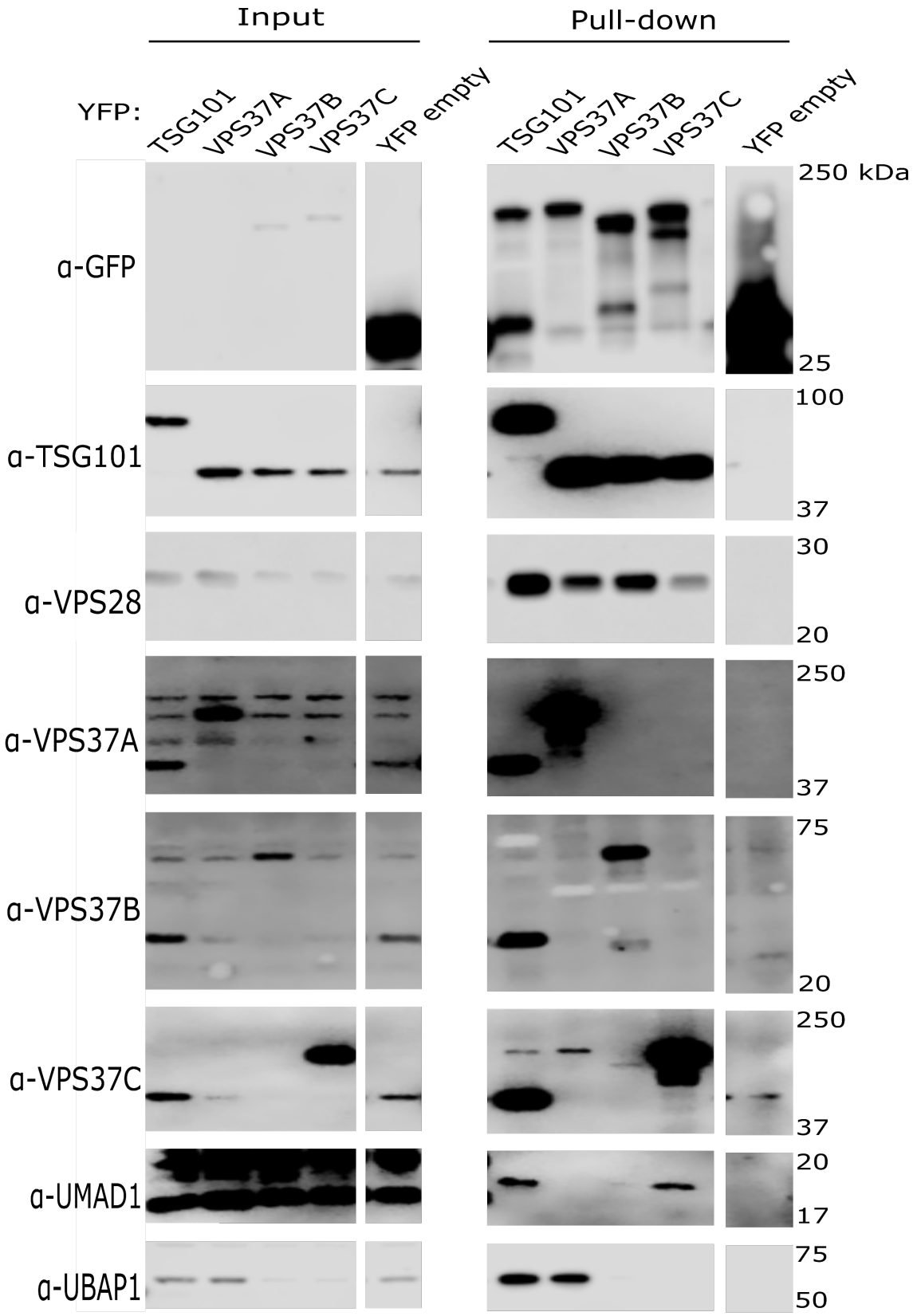

Figure 34. Pairing preference of UMAD1 for VPS37C is confirmed in physiological conditions
Lysates from HeLa cells stably expressing YFP tagged TSG101, VPS37A, VPS37B, VPS37C and YFP alone were purified by incubation with GFP trap beads. 1% cell lysates (input) and 10% bead eluates (pull-down) were resolved by SDS-PAGE and immunoblotting using α-GFP and antibodies against each of the ESCRT proteins shown was performed.

3.2.7. Compositional changes in ESCRT-I subunit stoichiometry

Results so far show preferential pairing with VPS37B and VPS37C, with a clear preference for VPS37C, by ESCRT-I complexes containing UMAD1. In order to characterise this further and potentially identify other differences in ESCRT-I stoichiometry and binding partners upon UMAD1 knockout, a further IP-TMT based mass spectrometry experiment was performed. GFP-trap immunoprecipitations using lysates from both HeLa and HeLaΔUMAD1 cells that stably express YFP-TSG101, together with cells expressing YFP alone as negative controls were performed. As for previous experiments, eluates were then digested with trypsin and prepared for mass spectrometry screening, labelling tryptic peptides from each eluate sample with a different TMT tag.

To determine binding partners specific to TSG101 in both cell backgrounds, a criterion based on the TMT tag reporter ion ratio for YFP-TSG101 to the YFP negative control was introduced. This time, a protein was defined as a specific binding partner if the ratio was ≥3 in either or both HeLa and HeLaΔUMAD1 backgrounds (Appendix 1). ESCRT-I proteins again showed the highest enrichment (Table 3) and all known ESCRT-I subunits, including UMAD1, except VPS37D and MVB12B were identified. Despite again being identified with only 1 peptide, UMAD1 was still identified as a binding partner using the 3-fold cut off value with a value at zero for the HeLaΔUMAD1 YFP-TSG101 repeat.

Following total normalisation of signal values across samples, signal values for the identified ESCRT protein binding partners in both HeLa and HeLaΔUMAD1 backgrounds were each divided by the mean values obtained for the corresponding YFP negative controls (Table 3). These values were further normalised to the levels of TSG101 protein in both backgrounds to facilitate examination of differences in subunit enrichment in the wild type vs UMAD1 knockout background (Figure 35). Results showed very clearly that UMAD1 is behaving as a novel alternative MVB12 subunit that competes with MVB12A and UBAP1 for binding to ESCRT-I, as shown by the obvious increase in signal for UBAP1 and MVB12A in the HeLaΔUMAD1 background compared to the HeLa background. Whilst signal for VPS37B remained relatively constant in both backgrounds, there was a slight decrease seen for VPS37C in the UMAD1 knockout background, consistent with the pairing preference of UMAD1 for VPS37C: presumably if UMAD1 is

knocked out, slightly less VPS37C binds ESCRT-I. VPS37A signal shows an increase in the UMAD1 knockout background because of increased binding of UBAP1, with which it specifically pairs. CEP55 shows a decrease in the HeLaΔUMAD1 background, potentially implicating UMAD1 in cytokinetic abscission. CEP55 is also actually listed as a potential interaction partner for UMAD1 on BioGRID3.5, from data obtained from a next generation interaction survey performed by Hein et al., 2015[693]. Surprisingly, VPS28 also shows an obvious decrease in the HeLaΔUMAD1 background. This is a surprising result given that incorporation of VPS28 into ESCRT-I has so far been described to be mediated primarily through its interaction with TSG101, with very little, if any, interaction with the other subunits[53,70,657,665–667].

Protein identity	HeLa YFP-TSG101/ HeLa YFP control	HeLa ΔUMAD1 YFP-TSG101/ HeLaΔYFP control
VPS37C	25.36952829	16.79412626
UMAD1	3.146558651	0
CEP55	4.315614564	2.345728325
VPS37A	18.66991004	42.62412162
TSG101	15.57974527	20.97823167
VPS37B	26.32217139	33.12642093
VPS28	26.54399472	9.89567091
UBAP1	44.47540609	126.0774306
MVB12A	18.60124359	55.16615724

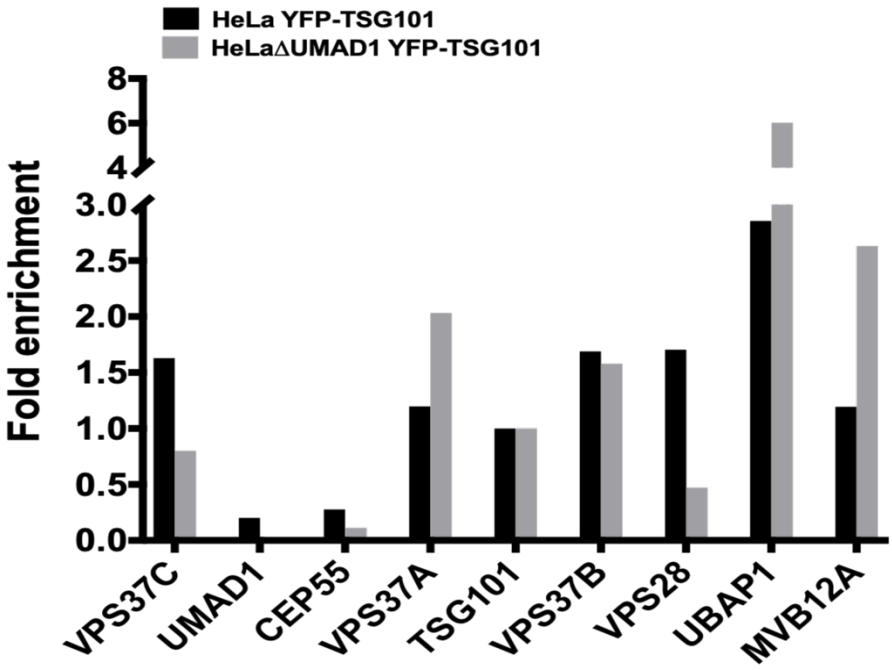

Table 3. Mass spectrometry determination of differences in ESCRT-I subunit enrichment when co-precipitated by YFP-TSG101 in HeLa and HeLaΔUMAD1 backgrounds
GFP trap immunoprecipitations using YFP-TSG101, in both a Hela and HeLaΔUMAD1 background, and together with appropriate YFP negative controls were performed. Eluates were analysed by multiplex IP-TMT based mass spectrometry following digestion with trypsin and isobaric TMT tag labelling. Following total normalisation of signal values across all 10 samples to eliminate variation in signal at the level of sample preparation and data acquisition, signal values for YFP-TSG101/YFP control were calculated for both HeLa and HeLaΔUMAD1 backgrounds.

Figure 35. Enrichment of ESCRT-I subunits is consistent with the identity of UMAD1 as a novel alternative MVB12 type subunit that pairs with VPS37B and VPS37C
A. Side by side comparison of fold enrichment of ESCRT-I proteins and CEP55 identified by multiplex IP-TMT based mass spectrometry using YFP-TSG101 as the bait protein in both a wild type HeLa and UMAD1 knockout background. Fold enrichment is calculated using the signal values presented in table 3 normalised to TSG101, given that this is the core ESCRT-I subunit present in all ESCRT-I complexes.

3.2.8. Further characterisation of affinity purified UMAD1 interaction partners

A further IP-TMT based mass spectrometry screen was performed with the aim of identifying further interaction partners for UMAD1 and confirming its interaction with ESCRT-I and pairing specificity with VPS37B and VPS37C. HeLaΔUMAD1 and 293TΔUMAD1 cells that stably re-express UMAD1 as YFP-UMAD1 were made in preparation for initial GFP-trap immunoprecipitations using YFP-UMAD1 as bait. Use of such cells ensures that only YFP-UMAD1 bait protein is expressed, with no interference from endogenous UMAD1. Two repeats of immunoprecipitations using lysates from both HeLaΔUMAD1 YFP-UMAD1 and 293TΔUMAD1 YFP-UMAD1 cells were performed, and eluates from each repeat, together with those from appropriate HeLaΔUMAD1 YFP and 293TΔUMAD1 YFP negative controls, were labelled using a different TMT tag.

To determine binding partners specific to UMAD1, a criterion based on the TMT tag reporter ion ratio for YFP-UMAD1 to YFP control was introduced. Following processing of the raw mass spectrometry data, including optimisation of the cut-off value relative to the YFP control, a protein was defined as a specific binding partner in this experiment if the ratio is ≥2 for both replicates using both HeLa and 293T cell lines. Using this cut-off, 24 proteins, including the UMAD1 bait, remained (Table 4). Results matched extremely well with previous findings regarding subunit pairing, showing identification of VPS37B and VPS37C but not VPS37A. As expected MVB12A and UBAP1 were not

identified, as they are outcompeted by UMAD1. TSG101, VPS28 and CEP55 were also identified. These expected binding partners showed the highest number of peptide spectrum matches (PSM) with good protein coverage and signal compared to controls. Once again, VPS37D was not identified at all in the screen, further confirming that this paralogue is either not expressed in HeLa and 293T cells or expressed at negligible levels. Aside from the expected ESCRT proteins, 8 of the 24 proteins were mitochondrial membrane carrier or transport proteins, involved in the transport of a variety of proteins, peptides, amino acids, small molecules and other metabolic intermediates across the inner or outer mitochondrial membrane (Table 4). The five mitochondrial carrier proteins (SLC25A6, SLC25A13, SLC25A3, SLC25A12 and SLC25A1) all belong to the same family of solute carriers, that typically catalyse the exchange of one molecule for another across the inner mitochondrial membrane and share a similar set of three tandem repeats of a SOLCAR domain, each consisting of approximately 100 residues which form two transmembrane regions.

Accession	Description	Coverage [%]	# Peptides	# PSMs	# Unique Peptides	# Protein Groups	Score Mascot	Score Sequest HT
Q99816	Tumor susceptibility gene 101 protein OS=Homo sapiens OX=9606 GN=TSG101 PE=1 SV=2	61	26	76	26	1	483	96.94
Q9H9H4	Vacuolar protein sorting-associated protein 37B OS=Homo sapiens OX=9606 GN=VPS37B PE=1 SV=1	72	15	35	15	1	372	53.53
Q9UK41	Vacuolar protein sorting-associated protein 28 homolog OS=Homo sapiens OX=9606 GN=VPS28 PE=1 SV=1	67	13	31	13	1	381	46.95
Q53EZ4	Centrosomal protein of 55 kDa OS=Homo sapiens OX=9606 GN=CEP55 PE=1 SV=3	30	12	19	12	1	208	20.45
C9J7I0	UBAP1-MVB12-associated (UMA)-domain containing protein 1 OS=Homo sapiens OX=9606 GN=UMAD1 PE=2 SV=2	58	8	40	8	1	675	40.76
A5D8V6	Vacuolar protein sorting-associated protein 37C OS=Homo sapiens OX=9606 GN=VPS37C PE=1 SV=2	27	7	15	7	1	230	24.34
P12236	ADP/ATP translocase 3 OS=Homo sapiens OX=9606 GN=SLC25A6 PE=1 SV=4	45	13	26	5	1	170	31.44
P46782	40S ribosomal protein S5 OS=Homo sapiens OX=9606 GN=RPS5 PE=1 SV=4	32	10	17	10	1	142	17.17
P08195	4F2 cell-surface antigen heavy chain OS=Homo sapiens OX=9606 GN=SLC3A2 PE=1 SV=3	14	6	10	6	1	50	8.31
Q9UJS0	Calcium-binding mitochondrial carrier protein Aralar2 OS=Homo sapiens OX=9606 GN=SLC25A13 PE=1 SV=2	13	6	13	4	1	102	15.69
Q92598	Heat shock protein 105 kDa OS=Homo sapiens OX=9606 GN=HSPH1 PE=1 SV=1	8	4	7	4	1	49	10.5
P11802	Cyclin-dependent kinase 4 OS=Homo sapiens OX=9606 GN=CDK4 PE=1 SV=2	17	4	8	3	1	38	7.94
Q9UPN3	Microtubule-actin cross-linking factor 1, isoforms 1/2/3/5 OS=Homo sapiens OX=9606 GN=MACF1 PE=1 SV=4	0	3	6	2	1	32	4.45
Q00325	Phosphate carrier protein, mitochondrial OS=Homo sapiens OX=9606 GN=SLC25A3 PE=1 SV=2	10	3	6	3	1	26	7.38
O75746	Calcium-binding mitochondrial carrier protein Aralar1 OS=Homo sapiens OX=9606 GN=SLC25A12 PE=1 SV=2	7	3	8	1	1	76	9.57
P53007	Tricarboxylate transport protein, mitochondrial OS=Homo sapiens OX=9606 GN=SLC25A1 PE=1 SV=2	6	2	3	2	1	0	3.42
Q9Y277	Voltage-dependent anion-selective channel protein 3 OS=Homo sapiens OX=9606 GN=VDAC3 PE=1 SV=1	8	2	4	2	1	47	1.8
O14980	Exportin-1 OS=Homo sapiens OX=9606 GN=XPO1 PE=1 SV=1	3	2	3	2	1	29	4.48
P42771	Cyclin-dependent kinase inhibitor 2A OS=Homo sapiens OX=9606 GN=CDKN2A PE=1 SV=2	19	2	4	2	1	72	4.93
O14925	Mitochondrial import inner membrane translocase subunit Tim23 OS=Homo sapiens OX=9606 GN=TIMM23 PE=1 SV=	12	2	3	2	1	41	3.15
Q9H9B4	Sideroflexin-1 OS=Homo sapiens OX=9606 GN=SFXN1 PE=1 SV=4	5	1	2	1	1	49	2.83
Q6YN16	Hydroxysteroid dehydrogenase-like protein 2 OS=Homo sapiens OX=9606 GN=HSDL2 PE=1 SV=1	2	1	2	1	1	37	1.89
Q969E2	Secretory carrier-associated membrane protein 4 OS=Homo sapiens OX=9606 GN=SCAMP4 PE=1 SV=1	5	1	2	1	1	24	2.35
O15427	Monocarboxylate transporter 4 OS=Homo sapiens OX=9606 GN=SLC16A3 PE=1 SV=1	2	1	2	1	1	0	2.02

ESCRT-I subunits and CEP55

Mitochondrial membrane carrier/transport proteins

Table 4. Proteins identified as potential UMAD1 interaction partners by IP-TMT based mass spectrometry

Tryptic peptides derived from eluates from two repeats of GFP trap immunoprecipitations using stably re-expressed YFP-UMAD1 as bait in both HeLaΔUMAD1 and 293TΔUMAD1 knockout cell backgrounds were subjected to LC-MS/MS. When a reporter ion ratio of ≥2 was applied for YFP-UMAD1:YFP for both repeats using both cell lines, 24 proteins remained, as shown. Expected binding partners are shown in yellow, placed at the top of the list. All other proteins are ordered according to the number of different tryptic peptides detected (# peptides). The no. of peptide spectrum matches (# PSMs) is nearly always greater than the no. of peptides, as certain peptides are detected more than once. # unique peptides refers to the no. of peptides specific to the particular protein shown and no other.

3.2.9. UMAD1 promotes interaction of ESCRT-I with CEP55

Hierarchical clustering of the 24 proteins identified in the previous section according to protein enrichment and reproducibility across cell types and repeats, revealed all ESCRT-I subunits and CEP55 to form a distinct cluster together, consistent with formation of a complex (Figure 36). Reproducibility across the two HeLaΔUMAD1 cell line repeats was better than across the two 293TΔUMAD1 cell line repeats. More detailed examination of this cluster shows further clustering together of VPS37B and C, with VPS37C above VPS37B, suggesting a higher enrichment of VPS37C, as would be consistent with the previously observed pairing preference (Figures 27A, 27B, 28 and 34). CEP55 and TSG101 also cluster together, consistent with their direct interaction[17,442].

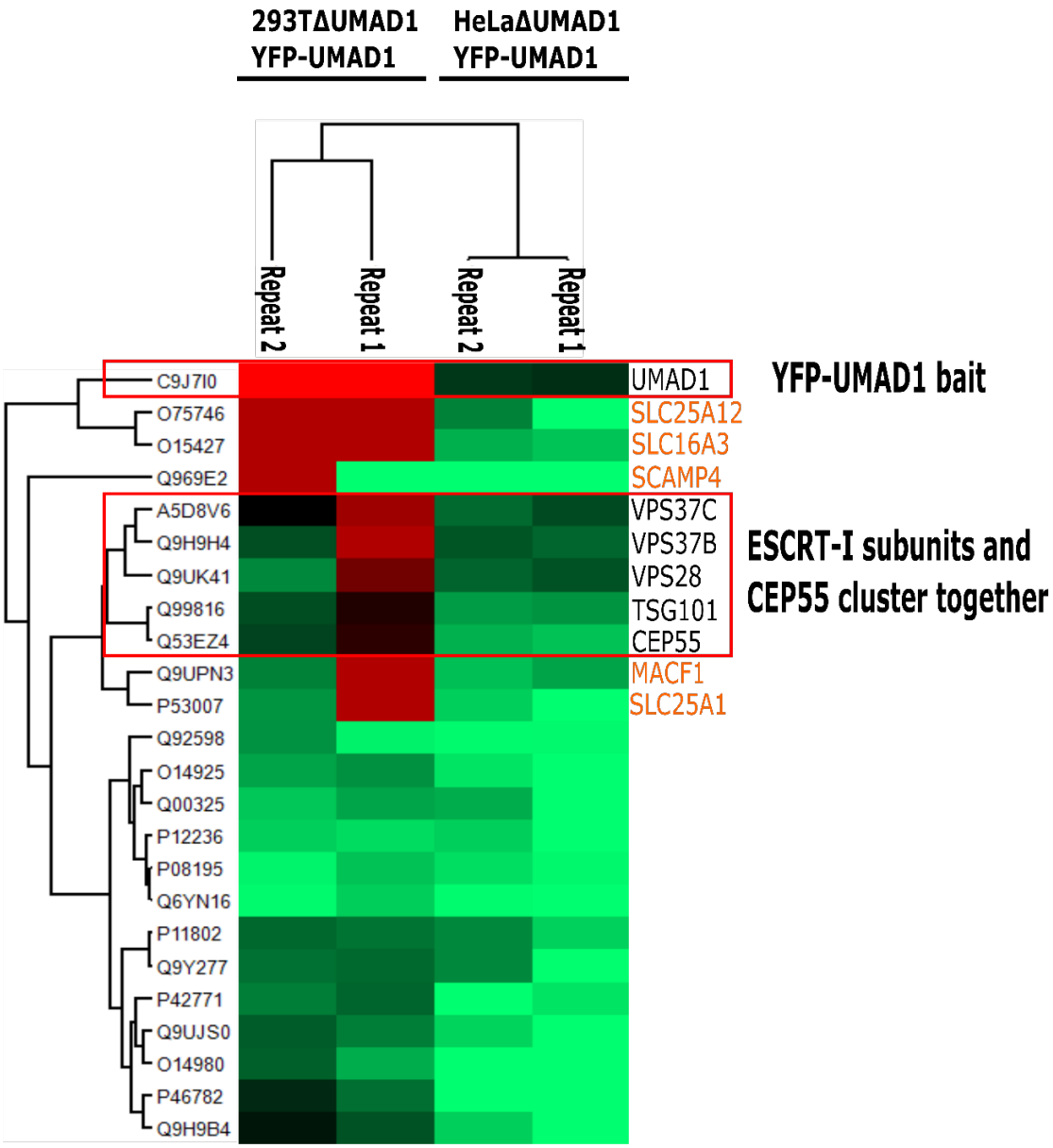

Figure 36. Hierarchical clustering analysis of 24 identified potential UMAD1 interaction partners by IP-TMT based mass spectrometry

Hierarchical clustering was applied to the 24 potential UMAD1 interaction partners identified by IP-TMT based mass spectrometry, ordering proteins according to enrichment and reproducibility across the two cell lines and repeats. ESCRT-I subunits and CEP55 form a distinct cluster, consistent with formation of a complex. Finer details of clustering within this group are also consistent with the CEP55-TSG101 interaction and the subunit pairing preference for VPS37C over VPS37B.

Following up on the observed decrease in co-precipitation of CEP55 by TSG101 in the HeLaΔUMAD1 background, observed by mass spectrometry (Table 3, Figure 35), we decided to repeat this co-precipitation and examine this reduced interaction by immunoblotting with α-CEP55 (Figure 37A). Four repeats of a side by side comparison of CEP55 co-precipitation by stably expressed YFP-TSG101 in HeLa and HeLaΔUMAD1 cells revealed an obvious decrease in the amount of CEP55 co-precipitated in the HeLaΔUMAD1 background compared to the HeLa background, for equal amounts of YFP-TSG101 immunoprecipitation. This matched perfectly with results from table 3 and figure 35.

A further co-precipitation assay using YFP-UMAD1 as the bait protein, stably re-expressed in HeLaΔUMAD1 cells, showed clear co-precipitation of CEP55 (Figure 37B bottom panel). Presumably this interaction occurs via TSG101, which binds directly to CEP55[17,442]. However, a direct interaction between CEP55 and UMAD1 cannot be ruled out either, and future work would involve testing this. These results strongly suggest a role for UMAD1 in ESCRT mediated cytokinetic abscission, potentially by forming a cytokinesis specific ESCRT-I complex in which it facilitates interaction between TSG101 and CEP55.

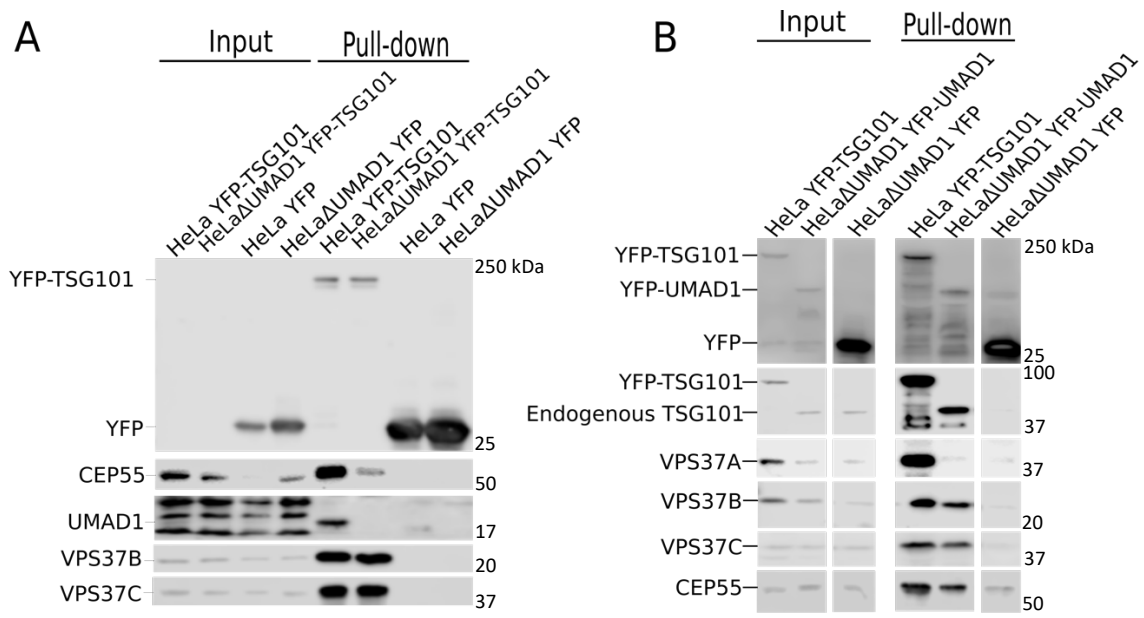

Figure 37. TSG101 shows reduced binding to CEP55 in a HeLaΔUMAD1 background.
A. An immunoprecipitation assay was performed as in A, using lysates from HeLaΔUMAD1 cells that stably re-express YFP-UMAD1 or HeLa cells that express YFP-TSG101/YFP as positive/negative controls respectively. Immunoblotting using α-GFP and antibodies against each of the proteins shown was performed. **B.** Lysates from HeLa or HeLaΔUMAD1 cells that stably express YFP-TSG101, or YFP alone were purified by incubation with GFP trap beads. 1% cell lysates (input) and 10% bead eluates (pull-down) were resolved by SDS-PAGE and immunoblotting using α-GFP and antibodies against each of the proteins shown was performed.

3.3. Discussion

In this chapter, I have presented strong evidence in the form of co-precipitation assays, mass spectrometry and a viral trans-complementation assay that UMAD1 is a genuinely expressed novel alternative MVB12 type subunit of ESCRT-I, that forms a functional ESCRT-I complex. UMAD1 pairs specifically with VPS37B and C with a preference for VPS37C, and its absence leads to reduced binding of TSG101 to CEP55. A picture for mammalian ESCRT-I subunit composition is starting to emerge, involving a combination of both stochastic and selective subunit pairing. Whilst there is strong evidence for selective preferred pairing of VPS37A with UBAP1[196,681], the preference of UMAD1 for pairing with VPS37C represents the second example of selective MVB12-VPS37 pairing, although binding to VPS37B is also observed. Although preferential pairing with VPS37C is clear from the experiments presented in this chapter, the ability of UMAD1 to also pair with VPS37B to a certain extent could exist to ensure that UMAD1 containing ESCRT-I complexes are still formed in tissues expressing low levels of VPS37C. Fine tuning of

VPS37B:VPS37C expression level ratios could also possibly act to determine the level of UMAD1 containing ESCRT-I formation in different cell types to accommodate specific functions.

Whilst VPS37A has been shown to preferentially pair with UBAP1 to form a specific ESCRT-I complex that is highly adapted for lysosomal sorting of ubiquitinated cargo, preferred pairing of the other VPS37 subunits with other MVB12-like subunits has not been seen until now. By analogy to ESCRT-I complexes that contain VPS37A with UBAP1, it is tempting to speculate that complexes containing UMAD1 with VPS37C could be involved in another specific ESCRT mediated process. Since UMAD1 also binds to VPS37B, however, like MVB12A and MVB12B[667,681], some redundancy in regard to function between UMAD1, MVB12A and MVB12B may exist, so future functional studies should involve examining the effects of co-depletion of pairs or all three MVB12A, MVB12B and UMAD1 subunits in addition to depletion of each individually. The UMAD1 CRISPR/Cas9 knockout cells generated in this chapter will be an invaluable tool for this, given that total abolishment of UMAD1 expression has extremely likely been achieved, thus removing the possibility of effects maintained by any residual UMAD1 expression that may be been using RNAi depletion. It should be remembered, however, that cells often adapt, displaying compensatory effects, when expression of a particular protein is knocked out. The UMAD1 knockout cells generated in this chapter were regularly checked for absence of the *UMAD1* locus by PCR, and absence of protein expression by lack of co-precipitation using YFP-TSG101. However, as presented in the following chapter, a possible compensatory effect manifested by increased ALIX expression in the UMAD1 knockout cells is observed (sections 4.2.3. and 4.2.4.). Future work should also involve generation of MVB12A and MVB12B CRISPR knockout cells, to be similarly tested side by side in functional studies if these cells are viable. Co-precipitation assays such as that presented in Figure 37A could also be performed using lysates from such knockout cells to investigate whether depletion of MVB12A and MVB12B also reduce binding of TSG101 to CEP55, or whether this is UMAD1 specific.

I have shown that UMAD1 binds ESCRT-I via a $V_{89}P_{90}F_{91}$ motif at the start of its UMA domain which is conserved with all other MVB12 proteins (Figure 29). This motif appears to be both necessary and sufficient for binding using overexpressed tagged ESCRT-I subunits. Although residues outside this VPF motif have been found to be important for

ESCRT-I binding in other MVB12-like proteins[196,658,667], mutations at the equivalent positions in UMAD1 (P108A and E130A, which is the UMA domain conserved C-terminal signature glutamate residue) did not disrupt binding of UMAD1 to ESCRT-I. It is possible that these residues are important for binding but are "accessory/secondary" binding sites and our experimental approach using overexpressed proteins masks the importance of interactions that are not as strong as that mediated by $V_{89}P_{90}F_{91}$, but still contribute to incorporation of UMAD1 into ESCRT-I. This is further suggested by the observation that the E130A mutant shows reduced binding to ESCRT-I, using this system. Further work should therefore involve testing the ability of these mutants to co-precipitate endogenous ESCRT-I, in co-precipitation assays such as those shown in figure 28 and 37B: immunoprecipitations using lysates from cells that stably express these YFP tagged mutants should be performed followed by blotting to detect endogenous ESCRT-I subunits. If P108A and E130A are found in these assays to be important for the incorporation of UMAD1 into ESCRT-I, it is likely that loss of binding mediated by these residues was previously masked by overexpression of the other ESCRT-I subunits. Alternatively, if these residues are genuinely found to be less crucial for incorporation of UMAD1 into ESCRT-I, it is likely that due to UMA domain structural differences in each of the MVB12-like subunits, these residues are more crucial for optimal interaction with ESCRT-I in the case of MVB12A, MVB12B and UBAP1. Perhaps binding via the VPF motif is enhanced in these subunits by additional VPS37B/VPS37C Mod(r) – TSG101 dimer contacts mediated by these residues.

Co-precipitation assays have shown that TSG101 appears to bind less well to CEP55 in the absence of UMAD1, and this has been reinforced by mass spectrometry experiments. The mechanism by which UMAD1 strengthens interaction of TSG101 with CEP55 remains to be elucidated. Two possibilities are that it either directly contributes to the interaction by providing a binding surface together with TSG101, or that it simply stabilises a cytokinesis specific ESCRT-I complex or promotes structural changes in TSG101 that favour its direct interaction with CEP55. Although a complete mammalian ESCRT-I structure is yet to be solved, structural information would also help clarify the relationship between UMAD1 with CEP55, and the reason for the pairing preference with VPS37C over VPS37B. Along these lines, another unanswered question is what the N-terminal ~85 residues of UMAD1, upstream of the UMA domain is for. Structural

information would help show whether this region, predicted to be largely unstructured, becomes more structured or stabilises interactions such as those with CEP55 or VPS37B/VPS37C-TSG101 dimers upon binding ESCRT-I. In the absence of a structure, further co-precipitation assays could also be performed to investigate this issue by side by side testing the ability of full-length UMAD1 and the UMA domain alone to co-precipitate CEP55 and each of the VPS37 proteins. Since a helical region downstream of the UMA domain in UBAP1 has been shown to confer specificity of binding to VPS37A, specifically by preventing binding of VPS37B and C[681], it follows that UMAD1, and MVB12A and B, most probably possess regions that prevent pairing with VPS37A. It is also worth noting that helical regions are predicted to exist either side of the $V_{89}P_{90}F_{91}$ motif in UMAD1, which are not predicted to occur in any of the other MVB12 proteins and are instead replaced by a short beta strand overlapping and extending just downstream of the VPF motif. It is therefore possible that such helical regions in UMAD1 could be involved in conferring specific interaction preferences or functions, and fragments encompassing these regions should be tested in co-precipitation assays.

My results suggest that the endogenous levels of VPS37 proteins are tightly regulated in cells. The mechanism similar to that of the steadiness box in TSG101, that appears to be controlling the total levels of VPS37 proteins further reinforces what is known about the inter-dependability of ESCRT-I subunits for stability[666], and further adds to the notion that subunits show precise levels of control at a post-translational level[669,672,694]. It is likely that specific ubiquitin ligases exist to ubiquitinate and target uncomplexed VPS37 proteins for degradation. By analogy to TSG101, perhaps sites of ubiquitination are located within the Mod(r) domains of VPS37 proteins which are occluded when this region binds to the rest of ESCRT-I. To investigate whether targeted proteosomal degradation by ubiquitination is regulating VPS37 levels, side by side transfections of cells with YFP-tagged VPS37 proteins with and without treatment with a proteasome inhibitor could be performed. If ubiquitination is necessary for steady state regulation, cells treated with the proteasome inhibitor would be expected not to lose expression of endogenous VPS37s upon transfection of increasing amounts of the YFP-tagged proteins.

The striking difference in enrichment of ESCRT-I proteins compared to other potential interaction partners identified in the mass spectrometry screens in this chapter suggests that genuine ESCRT-I binding partners other than its own subunits bind with a much

lower affinity or transiently. Perhaps a co-precipitation assay more suited to identification of weak interaction partners, such as BioID[695] would facilitate identification of weaker interaction partners such as potential ubiquitin ligases necessary for controlling the levels of VPS37 proteins.

Our mass spectrometry studies of affinity purified UMAD1 containing complexes have revealed a number of mitochondrial proteins identified as potential UMAD1 binding partners. We can speculate from this that perhaps UMAD1 could be involved in mitochondrial clearance. Damaged mitochondria must be promptly degraded to prevent their cytotoxicity leading to cell death. A number of pathways for mitochondrial clearance have been elucidated, most notably autophagy (mitophagy) regulated by Parkin – a ubiquitin ligase that marks damaged mitochondria for degradation. More recently, a Parkin mediated autophagy independent pathway for mitochondrial clearance has been described, in which damaged mitochondria are sequestered into Rab5 positive vesicles by the ESCRT machinery and later delivered to lysosomes for degradation[696,697]. Whether UMAD1 contributes to this pathway can be tested by comparing cell death in HeLa and HeLaΔUMAD1 cells following treatment with trifluoromethoxy carbonyl cyanide phenylhydrazone (FCCP) to depolarise mitochondria and stimulate their clearance. An increase in cell death due to accumulation of damaged mitochondria in HeLaΔUMAD1 cells would suggest a role for UMAD1 in clearance. HeLaΔUMAD1 cells would be expected to display a slower rate of mitochondrial clearance, hence mitochondrial proteins, over time following FCCP treatment. This could be measured by Western blotting.

Chapter 4 – UMAD1 in cytokinesis

4.1. Introduction

CEP55 represents the site-specific adaptor protein that recruits the ESCRT machinery to the midbody upon mitotic exit to function in cytokinetic abscission. This is mediated a direct interaction with either TSG101 or ALIX at the 'hinge' region of CEP55[17,442,451]. Initial testing of cytokinetic defects upon depletion of TSG101 or ALIX, by scoring of multinucleation showed the increase in multinucleation to be much greater upon depletion of ALIX than TSG101. Multinucleation levels could show as much as a >30-fold increase in the case of ALIX depletion, compared to around a 5-fold increase in the case of TSG101 depletion[17,442]. Furthermore, depletion of ESCRT-II appeared to show only very minor increases in cytokinetic defects[17,55,167,252]. Details of the exact pathways contributing to the recruitment of ESCRT-III were therefore further probed in a study by Christ et al 2016, through a series of more specific microscopy experiments to examine both CHMP4B recruitment to the midbody, and the time taken for abscission to occur upon knockdown of various ESCRT components[93].

The appearance of CHMP4B at the midbody was unperturbed upon single depletion of either TSG101 or ALIX but disappeared upon depletion of TSG101 in a CHMP4BΔALIX binding site background. Although localisation of CHMP4B to the midbody was unperturbed, further probing showed that depletion of ALIX or TSG101 displayed a delay in CHMP4B recruitment to the midbody, both by around 35 minutes. These initial experiments suggested overlapping roles for TSG101 and ALIX in CHMP4B recruitment. Experiments to examine effects on successful abscission timing revealed a delay in the time taken for midbody resolution upon TSG101 depletion, from approximately 74 minutes in wild type cells to 98 minutes upon TSG101 depletion, an even greater increase in the case of ALIX depletion to around 177 minutes. A synergistic increase upon depletion of both TSG101 and ALIX to around 338 minutes was observed. This suggested that TSG101 and ALIX constitute parts of two parallel pathways leading to abscission. Effects on abscission time were correlated with CHMP4B recruitment by the observation that TSG101 depletion in a CHMP4BΔALIX binding site background showed a much more pronounced increase in abscission time than in a wild type CHMP4B background.

Importantly, the effects of ESCRT-II depletion were re-visited in this study[93]. It was found that whilst wild type siRNA resistant VPS28 was able to rescue a slight delay in abscission seen upon depletion of endogenous VPS28, a rescue was not seen upon expression of truncated VPS28 that lacked the C-terminus, responsible for binding EAP45 (ESCRT-II) and CHMP6, or a mutant in which just the residues responsible for CHMP6 binding were mutated. CHMP6 localisation to the midbody was also not observed in the context of these mutant VPS28 constructs, and CHMP4B midbody recruitment was reduced upon co-depletion of ALIX and EAP30 (ESCRT-II). This was rescued upon re-expression of siRNA resistant EAP30. In another study by Goliand et al 2014, EAP45 was suggested to assume a position in between the Flemming body and secondary ingression during late cytokinesis, without ever reaching the secondary ingression like ESCRT-III[698]. This is consistent with a role for ESCRT-II in bridging ESCRT-I with ESCRT-III. Taken together, these studies point towards potential contribution of ESCRT-II in ESCRT-III recruitment for cytokinetic abscission, and suggest a model for ESCRT-III recruitment involving two partially redundant pathways that both contribute to ESCRT-III recruitment: A CEP55 – TSG101 (ESCRT-I) – ESCRT-II – CHMP6 – ESCRT-III branch and a CEP55 – ALIX – ESCRT-III branch (Figure 38). The above study by Christ et al 2016 also suggests interaction between VPS28 (ESCRT-I) and CHMP6 to contribute to abscission via a CEP55 – ESCRT-I – ESCRT-III pathway, bypassing ESCRT-II[93].

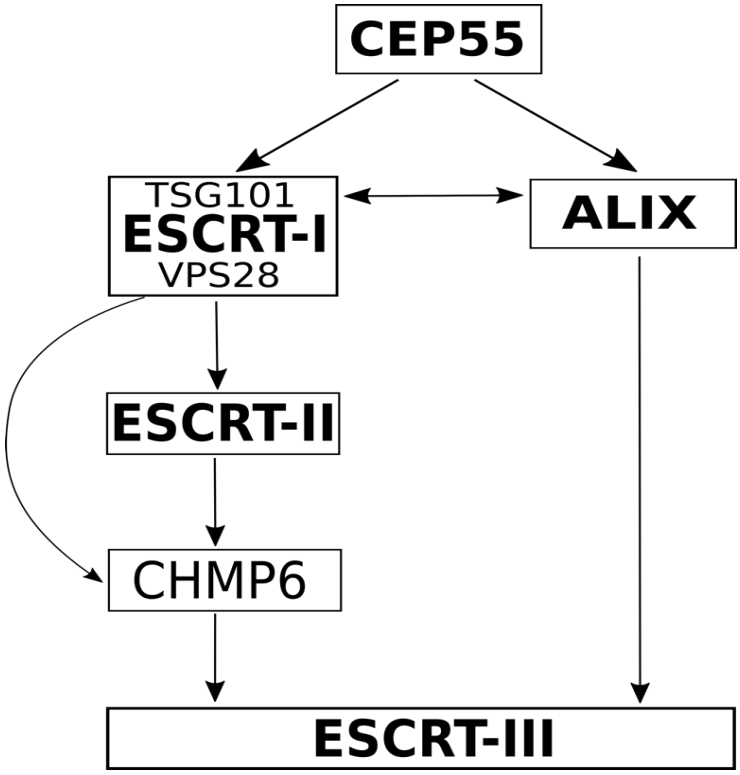

Figure 38. Proposed parallel arms of recruitment for ESCRT-III in cytokinetic abscission
ESCRT-III recruitment has been proposed by Christ et al 2016 to occur via two partially redundant parallel arms of recruitment involving a direct interaction between ALIX with CEP55 and CHMP4 proteins (ESCRT-III), or an interaction between CEP55 with TSG101, hence ESCRT-I, which then recruits ESCRT-II and CHMP6, which is able to nucleate ESCRT-III filament polymerisation. As part of the latter branch of recruitment, experiments using a re-expressed VPS28 mutant in which residues that disrupt CHMP6 binding were mutated (F206A D207S E209A), showed failure to rescue an observed delay in abscission seen upon endogenous VPS28 depletion. This mutant also displayed impairment of CHMP6 to the midbody. These results suggest the direct interaction between VPS28 and CHMP6 contributes to ESCRT-III recruitment and abscission. In addition to this model, work by Carlton et al. 2008 suggested that interaction between TSG101 and ALIX contributed to cytokinesis, as shown by the failure to rescue cytokinetic defects caused by endogenous ALIX depletion upon re-expression of ALIX with its TSG101 binding sites (^{717}PSAP^{720} and ^{852}PSYP^{855}) mutated. Direct effects on abscission, however, have not been investigated here.

Aside differences in binding partners described for TSG101 and ALIX that play roles in more upstream processes in cytokinesis (Section 1.5.6.), another reason for lack of complete redundancy between these proteins in abscission could be related to the interaction between them (Sections 3.1.1. and 1.3.5.2.). An earlier study by Carlton et al. 2008 of the roles for TSG101 and ALIX in cytokinesis suggested that the interaction between TSG101 and ALIX did somewhat contribute to cytokinesis[55]. This was

demonstrated by the incomplete ability of an ALIX construct in which its TSG101 binding ^{717}PSAP^{720} and ^{852}PSYP^{855} motifs were mutated to rescue cytokinetic defects seen upon endogenous ALIX depletion. In this way, TSG101 has additionally been proposed to play a role in the stabilisation of ALIX during cytokinesis. Along the same lines, another study by Okumura et al. 2013 showed the calcium binding protein ALG-2 to mediate a potential bridging interaction between TSG101 and ALIX[674]. ALG-2 is a homodimer, each monomer of which contains hydrophobic pockets capable of interacting with the PRR regions of TSG101 or ALIX in a calcium dependent manner, thus bridging these proteins[674–676]. Interestingly, this study also showed that VPS37B and VPS37C PRRs also interacted with ALG-2, more strongly than TSG101, and that even in the presence of the calcium chelating agent EGTA, some interaction with VPS37B and VPS37C was still seen[674]. As further discussed later in 'General discussion and future work', a potential parallel can be seen here with UMAD1, which specifically pairs with VPS37B and VPS37C and plays a role in cytokinesis as presented in this chapter.

4.2. Results

4.2.1. HeLaΔUMAD1 cells show a growth defect and increase in multinucleation

Experience passaging HeLaΔUMAD1 cells revealed noticeably slower growth compared to wild type, parental HeLa cells. We decided to compare the rate of cell growth of HeLaΔUMAD1 cells with that of wild type HeLa cells. To investigate this, a clonogenic assay was performed, in which an equal number of both HeLa and HeLaΔUMAD1 cells were plated and left to grow for 10 days, following which staining with crystal violet was performed and the area occupied by colonies on the base of wells was measured (Figure 39A). This assay allows quantification of cell growth based on the principle that single cells grow to form colonies, the size of which, after 10 days, will depend on their growth rate. HeLaΔUMAD1 cells displayed close to 4-fold less growth than wild type HeLa cells. Following the observation of reduced binding of CEP55 to TSG101 in the UMAD1 knockout background (Figure 37A) we hypothesised that, although unlikely to be the major contributor to defective cell growth of this scale, such defects could also, at least in part, be due to problems with cell division: CEP55 is the upstream adaptor required for recruitment of the ESCRT machinery to the midbody to function in abscission. In order to initially examine a more direct effect of UMAD1 on cytokinesis, HeLa cells and HeLaΔUMAD1 cells were plated and fixed on coverslips. Following staining with Hoechst, to visualise nuclei, and α-tubulin antibody, to visualise the cytoskeleton, cytokinetic defects were measured by scoring the number of cells with more than one nucleus and the number of midbody connected cells. Multinucleated cells form upon furrow regression. They can result from cytokinesis failure at both an early stage, such as during furrow ingression or midbody stabilisation, or a later stage such as abscission, following a prolonged period of daughter cell connection by midbodies. An increase in midbody connected cells is therefore indicative of a late stage phenotype, closer to abscission. HeLaΔUMAD1 cells displayed on average just over a 2-fold increase in multinucleated cells compared to wild type HeLa cells (Figure 39B/C). Experiments using siRNA to deplete UMAD1 did not display the same growth defect or increase in multinucleation (Appendix 1). However due to the lack of an antibody able to detect endogenous levels of UMAD1 expression, the efficiency of protein depletion could not be reliably tested,

and the lack of a phenotype seen in these experiments could be due to some residual UMAD1 expression that would be enough to prevent appearance of such phenotypes. Furthermore, the clonogenic assay was performed using only one dose of siRNA, which might not have depleted UMAD1 expression to the extent required to observe the growth defect. The reason for transfecting only one dose was to avoid inaccuracy when attempting to re-plate an equal number of cells for each condition following a further trypsinisation and siRNA transfection: cell counting using such a small volume of cells, from wells of a 24 well plate, would have been difficult and innacurate.

Examination of stably expressed YFP-UMAD1 localisation in fixed cells shows diffuse localisation throughout the cytoplasm, however midbody localisation in a pattern similar to that of TSG101 is observed: YFP-UMAD1 localises to the midbody at a single site at the centre of the Flemming body, as opposed to the concentric rings seen either side of the Flemming body as in the case of ESCRT-III proteins[17](Figure 39D). This localisation is therefore consistent with UMAD1's identity as an ESCRT-I subunit. Taken together these initial experiments are consistent with a potential role for UMAD1 in cytokinetic abscission.

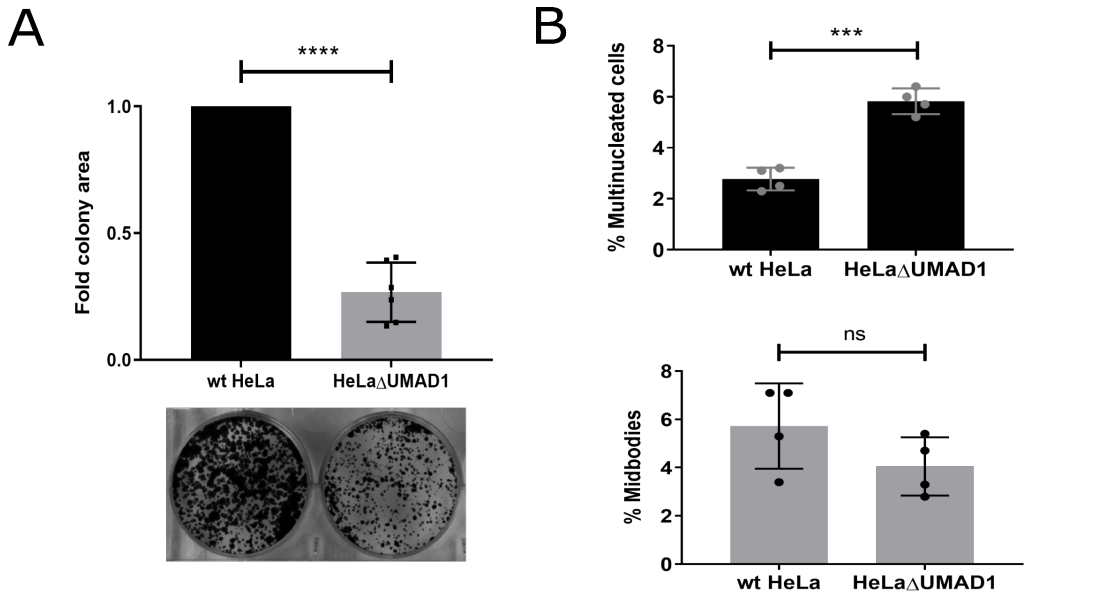
A
****
Fold colony area
1.0
0.5
0.0
wt HeLa
HeLaΔUMAD1
B
***
% Multinucleated cells
8
6
4
2
0
wt HeLa
HeLaΔUMAD1
ns
% Midbodies
8
6
4
2
0
wt HeLa
HeLaΔUMAD1

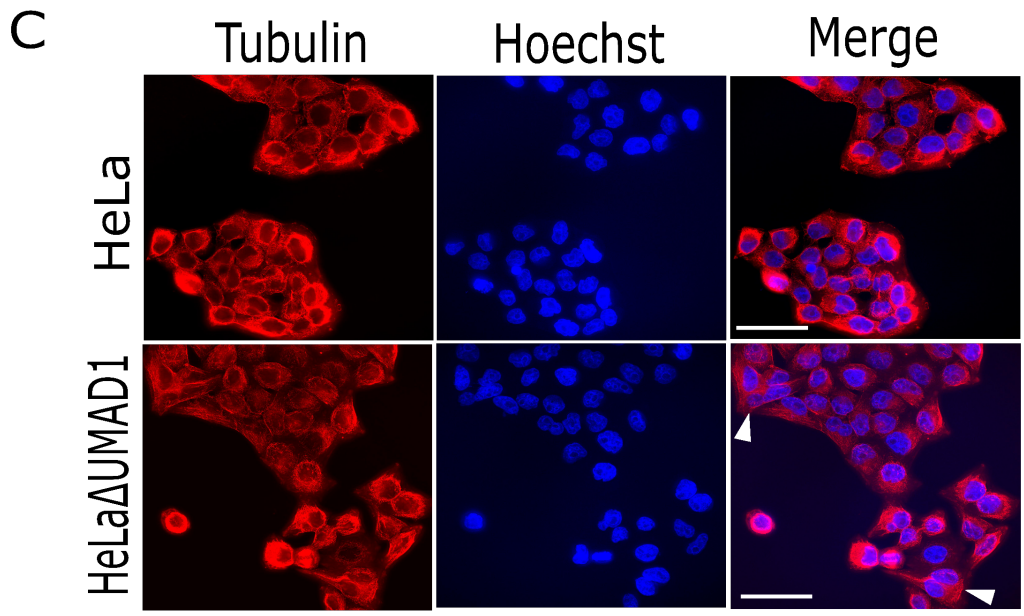
C
Tubulin
Hoechst
Merge
HeLa
HeLaΔUMAD1

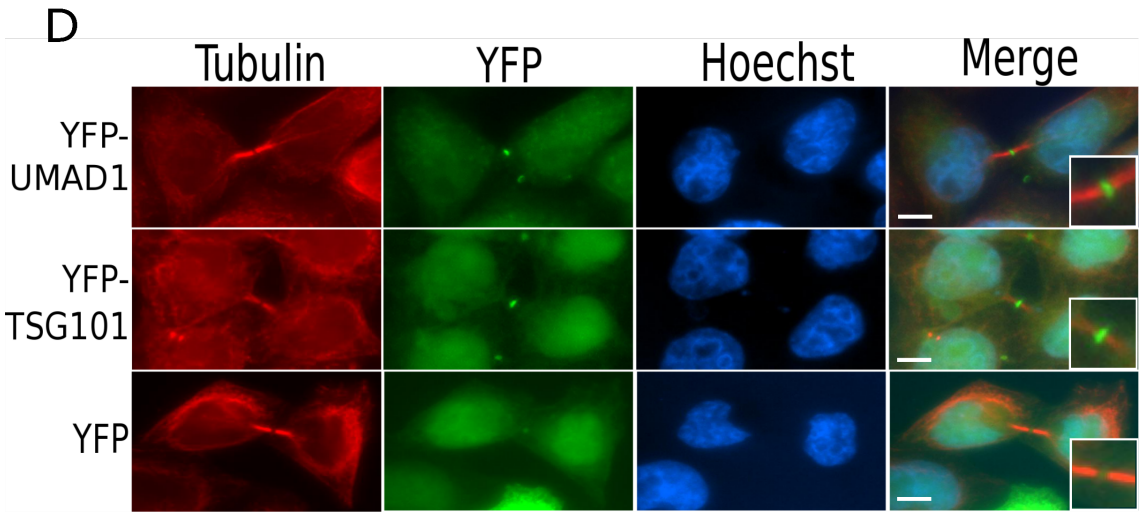
D
Tubulin
YFP
Hoechst
Merge
YFP-UMAD1
YFP-TSG101
YFP

Figure 39. HeLaΔUMAD1 cells show a growth defect and an increase in multinucleation
A. Clonogenic assay using HeLa cells and HeLaΔUMAD1 cells. 3000 HeLa or HeLaΔUMAD1 cells were seeded and resuspended in wells of a 6-well plate. Cell colonies were left to grow, following which colonies were fixed and stained with 0.5% w/v crystal violet in methanol. The area occupied by colonies on the base of each well was then measured. Graph shows the mean number obtained for six independent experimental repeats, and error bars represent the standard deviation from the mean. Values are normalised to those of wild type HeLa cells, set at 1-fold. HeLaΔUMAD1: 0.27±0.12-fold. Unpaired *t* test; ****, P < 0.0001 **B.** Quantification of cytokinetic defects in HeLa and HeLaΔUMAD1 cells. Graph shows the number of fixed cells with more than one nucleus and the number of midbody connected cells. The mean percentages for four independent repeats, with error bars representing the standard deviation from the mean are shown. n > 1200 cells per condition. HeLa multinucleated cells: 2.8±0.4%, HeLa midbodies: 5.7±1.8%, HeLaΔUMAD1 multinucleated cells: 5.8±0.5%, HeLaΔUMAD1 midbodies: 4.1±1.2%. Unpaired *t* test; ***, P = 0.0001. C. Representative images of Hela cells and HeLaΔUMAD1 cells used in B. Red = tubulin, Blue = Hoechst (Nuclei). Arrows indicate multinucleated cells, scale bar = 50μm. **D.** YFP-UMAD1 shows Flemming body localisation. HeLaΔUMAD1 cells that stably re-express YFP-UMAD1 were stained with Hoechst (blue) and α-Tubulin (red) to visualise the nucleus and cytoskeleton respectively, together with YFP-UMAD1 (green). HeLaΔUMAD1 cells expressing YFP-TSG101, or YFP alone were imaged as positive and negative controls, respectively. Scale bar = 10μm. Inset = Midbody

4.2.2. Depletion of VPS37C shows a growth defect and increase in multinucleation similar to HeLaΔUMAD1 cells

Given the pairing preference of UMAD1 for VPS37C, described in the previous chapter, further clonogenic and multinucleation assays were performed to compare cell growth and cytokinetic defects seen upon siRNA mediated depletion of VPS37C with those in HeLaΔUMAD1 cells (Figure 40A/B). Clonogenic assays showed growth of HeLa cells upon depletion of VPS37C to be almost identical to that of HeLaΔUMAD1 cells, with both displaying > 2-fold less growth than HeLa transfected with siNT control siRNA.

Although statistically insignificant, quantification of cytokinetic defects also initially suggested potentially similar levels of multinucleation in HeLaΔUMAD1 cells, with a mean of 7.6% multinucleation, and HeLa cells depleted of VPS37C, with a mean of 8.5% multinucleation compared to HeLa cells transfected with siNT control siRNA, which showed 3.3% multinucleation (Figure 40C/D).

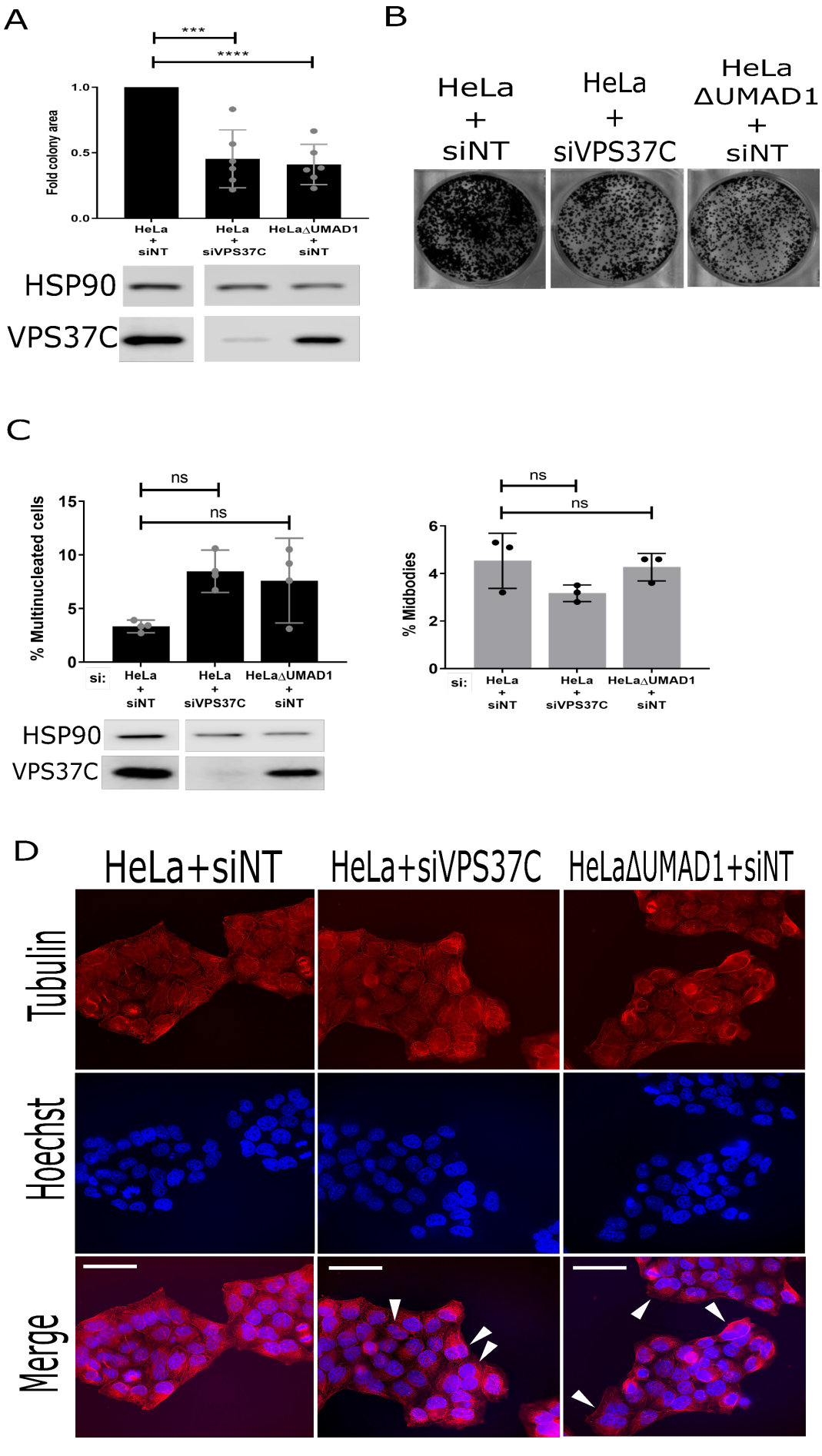
A
***
****
1.0
0.5
0.0
Fold colony area
HeLa + siNT
HeLa + siVPS37C
HeLaΔUMAD1 + siNT
HSP90
VPS37C
B
HeLa + siNT
HeLa + siVPS37C
HeLa ΔUMAD1 + siNT
C
ns
ns
15
10
5
0
% Multinucleated cells
si:
HeLa + siNT
HeLa + siVPS37C
HeLaΔUMAD1 + siNT
HSP90
VPS37C
ns
ns
6
4
2
0
% Midbodies
si:
HeLa + siNT
HeLa + siVPS37C
HeLaΔUMAD1 + siNT
D
HeLa+siNT
HeLa+siVPS37C
HeLaΔUMAD1+siNT
Tubulin
Hoechst
Merge

Figure 40. HeLaΔUMAD1 cells show a growth defect and increase in multinucleation comparable with that seen upon VPS37C depletion.
A. Clonogenic assay to compare cell growth upon siRNA mediated depletion of VPS37C with that of HeLaΔUMAD1 cells. HeLa and HeLaΔUMAD1 cells were transfected with a single dose of each siRNA shown. Cells were diluted 48 hrs later and colonies were left to grow for 10 days in wells of a 6-well plate. The mean area occupied by colonies on the base of each well is shown for 6 independent repeats, normalised to that of HeLa+siNT, set at 1-fold. Error bars represent the standard deviation from the mean. HeLa+siVPS37C: 0.454±0.221-fold, HeLaΔUMAD1+siNT: 0.410±0.153-fold. Unpaired *t* test; ***, P = 0.0001, ****, P < 0.0001 **B.** Representative image of cell colonies from A, fixed and stained with 0.5% w/v crystal violet in methanol following 10 days growth. **C.** Comparison of cytokinetic defects attained upon depletion of VPS37C with those in HeLaΔUMAD1 cells. HeLa cells and HeLaΔUMAD1 cells were transfected with two separate doses of each siRNA indicated. Following fixation and staining, the number of cells with more than one nucleus and the number of midbody connected cells were scored. The mean percentages for three independent experimental repeats are shown, with error bars representing the standard deviation from the mean. n > 900 cells per condition. HeLa+siNT: 3.3±0.6% multinucleated cells, 4.5±1.2% midbodies, HeLa+siVPS37C: 8.5±2.0% multinucleated cells, 3.2±0.4% midbodies, HeLaΔUMAD1+siNT: 7.6±4.0% multinucleated cells, 4.3±0.6% midbodies. Cell lysates were analysed by immunoblotting using rabbit α-VPS37C and α-HSP90. One-way ANOVA with Tukey's multiple comparisons test; ns, P is not significant. **D.** Representative images of fixed cells used in C. Red = Tubulin, Blue = Hoechst. Arrows indicate multinucleated cells, scale bar = 50μm

4.2.3. Determination of siRNA quantities suitable for a partial depletion of ALIX

ALIX and ESCRT-I have been proposed to constitute two parallel arms of ESCRT-III recruitment during cytokinetic abscission[93]. Interestingly, although statistically insignificant on this occasion, HeLaΔUMAD1 cells appeared to be expressing slightly elevated levels of ALIX compared to wild type HeLa cells (Figure 41A), as determined by immunoblotting using α-HSP90 and α-ALIX on the same membrane, normalising ALIX signal to HSP90 signal. We reasoned that this is likely to be a compensatory effect following depletion of UMAD1, under the hypothesis that UMAD1 contributes to the CEP55 – ESCRT-I – ESCRT-II – CHMP6 – ESCRT-III branch of ESCRT-III recruitment to the midbody whilst CEP55 – ALIX – ESCRT-III forms the second branch. Under this hypothesis and given the weak phenotype for cytokinesis defects upon knockout of UMAD1 alone, we decided to examine the effects of co-depletion of UMAD1 with ALIX.

Given the strength of the phenotype previously reported[17,183,442,699] and observed (Figure 41B) upon siRNA mediated depletion of ALIX using a single dose of 50 pmol, we decided to perform a titration using increasing quantities of siALIX to determine conditions that would lead to a significant increase in cytokinetic defects without reaching maximum levels (Figure 41B/C). This would allow for any synergistic effects of co-depletion of UMAD1 with ALIX to be observed. Given the observed elevation in ALIX

levels in HeLaΔUMAD1 cells, a second reason for performing a titration was to determine two separate quantities of siALIX that could be used side by side in further experiments, choosing the quantities that achieved ALIX depletion to the closest levels in HeLa and HeLaΔUMAD1 cells, in each experimental repeat. We decided to proceed with 5 pmol and 2.5 pmol quantities of siALIX for subsequent experiments.

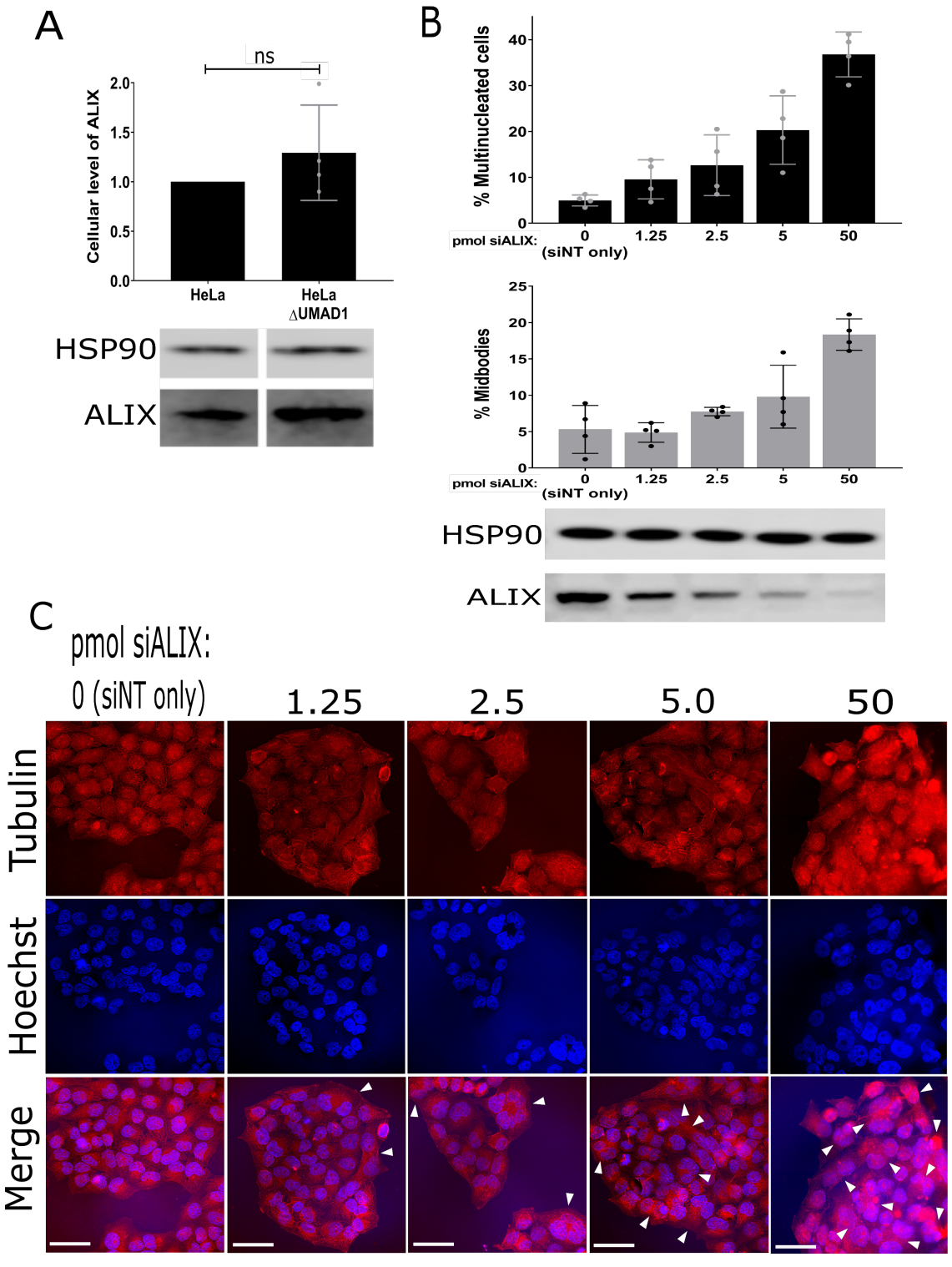

Figure 41. Titration of siRNA against ALIX to determine quantities to use for a suitable partial depletion

A. Quantification of ALIX levels in non-transfected HeLa and HeLaΔUMAD1 cells. Cell lysates from HeLa and HeLaΔUMAD1 cells were resolved by SDS-PAGE and immunoblotting with α-HSP90 and α-ALIX on the same gel was performed. ALIX levels in HeLaΔUMAD1 cells normalised to those in HeLa cells were then quantified according to band intensity. Graph shows the mean and standard deviation for 4 independent repeats. HeLaΔUMAD1 ALIX levels: 1.3±0.5-fold. Unpaired *t* test; ns, P is not significant. **B.** Titration of siALIX in HeLa cells. HeLa cells were transfected with the quantities of siALIX shown, using a single transfection per siALIX quantity. Following fixation and staining, the number of cells with more than one nucleus and the number of midbody connected cells were scored. The mean percentages for 4 independent experimental repeats are shown, with error bars representing the standard deviation from the mean. n > 1200 cells per condition. 0 pmol (siNT only): 5.0±1.2% multinucleated cells, 5.3±3.3% midbodies, 1.25 pmol siALIX: 9.6±4.3% multinucleated cells, 4.9±1.3% midbodies, 2.5 pmol siALIX: 12.6±6.6% multinucleated cells, 7.8±0.6% midbodies, 5 pmol siALIX: 20.3±7.4% multinucleated cells, 9.8±4.3% midbodies, 50 pmol siALIX: 36.8±4.9% multinucleated cells, 18.4±2.2% midbodies. Cell lysates were analysed by immunoblotting using α-HSP90 and α-ALIX. **C.** Representative images of fixed cells used in B. Red = Tubulin, Blue = Hoechst. Arrows indicate multinucleated cells, scale bar = 50μm

As further proof of principle for the use of a partial ALIX depletion under these conditions, before proceeding with experiments in HeLa and HeLaΔUMAD1 cells, an experiment to examine the effects of TSG101 depletion with a 5 pmol siALIX mediated partial depletion of ALIX was performed (Figure 42). Under these conditions, a synergistic increase in the number of multinucleated cells was observed, with a mean of 30.7% multinucleated cells compared to 13.4% in the case of the ALIX partial depletion alone, and 10.2% in the case of TSG101 depletion. This result contrasts with similar experiments using live cells performed by Christ et al. 2016, who concluded that there was no statistically significant increase in the number of cells that underwent multinucleation following depletion of TSG101 with ALIX[93]. These experiments, however, were performed with total depletion of ALIX rather than a partial depletion, suggesting that a synergistic effect was not seen due to reaching saturated levels of cytokinetic defects.

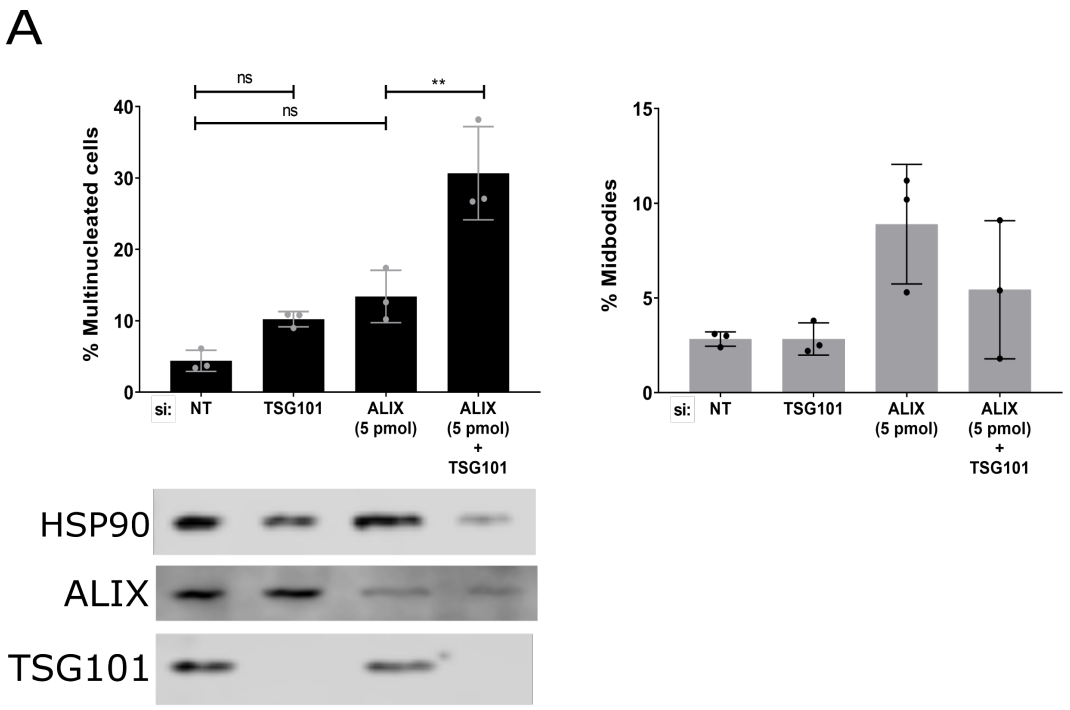
A
ns
ns
**
% Multinucleated cells
40
30
20
10
0
si:
NT
TSG101
ALIX (5 pmol)
ALIX (5 pmol) + TSG101
% Midbodies
15
10
5
0
HSP90
ALIX
TSG101

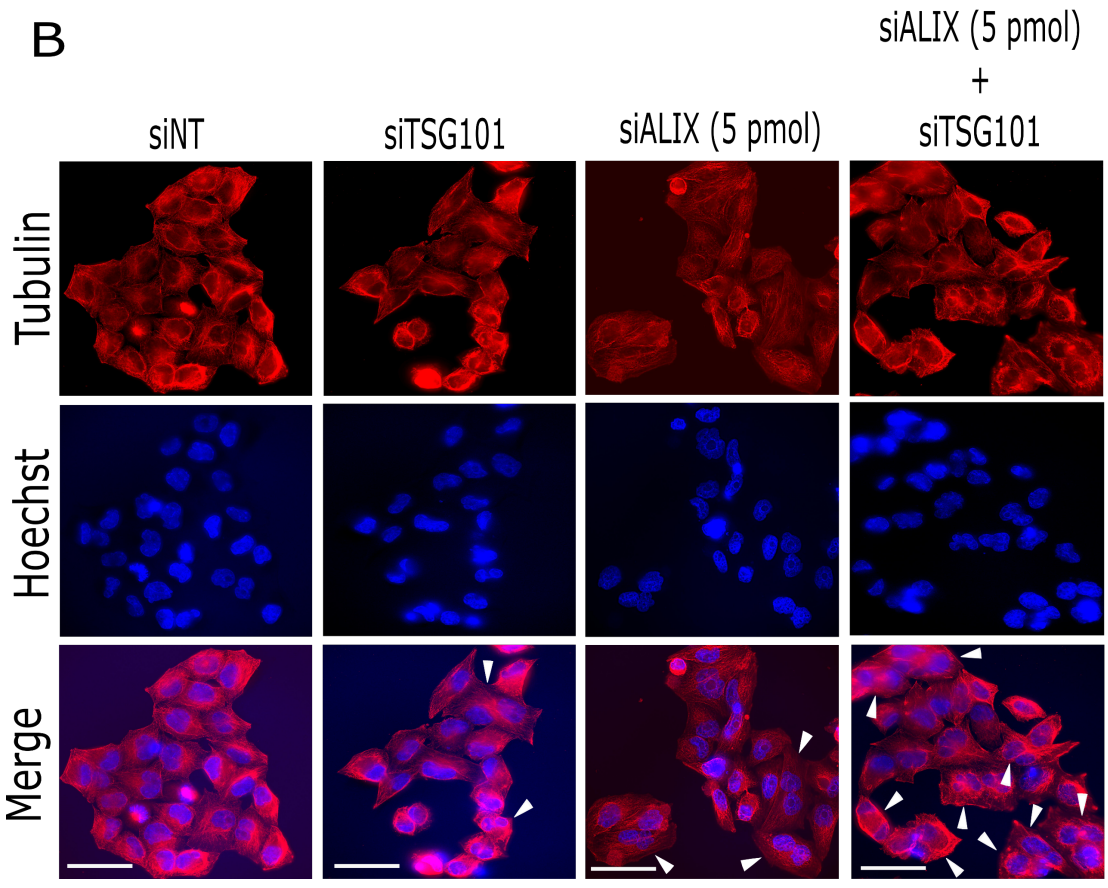
B
siALIX (5 pmol) + siTSG101
siNT
siTSG101
siALIX (5 pmol)
Tubulin
Hoechst
Merge

Figure 42. A synergistic increase in multinucleation is seen upon co-depletion of TSG101 with a partial depletion of ALIX

A. Quantification of cytokinetic defects upon co-depletion of TSG101 with a partial depletion of ALIX. A single transfection of HeLa cells was performed using the siRNA oligonucleotides shown. 50pmol siRNA was used for siNT and siTSG101 whilst 5pmol was used for siALIX, keeping the total volume of siRNA used per condition at 100pmol using siNT. Following fixation and staining, the number of cells with more than one nucleus and the number of midbody connected cells were scored. The mean percentages for 3 independent experimental repeats are shown, with error bars representing the standard deviation from the mean. n > 900 cells per condition. siNT: 4.4±1.5% multinucleated cells, 2.8±0.4% midbodies, siTSG101: 10.2±1.1% multinucleated cells, 2.8±0.9% midbodies, siALIX: 13.4±3.7% multinucleated cells, 8.9±3.2% midbodies, siALIX+siTSG101: 30.7±6.5% multinucleated cells, 5.4±3.7% midbodies. Cell lysates were analysed by immunoblotting using α-HSP90, α-ALIX and α-TSG101. One-way ANOVA with Tukey's multiple comparisons test; ns, P is not significant, **, P < 0.01 **B.** Representative images of fixed cells used in A. Red = Tubulin, Blue = Hoechst. Arrows indicate multinucleated cells, scale bar = 50μm.

4.2.4. Functional synergy between UMAD1 and ALIX in cytokinesis

Having determined suitable quantities of siALIX to use for obtaining a partial depletion of ALIX, the effects on cytokinesis of co-depletion of UMAD1 with ALIX were investigated. HeLaΔUMAD1 cells showed a substantial increase in both the number of multinucleated cells and midbodies, at 26.4% and 9.7% respectively, compared to wild type HeLa cells, at 13.8% and 7.5%, upon depletion of ALIX to approximately 24% of its normal expression level in wild type HeLa cells (Figure 43). This increase in multinucleation is not as strong as that seen upon co-depletion of TSG101 with ALIX (Figure 42A). However, the increases are significant, particularly given that the mean level to which ALIX is depleted for the 4 repeats is extremely close in HeLa and HeLaΔUMAD1 cells, at 24% and 23% respectively (Figure 43C). The elevated level of ALIX expression in HeLaΔUMAD1 cells is also clearer and statistically significant here, displaying a mean of 1.53-fold wild type HeLa levels, and elevated expression seen in all 4 repeats.

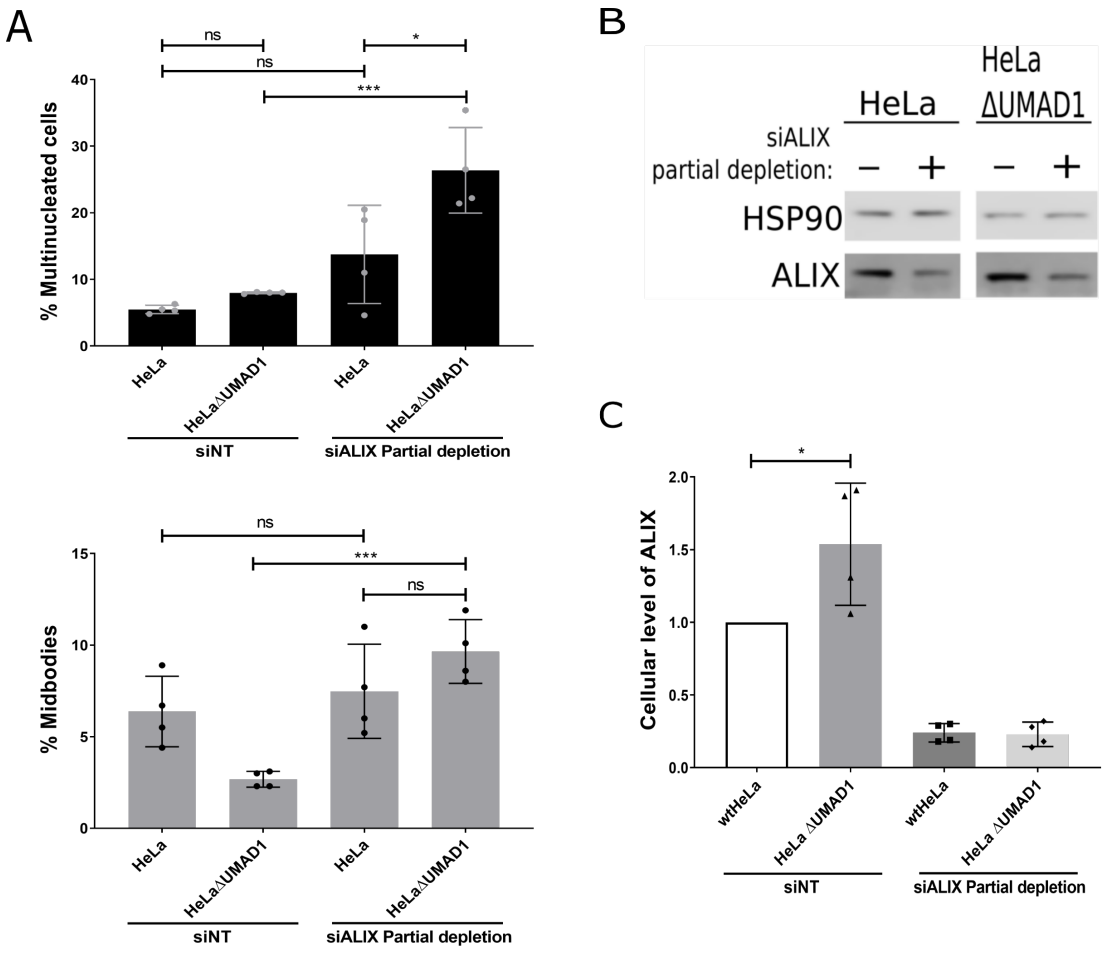
A
ns
ns
*
***
% Multinucleated cells
40
30
20
10
0
HeLa
HeLaΔUMAD1
HeLa
HeLaΔUMAD1
siNT
siALIX Partial depletion
ns
***
ns
% Midbodies
15
10
5
0
HeLa
HeLaΔUMAD1
HeLa
HeLaΔUMAD1
siNT
siALIX Partial depletion
B
HeLa
HeLa ΔUMAD1
siALIX
partial depletion:
–
+
–
+
HSP90
ALIX
C
*
Cellular level of ALIX
2.0
1.5
1.0
0.5
0.0
wtHeLa
HeLa ΔUMAD1
wtHeLa
HeLa ΔUMAD1
siNT
siALIX Partial depletion

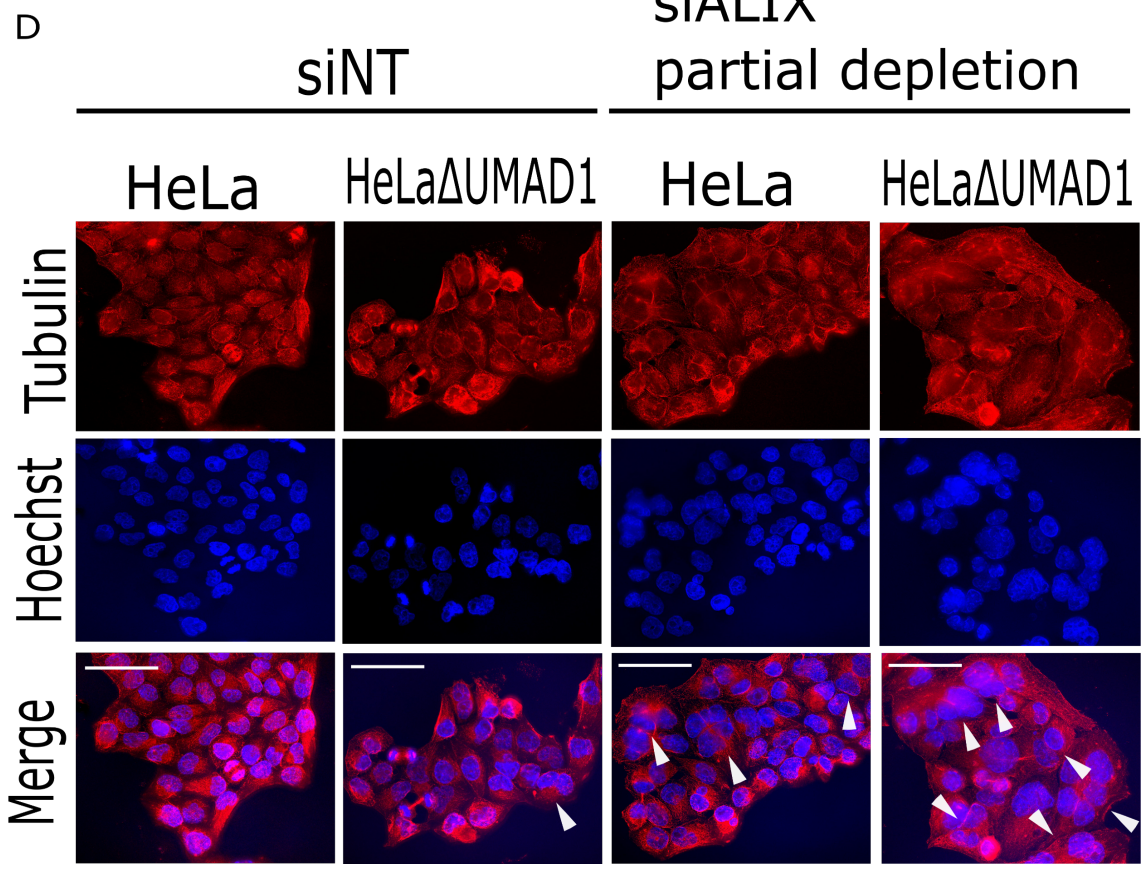
D
siNT
siALIX
partial depletion
HeLa
HeLaΔUMAD1
HeLa
HeLaΔUMAD1
Tubulin
Hoechst
Merge

Figure 43. Co-depletion of UMAD1 with a partial depletion of ALIX shows increased cytokinetic defects

A. Both HeLa and HeLaΔUMAD1 cells were transfected with siALIX, to obtain a partial depletion to equal levels in both cell types, or siNT control using a single dose of siRNA per condition. Following fixation and staining, the number of cells with more than one nucleus and the number of midbody connected cells were scored for conditions using the quantities of siALIX that showed depletion of ALIX to comparable levels in HeLa and HeLaΔUMAD1 cells (approximately 24% as shown in D), as determined by immunoblotting, as shown in C and D. The mean percentages for 4 independent experimental repeats are shown, with error bars representing the standard deviation from the mean. n > 1200 cells per condition. HeLa+siNT: 5.5±0.6% multinucleated cells, 6.4±1.9% midbodies, HeLaΔUMAD1+siNT: 8.0±0.1% multinucleated cells, 2.7±0.4% midbodies, HeLa+siALIX: 13.8±7.4% multinucleated cells, 7.5±2.6% midbodies, HeLaΔUMAD1+siALIX: 26.4±6.4% multinucleated cells, 9.7±1.7% midbodies. One-way ANOVA with Tukey's multiple comparisons test; *, $P < 0.05$, ***, $P < 0.001$, ns, P is not significant **B.** Cell lysates were analysed by immunoblotting using α-HSP90 and α-ALIX. Detection of HSP90 and ALIX signal on the same nitrocellulose membrane by fluorescence rather than enhanced chemiluminescence was performed to ensure optimal ALIX level quantification as shown in C. **C.** Quantification of cellular levels of ALIX used in A, as determined by immunoblotting. Mean ALIX levels are normalised to HeLa+siNT. Error bars represent the standard deviation from the mean. HeLaΔUMAD1+siNT: 1.53±0.42-fold, HeLa+siALIX partial depletion: 0.24±0.06, HeLaΔUMAD1+siALIX partial depletion: 0.23±0.08. Unpaired *t* test; *, $P < 0.05$ **D.** Representative images of fixed cells used in A. Red = Tubulin, Blue = Hoechst. Arrows indicate multinucleated cells, scale bar = 50μm.

4.2.5. Further synergy between UMAD1 and ALIX is seen in abscission timing

Having examined changes in cytokinetic defects representative of cytokinesis failure, we decided to more specifically examine effects on abscission by measuring abscission time in cells that successfully complete abscission. In addition to causing cytokinesis failure, depletion of TSG101 and ALIX have each been shown to delay successful abscission, and further display a synergistic increase in abscission time upon co-depletion of both proteins. Under the hypothesis that UMAD1 represents part of the branch for ESCRT-III recruitment including TSG101 (ESCRT-I), a possible prolonging of abscission time could be expected upon UMAD1 depletion, in addition to the above described phenotypes in cytokinetic failure. HeLa and HeLaΔUMAD1 cells that stably expressed mCherry-tubulin were made and sorted for comparable levels of low mCherry-tubulin expression. Live cell imaging of these cells was then performed for 24 hours to investigate differences in abscission timing upon partial depletion of ALIX with UMAD1. Imaging of asynchronous cells was started 12 hours post-transfection to avoid an undesirable number of multinucleated cells at the start of the experiment, caused in particular by depletion of ALIX, as shown in the previous figure. HeLa and HeLaΔUMAD1 cells were transfected

with siALIX, to obtain a partial depletion of ALIX to equal levels in both cell types (Section 4.2.3), or siNT control siRNA. Results for depletion of ALIX to comparable levels, of 28% and 30% wild type HeLa levels in HeLa and HeLaΔUMAD1 cells respectively, (Figure 44D/E) are shown, taking abscission time as the time from furrow ingression to midbody resolution (Figure 44A-C).

Abscission times showed a similar pattern to data obtained by Christ et al. 2016 for the effect of TSG101 and ALIX depletion on abscission timing[93]. An increase in median abscission time from 150 mins in HeLa cells to 170 mins in HeLaΔUMAD1 cells, 190 mins in HeLa cells with the partial ALIX depletion and a clearly synergistic increase to 240 mins in HeLaΔUMAD1 cells with the partial ALIX depletion was seen. Statistical analysis additionally revealed much higher degrees of confidence in this data, than for previous assays to measure cytokinetic defects in fixed cells. Such results are consistent with the hypothesis that UMAD1 and ALIX are part of two separate and partially redundant pathways for the recruitment of ESCRT-III to mediate abscission, with UMAD1 forming an ESCRT-I complex that contributes to cytokinetic abscission. In contrast to the previous figure, elevated levels of ALIX are not observed in HeLaΔUMAD1 cells on this occasion. A possible explanation for this could be that by this time, further adaptations to the absence of UMAD1 have occurred in the cells, thus no longer necessitating increased ALIX expression.

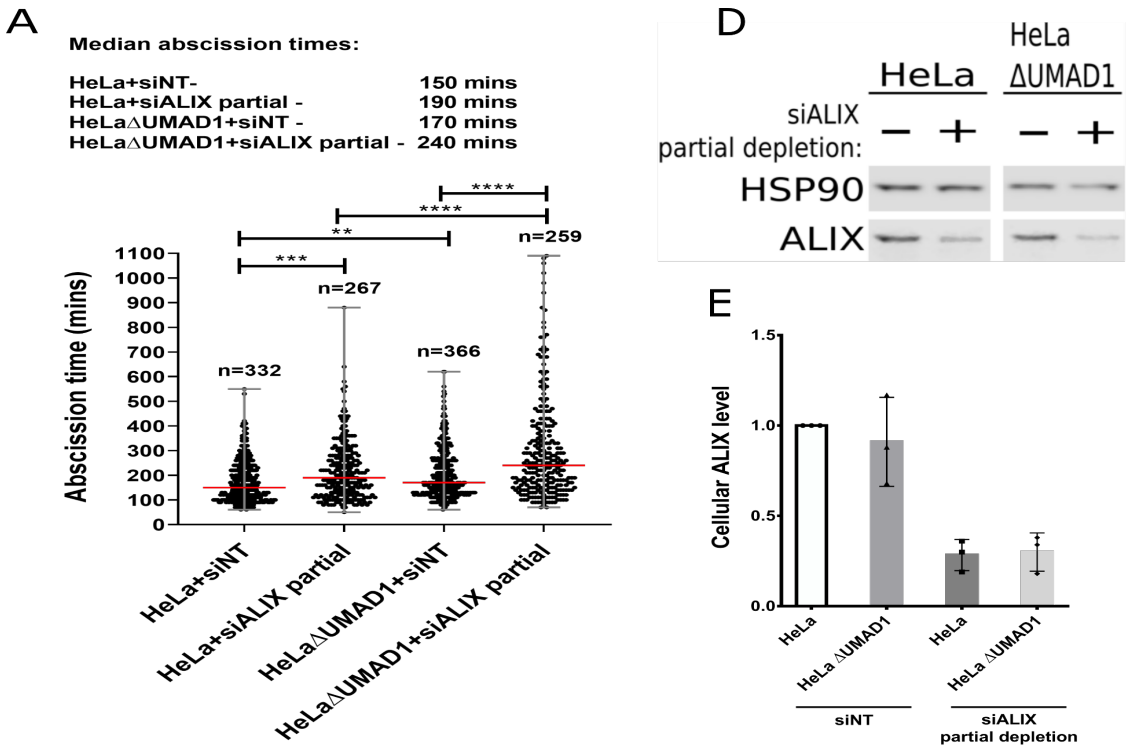
A
Median abscission times:
HeLa+siNT- 150 mins
HeLa+siALIX partial - 190 mins
HeLaΔUMAD1+siNT - 170 mins
HeLaΔUMAD1+siALIX partial - 240 mins
Abscission time (mins)
n=332
n=267
n=366
n=259
****
****
**
***
HeLa+siNT
HeLa+siALIX partial
HeLaΔUMAD1+siNT
HeLaΔUMAD1+siALIX partial
D
HeLa
HeLa ΔUMAD1
siALIX partial depletion:
HSP90
ALIX
E
Cellular ALIX level
HeLa
HeLa ΔUMAD1
siNT
siALIX partial depletion

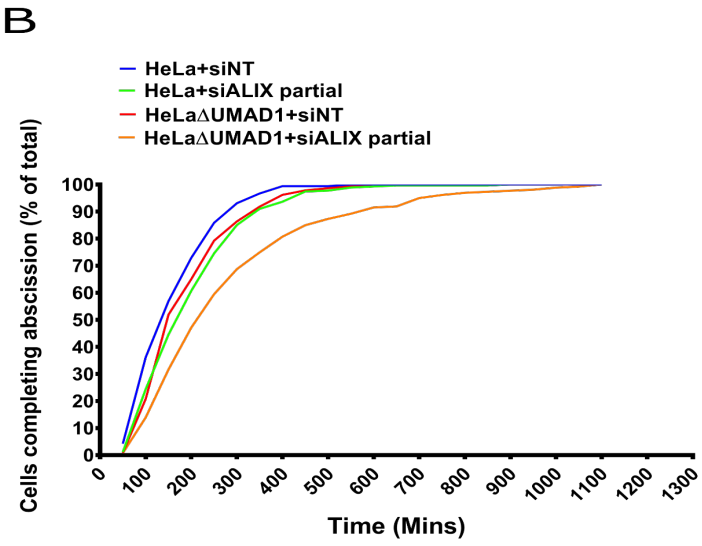
B
HeLa+siNT
HeLa+siALIX partial
HeLaΔUMAD1+siNT
HeLaΔUMAD1+siALIX partial
Cells completing abscission (% of total)
Time (Mins)

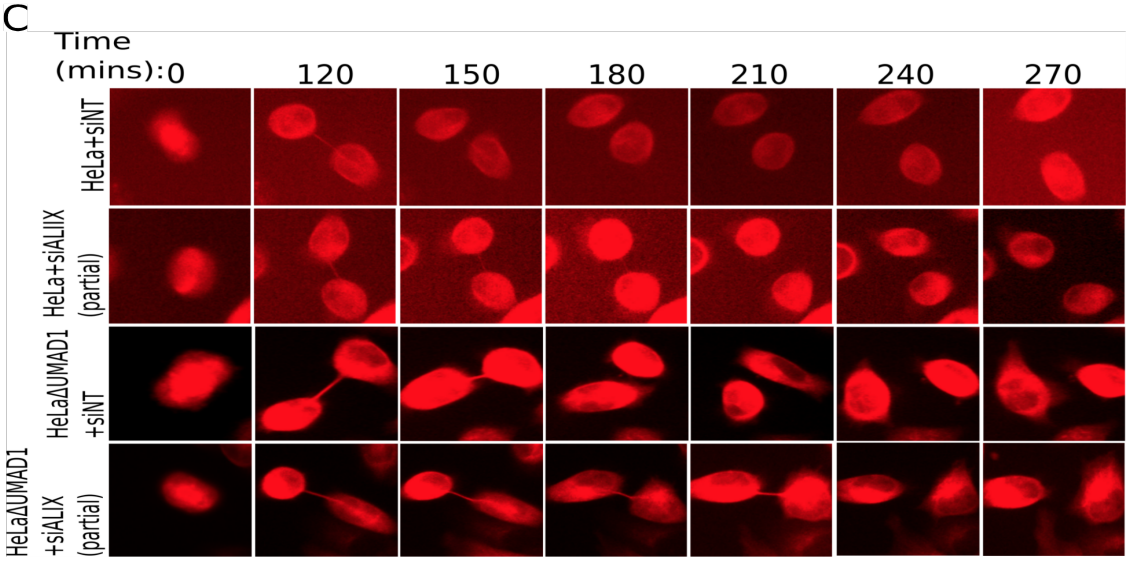
C
Time (mins):0
120
150
180
210
240
270
HeLa+siNT
HeLa+siALIIX (partial)
HeLaΔUMAD1 +siNT
HeLaΔUMAD1 +siALIX (partial)

Figure 44. A synergistic increase in abscission time is observed upon a partial co-depletion of ALIX with UMAD1.
A. 12 hours post-transfection with siNT or siALIX, to obtain a partial depletion, asynchronous HeLa or HeLaΔUMAD1 cells sorted for equal levels of low mCherry-Tubulin expression, were imaged live every 10 mins for 24 hrs. Midbody resolution times were scored for 3 independent experiments combined in the scatter plot shown, selecting for conditions using the quantities of siALIX that showed depletion of ALIX to comparable levels in HeLa and HeLaΔUMAD1 cells (approximately 29% as shown in C). Abscission times were taken as the interval between furrow ingression and midbody breakage. Bars indicate the median and range of abscission times. n = no. of events scored per condition. Kruskal-Wallis test with Dunn's multiple comparisons test; **, P < 0.01, ***, P < 0.001, ****, P < 0.0001. **B.** Data from A plotted as a cumulative frequency plot. **C**. Time-lapse images for HeLa and HeLaΔUMAD1 cells stably expressing equal levels of low mCherry-Tubulin, as used in A and B. Scale bar = 10μm **D.** Cell lysates were analysed by immunoblotting using α-HSP90 and α-ALIX. Detection of HSP90 and ALIX signal on the same nitrocellulose membrane by fluorescence rather than enhanced chemiluminescence was performed to ensure optimal ALIX level quantification, as shown in D. **E.** Quantification of cellular levels of ALIX used in A and B, determined by immunoblotting of cell lysates. The mean ALIX levels for the 3 independent experimental repeats are shown normalised to wild type HeLa+siNT. Error bars represent the standard deviation from the mean. HeLaΔUMAD1+siNT:0.91±0.25-fold, HeLa+siALIX partial depletion: 0.28±0.09-fold, HeLaΔUMAD1+siALIX partial depletion 0.30±0.11-fold.

4.2.6. Midbody localisation of CHMP4B upon UMAD1 and ALIX depletion

Under the hypothesis that UMAD1, as a component of ESCRT-I, and ALIX form parallel arms of ESCRT-III recruitment to the midbody, we decided to examine midbody localisation of CHMP4B-L-GFP in HeLa cells, initially following depletion of TSG101 or ALIX (Figure 45A/B).

As previously observed for fluorescently tagged ESCRT-III proteins[17], CHMP4B-L-GFP either displayed its characteristic localisation to two concentric rings at either side of the Flemming body or was absent, in cells transfected with non-targeting control siRNA. In the case of a partial depletion of ALIX, both localisation to two concentric rings and the absence from some midbodies was again observed. However, CHMP4B-L-GFP also showed a third type of localisation in 54.4% midbodies, as a single band at the centre of the Flemming body, similar to that seen for CEP55 and TSG101. This was also seen for TSG101 depletion, accounting for 32.6% midbodies.

In experiments using HeLaΔUMAD1 cells, a similar pattern of results was seen (Figure 45A/C). A slight increase from 2.0% in wild type cells transfected with non-targeting siRNA to 9.4% in HeLaΔUMAD1 cells transfected with non-targeting siRNA was seen for the number of cells showing CHMP4B-L-GFP localisation to a single band at the Flemming body. This figure was at 35.6% for cells transfected with 5pmol siALIX. It would therefore appear that both ALIX depletion and TSG101/UMAD1 depletion leads to

increases in this phenotype, with ALIX depletion showing a stronger phenotype than for TSG101/UMAD1 depletion. Whether this localisation represents midbodies that are still able to complete abscission or defective in abscission remains to be investigated. HeLaΔUMAD1 cells also show a more obvious increase in the number of midbodies in which CHMP4B is absent, compared to cells transfected with non-targetting control siRNA or siALIX.

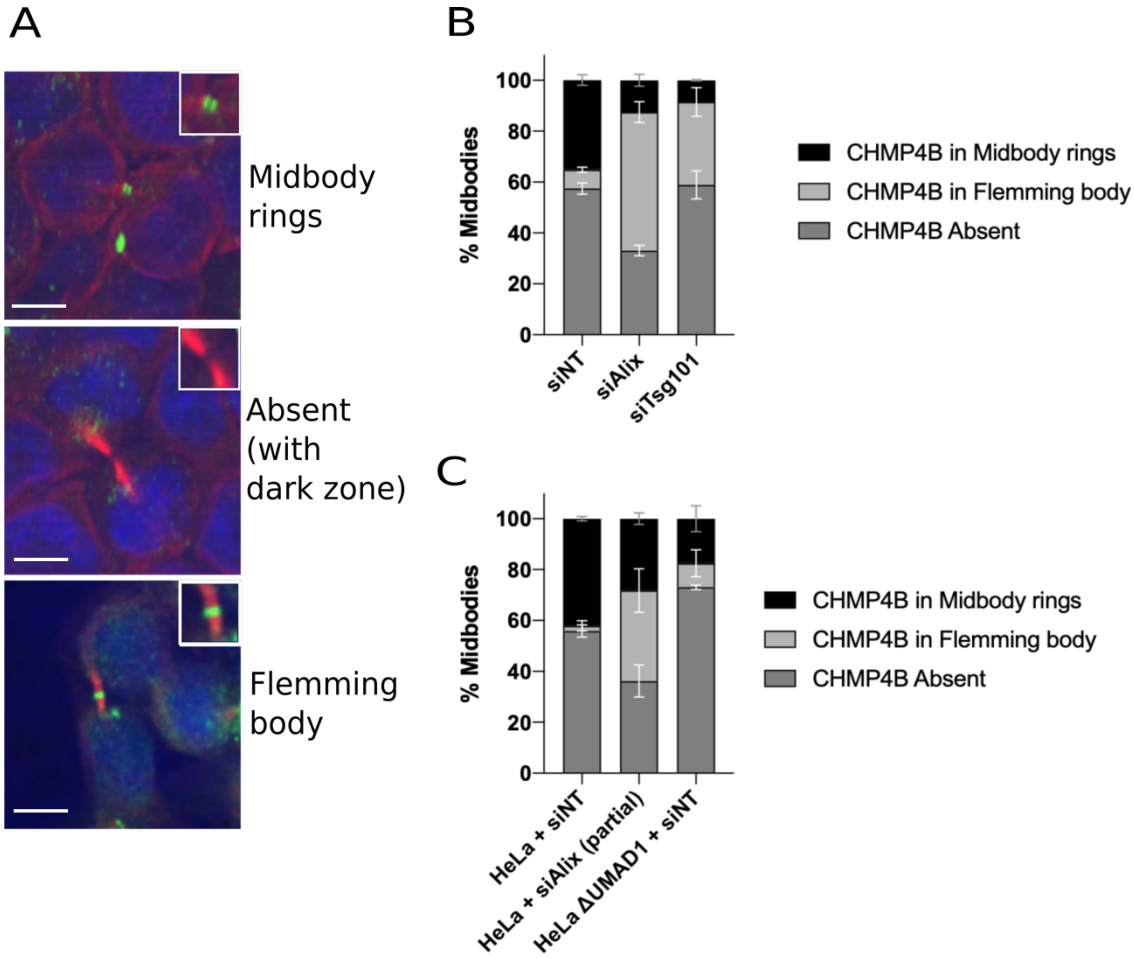

Figure 45. Effects of TSG101, UMAD1 and ALIX depletion on CHMP4B midbody localisation
A. Representative images of midbodies in HeLa cells stably expressing CHMP4B-L-GFP, as scored in B and C. Blue = Hoechst, Red = Tubulin, Green = CHMP4B-L-GFP. Scale bar = 10μm, Inset = Midbody. **B.** HeLa cells were transfected with one dose of each siRNA oligonucleotide shown. Following fixation and staining, the number of midbodies showing each type of CHMP4B-L-GFP localisation pattern were scored. The mean percentages for 3 independent experimental repeats is shown, with error bars representing the standard deviation from the mean. siNT: 57.5±3.9% Absent, 7.4±1.7% Flemming body, n=331, siALIX: 33.1±3.6% Absent, 54.4±7.1% Flemming body, n=829, siTSG101: 58.9±9.6% Absent, 32.6±9.8% Flemming body, n=275 **C.** Both HeLa and HeLaΔUMAD1 cells were transfected with one dose of each of siRNA oligonucleotides shown, using a partial depletion in the case of siALIX. Following fixation and staining, the number of midbodies showing each type of CHMP4B-L-GFP localisation pattern was scored. The mean percentages for 3 independent experimental repeats are shown, with error bars representing the standard deviation from the mean. HeLa+siNT: 55.9±4.1% Absent, 2.0±3.5% Flemming body, n=242, HeLa+siALIX (partial): 36.2±10.9% Absent, 35.6±14.8% Flemming body, n=432, HeLaΔUMAD1+siNT: 73.1±1.5% Absent, 9.4±9.2% Flemming body, n=217.

4.3. Discussion

Following the observation in the previous chapter that UMAD1 knockout reduces interaction of TSG101 with CEP55, the results presented in this chapter demonstrate that UMAD1 indeed contributes to cytokinesis. Time-lapse experiments have shown that UMAD1 functions in cytokinetic abscission. UMAD1 knockout leads to an increase in the median time taken for midbody resolution, and a synergistic increase in resolution time is observed upon a partial co-depletion with ALIX. Although not always statistically significant, results from assays to measure cytokinetic defects have additionally suggested a more generalised role for UMAD1 in mediating successful cytokinesis, as seen by increased multinucleation upon knockout of UMAD1. This could potentially explain some of the reason why retarded growth is seen in HeLaΔUMAD1 cells (Figure 39A). Despite undergoing increased multinucleation and an increase in time taken for abscission, it should be remembered that such cells would still enter G1 and G2 growth phases of the cell cycle. Additionally, such modest increases in cytokinetic defects upon knockout of UMAD1 alone are unlikely to fully explain the 4-fold growth defect observed. It is therefore likely that involvement of UMAD1 in additional cellular processes, uncharacterised here, other than cytokinesis could be contributing to the growth defect to a greater extent. Depletion of VPS37C shows a growth defect and increase in multinucleation similar to that seen upon UMAD1 knockout, consistent with the preferred pairing of UMAD1 with VPS37C, in the same ESCRT-I complex (Chapter 3/ Figure 40). The biggest question remaining here is whether increases in multinucleation upon UMAD1 knockdown occur more precisely at a stage closer to furrow ingression or to abscission, representing early or late cytokinetic defects, respectively, or both. This can be established by examination of multinucleation events in the time-lapse experiments presented in Figure 44, to specifically score the time intervals between furrow ingression and regression to form multinucleated cells.

If multinucleation events occur following a prolonged period of midbody connectivity (i.e. longer than the median time interval seen between furrow ingression and regression in wild type HeLa cells) involvement of UMAD1 closer to abscission would be implied. This would be consistent with the prolonged midbody resolution time seen in HeLaΔUMAD1 cells that do successfully complete abscission, as scored in time-lapse

experiments (Figure 44). Conversely, multinucleation events that occur closer to the time of furrow ingression (i.e. shorter than the median time interval seen between furrow ingression and regression in wild type HeLa cells) would be indicative of earlier failure, in furrow ingression or midbody stability. UMAD1 could also possibly be involved at both stages to a certain extent, like MITD1[511] (Section 1.5.6.). Interestingly, Morita et al. 2007 report both early and late furrow regression events upon depletion of TSG101 and ALIX[17]. Also, as presented in the same study and discussed in section 1.5.6., unique binding partners involved at early stages of cytokinesis have been identified for both TSG101 and ALIX. This suggests a potential dual role for the ESCRT machinery at both early and late stages of cytokinesis, coordinating abscission with more upstream events in cytokinesis and mitosis. The prolonged midbody resolution time and more statistically significant results for such time-lapse experiments, however, potentially suggests a more prominent role for UMAD1 in abscission.

A synergistic increase in midbody resolution time, in cells that successfully complete abscission, is seen upon co-depletion of UMAD1 with ALIX. This is consistent with the hypothesis that UMAD1 forms part of an ESCRT-I complex involved in abscission as part of a CEP55 – ESCRT-I – ESCRT-II – CHMP6 – ESCRT-III pathway of ESCRT-III recruitment (Figure 46). This is proposed to form a partially redundant branch of ESCRT-III recruitment in a dual axis together with a CEP55 – ALIX – ESCRT-III branch[93] (Figure 46). This hypothesis is also consistent with the elevated levels of ALIX expression in HeLaΔUMAD1 cells, seen most prominently in figure 43C, as a potential compensatory mechanism in cytokinesis. It will be interesting to similarly examine potential change in ALIX levels upon depletion of TSG101, VPS37B and VPS37C, given that these subunits form complexes with UMAD1 (Chapter 3), and VPS37C depletion shows a growth defect akin to that in HeLaΔUMAD1 cells (Figure 40A/B). A similar compensatory effect would yet again add to the notion that ESCRT proteins show tight regulation of expression and would shed light on an area for further investigation of control of ESCRT protein expression.

In addition to midbody resolution time, a synergistic increase is also seen in multinucleation upon codepletion of UMAD1 or TSG101 with a partial depletion of ALIX. This contrasts with similar experiments using live cells performed by Christ et al. 2016, who concluded that there was no statistically significant increase in the number of cells

that underwent multinucleation following depletion of TSG101 with ALIX[93]. These experiments, however, were performed with total depletion of ALIX rather than a partial depletion, suggesting that a synergistic effect might have been masked due to reaching saturated levels of multinucleation.

Experiments to examine localisation of CHMP4B-L-GFP have shown an increase in the localisation of CHMP4B-L-GFP to a single band at the Flemming body upon depletion of ALIX, TSG101 and UMAD1. An increase in midbodies in which CHMP4B is absent is also seen in HeLaΔUMAD1 cells. A possible explanation for this phenotype could be that localisation as a single band at the Flemming body might represent an intermediate stage of ESCRT-III localisation, prior to re-localisation to the concentric rings. Depletion of early ESCRTs such as ALIX, TSG101 and UMAD1 would lead to persistence at this stage, if they are required for appropriate positioning of ESCRT-III to the rings.

The different ratios of CHMP4B localisation to the Flemming body, concentric rings or absence from the midbody could also likely be due to differences in time taken for CHMP4B recruitment to the midbody and persistence at the midbody before the final scission event. For example, perhaps CHMP4B persists at the midbody for longer upon ALIX depletion than upon UMAD1 depletion, leading to the increased proportion of CHMP4B at the Flemming body and concentric rings compared to when UMAD1 is depleted. Time-lapse experiments would greatly help clarify this more accurately, by measuring the time interval between CEP55 and CHMP4B appearance at the midbody, and also how long CHMP4B persists at the midbody. Similarly, another potential method for measuring differences in the kinetics of CHMP4B recruitment to the midbody would be to perform fluorescence recovery after photobleaching (FRAP) experiments. In such experiments, high-power laser illumination would be used to specifically photobleach midbody localised CHMP4B-L-GFP. The time taken for fluorescence recovery, as non-bleached CHMP4B-L-GFP is recruited back to the midbody, would then be measured for wild type HeLa and HeLaΔUMAD1 cells. Time-lapse experiments would also help clarify whether localisation of CHMP4B to the Flemming body as a single band represents midbodies that are defective in abscission, and later undergo multinucleation, or represent midbodies that simply resolve later.

The fact that the phenotypes presented in this chapter are seen upon depletion of UMAD1 without codepletion of other MVB12 like subunits, suggests a potentially unique

role for UMAD1 in cytokinesis. Partial redundancy with other MVB12 like subunits, however, cannot be dismissed yet. Future multinucleation/midbody scoring assays and time-lapse experiments to measure abscission time should therefore be performed to further investigate whether similar phenotypes are seen upon depletion of MVB12A and MVB12B and whether stronger phenotypes are seen upon co-depletion of UMAD1 with MVB12A/B.

To further confirm that the phenotypes seen are genuinely due to UMAD1 knockout, future work should involve performing rescue experiments in which multinucleation assays and abscission time scoring experiments are performed using HeLaΔUMAD1 cells that re-express UMAD1 by lentiviral transduction. Decreases in multinucleation and abscission times would be expected in these cases. Also, in order to further attempt to discount a clone specific phenotype using a single CRISPR/Cas9 HeLaΔUMAD1 clone, experiments using siRNA knockdown of UMAD1 (Appendix 1) should also be reattempted for these experiments to measure abscission time. For completeness, time-lapse experiments to score abscission times upon depletion of UMAD1 binding partners VPS37B and VPS37C could also be attempted, to investigate whether abscission times similar to those seen upon UMAD1 depletion are observed.

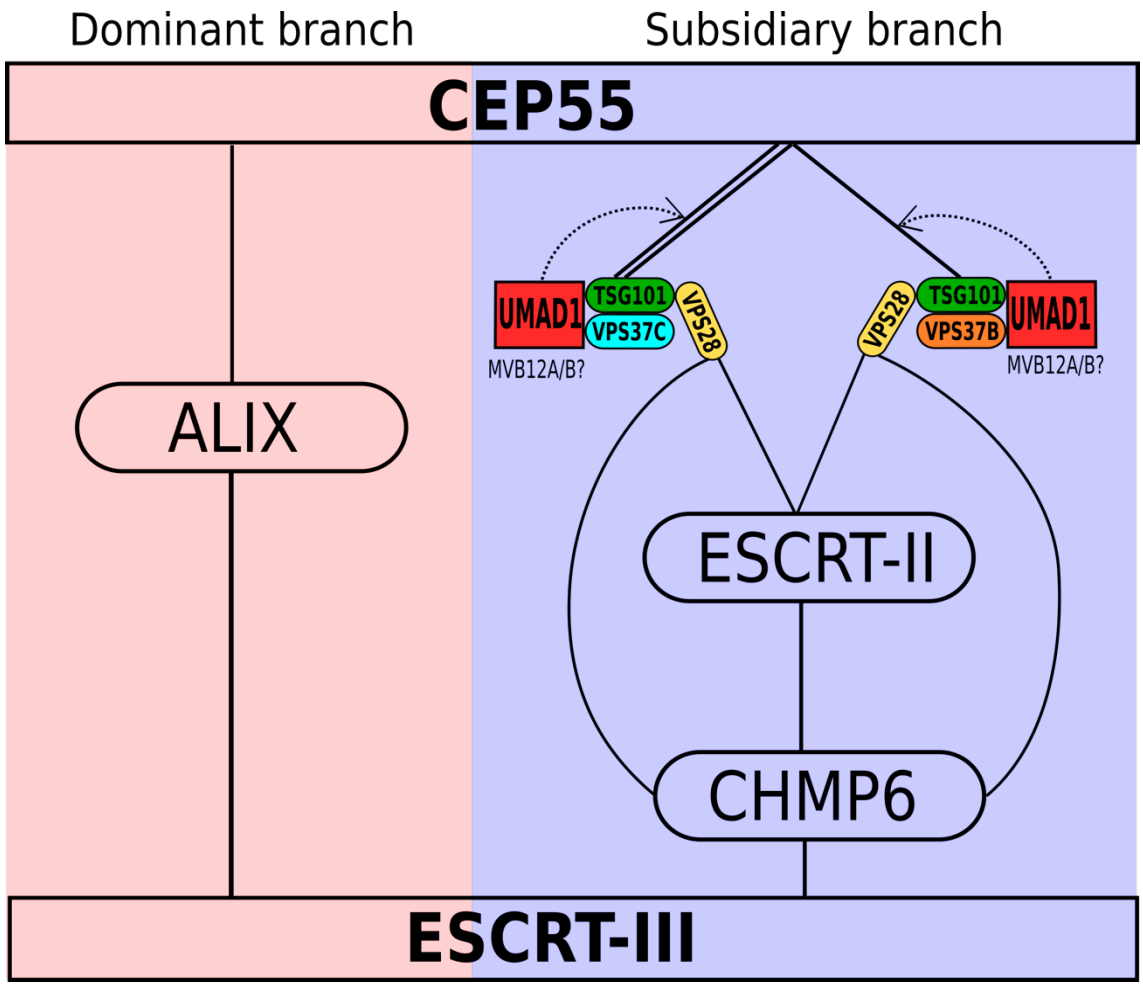

Figure 46. Proposed model for the role on UMAD1 in cytokinetic abscission
ESCRT-III is recruited by the two parallel partially redundant pathways proposed by Christ et al 2016 involving a dominant CEP55 – ALIX – ESCRT-III branch and a more subsidiary CEP55 – ESCRT-I – ESCRT-II – CHMP6 – ESCRT-III branch. UMAD1 contributes to cytokinesis through the more subsidiary branch, by incorporation into ESCRT-I complexes involved in cytokinesis containing VPS37B and VPS37C, with a preference for VPS37C (as shown by the double solid line, as opposed to the single solid line in the case of VPS37B). UMAD1 specifically strengthens the interaction between CEP55 with TSG101 (as shown by dashed arrows)

Chapter 5 – UMAD1 in viral budding

5.1. Introduction

5.1.1. HIV-1 assembly and Gag multimerisation

HIV-1 is a single-stranded positive-sense enveloped RNA virus that belongs to the *Lentivirus* genus of the *Retroviridae* family. Retroviruses are characterised by reverse transcription of their RNA genome into a double-stranded DNA intermediate by a virally encoded reverse transcriptase. The dsDNA provirus is then integrated into the host genome by a virally encoded integrase, such that transcription by the host cell machinery generates new ssRNA genomes for incorporation into new viral progeny. This host transcribed RNA also serves as mRNA for the production of new viral proteins, which assemble into the viral progeny.

The HIV-1 genome encodes 9 proteins: *Gag*, *Env*, *Pol*, *Tat*, *Rev*, *Vif*, *Vpu*, *Nef* and *Vpr*[700] (Figure 47). Gag and Env represent the main structural components of virions, with Gag accounting for approximately 50% of the virion mass[701]. Expression of Gag is sufficient for assembly of HIV-1 at the plasma membrane[702,703]. Env encodes the HIV-1 envelope glycoprotein that is processed to form gp120-gp41 that binds the HIV-1 receptor CD4 and co-receptors CXCR4 and CCR5, on cells of the immune system, via interaction with gp120[704,705]. Pol encodes the viral protease (PR), involved in maturation of the virus to form infectious virions, together with the viral reverse transcriptase (RT) and integrase (IN). Tat and Rev regulate gene expression, and the remaining Vif, Vpr, Vpu and Nef are known as accessory proteins, involved in evasion of host immune responses and fine tuning of viral replication[706–708]. Whilst unspliced RNA forms the viral genome for incorporation into progeny virions, it is also translated to form Gag and Gag-Pol polyprotein precursors. Singly spliced RNA is translated to produce Env at the ER, which is further glycosylated at the Golgi apparatus and cleaved to form gp120-gp41 prior to plasma membrane insertion[709–711]. Multiply spliced RNAs are translated to produce all other HIV-1 proteins[708].

Gag (p55) and Gag-Pol (p160) polyproteins (Figure 47) are generated by ribosomal frameshifting at the 3' end of the *Gag* open reading frame, such that Gag and Gag-Pol are produced in an approximately 20:1 ratio, ensuring appropriate stoichiometry of Gag

structural proteins and the viral enzymes[712]. Gag polyproteins consist of matrix protein (MA), capsid protein (CA) and nucleocapsid protein (NC) domains (Figure 47) separated by the flexible linkers spacer peptide 1 (SP1) and spacer peptide 2 (SP2) and the C-terminal p6 region which interacts with the ESCRT proteins TSG101 and ALIX to direct L-domain mediated viral budding[713] (Section 1.7.1.).

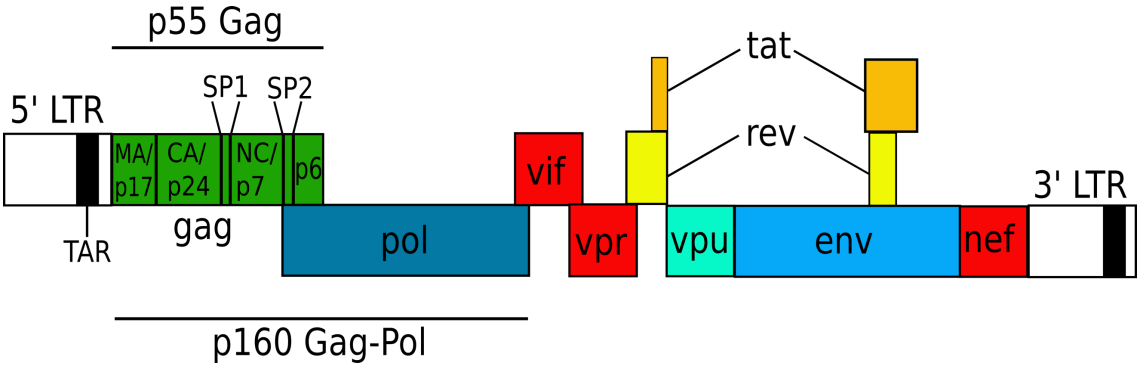

Figure 47. HIV-1 genome structure with p55 Gag proteolytic processing products
The HIV-1 genome encodes 9 proteins, as described in the text. Gag (p55) and Gag-Pol (p160) polyproteins are generated by ribosomal frameshifting, such that Gag (p55) and Gag-Pol (p160) are produced in an approximately 20:1 ratio. As relevant to this chapter, p55 Gag proteolytic processing products are shown.

Gag and Gag-Pol precursors traffic to the plasma membrane and are incorporated in a radial arrangement into domains of the membrane displaying specific lipid raft-like compositions (Figure 48). Such domains contain enriched PI(4,5)P_2, phosphatidylserine (PS), phosphatidylethanol, and cholesterol[714–717]. Gag MA domains provide interaction with the membrane through a basic patch in its N-terminus, which interacts with PI(3,4)P_2[713,718]. Further anchorage is mediated via an N-terminal myristoyl group which is exposed upon PI(3,4)P_2 binding[718,719]. Gag assembly into a spherical lattice is mediated primarily by lateral interactions between the CA-SP1 regions of Gag[720]. These form hexameric rings which curve to form the spherical immature virion[721,722]. The most inner layer of the immature virion contains the NC regions which package the viral genomic RNA dimers[723–725]. Genomic RNA dimers form in the cytoplasm prior to packaging and are formed through noncovalent interactions at the 5'UTRs. Packaging is directed through an interaction between another 5' region known as the ψ site, which forms stem loop structures that interact with two zinc finger motifs and basic clusters of residues within the NC region of Gag[726]. Binding to RNA also promotes Gag multimerisation[727,728].

Gag processing to form mature infectious virions occurs concomitantly with budding and involves cleavage of the Gag/Gag-Pol precursor proteins at PR cleavage sites, and reorganisation of the individual Gag components to form a characteristic HIV-1 conical capsid structure enclosing the genome[729,730] (Figure 48). Cleavage by PR occurs at 11 separate sites within Gag/Gag-Pol to produce MA, CA, NC, p6, PR, RT, and IN proteins. Whilst MA remains membrane associated, CA forms the capsid shell containing around 1500 CA copies[731,732]. The capsid shell encapsidates NC bound RNA, and the PR, RT and IN enzymes[733].

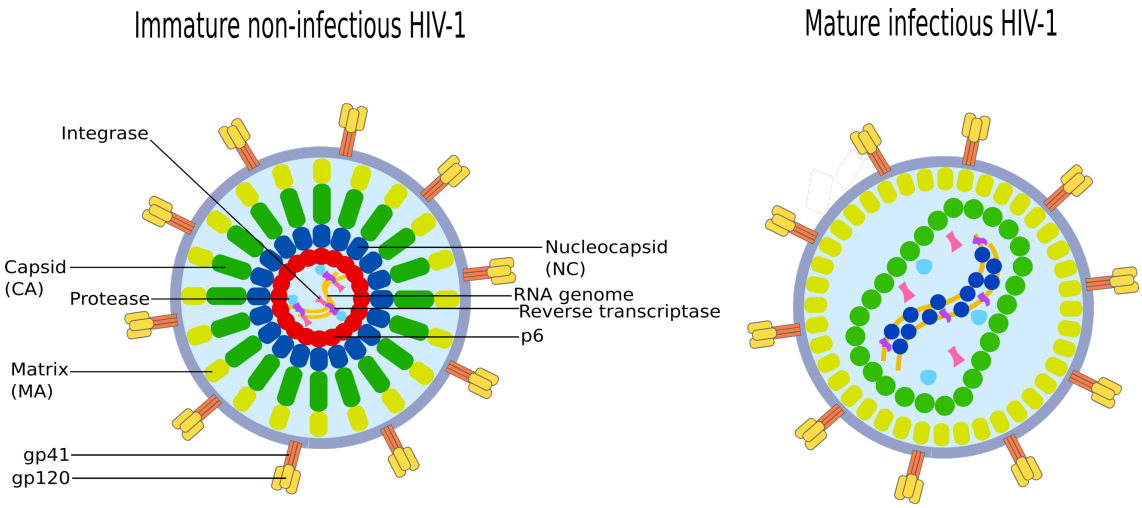

Figure 48. Arrangement of proteins in immature HIV-1 virions and mature infectious virions
During HIV-1 budding, Gag and Gag-Pol precursor polyproteins localise to lipid raft-like regions of the cell plasma membrane and form a radial arrangement. Whilst MA mediates interaction with the membrane, to become the viral envelope, CA-SP1 regions are primarily responsible for interaction with neighbouring Gag polyproteins for assembly into a spherical lattice, and NC is responsible for packaging of the viral RNA genome. Gag/Gag-Pol processing to form the mature infectious virion involves cleavage by the viral protease at 11 separate sites to produce MA, CA, NC, p6, PR, RT, and IN proteins. MA remains associated with the viral envelope, whilst CA forms the capsid shell encapdisating NC bound RNA, and the PR, RT and IN enzymes.

5.1.2. Contribution of ESCRT-I subunits to L-domain mediated viral budding

HIV-1 usurps the ESCRT machinery to facilitate its budding from the plasma membrane, as detailed in section 1.7. This is mediated primarily through a ^{7}PTAP^{10} L-domain and more auxilliary ^{35}LYPLTSL^{41} L-domain within p6 Gag, which bind directly to TSG101 and ALIX respectively. Accordingly, it comes as no surprise that depletion of TSG101 has

consistently shown a 10-50-fold reduction in infectious virus release from cells[12–14,76,734]. Overexpression of its N-terminus leads to similar reduction in release[15].

The importance of VPS28 in viral budding was initially suggested by the localisation of VPS28 to HIV-1 Gag, and later Ebola VP40, at the plasma membrane[565,735]. This interaction was abolished upon mutation of its interaction site on TSG101. It was further shown that truncation of the TSG101 C-terminus including the VPS28 binding region abolished HIV-1 budding[665,734].

A direct effect on HIV-1 budding upon specific depletion of VPS37A, VPS37B or VPS37C has not been examined. However, when an MLV virus was engineered to be dependent on ESCRT-I for budding, by replacing its PPPY L-domain with the PTAP L-domain and surrounding sequence from HIV-1, depletion of either VPS37B or VPS37C showed partial inhibition of viral budding and an even stronger inhibition than TSG101 depletion upon co-depletion of both VPS37B and VPS37C[657].

Whilst depletion of UBAP1 has been shown to have no effect on HIV-1 budding, consistent with its specific role in endosomal sorting[658], depletion of MVB12A or MVB12B, or co-depletion of both has been shown to reduce infectious virus release by a modest 2-5 fold, but not affect the actual level of budding, i.e. the overall release of virions[667]. Electron microscopy analysis of released virions revealed the reduction in infectious virus release to be due to an increase in budding of aberrant virions, that appeared electron dense and lacked discernible internal structures. A concomitant decrease in mature infectious virions with conical capsids was also seen[667]. This contrasts with depletion of TSG101 which shows a decrease in the overall levels of released virus, characteristic of defective ESCRT mediated viral budding. Interestingly, overexpression of MVB12A or MVB12B did cause a reduction in overall virus release that paralleled that of infectious virus release. Released virions also appeared mature. Unlike the phenotype seen upon TSG101 depletion, however, intracellular virions appeared to remain cell-associated but not directly connected to the plasma membrane, as seen for TSG101 overexpression[667]. Overall, these observations indicate that whilst MVB12A and MVB12B depletion appears to potentially perturb viral budding to a certain extent, the weaker phenotype and differences in terms of viral morphology, intracellular localisation and overall budding levels compared to TSG101 depletion indicates only a modest contribution to infectious virus release.

5.2. Results

5.2.1. The effect of UMAD1 knockout on HIV-1 budding

Given the importance of ESCRT-I, notably TSG101, for PT/SAP L-domain activity and previously described roles for MVB12A and MVB12B in ESCRT mediated viral budding (Section 5.1.2.), we decided to examine the effects of UMAD1 knockout on HIV-1 budding. Also, given that viral budding is largely unperturbed by ESCRT-II depletion, the identification of potential bridging factors that link ESCRT-I to ESCRT-III in L-domain mediated viral budding is of great interest. An initial TZM-bl assay to measure infectious virus release following transfection of producer 293T cells and 293TΔUMAD1 cells with the commonly used pNL-HxB full-length X4 strain HIV-1 infectious proviral plasmid appeared to show a 2-fold decrease in infectious virus release from 293TΔUMAD1 cells compared to 293T cells (Figure 49A). In this assay, infectious virus release is quantified by measuring β-galactosidase activity, since TZM-bl reporter cells express this enzyme under the control of an HIV-1 LTR promoter, which is responsive to the HIV-1 tat protein upon infection with HIV-1.

This modest decrease is similar to that previously reported for single depletion of either MVB12A or MVB12B[667], and immunoblotting using α-Gag revealed that band intensities for budded virus appeared to mirror the levels of infectious virus release. However, immunoblotting of producer cell lysates appeared to show less cellular Gag for the 293TΔUMAD1 cells (Figure 49A, lane 3) compared to the wild type 293T cells (lane 1), suggesting that fewer viable cells were present throughout the period of virus production compared to wild type 293T cells. 293TΔUMAD1 cells are noticeably more fragile than 293T cells, most likely due to the effects of UMAD1 knockout on cell division, so it is likely that despite seeding the same number of cells, more cell death occurred during seeding and throughout experimental repeats than for wild type 293T cells. This would have meant fewer producer cells, hence less virus production. From this it cannot be concluded that UMAD1 has an effect on viral budding.

An experiment performed the same way in HeLa and HeLaΔUMAD1 cells (which grow more slowly but are not as fragile as 293TΔUMAD1 cells) (Figure 49B) showed no difference in the levels of infectious virus release from HeLaΔUMAD1 cells. Immunoblotting of producer cell lysates and budded virions likewise revealed no clearly

visible difference in the levels of budded virus, or cellular gag. This finding makes it more likely that the decreased level of infectious virus release seen in 293TΔUMAD1 cells is due to cell death rather than a genuine role of UMAD1 in viral budding.

In contrast to 293T cells, transfection of HeLa cells with two doses of siTSG101, as a negative control, appeared to be considerably more toxic, causing substantial cell death, hence the absence of bands when blotting using cell lysates, and therefore virions.

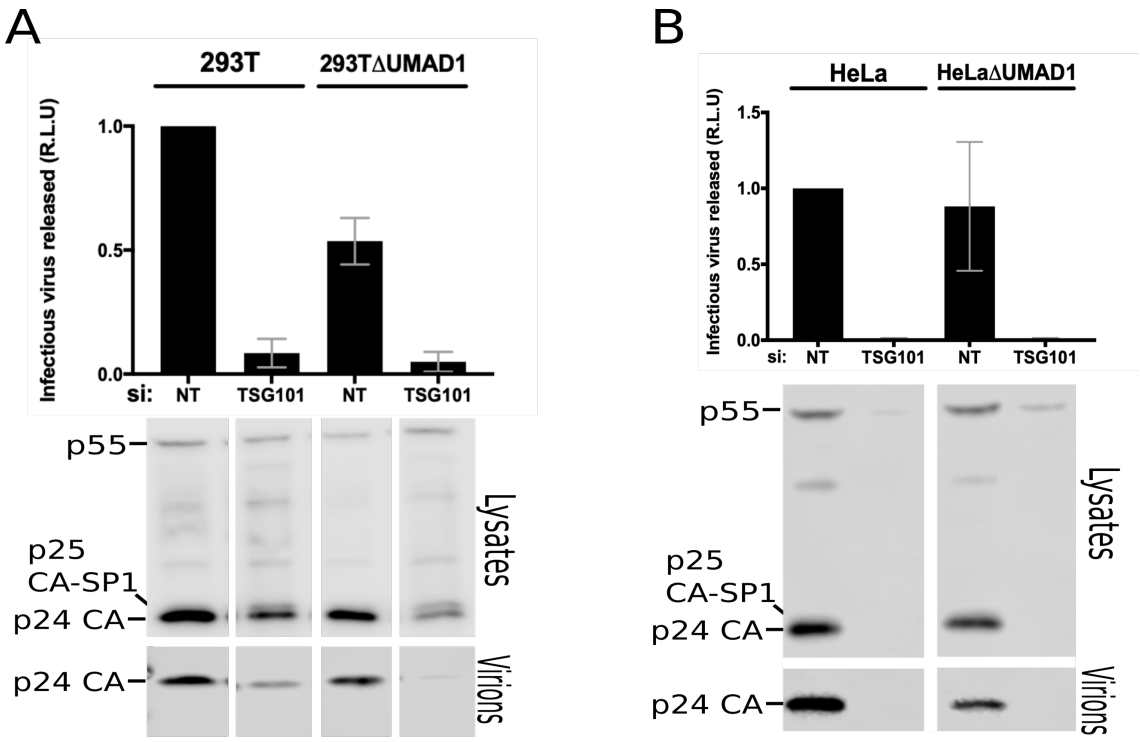

Figure 49. UMAD1 knockout appears to have to discernible effect on HIV-1 viral budding

A. The effect of UMAD1 knockout on HIV-1 viral budding is unclear using 293T cells. 293T and 293TΔUMAD1 cells were transfected with two doses of control siRNA (siNT) or siRNA against TSG101 (siTSG101) with co-transfection of pNL-HxB HIV-1 provirus with the second siRNA transfection. TZM-bl reporter cells were infected with clarified viral supernatant 48 hours later. TZM-bl cells were lysed a further 48 hours post-infection and infectious virus release readout was quantified by β-galactosidase activity. Graph shows the mean levels of infectious virus release for 5 independent repeats normalised to the levels attained using 293T+siNT. Error bars represent the standard deviation from the mean. 293T+siTSG101: 0.09±0.06-fold, 293TΔUMAD1+siNT: 0.54±0.09-fold, 293TΔUMAD1+siTSG101: 0.05±0.04-fold. Producer cell lysates were resolved by SDS-PAGE and immunoblotting using α-HIV-1 gag antibody was performed. Extracellular budded virions were purified by centrifugation through a 20% sucrose cushion and similarly analysed by SDS-PAGE and α-HIV-1 gag immunoblotting. **B.** UMAD1 knockout appears to be having no effect on HIV-1 budding using HeLa producer cells. An experiment performed exactly as in A, using HeLa and HeLaΔUMAD1 cells was performed. Graph shows mean levels of infectious virus release for 6 independent repeats normalised to the levels attained using HeLa+siNT. Error bars represent the standard deviation from the mean. HeLa+siTSG101: 0.01±0.01-fold, HeLaΔUMAD1+siNT: 0.88±0.43-fold, HeLaΔUMAD1+siTSG101: 0.01±0.01-fold.

5.2.2. The effect of UMAD1 knockout on L-domain dependent viral budding

Further viral budding assays were performed to explore the possibility that UMAD1 could be mediating more modest effects on PT/SAP L-domain dependent viral budding that are not so obvious using the experimental setup in figure 49. A side by side comparison of viral budding using pNL-HxB together with another full-length R9 HIV-1_{NL4-3} provirus, and the same construct with a mutated, non-functional YPxnL ALIX binding L-domain (R9ΔYPxnL) (Figure 50A) was performed, initially using 293T and 293TΔUMAD1 cells (Figure 50B). Since the ALIX binding YPxnL L-domain in R9ΔYPxnL is mutated, is it assumed that L-domain mediated viral budding is rendered entirely dependent on the PTAP motif in this case, and its interactions with TSG101, hence ESCRT-I. We hypothesised that this would therefore make any potentially more modest contributions to PTAP mediated HIV-1 budding by UMAD1 more obvious.

Whilst the same previously observed approximate 2-fold decrease in viral budding using pNL-HxB in 293TΔUMAD1 cells compared to 293T cells was recapitulated, the same phenotype was not seen using either R9 or R9ΔYPxnL proviruses (Figure 50B). Far from a decrease in viral budding, an increase was seen in 293TΔUMAD1 cells, although the standard deviations were large, again possibly due to varying amounts of cell death in 293TΔUMAD1 cells.

A similar experiment using HeLa cells was performed using an additional two R9 proviral constructs containing a mutated PTAP motif and both mutated PTAP and YPxnL motifs (Figure 50C), as alternative negative controls to use, given the toxicity previously seen upon two doses of siTSG101 in HeLa cells (Figure 49B). As expected, viral budding was abolished using both of these constructs (Figure 50C lanes 2, 4, 6 and 8 from the left). No difference in the levels of infectious virus release was seen for HeLaΔUMAD1 compared to HeLa cells using either R9 or R9ΔYPxnL proviruses, and the standard deviations were lower, showing better reproducibility than in figure 50B, using 293T cells.

Taken together, these assays show UMAD1 to be having no discernible effect on viral budding, L-domain dependent or otherwise.

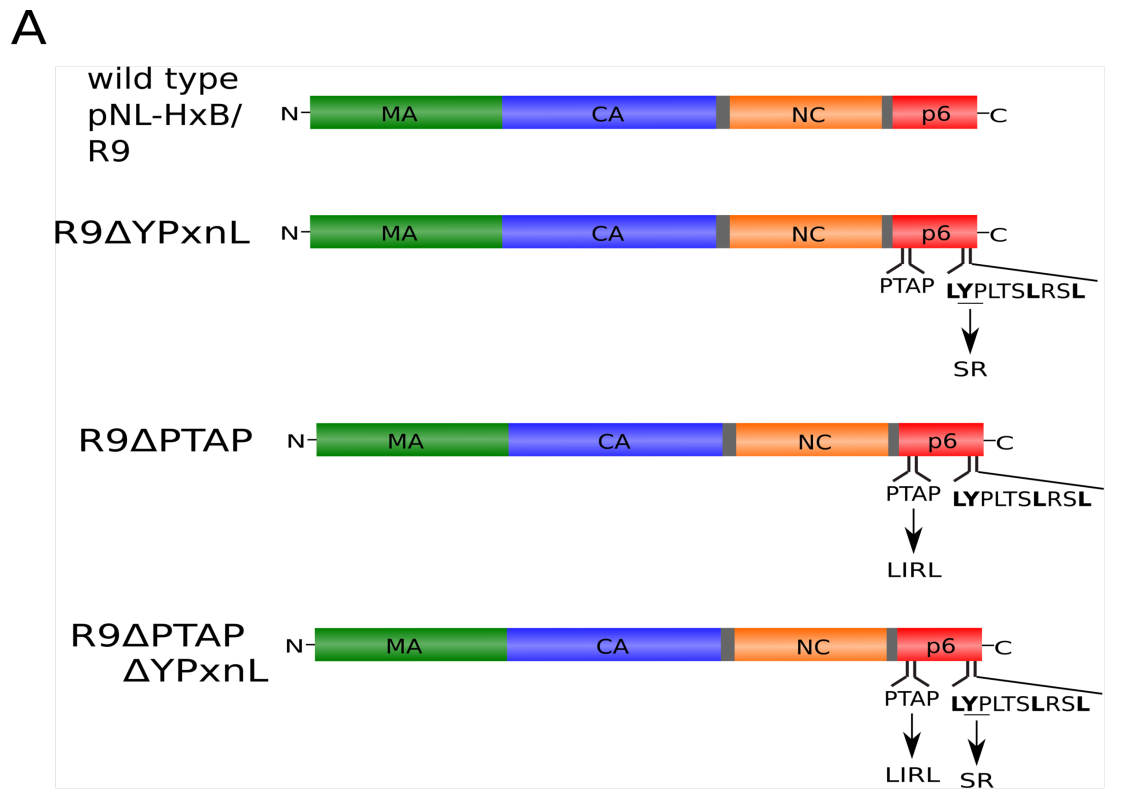
A
wild type
pNL-HxB/
R9
N
MA
CA
NC
p6
C
R9ΔYPxnL
PTAP
LYPLTSLRSL
SR
R9ΔPTAP
LIRL
R9ΔPTAP
ΔYPxnL

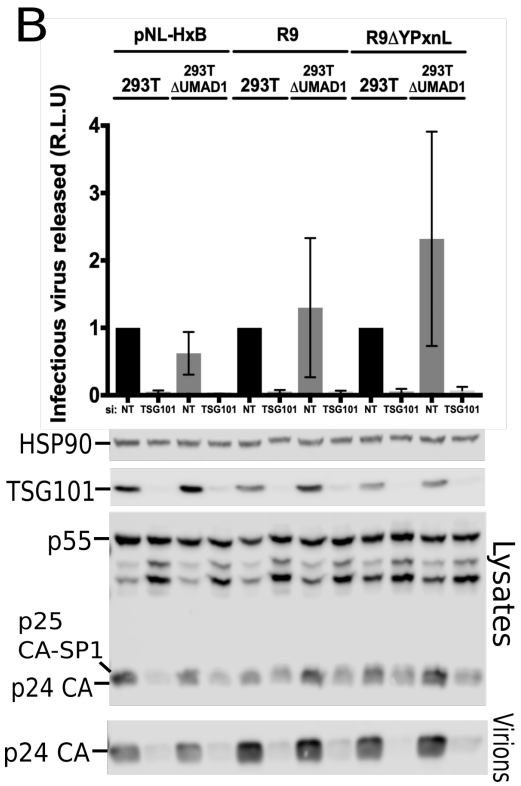
B
pNL-HxB
R9
R9ΔYPxnL
293T
293T ΔUMAD1
Infectious virus released (R.L.U)
si: NT TSG101 NT TSG101 NT TSG101 NT TSG101 NT TSG101 NT TSG101
HSP90
TSG101
p55
p25
CA-SP1
p24 CA
Lysates
p24 CA
Virions

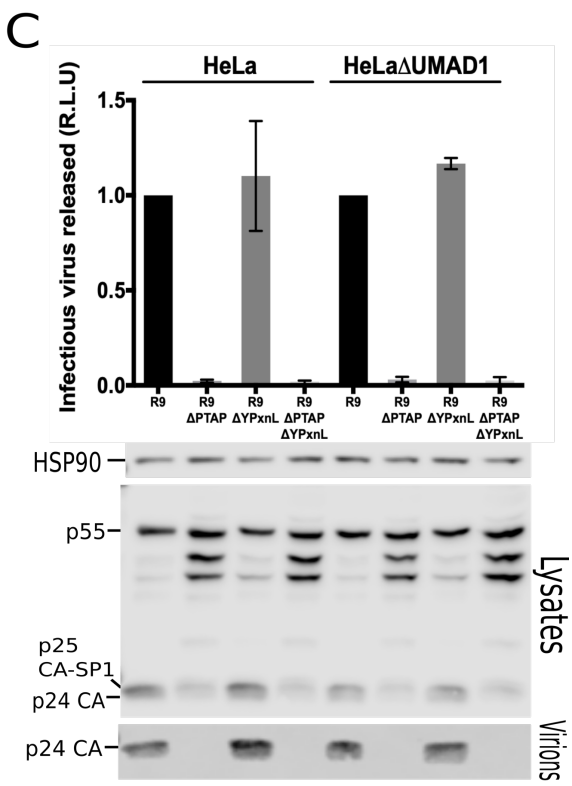
C
HeLa
HeLaΔUMAD1
Infectious virus released (R.L.U)
R9
R9 ΔPTAP
R9 ΔYPxnL
R9 ΔPTAP ΔYPxnL
HSP90
p55
p25
CA-SP1
p24 CA
Lysates
p24 CA
Virions

Figure 50. UMAD1 knockout appears to have no effect on L-domain dependent HIV-1 viral budding
A. Schematic showing HIV-1 Gag constructs encoded by each of the proviral constructs used in B and C. Mutation of the TSG101 binding PTAP L-domain and ALIX binding YPxnL L-domain is shown. **B.** UMAD1 knockout has no effect on PTAP L-domain dependent HIV-1 budding using 293T producer cells. 293T and 293TΔUMAD1 cells were transfected with two doses of control siRNA (siNT) or siRNA against TSG101 (siTSG101) with co-transfection of pNL-HxB, R9 or R9ΔYPxnL proviruses with the second siRNA transfection. TZM-bl reporter cells were infected with clarified viral supernatant 48 hours later and lysed a further 48 hours post-infection. Infectious virus release readout was quantified by β-galactosidase activity. Graph shows the mean levels of infectious virus release for 3 independent repeats normalised to the levels attained using 293T+siNT. Error bars represent the standard deviation from the mean. pNL-HxB 293TΔUMAD1+siNT: 0.62±0.32-fold, R9 293TΔUMAD1+siNT: 1.30±1.03-fold, R9ΔYPxnL 293TΔUMAD1+siNT: 2.32±1.59-fold. Producer cell lysates were resolved by SDS-PAGE and immunoblotting using α-HIV-1 gag antibody was performed. Extracellular budded virions were purified by centrifugation through a 20% sucrose cushion and similarly analysed by SDS-PAGE and α-HIV-1 gag immunoblotting. **C.** UMAD1 has no effect on L-domain dependent HIV-1 budding using HeLa producer cells. HeLa and HeLaΔUMAD1 cells were transfected with R9, R9ΔPTAP, R9ΔYPxnL and R9ΔPTAPΔYPxnL proviruses. TZM-bl reporter cells were infected with clarified viral supernatant 48 hours later and lysed a further 48 hours post-infection. Infectious virus release readout was quantified by β-galactosidase activity. Graph shows the mean levels of infectious virus release for 3 independent repeats normalised to the levels attained using R9 provirus. Error bars represent the standard deviation from the mean. HeLa R9ΔYPxnL: 1.10±0.29-fold, HeLaΔUMAD1 R9ΔYPxnL: 1.17±0.03-fold

5.3. Discussion

Results presented in this chapter suggest no apparent contribution of UMAD1 to HIV-1 budding. One potential avenue to explore further, however, is the possibility of redundancy with the other MVB12-like proteins. It is likely that any of the MVB12-like subunits can be co-opted by HIV-1 for viral budding, so co-depletion of UMAD1 with MVB12A, MVB12B, UBAP1 or combinations of more than one of these subunits could potentially show more obvious effects. Mass spectrometry data from chapter 3 suggesting that endogenous levels of UMAD1 expression are lower than that of MVB12A and UBAP1 also suggests that effects on viral budding upon co-depletion with other MVB12-like subunits could become more apparent.

Given the effects on cytokinesis upon co-depletion of UMAD1 with ALIX (Chapter 4), another exciting area to explore would be the same in HIV-1 budding, especially since HIV-1 encodes an auxiliary ALIX binding YPXnL motif in addition to its dominant TSG101 (ESCRT-I) binding PTAP motif, both of which have been shown to mediate L-domain activity (Section 1.7.1). Depletion of ALIX or mutation of the ALIX binding L-domain in HIV-1 has not been shown to significantly reduce HIV-1 budding, except in the context of a minimal proviral construct lacking the globular domain of MA and the N-terminal

domain of CA[568]. However, it is possible that co-depletion with UMAD1 could show more obvious effects, especially since depletion of UMAD1 does not show the same >10-fold decrease in budding seen upon TSG101 depletion: depletion of UMAD1 would not show a huge decrease in budding, allowing for more modest effects upon co-depletion with ALIX to be seen.

With reference to the study by Morita et al. 2007[667], on the effect of MVB12A and MVB12B depletion on HIV-1 budding, this study mainly observed a defect in virion infectivity, due to aberrant morphology, rather than budding. Similar analysis of virion morphology by electron microscopy is therefore another area for potential exploration. As for MVB12A/B depletion, a slightly elevated level of virions showing amorphous electron-dense morphology may be observed upon UMAD1 depletion, providing evidence for some involvement in viral budding in the form of a visual phenotype, that would not be clear from the assays to measure infectious virus release presented in this chapter. Since overexpression of MVB12A and MVB12B led to a reduction in virion release that was at least partially dependent upon ESCRT-I binding ability, similar overexpression studies could be performed using UMAD1 overexpression, using wild type UMAD1 and the UMAD1 $L_{86}S_{87}D_{88}$/AAA mutant (Chapter 3) that does not bind ESCRT-I.

General discussion and future work

The ESCRT machinery represents the only cellular apparatus so far identified for directing “reverse topology” membrane remodelling events away from the cytoplasm, by assembly inside cytoplasm filled stalks. Since their original discovery in MVB biogenesis and endosomal sorting, the last two decades have seen a vast expansion in the number of mammalian ESCRT mediated processes, ranging from viral budding and cytokinesis to nuclear envelope reformation and lysosome membrane repair. Such discoveries have reinforced the identity of the ESCRT machinery as a modular system, whereby site-specific adaptor proteins ultimately recruit ESCRT-III to target membranes. Links to mitosis and the abscission checkpoint, and the potential ability of a hIST1-CHMP1B polymer to direct ‘normal’ rather than ‘inside-out’ topology membrane remodelling have further demonstrated the essential role of ESCRTs as a key player in cell biology, and opened up many more avenues for future study.

The importance of ESCRT-I is clearly demonstrated by the inability of cells to survive upon its depletion. ESCRT-I shows precise regulation of its cellular levels, as demonstrated by the action of the TSG101 steadiness box. This thesis has demonstrated similar regulation of VPS37 subunit levels, as presented in chapter 3, and the increased expression of ALIX as a potential compensatory mechanism to account for UMAD1 knockout during cytokinesis also demonstrates tight control of ESCRT-I expression levels. Furthermore, ESCRT-I is conserved across species and is involved in many of the ever growing ESCRT mediated processes identified so far: endosomal sorting, cytokinetic abscission, viral budding, ARMM formation, lysosome membrane repair, neuron pruning, and potentially roles in plasma membrane repair and autophagy.

In this thesis, I have characterised the conserved protein UMAD1 as a novel MVB12-like subunit of ESCRT-I that binds ESCRT-I in a manner similar to other MVB12-like subunits via conserved residues within a C-terminal UMA domain. Prior to this work, preferred pairing between UBAP1 with VPS37A to form an ESCRT-I complex with a function specific to MVB biogenesis and endosomal sorting was well described. UMAD1 represents the second example of an MVB12-like subunit that shows a degree of preferred pairing, in this case with VPS37C, although pairing with VPS37B is also observed. My work on UMAD1 together with previous studies of ESCRT-I composition suggests that VPS37-

MVB12 pairing is mediated to varying extents in both selective and stochastic manners. Although preferred pairings with VPS37 subunits have not been seen for MVB12A and MVB12B, such pairings could likely become clearer by performing more finely tuned coprecipitation experiments. For example, immunoblotting using antibodies against MVB12A and MVB12B to examine levels of coprecipitation of these endogenous proteins by each of the VPS37 subunits, as performed for UMAD1 (Figure 34), could make any preferred pairing clearer.

UMAD1 knockout shows reduced binding of TSG101 to the adaptor protein for cytokinetic abscission, CEP55. Consistent with this are results for phenotypic studies from chapter 4 that show both an increase in time taken for successful midbody resolution, and an increase in multinucleation in HeLaΔUMAD1 cells. These results are indicative of a role in cytokinetic abscission and a more generalised role for UMAD1 in mediating successful cytokinesis, respectively. Whilst a similar role in cytokinesis cannot yet be excluded for MVB12A and MVB12B, this is equally likely to be a function specific role for UMAD1. This would represent a function specific role for UMAD1 in cytokinesis, similar to that seen in endosomal sorting for UBAP1. It is tempting in this way to speculate that specific MVB12-like subunits help determine function specific roles for ESCRT-I, mediated in part by their pairing preferences with VPS37 subunits. The ability to pair with more than one VPS37 subunit could potentially be to counteract tissue specific differences in expression levels of each of the VPS37 subunits. Alternatively, in cases where preferential binding to one VPS37 subunit over another is seen in the same cell type, this might be to ensure fine tuning of the levels of different MVB12-like subunit containing ESCRT-I complexes for a specific function, according to the ratio of the different VPS37 subunit levels.

Aside strengthening binding of TSG101 to CEP55, a function for UMAD1 in cytokinesis could also be conferred by other as yet unidentified binding partners, just as the interaction between UBAP1 with HD-PTP helps confer a function in endosomal sorting. As mentioned in chapter 3, results to IP-TMT based mass spectrometry experiments suggest that ESCRT-I binding partners other than its own subunits bind with a much lower affinity or transiently. A technique such as BioID, more suited to identifying weak interaction partners could therefore potentially help identify such partners for UMAD1. This together with characterisation of regions responsible for binding would help further

define the function of UMAD1, and potentially the uncharacterised N-terminus upstream of the UMA domain. If proteins known to be involved in cytokinesis are identified, this may help provide clues as to whether it is involved at early or late stages of cytokinesis, in addition to abscission, and would help direct further study of the role of UMAD1 in cytokinesis.

Other factors that could help define function specific roles for UMAD1 and the other MVB12-like proteins could include differences in localisation to specific membranes. This could be mediated by specific binding motifs, such as the MABP domains of MVB12A and MVB12B, or again via specific interaction partners.

A synergistic increase in midbody resolution time upon co-depletion of UMAD1 with a partial depletion of ALIX suggests that UMAD1 contributes to cytokinetic abscission through a CEP55 – ESCRT-I – ESCRT-II – CHMP6 – ESCRT-III pathway for ESCRT-III recruitment which acts in parallel with a CEP55 – ALIX – ESCRT-III pathway for ESCRT-III recruitment as two partially redundant pathways. Further work will firstly involve further characterisation of these phenotypes by determining when multinucleation takes place, hence whether UMAD1 is involved at early, late or both stages of cytokinesis, in addition to abscission. Further time-lapse experiments to investigate CHMP4B-L-GFP localisation upon UMAD1 depletion are also necessary, to examine differences in the recruitment kinetics and localisation of ESCRT-III in more detail. Rescue experiments in which cytokinetic defects and abscission times are measured upon UMAD1 re-expression in HeLaΔUMAD1 cells will also help strengthen findings.

Given the expansion of MVB12-like subunits in mammals, to include UBAP1, MVB12A, MVB12B and UMAD1, the potential for a degree of redundancy between these subunits suggests that similar testing of each of these proteins for roles in contributing to CEP55 binding and cytokinesis may prove fruitful, as single depletions or co-depletion with UMAD1. Whilst UBAP1 appears to be specifically required for endosomal sorting, further reason to test co-depletion of MVB12A and MVB12B with UMAD1 stems from the fact that MVB12A and MVB12B show only weak phenotypes in endosomal sorting and viral budding compared to UBAP1 and TSG101 respectively. Co-depletion with UMAD1 could therefore potentially display stronger phenotypes both in cytokinesis and viral budding. Consistent with this is the finding that yeast Mvb12 shows the weakest sorting defects compared to depletion of other ESCRT-I subunits, suggesting its main role to be in

stability of the ESCRT-I heterotetramer, even though more functional roles have been suggested.

As previously mentioned in section 4.1., a study by Okumura et al. 2013 showed a specific interaction between VPS37B and VPS37C paralogues with the calcium binding protein ALG-2, which had previously been shown to bind TSG101 and ALIX and proposed to act as a bridging protein between ESCRT-I and ALIX[674]. Interaction between ALG-2 with VPS37B/C appeared to be stronger than with TSG101, particularly the interaction with VPS37C[674]. An interesting parallel can be seen here with UMAD1, which also specifically pairs with VPS37B/C with a preference for VPS37C, and with the roles of UMAD1 and ALIX in cytokinetic abscission. The importance of an interaction between ESCRT-I with ALIX in cytokinesis is perhaps more consistent with the original proposal by Carlton et al. 2008[55] that ESCRT-I simply acts to stabilise ALIX, rather than each protein being part of separate pathways for ESCRT-III recruitment to the midbody. Nonetheless, such a striking parallel with UMAD1 suggests that UMAD1 could additionally be contributing to cytokinesis through stabilisation of ALIX via ALG-2 dimers. Since this bridging via ALG-2 requires calcium, further multinucleation and abscission time scoring experiments could be performed to examine differences in the effects of depleting each of the MVB12-like proteins with and without chelation of calcium, by addition of EGTA. Interestingly, the recently described role for the ESCRT machinery in lysosome membrane repair suggests involvement of both TSG101 and ALIX in this process, as manifested by a delay in recruitment of CHMP4B to damaged lysosome membranes upon depletion of TSG101, and abolishment of recruitment upon co-depletion of TSG101 and ALIX (Section 1.8.6.). This is similar to the effects of depletion of TSG101 and ALIX on cytokinetic abscission, although depletion of ALIX has consistently shown greater perturbation of cytokinesis than TSG101. Nonetheless, this interesting parallel also potentially suggests that testing contribution of UMAD1 to lysosomal repair could prove worthwhile, given the synergistic effects observed upon co-depletion of UMAD1 and ALIX in cytokinesis.

Although the marked increase in co-precipitated UBAP1 and MVB12A by TSG101 from HeLaΔUMAD1 cell lysate can be attributed to reduced competition for binding to ESCRT-I in the absence of UMAD1 (Chapter 3), this competition suggests that UMAD1 could potentially be involved in negative regulation of ubiquitin dependent endosomal sorting,

or other ESCRT-I mediated processes, as a subsidiary role. Given the comparatively small size and structural simplicity of UMAD1 compared to UBAP1, MVB12A or MVB12B, with the lack of any obvious ubiquitin binding motifs, one can speculate that UMAD1 could behave as a negative regulator by simply taking the place of UBAP1, or MVB12A/B within ESCRT-I. Pulse-chase experiments similar to those performed by Stefani et al. 2011[196] could be performed using wild type and UMAD1 knockout cells to compare EGF degradation and accumulation over time, to see if there is a decrease in accumulation/faster degradation of EGF in UMAD1 knockout cells. The cellular localisation of fluorescently tagged UMAD1 upon depletion of VPS4, or expression of VPS4 dominant negative catalytically inactive (E228Q) or ATP binding defective (K173Q) forms could also be examined for endosomal clustering phenotypes.

It is often overlooked that MVB12A was originally identified not as an ESCRT-I component but as a protein named CFBP (CIN85/CD2AP family binding protein) identified in a screen for proteins that are tyrosine-phosphorylated upon EGF stimulation[686]. Phorphorylation was shown to increase binding affinity of CIN85/CD2AP to CFBP and promote EGF receptor downregulation through recruitment of Cbl ubiquitin ligase to the CD2AP/CIN85 complex. Similar phosphorylation of MVB12B was also later observed, in response to EGF stimulation[667,685]. Such phosphorylations of MVB12A and MVB12B perhaps suggests that similar post-translational modifications of UMAD1 could be required for its function. Another area of future work could therefore be to identify whether this is the case, and if so, test whether abolishment of such modifications has an effect on the cytokinesis phenotypes presented in chapter 4, and interaction with ESCRT-I.

Our custom-made α-UMAD1 antibody does not detect endogenous levels of UMAD1 protein, making it unsuitable for immunofluorescence microscopy experiments. One way of examining endogenous UMAD1 localisation more accurately than using cells that stably express exogenous fluorescently tagged UMAD1 would be to create CRISPR knock-in cells for a fluorescent tag immediately upstream of the first *UMAD1* exon. This would ensure that fluorescently tagged UMAD1 is expressed at endogenous levels, thus minimising any undesirable effects due to overexpression, and UMAD1 localisation could be accurately observed in both fixed cells and time-lapse experiments. Time-lapse experiments to specifically examine localisation of fluorescently tagged UMAD1 to the

midbody would complement those to observe YFP-CHMP4B, as discussed in section 4.2.6., providing a more detailed profile of the spaciotemporal localisation of both proteins in relation to each other in cytokinetic abscission.

Although UMAD1 appears to be relatively ubiquitously expressed, according to the human protein atlas version 19, work could also be expanded to examination of UMAD1 in a number of other cell lines derived from other tissues. This could potentially uncover any cell type specific differences such as perhaps stronger cytokinesis phenotypes, as presented in chapter 4.

In conclusion, this thesis has characterised UMAD1 as a novel MVB12-like subunit that shows incorporation into a functional ESCRT-I complex, containing VPS37B or VPS37C with a preference for VPS37C. As is the case with the other characterised MVB12-like proteins, incorporation of UMAD1 into ESCRT-I is mediated via a conserved UMA domain at its C-terminus, through conserved residues. Regions conferring the preferred pairing with VPS37C remain to be discovered. The previously characterised interaction between TSG101 with CEP55 is reduced upon knockout of UMAD1 expression, and consistent with this are results from assays to measure time taken for abscission to occur, which demonstrate a role for UMAD1 in cytokinetic abscission. Quantification of cytokinetic defects in fixed cells has also demonstrated a more generalised role for UMAD1 in mediating successful cytokinesis, as seen by increased multinucleation upon UMAD1 knockdown. Synergistic increases in both multinucleated cells and time taken for successful abscission to occur are seen upon co-depletion of UMAD1 with ALIX. This has led to the hypothesis that UMAD1 contributes to abscission through a subsidiary CEP55 – ESCRT-I – ESCRT-II – CHMP6 – ESCRT-III branch of ESCRT-III recruitment to the midbody, which operates in conjunction with a more dominant partially redundant CEP55 – ALIX – ESCRT-III branch. Further microscopy has additionally demonstrated differences in the localisation patterns/presence of CHMP4B at the midbody upon UMAD1 depletion, further demonstrating a role for UMAD1 in ESCRT mediated cytokinetic abscission.

Bibliography and References

1. Raymond, C. K., I, H.-S., Vater, C. A. & Stevens, T. H. Morphological classification of the yeast vacuolar protein sorting mutants: evidence for a prevacuolar compartment in class E vps mutants. *Mol. Biol. Cell* **3**, 1389–1402 (1992).
2. Banta, L. M., Robinson, J. S., Klionsky, D. J. & Emr, S. D. Organelle assembly in yeast: characterization of yeast mutants defective in vacuolar biogenesis and protein sorting. *J. Cell Biol.* **107**, 1369–1383 (1988).
3. Davis, N. G., Horecka, J. L. & Sprague, G. F. Cis- and trans-acting functions required for endocytosis of the yeast pheromone receptors. *J. Cell Biol.* **122**, 53–65 (1993).
4. Rieder, S. E., Banta, L. M., Köhrer, K., McCaffery, J. M. & Emr, S. D. Multilamellar endosome-like compartment accumulates in the yeast vps28 vacuolar protein sorting mutant. *Mol. Biol. Cell* **7**, 985–99 (1996).
5. Rothman, J. H., Howald, I. & Stevens, T. H. Characterization of genes required for protein sorting and vacuolar function in the yeast Saccharomyces cerevisiae. *EMBO J.* **8**, 2057–2065 (1989).
6. Piper, R. C., Cooper, A. A., Yang, H. & Stevens, T. H. VPS27 controls vacuolar and endocytic traffic through a prevacuolar compartment in Saccharomyces cerevisiae. *J. Cell Biol.* **131**, 603–617 (1995).
7. Odorizzi, G., Babst, M. & Emr, S. D. Fab1p Ptdlns(3)P 5-kinase function essential for protein sorting in the multivesicular body. *Cell* (1998). doi:10.1016/S0092-8674(00)81707-9
8. Katzmann, D. J., Babst, M. & Emr, S. D. Ubiquitin-dependent sorting into the multivesicular body pathway requires the function of a conserved endosomal protein sorting complex, ESCRT-I. *Cell* **106**, 145–155 (2001).
9. Babst, M., Katzmann, D. J., Estepa-Sabal, E. J., Meerloo, T. & Emr, S. D. ESCRT-III: An endosome-associated heterooligomeric protein complex required for MVB sorting. *Dev. Cell* **3**, 271–282 (2002).
10. Babst, M., Katzmann, D. J., Snyder, W. B., Wendland, B. & Emr, S. D. Endosome-associated complex, ESCRT-II, recruits transport machinery for protein sorting at the multivesicular body. *Dev. Cell* **3**, 283–289 (2002).
11. Babst, M., Sato, T. K., Banta, L. M. & Emr, S. D. Endosomal transport function in yeast requires a novel AAA-type ATPase, Vps4p. *EMBO J.* (1997). doi:10.1093/emboj/16.8.1820
12. VerPlank, L. *et al.* Tsg101, a homologue of ubiquitin-conjugating (E2) enzymes, binds the L domain in HIV type 1 Pr55(Gag). *Proc. Natl. Acad. Sci. U. S. A.* **98**, 7724–9 (2001).
13. Garrus, J. E. *et al.* Tsg101 and the vacuolar protein sorting pathway are essential for HIV-1 budding. *Cell* **107**, 55–65 (2001).
14. Martin-Serrano, J., Zang, T. & Bieniasz, P. D. HIV-1 and Ebola virus encode small peptide motifs that recruit Tsg101 to sites of particle assembly to facilitate egress. *Nat. Med.* **7**, 1313–1319 (2001).
15. Demirov, D. G., Ono, A., Orenstein, J. M. & Freed, E. O. Overexpression of the N-terminal domain of TSG101 inhibits HIV-1 budding by blocking late domain function. *Proc. Natl. Acad. Sci. U. S. A.* **99**, 955–60 (2002).
16. Carlton, J. G. & Martin-serrano, J. Parallels Between Cytokinesis and the ESCRT

Machinery. *Science (80-.).* **316**, 1908–1912 (2007).
17. Morita, E. *et al.* Human ESCRT and ALIX proteins interact with proteins of the midbody and function in cytokinesis. *EMBO J.* **26**, 4215–27 (2007).
18. Olmos, Y., Hodgson, L., Mantell, J., Verkade, P. & Carlton, J. G. ESCRT-III controls nuclear envelope reformation. *Nature* **522**, 236–9 (2015).
19. Vietri, M. *et al.* Spastin and ESCRT-III coordinate mitotic spindle disassembly and nuclear envelope sealing. *Nature* **522**, 231–5 (2015).
20. Jimenez, A. J. *et al.* ESCRT Machinery Is Required for Plasma Membrane Repair. *Science (80-.).* **343**, 1247136–1247136 (2014).
21. Scheffer, L. L. *et al.* Mechanism of Ca2+-triggered ESCRT assembly and regulation of cell membrane repair. *Nat. Commun.* **5**, 5646 (2014).
22. Cocucci, E. & Meldolesi, J. Ectosomes and exosomes: Shedding the confusion between extracellular vesicles. *Trends in Cell Biology* **25**, 364–372 (2015).
23. Campelo, F. & Malhotra, V. Membrane Fission: The Biogenesis of Transport Carriers. *Annu. Rev. Biochem.* (2012). doi:10.1146/annurev-biochem-051710-094912
24. Brodsky, F. M. Diversity of Clathrin Function: New Tricks for an Old Protein. *Annu. Rev. Cell Dev. Biol.* (2012). doi:10.1146/annurev-cellbio-101011-155716
25. Popoff, V., Adolf, F., Brügge, B. & Wieland, F. COPI budding within the Golgi stack. *Cold Spring Harb. Perspect. Biol.* (2011). doi:10.1101/cshperspect.a005231
26. Faelber, K. *et al.* Structural insights into dynamin-mediated membrane fission. *Structure* (2012). doi:10.1016/j.str.2012.08.028
27. Scourfield, E. J. & Martin-Serrano, J. Growing functions of the ESCRT machinery in cell biology and viral replication. *Biochem. Soc. Trans.* **45**, 613–634 (2017).
28. Bache, K. G., Raiborg, C., Mehlum, A. & Stenmark, H. STAM and Hrs are subunits of a multivalent ubiquitin-binding complex on early endosomes. *J. Biol. Chem.* **278**, 12513–12521 (2003).
29. Mayers, J. R. *et al.* ESCRT-0 assembles as a heterotetrameric complex on membranes and binds multiple ubiquitinylated cargoes simultaneously. *J. Biol. Chem.* (2011). doi:10.1074/jbc.M110.185363
30. Asao, H. *et al.* Hrs is associated with STAM, a signal-transducing adaptor molecule. It's suppressive effect on cytokine-induced cell growth. *J. Biol. Chem.* (1997). doi:10.1074/jbc.272.52.32785
31. Prag, G. *et al.* The Vps27/Hse1 Complex Is a GAT Domain-Based Scaffold for Ubiquitin-Dependent Sorting. *Dev. Cell* (2007). doi:10.1016/j.devcel.2007.04.013
32. Raiborg, C. *et al.* FYVE and coiled-coil domains determine the specific localisation of Hrs to early endosomes. *J. Cell Sci.* (2001).
33. Gillooly, D. J. Localization of phosphatidylinositol 3-phosphate in yeast and mammalian cells. *EMBO J.* (2000). doi:10.1093/emboj/19.17.4577
34. Mizuno, E., Kawahata, K., Kato, M., Kitamura, N. & Komada, M. STAM proteins bind ubiquitinated proteins on the early endosome via the VHS domain and ubiquitin-interacting motif. *Mol. Biol. Cell* (2003). doi:10.1091/mbc.E02-12-0823
35. Bilodeau, P. S., Urbanowski, J. L., Winistorfer, S. C. & Piper, R. C. The Vps27p-Hse1p complex binds ubiquitin and mediates endosomal protein sorting. *Nat. Cell Biol.* **4**, 534–539 (2002).
36. Fisher, R. D. *et al.* Structure and ubiquitin binding of the ubiquitin-interacting

motif. *J. Biol. Chem.* (2003). doi:10.1074/jbc.M302596200
37. Hirano, S. *et al.* Double-sided ubiquitin binding of Hrs-UIM in endosomal protein sorting. *Nat. Struct. Mol. Biol.* (2006). doi:10.1038/nsmb1051
38. Ren, X. & Hurley, J. H. VHS domains of ESCRT-0 cooperate in high-avidity binding to polyubiquitinated cargo. *EMBO J.* (2010). doi:10.1038/emboj.2010.6
39. Raiborg, C. *et al.* Hrs sorts ubiquitinated proteins into clathrin-coated microdomains of early endosomes. *Nat. Cell Biol.* **4**, 394–8 (2002).
40. Raiborg, C., Wesche, J., Malerød, L. & Stenmark, H. Flat clathrin coats on endosomes mediate degradative protein sorting by scaffolding Hrs in dynamic microdomains. *J. Cell Sci.* (2006). doi:10.1242/jcs.02978
41. Sachse, M., Urbé, S., Oorschot, V., Strous, G. J. & Klumperman, J. Bilayered clathrin coats on endosomal vacuoles are involved in protein sorting toward lysosomes. *Mol. Biol. Cell* (2002). doi:10.1091/mbc.01-10-0525
42. Wenzel, E. M. *et al.* Concerted ESCRT and clathrin recruitment waves define the timing and morphology of intraluminal vesicle formation. *Nat. Commun.* (2018). doi:10.1038/s41467-018-05345-8
43. Im, Y. J. *et al.* Crystallographic and Functional Analysis of the ESCRT-I /HIV-1 Gag PTAP Interaction. *Structure* (2010). doi:10.1016/j.str.2010.08.010
44. Bache, K. G., Brech, A., Mehlum, A. & Stenmark, H. Hrs regulates multivesicular body formation via ESCRT recruitment to endosomes. *J. Cell Biol.* **162**, 435–442 (2003).
45. Lu, Q., Hope, L. W., Brasch, M., Reinhard, C. & Cohen, S. N. TSG101 interaction with HRS mediates endosomal trafficking and receptor down-regulation. *Proc. Natl. Acad. Sci. U. S. A.* **100**, 7626–31 (2003).
46. Katzmann, D. J., Stefan, C. J., Babst, M. & Emr, S. D. Vps27 recruits ESCRT machinery to endosomes during MVB sorting. *J. Cell Biol.* **162**, 413–423 (2003).
47. Pornillos, O. *et al.* HIV Gag mimics the Tsg101-recruiting activity of the human Hrs protein. *J. Cell Biol.* (2003). doi:10.1083/jcb.200302138
48. McCullough, J. *et al.* Activation of the endosome-associated ubiquitin isopeptidase AMSH by STAM, a component of the multivesicular body-sorting machinery. *Curr. Biol.* (2006). doi:10.1016/j.cub.2005.11.073
49. Row, P. E., Prior, I. A., McCullough, J., Clague, M. J. & Urbé, S. The ubiquitin isopeptidase UBPY regulates endosomal ubiquitin dynamics and is essential for receptor down-regulation. *J. Biol. Chem.* (2006). doi:10.1074/jbc.M512615200
50. Mizuno, E., Kobayashi, K., Yamamoto, A., Kitamura, N. & Komada, M. A deubiquitinating enzyme UBPY regulates the level of protein ubiquitination on endosomes. *Traffic* (2006). doi:10.1111/j.1600-0854.2006.00452.x
51. Babst, M., Odorizzi, G., Estepa, E. J. & Emr, S. D. Mammalian tumor susceptibility gene 101 (TSG101) and the yeast homologue, Vps23p, both function in late endosomal trafficking. *Traffic* **1**, 248–258 (2000).
52. Bishop, N., Horman, A. & Woodman, P. Mammalian class E vps proteins recognize ubiquitin and act in the removal of endosomal protein-ubiquitin conjugates. *J. Cell Biol.* (2002). doi:10.1083/jcb.200112080
53. Bishop, N. & Woodman, P. TSG101/Mammalian VPS23 and Mammalian VPS28 Interact Directly and Are Recruited to VPS4-induced Endosomes. *J. Biol. Chem.* **276**, 11735–11742 (2001).
54. Huang, M., Orenstein, J. M., Martin, M. A. & Freed, E. O. p6Gag is required for

particle production from full-length human immunodeficiency virus type 1 molecular clones expressing protease. *J. Virol.* **69**, 6810–8 (1995).
55. Carlton, J. G., Agromayor, M. & Martin-Serrano, J. Differential requirements for Alix and ESCRT-III in cytokinesis and HIV-1 release. *Proc. Natl. Acad. Sci. U. S. A.* **105**, 10541–10546 (2008).
56. Nabhan, J. F., Hu, R., Oh, R. S., Cohen, S. N. & Lu, Q. Formation and release of arrestin domain-containing protein 1-mediated microvesicles (ARMMs) at plasma membrane by recruitment of TSG101 protein. *Proc. Natl. Acad. Sci. U. S. A.* **109**, 4146–51 (2012).
57. Kuo, L. & Freed, E. O. ARRDC1 as a mediator of microvesicle budding. *Proc. Natl. Acad. Sci.* **109**, 4025–4026 (2012).
58. Rusten, T. E. *et al.* ESCRTs and Fab1 Regulate Distinct Steps of Autophagy. *Curr. Biol.* (2007). doi:10.1016/j.cub.2007.09.032
59. Lee, J. A., Beigneux, A., Ahmad, S. T., Young, S. G. & Gao, F. B. ESCRT-III Dysfunction Causes Autophagosome Accumulation and Neurodegeneration. *Curr. Biol.* (2007). doi:10.1016/j.cub.2007.07.029
60. Djeddi, A. *et al.* Induction of autophagy in ESCRT mutants is an adaptive response for cell survival in C. Elegans. *J. Cell Sci.* (2012). doi:10.1242/jcs.091702
61. Sahu, R. *et al.* Microautophagy of Cytosolic Proteins by Late Endosomes. *Dev. Cell* (2011). doi:10.1016/j.devcel.2010.12.003
62. Skowyra, M. L., Schlesinger, P. H., Naismith, T. V. & Hanson, P. I. Triggered recruitment of ESCRT machinery promotes endolysosomal repair. *Science (80-.).* **360**, (2018).
63. Radulovic, M., Bongiovanni, A., Schink, K. O. & Nähse, V. ESCRT-mediated lysosome repair precedes lysophagy and promotes cell survival. (2018).
64. Kostelansky, M. S. *et al.* Molecular Architecture and Functional Model of the Complete Yeast ESCRT-I Heterotetramer. *Cell* **129**, 485–498 (2007).
65. Chu, T., Sun, J., Saksena, S. & Emr, S. D. New component of ESCRT-I regulates endosomal sorting complex assembly. *J. Cell Biol.* **175**, 815–823 (2006).
66. Curtiss, M., Jones, C. & Babst, M. Efficient Cargo Sorting by ESCRT-I and the Subsequent Release of ESCRT-I from Multivesicular Bodies Requires the Subunit Mvb12 □. **18**, 636–645 (2007).
67. Oestreich, A. J., Davies, B. A., Payne, J. A. & Katzmann, D. J. Mvb12 Is a Novel Member of ESCRT-I Involved in Cargo Selection by the Multivesicular Body Pathway □. **18**, 646–657 (2007).
68. Teo, H. *et al.* ESCRT-I Core and ESCRT-II GLUE Domain Structures Reveal Role for GLUE in Linking to ESCRT-I and Membranes. *Cell* (2006). doi:10.1016/j.cell.2006.01.047
69. Pineda-Molina, E. *et al.* The crystal structure of the C-terminal domain of Vps28 reveals a conserved surface required for Vps20 recruitment. *Traffic* **7**, 1007–1016 (2006).
70. Kostelansky, M. S. *et al.* Structural and Functional Organization of the ESCRT-I Trafficking Complex. *Cell* **125**, 113–126 (2006).
71. VanDemark, A. P., Hofmann, R. M., Tsui, C., Pickart, C. M. & Wolberger, C. Molecular insights into polyubiquitin chain assembly: Crystal structure of the Mms2/Ubc13 heterodimer. *Cell* (2001). doi:10.1016/S0092-8674(01)00387-7
72. Sancho, E. *et al.* Role of UEV-1, an Inactive Variant of the E2

UbiquitinConjugating Enzymes, in In Vitro Differentiation and Cell Cycle Behavior of HT-29-M6 Intestinal Mucosecretory Cells. *Mol. Cell. Biol.* (1998). doi:10.1128/mcb.18.1.576

73. Teo, H., Veprintsev, D. B. & Williams, R. L. Structural insights into endosomal sorting complex required for transport (ESCRT-I) recognition of ubiquitinated proteins. *J. Biol. Chem.* **279**, 28689–28696 (2004).
74. Ren, X. & Hurley, J. H. Structural basis for endosomal recruitment of ESCRT-I by ESCRT-0 in yeast. *EMBO J.* (2011). doi:10.1038/emboj.2011.122
75. Pornillos, O., Alam, S. L., Davis, D. R. & Sundquist, W. I. Structure of the Tsg101 UEV domain in complex with the PTAP motif of the HIV-1 p6 protein. *Nat. Struct. Biol.* **9**, 812–817 (2002).
76. Pornillos, O. *et al.* Structure and functional interactions of the Tsg101 UEV domain. *EMBO J.* **21**, 2397–2406 (2002).
77. Alam, S. L. *et al.* Ubiquitin interactions of NZF zinc fingers. *EMBO J.* (2004). doi:10.1038/sj.emboj.7600114
78. Meyer, H. H., Wang, Y. & Warren, G. Direct binding of ubiquitin conjugates by the mammalian p97 adaptor complexes, p47 and Ufd1-Npl4. *EMBO J.* (2002). doi:10.1093/emboj/cdf579
79. Gill, D. J. *et al.* Structural insight into the ESCRT-I/-II link and its role in MVB trafficking. *EMBO J.* (2007). doi:10.1038/sj.emboj.7601501
80. Shields, S. B. *et al.* ESCRT ubiquitin-binding domains function cooperatively during MVB cargo sorting. *J. Cell Biol.* (2009). doi:10.1083/jcb.200811130
81. Hierro, A. *et al.* Structure of the ESCRT-II endosomal trafficking complex. *Nature* **431**, 221–225 (2004).
82. Teo, H., Perisic, O., González, B. & Williams, R. L. ESCRT-II, an endosome-associated complex required for protein sorting: Crystal structure and interactions with ESCRT-III and membranes. *Dev. Cell* **7**, 559–569 (2004).
83. Im, Y. J. & Hurley, J. H. Integrated Structural Model and Membrane Targeting Mechanism of the Human ESCRT-II Complex. *Dev. Cell* **14**, 902–913 (2008).
84. Boura, E. *et al.* Solution structure of the ESCRT-I and -II supercomplex: Implications for membrane budding and scission. *Structure* **20**, 874–886 (2012).
85. Slagsvold, T. *et al.* Eap45 in mammalian ESCRT-II binds ubiquitin via a phosphoinositide- interacting GLUE domain. *J. Biol. Chem.* **280**, 19600–19606 (2005).
86. Alam, S. L. *et al.* Structural basis for ubiquitin recognition by the human ESCRT-II EAP45 GLUE domain. *Nat. Struct. Mol. Biol.* (2006). doi:10.1038/nsmb1160
87. Hirano, S. *et al.* Structural basis of ubiquitin recognition by mammalian Eap45 GLUE domain. *Nat. Struct. Mol. Biol.* (2006). doi:10.1038/nsmb1163
88. Im, Y. J., Wollert, T., Boura, E. & Hurley, J. H. Structure and Function of the ESCRT-II-III Interface in Multivesicular Body Biogenesis. *Dev. Cell* **17**, 234–243 (2009).
89. Saksena, S., Wahlman, J., Teis, D., Johnson, A. E. & Emr, S. D. Functional Reconstitution of ESCRT-III Assembly and Disassembly. *Cell* **136**, 97–109 (2009).
90. Bowers, K. *et al.* Degradation of endocytosed epidermal growth factor and virally ubiquitinated major histocompatibility complex class I is independent of mammalian ESCRTII. *J. Biol. Chem.* (2006). doi:10.1074/jbc.M508632200
91. Langelier, C. *et al.* Human ESCRT-II Complex and Its Role in Human

Immunodeficiency Virus Type 1 Release. *J. Virol.* **80**, 9465–9480 (2006).
92. Malerød, L., Stuffers, S., Brech, A. & Stenmark, H. Vps22/EAP30 in ESCRT-II mediates endosomal sorting of growth factor and chemokine receptors destined for lysosomal degradation. *Traffic* (2007). doi:10.1111/j.1600-0854.2007.00630.x
93. Christ, L. *et al.* ALIX and ESCRT-I/II function as parallel ESCRT-III recruiters in cytokinetic abscission. *J. Cell Biol.* **212**, 499–513 (2016).
94. Lini, Y., Kimpler, L. A., Naismith, T. V., Lauer, J. M. & Hanson, P. I. Interaction of the mammalian Endosomal Sorting Complex Required for Transport (ESCRT) III protein hSnf7-1 with itself, membranes, and the AAA + ATPase SKD1. *J. Biol. Chem.* (2005). doi:10.1074/jbc.M413968200
95. Zamborlini, A. *et al.* Release of autoinhibition converts ESCRT-III components into potent inhibitors of HIV-1 budding. *Proc. Natl. Acad. Sci. U. S. A.* **103**, 19140–5 (2006).
96. Shim, S., Kimpler, L. A. & Hanson, P. I. Structure/function analysis of four core ESCRT-III proteins reveals common regulatory role for extreme C-terminal domain. *Traffic* **8**, 1068–1079 (2007).
97. Hanson, P. I., Roth, R., Lin, Y. & Heuser, J. E. Plasma membrane deformation by circular arrays of ESCRT-III protein filaments. *J. Cell Biol.* **180**, 389–402 (2008).
98. Bajorek, M. *et al.* Structural basis for ESCRT-III protein autoinhibition. *Nat. Struct. Mol. Biol.* **16**, 754–762 (2009).
99. Muzioł, T. *et al.* Structural Basis for Budding by the ESCRT-III Factor CHMP3. *Dev. Cell* **10**, 821–830 (2006).
100. Tang, S. *et al.* Structural basis for activation, assembly and membrane binding of ESCRT-III Snf7 filaments. (2015). doi:10.7554/eLife.12548.001
101. Xiao, J. *et al.* Structural basis of Ist1 function and Ist1-Did2 interaction in the multivesicular body pathway and cytokinesis. *Mol. Biol. Cell* **20**, 3514–24 (2009).
102. McCullough, J. *et al.* Structure and membrane remodeling activity of ESCRT-III helical polymers.-suppl. *Science* **350**, 1548–51 (2015).
103. Guo, E. Z. & Xu, Z. Distinct mechanisms of recognizing endosomal sorting complex required for transport III (ESCRT-III) protein IST1 by different microtubule interacting and trafficking (MIT) domains. *J. Biol. Chem.* (2015). doi:10.1074/jbc.M114.607903
104. Henne, W. M., Buchkovich, N. J., Zhao, Y. & Emr, S. D. The endosomal sorting complex ESCRT-II mediates the assembly and architecture of ESCRT-III helices. *Cell* **151**, 356–371 (2012).
105. Ghazi-Tabatabai, S. *et al.* Structure and Disassembly of Filaments Formed by the ESCRT-III Subunit Vps24. *Structure* **16**, 1345–1356 (2008).
106. Lata, S. *et al.* Helical structures of ESCRT-III are disassembled by VPS4. *Science (80-.).* **321**, 1354–7 (2008).
107. Teis, D., Saksena, S. & Emr, S. D. Ordered Assembly of the ESCRT-III Complex on Endosomes Is Required to Sequester Cargo during MVB Formation. *Dev. Cell* **15**, 578–589 (2008).
108. Teis, D., Saksena, S., Judson, B. L. & Emr, S. D. ESCRT-II coordinates the assembly of ESCRT-III filaments for cargo sorting and multivesicular body vesicle formation. *EMBO J.* **29**, 871–83 (2010).
109. Yorikawa, C. *et al.* Human CHMP6, a myristoylated ESCRT-III protein, interacts

directly with an ESCRT-II component EAP20 and regulates endosomal cargo sorting. *Biochem. J.* **387**, 17–26 (2005).
110. Lee, I.-H. H., Kai, H., Carlson, L.-A. A., Groves, J. T. & Hurley, J. H. Negative membrane curvature catalyzes nucleation of endosomal sorting complex required for transport (ESCRT)-III assembly. *Proc. Natl. Acad. Sci. U. S. A.* **112**, 15892–15897 (2015).
111. Fyfe, I., Schuh, A. L., Edwardson, J. M. & Audhya, A. Association of the endosomal sorting complex ESCRT-II with the Vps20 subunit of ESCRT-III generates a curvature-sensitive complex capable of nucleating ESCRT-III filaments. *J. Biol. Chem.* **286**, 34262–34270 (2011).
112. McCullough, J., Frost, A. & Sundquist, W. I. Structures, Functions, and Dynamics of ESCRT-III/Vps4 Membrane Remodeling and Fission Complexes. *Annu. Rev. Cell Dev. Biol.* (2018). doi:10.1146/annurev-cellbio-100616-060600
113. Olmos, Y. *et al.* Membrane Binding by CHMP7 Coordinates ESCRT- III-Dependent Nuclear Envelope Reformation Report Membrane Binding by CHMP7 Coordinates ESCRT-III-Dependent Nuclear Envelope Reformation. *Curr. Biol.* **26**, 1–7 (2016).
114. Pires, R. *et al.* A Crescent-Shaped ALIX Dimer Targets ESCRT-III CHMP4 Filaments. *Structure* **17**, 843–856 (2009).
115. Hurley, J. H. & Hanson, P. I. Membrane budding and scission by the ESCRT machinery: it's all in the neck. *Nat. Rev. Mol. Cell Biol.* **11**, 556–66 (2010).
116. Peel, S., Macheboeuf, P., Martinelli, N. & Weissenhorn, W. Divergent pathways lead to ESCRT-III-catalyzed membrane fission. *Trends in Biochemical Sciences* (2011). doi:10.1016/j.tibs.2010.09.004
117. Mierzwa, B. E. *et al.* Dynamic subunit turnover in ESCRT-III assemblies is regulated by Vps4 to mediate membrane remodelling during cytokinesis. *Nat. Cell Biol.* (2017). doi:10.1038/ncb3559
118. Guizetti, J. *et al.* Cortical constriction during abscission involves helices of ESCRT-III-dependent filaments. *Science (80-.).* **331**, 1616–20 (2011).
119. Shen, Q.-T. *et al.* Structural analysis and modeling reveals new mechanisms governing ESCRT-III spiral filament assembly. *J. Cell Biol.* **206**, 763–77 (2014).
120. Effantin, G. *et al.* ESCRT-III CHMP2A and CHMP3 form variable helical polymers in vitro and act synergistically during HIV-1 budding. *Cell. Microbiol.* **15**, 213–226 (2013).
121. Elia, N., Sougrat, R., Spurlin, T. A., Hurley, J. H. & Lippincott-schwartz, J. Dynamics of endosomal sorting complex required for transport (ESCRT) machinery during cytokinesis and its role in abscission. *Proc. Natl. Acad. Sci. U. S. A.* **108**, (2011).
122. Cashikar, A. G. *et al.* Structure of cellular ESCRT-III spirals and their relationship to HIV budding. *Elife* **3**, e02184 (2014).
123. Chiaruttini, N. *et al.* Relaxation of Loaded ESCRT-III Spiral Springs Drives Membrane Deformation. *Cell* **163**, 866–879 (2015).
124. Bodon, G. *et al.* Charged Multivesicular Body Protein 2B (CHMP2B) of the Endosomal Sorting Complex Required for Transport-III (ESCRT-III) polymerizes into helical structures deforming the plasma membrane. *J. Biol. Chem.* **286**, 40276–40286 (2011).
125. Dobro, M. J. *et al.* Electron cryotomography of ESCRT assemblies and dividing

Sulfolobus cells suggests that spiraling filaments are involved in membrane scission. *Mol. Biol. Cell* **24**, 2319–27 (2013).
126. Kieffer, C. *et al.* Two Distinct Modes of ESCRT-III Recognition Are Required for VPS4 Functions in Lysosomal Protein Targeting and HIV-1 Budding. *Dev. Cell* (2008). doi:10.1016/j.devcel.2008.05.014
127. Wollert, T., Wunder, C., Lippincott-schwartz, J., Hurley, J. H. J. H. & H, J. Membrane scission by the ESCRT-III complex. *Nature* **458**, 172–7 (2009).
128. Fabrikant, G. *et al.* Computational model of membrane fission catalyzed by ESCRT-III. *PLoS Comput. Biol.* **5**, (2009).
129. Schöneberg, J., Lee, I.-H., Iwasa, J. H. & Hurley, J. H. Reverse-topology membrane scission by the ESCRT proteins. *Nat. Rev. Mol. Cell Biol.* (2016). doi:10.1038/nrm.2016.121
130. Henne, W. M., Buchkovich, N. J. & Emr, S. D. The ESCRT Pathway. *Dev. Cell* **21**, 77–91 (2011).
131. Lenz, M., Crow, D. J. G. & Joanny, J. F. Membrane Buckling Induced by Curved Filaments. *Phys. Rev. Lett.* **103**, (2009).
132. Caspi, Y. & Dekker, C. Dividing the archaeal way: The ancient Cdv cell-division machinery. *Frontiers in Microbiology* (2018). doi:10.3389/fmicb.2018.00174
133. Lata, S. *et al.* Structure and function of ESCRT-III. *Biochem Soc Trans* **37**, 156–160 (2009).
134. Scott, A. *et al.* Structure and ESCRT-III protein interactions of the MIT domain of human VPS4A. *Proc. Natl. Acad. Sci. U. S. A.* **102**, 13813–8 (2005).
135. Shim, S., Merrill, S. A. & Hanson, P. I. Novel interactions of ESCRT-III with LIP5 and VPS4 and their implications for ESCRT-III disassembly. *Mol. Biol. Cell* (2008). doi:10.1091/mbc.E07-12-1263
136. Obita, T. *et al.* Structural basis for selective recognition of ESCRT-III by the AAA ATPase Vps4. *Nature* **449**, 735–739 (2007).
137. Stuchell-Brereton, M. D. *et al.* ESCRT-III recognition by VPS4 ATPases. *Nature* **449**, 740–744 (2007).
138. Han, H. *et al.* Binding of substrates to the central pore of the Vps4 ATPase is autoinhibited by the Microtubule Interacting and Trafficking (MIT) domain and activated by MIT Interacting Motifs (MIMs). *J. Biol. Chem.* (2015). doi:10.1074/jbc.M115.642355
139. Han, H., Monroe, N., Sundquist, W. I., Shen, P. S. & Hill, C. P. The AAA ATPase Vps4 binds ESCRT-III substrates through a repeating array of dipeptide-binding pockets. *Elife* (2017). doi:10.7554/eLife.31324
140. Su, M. *et al.* Mechanism of Vps4 hexamer function revealed by cryo-EM. *Sci. Adv.* (2017). doi:10.1126/sciadv.1700325
141. Monroe, N., Han, H., Shen, P. S., Sundquist, W. I. & Hill, C. P. Structural basis of protein translocation by the Vps4-Vta1 AAA ATPase. *Elife* (2017). doi:10.7554/eLife.24487
142. Sun, S. *et al.* Cryo-EM structures of the ATP-bound Vps4E233Q hexamer and its complex with Vta1 at near-atomic resolution. *Nat. Commun.* (2017). doi:10.1038/ncomms16064
143. Yu, Z., Gonciarz, M. D., Sundquist, W. I., Hill, C. P. & Jensen, G. J. Cryo-EM Structure of Dodecameric Vps4p and Its 2:1 Complex with Vta1p. *J. Mol. Biol.* (2008). doi:10.1016/j.jmb.2008.01.009

144. Monroe, N. & Hill, C. P. Meiotic Clade AAA ATPases: Protein Polymer Disassembly Machines. *Journal of Molecular Biology* **428**, 1897–1911 (2016).
145. Scott, A. *et al.* Structural and mechanistic studies of VPS4 proteins. *EMBO J.* **24**, 3658–3669 (2005).
146. Yang, D. & Hurley, J. H. Structural role of the Vps4-Vta1 interface in ESCRT-III recycling. *Structure* (2010). doi:10.1016/j.str.2010.04.014
147. Xiao, J. *et al.* Structural Basis of Vta1 Function in the Multivesicular Body Sorting Pathway. *Dev. Cell* (2008). doi:10.1016/j.devcel.2007.10.013
148. Skalicky, J. J. *et al.* Interactions of the human LIP5 regulatory protein with endosomal sorting complexes required for transport. *J. Biol. Chem.* (2012). doi:10.1074/jbc.M112.417899
149. Yang, Z. *et al.* Structural basis of molecular recognition between ESCRT-III-like protein Vps60 and AAA-ATPase regulator Vta1 in the multivesicular body pathway. *J. Biol. Chem.* (2012). doi:10.1074/jbc.M112.390724
150. Merrill, S. A. & Hanson, P. I. Activation of human VPS4A by ESCRT-III proteins reveals ability of substrates to relieve enzyme autoinhibition. *J. Biol. Chem.* **285**, 35428–35438 (2010).
151. Babst, M., Davies, B. A. & Katzmann, D. J. Regulation of Vps4 during MVB sorting and cytokinesis. *Traffic* **12**, (2011).
152. Fisher, R. D. *et al.* Structural and Biochemical Studies of ALIX/AIP1 and Its Role in Retrovirus Budding. *Cell* **128**, 841–852 (2007).
153. Kim, J. *et al.* Structural basis for endosomal targeting by the Bro1 domain. *Dev. Cell* (2005). doi:10.1016/j.devcel.2005.04.001
154. Zhai, Q., Landesman, M. B., Robinson, H., Sundquist, W. I. & Hill, C. P. Structure of the Bro1 domain protein BROX and functional analyses of the ALIX Bro1 domain in HIV-1 budding. *PLoS One* (2011). doi:10.1371/journal.pone.0027466
155. Odorizzi, G., Katzmann, D. J., Babst, M., Audhya, A. & Emr, S. D. Bro1 is an endosome-associated protein that functions in the MVB pathway in Saccharomyces cerevisiae. *J. Cell Sci.* (2003). doi:10.1242/jcs.00395
156. Springael, J. Y., Nikko, E., André, B. & Marini, A. M. Yeast Npi3/Bro1 is involved in ubiquitin-dependent control of permease trafficking. *FEBS Lett.* (2002). doi:10.1016/S0014-5793(02)02586-3
157. Wemmer, M. *et al.* Bro1 binding to Snf7 regulates ESCRT-III membrane scission activity in yeast. *J. Cell Biol.* **192**, 295–306 (2011).
158. Luhtala, N. & Odorizzi, G. Bro1 coordinates deubiquitination in the multivesicular body pathway by recruiting Doa4 to endosomes. *J. Cell Biol.* (2004). doi:10.1083/jcb.200403139
159. Richter, C., West, M. & Odorizzi, G. Dual mechanisms specify Doa4-mediated deubiquitination at multivesicular bodies. *EMBO J.* (2007). doi:10.1038/sj.emboj.7601692
160. Richter, C. M., West, M. & Odorizzi, G. Doa4 function in ILV budding is restricted through its interaction with the Vps20 subunit of ESCRT-III. *J. Cell Sci.* (2013). doi:10.1242/jcs.122499
161. Pashkova, N. *et al.* The yeast alix homolog bro1 functions as a ubiquitin receptor for protein sorting into multivesicular endosomes. *Dev. Cell* (2013). doi:10.1016/j.devcel.2013.04.007
162. Kimura, Y., Kawawaki, J., Kakiyama, Y., Shimoda, A. & Tanaka, K. The ESCRT-III

adaptor protein Bro1 controls functions of regulator for free ubiquitin chains 1 (Rfu1) in ubiquitin homeostasis. *J. Biol. Chem.* (2014). doi:10.1074/jbc.M114.550871
163. Nikko, E. & André, B. Split-ubiquitin two-hybrid assay to analyze protein-protein interactions at the endosome: Application to Saccharomyces cerevisiae Bro1 interacting with ESCRT complexes, the Doa4 ubiquitin hydrolase, and the Rsp5 ubiquitin ligase. *Eukaryot. Cell* (2007). doi:10.1128/EC.00024-07
164. Sette, P. *et al.* The Phe105 loop of Alix bro1 domain plays a key role in HIV-1 release. *Structure* **19**, 1485–1495 (2011).
165. Missotten, M., Nichols, A., Rieger, K. & Sadoul, R. Alix, a novel mouse protein undergoing calcium-dependent interaction with the apoptosis-linked-gene 2 (ALG-2) protein. *Cell Death Differ.* (1999). doi:10.1038/sj.cdd.4400456
166. Vito, P., Pellegrini, L., Guiet, C. & D'Adamio, L. Cloning of AIP1, a novel protein that associates with the apoptosis- linked gene ALG-2 in a Ca 2+ -dependent reaction. *J. Biol. Chem.* (1999). doi:10.1074/jbc.274.3.1533
167. McCullough, J., Fisher, R. D., Whitby, F. G., Sundquist, W. I. & Hill, C. P. ALIX-CHMP4 interactions in the human ESCRT pathway. *Proc. Natl. Acad. Sci. U. S. A.* **105**, 7687–7691 (2008).
168. Dussupt, V. *et al.* The nucleocapsid region of HIV-1 gag cooperates with the PTAP and LYPX nL late domains to recruit the cellular machinery necessary for viral budding. *PLoS Pathog.* **5**, (2009).
169. Dussupt, V. *et al.* Basic Residues in the Nucleocapsid Domain of Gag Are Critical for Late Events of HIV-1 Budding. *J. Virol.* (2011). doi:10.1128/jvi.01562-10
170. Popov, S., Popova, E., Inoue, M. & Gottlinger, H. G. Human Immunodeficiency Virus Type 1 Gag Engages the Bro1 Domain of ALIX/AIP1 through the Nucleocapsid. *J. Virol.* (2008). doi:10.1128/jvi.01912-07
171. Bissig, C. *et al.* Viral Infection Controlled by a Calcium-Dependent Lipid-Binding Module in ALIX. *Dev. Cell* (2013). doi:10.1016/j.devcel.2013.04.003
172. Schmidt, M. H. H., Dikic, I. & Bögler, O. Src phosphorylation of Alix/AIP1 modulates its interaction with binding partners and antagonizes its activities. *J. Biol. Chem.* (2005). doi:10.1074/jbc.M409839200
173. Lee, S., Joshi, A., Nagashima, K., Freed, E. O. & Hurley, J. H. Structural basis for viral late-domain binding to Alix. *Nat. Struct. Mol. Biol.* (2007). doi:10.1038/nsmb1203
174. Zhai, Q. *et al.* Structural and functional studies of ALIX interactions with YPX nL late domains of HIV-1 and EIAV. *Nat. Struct. Mol. Biol.* **15**, 43–49 (2008).
175. Dowlatshahi, D. P. *et al.* ALIX Is a Lys63-Specific Polyubiquitin Binding Protein that Functions in Retrovirus Budding. *Dev. Cell* **23**, 1247–1254 (2012).
176. Keren-Kaplan, T. *et al.* Structure-based in silico identification of ubiquitin-binding domains provides insights into the ALIX-V:ubiquitin complex and retrovirus budding. *EMBO J.* **32**, 538–51 (2013).
177. Dores, M. R. *et al.* ALIX binds a YPX 3L motif of the GPCR PAR1 and mediates ubiquitin-independent ESCRT-III/MVB sorting. *J. Cell Biol.* (2012). doi:10.1083/jcb.201110031
178. Odorizzi, G. The multiple personalities of Alix. *J. Cell Sci.* (2006). doi:10.1242/jcs.03072
179. Bissig, C. & Gruenberg, J. ALIX and the multivesicular endosome: ALIX in

Wonderland. *Trends Cell Biol.* (2014). doi:10.1016/j.tcb.2013.10.009
180. Zhai, Q. *et al.* Activation of the Retroviral Budding Factor ALIX. *J. Virol.* (2011). doi:10.1128/jvi.02653-10
181. Sun, S. *et al.* Phosphorylation-Dependent Activation of the ESCRT Function of ALIX in Cytokinetic Abscission and Retroviral Budding. *Dev. Cell* **36**, 331–343 (2016).
182. Sun, S. *et al.* ALG-2 activates the MVB sorting function of ALIX through relieving its intramolecular interaction. *Cell Discov.* (2015). doi:10.1038/celldisc.2015.18
183. Cabezas, A., Bache, K. G., Brech, A. & Stenmark, H. Alix regulates cortical actin and the spatial distribution of endosomes. *J. Cell Sci.* (2005). doi:10.1242/jcs.02382
184. Doyotte, A., Mironov, A., McKenzie, E. & Woodman, P. The Bro1-related protein HD-PTP/PTPN23 is required for endosomal cargo sorting and multivesicular body morphogenesis. *Proc. Natl. Acad. Sci. U. S. A.* (2008). doi:10.1073/pnas.0707601105
185. Sun, S., Zhou, X., Zhang, W., Gallick, G. E. & Kuang, J. Unraveling the pivotal role of ALIX in MVB sorting and silencing of activated EGFR HHS Public Access. **466**, 475–487 (2015).
186. Chen, B., Borinstein, S. C., Gillis, J., Sykes, V. W. & Bogler, O. The glioma-associated protein SETA interacts with AIP1/Alix and ALG-2 and modulates apoptosis in astrocytes. *J. Biol. Chem.* (2000). doi:10.1074/jbc.M908994199
187. Kowanetz, K. *et al.* Identification of a novel proline-arginine motif involved in CIN85-dependent clustering of Cbl and down-regulation of epidermal growth factor receptors. *J. Biol. Chem.* (2003). doi:10.1074/jbc.M304541200
188. Schmidt, M. H. H. *et al.* Alix/AIP1 Antagonizes Epidermal Growth Factor Receptor Downregulation by the Cbl-SETA/CIN85 Complex. *Mol. Cell. Biol.* (2004). doi:10.1128/mcb.24.20.8981-8993.2004
189. Soubeyran, P., Kowanetz, K., Szymkiewicz, I., Langdon, W. Y. & Dikic, I. Cbl-CIN85-endophilin complex mediates ligand-induced downregulation of EGF receptors. *Nature* (2002). doi:10.1038/416183a
190. Chatellard-Causse, C. *et al.* Alix (ALG-2-interacting protein X), a protein involved in apoptosis, binds to endophilins and induces cytoplasmic vacuolization. *J. Biol. Chem.* (2002). doi:10.1074/jbc.M204019200
191. Dores, M. R. *et al.* AP-3 regulates PAR1 ubiquitin-independent MVB/lysosomal sorting via an ALIX-mediated pathway. *Mol. Biol. Cell* (2012). doi:10.1091/mbc.E12-03-0251
192. Toyooka, S. ichi *et al.* HD-PTP: A novel protein tyrosine phosphatase gene on human chromosome 3p21.3. *Biochem. Biophys. Res. Commun.* (2000). doi:10.1006/bbrc.2000.3870
193. Ma, H. *et al.* Histidine-domain-containing protein tyrosine phosphatase regulates platelet-derived growth factor receptor intracellular sorting and degradation. *Cell. Signal.* (2015). doi:10.1016/j.cellsig.2015.07.020
194. Parkinson, M. D. J. *et al.* A non-canonical ESCRT pathway, including histidine domain phosphotyrosine phosphatase (HD-PTP), is used for down-regulation of virally ubiquitinated MHC class I. *Biochem. J.* (2015). doi:10.1042/BJ20150336
195. Kharitidi, D. *et al.* Interplay of Endosomal pH and Ligand Occupancy in Integrin α5β1 Ubiquitination, Endocytic Sorting, and Cell Migration. *Cell Rep.* (2015).

doi:10.1016/j.celrep.2015.09.024
196. Stefani, F. *et al.* UBAP1 is a component of an endosome-specific ESCRT-I complex that is essential for MVB sorting. *Curr. Biol.* **21**, 1245–1250 (2011).
197. Ali, N. *et al.* Recruitment of UBPY and ESCRT exchange drive hd-ptp-dependent sorting of egfr to the mvb. *Curr. Biol.* **23**, 453–461 (2013).
198. Gahloth, D. *et al.* The open architecture of HD-PTP phosphatase provides new insights into the mechanism of regulation of ESCRT function. *Sci. Rep.* (2017). doi:10.1038/s41598-017-09467-9
199. Gahloth, D. *et al.* Structural Basis for Selective Interaction between the ESCRT Regulator HD-PTP and UBAP1. *Structure* (2016). doi:10.1016/j.str.2016.10.006
200. Lee, J. *et al.* Structural study of the HD-PTP bro1 domain in a complex with the core region of STAM2, a subunit of ESCRT-0. *PLoS One* **11**, 1–14 (2016).
201. Gahloth, D. *et al.* Structural Basis for Specific Interaction of TGFβ Signaling Regulators SARA/Endofin with HD-PTP. *Structure* (2017). doi:10.1016/j.str.2017.05.005
202. Tanase, C. A. Histidine domain-protein tyrosine phosphatase interacts with Grb2 and GrpL. *PLoS One* (2010). doi:10.1371/journal.pone.0014339
203. Gingras, M. C., Kazan, J. M. & Pause, A. Role of ESCRT component HD-PTP/PTPN23 in cancer. *Biochemical Society Transactions* (2017). doi:10.1042/BST20160332
204. Zhang, S. *et al.* Suppression of protein tyrosine phosphatase N23 predisposes to breast tumorigenesis via activation of FYN kinase. *Genes Dev.* (2017). doi:10.1101/gad.304261.117
205. Tabernero, L. & Woodman, P. Dissecting the role of His domain protein tyrosine phosphatase/PTPN23 and ESCRTs in sorting activated epidermal growth factor receptor to the multivesicular body. (2018). doi:10.1042/BST20170443
206. Ichioka, F., Kobayashi, R., Katoh, K., Shibata, H. & Maki, M. Brox, a novel farnesylated Bro1 domain-containing protein that associates with charged multivesicular body protein 4 (CHMP4). *FEBS J.* **275**, 682–692 (2008).
207. Mu, R. *et al.* Two Distinct Binding Modes Define The Interaction of Brox with The C-Terminal Tails of CHMP5 and CHMP4B. doi:10.1016/j.str.2012.03.001
208. Huotari, J. & Helenius, A. Endosome maturation. *EMBO Journal* (2011). doi:10.1038/emboj.2011.286
209. Zerial, M. & McBride, H. Rab proteins as membrane organizers. *Nature Reviews Molecular Cell Biology* (2001). doi:10.1038/35052055
210. Vonderheit, A. & Helenius, A. Rab7 associates with early endosomes to mediate sorting and transport of Semliki forest virus to late endosomes. *PLoS Biol.* (2005). doi:10.1371/journal.pbio.0030233
211. Rojas, R. *et al.* Regulation of retromer recruitment to endosomes by sequential action of Rab5 and Rab7. *J. Cell Biol.* (2008). doi:10.1083/jcb.200804048
212. Hayer, A. *et al.* Caveolin-1 is ubiquitinated and targeted to intralumenal vesicles in endolysosomes for degradation. *J. Cell Biol.* (2010). doi:10.1083/jcb.201003086
213. Christoforidis, S. *et al.* Phosphatidylinositol-3-OH kinases are Rab5 effectors. *Nat. Cell Biol.* (1999). doi:10.1038/12075
214. Behnia, R. & Munro, S. Organelle identity and the signposts for membrane traffic. *Nature* (2005). doi:10.1038/nature04397

215. Stenmark, H., Aasland, R., Toh, B. H. & D'Arrigo, A. Endosomal localization of the autoantigen EEA1 is mediated by a zinc- binding FYVE finger. *J. Biol. Chem.* (1996). doi:10.1074/jbc.271.39.24048
216. Patki, V. *et al.* Identification of an early endosomal protein regulated by phosphatidylinositol 3-kinase. *Proc. Natl. Acad. Sci. U. S. A.* (1997). doi:10.1073/pnas.94.14.7326
217. Simonsen, A. *et al.* EEA1 links PI(3)K function to Rab5 regulation of endosome fusion. *Nature* (1998). doi:10.1038/28879
218. Rubino, M., Miaczynska, M., Lippé, R. & Zerial, M. Selective membrane recruitment of EEA1 suggests a role in directional transport of clathrin-coated vesicles to early endosomes. *J. Biol. Chem.* (2000). doi:10.1074/jbc.275.6.3745
219. Balderhaar, H. J. klein. & Ungermann, C. CORVET and HOPS tethering complexes - coordinators of endosome and lysosome fusion. *Journal of Cell Science* (2013). doi:10.1242/jcs.107805
220. Jovic, M., Sharma, M., Rahajeng, J. & Caplan, S. The early endosome: A busy sorting station for proteins at the crossroads. *Histology and Histopathology* (2010). doi:10.14670/HH-25.99
221. Solinger, J. A. & Spang, A. Tethering complexes in the endocytic pathway: CORVET and HOPS. *FEBS Journal* (2013). doi:10.1111/febs.12151
222. Rizo, J. & Südhof, T. C. The Membrane Fusion Enigma: SNAREs, Sec1/Munc18 Proteins, and Their Accomplices—Guilty as Charged? *Annu. Rev. Cell Dev. Biol.* (2012). doi:10.1146/annurev-cellbio-101011-155818
223. Maxfield, F. R. & Yamashiro, D. J. Endosome acidification and the pathways of receptor-mediated endocytosis. *Advances in experimental medicine and biology* (1987). doi:10.1007/978-1-4684-5442-0_16
224. Trombetta, E. S., Ebersold, M., Garrett, W., Pypaert, M. & Mellman, I. Activation of lysosomal function during dendritic cell maturation. *Science (80-.).* (2003). doi:10.1126/science.1080106
225. Kane, P. M. The Where, When, and How of Organelle Acidification by the Yeast Vacuolar H+-ATPase. *Microbiol. Mol. Biol. Rev.* (2006). doi:10.1128/mmbr.70.1.177-191.2006
226. Lafourcade, C., Sobo, K., Kieffer-Jaquinod, S., Garin, J. & van der Goot, F. G. Regulation of the V-ATPase along the endocytic pathway occurs through reversible subunit association and membrane localization. *PLoS One* (2008). doi:10.1371/journal.pone.0002758
227. Rink, J., Ghigo, E., Kalaidzidis, Y. & Zerial, M. Rab conversion as a mechanism of progression from early to late endosomes. *Cell* (2005). doi:10.1016/j.cell.2005.06.043
228. Vicinanza, M., D'Angelo, G., Di Campli, A. & De Matteis, M. A. Function and dysfunction of the PI system in membrane trafficking. *EMBO Journal* (2008). doi:10.1038/emboj.2008.169
229. Kinchen, J. M. & Ravichandran, K. S. Identification of two evolutionarily conserved genes regulating processing of engulfed apoptotic cells. *Nature* (2010). doi:10.1038/nature08853
230. Poteryaev, D., Datta, S., Ackema, K., Zerial, M. & Spang, A. Identification of the switch in early-to-late endosome transition. *Cell* (2010). doi:10.1016/j.cell.2010.03.011

231. Gary, J. D., Wurmser, A. E., Bonangelino, C. J., Weisman, L. S. & Emr, S. D. Fab1p is essential for PtdIns(3)P 5-kinase activity and the maintenance of vacuolar size and membrane homeostasis. *J. Cell Biol.* (1998). doi:10.1083/jcb.143.1.65
232. Shisheva, A. PIKfyve: Partners, significance, debates and paradoxes. *Cell Biology International* (2008). doi:10.1016/j.cellbi.2008.01.006
233. Nickerson, D. P., Brett, C. L. & Merz, A. J. Vps-C complexes: gatekeepers of endolysosomal traffic. *Current Opinion in Cell Biology* (2009). doi:10.1016/j.ceb.2009.05.007
234. Scott, C. C., Vacca, F. & Gruenberg, J. Endosome maturation, transport and functions. *Seminars in Cell and Developmental Biology* (2014). doi:10.1016/j.semcdb.2014.03.034
235. Zheng, N. & Shabek, N. Ubiquitin Ligases: Structure, Function, and Regulation. *Annu. Rev. Biochem.* (2017). doi:10.1146/annurev-biochem-060815-014922
236. Katzmann, D. J., Odorizzi, G. & Emr, S. D. Receptor downregulation and multivesicular-body sorting. *Nature Reviews Molecular Cell Biology* (2002). doi:10.1038/nrm973
237. Raiborg, C. & Stenmark, H. The ESCRT machinery in endosomal sorting of ubiquitylated membrane proteins. *Nature* **458**, 445–52 (2009).
238. Hurley, J. H. & Stenmark, H. Molecular Mechanisms of Ubiquitin-Dependent Membrane Traffic. *Annu. Rev. Biophys.* (2011). doi:10.1146/annurev-biophys-042910-155404
239. Williams, R. L. & Urbé, S. The emerging shape of the ESCRT machinery. *Nat. Rev. Mol. Cell Biol.* **8**, 355–68 (2007).
240. Levkowitz, G. *et al.* Ubiquitin ligase activity and tyrosine phosphorylation underlie suppression of growth factor signaling by c-Cbl/Sli-1. *Mol. Cell* (1999). doi:10.1016/S1097-2765(00)80231-2
241. Shenoy, S. K. *et al.* Nedd4 mediates agonist-dependent ubiquitination, lysosomal targeting, and degradation of the β2-adrenergic receptor. *J. Biol. Chem.* (2008). doi:10.1074/jbc.M709668200
242. Guiney, E. L., Klecker, T. & Emr, S. D. Identification of the endocytic sorting signal recognized by the Art1-Rsp5 ubiquitin ligase complex. *Mol. Biol. Cell* (2016). doi:10.1091/mbc.E16-08-0570
243. Reggiori, F. & Pelham, H. R. B. Sorting of proteins into multivesicular bodies: Ubiquitin-dependent and -independent targeting. *EMBO J.* (2001). doi:10.1093/emboj/20.18.5176
244. Sobo, K., Chevallier, J., Parton, R. G., Gruenberg, J. & van der Goot, F. G. Diversity of raft-like domains in late endosomes. *PLoS One* (2007). doi:10.1371/journal.pone.0000391
245. Kobayashi, T. *et al.* A lipid associated with the antiphospholipid syndrome regulates endosome structure and function. *Nature* (1998). doi:10.1038/32440
246. Möbius, W. *et al.* Recycling compartments and the internal vesicles of multivesicular bodies harbor most of the cholesterol found in the endocytic pathway. *Traffic* (2003). doi:10.1034/j.1600-0854.2003.00072.x
247. Trajkovic, K. *et al.* Ceramide triggers budding of exosome vesicles into multivesicular endosomes. *Science (80-.).* (2008). doi:10.1126/science.1153124
248. Gill, D. J. *et al.* Structural studies of phosphoinositide 3-kinase-dependent traffic to multivesicular bodies. *Biochem Soc Symp* 47–57 (2007).

doi:10.1042/BSS0740047
249. Bilodeau, P. S., Winistorfer, S. C., Kearney, W. R., Robertson, A. D. & Piper, R. C. Vps27-Hse1 and ESCRT-I complexes cooperate to increase efficiency of sorting ubiquitinated proteins at the endosome. *J. Cell Biol.* (2003). doi:10.1083/jcb.200305007
250. Shih, S. C. *et al.* Epsins and Vps27p/Hrs contain ubiquitin-binding domains that function in receptor endocytosis. *Nat. Cell Biol.* (2002). doi:10.1038/ncb790
251. Mageswaran, S. K. *et al.* Constitutively active ESCRT-II suppresses the MVB-sorting phenotype of ESCRT-0 and ESCRT-I mutants. *Mol. Biol. Cell* **26**, 554–68 (2015).
252. Schuh, A. L. & Audhya, A. The ESCRT machinery: from the plasma membrane to endosomes and back again. *Crit. Rev. Biochem. Mol. Biol.* **49**, 242–61 (2014).
253. Wollert, T. & Hurley, J. H. Molecular mechanism of multivesicular body biogenesis by ESCRT complexes. *Nature* **464**, 864–869 (2010).
254. Babst, M. MVB Vesicle Formation: ESCRT-Dependent, ESCRT-Independent and Everything in Between. *Curr. Opin. Cell Biol.* **23**, 452–457 (2011).
255. Matsuo, H. *et al.* Role of LBPA and Alix in Multivesicular Liposome Formation and Endosome Organization. *Science (80-.).* (2004). doi:10.1126/science.1092425
256. Stuffers, S., Sem Wegner, C., Stenmark, H. & Brech, A. Multivesicular endosome biogenesis in the absence of ESCRTs. *Traffic* (2009). doi:10.1111/j.1600-0854.2009.00920.x
257. Adell, M. A. Y. *et al.* Recruitment dynamics of ESCRT-III and Vps4 to endosomes and implications for reverse membrane budding. *Elife* (2017). doi:10.7554/eLife.31652
258. Quinney, K. B. *et al.* Growth factor stimulation promotes multivesicular endosome biogenesis by prolonging recruitment of the late-acting ESCRT machinery. *Proc. Natl. Acad. Sci. U. S. A.* (2019). doi:10.1073/pnas.1817898116
259. Agromayor, M. & Martin-Serrano, J. Interaction of AMSH with ESCRT-III and deubiquitination of endosomal cargo. *J. Biol. Chem.* (2006). doi:10.1074/jbc.M513803200
260. Solomons, J. *et al.* Structural basis for ESCRT-III CHMP3 recruitment of AMSH. *Structure* (2011). doi:10.1016/j.str.2011.05.011
261. McCullough, J., Clague, M. J. & Urbé, S. AMSH is an endosome-associated ubiquitin isopeptidase. *J. Cell Biol.* (2004). doi:10.1083/jcb.200401141
262. Yu, M. M. *et al.* Targeting of AMSH to endosomes is required for epidermal growth factor receptor degradation. *J. Biol. Chem.* (2007). doi:10.1074/jbc.M611635200
263. Row, P. E. *et al.* The MIT domain of UBPY constitutes a CHMP binding and endosomal localization signal required for efficient epidermal growth factor receptor degradation. *J. Biol. Chem.* (2007). doi:10.1074/jbc.M704009200
264. Tsang, H. T. H. H. *et al.* A systematic analysis of human CHMP protein interactions: Additional MIT domain-containing proteins bind to multiple components of the human ESCRT III complex. *Genomics* (2006). doi:10.1016/j.ygeno.2006.04.003
265. Amerik, A., Sindhi, N. & Hochstrasser, M. A conserved late endosome-targeting signal required for Doa4 deubiquitylating enzyme function. *J. Cell Biol.* (2006).

doi:10.1083/jcb.200605134
266. Pareja, F. *et al.* Deubiquitination of EGFR by Cezanne-1 contributes to cancer progression. *Oncogene* (2012). doi:10.1038/onc.2011.587
267. Alwan, H. A. J. & Van Leeuwen, J. E. M. UBPY-mediated Epidermal Growth Factor Receptor (EGFR) de-ubiquitination promotes EGFR degradation. *J. Biol. Chem.* (2007). doi:10.1074/jbc.M604711200
268. Berlin, I., Schwartz, H. & Nash, P. D. Regulation of epidermal growth factor receptor ubiquitination and trafficking by the USP8·STAM complex. *J. Biol. Chem.* (2010). doi:10.1074/jbc.M109.016287
269. Mizuno, E. *et al.* Regulation of epidermal growth factor receptor down-regulation by UBPY-mediated deubiquitination at endosomes. *Mol. Biol. Cell* (2005). doi:10.1091/mbc.E05-06-0560
270. Zhang, J., Du, J., Lei, C., Liu, M. & Zhu, A. J. Ubpy controls the stability of the ESCRT-0 subunit Hrs in development. *Dev.* (2014). doi:10.1242/dev.099564
271. Soediono, B. Alberts - Molecular Biology Of The Cell 4th Ed. *J. Chem. Inf. Model.* (1989). doi:10.1017/CBO9781107415324.004
272. Mitchison, T. J. & Salmon, E. D. Mitosis: A history of division. *Nature Cell Biology* (2001). doi:10.1038/35050656
273. Flemming, W. Zellsubstanz, kern und zelltheilung. *F.C.W. Vogel, Leipzig,* (1882).
274. Gershony, O., Péer, T., Noach-Hirsh, M., Elia, N. & Tzur, A. Cytokinetic abscission is an acute G1 event. *Cell Cycle* (2014). doi:10.4161/15384101.2014.956486
275. Eikenes, Å. H. *et al.* ALIX and ESCRT-III Coordinately Control Cytokinetic Abscission during Germline Stem Cell Division In Vivo. *PLoS Genet.* **11**, (2015).
276. Park, J. The Cell: A Molecular Approach, Second Edition. (2001).
277. D'Adda Di Fagagna, F. Living on a break: Cellular senescence as a DNA-damage response. *Nature Reviews Cancer* (2008). doi:10.1038/nrc2440
278. Goloborodko, A., Imakaev, M. V., Marko, J. F. & Mirny, L. Compaction and segregation of sister chromatids via active loop extrusion. *Elife* (2016). doi:10.7554/eLife.14864
279. Hauf, S. *et al.* Dissociation of cohesin from chromosome arms and loss of arm cohesion during early mitosis depends on phosphorylation of SA2. in *PLoS Biology* (2005). doi:10.1371/journal.pbio.0030069
280. Dewar, H., Tanaka, K., Nasmyth, K. & Tanaka, T. U. Tension between two kinetochores suffices for their bi-orientation on the mitotic spindle. *Nature* (2004). doi:10.1038/nature02328
281. Gregan, J., Polakova, S., Zhang, L., Tolić-Nørrelykke, I. M. & Cimini, D. Merotelic kinetochore attachment: Causes and effects. *Trends in Cell Biology* (2011). doi:10.1016/j.tcb.2011.01.003
282. Uhlmann, F., Lottspelch, F. & Nasmyth, K. Sister-chromatid separation at anaphase onset is promoted by cleavage of the cohesin subunit Scc1. *Nature* (1999). doi:10.1038/21831
283. Waizenegger, I. C., Hauf, S., Meinke, A. & Peters, J. M. Two distinct pathways remove mammalian cohesin from chromosome arms in prophase and from centromeres in anaphase. *Cell* (2000). doi:10.1016/S0092-8674(00)00132-X
284. Vermeulen, K., Van Bockstaele, D. R. & Berneman, Z. N. The cell cycle: A review of regulation, deregulation and therapeutic targets in cancer. *Cell Prolif.* **36**, 131–149 (2003).

285. Morgan, D. O. Principles of CDK regulation. *Nature* (1995). doi:10.1038/374131a0
286. Lee, M. G. & Nurse, P. Complementation used to clone a human homologue of the fission yeast cell cycle control gene cdc2. *Nature* (1987). doi:10.1038/327031a0
287. Sherr, C. J. G1 phase progression: Cycling on cue. *Cell* (1994). doi:10.1016/0092-8674(94)90540-1
288. Buchkovich, K., Duffy, L. A. & Harlow, E. The retinoblastoma protein is phosphorylated during specific phases of the cell cycle. *Cell* (1989). doi:10.1016/0092-8674(89)90508-4
289. Kato, J., Matsushime, H., Hiebert, S. W., Ewen, M. E. & Sherr, C. J. Direct binding of cyclin D to the retinoblastoma gene product (pRb) and pRb phosphorylation by the cyclin D-dependent kinase CDK4. *Genes Dev.* (1993). doi:10.1101/gad.7.3.331
290. Brehm, A. *et al.* Retinoblastoma protein recruits histone deacetylase to repress transcription. *Nature* (1998). doi:10.1038/35404
291. Girard, F., Strausfeld, U., Fernandez, A. & Lamb, N. J. C. Cyclin a is required for the onset of DNA replication in mammalian fibroblasts. *Cell* (1991). doi:10.1016/0092-8674(91)90293-8
292. Walker, D. H. & Maller, J. L. Role for cyclin A in the dependence of mitosis on completion of DMA replication. *Nature* (1991). doi:10.1038/354314a0
293. King, R. W., Jackson, P. K. & Kirschner, M. W. Mitosis in transition. *Cell* (1994). doi:10.1016/0092-8674(94)90542-8
294. Arellano, M. & Moreno, S. Regulation of CDK/cyclin complexes during the cell cycle. *International Journal of Biochemistry and Cell Biology* (1997). doi:10.1016/S1357-2725(96)00178-1
295. Fisher, R. P. & Morgan, D. O. A novel cyclin associates with M015/CDK7 to form the CDK-activating kinase. *Cell* (1994). doi:10.1016/0092-8674(94)90535-5
296. Pines, J. Cyclins and cyclin-dependent kinases: Theme and variations. *Advances in Cancer Research* (1995). doi:10.1016/s0065-230x(08)60254-7
297. Lew, D. J. & Kornbluth, S. Regulatory roles of cyclin dependent kinase phosphorylation in cell cycle control. *Curr. Opin. Cell Biol.* (1996). doi:10.1016/S0955-0674(96)80080-9
298. Sherr, C. J. & Roberts, J. M. Inhibitors of mammalian G1 cyclin-dependent kinases. *Genes and Development* (1995). doi:10.1101/gad.9.10.1149
299. Polyak, K. *et al.* Cloning of p27Kip1, a cyclin-dependent kinase inhibitor and a potential mediator of extracellular antimitogenic signals. *Cell* (1994). doi:10.1016/0092-8674(94)90572-X
300. Harper, J. W. *et al.* Inhibition of cyclin-dependent kinases by p21. *Mol. Biol. Cell* (1995). doi:10.1091/mbc.6.4.387
301. Lee, M. H., Reynisdottir, I. & Massague, J. Cloning of p57(KIP2), a cyclin-dependent kinase inhibitor with unique domain structure and tissue distribution. *Genes Dev.* (1995). doi:10.1101/gad.9.6.639
302. Pardee, A. B. A restriction point for control of normal animal cell proliferation. *Proc. Natl. Acad. Sci. U. S. A.* (1974). doi:10.1073/pnas.71.4.1286
303. Levine, A. J. p53, the cellular gatekeeper for growth and division. *Cell* (1997). doi:10.1016/S0092-8674(00)81871-1

304. Siliciano, J. D. *et al.* DNA damage induces phosphorylation of the amino terminus of p53. *Genes Dev.* (1997). doi:10.1101/gad.11.24.3471
305. Durocher, D. & Jackson, S. P. DNA-PK, ATM and ATR as sensors of DNA damage: Variations on a theme? *Current Opinion in Cell Biology* (2001). doi:10.1016/S0955-0674(00)00201-5
306. Pan, Z. Q. *et al.* Inhibition of nucleotide excision repair by the cyclin-dependent kinase inhibitor p21. *J. Biol. Chem.* (1995). doi:10.1074/jbc.270.37.22008
307. Sanchez, Y. *et al.* Conservation of the Chk1 checkpoint pathway in mammals: Linkage of DNA damage to Cdk regulation through Cdc25. *Science (80-.).* (1997). doi:10.1126/science.277.5331.1497
308. Zeng, Y. *et al.* Replication checkpoint requires phosphorylation of the phosphatase Cdc25 by Cds1 or Chk1. *Nature* (1998). doi:10.1038/26766
309. Lu, X., Nannenga, B. & Donehower, L. A. PPM1D dephosphorylates Chk1 and p53 and abrogates cell cycle checkpoints. *Genes Dev.* (2005). doi:10.1101/gad.1291305
310. Den Elzen, N., Kosoy, A., Christopoulos, H. & O'Connell, M. J. Resisting arrest: Recovery from checkpoint arrest through dephosphorylation of Chk1 by PP1. *Cell Cycle* (2004). doi:10.4161/cc.3.5.820
311. Den Elzen, N. R. & O'Connell, M. J. Recovery from DNA damage checkpoint arrest by PP1-mediated inhibition of Chk1. *EMBO J.* (2004). doi:10.1038/sj.emboj.7600105
312. Pines, J. Cubism and the cell cycle: The many faces of the APC/C. *Nature Reviews Molecular Cell Biology* (2011). doi:10.1038/nrm3132
313. McLean, J. R., Chaix, D., Ohi, M. D. & Gould, K. L. State of the APC/C: Organization, function, and structure. *Critical Reviews in Biochemistry and Molecular Biology* (2011). doi:10.3109/10409238.2010.541420
314. Hagting, A. *et al.* Human securin proteolysis is controlled by the spindle checkpoint and reveals when the APC/C switches from activation by Cdc20 to Cdh1. *J. Cell Biol.* (2002). doi:10.1083/jcb.200111001
315. Cohen-Fix, O. & Koshland, D. The anaphase inhibitor of Saccharomyces cerevisiae Pds1p is a target of the DNA damage checkpoint pathway. *Proc. Natl. Acad. Sci. U. S. A.* (1997). doi:10.1073/pnas.94.26.14361
316. Fang, G., Yu, H. & Kirschner, M. W. The checkpoint protein MAD2 and the mitotic regulator CDC20 form a ternary complex with the anaphase-promoting complex to control anaphase initiation. *Genes Dev.* (1998). doi:10.1101/gad.12.12.1871
317. Bement, W. M., Benink, H. A. & Von Dassow, G. A microtubule-dependent zone of active RhoA during cleavage plane specification. *J. Cell Biol.* (2005). doi:10.1083/jcb.200501131
318. Euteneuer, U., McIntosh, J. R. & Richard Mcintosh, J. Polarity of midbody and phragmoplast microtubules. *J. Cell Biol.* **87**, 509–515 (1980).
319. Kamasaki, T. *et al.* Augmin-dependent microtubule nucleation at microtubule walls in the spindle. *J. Cell Biol.* (2013). doi:10.1083/jcb.201304031
320. Uehara, R. *et al.* The augmin complex plays a critical role in spindle microtubule generation for mitotic progression and cytokinesis in human cells. *Proc. Natl. Acad. Sci. U. S. A.* (2009). doi:10.1073/pnas.0901587106
321. Uehara, R. & Goshima, G. Functional central spindle assembly requires de novo

microtubule generation in the interchromosomal region during anaphase. *J. Cell Biol.* (2010). doi:10.1083/jcb.201004150
322. Earnshaw, W. C. & Bernat, R. L. Chromosomal passengers: Toward an integrated view of mitosis. *Chromosoma* (1991). doi:10.1007/BF00337241
323. Adams, R. R., Carmena, M. & Earnshaw, W. C. Chromosomal passengers and the (aurora) ABCs of mitosis. *Trends in Cell Biology* (2001). doi:10.1016/S0962-8924(00)01880-8
324. Bieling, P., Telley, I. A. & Surrey, T. A minimal midzone protein module controls formation and length of antiparallel microtubule overlaps. *Cell* (2010). doi:10.1016/j.cell.2010.06.033
325. Cundell, M. J. *et al.* The BEG (PP2A-B55/ENSA/Greatwall) Pathway Ensures Cytokinesis follows Chromosome Separation. *Mol. Cell* (2013). doi:10.1016/j.molcel.2013.09.005
326. Jiang, W. *et al.* PRC1: A human mitotic spindle-associated CDK substrate protein required for cytokinesis. *Mol. Cell* (1998). doi:10.1016/s1097-2765(00)80302-0
327. Mollinari, C. *et al.* PRC1 is a microtubule binding and bundling protein essential to maintain the mitotic spindle midzone. *J. Cell Biol.* (2002). doi:10.1083/jcb.200111052
328. Neef, R. *et al.* Choice of Plk1 docking partners during mitosis and cytokinesis is controlled by the activation state of Cdk1. *Nat. Cell Biol.* (2007). doi:10.1038/ncb1557
329. Subramanian, R. *et al.* Insights into antiparallel microtubule crosslinking by PRC1, a conserved nonmotor microtubule binding protein. *Cell* (2010). doi:10.1016/j.cell.2010.07.012
330. Zhu, C., Lau, E., Schwarzenbacher, R., Bossy-Wetzel, E. & Jiang, W. Spatiotemporal control of spindle midzone formation by PRC1 in human cells. *Proc. Natl. Acad. Sci. U. S. A.* (2006). doi:10.1073/pnas.0506926103
331. Mishima, M., Kaitna, S. & Glotzer, M. Central spindle assembly and cytokinesis require a kinesin-like protein/RhoGAP complex with microtubule bundling activity. *Dev. Cell* (2002). doi:10.1016/S1534-5807(01)00110-1
332. Pavicic-Kaltenbrunner, V., Mishima, M. & Glotzer, M. Cooperative assembly of CYK-4/MgcRacGAP and ZEN-4/MKLP1 to form the centralspindlin complex. *Mol. Biol. Cell* **18**, 4992–5003 (2007).
333. Douglas, M. E., Davies, T., Joseph, N. & Mishima, M. Aurora B and 14-3-3 Coordinately Regulate Clustering of Centralspindlin during Cytokinesis. *Curr. Biol.* (2010). doi:10.1016/j.cub.2010.03.055
334. Hutterer, A., Glotzer, M. & Mishima, M. Clustering of Centralspindlin Is Essential for Its Accumulation to the Central Spindle and the Midbody. *Curr. Biol.* (2009). doi:10.1016/j.cub.2009.10.050
335. Carmena, M., Wheelock, M., Funabiki, H. & Earnshaw, W. C. The chromosomal passenger complex (CPC): From easy rider to the godfather of mitosis. *Nat. Rev. Mol. Cell Biol.* **13**, 789–803 (2012).
336. Haase, J., Bonner, M. K., Halas, H. & Kelly, A. E. Distinct Roles of the Chromosomal Passenger Complex in the Detection of and Response to Errors in Kinetochore-Microtubule Attachment. *Dev. Cell* (2017). doi:10.1016/j.devcel.2017.08.022
337. Hümmer, S. & Mayer, T. U. Cdk1 Negatively Regulates Midzone Localization of

the Mitotic Kinesin Mklp2 and the Chromosomal Passenger Complex. *Curr. Biol.* **19**, 607–612 (2009).
338. Kaitna, S., Mendoza, M., Jantsch-Plunger, V. & Glotzer, M. Incenp and an Aurora-like kinase form a complex essential for chromosome segregation and efficient completion of cytokinesis. *Curr. Biol.* (2000). doi:10.1016/S0960-9822(00)00721-1
339. Mishima, M. *et al.* Cell cycle regulation of central spindle assembly. *Nature* **430**, 908–913 (2004).
340. Guse, A., Mishima, M. & Glotzer, M. Phosphorylation of ZEN-4/MKLP1 by aurora B regulates completion of cytokinesis. *Curr. Biol.* **15**, 778–786 (2005).
341. Uehara, R. *et al.* Aurora B and Kif2A control microtubule length for assembly of a functional central spindle during anaphase. *J. Cell Biol.* (2013). doi:10.1083/jcb.201302123
342. Burkard, M. E. *et al.* Plk1 self-organization and priming phosphorylation of HsCYK-4 at the spindle midzone regulate the onset of division in human cells. *PLoS Biol.* (2009). doi:10.1371/journal.pbio.1000111
343. Su, K. C., Takaki, T. & Petronczki, M. Targeting of the RhoGEF Ect2 to the Equatorial Membrane Controls Cleavage Furrow Formation during Cytokinesis. *Dev. Cell* **21**, 1104–1115 (2011).
344. Wolfe, B. A., Takaki, T., Petronczki, M. & Glotzer, M. Polo-like kinase 1 directs assembly of the HsCyk-4 RhoGAP/Ect2 RhoGEF complex to initiate cleavage furrow formation. *PLoS Biol.* (2009). doi:10.1371/journal.pbio.1000110
345. Yüce, Ö., Piekny, A. & Glotzer, M. An ECT2-centralspindlin complex regulates the localization and function of RhoA. *J. Cell Biol.* (2005). doi:10.1083/jcb.200501097
346. Kotýnková, K., Su, K. C., West, S. C. & Petronczki, M. Plasma Membrane Association but Not Midzone Recruitment of RhoGEF ECT2 Is Essential for Cytokinesis. *Cell Rep.* (2016). doi:10.1016/j.celrep.2016.11.029
347. Loria, A., Longhini, K. M. & Glotzer, M. The RhoGAP domain of CYK-4 Has an essential role in RhoA activation. *Curr. Biol.* (2012). doi:10.1016/j.cub.2011.12.019
348. Miller, A. L. & Bement, W. M. Regulation of cytokinesis by Rho GTPase flux. *Nat. Cell Biol.* (2009). doi:10.1038/ncb1814
349. Bastos, R. N., Penate, X., Bates, M., Hammond, D. & Barr, F. A. CYK4 inhibits Rac1-dependent PAK1 and ARHGEF7 effector pathways during cytokinesis. *J. Cell Biol.* (2012). doi:10.1083/jcb.201204107
350. Canman, J. C. *et al.* Inhibition of Rac by the GAP activity of centralspindlin is essential for cytokinesis. *Science (80-.).* (2008). doi:10.1126/science.1163086
351. Pollard, T. D. Regulation of actin filament assembly by Arp2/3 complex and formins. *Annual Review of Biophysics and Biomolecular Structure* (2007). doi:10.1146/annurev.biophys.35.040405.101936
352. Davies, T. & Canman, J. C. Stuck in the middle: Rac, adhesion, and cytokinesis. *Journal of Cell Biology* (2012). doi:10.1083/jcb.201207197
353. Dechant, R. & Glotzer, M. Centrosome separation and central spindle assembly act in redundant pathways that regulate microtubule density and trigger cleavage furrow formation. *Dev. Cell* (2003). doi:10.1016/S1534-5807(03)00057-1

354. Foe, V. E. & Von Dassow, G. Stable and dynamic microtubules coordinately shape the myosin activation zone during cytokinetic furrow formation. *J. Cell Biol.* (2008). doi:10.1083/jcb.200807128
355. Werner, M., Munro, E. & Glotzer, M. Astral Signals Spatially Bias Cortical Myosin Recruitment to Break Symmetry and Promote Cytokinesis. *Curr. Biol.* (2007). doi:10.1016/j.cub.2007.06.070
356. Castrillon, D. H. & Wasserman, S. A. diaphanous is required for cytokinesis in Drosophila and shares domains of similarity with the products of the limb deformity gene. *Development* (1994).
357. Severson, A. F., Baillie, D. L. & Bowerman, B. A Formin Homology protein and a profilin are required for cytokinesis and Arp2/3-independent assembly of cortical microfilaments in C. elegans. *Curr. Biol.* (2002). doi:10.1016/S0960-9822(02)01355-6
358. Watanabe, S. *et al.* mDia2 induces the actin scaffold for the contractile ring and stabilizes its position during cytokinesis in NIH 3T3 cells. *Mol. Biol. Cell* **19**, 2328–2338 (2008).
359. Matsumura, F. Regulation of myosin II during cytokinesis in higher eukaryotes. *Trends in Cell Biology* **15**, 371–377 (2005).
360. Kimura, K. *et al.* Regulation of myosin phosphatase by Rho and Rho-associated kinase (Rho- kinase). *Science (80-.).* (1996). doi:10.1126/science.273.5272.245
361. Field, C. M. & Alberts, B. M. Anillin, a contractile ring protein that cycles from the nucleus to the cell cortex. *J. Cell Biol.* (1995). doi:10.1083/jcb.131.1.165
362. Piekny, A. J. & Maddox, A. S. The myriad roles of Anillin during cytokinesis. *Seminars in Cell and Developmental Biology* (2010). doi:10.1016/j.semcdb.2010.08.002
363. D'Avino, P. P. *et al.* Interaction between Anillin and RacGAP50C connects the actomyosin contractile ring with spindle microtubules at the cell division site. *J. Cell Sci.* (2008). doi:10.1242/jcs.026716
364. Gregory, S. L. *et al.* Cell Division Requires a Direct Link between Microtubule-Bound RacGAP and Anillin in the Contractile Ring. *Curr. Biol.* (2008). doi:10.1016/j.cub.2007.11.050
365. Bassi, Z. I. *et al.* Sticky/Citron kinase maintains proper RhoA localization at the cleavage site during cytokinesis. *J. Cell Biol.* (2011). doi:10.1083/jcb.201105136
366. Schroeder, T. E. The contractile ring: II. determining its brief existence, volumetric changes, and vital role in cleaving arbacia eggs. *J. Cell Biol.* (1972). doi:10.1083/jcb.53.2.419
367. Tucker, J. B. Microtubules and a contractile ring of microfilaments associated with a cleavage furrow. *J. Cell Sci.* (1971).
368. Maupin, P. & Pollard, T. D. Arrangement of actin filaments and myosin-like filaments in the contractile ring and of actin-like filaments in the mitotic spindle of dividing HeLa cells. *J. Ultrastruct. Res. Mol. Struct. Res.* (1986). doi:10.1016/0889-1605(86)90055-8
369. Kamasaki, T., Osumi, M. & Mabuchi, I. Three-dimensional arrangement of F-actin in the contractile ring of fission yeast. *J. Cell Biol.* (2007). doi:10.1083/jcb.200612018
370. Reichl, E. M. *et al.* Interactions between Myosin and Actin Crosslinkers Control Cytokinesis Contractility Dynamics and Mechanics. *Curr. Biol.* (2008).

doi:10.1016/j.cub.2008.02.056
371. Fishkind, D. J. & Wang, Y. L. Orientation and three-dimensional organization of actin filaments in dividing cultured cells. *J. Cell Biol.* (1993). doi:10.1083/jcb.123.4.837
372. Kruse, K. & Jülicher, F. Self-organization and mechanical properties of active filament bundles. *Phys. Rev. E - Stat. Physics, Plasmas, Fluids, Relat. Interdiscip. Top.* (2003). doi:10.1103/PhysRevE.67.051913
373. Murthy, K. & Wadsworth, P. Myosin-II-dependent localization and dynamics of F-actin during cytokinesis. *Curr. Biol.* (2005). doi:10.1016/j.cub.2005.02.055
374. Carvalho, A., Desai, A. & Oegema, K. Structural Memory in the Contractile Ring Makes the Duration of Cytokinesis Independent of Cell Size. *Cell* (2009). doi:10.1016/j.cell.2009.03.021
375. Biron, D., Alvarez-Lacalle, E., Tlusty, T. & Moses, E. Molecular model of the contractile ring. *Phys. Rev. Lett.* (2005). doi:10.1103/PhysRevLett.95.098102
376. Zumdieck, A., Kruse, K., Bringmann, H., Hyman, A. A. & Jülicher, F. Stress generation and filamnet turnover during actin ring constriction. *PLoS One* (2007). doi:10.1371/journal.pone.0000696
377. Joo, E., Surka, M. C. & Trimble, W. S. Mammalian SEPT2 Is Required for Scaffolding Nonmuscle Myosin II and Its Kinases. *Dev. Cell* (2007). doi:10.1016/j.devcel.2007.09.001
378. Estey, M. P., Di Ciano-Oliveira, C., Froese, C. D., Bejide, M. T. & Trimble, W. S. Distinct roles of septins in cytokinesis: SEPT9 mediates midbody abscission. *J. Cell Biol.* (2010). doi:10.1083/jcb.201006031
379. Farkas, R. M., Giansanti, M. G., Gatti, M. & Fuller, M. T. The Drosophila Cog5 homologue is required for cytokinesis, cell elongation, and assembly of specialized golgi architecture during spermatogenesis. *Mol. Biol. Cell* (2003). doi:10.1091/mbc.E02-06-0343
380. Belloni, G. *et al.* Mutations in Cog7 affect Golgi structure, meiotic cytokinesis and sperm development during Drosophila spermatogenesis. *J. Cell Sci.* (2012). doi:10.1242/jcs.108878
381. Xu, H. *et al.* Syntaxin 5 is required for cytokinesis and spermatid differentiation in Drosophila. *Dev. Biol.* (2002). doi:10.1006/dbio.2002.0830
382. Robinett, C. C., Giansanti, M. G., Gatti, M. & Fuller, M. T. TRAPPII is required for cleavage furrow ingression and localization of Rab11 in dividing male meiotic cells of Drosophila. *J. Cell Sci.* (2009). doi:10.1242/jcs.054536
383. Giansanti, M. G., Belloni, G. & Gatti, M. Rab11 is required for membrane trafficking and actomyosin ring constriction in meiotic cytokinesis of Drosophila males. *Mol. Biol. Cell* (2007). doi:10.1091/mbc.E07-05-0415
384. Dyer, N. *et al.* Spermatocyte cytokinesis requires rapid membrane addition mediated by ARF6 on central spindle recycling endosomes. *Development* (2007). doi:10.1242/dev.010983
385. Kitazawa, D., Yamaguchi, M., Mori, H. & Inoue, Y. H. COPI-mediated membrane trafficking is required for cytokinesis in drosophila male meiotic divisions. *J. Cell Sci.* (2012). doi:10.1242/jcs.103317
386. Giansanti, M. G. *et al.* Exocyst-Dependent Membrane Addition Is Required for Anaphase Cell Elongation and Cytokinesis in Drosophila. *PLoS Genet.* (2015). doi:10.1371/journal.pgen.1005632

387. Konopka, C. A., Schleede, J. B., Skop, A. R. & Bednarek, S. Y. Dynamin and cytokinesis. *Traffic* (2006). doi:10.1111/j.1600-0854.2006.00385.x
388. Albertson, R., Riggs, B. & Sullivan, W. Membrane traffic: A driving force in cytokinesis. *Trends in Cell Biology* (2005). doi:10.1016/j.tcb.2004.12.008
389. Joo, E., Tsang, C. W. & Trimble, W. S. Septins: Traffic control at the cytokinesis intersection. *Traffic* (2005). doi:10.1111/j.1600-0854.2005.00305.x
390. Pelissier, A., Chauvin, J. P. & Lecuit, T. Trafficking through Rab11 Endosomes Is Required for Cellularization during Drosophila Embryogenesis. *Curr. Biol.* (2003). doi:10.1016/j.cub.2003.10.023
391. Riggs, B. *et al.* Actin cytoskeleton remodeling during early Drosophila furrow formation requires recycling endosomal components Nuclear-fallout and Rab11. *J. Cell Biol.* (2003). doi:10.1083/jcb.200305115
392. Frémont, S. & Echard, A. Membrane Traffic in the Late Steps of Cytokinesis. *Curr. Biol.* **28**, R458–R470 (2018).
393. Szafer-Glusman, E. *et al.* A Role for Very-Long-Chain Fatty Acids in Furrow Ingression during Cytokinesis in Drosophila Spermatocytes. *Curr. Biol.* (2008). doi:10.1016/j.cub.2008.08.061
394. Dambournet, D. *et al.* Rab35 GTPase and OCRL phosphatase remodel lipids and F-actin for successful cytokinesis. *Nat. Cell Biol.* **13**, 981–988 (2011).
395. Emoto, K., Inadome, H., Kanaho, Y., Narumiya, S. & Umeda, M. Local change in phospholipid composition at the cleavage furrow is essential for completion of cytokinesis. *J. Biol. Chem.* (2005). doi:10.1074/jbc.M504282200
396. Field, S. J. *et al.* PtdIns(4,5)P2 functions at the cleavage furrow during cytokinesis. *Curr. Biol.* (2005). doi:10.1016/j.cub.2005.06.059
397. Kouranti, I., Sachse, M., Arouche, N., Goud, B. & Echard, A. Rab35 Regulates an Endocytic Recycling Pathway Essential for the Terminal Steps of Cytokinesis. *Curr. Biol.* (2006). doi:10.1016/j.cub.2006.07.020
398. Yonezawa, N., Nishida, E., Iida, K., Yahara, I. & Sakai, H. Inhibition of the interactions of cofilin, destrin, and deoxyribonuclease I with actin by phosphoinositides. *J. Biol. Chem.* (1990).
399. Schafer, D. A., Jennings, P. B. & Cooper, J. A. Dynamics of capping protein and actin assembly in vitro: Uncapping barbed ends by polyphosphoinositides. *J. Cell Biol.* (1996). doi:10.1083/jcb.135.1.169
400. Lassing, I. & Lindberg, U. Specific interaction between phosphatidylinositol 4,5-bisphosphate and profilactin. *Nature* (1985). doi:10.1038/314472a0
401. Flemming, W. Neue Beiträge zur Kenntniss der Zelle. II. Theil. *Arch. für mikroskopische Anat.* (1891). doi:10.1007/BF02954311
402. Piperno, G., LeDizet, M. & Chang, X. J. Microtubules containing acetylated alpha-tubulin in mammalian cells in culture. *J. Cell Biol.* (1987). doi:10.1083/jcb.104.2.289
403. Elad, N., Abramovitch, S., Sabanay, H. & Medalia, O. Microtubule organization in the final stages of cytokinesis as revealed by cryo-electron tomography. *J. Cell Sci.* (2011). doi:10.1242/jcs.073486
404. Gruneberg, U., Neef, R., Honda, R., Nigg, E. A. & Barr, F. A. Relocation of Aurora B from centromeres to the central spindle at the metaphase to anaphase transition requires MKlp2. *J. Cell Biol.* (2004). doi:10.1083/jcb.200403084
405. Hu, C. K., Coughlin, M. & Mitchison, T. J. Midbody assembly and its regulation

during cytokinesis. *Mol. Biol. Cell* (2012). doi:10.1091/mbc.E11-08-0721
406. Yen, T. J. *et al.* CENP-E, a novel human centromere-associated protein required for progression from metaphase to anaphase. *EMBO J.* (1991). doi:10.1002/j.1460-2075.1991.tb08066.x
407. Gai, M. *et al.* Citron kinase controls abscission through RhoA and anillin. *Mol. Biol. Cell* (2011). doi:10.1091/mbc.E10-12-0952
408. Kechad, A., Jananji, S., Ruella, Y. & Hickson, G. R. X. Anillin acts as a bifunctional linker coordinating midbody ring biogenesis during cytokinesis. *Curr. Biol.* (2012). doi:10.1016/j.cub.2011.11.062
409. Echard, A. Membrane traffic and polarization of lipid domains during cytokinesis. in *Biochemical Society Transactions* (2008). doi:10.1042/BST0360395
410. Emoto, K. *et al.* Redistribution of phosphatidylethanolamine at the cleavage furrow of dividing cells during cytokinesis. *Proc. Natl. Acad. Sci. U. S. A.* (1996). doi:10.1073/pnas.93.23.12867
411. Wong, R. *et al.* PIP2 hydrolysis and calcium release are required for cytokinesis in Drosophila spermatocytes. *Curr. Biol.* (2005). doi:10.1016/j.cub.2005.06.060
412. Janetopoulos, C. & Devreotes, P. Phosphoinositide signaling plays a key role in cytokinesis. *Journal of Cell Biology* (2006). doi:10.1083/jcb.200603156
413. Logan, M. R. & Mandato, C. A. Regulation of the actin cytoskeleton by PIP2 in cytokinesis. *Biol. Cell* (2006). doi:10.1042/bc20050081
414. Emoto, K. & Umeda, M. An essential role for a membrane lipid in cytokinesis: Regulation of contractile ring disassembly by redistribution of phosphatidylethanolamine. *J. Cell Biol.* (2000). doi:10.1083/jcb.149.6.1215
415. Sagona, A. P. *et al.* PtdIns(3)P controls cytokinesis through KIF13A-mediated recruitment of FYVE-CENT to the midbody. *Nat. Cell Biol.* (2010). doi:10.1038/ncb2036
416. Thoresen, S. B., Pedersen, N. M., Liestøl, K. & Stenmark, H. A phosphatidylinositol 3-kinase class III sub-complex containing VPS15, VPS34, Beclin 1, UVRAG and BIF-1 regulates cytokinesis and degradative endocytic traffic. *Exp. Cell Res.* (2010). doi:10.1016/j.yexcr.2010.07.008
417. You, S. Y. *et al.* Beclin-1 knockdown shows abscission failure but not autophagy defect during oocyte meiotic maturation. *Cell Cycle* (2016). doi:10.1080/15384101.2016.1181235
418. Saurin, A. T. *et al.* The regulated assembly of a PKCepsilon complex controls the completion of cytokinesis. *Nat. Cell Biol.* **10**, 891–901 (2008).
419. Echard, A. Phosphoinositides and cytokinesis: The 'PIP' of the iceberg. *Cytoskeleton* (2012). doi:10.1002/cm.21067
420. Kinoshita, M., Field, C. M., Coughlin, M. L., Straight, A. F. & Mitchison, T. J. Self- and actin-templated assembly of mammalian septins. *Dev. Cell* (2002). doi:10.1016/S1534-5807(02)00366-0
421. Hickson, G. R. X. & O'Farrell, P. H. Rho-dependent control of anillin behavior during cytokinesis. *J. Cell Biol.* (2008). doi:10.1083/jcb.200709005
422. Field, C. M., Coughlin, M., Doberstein, S., Marty, T. & Sullivan, W. Characterization of anillin mutants reveals essential roles in septin localization and plasma membrane integrity. *Development* (2005). doi:10.1242/dev.01843
423. Bassi, Z. I., Audusseau, M., Riparbelli, M. G., Callaini, G. & D'Avino, P. P. Citron

kinase controls a molecular network required for midbody formation in cytokinesis. *Proc. Natl. Acad. Sci. U. S. A.* (2013). doi:10.1073/pnas.1301328110
424. Watanabe, S., De Zan, T., Ishizaki, T. & Narumiya, S. Citron kinase mediates transition from constriction to abscission through its coiled-coil domain. *J. Cell Sci.* (2013). doi:10.1242/jcs.116608
425. Makyio, H. *et al.* Structural basis for Arf6-MKLP1 complex formation on the Flemming body responsible for cytokinesis. *EMBO J.* (2012). doi:10.1038/emboj.2012.89
426. Joseph, N., Hutterer, A., Poser, I. & Mishima, M. ARF6 GTPase protects the post-mitotic midbody from 14-3-3-mediated disintegration. *EMBO J.* (2012). doi:10.1038/emboj.2012.139
427. Lekomtsev, S. *et al.* Centralspindlin links the mitotic spindle to the plasma membrane during cytokinesis. *Nature* (2012). doi:10.1038/nature11773
428. Wilson, G. M. *et al.* The FIP3-Rab11 protein complex regulates recycling endosome targeting to the cleavage furrow during late cytokinesis. *Mol. Biol. Cell* **16**, 849–60 (2005).
429. Schiel, J. A. *et al.* FIP3-endosome-dependent formation of the secondary ingression mediates ESCRT-III recruitment during cytokinesis. *Nat. Cell Biol.* **14**, 1068–78 (2012).
430. Simon, G. C. *et al.* Sequential Cyk-4 binding to ECT2 and FIP3 regulates cleavage furrow ingression and abscission during cytokinesis. *EMBO J.* (2008). doi:10.1038/emboj.2008.112
431. Prigent, M. *et al.* ARF6 controls post-endocytic recycling through its downstream exocyst complex effector. *J. Cell Biol.* (2003). doi:10.1083/jcb.200305029
432. Wu, S., Mehta, S. Q., Pichaud, F., Bellen, H. J. & Quiocho, F. A. Sec15 interacts with Rab11 via a novel domain and affects Rab11 localization in vivo. *Nat. Struct. Mol. Biol.* (2005). doi:10.1038/nsmb987
433. Fielding, A. B. *et al.* Rab11-FIP3 and FIP4 interact with Arf6 and the Exocyst to control membrane traffic in cytokinesis. *EMBO J.* **24**, 3389–3399 (2005).
434. Gromley, A. *et al.* Centriolin anchoring of exocyst and SNARE complexes at the midbody is required for secretory-vesicle-mediated abscission. *Cell* **123**, 75–87 (2005).
435. Neto, H., Kaupisch, A., Collins, L. L. & Gould, G. W. Syntaxin 16 is a master recruitment factor for cytokinesis. *Mol. Biol. Cell* (2013). doi:10.1091/mbc.E13-06-0302
436. Horgan, C. P., Hanscom, S. R., Kelly, E. E. & McCaffrey, M. W. Tumor susceptibility gene 101 (TSG101) is a novel binding-partner for the class II Rab11-FIPs. *PLoS One* (2012). doi:10.1371/journal.pone.0032030
437. Pohl, C. & Jentsch, S. Final Stages of Cytokinesis and Midbody Ring Formation Are Controlled by BRUCE. *Cell* (2008). doi:10.1016/j.cell.2008.01.012
438. Schiel, J. a *et al.* Endocytic membrane fusion and buckling-induced microtubule severing mediate cell abscission. *J. Cell Sci.* **124**, 1411–1424 (2011).
439. Goss, J. W. & Toomre, D. K. Both daughter cells traffic and exocytose membrane at the cleavage furrow during mammalian cytokinesis. *J. Cell Biol.* **181**, 1047–1054 (2008).
440. Darenfed, H. & Mandato, C. A. Wound-induced contractile ring: A model for cytokinesis. in *Biochemistry and Cell Biology* (2005). doi:10.1139/o05-164

441. Xie, W., Li, L. & Cohen, S. N. Cell cycle-dependent subcellular localization of the TSG101 protein and mitotic and nuclear abnormalities associated with TSG101 deficiency. *Proc. Natl. Acad. Sci. U. S. A.* (1998). doi:10.1073/pnas.95.4.1595
442. Carlton, J. G. & Martin-Serrano, J. Parallels between cytokinesis and retroviral budding: a role for the ESCRT machinery. *Science* **316**, 1908–1912 (2007).
443. Bastos, R. N. & Barr, F. A. Plk1 negatively regulates Cep55 recruitment to the midbody to ensure orderly abscission. *J. Cell Biol.* **191**, 751–760 (2010).
444. Fabbro, M. *et al.* Cdk1/Erk2- and Plk1-dependent phosphorylation of a centrosome protein, Cep55, is required for its recruitment to midbody and cytokinesis. *Dev. Cell* **9**, 477–488 (2005).
445. Martinez-Garay, I., Rustom, A., Gerdes, H. H. & Kutsche, K. The novel centrosomal associated protein CEP55 is present in the spindle midzone and the midbody. *Genomics* (2006). doi:10.1016/j.ygeno.2005.11.006
446. Zhao, W. M., Seki, A. & Fang, G. Cep55, a microtubule-bundling protein, associates with centralspindlin to control the midbody integrity and cell abscission during cytokinesis. *Mol. Biol. Cell* **17**, 3881–3896 (2006).
447. Dukes, J. D., Richardson, J. D., Simmons, R. & Whitley, P. A dominant-negative ESCRT-III protein perturbs cytokinesis and trafficking to lysosomes. *Biochem. J.* (2008). doi:10.1042/BJ20071296
448. Samson, R. Y., Obita, T., Freund, S. M., Williams, R. L. & Bell, S. D. A role for the ESCRT system in cell division in archaea. *Science* **322**, 1710–3 (2008).
449. Lindås, A.-C., Karlsson, E. a, Lindgren, M. T., Ettema, T. J. G. & Bernander, R. A unique cell division machinery in the Archaea. *Proc. Natl. Acad. Sci. U. S. A.* **105**, 18942–6 (2008).
450. Snyder, J. C., Samson, R. Y., Brumfield, S. K., Bell, S. D. & Young, M. J. Functional interplay between a virus and the ESCRT machinery in archaea. *Proc. Natl. Acad. Sci. U. S. A.* **110**, 10783–7 (2013).
451. Lee, H. H., Elia, N., Ghirlando, R., Lippincott-Schwartz, J. & Hurley, J. H. Midbody targeting of the ESCRT machinery by a noncanonical coiled coil in CEP55. *Science* **322**, 576–580 (2008).
452. Mullins, J. M. & Biesele, J. J. Terminal phase of cytokinesis in D-98s cells. *J. Cell Biol.* **73**, 672–84 (1977).
453. Matuliene, J. & Kuriyama, R. Kinesin-like protein CHO1 is required for the formation of midbody matrix and the completion of cytokinesis in mammalian cells. *Mol. Biol. Cell* (2002). doi:10.1091/mbc.01-10-0504
454. Morita, E. *et al.* Human ESCRT-III and VPS4 proteins are required for centrosome and spindle maintenance. *Proc. Natl. Acad. Sci. U. S. A.* **107**, 12889–94 (2010).
455. Nakamura, A., Arai, H. & Fujita, N. Centrosomal Aki1 and cohesin function in separase-regulated centriole disengagement. *J. Cell Biol.* (2009). doi:10.1083/jcb.200906019
456. Ott, C. *et al.* VPS4 is a dynamic component of the centrosome that regulates centrosome localization of γ-tubulin, centriolar satellite stability and ciliogenesis. *Sci. Rep.* (2018). doi:10.1038/s41598-018-21491-x
457. Malerød, L. *et al.* Centrosomal ALIX regulates mitotic spindle orientation by modulating astral microtubule dynamics. *EMBO J.* (2018). doi:10.15252/embj.201797741
458. Dionisio-Vicuña, M. N., Gutiérrez-López, T. Y., Adame-García, S. R., Vázquez-

Prado, J. & Reyes-Cruz, G. VPS28, an ESCRT-I protein, regulates mitotic spindle organization via Gβγ EG5 and TPX2. *Biochim. Biophys. Acta - Mol. Cell Res.* (2018). doi:10.1016/j.bbamcr.2018.03.005
459. Petsalaki, E., Dandoulaki, M. & Zachos, G. The ESC RT protein Chmp4c regulates mitotic spindle checkpoint signaling. *J. Cell Biol.* (2018). doi:10.1083/jcb.201709005
460. Sherman, S. *et al.* Resolving new ultrastructural features of cytokinetic abscission with soft-X-ray cryo-tomography. *Sci. Rep.* (2016). doi:10.1038/srep27629
461. Elia, N., Fabrikant, G., Kozlov, M. M. & Lippincott-Schwartz, J. Computational model of cytokinetic abscission driven by ESCRT-III polymerization and remodeling. *Biophys. J.* **102**, 2309–2320 (2012).
462. Goliand, I. *et al.* Resolving ESCRT-III Spirals at the Intercellular Bridge of Dividing Cells Using 3D STORM. *Cell Rep.* **24**, 1756–1764 (2018).
463. Dubreuil, V., Marzesco, A. M., Corbeil, D., Huttner, W. B. & Wilsch-Bräuninger, M. Midbody and primary cilium of neural progenitors release extracellular membrane particles enriched in the stem cell marker prominin-1. *J. Cell Biol.* (2007). doi:10.1083/jcb.200608137
464. Karasmanis, E. P. *et al.* Report A Septin Double Ring Controls the Spatiotemporal Organization of the ESCRT Machinery in Cytokinetic Report A Septin Double Ring Controls the Spatiotemporal Organization of the ESCRT Machinery in Cytokinetic Abscission. *Curr. Biol.* **29**, 2174-2182.e7 (2019).
465. Bondeson, M. L. *et al.* A nonsense mutation in CEP55 defines a new locus for a Meckel-like syndrome, an autosomal recessive lethal fetal ciliopathy. *Clin. Genet.* **92**, 510–516 (2017).
466. Frosk, P. *et al.* A truncating mutation in CEP55 is the likely cause of MARCH, a novel syndrome affecting neuronal mitosis. *J. Med. Genet.* **54**, 490–501 (2017).
467. Rawlins, L. E. *et al.* An Amish founder variant consolidates disruption of CEP55 as a cause of hydranencephaly and renal dysplasia. *Eur. J. Hum. Genet.* **27**, 657–662 (2019).
468. Chen, C. H. *et al.* FLJ10540-elicited cell transformation is through the activation of PI3-kinase/AKT pathway. *Oncogene* (2007). doi:10.1038/sj.onc.1210207
469. Jeffery, J. *et al.* Cep55 regulates embryonic growth and development by promoting Akt stability in zebrafish. *FASEB J.* (2015). doi:10.1096/fj.14-265090
470. Tedeschi, A. *et al.* Cep55 promotes cytokinesis of neural progenitors but is dispensable for most mammalian cell divisions. *Nat. Commun.* **11**, 1746 (2020).
471. König, J., Frankel, E. B., Audhya, A. & Müller-Reichert, T. Membrane remodeling during embryonic abscission in Caenorhabditis elegans. *J. Cell Biol.* (2017). doi:10.1083/jcb.201607030
472. Lie-Jensen, A. *et al.* Centralspindlin Recruits ALIX to the Midbody during Cytokinetic Abscission in Drosophila via a Mechanism Analogous to Virus Budding. *Curr. Biol.* (2019). doi:10.1016/j.cub.2019.09.025
473. Amine, N. El, Kechad, A., Jananji, S. & Hickson, G. R. X. Opposing actions of septins and Sticky on Anillin promote the transition from contractile to midbody ring. *J. Cell Biol.* (2013). doi:10.1083/jcb.201305053
474. Stéphane, S., Frémont, F., Romet-Lemonne, G., Houdusse, A. & Echard, A. Emerging roles of MICAL family proteins-from actin oxidation to membrane

trafficking during cytokinesis. (2017). doi:10.1242/jcs.202028
475. Suzuki, T. *et al.* MICAL, a novel CasL interacting molecule, associates with vimentin. *J. Biol. Chem.* (2002). doi:10.1074/jbc.M111842200
476. Fischer, J., Weide, T. & Barnekow, A. The MICAL proteins and rab1: A possible link to the cytoskeleton? *Biochem. Biophys. Res. Commun.* (2005). doi:10.1016/j.bbrc.2004.12.182
477. Pasterkamp, R. J. *et al.* MICAL flavoprotein monooxygenases: Expression during neural development and following spinal cord injuries in the rat. *Mol. Cell. Neurosci.* (2006). doi:10.1016/j.mcn.2005.09.001
478. Terman, J. R., Mao, T., Pasterkamp, R. J., Yu, H. H. & Kolodkin, A. L. MICALs, a Family of Conserved Flavoprotein Oxidoreductases, Function in Plexin-Mediated Axonal Repulsion. *Cell* (2002). doi:10.1016/S0092-8674(02)00794-8
479. Weide, T., Teuber, J., Bayer, M. & Barnekow, A. MICAL-1 isoforms, novel rab1 interacting proteins. *Biochem. Biophys. Res. Commun.* (2003). doi:10.1016/S0006-291X(03)00918-5
480. Nakatsuji, H., Nishimura, N., Yamamura, R., Kanayama, H. -o. & Sasaki, T. Involvement of Actinin-4 in the Recruitment of JRAB/MICAL-L2 to Cell-Cell Junctions and the Formation of Functional Tight Junctions. *Mol. Cell. Biol.* (2008). doi:10.1128/mcb.00144-08
481. Sharma, M., Giridharan, S. S. P., Rahajeng, J., Naslavsky, N. & Caplan, S. MICAL-L1 links EHD1 to tubular recycling endosomes and regulates receptor recycling. *Mol. Biol. Cell* (2009). doi:10.1091/mbc.E09-06-0535
482. Terai, T., Nishimura, N., Kanda, I., Yasui, N. & Sasaki, T. JRAB/MICAL-L2 is a junctional Rab13-binding protein mediating the endocytic recycling of occludin. *Mol. Biol. Cell* (2006). doi:10.1091/mbc.E05-09-0826
483. Alqassim, S. S. *et al.* Modulation of MICAL Monooxygenase Activity by its Calponin Homology Domain: Structural and Mechanistic Insights. *Sci. Rep.* (2016). doi:10.1038/srep22176
484. Nadella, M., Bianchet, M. A., Gabelli, S. B., Barrila, J. & Amzel, L. M. Structure and activity of the axon guidance protein MICAL. *Proc. Natl. Acad. Sci. U. S. A.* (2005). doi:10.1073/pnas.0504838102
485. Siebold, C. *et al.* High-resolution structure of the catalytic region of MICAL (molecule interacting with CasL), a multidomain flavoenzyme-signaling molecule. *Proc. Natl. Acad. Sci. U. S. A.* (2005). doi:10.1073/pnas.0504997102
486. Giridharan, S. S. P., Rohn, J. L., Naslavsky, N. & Caplan, S. Differential regulation of actin microfilaments by human MICAL proteins. *J. Cell Sci.* (2012). doi:10.1242/jcs.089367
487. Wilson, C., Terman, J. R., González-Billault, C. & Ahmed, G. Actin filaments—A target for redox regulation. *Cytoskeleton* (2016). doi:10.1002/cm.21315
488. Hung, R. J. *et al.* Mical links semaphorins to F-actin disassembly. *Nature* (2010). doi:10.1038/nature08724
489. Hung, R. J., Pak, C. W. & Terman, J. R. Direct redox regulation of F-actin assembly and disassembly by Mical. *Science (80-.).* (2011). doi:10.1126/science.1211956
490. Fedorova, M., Todorovsky, T., Kuleva, N. & Hoffmann, R. Quantitative evaluation of tryptophan oxidation in actin and troponin I from skeletal muscles using a rat model of acute oxidative stress. *Proteomics* (2010).

doi:10.1002/pmic.201000147
491. Milzani, A. *et al.* The oxidation produced by hydrogen peroxide on Ca-ATP-G-actin. *Protein Sci.* (2000). doi:10.1110/ps.9.9.1774
492. Frémont, S. *et al.* Oxidation of F-actin controls the terminal steps of cytokinesis. *Nat. Commun.* (2017). doi:10.1038/ncomms14528
493. Frémont, S. & Echard, A. Studying cytokinesis and midbody remnants using correlative light/scanning EM. *Methods Cell Biol.* (2017). doi:10.1016/bs.mcb.2016.03.028
494. Crowell, E. F., Gaffuri, A. L., Gayraud-Morel, B., Tajbakhsh, S. & Echard, A. Engulfment of the midbody remnant after cytokinesis in mammalian cells. *J. Cell Sci.* (2014). doi:10.1242/jcs.154732
495. Deng, W. *et al.* MICAL1 controls cell invasive phenotype via regulating oxidative stress in breast cancer cells. *BMC Cancer* (2016). doi:10.1186/s12885-016-2553-1
496. Fukuda, M., Kanno, E., Ishibashi, K. & Itoh, T. Large scale screening for novel rab effectors reveals unexpected broad rab binding specificity. *Mol. Cell. Proteomics* (2008). doi:10.1074/mcp.M700569-MCP200
497. Liu, Q. *et al.* MICAL3 flavoprotein monooxygenase forms a complex with centralspindlin and regulates cytokinesis. *J. Biol. Chem.* (2016). doi:10.1074/jbc.M116.748186
498. Reinecke, J. B., Katafiasz, D., Naslavsky, N. & Caplan, S. Novel Functions for the Endocytic Regulatory Proteins MICAL-L1 and EHD1 in Mitosis. *Traffic* (2015). doi:10.1111/tra.12234
499. Rahajeng, J., Panapakkam Giridharan, S. S., Cai, B., Naslavsky, N. & Caplan, S. MICAL-L1 is a tubular endosomal membrane hub that connects Rab35 and Arf6 with Rab8a. *Traffic* (2012). doi:10.1111/j.1600-0854.2011.01294.x
500. Giridharan, S. S. P., Cai, B., Naslavsky, N. & Caplan, S. Trafficking cascades mediated by Rab35 and its membrane hub effector, MICAL-L1. *Commun. Integr. Biol.* (2012). doi:10.4161/cib.20064
501. Kobayashi, H., Etoh, K., Ohbayashi, N. & Fukuda, M. Rab35 promotes the recruitment of Rab8, Rab13 and Rab36 to recycling endosomes through MICAL-L1 during neurite outgrowth. *Biol. Open* (2014). doi:10.1242/bio.20148771
502. McDermott, C. J. *et al.* Clinical features of hereditary spastic paraplegia due to spastin mutation. *Neurology* (2006). doi:10.1212/01.wnl.0000223315.62404.00
503. Roll-Mecak, A. & Vale, R. D. Structural basis of microtubule severing by the hereditary spastic paraplegia protein spastin. *Nature* (2008). doi:10.1038/nature06482
504. Connell, J. W., Lindon, C., Luzio, J. P. & Reid, E. Spastin couples microtubule severing to membrane traffic in completion of cytokinesis and secretion. *Traffic* **10**, 42–56 (2009).
505. Yang, D. *et al.* Structural basis for midbody targeting of spastin by the ESCRT-III protein CHMP1B. *Nat. Struct. Mol. Biol.* **15**, (2008).
506. Reid, E. *et al.* The hereditary spastic paraplegia protein spastin interacts with the ESCRT-III complex-associated endosomal protein CHMP-1B. *Hum. Mol. Genet.* (2005). doi:10.1093/hmg/ddi003
507. Agromayor, M. *et al.* Essential Role of hIST1 in Cytokinesis. *Mol. Biol. Cell* **20**, 1374–87 (2009).

508. Bajorek, M. *et al.* Biochemical Analyses of Human IST1 and Its Function in Cytokinesis. *Mol. Biol. Cell* **20**, 1360–1373 (2009).
509. Dimaano, C., Jones, C. B., Hanono, A., Curtiss, M. & Babst, M. Ist1 Regulates Vps4 Localization and Assembly. *Mol. Biol. Cell* **19**, 465–474 (2008).
510. Renvoisé, B. *et al.* SPG20 protein spartin is recruited to midbodies by ESCRT-III protein Ist1 and participates in cytokinesis. *Mol. Biol. Cell* (2010). doi:10.1091/mbc.E09-10-0879
511. Hadders, M. A. *et al.* ESCRT-III binding protein MITD1 is involved in cytokinesis and has an unanticipated PLD fold that binds membranes. doi:10.1073/pnas.1206839109
512. Lee, S. *et al.* MITD1 is recruited to midbodies by ESCRT-III and participates in cytokinesis. *Mol. Biol. Cell* **23**, 4347–61 (2012).
513. Mondal, G. *et al.* BRCA2 Localization to the Midbody by Filamin A Regulates CEP55 Signaling and Completion of Cytokinesis. *Dev. Cell* (2012). doi:10.1016/j.devcel.2012.05.008
514. Mendoza, M. *et al.* A mechanism for chromosome segregation sensing by the NoCut checkpoint. *Nat. Cell Biol.* **11**, 477–483 (2009).
515. Norden, C. *et al.* The NoCut Pathway Links Completion of Cytokinesis to Spindle Midzone Function to Prevent Chromosome Breakage. *Cell* **125**, 85–98 (2006).
516. Steigemann, P. *et al.* Aurora B-Mediated Abscission Checkpoint Protects against Tetraploidization. *Cell* **136**, 473–484 (2009).
517. Mendoza, M. & Barral, Y. Co-ordination of cytokinesis with chromosome segregation. in *Biochemical Society Transactions* (2008). doi:10.1042/BST0360387
518. Mackay, D. R., Makise, M. & Ullman, K. S. Defects in nuclear pore assembly lead to activation of an Aurora B-mediated abscission checkpoint. *J. Cell Biol.* **191**, 923–931 (2010).
519. Lafaurie-Janvore, Julie Paolo Maiuri, Irène Wang, Mathieu Pinot, J.-B. M. *et al.* ESCRT-III Assembly and Cytokinetic Abscission Are Induced by Tension Release in the Intercellular Bridge. *Science (80-.).* **339**, 1625–1629 (2013).
520. Caballe, A. *et al.* ULK3 regulates cytokinetic abscission by phosphorylating ESCRT-III proteins. *Elife* **4**, 1–70 (2015).
521. Carlton, J. G., Caballe, A., Agromayor, M., Kloc, M. & Martin-Serrano, J. ESCRT-III governs the Aurora B-mediated abscission checkpoint through CHMP4C. *Science (80-.).* **336**, 220–5 (2012).
522. Capalbo, L. *et al.* The chromosomal passenger complex controls the function of endosomal sorting complex required for transport-III Snf7 proteins during cytokinesis. *Open Biol.* **2**, 120070 (2012).
523. Capalbo, L. *et al.* Coordinated regulation of the ESCRT-III component CHMP4C by the chromosomal passenger complex and centralspindlin during cytokinesis. (2016).
524. Sadler, J. B. A. *et al.* A cancer-associated polymorphism in ESCRT-III disrupts the abscission checkpoint and promotes genome instability. *Proc. Natl. Acad. Sci. U. S. A.* (2018). doi:10.1073/pnas.1805504115
525. Thoresen, S. B. *et al.* ANCHR mediates Aurora-B-dependent abscission checkpoint control through retention of VPS4. *Nat. Cell Biol.* **16**, (2014).
526. Hetzer, M. W. The nuclear envelope. *Cold Spring Harbor perspectives in biology*

2, (2010).
527. Wandke, C. & Kutay, U. Enclosing chromatin: Reassembly of the nucleus after open mitosis. *Cell* **152**, 1222–1225 (2013).
528. Güttinger, S., Laurell, E. & Kutay, U. Orchestrating nuclear envelope disassembly and reassembly during mitosis. *Nat. Rev. Mol. Cell Biol.* **10**, 178–191 (2009).
529. Kutay, U. & Hetzer, M. W. Reorganization of the nuclear envelope during open mitosis. *Current Opinion in Cell Biology* **20**, 669–677 (2008).
530. Mierzwa, B. & Gerlich, D. W. Cytokinetic Abscission: Molecular Mechanisms and Temporal Control. *Dev. Cell* **31**, 525–538 (2014).
531. Schellhaus, A. K., De Magistris, P. & Antonin, W. Nuclear Reformation at the End of Mitosis. *Journal of Molecular Biology* **428**, 1962–1985 (2016).
532. Anderson, D. J. & Hetzer, M. W. Nuclear envelope formation by chromatin-mediated reorganization of the endoplasmic reticulum. *Nat. Cell Biol.* **9**, 1160–1166 (2007).
533. Anderson, D. J. & Hetzer, M. W. Reshaping of the endoplasmic reticulum limits the rate for nuclear envelope formation. *J. Cell Biol.* **182**, 911–924 (2008).
534. Lu, L., Ladinsky, M. S. & Kirchhausen, T. Formation of the postmitotic nuclear envelope from extended ER cisternae precedes nuclear pore assembly. *J. Cell Biol.* **194**, 425–440 (2011).
535. Hetzer, M. *et al.* Distinct AAA-ATPase p97 complexes function in discrete steps of nuclear assembly. *Nat Cell Biol* **3**, 1086–1091 (2001).
536. Ramadan, K. *et al.* Cdc48/p97 promotes reformation of the nucleus by extracting the kinase Aurora B from chromatin. *Nature* **450**, 1258–1262 (2007).
537. Bauer, I., Brune, T., Preiss, R. & Kölling, R. Evidence for a nonendosomal function of the saccharomyces cerevisiae ESCRT-III-Like protein Chm7. *Genetics* **201**, 1439–1452 (2015).
538. Olmos, Y. & Carlton, J. G. The ESCRT machinery: New roles at new holes. *Curr. Opin. Cell Biol.* **38**, 1–11 (2016).
539. Horii, M. *et al.* CHMP7, a novel ESCRT-III-related protein, associates with CHMP4b and functions in the endosomal sorting pathway. *Biochem. J.* (2006). doi:10.1042/BJ20060897
540. Pieper, G. H., Sprenger, S., Teis, D. & Oliferenko, S. ESCRT-III/Vps4 Controls Heterochromatin-Nuclear Envelope Attachments. *Dev. Cell* (2020). doi:10.1016/j.devcel.2020.01.028
541. Vietri, M. *et al.* Unrestrained ESCRT-III drives chromosome fragmentation and micronuclear catastrophe. *bioRxiv* (2019). doi:10.1101/517011
542. Gu, M. *et al.* LEM2 recruits CHMP7 for ESCRT-mediated nuclear envelope closure in fission yeast and human cells. *Proc. Natl. Acad. Sci. USA* (2017). doi:10.1073/pnas.1613916114
543. Thaller, D. J. *et al.* An escrt-lem protein surveillance system is poised to directly monitor the nuclear envelope and nuclear transport system. *Elife* (2019). doi:10.7554/eLife.45284
544. Ventimiglia, L. N. *et al.* CC2D1B Coordinates ESCRT-III Activity during the Mitotic Reformation of the Nuclear Envelope. *Dev. Cell* (2018). doi:10.1016/j.devcel.2018.11.012
545. Martinelli, N. *et al.* CC2D1A is a regulator of ESCRT-III CHMP4B. *J. Mol. Biol.* (2012). doi:10.1016/j.jmb.2012.02.044

546. Troost, T., Jaeckel, S., Ohlenhard, N. & Klein, T. The tumour suppressor Lethal (2) giant discs is required for the function of the ESCRT-III component Shrub/CHMP4. *J. Cell Sci.* (2012). doi:10.1242/jcs.097261
547. Usami, Y. *et al.* Regulation of CHMP4/ESCRT-III Function in Human Immunodeficiency Virus Type 1 Budding by CC2D1A. *J. Virol.* (2012). doi:10.1128/jvi.06539-11
548. Raab, M. *et al.* ESCRT III repairs nuclear envelope ruptures during cell migration to limit DNA damage and cell death. *Science* **352**, (2016).
549. C.M. Denais, R. M. Gilbert, P. Isermann, A. L. McGregor, M. te Lindert, B. Weigelin, P. M. Davidson, P. Friedl, K.Wolf, J. L. 2016 Nuclear envelope rupture and repair during cancer cell migration. *Science (80-.).* **352**, 353–358 (2016).
550. Halfmann, C. T. *et al.* Repair of nuclear ruptures requires barrier-to-autointegration factor. *J. Cell Biol.* (2019). doi:10.1083/jcb.201901116
551. Webster, B. M., Colombi, P., Jager, J. & Lusk, C. P. Surveillance of Nuclear Pore Complex Assembly by ESCRT-III/Vps4. *Cell* **159**, 388–401 (2014).
552. Webster, B. M. & Lusk, C. P. Border Safety: Quality Control at the Nuclear Envelope. *Trends in Cell Biology* **26**, 29–39 (2016).
553. Frost, A. *et al.* Functional repurposing revealed by comparing S. pombe and S. cerevisiae genetic interactions. *Cell* **149**, 1339–1352 (2012).
554. Webster, B. M. & Lusk, C. P. ESCRTs breach the nuclear border. *Nucleus* **6**, 197–202 (2015).
555. Hurt, E. & Beck, M. Towards understanding nuclear pore complex architecture and dynamics in the age of integrative structural analysis. *Current Opinion in Cell Biology* **34**, 31–38 (2015).
556. Alber, F. *et al.* The molecular architecture of the nuclear pore complex. *Nature* **450**, 695–701 (2007).
557. Bui, K. H. H. *et al.* Integrated Structural Analysis of the Human Nuclear Pore Complex Scaffold. *Cell* **155**, 1233–1243 (2013).
558. Webster, B. M. *et al.* Chm7 and Heh1 collaborate to link nuclear pore complex quality control with nuclear envelope sealing. *EMBO J.* **35**, 2447 LP – 2467 (2016).
559. Yewdell, W. T., Colombi, P., Makhnevych, T. & Lusk, C. P. Lumenal interactions in nuclear pore complex assembly and stability. *Mol. Biol. Cell* **22**, 1375–1388 (2011).
560. Göttlinger, H. G., Dorfman, T., Sodroski, J. G. & Haseltine, W. a. Effect of mutations affecting the p6 gag protein on human immunodeficiency virus particle release. *Proc. Natl. Acad. Sci. U. S. A.* **88**, 3195–3199 (1991).
561. Puffer, B. a, Parent, L. J., Wills, J. W. & Montelaro, R. C. Equine infectious anemia virus utilizes a YXXL motif within the late assembly domain of the Gag p9 protein. *J. Virol.* **71**, 6541–6546 (1997).
562. Xiang, Y., Cameron, C. E., Wills, J. W. & Leis, J. Fine mapping and characterization of the Rous sarcoma virus Pr76gag late assembly domain. *J. Virol.* **70**, 5695–700 (1996).
563. Parent, L. J. *et al.* Positionally independent and exchangeable late budding functions of the Rous sarcoma virus and human immunodeficiency virus Gag proteins. *J. Virol.* **69**, 5455–5460 (1995).
564. Yuan, B., Campbell, S., Bacharach, E., Rein, A. & Goff, S. P. Infectivity of Moloney

murine leukemia virus defective in late assembly events is restored by late assembly domains of other retroviruses. *J. Virol.* **74**, 7250–7260 (2000).
565. Martin-Serrano, J., Zang, T. & Bieniasz, P. D. Role of ESCRT-I in retroviral budding. *J. Virol.* **77**, 4794–804 (2003).
566. Von Schwedler, U. K. *et al.* The protein network of HIV budding. *Cell* **114**, 701–713 (2003).
567. Martin-Serrano, J., Yarovoy, A., Perez-Caballero, D., Bieniasz, P. D. & Yaravoy, A. Divergent retroviral late-budding domains recruit vacuolar protein sorting factors by using alternative adaptor proteins. *Proc. Natl. Acad. Sci. U. S. A.* **100**, 12414–9 (2003).
568. Strack, B., Calistri, A., Craig, S., Popova, E. & Göttlinger, H. G. AIP1/ALIX is a binding partner for HIV-1 p6 and EIAV p9 functioning in virus budding. *Cell* **114**, 689–699 (2003).
569. Martin-Serrano, J., Eastman, S. W., Chung, W. & Bieniasz, P. D. HECT ubiquitin ligases link viral and cellular PPXY motifs to the vacuolar protein-sorting pathway. *J. Cell Biol.* **168**, 89–101 (2005).
570. Kikonyogo, A. *et al.* Proteins related to the Nedd4 family of ubiquitin protein ligases interact with the L domain of Rous sarcoma virus and are required for Gag budding from cells. *Proc. Natl. Acad. Sci. U. S. A.* **98**, 11199–11204 (2001).
571. Chen, B. J. & Lamb, R. A. Mechanisms for enveloped virus budding: Can some viruses do without an ESCRT? *Virology* (2008). doi:10.1016/j.virol.2007.11.008
572. Tanzi, G. O., Piefer, A. J. & Bates, P. Equine infectious anemia virus utilizes host vesicular protein sorting machinery during particle release. *J.Virol.* **77**, 8440–8447 (2003).
573. Morita, E. *et al.* ESCRT-III protein requirements for HIV-1 budding. *Cell Host Microbe* **9**, 235–242 (2011).
574. Sandrin, V. & Sundquist, W. I. ESCRT requirements for EIAV budding. *Retrovirology* **10**, 104 (2013).
575. Martin-Serrano, J. & Bieniasz, P. D. A bipartite late-budding domain in human immunodeficiency virus type 1. *J Virol* **77**, 12373–12377 (2003).
576. Usami, Y., Popov, S., Popova, E. & Göttlinger, H. G. Efficient and specific rescue of human immunodeficiency virus type 1 budding defects by a Nedd4-like ubiquitin ligase. *J. Virol.* **82**, 4898–907 (2008).
577. Chung, H.-Y. *et al.* NEDD4L overexpression rescues the release and infectivity of human immunodeficiency virus type 1 constructs lacking PTAP and YPXL late domains. *J. Virol.* **82**, 4884–97 (2008).
578. Weiss, E. R. *et al.* Rescue of HIV-1 release by targeting widely divergent NEDD4-type ubiquitin ligases and isolated catalytic HECT domains to gag. *PLoS Pathog.* **6**, (2010).
579. Segura-Morales, C. *et al.* Tsg101 and Alix interact with murine leukemia virus Gag and cooperate with Nedd4 ubiquitin ligases during budding. *J. Biol. Chem.* **280**, 27004–27012 (2005).
580. Licata, J. M. *et al.* Overlapping motifs (PTAP and PPEY) within the Ebola virus VP40 protein function independently as late budding domains: involvement of host proteins TSG101 and VPS-4. *J. Virol.* **77**, 1812–9 (2003).
581. Han, Z. *et al.* ALIX Rescues Budding of a Double PTAP/PPEY L-Domain Deletion Mutant of Ebola VP40: A Role for ALIX in Ebola Virus Egress. *J. Infect. Dis.* **212**,

S138–S145 (2015).
582. Fujii, K. *et al.* Functional role of Alix in HIV-1 replication. *Virology* **391**, 284–292 (2009).
583. Pincetic, A., Medina, G., Carter, C. & Leis, J. Avian sarcoma virus and human immunodeficiency virus, type 1 use different subsets of ESCRT proteins to facilitate the budding process. *J. Biol. Chem.* **283**, 29822–29830 (2008).
584. Carlson, L. A. & Hurley, J. H. In vitro reconstitution of the ordered assembly of the endosomal sorting complex required for transport at membrane-bound HIV-1 Gag clusters. *Proc. Natl. Acad. Sci. U. S. A.* (2012). doi:10.1073/pnas.1211759109
585. Meng, B., Ip, N. C. Y., Prestwood, L. J., Abbink, T. E. M. & Lever, A. M. L. Evidence that the endosomal sorting complex required for transport-II (ESCRT-II) is required for efficient human immunodeficiency virus-1 (HIV-1) production. *Retrovirology* **12**, 72 (2015).
586. Bartusch, C. & Prange, R. ESCRT requirements for murine leukemia virus release. *Viruses* **8**, 103 (2016).
587. Ghoujal, B., Milev, M. P., Ajamian, L., Abel, K. & Mouland, A. J. ESCRT-II's involvement in HIV-1 genomic RNA trafficking and assembly. *Biol. Cell* **104**, 706–721 (2012).
588. Gottwein, E., Jager, S., Habermann, A. & Krausslich, H.-G. Cumulative Mutations of Ubiquitin Acceptor Sites in Human Immunodeficiency Virus Type 1 Gag Cause a Late Budding Defect. *J. Virol.* (2006). doi:10.1128/jvi.02177-05
589. Spidel, J. L. *et al.* Lysines close to the Rous sarcoma virus late domain critical for budding. *J. Virol.* **78**, 10606–10616 (2004).
590. Martin-serrano, J., Perez-caballero, D. & Bieniasz, P. D. Context-dependent effects of L domains and ubiquitination on viral budding. *J Virol* **78**, 5554–5563 (2004).
591. Joshi, A., Munshi, U., Ablan, S. D., Nagashima, K. & Freed, E. O. Functional replacement of a retroviral late domain by ubiquitin fusion. *Traffic* **9**, 1972–1983 (2008).
592. Strack, B., Calistri, A., Accola, M. A., Palu, G. & Gottlinger, H. G. A role for ubiquitin ligase recruitment in retrovirus release. *Proc. Natl. Acad. Sci. U. S. A.* **97**, 13063–8 (2000).
593. Zhadina, M., Mcclure, M. O., Johnson, M. C. & Bieniasz, P. D. Ubiquitindependent virus particle budding without viral protein ubiquitination. *Proc. Natl. Acad. Sci. U. S. A.* **104**, 20031–6 (2007).
594. Zhadina, M. & Bieniasz, P. D. Functional interchangeability of late domains, late domain cofactors and ubiquitin in viral budding. *PLoS Pathog.* **6**, (2010).
595. Rauch, S. & Martin-Serrano, J. Multiple interactions between the ESCRT machinery and arrestin-related proteins: implications for PPXY-dependent budding. *J. Virol.* **85**, 3546–3556 (2011).
596. Van Engelenburg, S. B. *et al.* Distribution of ESCRT machinery at HIV assembly sites reveals virus scaffolding of ESCRT subunits. *Science (80-.).* (2014). doi:10.1126/science.1247786
597. Baumgärtel, V. *et al.* Live-cell visualization of dynamics of HIV budding site interactions with an ESCRT component. *Nat. Cell Biol.* **13**, 469–474 (2011).
598. Jouvenet, N., Zhadina, M., Bieniasz, P. D. & Simon, S. M. Dynamics of ESCRT

protein recruitment during retroviral assembly. *Nat. Cell Biol.* **13**, 394–401 (2011).
599. Carlson, L. A., Shen, Q. T., Pavlin, M. R. & Hurley, J. H. ESCRT Filaments as Spiral Springs. *Developmental Cell* **35**, 397–398 (2015).
600. Lee, J. A. & Gao, F. B. Roles of ESCRT in autophagy-associated neurodegeneration. *Autophagy* (2008). doi:10.4161/auto.5384
601. Mizushima, N., Levine, B., Cuervo, A. M. & Klionsky, D. J. Autophagy fights disease through cellular self-digestion. *Nature* (2008). doi:10.1038/nature06639
602. Rusten, T. E., Filimonenko, M., Rodahl, L. M., Stenmark, H. & Simonsen, A. ESCRTing autophagic clearance of aggregating proteins. *Autophagy* (2008). doi:10.4161/auto.5396
603. Spitzer, C. *et al.* The endosomal protein CHARGED MULTIVESICULAR BODY PROTEIN1 regulates the autophagic turnover of plastids in arabidopsis. *Plant Cell* (2015). doi:10.1105/tpc.114.135939
604. Filimonenko, M. *et al.* Functional multivesicular bodies are required for autophagic clearance of protein aggregates associated with neurodegenerative disease. *J. Cell Biol.* (2007). doi:10.1083/jcb.200702115
605. Nara, A. *et al.* SKD1 AAA ATPase-dependent endosomal transport is involved in autolysosome formation. *Cell Struct. Funct.* (2002). doi:10.1247/csf.27.29
606. Rusten, T. E. & Stenmark, H. How do ESCRT proteins control autophagy? *J. Cell Sci.* (2009). doi:10.1242/jcs.050021
607. Takahashi, Y. *et al.* An autophagy assay reveals the ESCRT-III component CHMP2A as a regulator of phagophore closure. *Nat. Commun.* (2018). doi:10.1038/s41467-018-05254-w
608. Zhen, Y. *et al.* ESCRT-mediated phagophore sealing during mitophagy. *Autophagy* (2019). doi:10.1080/15548627.2019.1639301
609. Zhou, F., Wu, Z., Zhao, M., Segev, N. & Liang, Y. Autophagosome closure by ESCRT: Vps21/RAB5-regulated ESCRT recruitment via an Atg17-Snf7 interaction. *Autophagy* (2019). doi:10.1080/15548627.2019.1628547
610. Keyel, P. A. *et al.* Streptolysin O clearance through sequestration into blebs that bud passively from the plasma membrane. *J. Cell Sci.* **124**, 2414–23 (2011).
611. Babiychuk, E. B., Monastyrskaya, K., Potez, S. & Draeger, a. Intracellular Ca(2+) operates a switch between repair and lysis of streptolysin O-perforated cells. *Cell Death Differ.* **16**, 1126–34 (2009).
612. McNeil, P. L. & Khakee, R. Disruptions of muscle fiber plasma membranes. Role in exercise-induced damage. *Am J Pathol* **140**, 1097–1109 (1992).
613. McNeil, P. L. & Steinhardt, R. A. Plasma Membrane Disruption: Repair, Prevention, Adaptation. *Annu. Rev. Cell Dev. Biol.* **19**, 697–731 (2003).
614. Jimenez, A. J. *et al.* ESCRT machinery is required for plasma membrane repair. Supplement. *Science* **343**, 1247136 (2014).
615. Wehman, A. M., Poggioli, C., Schweinsberg, P., Grant, B. D. & Nance, J. The P4-ATPase TAT-5 inhibits the budding of extracellular vesicles in C. elegans embryos. *Curr. Biol.* **21**, 1951–1959 (2011).
616. Baietti, M. F. *et al.* Syndecan–syntenin–ALIX regulates the biogenesis of exosomes. *Nat. Cell Biol.* **14**, 677–685 (2012).
617. Hurley, J. H. & Odorizzi, G. Get on the exosome bus with ALIX. *Nat. Cell Biol.* **14**, 654–5 (2012).

618. Issman-Zecharya, N. & Schuldiner, O. The PI3K class III complex promotes axon pruning by downregulating a ptc-derived signal via endosome-lysosomal degradation. *Dev. Cell* **31**, 461–473 (2014).
619. Zhang, H. *et al.* Endocytic Pathways Downregulate the L1-type Cell Adhesion Molecule Neuroglian to Promote Dendrite Pruning in Drosophila. *Dev. Cell* **30**, 463–478 (2014).
620. Loncle, N., Agromayor, M., Martin-Serrano, J. & Williams, D. W. An ESCRT module is required for neuron pruning. *Sci. Rep.* **5**, 8461 (2015).
621. Thiele, D. L. & Lipsky, P. E. Mechanism of L-leucyl-L-leucine methyl ester-mediated killing of cytotoxic lymphocytes: Dependence on a lysosomal thiol protease, dipeptidyl peptidase I, that is enriched in these cells. *Proc. Natl. Acad. Sci. U. S. A.* (1990). doi:10.1073/pnas.87.1.83
622. Rusten, T. E. & Simonsen, A. ESCRT functions in autophagy and associated disease. *Cell Cycle* **7**, 1166–1172 (2008).
623. Saksena, S. & Emr, S. D. ESCRTs and human disease. *Biochem. Soc. Trans.* **37**, 167–72 (2009).
624. Stuffers, S., Brech, A. & Stenmark, H. ESCRT proteins in physiology and disease. *Experimental Cell Research* (2009). doi:10.1016/j.yexcr.2008.10.013
625. Skibinski, G. *et al.* Mutations in the endosomal ESCRTIII-complex subunit CHMP2B in frontotemporal dementia. *Nat. Genet.* **37**, 806–808 (2005).
626. Parkinson, N. *et al.* ALS phenotypes with mutations in CHMP2B (charged multivesicular body protein 2B). *Neurology* (2006). doi:10.1212/01.wnl.0000231510.89311.8b
627. Hara, T. *et al.* Suppression of basal autophagy in neural cells causes neurodegenerative disease in mice. *Nature* (2006). doi:10.1038/nature04724
628. Komatsu, M. *et al.* Loss of autophagy in the central nervous system causes neurodegeneration in mice. *Nature* (2006). doi:10.1038/nature04723
629. Juhász, G., Érdi, B., Sass, M. & Neufeld, T. P. Atg7-dependent autophagy promotes neuronal health, stress tolerance, and longevity but is dispensable for metamorphosis in Drosophila. *Genes Dev.* (2007). doi:10.1101/gad.1600707
630. Simonsen, A. *et al.* Promoting basal levels of autophagy in the nervous system enhances longevity and oxidant resistance in adult Drosophila. *Autophagy* (2008). doi:10.4161/auto.5269
631. Ravikumar, B. *et al.* Inhibition of mTOR induces autophagy and reduces toxicity of polyglutamine expansions in fly and mouse models of Huntington disease. *Nat. Genet.* (2004). doi:10.1038/ng1362
632. Yamamoto, A., Cremona, M. L. & Rothman, J. E. Autophagy-mediated clearance of huntingtin aggregates triggered by the insulin-signaling pathway. *J. Cell Biol.* (2006). doi:10.1083/jcb.200510065
633. Bong, Y. K., Olzmann, J. A., Barsh, G. S., Chin, L. S. & Li, L. Spongiform neurodegeneration-associated E3 ligase mahogunin ubiquitylates TSG101 and regulates endosomal trafficking. *Mol. Biol. Cell* (2007). doi:10.1091/mbc.E06-09-0787
634. Patel, H. *et al.* SPG20 is mutated in Troyer syndrome, an hereditary spastic paraplegia. *Nat. Genet.* (2002). doi:10.1038/ng937
635. Li, L. & Cohen, S. N. tsg101: A novel tumor susceptibility gene isolated by controlled homozygous functional knockout of allelic loci in mammalian cells.

Cell (1996). doi:10.1016/S0092-8674(00)81111-3
636. Moberg, K. H., Schelble, S., Burdick, S. K. & Hariharan, I. K. Mutations in erupted, the Drosophila ortholog of mammalian tumor susceptibility gene 101, elicit non-cell-autonomous overgrowth. *Dev. Cell* (2005). doi:10.1016/j.devcel.2005.09.018
637. Xu, Z., Liang, L., Wang, H., Li, T. & Zhao, M. HCRP1, a novel gene that is downregulated in hepatocellular carcinoma, encodes a growth-inhibitory protein. *Biochem. Biophys. Res. Commun.* (2003). doi:10.1016/j.bbrc.2003.10.109
638. Li, J., Belogortseva, N., Porter, D. & Park, M. Chmp1A functions as a novel tumor suppressor gene in human embryonic kidney and ductal pancreatic tumor cells. *Cell Cycle* (2008). doi:10.4161/cc.7.18.6677
639. Lin, H. H. *et al.* Identification of an AAA ATPase VPS4B-Dependent Pathway That Modulates Epidermal Growth Factor Receptor Abundance and Signaling during Hypoxia. *Mol. Cell. Biol.* (2012). doi:10.1128/mcb.06053-11
640. Krempler, A., Henry, M. D., Triplett, A. A. & Wagner, K. U. Targeted deletion of the Tsg101 gene results in cell cycle arrest at G1/S and p53-independent cell death. *J. Biol. Chem.* (2002). doi:10.1074/jbc.M207662200
641. Wagner, K.-U. *et al.* Tsg101 Is Essential for Cell Growth, Proliferation, and Cell Survival of Embryonic and Adult Tissues. *Mol. Cell. Biol.* (2003). doi:10.1128/mcb.23.1.150-162.2003
642. Thompson, B. J. *et al.* Tumor suppressor properties of the ESCRT-II complex component Vps25 in Drosophila. *Dev. Cell* (2005). doi:10.1016/j.devcel.2005.09.020
643. Vaccari, T. & Bilder, D. The Drosophila tumor suppressor vps25 prevents nonautonomous overproliferation by tegulating Notch trafficking. *Dev. Cell* (2005). doi:10.1016/j.devcel.2005.09.019
644. Lloyd, T. E. *et al.* Hrs regulates endosome membrane invagination and tyrosine kinase receptor signaling in Drosophila. *Cell* (2002). doi:10.1016/S0092-8674(02)00611-6
645. Buchanan, S. M., Schalm, S. S. & Maniatis, T. Proteolytic processing of protocadherin proteins requires endocytosis. *Proc. Natl. Acad. Sci. U. S. A.* (2010). doi:10.1073/pnas.1013105107
646. Toyoshima, M. *et al.* Inhibition of tumor growth and metastasis by depletion of vesicular sorting protein Hrs: Its regulatory role on E-cadherin and β-catenin. *Cancer Res.* (2007). doi:10.1158/0008-5472.CAN-06-2756
647. Brown, C. J., Lain, S., Verma, C. S., Fersht, A. R. & Lane, D. P. Awakening guardian angels: Drugging the P53 pathway. *Nature Reviews Cancer* (2009). doi:10.1038/nrc2763
648. Li, L., Liao, J., Ruland, J., Mak, T. W. & Cohen, S. N. A TSG101/MDM2 regulatory loop modulates MDM2 degradation and MDM2/p53 feedback control. *Proc. Natl. Acad. Sci. U. S. A.* (2001). doi:10.1073/pnas.98.4.1619
649. Komada, M. & Soriano, P. Hrs, a FYVE finger protein localized to early endosomes, is implicated in vesicular traffic and required for ventral folding morphogenesis. *Genes Dev.* (1999). doi:10.1101/gad.13.11.1475
650. Yamada, M. *et al.* Signal-Transducing Adaptor Molecules STAM1 and STAM2 Are Required for T-Cell Development and Survival. *Mol. Cell. Biol.* (2002).

doi:10.1128/mcb.22.24.8648-8658.2002
651. Mochida, G. H. *et al.* CHMP1A encodes an essential regulator of BMI1-INK4A in cerebellar development. *Nat. Genet.* (2012). doi:10.1038/ng.2425
652. Zivony-Elboum, Y. *et al.* A founder mutation in Vps37A causes autosomal recessive complex hereditary spastic paraparesis. *J. Med. Genet.* (2012). doi:10.1136/jmedgenet-2012-100742
653. Vieira, O. V. *et al.* Acquisition of Hrs, an Essential Component of Phagosomal Maturation, Is Impaired by Mycobacteria. *Mol. Cell. Biol.* (2004). doi:10.1128/mcb.24.10.4593-4604.2004
654. Philips, J. A., Porto, M. C., Wang, H., Rubin, E. J. & Perrimon, N. ESCRT factors restrict mycobacterial growth. *Proc. Natl. Acad. Sci. U. S. A.* (2008). doi:10.1073/pnas.0707206105
655. Pear, W. S. *et al.* Efficient and rapid induction of a chronic myelogenous leukemia-like myeloproliferative disease in mice receiving p210 bcr/abl-transduced bone marrow. *Blood* (1998). doi:10.1182/blood.v92.10.3780.422k15_3780_3792
656. Soneoka, Y. *et al.* A transient three-plasmid expression system for the production of high titer retroviral vectors. *Nucleic Acids Research* (1995). doi:10.1093/nar/23.4.628
657. Eastman, S. W., Martin-Serrano, J., Chung, W., Zang, T. & Bieniasz, P. D. Identification of human VPS37C, a component of endosomal sorting complex required for transport-I important for viral budding. *J. Biol. Chem.* **280**, 628–636 (2005).
658. Agromayor, M. *et al.* The UBAP1 subunit of ESCRT-I interacts with ubiquitin via a SOUBA domain. *Structure* **20**, 414–428 (2012).
659. Kim, D. I. *et al.* An improved smaller biotin ligase for BioID proximity labeling. *Mol. Biol. Cell* (2016). doi:10.1091/mbc.E15-12-0844
660. Sanjana, N. E., Shalem, O. & Zhang, F. Improved vectors and genome-wide libraries for CRISPR screening. *Nature Methods* (2014). doi:10.1038/nmeth.3047
661. Shalem, O. *et al.* Genome-scale CRISPR-Cas9 knockout screening in human cells. *Science (80-.).* (2014). doi:10.1126/science.1247005
662. Walter, J. M., Chandran, S. S. & Horwitz, A. A. CRISPR-Cas-Assisted Multiplexing (CAM): Simple Same-Day Multi-Locus Engineering in Yeast. *J. Cell. Physiol.* (2016). doi:10.1002/jcp.25375
663. Derdeyn, C. A. *et al.* Sensitivity of Human Immunodeficiency Virus Type 1 to the Fusion Inhibitor T-20 Is Modulated by Coreceptor Specificity Defined by the V3 Loop of gp120. *J. Virol.* **74**, 8358–8367 (2000).
664. Tyanova, S. *et al.* The Perseus computational platform for comprehensive analysis of (prote)omics data. *Nature Methods* (2016). doi:10.1038/nmeth.3901
665. Stuchell, M. D. *et al.* The human endosomal sorting complex required for transport (ESCRT-I) and its role in HIV-1 budding. *J. Biol. Chem.* **279**, 36059–36071 (2004).
666. Bache, K. G. *et al.* The growth-regulatory protein HCRP1/hVps37A is a subunit of mammalian ESCRT-I and mediates receptor down-regulation. *Mol. Biol. Cell* **15**, 4337–46 (2004).
667. Morita, E. *et al.* Identification of Human MVB12 Proteins as ESCRT-I Subunits that Function in HIV Budding. *Cell Host Microbe* **2**, 41–53 (2007).

668. Ichioka, F. *et al.* HD-PTP and Alix share some membrane-traffic related proteins that interact with their Bro1 domains or proline-rich regions. *Arch. Biochem. Biophys.* **457**, 142–149 (2007).
669. McDonald, B. & Martin-Serrano, J. Regulation of Tsg101 expression by the steadiness box: A role of Tsg101-associated ligase. *Mol. Biol. Cell* (2008). doi:10.1091/mbc.E07-09-0957
670. Razi, M. & Futter, C. E. Distinct roles for Tsg101 and Hrs in multivesicular body formation and inward vesiculation. *Mol. Biol. Cell* (2006). doi:10.1091/mbc.E05-11-1054
671. Rush, J. S. & Ceresa, B. P. RAB7 and TSG101 are required for the constitutive recycling of unliganded EGFRs via distinct mechanisms. *Mol. Cell. Endocrinol.* (2013). doi:10.1016/j.mce.2013.07.029
672. Feng, G. H., Lih, C. J. & Cohen, S. N. TSG101 protein steady-state level is regulated posttranslationally by an evolutionarily conserved COOH-terminal sequence. *Cancer Res.* (2000).
673. Palencia, A., Martinez, J. C., Mateo, P. L., Luque, I. & Camara-Artigas, A. Structure of human TSG101 UEV domain. *Acta Crystallogr. Sect. D Biol. Crystallogr.* (2006). doi:10.1107/S0907444906005221
674. Okumura, M., Katsuyama, A. M., Shibata, H. & Maki, M. VPS37 isoforms differentially modulate the ternary complex formation of ALIX, ALG-2, and ESCRT-I. *Biosci. Biotechnol. Biochem.* (2013). doi:10.1271/bbb.130280
675. Okumura, M. *et al.* Penta-EF-hand protein ALG-2 functions as a Ca2+-dependent adaptor that bridges Alix and TSG101. *Biochem. Biophys. Res. Commun.* (2009). doi:10.1016/j.bbrc.2009.06.015
676. Maki, M., Suzuki, H. & Shibata, H. Structure and function of ALG-2, a penta-EF-hand calcium-dependent adaptor protein. *Science China Life Sciences* (2011). doi:10.1007/s11427-011-4204-8
677. Begley, D., Murphy, A. M., Hiu, C. & Tsubota, S. I. Modifier of rudimentaryp1, mod(r)p1, a trans-acting regulatory mutation of rudimentary. *Mol. Gen. Genet. MGG* (1995). doi:10.1007/BF02456615
678. Pashkova, N. & Piper, R. C. UBAP1: A new ESCRT member joins the cl-Ub. *Structure* **20**, 383–385 (2012).
679. Boura, E. & Hurley, J. H. Structural basis for membrane targeting by the MVB12-associated beta-prism domain of the human ESCRT-I MVB12 subunit. *Proc. Natl. Acad. Sci. U. S. A.* **109**, 1901–1906 (2012).
680. de Souza, R. F. & Aravind, L. UMA and MABP domains throw light on receptor endocytosis and selection of endosomal cargoes. *Bioinformatics* **26**, 1477–1480 (2010).
681. Wunderley, L., Brownhill, K., Stefani, F., Tabernero, L. & Woodman, P. The molecular basis for selective assembly of the UBAP1-containing, endosome-specific ESCRT-I complex. *J. Cell Sci.* **127**, 663–672 (2013).
682. Hofmann, K. & Bucher, P. The UBA domain: A sequence motif present in multiple enzyme classes of the ubiquitination pathway. *Trends Biochem. Sci.* (1996). doi:10.1016/S0968-0004(96)30015-7
683. Mueller, T. D. & Feigon, J. Solution structures of UBA domains reveal a conserved hydrophobic surface for protein-protein interactions. *J. Mol. Biol.* (2002). doi:10.1016/S0022-2836(02)00302-9

684. Ohno, A. *et al.* Structure of the UBA domain of Dsk2p in complex with ubiquitin: Molecular determinants for ubiquitin recognition. *Structure* (2005). doi:10.1016/j.str.2005.01.011
685. Tsunematsu, T. *et al.* Distinct functions of human MVB12A and MVB12B in the ESCRT-I dependent on their posttranslational modifications. *Biochem. Biophys. Res. Commun.* **399**, 232–237 (2010).
686. Konishi, H. *et al.* CFBP is a novel tyrosine-phosphorylated protein that might function as a regulator of CIN85/CD2AP. *J. Biol. Chem.* **281**, 28919–28931 (2006).
687. Goujon, M. *et al.* A new bioinformatics analysis tools framework at EMBL-EBI. *Nucleic Acids Res.* (2010). doi:10.1093/nar/gkq313
688. Sievers, F. *et al.* Fast, scalable generation of high-quality protein multiple sequence alignments using Clustal Omega. *Mol. Syst. Biol.* (2011). doi:10.1038/msb.2011.75
689. Tym, J. E. *et al.* canSAR: An updated cancer research and drug discovery knowledgebase. *Nucleic Acids Res.* (2016). doi:10.1093/nar/gkv1030
690. Aboussekhra, A. *et al.* Mammalian DNA nucleotide excision repair reconstituted with purified protein components. *Cell* (1995). doi:10.1016/0092-8674(95)90289-9
691. Lin, Y. L. *et al.* The evolutionarily conserved zinc finger motif in the largest subunit of human replication protein A is required for DNA replication and mismatch repair but not for nucleotide excision repair. *J. Biol. Chem.* (1998). doi:10.1074/jbc.273.3.1453
692. DeMott, M. S., Zigman, S. & Bambara, R. A. Replication protein A stimulates long patch DNA base excision repair. *J. Biol. Chem.* (1998). doi:10.1074/jbc.273.42.27492
693. Hein, M. Y. *et al.* A Human Interactome in Three Quantitative Dimensions Organized by Stoichiometries and Abundances. *Cell* (2015). doi:10.1016/j.cell.2015.09.053
694. Amit, I. *et al.* Tal, a Tsg101-specific E3 ubiquitin ligase, regulates receptor endocytosis and retrovirus budding. *Genes Dev.* (2004). doi:10.1101/gad.294904
695. Roux, K. J., Kim, D. I., Raida, M. & Burke, B. A promiscuous biotin ligase fusion protein identifies proximal and interacting proteins in mammalian cells. *J. Cell Biol.* **196**, 801–810 (2012).
696. Hammerling, B. C. *et al.* A Rab5 endosomal pathway mediates Parkin-dependent mitochondrial clearance. *Nat. Commun.* **8**, 14050 (2017).
697. Hammerling, B. C., Shires, S. E., Leon, L. J., Cortez, M. Q. & Gustafsson, Å. B. Isolation of Rab5-positive endosomes reveals a new mitochondrial degradation pathway utilized by BNIP3 and Parkin. *Small GTPases* (2017). doi:10.1080/21541248.2017.1342749
698. Goliand, I., Nachmias, D., Gershony, O. & Elia, N. Inhibition of ESCRT-II-CHMP6 interactions impedes cytokinetic abscission and leads to cell death. *Mol. Biol. Cell* **25**, 3740–3748 (2014).
699. Chu, D. *et al.* AIP1 acts with cofilin to control actin dynamics during epithelial morphogenesis. *Dev.* (2012). doi:10.1242/dev.079491
700. Frankel, A. D. & Young, J. A. T. HIV-1: Fifteen Proteins and an RNA. *Annu. Rev. Biochem.* (1998). doi:10.1146/annurev.biochem.67.1.1

701. Carlson, L. A. *et al.* Three-Dimensional Analysis of Budding Sites and Released Virus Suggests a Revised Model for HIV-1 Morphogenesis. *Cell Host Microbe* **4**, 592–599 (2008).
702. Gheysen, D. *et al.* Assembly and release of HIV-1 precursor Pr55gag virus-like particles from recombinant baculovirus-infected insect cells. *Cell* (1989). doi:10.1016/0092-8674(89)90873-8
703. Campbell, S. & Vogt, V. M. Self-assembly in vitro of purified CA-NC proteins from Rous sarcoma virus and human immunodeficiency virus type 1. *J. Virol.* (1995).
704. Kwong, P. D. *et al.* Structure of an HIV gp 120 envelope glycoprotein in complex with the CD4 receptor and a neutralizing human antibody. *Nature* (1998). doi:10.1038/31405
705. Rizzuto, C. D. *et al.* A conserved HIV gp120 glycoprotein structure involved in chemokine receptor binding. *Science (80-.).* (1998). doi:10.1126/science.280.5371.1949
706. Martin-Serrano, J. & Neil, S. J. D. Host factors involved in retroviral budding and release. *Nat. Rev. Microbiol.* **9**, 519–531 (2011).
707. Freed, E. O. HIV-1 assembly, release and maturation. *Nat. Publ. Gr.* **13**, (2015).
708. Sundquist, W. I. & Kr??usslich, H. G. HIV-1 assembly, budding, and maturation. *Cold Spring Harbor Perspectives in Medicine* **2**, (2012).
709. Freed, E. O. & Martin, M. A. The role of human immunodeficiency virus type 1 envelope glycoproteins in virus infection. *Journal of Biological Chemistry* (1995). doi:10.1074/jbc.270.41.23883
710. Delwart, E. Principles of Virology . Volume I: Molecular Biology and Volume II: Pathogenesis and Control. Third Edition. By S. J. Flint, L. W. Enquist, V. R. Racaniello, and A. M. Skalka. Washington (DC): ASM Press. $99.95 (paper); $169.95 (two-volume set). Volume I. *Q. Rev. Biol.* (2011). doi:10.1086/659935
711. Engelman, A. & Cherepanov, P. The structural biology of HIV-1: Mechanistic and therapeutic insights. *Nature Reviews Microbiology* (2012). doi:10.1038/nrmicro2747
712. Jacks, T. *et al.* Characterization of ribosomal frameshifting in HIV-1 gag-pol expression. *Nature* (1988). doi:10.1038/331280a0
713. Göttlinger, H. G. The HIV-1 assembly machine. *AIDS* (2001). doi:10.1097/00002030-200100005-00003
714. Ono, A. & Freed, E. O. Plasma membrane rafts play a critical role in HIV-1 assembly and release. *Proc. Natl. Acad. Sci. U. S. A.* (2001). doi:10.1073/pnas.241320298
715. Ono, A. HIV-1 assembly at the plasma membrane: Gag trafficking and localization. *Future Virology* (2009). doi:10.2217/fvl.09.4
716. Hogue, I. B., Grover, J. R., Soheilian, F., Nagashima, K. & Ono, A. Gag Induces the Coalescence of Clustered Lipid Rafts and Tetraspanin-Enriched Microdomains at HIV-1 Assembly Sites on the Plasma Membrane. *J. Virol.* (2011). doi:10.1128/jvi.00743-11
717. Nguyen, D. H. & Hildreth, J. E. K. Evidence for Budding of Human Immunodeficiency Virus Type 1 Selectively from Glycolipid-Enriched Membrane Lipid Rafts. *J. Virol.* (2000). doi:10.1128/jvi.74.7.3264-3272.2000
718. Saad, J. S. *et al.* Structural basis for targeting HIV-1 Gag proteins to the plasma membrane for virus assembly. *Proc. Natl. Acad. Sci. U. S. A.* (2006).

doi:10.1073/pnas.0602818103
719. Gottlinger, H. G., Sodroski, J. G. & Haseltine, W. A. Role of capsid precursor processing and myristoylation in morphogenesis and infectivity of human immunodeficiency virus type 1. *Proc. Natl. Acad. Sci. U. S. A.* (1989). doi:10.1073/pnas.86.15.5781
720. Ganser-Pornillos, B. K., Yeager, M. & Sundquist, W. I. The structural biology of HIV assembly. *Current Opinion in Structural Biology* (2008). doi:10.1016/j.sbi.2008.02.001
721. Briggs, J. A. G. *et al.* Structure and assembly of immature HIV. *Proc. Natl. Acad. Sci. U. S. A.* (2009). doi:10.1073/pnas.0903535106
722. Wright, E. R. *et al.* Electron cryotomography of immature HIV-1 virions reveals the structure of the CA and SP1 Gag shells. *EMBO J.* (2007). doi:10.1038/sj.emboj.7601664
723. Johnson, S. F. & Telesnitsky, A. Retroviral RNA dimerization and packaging: The what, how, when, where, and why. *PLoS Pathog.* (2010). doi:10.1371/journal.ppat.1001007
724. Lever, A. M. L. HIV-1 RNA Packaging. *Advances in Pharmacology* (2007). doi:10.1016/S1054-3589(07)55001-5
725. Chen, J. *et al.* High efficiency of HIV-1 genomic RNA packaging and heterozygote formation revealed by single virion analysis. *Proc. Natl. Acad. Sci. U. S. A.* (2009). doi:10.1073/pnas.0906822106
726. D'Souza, V. & Summers, M. F. How retroviruses select their genomes. *Nature Reviews Microbiology* (2005). doi:10.1038/nrmicro1210
727. Accola, M. A., Strack, B. & Gottlinger, H. G. Efficient Particle Production by Minimal Gag Constructs Which Retain the Carboxy-Terminal Domain of Human Immunodeficiency Virus Type 1 Capsid-p2 and a Late Assembly Domain. *J. Virol.* (2000). doi:10.1128/jvi.74.12.5395-5402.2000
728. Gross, I., Hohenberg, H. & Kräusslich, H. G. In vitro assembly properties of purified bacterially expressed capsid proteins of human immunodeficiency virus. *Eur. J. Biochem.* (1997). doi:10.1111/j.1432-1033.1997.t01-1-00592.x
729. Hill, M., Tachedjian, G. & Mak, J. The Packaging and Maturation of the HIV-1 Pol Proteins. *Curr. HIV Res.* (2005). doi:10.2174/1570162052772942
730. Swanstrom, R. & Wills, J. *Synthesis, Assembly, and Processing of Viral Proteins*. *Retroviruses* (1997).
731. Briggs, J. A. G., Wilk, T., Welker, R., Kräusslich, H. G. & Fuller, S. D. Structural organization of authentic, mature HIV-1 virions and cores. *EMBO J.* (2003). doi:10.1093/emboj/cdg143
732. Benjamin, J., Ganser-Pornillos, B. K., Tivol, W. F., Sundquist, W. I. & Jensen, G. J. Three-dimensional structure of HIV-1 virus-like particles by electron cryotomography. *J. Mol. Biol.* (2005). doi:10.1016/j.jmb.2004.11.064
733. Briggs, J. A. G. *et al.* The mechanism of HIV-1 core assembly: Insights from three-dimensional reconstructions of authentic virions. *Structure* (2006). doi:10.1016/j.str.2005.09.010
734. Goila-Gaur, R., Demirov, D. G., Orenstein, J. M., Ono, A. & Freed, E. O. Defects in human immunodeficiency virus budding and endosomal sorting induced by TSG101 overexpression. *J. Virol.* **77**, 6507–19 (2003).
735. Silvestri, L. S. *et al.* Involvement of Vacuolar Protein Sorting Pathway in Ebola

Virus Release Independent of TSG101 Interaction. *J. Infect. Dis.* (2007). doi:10.1086/520610

Appendix 1 – Supplementary material

Oligonucleotides used in this thesis

Primers for cloning and mutagenesis

UMAD1 5’ Fwd	CTCCTCGAATTCATGTTTCACTTCTTCAG
UMAD1 3’ Rev	ATATATCTCGAGTTATGAATCACAGAGCACTG
UMAD1 $L_{86}S_{87}D_{88}$/AAA 5’ Fwd	TTAATGGCCGAGCTCGCAGCAGCAGTGCCGTTCACCCTG
UMAD1 $L_{86}S_{87}D_{88}$/AAA 3’ Rev	CAGGGTGAACGGCACTGCTGCTGCGAGCTCGGCCATTAA
UMAD1 $V_{89}P_{90}F_{91}$/AAA 5’ Fwd	GCCGAGCTCCTGAGCGATGCAGCAGCAACCCTGGCCCCGCATGTG
UMAD1 $V_{89}P_{90}F_{91}$/AAA 3’ Rev	CACATGCGGGGCCAGGGTTGCTGCTGCATCGCTCAGGAGCTCGGC
UMAD1 P108A 5’ Fwd	ATCACTGACCTTGCAGACCACTTACTC
UMAD1 P108A 3’ Rev	GAGTAAGTGGTCTGCAAGGTCAGTGAT
UMAD1 Y125A 5’ Fwd	TATCACGGTTTTGGGCAGATTTCACTCTTGAA
UMAD1 Y125A 3’ Rev	TTCAAGAGTGAAATCTGCCCAAAACCGTGATA
UMAD1 F127A 5’ Fwd	CGGTTTTGGTATGATGCAACTCTTGAAAATTCA
UMAD1 F127A 3’ Rev	TGAATTTTCAAGAGTTGCATCATACCAAAACCG
UMAD1 E130A 5’ Fwd	TATGATTTCACTCTTGCAAATTCAGTGCTCTGT
UMAD1 E130A 3’ Rev	ACAGAGCACTGAATTTGCAAGAGTGAAATCATA
RPA3 5’ Fwd	CTCCTCGAATTCATGGTGGACATGATG
RPA3 3’ Rev	ATATATCTCGAGTCAATCATGTTGCACAATC

Primers for sequencing

pCR3.1 Rev	TAGAAGGCACAGTCGAGG
pCMS28 Fwd	CTTGAACCTCCTCGTTCGACC
pCMS28 Rev	GCTTCGGCCAGTAACGTTAGG
pLKO1 Fwd	GACTATCATATGCTTACCGT

siRNA oligos

Non-targeting siRNA	ON-TARGETplus Non-targeting (Cat. No. D-001810-01, Dharmacon)
siVPS37C	CAGUCCUGGUUAUCCUCAAUU Cat. No. S104156096, Qiagen
siTSG101	CCUCCAGUCUUCUCUCGUC (custom order siRNA, Dharmacon)
siALIX	GAAGGAUGCUUUCGAUAAAUU (custom order siRNA, Dharmacon)
siUMAD1	GCGAAAACUUAUCACGGUU (Cat. No. N-183515-16, Dharmacon)

All sequences are shown 5’ – 3’
Fwd = Forward
Rev = Reverse

Plasmids used in this thesis

Gene	Vector	Restriction sites	Resistance genes	Applications
Wild type UMAD1	pCR3.1 HA	EcoRI/XhoI	Ampicillin	Coprecipitations
	pCMS28 YFP	EcoRI/XhoI	Ampicillin/Puro	Immunoprecipitations, Imaging
	pHxB	EcoRI/XhoI	Ampicillin	Viral trans-complementation
UMAD1 point mutants (Section 3.2.4.)	pCR3.1 HA	EcoRI/XhoI	Ampicillin	Coprecipitations
VPS28	pCR3.1 Myc	NotI/NotI	Ampicillin	Coprecipitations
VPS37A	pCR3.1 HA	EcoRI/XhoI	Ampicillin	Coprecipitations
	pCMS28 YFP	EcoRI/XhoI	Ampicillin/Puro	Immunoprecipitations
VPS37B	pCR3.1 HA	EcoRI/XhoI	Ampicillin	Coprecipitations
	pCMS28 YFP	EcoRI/XhoI	Ampicillin/Puro	Immunoprecipitations
VPS37C	pCR3.1 HA	EcoRI/XhoI	Ampicillin	Coprecipitations
	pCMS28 YFP	EcoRI/XhoI	Ampicillin/Puro	Immunoprecipitations
VPS37D	pCR3.1 HA	EcoRI/XhoI	Ampicillin	Coprecipitations
TSG101	pCAGGS GST	EcoRI/XhoI	Ampicillin	Coprecipitations
	pCMS28 YFP	EcoRI/XhoI	Ampicillin/Puro	Immunoprecipitations, Imaging
	pHxB	EcoRI/XhoI	Ampicillin	Viral trans-complementation
UBAP1	pHxB	NotI/NotI	Ampicillin	Viral trans-complementation
HIV-1 Gag p6	pHxB	EcoRI/XhoI	Ampicillin	Viral trans-complementation
RPA3	pNG72	EcoRI/XhoI	Ampicillin/G418	Testing α-RPA3 antibody
	pNG72 YFP	EcoRI/XhoI	Ampicillin/G418	Testing α-RPA3 antibody
Tubulin	pCMS28 mCherry	NotI/NotI	Ampicillin/Puro	Imaging
CHMP4B	pNG72-linker GFP	EcoRI/XhoI	Ampicillin/G418	Imaging

Antibodies used in this thesis

Primary antibodies

Antibody	Species	Source	Dilution	Application
α-Tubulin	Mouse, monoclonal	Sigma (DM1a) Cell signalling	1:1000	IF
α-HA	Mouse, monoclonal	Covance (HA.11, 16B12)	1:1000	WB
α-HSP90	Mouse, monoclonal	Santa Cruz Biotechnology sc-13119	1:1000	WB
α-GFP	Mouse, monoclonal	Roche (7.1/13.1)	1:5000	WB
α-TSG101	Mouse, monoclonal	Abcam (4A10)	1:1000	WB
α-VPS37A	Rabbit, polyclonal	Proteintech 11870-1-AP	1:1000	WB
α-VPS37B	Rabbit, polyclonal	Proteintech 15613-1-AP	1:1000	WB
α-VPS37C	Rabbit, polyclonal	Gifted from Prof. Philip Woodman	1:1000	WB
α-CEP55	Mouse, polyclonal	Abnova	1:500	WB
α-HIV-1 p24 Gag	Mouse, monoclonal	NIH AIDS Reagent Program (183-H12-5C)	1:100	WB
α-UBAP1	Rabbit, polyclonal	Proteintech 12385-1-AP	1:1000	WB
α-RPA3	Rabbit, polyclonal	Proteintech 10692-1-AP	1:1000	WB
α-UMAD1	Rabbit, polyclonal	Custom made by Lampire Biologicals* against residues 6-23	1:100	WB
α-ALIX	Rabbit, polyclonal	Gifted from Prof. Wesley Sundquist	1:1000	WB

Secondary antibodies

Antibody	Conjugation	Source	Dilution	Application
α-mouse IgG	HRP-linked	Cell Signalling Technology	1:1000	WB, LI-COR Odyssey
α-rabbit IgG	HRP-linked	Cell Signalling Technology	1:1000	WB, LI-COR Odyssey
Goat α-mouse	680nm IRDye®	LI-COR Biosciences	1:10000	WB, LI-COR Odyssey
Goat α-rabbit	800nm IRDye®	LI-COR Biosciences	1:10000	WB, LI-COR Odyssey
Donkey α-Mouse IgG (H+L)	Alexa Fluor® 594	Invitrogen Life Technologies	1:5000	IF

IF = Immunofluorescence
WB = Western blotting
* Only detects overexpressed/concentrated protein

Mass spectrometry results

Gene Symbol	Protein FDR Confidence: Combined	Coverage [%]	# Peptides	# PSMs	# Unique Peptides	# AAs	MW [kDa]	calc. pI	Score Mascot: Mascot	Score Sequest HT: Sequest HT	Abundances (Grouped): F1, 126 HelaΔUMAD1 YFP empty repeat 1	Abundances (Grouped): F1, 127N HelaΔUMA D1 YFP empty repeat 2	Abundances (Grouped): F1, 127C HelaΔUMA D1 YFP-TSG101 repeat 1	Abundances (Grouped): F1, 128N HelaΔUMA D1 YFP-TSG101 repeat 2	Abundances (Grouped): F1, 128C HeLa YFP empty repeat 1	Abundances (Grouped): F1, 129N HeLa YFP empty repeat 2	Abundances (Grouped): F1, 129C HeLa YFP-TSG101 repeat 1	Abundances (Grouped): F1, 130N HeLa YFP-TSG101 repeat 2	Abundances (Grouped): F1, 130C HeLa YFP-VPS37C repeat 1	Abundances (Grouped): F1, 131 HeLa YFP-VPS37C repeat 2
VPS37C	High	12	5	10	5	355	38.6	5.21	99	10.34	53.1	33	234.2	279.3	53.7	36.5	409.6	609	3331.3	4762.9
UMAD1	High	17	1	1	1	137	15.2	4.48	54	NaN	11.2	8.6	NaN	2.6	11.6	5.8	9.8	26.1	14.7	28.2
CEP55	High	6	2	4	2	464	54.1	7.01	36	2.77	106.3	66.1	65.5	99.8	117	44.3	124.6	307.9	105.8	174.5
VPS37A	High	12	4	10	4	397	44.3	5.57	91	13.23	79.1	50.7	896.1	1043	128.6	103.1	774.3	1055.4	22.1	127.9
TSG101	High	37	14	32	14	390	43.9	6.46	376	40.71	245.1	232.3	1622.1	2523.9	232.8	248.5	1342.2	2799.1	3121.4	4592.1
VPS37B	High	6	1	2	1	285	31.3	7.34	29	3.18	2.6	NaN	27.9	43.6	NaN	2.6	24.5	43.7	NaN	2.3
VPS28	High	39	6	14	6	221	25.4	5.54	201	19.83	20.1	23.2	69.4	128.4	19.2	21	191	355.8	121.6	211.5
UBAP1	High	21	7	14	7	502	55	5.11	163	22.94	31.1	38.6	1423.3	1916.6	17.4	151.3	1343	2141.2	20.8	83.3
FAM125A;MVB12A	High	42	9	22	9	273	28.8	8.91	279	33.18	71	69.2	1252.7	1834.5	99.3	128.6	758.8	845.3	1244.9	2276.2
PLEC	High	50	224	438	219	4684	531.5	5.96	4174	499.96	22895.1	9038.1	2607.6	3404.3	36120.4	4708	18067.5	61262.6	7534	181479
DSP	High	22	50	97	50	2871	331.6	6.81	932	86.84	3328.1	1717.1	431.1	897.1	3781.1	1058.6	2204.7	10654.2	1529.2	4119.8
KRT8	High	80	49	157	40	483	53.7	5.59	1536	189.59	12441.1	4052	915.3	1768.3	10992.4	1843.9	7488.4	24938.3	3963.6	9613.8
KRT18	High	87	46	123	46	430	48	5.45	1267	144.38	9580.4	2957.8	793.9	1182.2	8439.6	1216.9	6715.6	19796	2752.7	6175.4
TUBB	High	76	30	107	6	444	49.6	4.89	963	113.18	7443.4	1834.1	1097.8	2068.6	6771.9	1592.8	3599.5	16109.7	5102.9	2792.6
TUBB4B	High	68	28	91	3	445	49.8	4.89	789	89.73	583.4	150.5	116	203.1	502	140.5	255.1	1240.7	460.5	310.2
TUBA1C	High	56	23	71	10	449	49.9	5.1	707	99.99	5205.9	1241.1	615.9	1164.3	3256.3	824.6	2104.8	10640.2	3506.1	2228.3
TUBA4A	High	54	19	63	6	448	49.9	5.06	590	92.84	1176.8	256.5	144.2	260.2	759.5	181.4	524.3	2697.4	792.7	452.1
MYO1C	High	20	18	32	18	1063	121.6	9.41	299	41.54	1148.6	536.8	155.2	238.2	1615.9	250.3	923.3	3401.7	689.3	1799.9
ACTC1	High	33	17	98	2	377	42	5.39	831	108.85	977.3	218.7	74.6	79.4	409.1	67	358.2	1318.5	181.4	778.7
ACTN4	High	15	13	24	6	911	104.8	5.44	112	17.02	1033.2	605.8	207.6	272.9	1640.6	310.4	874.4	3271.2	510.8	1692.2
MYO1E	High	13	9	18	9	1108	127	8.92	156	20.85	298.4	134.4	33.2	42.4	342.6	63.5	207.2	853.9	155	311
TUBB6	High	20	8	31	2	446	49.8	4.88	258	28.67	70.9	17.7	12	20.3	110.6	12.3	48.1	275.6	62.6	33.5
MYL6	High	52	7	13	7	151	16.9	4.65	144	17.35	1327.5	633.5	37.6	143.5	1451.1	193.1	728.8	3234.4	341.3	1152.2
PKP2	High	11	7	10	7	881	97.4	9.33	49	5.95	233.8	99.3	45.1	52	267.5	62.1	181.3	611	99	217.7
HSPB1	High	33	6	12	6	205	22.8	6.4	115	14.18	199.5	310	39.4	144.4	313.4	178.5	200.9	2144.4	48.5	579.5
LMNA	High	9	5	10	5	664	74.1	7.02	43	8.88	293.1	142.8	105.2	122.7	219.1	131	190.2	525.7	160.4	281.9
SNRPA1	High	17	5	7	5	255	28.4	8.62	87	2.03	154.5	221.2	356.2	705.3	309.4	393.5	449.2	903.2	602.1	1346.1
JUP	High	9	5	10	5	745	81.7	6.14	138	9.82	178.2	122.9	25.7	35.9	184.7	58.1	96	465.9	35.9	222.3
CAD	High	2	5	9	5	2225	242.8	6.46	140	6.25	361	169.7	81.6	110.4	95.1	54.2	192.2	707.3	238.7	214.1
ITPR3	High	2	5	10	2	2671	303.9	6.48	115	10.62	241	105.4	40.9	54.4	328.1	54.2	186.4	700	113.1	251.4
NPM1	High	19	4	7	4	294	32.6	4.78	27	8.01	148.9	95.9	74.3	85.1	215.6	79.2	124.3	469.1	95.2	193
HNRNPF	High	16	4	9	3	415	45.6	5.58	106	9.42	188.4	120.2	59.2	112.3	139.7	58	153	459	172.5	298.8
RPS18	High	20	4	7	4	152	17.7	10.99	44	4.18	317.8	207.5	100.9	125.7	241.1	101.1	168.1	517.1	213.7	402.9
HIST1H4A	High	33	4	8	4	103	11.4	11.36	60	5.56	679.9	232.5	51.8	74.2	501.2	126.6	375.5	2872	214	591.6
EEF1A1	High	11	4	9	4	462	50.1	9.01	65	4.7	487.7	432.6	206	446.4	234.2	183.5	223.4	817	507.2	980.1
LGALS3BP	High	11	4	7	4	585	65.3	5.27	50	8.62	117.5	123.6	109.3	144.2	80.2	66.4	85.3	171	203.8	296.6
ITPR1	High	1	4	8	1	2758	313.7	6.04	79	8.13	32.5	18.3	5.5	8.5	36.4	8	17.9	90.8	11.1	33.4
MYL12A;MYL12B	High	28	3	6	3	172	19.8	4.84	97	10.35	134.6	73	9.1	13.8	180.6	20.3	72.8	342.1	41.5	112.9
HIST1H2BK	High	25	3	4	3	126	13.9	10.32	67	0	98.7	68.9	17.2	21.6	56.9	33.5	42.5	373.8	13.2	74.8
HNRNPA1	High	14	3	4	3	372	38.7	9.13	105	7.27	135.6	123.6	67.1	94	130.6	113	120.4	488.9	143.7	216.9
MCM3	High	5	3	6	3	808	90.9	5.77	54	1.72	100.8	99.4	133.7	281.2	131.9	156.5	145.7	461.1	232	326.1
KRT85	High	6	3	5	2	507	55.8	6.55	47	6.4	9.5	11.1	16.8	4.4	12.6	6.6	10.5	20.7	67.8	9
FSCN1	High	6	3	6	3	493	54.5	7.24	47	5.37	1039.9	132.3	99.7	71.4	119.9	65.4	232.3	667.9	158.5	407
H2AFZ	High	18	2	4	2	128	13.5	10.58	59	2.09	347.2	128.6	40.6	40.4	363.6	76.4	224.9	1229	70.7	251.3
HIST1H1E	High	10	2	2	2	219	21.9	11.03	60	NaN	149.8	57.2	44.5	54.5	111.4	83.1	86.2	855.9	15.3	204.5
PLS3	High	4	2	4	2	630	70.8	5.6	28	2.83	153	73.9	26.7	39.3	113.2	34.3	60.6	254.3	49.2	162
HNRNPA2B1	High	10	2	4	2	353	37.4	8.95	66	6.74	38.8	32.6	4.4	13.7	19.3	19.5	13.2	107.4	13.4	27.9
HNRNPM	High	3	2	3	2	730	77.5	8.7	34	0	92	41.8	16	18.8	61.3	18.8	37.6	156.2	49.8	82.6
RPS27A	High	16	2	4	2	156	18	9.64	42	2.3	116.6	71.1	115.2	203.5	67.2	53.7	121.3	351.7	216.6	386.6
CALD1	High	4	2	4	2	793	93.2	5.66	40	3.58	37.6	25	5.6	8.9	28.8	6.6	24.6	67.1	15.7	22.4
RBBP4	High	2	2	3	2	425	47.6	4.89	27	2.02	107.3	81.1	70.4	111.1	115.6	80.3	115.9	366.3	138.7	194.7

Gene Symbol	Normalised HeLaΔUMAD1 YFP-TSG101/YFP control repeat 1	Normalised HeLaΔUMAD1 YFP-TSG101/YFP control repeat 2	Normalised HeLa YFP-TSG101/YFP control repeat 1	Normalised HeLa YFP-TSG101/YFP control repeat 2	Normalised HeLa YFP-VPS37C/YFP control repeat 1	Normalised HeLa YFP-VPS37C/YFP control repeat 2
VPS37C	16.79412626	14.28615139	25.36952829	13.50332642	156.4856277	142.1522823
UMAD1	0	0.578303229	3.146558651	3	3.579606866	4.363035781
CEP55	2.345728325	2.549416295	4.315614564	3.817730904	2.779191864	2.912392887
VPS37A	42.62412162	35.38808797	18.66991004	9.110055923	0.404141535	1.48605002
TSG101	20.97823167	23.28290699	15.57974527	11.63141537	27.47899204	25.68528545
VPS37B	33.12642093	36.92585721	26.32217139	16.80769157	0	1.190730293
VPS28	9.89567091	13.05944131	26.54399472	17.70149231	12.81665716	14.16358706
UBAP1	126.0774306	121.1005674	44.47540609	25.3847065	0.522414828	1.329287254
FAM125A;MVB12A	55.16615724	57.62582704	18.60124359	7.418165684	23.14501004	26.88778402
PLEC	0.504164417	0.469497021	2.472263117	3.000979662	0.781862679	1.196610861
DSP	0.527561763	0.783086862	2.545013264	4.402834892	1.338791967	2.291641193
KRT8	0.342637438	0.472172969	3.259178583	3.885590076	1.308329767	2.016248855
KRT18	0.390934741	0.41524387	3.885295416	4.100036144	1.207831541	1.721607957
TUBB	0.730576894	0.98195823	2.404090333	3.851829767	2.584841518	0.898767325
TUBB4B	0.97587631	1.218766472	2.218177636	3.862101078	3.036852703	1.299743286
TUBA1C	0.58982909	0.795343397	2.881468483	5.214633942	3.640286798	1.469963822
TUBA4A	0.621157635	0.799498493	3.113116524	5.733659267	3.569707411	1.293540272
MYO1C	0.568541792	0.622423855	2.764035593	3.645590067	1.565010838	2.596444877
ACTC1	0.385106898	0.292372674	4.203261362	5.538752556	1.614382087	4.40312403
ACTN4	0.782027541	0.733283724	2.503870436	3.353357315	1.109330228	2.334981021
MYO1E	0.473613973	0.431445633	2.850465218	4.205368042	1.617208248	2.061656541
TUBB6	0.83622125	1.009043265	2.18651354	4.484947205	2.15819014	0.733807017
MYL6	0.118381516	0.322271402	2.476353807	3.934314489	0.87952641	1.886523177
PKP2	0.835940923	0.687505482	3.073049772	3.7075243	1.27266832	1.778116163
HSPB1	0.477447573	1.248160579	2.281718611	8.718845367	0.417765091	3.171505993
LMNA	1.4900558	1.239667294	3.035130512	3.00314188	1.941241243	2.167663542
SNRPA1	5.853644894	8.267613315	3.570303791	2.569924593	3.629462506	5.1555226
JUP	0.526982293	0.525086883	2.208927838	3.837726593	0.626488372	2.464788695
CAD	0.949324563	0.916151844	2.812395777	3.705081224	2.649010934	1.50962701
ITPR3	0.728985824	0.691621466	2.723959184	3.662045479	1.253503438	1.770312311
NPM1	1.873920107	1.530966183	2.35560594	3.182496548	1.368285512	1.762457914
HNRNPF	1.184402868	1.602622752	4.323582494	4.643399239	3.697001948	4.068767313
RPS18	1.185925581	1.053841598	2.744395485	3.022209167	2.64601165	3.169612555
HIST1H4A	0.350524315	0.35815094	3.341547156	9.149410248	1.444307603	2.536855824
EEF1A1	1.382010901	2.136201607	2.987979936	3.911898375	5.144959909	6.31676637
LGALS3BP	2.798959465	2.633998443	3.250678859	2.33287859	5.890300577	5.446607846
ITPR1	0.668455712	0.73689	2.25231456	4.090090275	1.059271412	2.025127795
MYL12A;MYL12B	0.270637322	0.292751558	2.024465672	3.405674458	0.875256611	1.512874577
HIST1H2BK	0.633618837	0.567580147	2.626512551	8.269911766	0.618689503	2.227522491
HNRNPA1	1.598310646	1.597130224	2.761265565	4.0139575	2.499463208	2.397017423
MCM3	4.12326276	6.185840208	2.822430614	3.197642088	3.408473945	3.043998685
KRT85	5.035188443	0.940660517	3.055252132	2.15625	14.96220869	1.261915288
FSCN1	0.525130308	0.268252613	7.003784831	7.208850384	3.624274624	5.913000718
H2AFZ	0.526835781	0.373942122	2.855589362	5.586363792	0.680822608	1.537548157
HIST1H1E	1.327282388	1.159507597	2.475977188	8.801028252	0.333302874	2.830496569
PLS3	0.726524745	0.762790902	2.295300688	3.448135614	1.413319468	2.956731743
HNRNPA2B1	0.380476751	0.845025523	1.90064575	5.536082268	1.463323354	1.935804066
HNRNPM	0.738307944	0.618798417	2.622492789	3.900124788	2.634292826	2.776108693
RPS27A	3.789325053	4.774716739	5.605230701	5.818031311	7.591007027	8.608440298
CALD1	0.552315668	0.626128044	3.882315435	3.79096055	1.879159406	1.703466738
RBBP4	2.307094604	2.597051979	3.305277891	3.739663124	2.999917268	2.675595389

Complete list of mass spectrometry data for potential TSG101 interaction partners identified in sections 3.2.1. and 3.2.7.

ESCRT proteins are highlighted in yellow. All proteins identified with >1 peptide are shown. Signal values for each identified protein, and the isobaric tandem mass tag (TMT) used for each sample are indicated. # Peptides = No. of different tryptic peptides detected. # PSM = Peptide Spectrum Matches, i.e. the total number of tryptic peptides identified for a protein (including those identified more than once). # Unique peptides = No. of peptides specific to the protein shown and no other protein.

Experiments using siRNA against UMAD1

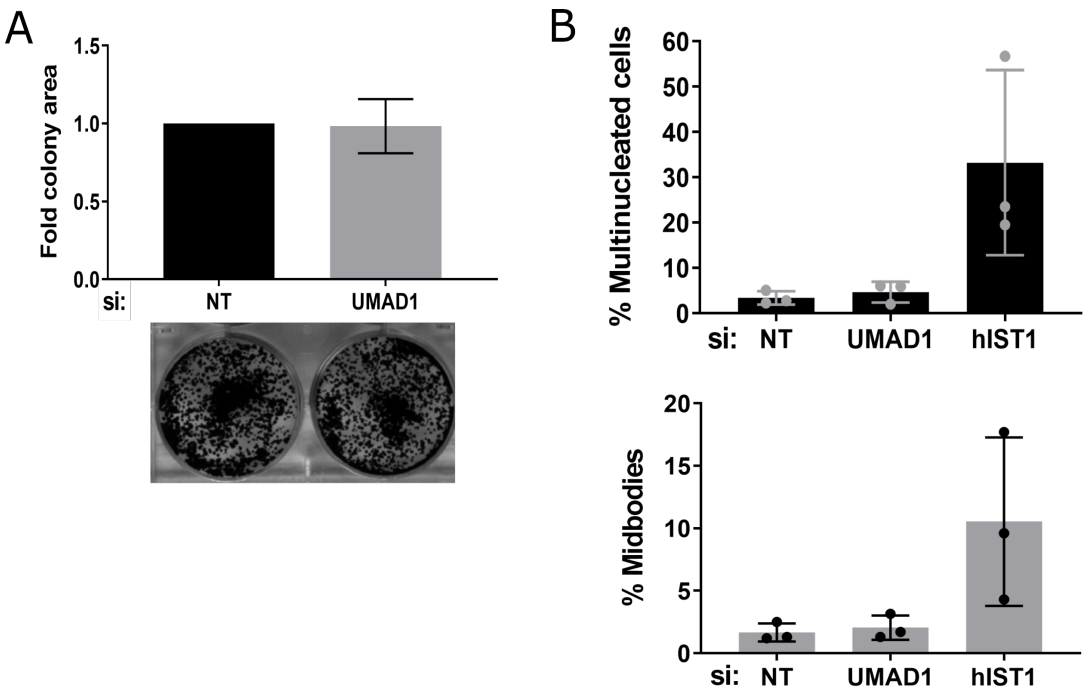

Experiments using siRNA against UMAD1

A. Clonogenic assay to compare cell growth upon transfection of siRNA against UMAD1. HeLa cells were transfected with a single dose of each siRNA shown. Cells were diluted 48 hrs later and colonies were left to grow for 10 days in wells of a 6-well plate. The mean area occupied by colonies on the base of each well is shown for 3 independent repeats, normalised to that of siNT, set at 1-fold. Error bars represent the standard deviation from the mean. siUMAD1: 0.983±0.174-fold. **B.** Quantification of cytokinetic defects attained upon transfection of siUMAD1. HeLa cells were transfected with two separate doses of each siRNA indicated. Following fixation and staining, the number of cells with more than one nucleus and the number of midbody connected cells were scored. The mean percentages for three independent experimental repeats are shown, with error bars representing the standard deviation from the mean. n > 900 cells per condition. sihIST1 was used as a positive control. siNT: 3.400±1.493% multinucleated cells, 1.667±0.723% midbodies, siUMAD1: 4.667±2.312% multinucleated cells, 2.050±0.973% midbodies, sihIST1: 33.233±20.421% multinucleated cells, 10.533±6.749% midbodies.

Appendix 2 – Publication during PhD

Biochemical Society Transactions (2017) **45** 613–634
DOI: 10.1042/BST20160479

Review Article

Growing functions of the ESCRT machinery in cell biology and viral replication

Edward J. Scourfield and Juan Martin-Serrano

Faculty of Life Sciences & Medicine, Department of Infectious Diseases, King's College London, London, U.K.

Correspondence: Juan Martin-Serrano (juan.martin_serrano@kcl.ac.uk)

The vast expansion in recent years of the cellular processes promoted by the endosomal sorting complex required for transport (ESCRT) machinery has reinforced its identity as a modular system that uses multiple adaptors to recruit the core membrane remodelling activity at different intracellular sites and facilitate membrane scission. Functional connections to processes such as the aurora B-dependent abscission checkpoint also highlight the importance of the spatiotemporal regulation of the ESCRT machinery. Here, we summarise the role of ESCRTs in viral budding, and what we have learned about the ESCRT pathway from studying this process. These advances are discussed in the context of areas of cell biology that have been transformed by research in the ESCRT field, including cytokinetic abscission, nuclear envelope resealing and plasma membrane repair.

Introduction

Seminal work in yeast identified the endosomal sorting complex required for transport (ESCRT) through a series of studies of ∼40 vacuolar protein sorting (*VPS*) mutants that showed defective sorting of proteins to the vacuole [1]. In a subset of these mutants, membrane proteins that were normally trafficked to the vacuole for degradation did not reach this compartment and accumulated in a perivacuolar structure termed the class E compartment [1–4]. These class E *VPS* genes were subsequently found to encode components of four ESCRT complexes, ESCRT-0, -I, -II and -III, that are necessary to recognise the ubiquitinated cargo and sort it into intralumenal vesicles (ILVs) at multivesicular bodies (MVBs) through inward invagination and budding of the limiting membrane away from the cytoplasm [5–10].

The ESCRT proteins are conserved from yeast to humans [8,11,12], although a gene expansion can be seen in higher eukaryotes. For example, ESCRT-III in humans possesses eight charged multivesicular body protein (CHMP) families, namely CHMP1–7 and human increased sodium tolerance 1 (hIST1). Additional genes for CHMP1 (CHMP1A and B), CHMP2 (CHMP2A and 2B) and CHMP4 (CHMP4A, 4B and 4C) exist, totalling 12 different ESCRT-III subunits identified so far. A key component required for ESCRT function throughout evolution is VPS4, an ATPase that maintains the activity of ESCRT-III by promoting its disassembly for recycling purposes [13–15].

In addition to their role in MVB formation, ESCRTs were subsequently found to be involved in topologically equivalent membrane remodelling events, notably facilitation of enveloped virus budding [16–19] and cytokinetic abscission [20,21]. Over the last decade, the number of discovered ESCRT-mediated processes has continued to expand to include plasma membrane repair [22,23], axonal pruning [24–26], nuclear envelope (NE) resealing [27,28] and defective nuclear pore complex (NPC) removal [29]. In each of these cases, the ESCRT machinery must assemble on the cytosolic side of the limiting membrane, within membranous stalks, to stabilise negative membrane curvature and mediate budding and scission away from the cytosol.

This review will first summarise what is known about the role of ESCRTs in viral budding and how studies in this area have furthered our understanding of the ESCRT pathway. Focus will be paid to areas of cell biology that have been transformed by research in the ESCRT field, such as cytokinesis

Juan Martin-Serrano was awarded the Biochemical Society's GlaxoSmithKline Award in 2014; this review is based on the Award Lecture.

Received: 12 December 2016
Revised: 17 February 2017
Accepted: 21 February 2017

Version of Record published: 15 June 2017

Biochemical Society Transactions (2017) **45** 613–634
DOI: 10.1042/BST20160479

and NE resealing, together with spaciotemporal regulation of the ESCRTs and their coordination with the abscission checkpoint. Finally, the role of ESCRTs in plasma membrane repair and modes of ESCRT-III polymerisation that may be relevant for membrane remodelling will be discussed.

ESCRTs in viral budding

The pioneering work by Göttlinger et al. [30] showed that the p6 region of the main human immunodeficiency virus-1 (HIV-1) structural protein, Gag, is essential for viral release. The deletion of p6 resulted in tethering of nascent virions to the plasma membrane by thin membranous stalks, thus suggesting that membrane remodelling events required at the last step of viral assembly were impaired in these mutants. Subsequent work established that this phenotype could be largely attributed to a conserved N-terminal ^{7}PTAP^{10} motif in p6 [31]. Other conserved short amino acid motifs that were necessary for viral budding were soon identified, notably a YPx$_n$L motif in equine infectious anaemia virus (EIAV) p9-Gag [32] and a PPxY motif in Rous sarcoma virus (RSV) p2b-Gag [33,34]. Given their activity in the final events of viral assembly, these motifs were termed late budding domains (L-domains). The short length and proline-rich nature of these motifs suggested that their role in viral budding could involve the recruitment of cellular proteins. This notion was further supported by observations that L-domains were interchangeable and position independent within retroviral Gag proteins [32,35,36].

The cellular pathway recruited by L-domains was revealed by the identification of the essential interaction between PT/SAP motifs in HIV-1 and Ebola virus with the ESCRT-I subunit tumour susceptibility gene 101 (Tsg101), via its ubiquitin enzyme variant (UEV) domain [16–19,37,38]. YPx$_n$L motifs on the other hand were shown to recruit the ESCRT-associated protein ALG-2-interacting protein X (ALIX) via its V domain [11,12,39,40], whereas PPxY motifs promote viral budding by binding to members of the NEDD4 (neural precursor cell expressed developmentally down-regulated protein 4)-like HECT domain E3 ubiquitin ligases, notably WWP1 (WW domain-containing E3 ubiquitin protein ligase 1), WWP2 (WW domain-containing E3 ubiquitin protein ligase 2) and Itch via their WW domains [41,42]. Although functional redundancy between these ubiquitinases in viral budding was originally suggested, a recent study has shown a preference for NEDD4-1 and Itch ubiquitin ligases for Ebola virus budding [43], which encodes overlapping PTAP and PPEY motifs [18,44]. The striking discovery of a primordial ESCRT system in Archae of the genus *Sulfolobus* has revealed that the CHMP4 and VPS4 homologues are necessary for *Sulphobus* turreted icosahedral virus replication and budding [45–47]. These findings demonstrate an ancient, conserved role for ESCRTs in viral budding.

The widely conserved requirement in the release of enveloped viruses suggested a membrane remodelling function of the ESCRT machinery, in particular of ESCRT-III. Importantly, ALIX recruitment to YPx$_n$L L-domains provides a direct link to ESCRT-III by directly binding to the CHMP4 proteins [11,12,40,48,49]. However, definitive pathways for ESCRT-III recruitment for the other two L-domains remain less clear. ESCRT-II has been suggested as a necessary activity for HIV-1 genomic RNA trafficking [50], and subsequent work has proposed a role for ESCRT-II as a potential bridging complex between ESCRT-I and ESCRT-III in PTAP-dependent budding [51,52]. However, these hypotheses remain controversial as other studies do not observe deleterious effects in viral assembly upon depletion of ESCRT-II [53,54]. Crucially, siRNA approaches and VPS4 dominant-negative expression have established the essential role of ESCRT-III in each case [17,37,55–57]. These findings together with the specificity found at the adaptor/L-domain level have given rise to the concept that the ESCRT pathway operates as a modular machinery that uses different adaptor proteins to recruit a core membrane remodelling activity at specific sites (Figure 1).

Detailed functional analysis of HIV-1, murine leukaemia virus (MLV) and EIAV assembly has shown that viral budding requires only a small subset of the 12 mammalian ESCRT-III subunits. In particular, a prominent role for CHMP2 and CHMP4 family members in L-domain activity has been demonstrated for HIV-1 and MLV [52,56]. Accordingly, an axis that involves Gag–ALIX–CHMP4B–CHMP2A–VPS4 interactions is required for EIAV release [57]. The involvement of other ESCRT-III subunits in retroviral budding is less clear, as depletion of CHMP6, CHMP3 and the CHMP1A/B proteins only results in modest phenotypes at best [52,54,56,57]. These studies strongly suggest that the core membrane remodelling activity only requires the CHMP4–CHMP2 complex, while other ESCRT-III subunits may play accessory roles that are not required for retroviral release.

Many viruses such as HIV-1, Ebola virus and MLV encode multiple L-domains. In each case, one appears to show dominance whilst others seem to play subsidiary roles. For example, HIV-1 Gag has an ALIX-binding LYPx$_n$L motif in p6, in addition to its PTAP motif [11,39,58]. The PTAP–Tsg101 interaction appears to be its

dominant mode of ESCRT recruitment, but ALIX overexpression can rescue budding of PTAP mutant HIV-1 [40,49]. A similar phenomenon has been described for MLV, whose Gag encodes PPPY, PSAP and LYPx$_n$L motifs, although the PPPY L-domain activity shows a clear dominance [59]. Ebola VP40 contains a PTAPPEY sequence that binds Tsg101 and HECT ubiquitin ligases, and both activities are required for efficient viral release [18,41,60]. Similar to HIV-1 and MLV, a third L-domain in VP40 interacts with ALIX and plays an auxiliary function in viral release [61]. Possession of multiple L-domains may have evolved to confer an evolutionary advantage to ensure viral propagation in the event of loss-of-function mutations of the dominant L-domain, albeit at reduced levels. Another advantage would be to broaden viral tropism such that alternative L-domains may exhibit differential dominance in multiple cell types, as has been shown for the LYPx$_n$L motif of HIV-1 in T cells [62].

One intriguing question that still needs to be fully answered is the role of ubiquitin in L-domain activity. Evidence supporting a role here includes the enrichment of ubiquitin observed in many virus particles [63,64], the discovery of ubiquitin ligases as host factors for PPXY type L-domains [41,42,65] and the substitution of L-domain activity by attachment of ubiquitin to Gag [66,67]. Defining the mechanism and most relevant substrates for ubiquitination has proved challenging, perhaps suggesting considerable redundancy in substrate requirements. The importance of ubiquitination in viral budding is supported by the strong correlation between viral budding and Gag ubiquitination in those viruses that exhibit PPXY motifs [65,68]. Accordingly, mutation of ubiquitin acceptor sites in RSV Gag abolishes budding, particularly in the NC-p2 region that lies close to the L-domains [69]. Importantly, L-domain-deficient EIAV and human T-lymphotropic virus can be rescued by fusion of ubiquitin to Gag [66]. In the case of HIV-1, ubiquitination of residues in the vicinity of the PTAP motif increases Tsg101 binding [70]. However, increased ubiquitination of Gag by introduction of a PPXY motif does not enhance budding in the HIV-1 context [68]. In contrast, NEDD4-2 overexpression can rescue budding of an HIV-1 that lacks L-domains by conjugating K63-linked polyubiquitin chains, despite the lack of a PPXY motif [71]. Subsequent work has shown that the truncated C2 domain of NEDD4-2 provides a natural Gag-targeting module, thus explaining an L-domain-independent recruitment of ubiquitin ligases to the sites of viral budding [72,73].

One possible scenario contemplates that Gag ubiquitination could serve as a docking site for ubiquitin-binding activities in ESCRT-I [Tsg101, UBAP1 (ubiquitin-associated protein 1)], ESCRT-II (Eap45) and ALIX [70,74–77]. Accordingly, Tsg101 depletion abolished the ability of NEDD4-2 to rescue an L-domain-deficient HIV-1 [73], and residues in the UEV domain of Tsg101 that bind ubiquitin are necessary for rescue of an L-domain-deficient EIAV [66]. Moreover, mutation of the ubiquitin-binding sites in the V domain of ALIX impairs retroviral budding [77]. A second scenario involving ubiquitination of *trans*-acting factors is also supported by data showing that NEDD4-2 overexpression induces the ubiquitination of ESCRT-I subunits [73]. Conversely, the fusion of a deubiquitinating activity to either Tsg101 or ALIX inhibits HIV-1 budding [78]. A more compelling example of the importance of *trans*-acting factor ubiquitination in viral budding has been provided by studies that used an engineered prototypic foamy virus Gag devoid of its single ubiquitination site, which was fully functional in viral budding [79]. Ubiquitination-resistant foamy virus Gag was also capable of budding when the PSAP motif was replaced with a PPPY motif derived from MLV, and viral budding in this context was also enhanced by a catalytically active YFP-WWP1 in the absence of Gag ubiquitination [67,79]. Thus, a *trans*-acting factor must be the target of ubiquitination since Gag cannot be ubiquitinated in this context. Some plausible candidates for ubiquitinated *trans*-acting factors are the arrestin-related trafficking (ART) proteins. This family of proteins interacts both with HECT domain ubiquitin ligases (WWP1, WWP2, Itch and NEDD4) and ESCRT-associated proteins (Tsg101, ALIX and ubiquitin), therefore providing potential bridging interactions with the ESCRT machinery [41,80]. ARTs can be recruited to sites of viral budding and they reduce MLV budding when overexpressed, but more definitive evidence is needed to support their role in PPXY-dependent budding [80]. One related hypothesis is that the identity of the ubiquitinated protein may not be critical for viral budding to proceed, as long as it is located in close proximity to Gag to allow the recruitment of ubiquitin-binding components in the ESCRT pathway [67].

In addition to the established role in viral particle release at the plasma membrane, ESCRTs have also been implicated in intracellular viral replication events that include both RNA and DNA viruses. The positive-strand RNA plant viruses including Tomato bushy stunt virus and Brome mosaic virus recruit ESCRT-III to facilitate inward invagination of peroxisome or endoplasmic reticulum (ER) membranes, respectively, to form replication compartments [81,82]. These compartments are thought both to provide a protective environment, away from viral RNA sensing host defence mechanisms, and to concentrate components necessary for viral replication.

Biochemical Society Transactions (2017) **45** 613–634
DOI: 10.1042/BST20160479

Unlike other ESCRT-mediated processes, no membrane scission is involved in the formation of the replication organelles, as this compartment remains attached to the membrane. How this incomplete budding event is controlled remains unknown but potential clues have been provided by the functional characterisation of ESCRT requirement in flavivirus replication. Propagation of dengue virus and Japanese encephalitis virus was inhibited by depletion of Tsg101 or ESCRT-III subunits. However, unlike other enveloped viruses, VPS4 is dispensable for flavivirus replication, perhaps suggesting that unknown viral mechanisms inhibit the recruitment of VPS4 in this context to prevent membrane scission by ESCRT-III [83].

Other uses of the ESCRT machinery in viral replication include herpesviruses. This family of viruses requires two separate envelopment stages for assembly and egress [84]. Primary envelopment allows nucleocapsids to exit the nucleus through budding at the inner nuclear membrane (INM) and fusion of the resulting perinuclear virion with the outer nuclear membrane, subsequently releasing nucleocapsids into the cytoplasm. Secondary envelopment promotes budding of nucleocapsids, together with viral tegument proteins, into the lumen of cytoplasmic membrane compartments that contain the viral envelope proteins [84]. Herpesviruses are likely to use the ESCRT machinery at multiple stages during assembly, as Epstein-Barr virus recruits ALIX through the viral protein BFRF1 for nuclear egress [85,86], whereas herpes simplex virus-1 (HSV-1) requires ESCRT-III for secondary envelopment at the *trans*-Golgi network/endosomal compartments [87]. Although HSV-1 encodes potential L-domain motifs, the viral mechanisms that recruit ESCRT-III to promote secondary envelopment remain unclear [88].

ESCRTs in cytokinesis

Cytokinesis begins with the establishment of the spindle midzone, which derives from the metaphase spindle after mitosis. The central area of the spindle midzone, or central spindle, is formed by microtubules overlapping at their plus ends. The central spindle subsequently acts as a signalling hub from which signals to the cell cortex emanate to specify the central cleavage plane, where the cleavage furrow is constricted by an actomyosin ring [89,90]. Two important components of the central spindle orchestrate the cytokinetic process. The centralspindlin complex is composed of two mitotic kinesin-like protein 1 (MKLP1) kinesin-6 motor subunits and two cytokeratin-4 (CYK-4) Rho-family GTPase-activating subunits [91]. The chromosomal passenger complex (CPC) is composed of Aurora B kinase, INCENP (inner centromere protein), Borealin and Survivin [92]. Both centralspindlin and the CPC play roles in stabilising the central spindle and they are activated by dephosphorylation of cyclin-dependent kinase 1 (CDK1) substrate residues [93,94]. Aurora B-mediated phosphorylations of centralspindlin and other components of the spindle midzone are also important in central spindle maintenance [95]. The guanine-nucleotide exchange factor ECT2 (epithelial cell-transforming sequence 2 oncogene) binds to the CYK-4 component of centralspindlin and thereby induces localised activation of the GTPase RhoA at the cell cortex in response to decreasing CDK1 activity [96]. This localised RhoA activity determines the cleavage plane at which actomyosin ring formation occurs through nucleation of actin and myosin II filaments [97,98]. These filaments contract to eventually form a thin intercellular bridge connecting daughter cells known as the midbody, with a central electron dense region corresponding to the compacted microtubules of the central spindle known as the Flemming body [99,100]. Once the midbody is formed, the actomyosin ring is disassembled through inactivation of RhoA by PKCε [101], and a decrease in membrane associated PI(4,5)P2 levels that result from the action of Rab35 and p50RhoGAP, which are delivered to the midbody by RAB11 (Ras-related protein Rab-11A)/FIP3 (Rab11 family-interacting protein 3)-positive endosomes [102,103].

The final event in cytokinesis is termed abscission and requires the resolution of the midbody to facilitate the physical separation of the daughter cells [104,105]. The molecular mechanism underlying abscission has remained elusive until recently as the identity of the membrane remodelling activities involved in this process was not clear. An important clue to better understand abscission was the identification of centrosomal protein 55 (CEP55) as an essential adaptor protein required for midbody resolution [106,107]. In agreement with this role, CEP55 stays inhibited during the early stages of cytokinesis via its phosphorylation by Polo-like kinase 1 (PLK-1), which inhibits the interaction with MKLP-1 to prevent the premature recruitment of CEP55 to the midbody [108]. Towards the end of anaphase, PLK-1 is targeted for proteasomal degradation as a consequence of its ubiquitination by the anaphase-promoting complex. As the level of PLK1 decreases, cytokinesis progresses and CEP55 is dephosphorylated to allow the interaction with MKLP-1 at the Flemming body [108].

Functional analogies with viral budding and the interaction with CEP55 were instrumental to uncover the essential role of the ESCRT machinery in cytokinetic abscission [20,21]. This discovery was quickly followed by the surprising identification of CHMP4 and VPS4 homologues that are involved in cell division in Archaea of

the genus *Sulfolobus*, thus suggesting that abscission is the ancestral role for ESCRT proteins as these organisms lack endosomal systems [45,46]. In mammalian cells, CEP55 works as the adaptor protein, analogous to viral Gag proteins, that recruits the ESCRT machinery to the midbody by directly binding to Tsg101 and ALIX [20,21,109,110]. Like MVB formation and viral budding, ESCRT-III activity is required for abscission, as indicated by the requirement for the ALIX–CHMP4B interaction in this process [21,109]. More recent work has suggested that ALIX and the Tsg101/ESCRT-II axis constitute parallel arms that promote CHMP4B recruitment [111], although this model requires further validation. Abscission requires midbody maturation and thinning from an approximate diameter of 1.5–2 μm to ∼100 nm (Figure 2). This constriction can occur at either side of the Flemming body at an approximate distance of 1 μm and it always forms ∼10–20 min before abscission [112,113]. These secondary ingression zones coincide with the site of abscission and one model suggests that they are formed by fusion of Golgi and recycling endosomes with the membrane. This is thought to be facilitated by members of the exocyst complex and SNAREs [SNAP (soluble NSF attachment protein) receptor], which localise to the midbody via interaction with centriolin rings [114–116]. Alternatively, it has been proposed that ESCRT-III polymerisation itself drives secondary ingression [117], perhaps facilitated by hIST1 — an ESCRT-III subunit specific to cytokinesis that can direct polymerisation of filaments large enough to promote abscission [118–120].

Time-lapse experiments have shown that whilst MKLP-1 and CEP55 are present at the Flemming body from the time of its appearance, ESCRT proteins localise to the Flemming body at times closer to midbody resolution [112,113]. Importantly, monitoring of fluorescently tagged CHMP4B and CHMP4A shows that closer to the time of abscission, a separate pool of ESCRT-III appears specifically at the secondary ingression site at which abscission occurs [113,121]. Here, the membrane appears rippled containing 17 nm diameter filaments, which are likely to be those of ESCRT-III since they are not observed in CHMP2A-depleted cells [112]. Interestingly, the appearance of this separate ring of ESCRT-III is preceded by an increase in the fluorescence of CHMP4B at the Flemming body, at the same side as the distal pool. VPS4 shows a similar localisation pattern, but appears at the secondary ingression just after CHMP4B, consistent with its role in ESCRT disassembly and recycling following abscission [113]. This ESCRT-III localisation pattern is consistent with a model whereby nucleation of ESCRT-III polymerisation at the Flemming body first occurs followed by VPS4-mediated breakage and constriction of outer ESCRT-III spirals, thus propelling them away from the Flemming body to form the secondary ingression at an equilibrium position. VPS4-mediated disassembly would then mediate the final scission event [121]. Other models have been proposed, such as continuous polymerisation and constriction of ESCRT-III spirals away from the Flemming body to deform the membrane and form the secondary ingression [112]. Schiel et al. propose a model whereby ESCRT-III polymerisation instead stabilises a pre-formed secondary ingression formed by vesicle fusion, such as by FIP3-positive endosomes [103,122]. However, the importance of vesicle fusion remains controversial as the addition of vesicle fusion inhibitors has no effect on abscission [112].

Cytokinesis is characterised by a tight spatiotemporal regulation, perhaps explaining the requirement for most of the ESCRT-III subunits, in contrast with viral budding which only requires the core membrane remodelling subunits of ESCRT-III [123]. Completion of cytokinesis requires a complex coordination with activities upstream of scission, such as furrow ingression and those involved in membrane binding, midbody stabilisation and microtubule disassembly. In this context, severing of microtubules derived from the spindle midzone has been shown to be a rate-limiting essential step in cytokinesis and its occurrence at secondary ingression sites correlates closely with completion of abscission [112,124]. The microtubule severing AAA-ATPase Spastin plays an essential role in this process, and when depleted, abscission is delayed [112,124]. All ESCRT-III subunits encode microtubule-interacting and trafficking (MIT) domain-interacting motifs (MIMs) that interact with MIT domain containing effector proteins, notably VPS4A/B and its effector LYST-interacting protein 5 (LIP5) [125,126]. In addition to VPS4, Spastin is another MIT domain-containing protein that is specifically recruited to sites of abscission via the MIMs of CHMP1B and hIST1 [124,127]. These interactions would be consistent with a role for Spastin in abscission, thus suggesting a mechanism that co-ordinates microtubule severing with ESCRT-III-mediated scission. An alternative model suggests that buckling of microtubules by spastin contributes to abscission, rather than microtubule severing. This result is based on the disorganisation of the central spindle microtubules in Spastin-depleted cells [128]. However, subsequent work has shown that Spastin plays another key role during mitotic exit by coordinating NE sealing and spindle disassembly at NE–microtubule intersection sites, perhaps explaining the disorganised spindle in Spastin-depleted cells [28].

Biochemical Society Transactions (2017) **45** 613–634
DOI: 10.1042/BST20160479

The ESCRT-III–Spastin interaction highlights an example of the adaptability of the ESCRT machinery that is required to facilitate cytokinetic abscission. A second adaptation of the ESCRT machinery is illustrated by MIT domain containing 1 (MITD1), which binds MIMs encoded by several ESCRT-III subunits, including CHMP1A, 1B, 2A and hIST1 [129,130]. Whilst the N-terminal MIT domain in MITD1 mediates the interactions with ESCRT-III, the C-terminal domain has a phospholipase D-like fold with a positively charged surface patch that interacts with PtdIns (phosphatidylinositol)-containing membranes. The phenotypic characterisation of MITD1-depleted cells suggests multiple roles in cytokinesis as evidenced by premature abscission, increased cortical blebbing and cytokinesis failure. These phenotypes are consistent with a role of MITD1 in maintaining the stability of the midbody and coordinating abscission with earlier cytokinetic events, perhaps by stabilising ESCRT-III filaments and regulating the actin cytoskeleton [129,131].

The different MIT domain-containing proteins involved in abscission could be brought into close proximity by interacting with the multiple MIMs that are present in the ESCRT filaments to couple activation of VPS4, membrane scission and microtubule severing (Figure 2). However, despite this progress in our understanding of abscission, some important questions remain unanswered. For example, the midbody persists from 80 min to several hours before abscission, depending on the cell type. The events that occur during this time remain largely unknown. A partial clue comes from the regulation of abscission by midbody tension [132], which can explain an ∼30 min delay in HeLa cells, but we still do not understand the events that precede abscission in these cells. It will also be important to understand how the recruitment of each of the ESCRT subunits is co-ordinated, and the nature of the signal that triggers the polymerisation of ESCRT-III in the final moments of abscission.

ESCRTs and the abscission checkpoint

One of the most striking adaptations of the ESCRT machinery for coordinating cytokinetic abscission comes from its interaction with the Aurora B-dependent abscission checkpoint, also known as NoCut [104,131]. This evolutionarily conserved control system ensures that abscission is delayed until anaphase chromatin bridges, caused by segregation errors, have been removed from the intercellular bridge connecting daughter cells [133–135]. Such segregation errors are often caused by defects in chromosome architecture, such as impaired decatenation of DNA and dicentric chromosomes [136–138]. Failure to restrain abscission until clearance from the midbody leads to cleavage furrow regression, tetraploidisation and DNA damage. NoCut was originally identified in yeast, in which the Aurora B homologue, Ipl1 kinase, was shown to inhibit septin-mediated abscission upon interaction with chromatin [133]. In addition to chromatin bridges, the abscission checkpoint also delays midbody resolution in response to defective NPC assembly [139] and high levels of midbody tension that result from cell growth at low densities [140].

Aurora B plays a crucial role in the coordination of cytokinesis [92]. One of its critical functions in this process is the phosphorylation of MKLP1 to stabilise the cleavage furrow, while the subsequent inactivation of Aurora B triggers abscission [135]. Crucially, Aurora B activity is sustained in the presence of chromatin bridges to delay midbody resolution, although how this activity is regulated by chromatin is not known [133,135,141]. The signal by chromatin, however, is thought to be specific, since asbestos fibres within the intercellular bridge do not sustain the checkpoint [135]. Intriguingly, the molecular origin of the chromatin bridges has an important effect on checkpoint induction. Whilst chromatin bridges induced by replication stress, condensation or decatenation defects sustain the abscission checkpoint, those due to the formation of dicentric chromosomes are not detected by NoCut, thus resulting in chromosome damage by the abscission machinery [142].

The physical connection between the abscission checkpoint and the abscission machinery was demonstrated by the functional interaction between regulatory subunits in the ESCRT pathway and components of the abscission checkpoint. More specifically, abscission delays induced by nucleopore disruption and chromatin bridges are abrogated by depletion of CHMP4C [141], a human ESCRT-III subunit that is closely related to the polymer forming CHMP4B. At a molecular level, CHMP4C engages the CPC by binding to Borealin and this interaction delays abscission via the Aurora B-dependent phosphorylation of CHMP4C at a unique insertion that is not present in CHMP4B [141,143]. Importantly, the interaction of ESCRT-III with the CPC is conserved from *Drosophila* to humans [143], and human polymorphisms in the CHMP4C gene are associated with increased risk for ovarian cancer [144], thus highlighting the importance of this damage preventing regulatory mechanism.

Abscission/NoCut Checkpoint Regulator (ANCHR) has been recently identified as another key component of the abscission checkpoint [145]. ANCHR encodes two MIM sequences that interact with the MIT domain

of VPS4 in an Aurora B-dependent manner. This interaction allows the formation of a ternary complex with CHMP4C that retains VPS4 at the Flemming body, thus inhibiting its localisation to the secondary ingressions that mark the abscission sites [145]. Unc-51-like kinase 3 (ULK3) was subsequently identified as an essential regulator of the abscission checkpoint and its kinase activity is required for this function [140]. ULK3 acts downstream from Aurora B to regulate abscission in a CHMP4C-dependent manner. Accordingly, ULK3 phosphorylates CHMP4C at sites distinct from those targeted by Aurora B. A subset of other ESCRT-III subunits is also phosphorylated by ULK3, although the preferred substrate is thought to be hIST1, which binds ULK3 via an especially strong MIT–MIM interaction. Critically, ULK3 phosphorylation of hIST1 is required to sustain the checkpoint in response to lagging chromosomes and nucleopore disruption. However, a mutated version of hIST1 that cannot be phosphorylated by ULK3 still supports abscission delays when the checkpoint is sustained by low cell tension, suggesting that some downstream factors involved in maintaining the checkpoint may differ depending on the stimuli [140]. The exact mechanism by which the various phosphorylation events inhibit abscission is still unclear. One possible scenario is that the initial phosphorylation of CHMP4C by Aurora B could be subsequently 'amplified' to other ESCRT-III subunits by ULK3 (Figure 3). These phosphorylations could lock the ESCRT-III subunits such as hIST1 in their 'closed' inactive forms. It is also possible that the various phosphorylations may retain ESCRT-III and VPS4 at the Flemming body, thus preventing its polymerisation and scission activity at the secondary ingression sites. In agreement with this model, phosphomimetic mutations enhance the hIST1 interactions with VPS4 and LIP5 [140], a cofactor that promotes VPS4 oligomerisation and ATP hydrolysis [146–148].

One important question that remains open is the relevant subcellular location where CHMP4C inhibits abscission. One possibility is that CHMP4C might form an inhibitory complex in the cytoplasm, as suggested by the distinctive localisation of Aurora B to cytoplasmic foci in cells arrested by the abscission checkpoint [139]. An independent line of evidence suggests that abscission regulation would require the midbody localisation of CHMP4C [141], which would be facilitated by ALIX and MKLP1 [111,149]. Once recruited to the midbody, CHMP4C is initially found in the midbody arms, whereas the phosphorylation of serine 210 by Aurora B allows its subsequent localisation to the Flemming body [141]. Interestingly, the CHMP4C subset found at the midbody arms is phosphorylated at residues 214, 215 and 210, whereas the phosphorylation of residues 214 and 215 is lost in the transition to the Flemming body [149]. In agreement with this notion, the mitotic phosphorylation of CHMP4C decreases around the time of abscission [140,141], suggesting that a phosphatase activity of unknown identity may be required to reverse the inhibitory activity of CHMP4C, thus allowing abscission in midbodies that are arrested by the abscission checkpoint.

ESCRTs at the nuclear envelope

The nuclear envelope (NE) is a double membrane structure continuous with the ER that acts as a barrier, establishing both nucleo-cytoplasmic compartmentalisation and protection of the genome from cytoplasmic nucleases [150]. Whilst yeast undergoes a closed mitosis, mammalian cells undergo an open mitosis, in which the NE and the nuclear lamina that lines the inner nuclear membrane (INM) are disassembled, allowing chromosomes to access the mitotic spindle at prometaphase [150–153]. Dynein-mediated microtubule tearing breaks down the NE, co-ordinated by numerous kinases including regulators that are shared with cytokinesis, such as CDK1, Aurora B and PLK-1 [152]. The broken down NE is incorporated into the mitotic ER, which remains intact, away from the spindle and segregating chromosomes [154–159]. Opposite events occur during NE reformation, during which Aurora B and PLK-1 relocate to the central spindle and midbody, to control cytokinesis, and CDK1 is inactivated [104]. The NE is reformed from the ER by attachment of ER tubules to decondensing chromosomes [160]. These tubules flatten and enclose chromatin, leaving discontinuities of the double membrane primarily at sites of mitotic spindle attachment [157,160–162]. Annular fusion must therefore take place to seal such holes in close coordination with microtubule severing. Two ground breaking studies have recently established the essential role of the ESCRT machinery in this process.

As observed for other functions of the ESCRT pathway, NE resealing requires the core membrane remodelling activity of ESCRT-III [27,28]. Accordingly, knockdown of ESCRT-III subunits disrupts the integrity of the NE and this phenotype correlates with increased DNA damage. This function is further supported by the localisation of CHMP2A and CHMP4B to the reforming NE into nucleo-cytoplasmic channels that are topologically equivalent to other membrane tethers resolved by the ESCRT pathway [27,28]. In a striking parallel with cytokinesis, hIST1 is required in NE reformation to recruit spastin and promote the disassembly of spindle microtubules [28]. As observed in cytokinesis, microtubule severing is a rate-limiting step of the NE resealing

Biochemical Society Transactions (2017) 45 613–634
DOI: 10.1042/BST20160479

process, as CHMP4B–eGFP persisted at unsealed holes upon inhibition of spastin activity [28]. In contrast with cytokinesis, CHMP1B depletion did not perturb spastin localisation to the nucleus, suggesting differential routes of recruitment in these two processes [28].

The two most likely candidates identified so far as adaptor proteins responsible for ESCRT-III recruitment to the NE are ubiquitin fusion degradation protein 1 (UFD1) and CHMP7. UFD1 is an adaptor protein of the p97/UFD1/NPL4 AAA-ATPase that has previously been implicated in NE resealing [163,164]. Prior to this, a related complex containing p97 and p47 is involved in ER membrane recruitment to chromatin [163]. P97/UFD1/NPL4 is also known to facilitate removal of Aurora B from chromatin to allow chromosome decondensation [163,164]. UFD1 was shown to be necessary for ESCRT-III recruitment to the reforming NE, and this function correlates with its interaction with CHMP2A [27]. CHMP7 is essential for ESCRT-III recruitment to the NE, and this function correlates with a potential interaction with CHMP4B [28]. Closer examination of its structure reveals a C-terminus similar to CHMP6 that is necessary for binding to CHMP4B, whereas the extended N-terminus contains tandem winged-helix domains that resemble the ESCRT-II subunit ELL-associated protein of ∼20 kDa (EAP20) [165,166]. The first of these tandem domains contains an extended loop between the β2–β3 hairpin that is important for the specific localisation of CHMP7 at the ER membrane [166]. The continuity of the ER with the NE suggests a model whereby CHMP7 provides a platform that orchestrates the recruitment of ESCRT-III to the reforming NE.

The emerging role of the ESCRT pathway in establishing NE integrity has been extended beyond the mitotic nuclear regeneration. NE breakdown is thought to be a rare event outside mitosis [167], but recent work has shown that NE rupture occurs during migration of cells of the immune system, and similar nuclear ruptures have been observed in cancer cells during metastasis [168,169]. Studies monitoring cell migration through confined spaces have shown that NE blebbing occurs at the leading end of the cell in response to increased nuclear hydrostatic pressure, and the NE is forced through ruptures in the nuclear lamina [168]. These blebs eventually burst resulting in nucleo-cytoplasmic mixing and DNA damage. The rapid localisation of ESCRT-III to the site of NE rupture is associated with a repair function that results in nucleo-cytoplasmic re-compartmentalisation and reduced DNA damage. Following the repair by ESCRT-III, the accumulation of lamin A forms 'lamin scars' that increase the local resistance of the NE to protect against subsequent rupture at the same sites [169].

The quality control of nuclear pore complexes (NPCs) has been identified as another function of the ESCRT pathway to maintain nucleo-cytoplasmic compartmentalisation [170]. NPCs are central to maintaining nuclear identity by controlling entry and exit of proteins and RNA, and consist of ∼600–700 individual subunits from a repertoire of ∼30 different nucleoporins (Nups) [171–173]. Epistasis screens in yeast have uncovered a role for ESCRT-III in the clearance of defectively assembled early NPC intermediates [29,174]. Since yeast undergoes a closed mitosis, involving asymmetric division in which the NE is not broken down and reassembled, such a quality control mechanism is thought to be essential to re-establish a fully functional NE [29,170,175]. As yet, there is no evidence for an equivalent role for ESCRT-III in mammals, perhaps due to less demand as a consequence of the open mitosis in these cells.

The initial clue to uncovering the role of ESCRTs in NPC surveillance was provided by the conserved genetic interaction in fission and budding yeast between Vps4 and the transmembrane nucleoporin POM152 [174]. Additional genetic interactions were subsequently observed between POM152, Nup170 and the ESCRT-III subunits sucrose nonfermenting protein 7 (Snf7) (CHMP4), Vps24 (CHMP3) and Vps2 (CHMP2) [29]. Snf7 and, more recently, Chm7 (CHMP7) [176], were also found to interact with the INM LEM (LAP2, emerin, MAN1) domain proteins Heh1 and Heh2, both of which interact with Nup170, perhaps during NPC assembly [177]. Chm7 was shown to be recruited to sites of incomplete NPC assembly [176], and its recruitment was shown to require Heh1/2 [176]. This strongly suggests that Heh1/2 acts as putative adaptors for ESCRT-III recruitment to the NPC [29]. In agreement with this model, deletion of Heh2, ESCRT-III or Vps4 leads to clustering of malformed NPCs in a structure termed the storage of improperly assembled NPCs (SINCs) [29]. Conversely, Chm7 deletion prevents SINC formation suggesting a role in defective NPC clearance [176]. This storage structure forms at a single location at the NE and is therefore not inherited by the daughter cells, thus representing an additional level of quality control of the NE in yeast [29,170]. Importantly, Chm7 is also required for sealing of the NE over the top of malformed NPCs [176]. This demonstrates a conserved mode of action in both NE resealing/repair and defective NPC removal through sealing of the NE to maintain nucleo-cytoplasmic compartmentalisation.

How ESCRT-III and Vps4 could also potentially direct removal of defective NPCs is not clear. The catalytic activity of Vps4 has been suggested to disassemble the defective intermediates, either directly or through the

removal of NPC-bound ESCRT-III [29,170,178]. An alternative model would involve the ESCRT-III-dependent budding of vesicles that contain the defective NPCs into the intermembrane space, a process that may resemble the nuclear egress of Epstein–Barr virus [85,86].

ESCRTs at the plasma membrane

A direct role of the ESCRT pathway in remodelling the plasma membrane in diverse functional contexts has emerged in the last few years. One of these processes bears striking resemblance to viral budding, namely the formation of arrestin domain containing 1 (ARRDC1)-mediated microvesicles (ARMMs) [179,180]. A central PSAP motif in ARRDC1 mediates interaction with Tsg101, as in viral budding, whereas localisation to the plasma membrane is directed via an N-terminal arrestin domain. Furthermore, two C-terminal PPXY motifs mediate interaction with WWP2 ubiquitin ligase, which ubiquitinates ARRDC1 and confers optimal ARMM release [179]. ARMM formation is likely to require the core ESCRT machinery since vesicle release is inhibited by catalytically inactive VPS4. However, the subset of ESCRT-III units required for this process needs to be determined [179]. Whilst the function of ARMM release remains uncharacterised, ARRDC1 can be transferred from donor to recipient cells, suggesting a role for ARMM contents or membrane-bound proteins in intercellular communication [179]. This transfer of material between cells also raises the question of how the released vesicles fuse with the target cells. It is tempting to speculate that cellular fusogens may resemble the fusion activity of viral envelope proteins, to deliver the microvesicle content into the target cells. ESCRTs have also been implicated in shedding of ubiquitinated T-cell receptor (TCR) containing microvesicles from T cells at immunological synapses, although the involvement of ARRDC1 in this budding event is not clear. This mechanism facilitates the interaction of TCRs with major histocompatibility complex-bound antigens on antigen-presenting cells and promotes signal transduction [181].

Another ESCRT-mediated event at the plasma membrane is the microvesicle shedding induced by depletion of the lipid flippase TAT-5 [182]. Loss of this P4-ATPase disrupts phosphatidylethanolamine symmetry leading to accumulation of this lipid on the exterior side of the plasma membrane (PM). This lipid asymmetry in turn triggers loss of cell adhesion and increased vesicle shedding, leading to a thickened appearance of the membrane, which contains components of the ESCRT machinery [182]. Although the relevant adaptor protein is unknown, ESCRT-0 and ESCRT-I are thought to be necessary for membrane thickening, but the role of ESCRT-III in ectosome release needs to be established [182].

In addition to formation and shedding of microvesicles, ESCRTs have been implicated in PM repair by an analogous process that involves pinching out of the damaged regions of membrane followed by scission and shedding [22]. The plasma membrane can be damaged by exposure to bacterial pore forming toxins [183,184] and mechanical stress, such as that seen in muscle tissue [185,186]. Experimental approaches to induce membrane wounding include laser ablation, detergents and micropipettes. All membrane repair mechanisms described so far share a dependence of calcium influx into the cytoplasm following wounding [186,187]. Such mechanisms include clotting, patching and endocytosis or exocytosis of damaged regions [188–191]. Likewise, the rapid recruitment of ESCRT-III to sites of wounding is calcium-dependent [22,23]. Whilst ESCRT-0 and ESCRT-II are not involved in PM repair, Tsg101, ALIX, CHMP3, 2A, 2B, 1A and importantly 4B have all been shown to localise to the PM upon wounding, and wound closure correlates with maximum CHMP4B levels at the repair site [22,23]. ALIX is thought to play an important role in wound repair by bridging the calcium-sensing protein apoptosis-linked gene-2 (ALG-2) with ESCRT-III at the PM, perhaps nucleating ESCRT-III polymers via its interaction with CHMP4B [22,23]. ALG-2 therefore appears to act as the adaptor for ESCRT recruitment to the PM. This model is consistent with the sequential recruitment of ALG-2, ALIX, ESCRT-III and VPS4 to sites of wounding, as shown by confocal microscopy and TIRF imaging [22,23].

Finally, ESCRTs also play indirect roles at the plasma membrane, for example, by promoting the release of exosomes [192]. This function requires binding of the intracellular adaptor protein syntenin and ALIX, and this interaction promotes the release of exosomes as ILVs into multivesicular bodies by remodelling the endosomal membranes [193,194]. These late endosomal compartments subsequently fuse with the plasma membrane in an ESCRT-independent manner, thus releasing the exosomes to the extracellular medium.

ESCRT-III and membrane remodelling

In contrast with ESCRT-0, -I and -II, ESCRT-III does not form a stable complex, instead forming a transient assembly at sites of membrane remodelling to direct scission [195]. The domain organisation and structure of CHMP proteins has been well characterised [120,196], and studying MVB formation and viral budding has

Biochemical Society Transactions (2017) **45** 613–634
DOI: 10.1042/BST20160479

helped define the core CHMP proteins required for all ESCRT-mediated processes. Despite this progress, a defined, unified mechanism for membrane sculpting and severing by ESCRT-III remains to be established. Likewise, functional studies in cytokinesis indicate that each of the CHMP proteins may play differential roles and cannot compensate for one another [117,131,197]. However, precise roles for each of the CHMPs in ESCRT-III polymerisation and membrane remodelling remain to be defined.

Crystal structures for CHMP1B, 3, 4 and hIST1 have revealed that all CHMPs share a similar structure [120,196,198–200]. In their 'closed' soluble autoinhibited conformation, they consist of a highly structured N-terminal 4-helix bundle and an unstructured C-terminus, containing another two helices [120,196,199,201,202]. In their 'open' polymerisation competent forms, the second and third helices from the N-terminal bundle form a single elongated helix which forms a positively charged hairpin, together with helix one [198], which binds acidic lipids to promote membrane binding [120,196]. Interactions between ESCRT-III subunits are also mediated by this hairpin, particularly at the tip [120,196,199]. Other regions involved in inter-subunit interactions remain to be confirmed but are likely to include other surfaces of the first four helices that together comprise the core structure [56,198,200] and the fifth helix [120,196,201,203,204]. The fifth helix is, however, more commonly associated with an autoinhibitory function, maintaining CHMPs in their 'closed' monomeric conformation in the cytoplasm when not in use. The fifth helix folds back on the four helix bundle forming numerous contacts with the helices [120,196,201,202,204,205]. MIM domains are present in the C-terminus of all CHMPs except CHMP3 [199,202,206]. MIT domain-containing proteins can stabilise the open conformation of the CHMPs by binding to the conserved C-terminal MIM [201].

Studies in yeast initially showed the highly ordered assembly of CHMPs in a sequence that starts with Vps20 (CHMP6) and follows with Snf7 (CHMP4), Vps24 (CHMP3) and Vps2 (CHMP2), which recruits Vps4 to promote ESCRT-III disassembly [9,195]. According to this model, Vps20 would act as the nucleator for initial polymerisation of Snf7, which is thought to be the main constituent of the ESCRT-III filaments [204,207]. These polymers would be capped by the Vps24/Vps2 dimer that in turn recruits Vps4 for filament disassembly [125,195,208]. The specific roles of these core subunits are thought to be conserved in mammals [209,210], although additional proteins, such as ALIX and CHMP7, may also have nucleating activity in higher eukaryotes [28,40,165,211]. Nucleation of ESCRT-III involves transition of CHMPs from 'closed' to 'open' forms as a result of structural reorganisation upon binding to ESCRT-II/ALIX [195,207,212–214]. Membrane curvature has also been shown to promote nucleation [213,215]. One interesting feature observed in some of the nucleating factors is their ability to dimerise. For example, ESCRT-II contains two EAP20 subunits which are each able to bind separate CHMP6 molecules and therefore nucleate two ESCRT-III filaments [207,212,214,216,217]. ALIX can also dimerise through its V domain and bind two CHMP4 subunits [211]. Such pairing of ESCRT-III filaments is likely to account for some of the diversity in filament width that is observed *in vitro* and *in vivo* [112,200,203,218,219]. In fact, ALIX has been shown to bundle pairs of 3 nm CHMP4B filaments *in vitro* [205,211], whereas the spiral filaments formed *in vivo* when CHMP4B is overexpressed have an approximate width of 6 nm [203], perhaps suggesting that bundling of two ESCRT-III filaments could underlie the formation of these structures. Similar observations have been made in the context of yeast Snf7, whereby bundling produces proto-filaments wider than 9 nm [204].

Electron microscopy has shown a variety of structures, both *in vitro* and *in vivo* for various ESCRT-III filaments, including spirals, tubes, coils, cones and domes [200,204,208,218–220]. The overexpression of CHMP4A in COS-7 cells forms flat spirals, which form tubes projecting from the plasma membrane when a VPS4 dominant-negative mutant is expressed, consistent with membrane budding away from the cytoplasm [203]. Yeast Snf7 forms a variety of filaments, rings and sheets *in vitro* [205,211]. A recent study showed that, when incubated with membranes, Snf7 forms spirals in which the inner ring is over bent, hence storing less energy than outer rings which are underbent [221]. Such spirals showed spring-like buckling activity when they eventually covered the entire membrane, pushing ESCRT-III outwards, suggesting that lateral compression causes the spirals to deform into tubes, releasing stored elastic energy to remodel membranes [221]. Like CHMP4, CHMP2A also forms spirals when the C-terminal autoinhibitory region is removed [208,219], whereas CHMP2B forms tubes of varying diameters when overexpressed [222]. Importantly, coexpression of CHMP2A and CHMP3 forms heteropolymeric tubes that end in dome-shaped caps [203,208,223]. Another fascinating study has recently determined a high-resolution hIST1–CHMP1B structure by cryo-electron microscopy [200]. The tubular structure of this straight heteropolymer revealed an outer surface of 'closed' hIST1 that is negatively charged, whilst CHMP1B assumed an 'open' state in the inner surface that forms a cationic interior [200]. Remarkably, the inner surface was able to bind membranes and promote scission of membrane tubules

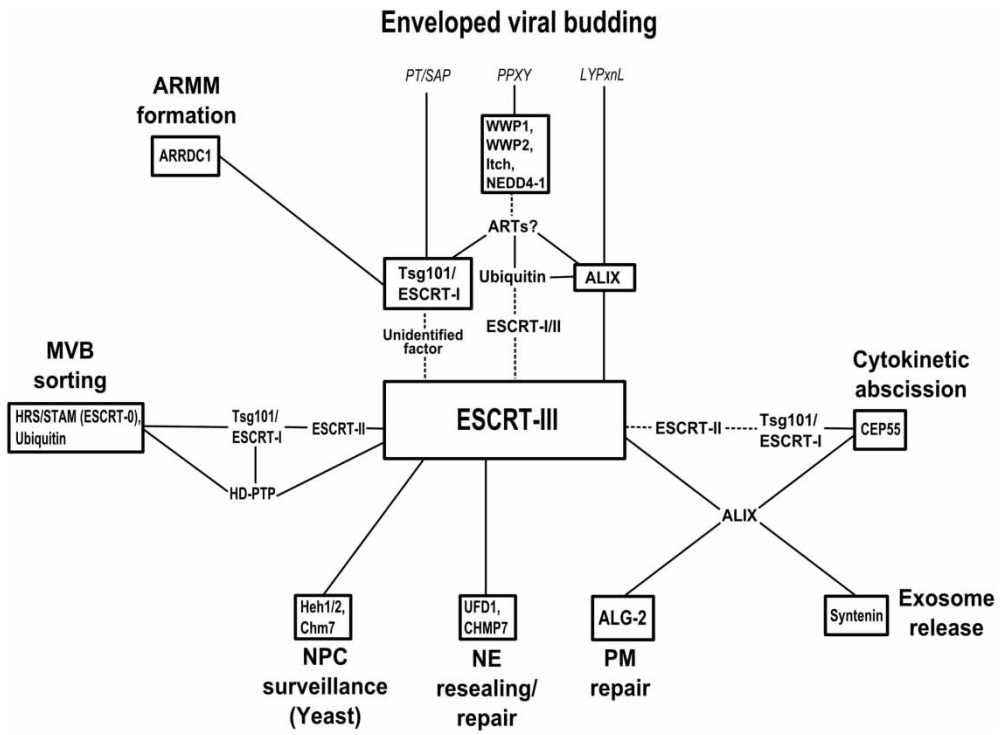

Figure 1. Site specific adaptors and pathways for ESCRT-III recruitment.

Schematic depicting adaptor proteins necessary for recruitment of ESCRT-III to sites of membrane remodelling and pathways for ESCRT-III recruitment that are both well established and speculative/require further validation. Adaptors are boxed, adjacent to their relevant ESCRT-mediated process. Solid lines represent established interactions. Dashed lines represent interactions that are either speculative or require further validation, such as the role of ESCRT-II in viral budding/cytokinetic abscission.

with normal topology, i.e. scission from the outside of the membrane rather than from the inside, as commonly associated with the ESCRT machinery [200]. This study raises the question of whether closed CHMP conformations always correspond to autoinhibited incompetent forms, or just membrane-binding forms. Secondly, it raises the surprising possibility that CHMPs are indeed capable of directing membrane scission in diverse topological contexts, a model supported by increased endosomal tubulation in hIST1-depleted cells [224].

Various models for ESCRT-III action have been proposed based on the structures observed so far [225]. These models take also into account the importance of CHMP4 and CHMP2/3 subunits, energetic considerations and localisation of subunits in relation to cargo in MVB formation, as well as observations in the context of viral budding. The 'whorl' model of ESCRT-III assembly was proposed to accommodate the initial role of ESCRT-I and -II in initial membrane stabilisation at bud necks of ILVs [226]. ESCRT-I and -II form a crescent-shaped supercomplex that is believed to facilitate initial membrane bending that aids ESCRT-III nucleation. Pairs of ESCRT-III filaments are proposed to form spokes that extend away from each ESCRT-I–ESCRT-II complex, meeting at the site of scission [226]. The natural propensity for filaments to bend would allow the ESCRT-III filaments to form a 'whorl' shaped structure that would constrict the membrane towards the site of scission. VPS4 has been suggested to play an organisational role in this context by clustering the ends of the spokes at the site of scission [226]. Dome models have gained more plausibility given the strong experimental evidence that supports dome-shaped caps at the ends of tubular structures formed by CHMP2/CHMP3 [208,227]. Crucially, this model has the potential to explain how ESCRT-III could remodel membrane necks of different diameters ranging from 50 nm, as required for viral budding, to 1 μm in cytokinesis. Dome models involve binding of membrane to the outside of dome-shaped caps of tubules, which pull opposing membranes together to constrict bud necks and drive scission [208,225,227,228]. Whether membrane scission requires VPS4 in this context is unclear at present [200,228]. It is also unclear whether CHMP2 and 3 are incorporated into growing CHMP4 filaments or whether they form a separate dome-shaped cap on the end of the tubes [112,204,208,229]. This

Biochemical Society Transactions (2017) **45** 613–634
DOI: 10.1042/BST20160479

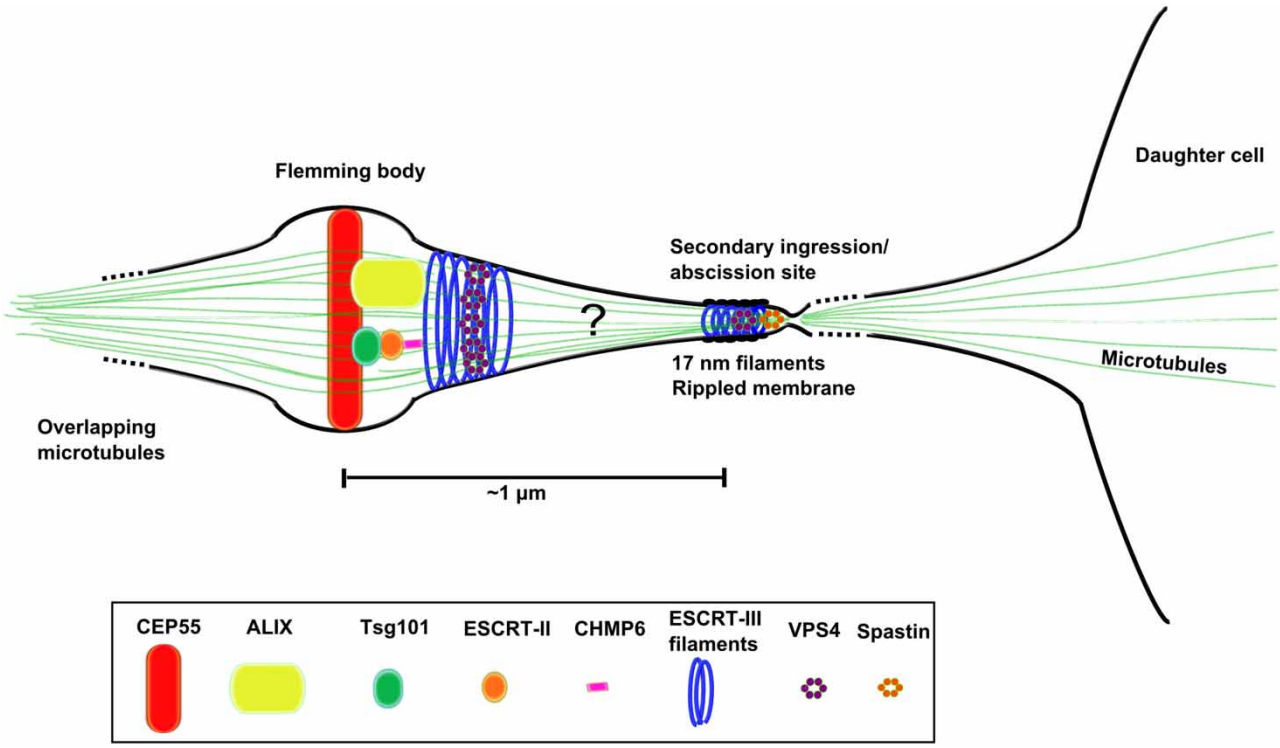

Figure 2. Localisation and action of the ESCRT machinery during cytokinetic abscission.

The adaptor protein CEP55 recruits ALIX and Tsg101 to the Flemming body — an electron dense structure formed at the centre of the midbody, where microtubules derived from the central spindle overlap. ALIX–CHMP4B and Tsg101 (ESCRT-I)-ESCRT-II-CHMP6 have been proposed to form parallel arms of recruitment for ESCRT-III to the midbody. Prior to abscission, ESCRT-III and VPS4 appear both at the sides of the Flemming body and in distal pools as 17 nm filaments ~1 μm away from the Flemming body, where the membrane appears rippled. These distal sites correspond to the sites of abscission and are known as secondary ingressions because the membrane tube is thinned from 1.5–2 μm to ~100 nm here, possibly by vesicle fusion with the membrane prior to ESCRT-III arrival, or directly by ESCRT-III constriction. The 'cut and slide' model for abscission proposes VPS4-mediated breakage of ESCRT-III filaments at the initial pool at the sides of the Flemming body, followed by constriction, leading to propulsion away from the Flemming body to form/reach pre-formed secondary ingression sites. Here, continued polymerisation would mediate scission. Alternatively, continuous ESCRT-III polymerisation from the Flemming body to the secondary ingression sites has been proposed, as has independent nucleation of ESCRT-III at pre-formed secondary ingression sites. Microtubule severing is a rate-limiting step of abscission and is performed by spastin that binds CHMP1B and hIST1 via MIT–MIM interactions.

aspect could have profound implications in this model as a switch from CHMP4 homopolymerisation to heteropolymerisation of CHMP2/3 would be required to achieve membrane scission.

In addition to 'whorl' and 'dome' models, inverse buckling of ESCRT-III cones/domes has been suggested to drive membrane scission [221,230]. In this model, over bent filaments at the tip of the cones are severed from upstream ESCRTs, such as ESCRT-I, ESCRT-II and ALIX, by the action of VPS4, causing stored energy to be released by inverse buckling, back into 2D spirals [225,230]. Release of energy stored in the bent membranes would simultaneously drive scission. This model would require outward growth of filaments from the narrow tip towards the wider end of the cone, consistent with tapering of the cone towards HIV-1 Gag seen by deep-etch electron microscopy (DEEM) [220]. However, it would be difficult to apply this model to cytokinesis, where ESCRT-I, ESCRT-II and ALIX localise to the Flemming body and have not been observed at the abscission sites [112,113]. The orientation of ESCRT-I and -II complex-bound cargo in relation to the ESCRT-III cones also makes this model attractive in terms of providing an explanation for how MVB sorted cargo is sorted into ILVs whilst ESCRT-III monomers are recycled to the cytoplasm [225,231].

Whilst the role of VPS4 in disassembly and recycling of ESCRT-III is well established, it is still unclear whether or not it plays a direct role in membrane deformation and/or the actual membrane scission event. Neither Vps4 nor Vps2 appears to be required for scission of ILVs in yeast, but both are required for

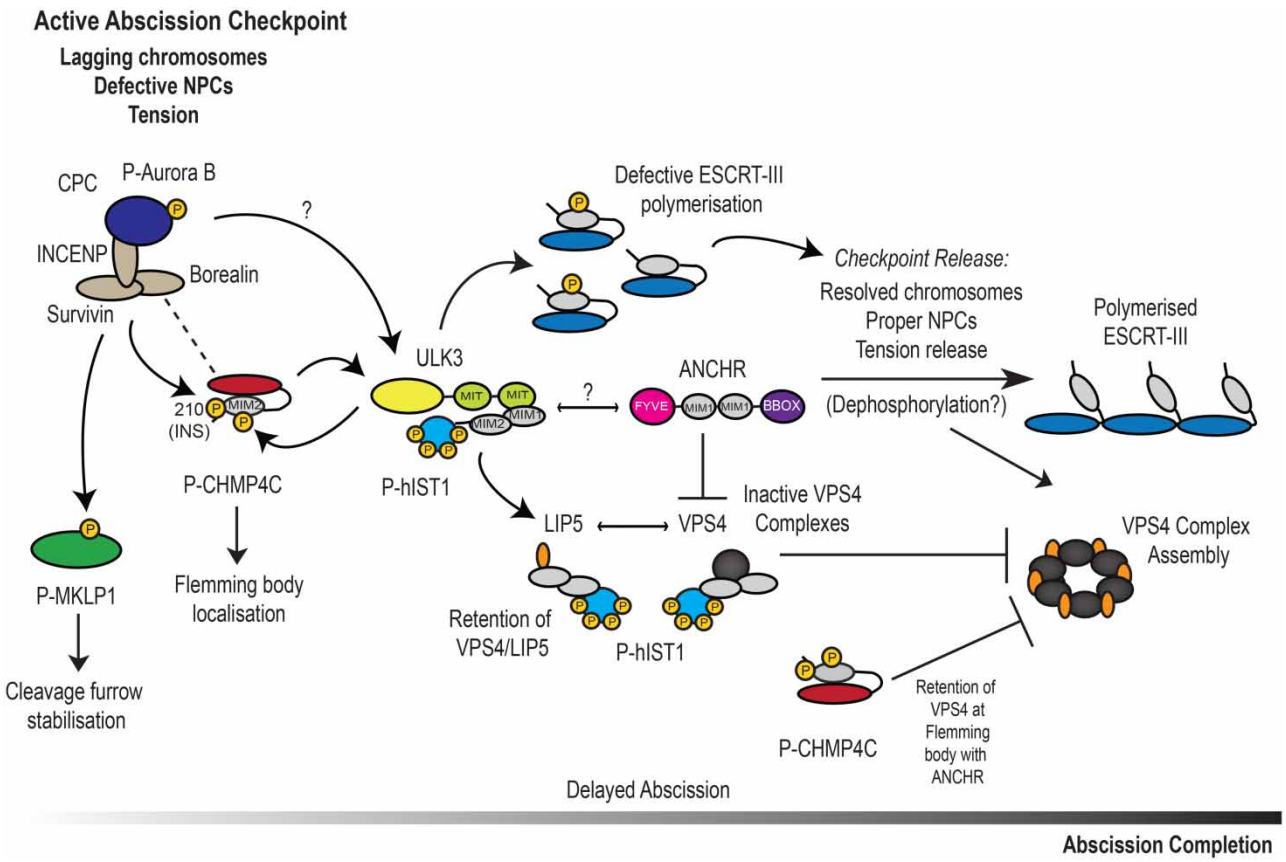

Figure 3. The ESCRT machinery in the NoCut Aurora B-dependent abscission checkpoint.

Aurora B kinase, a component of the CPC, is activated by phosphorylation. Activated Aurora B phosphorylates MKLP1, which ensures cleavage furrow stabilisation. Aurora B also phosphorylates CHMP4C which is brought into the proximity of Aurora B via its interaction with Borealin, another CPC component. Phosphorylation at residue 210 of CHMP4C is important here, within an insertion specific to CHMP4C between the MIM- and ALIX-binding regions. CHMP4C acts upstream of and is necessary for ULK3 kinase activity. ULK3 also phosphorylates CHMP4C, at separate sites within the MIM, and other ESCRT-III subunits. However, its best characterised substrate is hIST1, with which it interacts via a strong C-terminal MIT–MIM interaction. These phosphorylations have been proposed to halt abscission by potentially binding to VPS4 and retaining it at the Flemming body and/or preventing VPS4 activation through inhibition of assembly, and/or maintaining ESCRT-III subunits in 'closed' inactive forms incapable of polymerisation. ANCHR is another component of the checkpoint that has been proposed to act in concert with CHMP4C to bind and retain VPS4 at the midbody in an Aurora B-dependent manner. Question marks represent speculative interactions that have not been validated.

subsequent rounds of scission, arguing for an ESCRT-III recycling role for Vps4 [229,232]. Furthermore, the hIST1–CHMP1B helical tubes discussed above could be formed in the absence of VPS4, suggesting a dispensable role for polymer assembly, at least *in vitro* [200]. Despite this evidence, the role of VPS4 remains an open question, and a more direct role in membrane remodelling is possible, given its localisation to sites of membrane scission such as the stalks of budding HIV-1 virions [233,234] and abscission sites during cytokinesis prior to scission [113]. One simple model that could unify several observations is the sequential removal of ESCRT-III subunits by VPS4, which could drive membrane constriction perhaps by constricting the ESCRT-III filaments up to a point where spontaneous membrane scission can occur [227,235].

As summarised in this section, there has been spectacular progress over the last few years in our understanding of the molecular mechanisms employed by ESCRT-III to promote membrane scission. However, the mechanism of ESCRT-III polymerisation should be treated with caution at this stage due to the overexpressed nature of some of the experimental systems, as well as the limitation posed by the lack of the entire set of ESCRT-III subunits that are found in physiological conditions. In these respects, greater effort should be devoted to better understanding the structure of the ESCRT-III filaments assembled under strict physiological conditions. Cytokinetic abscission

Biochemical Society Transactions (2017) **45** 613–634
DOI: 10.1042/BST20160479

perhaps represents an interesting area that could benefit from such work, given the large size of the polymeric ESCRT-III structures that are proposed to promote the physical separation of daughter cells.

Concluding remarks

The co-option of the ESCRT machinery by an increasing number of intracellular processes, together with the identification of various adaptors for recruitment of ESCRT-III to specific sites, has reinforced the modular nature of the ESCRT machinery. The control in cytokinesis by the abscission checkpoint, as well as the role of ESCRTs in multiple events at the NE, has demonstrated the interplay and precise spatiotemporal coordination of the ESCRT machinery with cellular processes that are involved in quality control.

The binding partners of the different L-domains and the essential ESCRT-III subunits required for viral budding are well established. However, the biggest remaining question in this field is exactly how ESCRT-III is recruited to the sites of viral budding, and how membrane remodelling is achieved in this context. Whilst ALIX provides direct bridging of viral structural proteins with ESCRT-III, we still lack a clear consensus regarding ESCRT-III recruitment in PTAP and PPXY-dependent budding. Questions that remain unanswered in cytokinetic abscission include how ESCRT-III is recruited to the sites of abscission that are adjacent to the Flemming body, and how the membrane tube of ∼1 μm is severed, given that the diameters resolved in other ESCRT-mediated processes are much smaller, in the range of 50–100 nm. Why the midbody persists for so long before abscission occurs, and what triggers the final cut is also unclear. Intriguing connections between the nucleus and the midbody are suggested by the delays in abscission that are induced upon disruption of the nucleopores, and the nature of this signal needs to be uncovered. This connection is further highlighted by the recent discoveries that demonstrate the essential role of the ESCRT machinery in establishing and maintaining the integrity of the NE, suggesting that a tight coordination of the ESCRT complexes is needed at multiple steps during the final events of cell division. In fact, this coordination might be required in other cellular compartments, as the localisation of CHMP7 in interphase strongly suggests potential roles of the ESCRT pathway at the ER.

The variety of structures seen for homo and heteropolymers of CHMP proteins *in vitro* and *in vivo* has provided the basis to better understand the dynamic conformation of ESCRT-III and the mechanism that promotes membrane scission. However, a better characterisation of the polymers formed *in vivo* is required to understand membrane remodelling by ESCRT-III; it is even possible that different structures might be adopted by ESCRT-III at different sites of action. Further insights into the mechanism of ESCRT-III action is likely to come from higher resolution microscopy techniques, such as the DEEM employed so far, and newly developed super-resolution microscopy will be better suited to address these issues.

In terms of the clinical implications of ESCRTs, their role in viral maturation and budding presents potential avenues for therapeutic intervention in HIV-1, Ebola, Hepatitis C and other emerging viral infections. Changes in expression levels of several ESCRT proteins have also been linked to various forms of cancer, and the connection between polymorphisms in human CHMP4C and increased risk for ovarian cancer is particularly exciting. Other relevant connections with human disease that need to be further explored include the link between CHMP2B and neurodegenerative diseases such as frontotemporal dementia and Alzheimer's disease [236–238].

Abbreviations

ALG-2, apoptosis-linked gene-2; ALIX, ALG-2-interacting protein X; ANCHR, Abscission/NoCut Checkpoint Regulator; ARMM, ARRDC1-mediated microvesicle; ARRDC1, arrestin domain containing 1; ART, arrestin-related trafficking; CDK1, cyclin-dependent kinase 1; CEP55, centrosomal protein of 55 kDa; CHMP, charged multivesicular body protein; CPC, chromosomal passenger complex; CYK-4, cytokeratin-4; DEEM, deep-etch electron microscopy; EAP20, ELL-associated protein of 20 kDa; EAP45, ELL-associated protein of 45 kDa; EIAV, equine infectious anaemia virus; ER, endoplasmic reticulum; ESCRT, endosomal sorting complex required for transport; HECT, homologous to the E6-AP carboxyl terminus; hIST1, human Increased sodium tolerance 1; HIV, human immunodeficiency virus; HSV-1, herpes simplex virus-1; ILV, intralumenal vesicle; INM, inner nuclear membrane; LIP5, LYST-interacting protein 5; MHC, major histocompatibility complex; MIM, MIT domain-interacting motif; MIT, microtubule-interacting and trafficking; MITD1, MIT domain containing 1; MKLP1, mitotic kinesin-like protein 1; MLV, murine leukaemia virus; MVB, multivesicular body; NE, nuclear envelope; NEDD4, neural precursor cell expressed developmentally down-regulated protein 4; NPC, nuclear pore complex; Nup, nucleoporin; PLK-1, Polo-like kinase 1; PM, plasma membrane; RSV, Rous sarcoma virus; SINC, storage of improperly assembled NPCs; Snf7, sucrose nonfermenting protein 7; TCR, T-cell receptor; TIRF, total internal

reflection fluorescence microscopy; Tsg101, tumour susceptibility gene 101; UEV, ubiquitin enzyme variant; UFD1, ubiquitin fusion degradation protein 1; ULK3, Unc-51-like kinase 3; VPS, vacuole protein sorting; WWP1, WW domain containing E3 ubiquitin protein ligase 1; WWP2, WW domain containing E3 ubiquitin protein ligase 2.

Funding
Work in J.M.-S.'s laboratory is funded by the Wellcome Trust [WT093056MA].

Acknowledgements
We thank Monica Agromayor for critical reading of the manuscript and Anna Caballe for help with the figures.

Competing Interests
The Authors declare that there are no competing interests associated with the manuscript.

References
1 Raymond, C.K., Howald-Stevenson, I., Vater, C.A. and Stevens, T.H. (1992) Morphological classification of the yeast vacuolar protein sorting mutants: evidence for a prevacuolar compartment in class E vps mutants. *Mol. Biol. Cell.* **3**, 1389–1402 doi:10.1091/mbc.3.12.1389
2 Banta, L.M., Robinson, J.S., Klionsky, D.J. and Emr, S.D. (1988) Organelle assembly in yeast: characterization of yeast mutants defective in vacuolar biogenesis and protein sorting. *J. Cell Biol.* **107**, 1369–1383 doi:10.1083/jcb.107.4.1369
3 Davis, N.G., Horecka, J.L. and Sprague, G.F. (1993) Cis- and trans-acting functions required for endocytosis of the yeast pheromone receptors. *J. Cell Biol.* **122**, 53–65 doi:10.1083/jcb.122.1.53
4 Rieder, S.E., Banta, L.M., Köhrer, K., McCaffery, J.M. and Emr, S.D. (1996) Multilamellar endosome-like compartment accumulates in the yeast vps28 vacuolar protein sorting mutant. *Mol. Biol. Cell* **7**, 985–999 doi:10.1091/mbc.7.6.985
5 Katzmann, D.J., Babst, M. and Emr, S.D. (2001) Ubiquitin-dependent sorting into the multivesicular body pathway requires the function of a conserved endosomal protein sorting complex, ESCRT-I. *Cell* **106**, 145–155 doi:10.1016/S0092-8674(01)00434-2
6 Katzmann, D.J., Stefan, C.J., Babst, M. and Emr, S.D. (2003) Vps27 recruits ESCRT machinery to endosomes during MVB sorting. *J. Cell Biol.* **162**, 413–423 doi:10.1083/jcb.200302136
7 Bilodeau, P.S., Urbanowski, J.L., Winistorfer, S.C. and Piper, R.C. (2002) The Vps27p Hse1p complex binds ubiquitin and mediates endosomal protein sorting. *Nat. Cell Biol.* **4**, 534–539 doi:10.1038/ncb815
8 Bowers, K., Lottridge, J., Helliwell, S.B., Goldthwaite, L.M., Luzio, J.P. and Stevens, T.H. (2004) Protein-protein interactions of ESCRT complexes in the yeast *Saccharomyces cerevisiae*. *Traffic* **5**, 194–210 doi:10.1111/j.1600-0854.2004.00169.x
9 Babst, M., Katzmann, D.J., Estepa-Sabal, E.J., Meerloo, T. and Emr, S.D. (2002) ESCRT-III: an endosome-associated heterooligomeric protein complex required for MVB sorting. *Dev. Cell* **3**, 271–282 doi:10.1016/S1534-5807(02)00220-4
10 Babst, M., Katzmann, D.J., Snyder, W.B., Wendland, B. and Emr, S.D. (2002) Endosome-associated complex, ESCRT-II, recruits transport machinery for protein sorting at the multivesicular body. *Dev. Cell* **3**, 283–289 doi:10.1016/S1534-5807(02)00219-8
11 von Schwedler, U.K., Stuchell, M., Müller, B., Ward, D.M., Chung, H.-Y., Morita, E. et al. (2003) The protein network of HIV budding. *Cell* **114**, 701–713 doi:10.1016/S0092-8674(03)00714-1
12 Martin-Serrano, J., Yarovoy, A., Perez-Caballero, D., Bieniasz, P.D. and Yaravoy, A. (2003) Divergent retroviral late-budding domains recruit vacuolar protein sorting factors by using alternative adaptor proteins. *Proc. Natl Acad. Sci. U.S.A.* **100**, 12414–12419 doi:10.1073/pnas.2133846100
13 Babst, M., Wendland, B., Estepa, E.J. and Emr, S.D. (1998) The Vps4p AAA ATPase regulates membrane association of a Vps protein complex required for normal endosome function. *EMBO J.* **17**, 2982–2993 doi:10.1093/emboj/17.11.2982
14 Monroe, N. and Hill, C.P. (2016) Meiotic clade AAA ATPases: protein polymer disassembly machines. *J. Mol. Biol.* **428**, 1897–1911 doi:10.1016/j.jmb.2015.11.004
15 Scott, A., Chung, H.-Y., Gonciarz-Swiatek, M., Hill, G.C., Whitby, F.G., Gaspar, J. et al. (2005) Structural and mechanistic studies of VPS4 proteins. *EMBO J.* **24**, 3658–3669 doi:10.1038/sj.emboj.7600818
16 VerPlank, L., Bouamr, F., LaGrassa, T.J., Agresta, B., Kikonyogo, A., Leis, J. et al. (2001) Tsg101, a homologue of ubiquitin-conjugating (E2) enzymes, binds the L domain in HIV type 1 $Pr55^{Gag}$. *Proc. Natl Acad. Sci. U.S.A.* **98**, 7724–7729 doi:10.1073/pnas.131059198
17 Garrus, J.E., von Schwedler, U.K., Pornillos, O.W., Morham, S.G., Zavitz, K.H., Wang, H.E. et al. (2001) Tsg101 and the vacuolar protein sorting pathway are essential for HIV-1 budding. *Cell* **107**, 55–65 doi:10.1016/S0092-8674(01)00506-2
18 Martin-Serrano, J., Zang, T. and Bieniasz, P.D. (2001) HIV-1 and Ebola virus encode small peptide motifs that recruit Tsg101 to sites of particle assembly to facilitate egress. *Nat. Med.* **7**, 1313–1319 doi:10.1038/nm1201-1313
19 Demirov, D.G., Ono, A., Orenstein, J.M. and Freed, E.O. (2002) Overexpression of the N-terminal domain of TSG101 inhibits HIV-1 budding by blocking late domain function. *Proc. Natl Acad. Sci. U.S.A.* **99**, 955–960 doi:10.1073/pnas.032511899
20 Carlton, J.G. and Martin-Serrano, J. (2007) Parallels between cytokinesis and retroviral budding: a role for the ESCRT machinery. *Science* **316**, 1908–1912 doi:10.1126/science.1143422
21 Morita, E., Sandrin, V., Chung, H.-Y., Morham, S.G., Gygi, S.P., Rodesch, C.K. et al. (2007) Human ESCRT and ALIX proteins interact with proteins of the midbody and function in cytokinesis. *EMBO J.* **26**, 4215–4227 doi:10.1038/sj.emboj.7601850
22 Jimenez, A.J., Maiuri, P., Lafaurie-Janvore, J., Divoux, S., Piel, M. and Perez, F. (2014) ESCRT machinery is required for plasma membrane repair. *Science* **343**, 1247136 doi:10.1126/science.1247136
23 Scheffer, L.L., Sreetama, S.C., Sharma, N., Medikayala, S., Brown, K.J., Defour, A. et al. (2014) Mechanism of Ca^{2+}-triggered ESCRT assembly and regulation of cell membrane repair. *Nat. Commun.* **5**, 5646 doi:10.1038/ncomms6646
24 Loncle, N., Agromayor, M., Martin-Serrano, J. and Williams, D.W. (2015) An ESCRT module is required for neuron pruning. *Sci. Rep.* **5**, 8461 doi:10.1038/srep08461

Biochemical Society Transactions (2017) **45** 613–634
DOI: 10.1042/BST20160479

25 Zhang, H., Wang, Y., Wong, J.J.L., Lim, K.-L., Liou, Y.-C., Wang, H. et al. (2014) Endocytic pathways downregulate the L1-type cell adhesion molecule neuroglian to promote dendrite pruning in *Drosophila*. *Dev. Cell* **30**, 463–478 doi:10.1016/j.devcel.2014.06.014

26 Issman-Zecharya, N. and Schuldiner, O. (2014) The PI3K class III complex promotes axon pruning by downregulating a ptc-derived signal via endosome-lysosomal degradation. *Dev. Cell* **31**, 461–473 doi:10.1016/j.devcel.2014.10.013

27 Olmos, Y., Hodgson, L., Mantell, J., Verkade, P. and Carlton, J.G. (2015) ESCRT-III controls nuclear envelope reformation. *Nature* **522**, 236–239 doi:10.1038/nature14503

28 Vietri, M., Schink, K.O., Campsteijn, C., Wegner, C.S., Schultz, S.W., Christ, L. et al. (2015) Spastin and ESCRT-III coordinate mitotic spindle disassembly and nuclear envelope sealing. *Nature* **522**, 231–235 doi:10.1038/nature14408

29 Webster, B.M., Colombi, P., Jäger, J. and Lusk, C.P. (2014) Surveillance of nuclear pore complex assembly by ESCRT-III/Vps4. *Cell* **159**, 388–401 doi:10.1016/j.cell.2014.09.012

30 Göttlinger, H.G., Dorfman, T., Sodroski, J.G. and Haseltine, W.A. (1991) Effect of mutations affecting the p6 gag protein on human immunodeficiency virus particle release. *Proc. Natl Acad. Sci. U.S.A.* **88**, 3195–3199 doi:10.1073/pnas.88.8.3195

31 Huang, M., Orenstein, J.M., Martin, M.A. and Freed, E.O. (1995) P6gag is required for particle production from full-length human immunodeficiency virus type 1 molecular clones expressing protease. *J. Virol.* **69**, 6810–6818 PMCID:189593

32 Puffer, B.A., Parent, L.J., Wills, J.W. and Montelaro, R.C. (1997) Equine infectious anemia virus utilizes a YXXL motif within the late assembly domain of the Gag p9 protein. *J. Virol.* **71**, 6541–6546 PMID:9261374

33 Xiang, Y., Cameron, C.E., Wills, J.W. and Leis, J. (1996) Fine mapping and characterization of the Rous sarcoma virus Pr76gag late assembly domain. *J. Virol.* **70**, 5695–5700 PMID:876409134.

34 Wills, J.W., Cameron, C.E., Wilson, C.B., Xiang, Y., Bennett, R.P. and Leis, J. (1994) An assembly domain of the Rous sarcoma virus Gag protein required late in budding. *J. Virol.* **68**, 6605–6618 PMID:8083996

35 Parent, L.J., Bennett, R.P., Craven, R.C., Nelle, T.D., Krishna, N.K., Bowzard, J.B. et al. (1995) Positionally independent and exchangeable late budding functions of the Rous sarcoma virus and human immunodeficiency virus Gag proteins. *J. Virol.* **69**, 5455–5460 PMID:7636991

36 Yuan, B., Campbell, S., Bacharach, E., Rein, A. and Goff, S.P. (2000) Infectivity of Moloney murine leukemia virus defective in late assembly events is restored by late assembly domains of other retroviruses. *J. Virol.* **74**, 7250–7260 doi:10.1128/JVI.74.16.7250-7260.2000

37 Martin-Serrano, J., Zang, T. and Bieniasz, P.D. (2003) Role of ESCRT-I in retroviral budding. *J. Virol.* **77**, 4794–4804 doi:10.1128/JVI.77.8.4794-4804.2003

38 Pornillos, O., Alam, S.L., Davis, D.R. and Sundquist, W.I. (2002) Structure of the Tsg101 UEV domain in complex with the PTAP motif of the HIV-1 p6 protein. *Nat. Struct. Mol. Biol.* **9**, 812–817 doi:10.1038/nsb856

39 Strack, B., Calistri, A., Craig, S., Popova, E. and Göttlinger, H.G. (2003) AIP1/ALIX is a binding partner for HIV-1 p6 and EIAV p9 functioning in virus budding. *Cell* **114**, 689–699 doi:10.1016/S0092-8674(03)00653-6

40 Fisher, R.D., Chung, H.-Y., Zhai, Q., Robinson, H., Sundquist, W.I. and Hill, C.P. (2007) Structural and biochemical studies of ALIX/AIP1 and its role in retrovirus budding. *Cell* **128**, 841–852 doi:10.1016/j.cell.2007.01.035

41 Martin-Serrano, J., Eastman, S.W., Chung, W. and Bieniasz, P.D. (2005) HECT ubiquitin ligases link viral and cellular PPXY motifs to the vacuolar protein-sorting pathway. *J. Cell Biol.* **168**, 89–101 doi:10.1083/jcb.200408155

42 Kikonyogo, A., Bouamr, F., Vana, M.L., Xiang, Y., Aiyar, A., Carter, C. et al. (2001) Proteins related to the Nedd4 family of ubiquitin protein ligases interact with the L domain of Rous sarcoma virus and are required for Gag budding from cells. *Proc. Natl Acad. Sci. U.S.A.* **98**, 11199–11204 doi:10.1073/pnas.201268998

43 Han, Z., Sagum, C.A., Bedford, M.T., Sidhu, S.S., Sudol, M. and Harty, R.N. (2016) ITCH e3 ubiquitin ligase interacts with ebola virus VP40 to regulate budding. *J. Virol.* **90**, 9163–9171 doi: 10.1128/JVI.01078-16

44 Harty, R.N., Brown, M.E., Wang, G., Huibregtse, J. and Hayes, F.P. (2000) A PPxY motif within the VP40 protein of Ebola virus interacts physically and functionally with a ubiquitin ligase: implications for filovirus budding. *Proc. Natl Acad. Sci. U.S.A.* **97**, 13871–13876 doi:10.1073/pnas.250277297

45 Samson, R.Y., Obita, T., Freund, S.M., Williams, R.L. and Bell, S.D. (2008) A role for the ESCRT system in cell division in archaea. *Science* **322**, 1710–1713 doi:10.1126/science.1165322

46 Lindås, A.-C., Karlsson, E.A., Lindgren, M.T., Ettema, T.J.G. and Bernander, R. (2008) A unique cell division machinery in the Archaea. *Proc. Natl Acad. Sci. U.S.A.* **105**, 18942–18946 doi:10.1073/pnas.0809467105

47 Snyder, J.C., Samson, R.Y., Brumfield, S.K., Bell, S.D. and Young, M.J. (2013) Functional interplay between a virus and the ESCRT machinery in archaea. *Proc. Natl Acad. Sci. U.S.A.* **110**, 10783–10787 doi:10.1073/pnas.1301605110

48 McCullough, J., Fisher, R.D., Whitby, F.G., Sundquist, W.I. and Hill, C.P. (2008) ALIX-CHMP4 interactions in the human ESCRT pathway. *Proc. Natl Acad. Sci. U.S.A.* **105**, 7687–7691 doi:10.1073/pnas.0801567105

49 Usami, Y., Popov, S. and Göttlinger, H.G. (2007) Potent rescue of human immunodeficiency virus type 1 late domain mutants by ALIX/AIP1 depends on its CHMP4 binding site. *J. Virol.* **81**, 6614–6622 doi:10.1128/JVI.00314-07

50 Ghoujal, B., Milev, M.P., Ajamian, L., Abel, K. and Mouland, A.J. (2012) ESCRT-II's involvement in HIV-1 genomic RNA trafficking and assembly. *Biol. Cell* **104**, 706–721 doi:10.1111/boc.201200021

51 Meng, B., Ip, N.C.Y., Prestwood, L.J., Abbink, T.E.M. and Lever, A.M.L. (2015) Evidence that the endosomal sorting complex required for transport-II (ESCRT-II) is required for efficient human immunodeficiency virus-1 (HIV-1) production. *Retrovirology* **12**, 72 doi:10.1186/s12977-015-0197-x

52 Bartusch, C. and Prange, R. (2016) ESCRT requirements for murine leukemia virus release. *Viruses* **8**, 103 doi: 10.3390/v8040103

53 Langelier, C., von Schwedler, U.K., Fisher, R.D., De Domenico, I., White, P.L., Hill, C.P. et al. (2006) Human ESCRT-II complex and its role in human immunodeficiency virus type 1 release. *J. Virol.* **80**, 9465–9480 doi:10.1128/JVI.01049-06

54 Pincetic, A., Medina, G., Carter, C. and Leis, J. (2008) Avian sarcoma virus and human immunodeficiency virus, type 1 use different subsets of ESCRT proteins to facilitate the budding process. *J. Biol. Chem.* **283**, 29822–29830 doi:10.1074/jbc.M804157200

55 Tanzi, G.O., Piefer, A.J. and Bates, P. (2003) Equine infectious anemia virus utilizes host vesicular protein sorting machinery during particle release. *J. Virol.* **77**, 8440–8447 doi:10.1128/JVI.77.15.8440-8447.2003

56 Morita, E., Sandrin, V., McCullough, J., Katsuyama, A., Baci Hamilton, I. and Sundquist, W.I. (2011) ESCRT-III protein requirements for HIV-1 budding. *Cell Host Microbe* **9**, 235–242 doi:10.1016/j.chom.2011.02.004

57 Sandrin, V. and Sundquist, W.I. (2013) ESCRT requirements for EIAV budding. *Retrovirology* **10**, 104 doi:10.1186/1742-4690-10-104
58 Martin-Serrano, J. and Bieniasz, P.D. (2003) A bipartite late-budding domain in human immunodeficiency virus type 1. *J Virol.* **77**, 12373–12377 doi:10.1128/JVI.77.22.12373-12377.2003
59 Segura-Morales, C., Pescia, C., Chatellard-Causse, C., Sadoul, R., Bertrand, E. and Basyuk, E. (2005) Tsg101 and Alix interact with murine leukemia virus Gag and cooperate with Nedd4 ubiquitin ligases during budding. *J. Biol. Chem.* **280**, 27004–27012 doi:10.1074/jbc.M413735200
60 Licata, J.M., Simpson-Holley, M., Wright, N.T., Han, Z., Paragas, J. and Harty, R.N. (2003) Overlapping motifs (PTAP and PPEY) within the Ebola virus VP40 protein function independently as late budding domains: involvement of host proteins TSG101 and VPS-4. *J. Virol.* **77**, 1812–1819 doi:10.1128/JVI.77.3.1812-1819.2003
61 Han, Z., Madara, J.J., Liu, Y., Liu, W., Ruthel, G., Freedman, B.D. et al. (2015) ALIX rescues budding of a double PTAP/PPEY L-domain deletion mutant of Ebola VP40: a role for ALIX in Ebola virus egress. *J. Infect. Dis.* **212**(Suppl 2), S138–S145 doi:10.1093/infdis/jiu838
62 Fujii, K., Munshi, U.M., Ablan, S.D., Demirov, D.G., Soheilian, F., Nagashima, K. et al. (2009) Functional role of Alix in HIV-1 replication. *Virology* **391**, 284–292 doi:10.1016/j.virol.2009.06.016
63 Ott, D.E., Coren, L.V., Copeland, T.D., Kane, B.P., Johnson, D.G., Sowder, II, R.C. et al. (1998) Ubiquitin is covalently attached to the p6Gag proteins of human immunodeficiency virus type 1 and simian immunodeficiency virus and to the p12Gag protein of Moloney murine leukemia virus. *J. Virol.* **72**, 2962–2968 PMID:9525617
64 Putterman, D., Pepinsky, R.B. and Vogt, V.M. (1990) Ubiquitin in avian leukosis virus particles. *Virology* **176**, 633–637 doi:10.1016/0042-6822(90)90035-P
65 Strack, B., Calistri, A., Accola, M.A., Palu, G. and Gottlinger, H.G. (2000) A role for ubiquitin ligase recruitment in retrovirus release. *Proc. Natl Acad. Sci. U.S.A.* **97**, 13063–13068 doi:10.1073/pnas.97.24.13063
66 Joshi, A., Munshi, U., Ablan, S.D., Nagashima, K. and Freed, E.O. (2008) Functional replacement of a retroviral late domain by ubiquitin fusion. *Traffic* **9**, 1972–1983 doi:10.1111/j.1600-0854.2008.00817.x
67 Zhadina, M. and Bieniasz, P.D. (2010) Functional interchangeability of late domains, late domain cofactors and ubiquitin in viral budding. *PLoS Pathog.* **6**, e1001153 doi:10.1371/journal.ppat.1001153
68 Martin-serrano, J., Perez-caballero, D. and Bieniasz, P.D. (2004) Context-dependent effects of L domains and ubiquitination on viral budding. *J. Virol.* **78**, 5554–5563 doi:10.1128/JVI.78.11.5554-5563.2004
69 Spidel, J.L., Craven, R.C., Wilson, C.B., Patnaik, A., Wang, H., Mansky, L.M. et al. (2004) Lysines close to the Rous sarcoma virus late domain critical for budding. *J. Virol.* **78**, 10606–10616 doi:10.1128/JVI.78.19.10606-10616.2004
70 Pornillos, O., Alam, S.L., Rich, R.L., Myszka, D.G., Davis, D.R. and Sundquist, W.I. (2002) Structure and functional interactions of the Tsg101 UEV domain. *EMBO J.* **21**, 2397–2406 doi:10.1093/emboj/21.10.2397
71 Weiss, E.R., Popova, E., Yamanaka, H., Kim, H.C., Huibregtse, J.M., Göttlinger, H. et al. (2010) Rescue of HIV-1 release by targeting widely divergent NEDD4-type ubiquitin ligases and isolated catalytic HECT domains to gag. *PLoS Pathog.* **6**, e1001107 doi: 10.1371/journal.ppat.1001107
72 Usami, Y., Popov, S., Popova, E. and Göttlinger, H.G. (2008) Efficient and specific rescue of human immunodeficiency virus type 1 budding defects by a Nedd4-like ubiquitin ligase. *J. Virol.* **82**, 4898–4907 doi:10.1128/JVI.02675-07
73 Chung, H.-Y., Morita, E., von Schwedler, U., Müller, B., Kräusslich, H.-G. and Sundquist, W.I. (2008) NEDD4L overexpression rescues the release and infectivity of human immunodeficiency virus type 1 constructs lacking PTAP and YPXL late domains. *J. Virol.* **82**, 4884–4897 doi:10.1128/JVI.02667-07
74 Agromayor, M., Soler, N., Caballe, A., Kueck, T., Freund, S.M., Allen, M.D. et al. (2012) The UBAP1 subunit of ESCRT-I interacts with ubiquitin via a SOUBA domain. *Structure* **20**, 414–428 doi:10.1016/j.str.2011.12.013
75 Slagsvold, T., Aasland, R., Hirano, S., Bache, K.G., Raiborg, C., Trambaiolo, D. et al. (2005) Eap45 in mammalian ESCRT-II binds ubiquitin via a phosphoinositide-interacting GLUE domain. *J. Biol. Chem.* **280**, e99924 doi:10.1074/jbc.M501510200
76 Keren-Kaplan, T., Attali, I., Estrin, M., Kuo, L.S., Farkash, E., Jerabek-Willemsen, M. et al. (2013) Structure-based in silico identification of ubiquitin-binding domains provides insights into the ALIX-V:ubiquitin complex and retrovirus budding. *EMBO J.* **32**, 538–551 doi:10.1038/emboj.2013.4
77 Dowlatshahi, D.P., Sandrin, V., Vivona, S., Shaler, T.A., Kaiser, S.E., Melandri, F. et al. (2012) ALIX is a Lys63-specific polyubiquitin binding protein that functions in retrovirus budding. *Dev. Cell* **23**, 1247–1254 doi:10.1016/j.devcel.2012.10.023
78 Sette, P., Nagashima, K., Piper, R.C. and Bouamr, F. (2013) Ubiquitin conjugation to Gag is essential for ESCRT-mediated HIV-1 budding. *Retrovirology* **10**, 79 doi:10.1186/1742-4690-10-79
79 Zhadina, M., McClure, M.O., Johnson, M.C. and Bieniasz, P.D. (2007) Ubiquitin-dependent virus particle budding without viral protein ubiquitination. *Proc. Natl Acad. Sci. U.S.A.* **104**, 20031–20036 doi:10.1073/pnas.0708002104
80 Rauch, S. and Martin-Serrano, J. (2011) Multiple interactions between the ESCRT machinery and arrestin-related proteins: implications for PPXY-dependent budding. *J. Virol.* **85**, 3546–3556 doi:10.1128/JVI.02045-10
81 Barajas, D., Jiang, Y., Nagy, P.D. and Nelson, J.A. (2009) A unique role for the host ESCRT proteins in replication of tomato bushy stunt virus. *PLoS Pathog.* **5**, e1000705 doi:10.1371/journal.ppat.1000705
82 Diaz, A., Zhang, J., Ollwerther, A., Wang, X. and Ahlquist, P. (2015) Host ESCRT proteins are required for bromovirus RNA replication compartment assembly and function. *PLoS Pathog.* **11**, e1004845 doi:10.1371/journal.ppat.1004845
83 Tabata, K., Arimoto, M., Arakawa, M., Nara, A., Saito, K., Omori, H. et al. (2016) Unique requirement for ESCRT factors in flavivirus particle formation on the endoplasmic reticulum. *Cell Rep.* **16**, 2339–2347 doi:10.1016/j.celrep.2016.07.068
84 Owen, D.J., Crump, C.M. and Graham, S.C. (2015) Tegument assembly and secondary envelopment of alphaherpesviruses. *Viruses* **7**, 5084–5114 doi:10.3390/v7092861
85 Lee, C.-P., Liu, P.-T., Kung, H.-N., Su, M.-T., Chua, H.-H., Chang, Y.-H. et al. (2012) The ESCRT machinery is recruited by the viral BFRF1 protein to the nucleus-associated membrane for the maturation of Epstein-Barr virus. *PLoS Pathog.* **8**, e1002904 doi.org/10.1371/journal.ppat.1002904
86 Schulz, K.S., Klupp, B.G., Granzow, H., Paßvogel, L. and Mettenleiter, T.C. (2015) Herpesvirus nuclear egress: Pseudorabies virus can simultaneously induce nuclear envelope breakdown and exit the nucleus via the envelopment-deenvelopment-pathway. *Virus Res.* **209**, 76–86 doi:10.1016/j.virusres.2015.02.001

Biochemical Society Transactions (2017) **45** 613–634
DOI: 10.1042/BST20160479

87 Crump, C.M., Yates, C. and Minson, T. (2007) Herpes simplex virus type 1 cytoplasmic envelopment requires functional Vps4. *J. Virol.* **81**, 7380–7387 doi:10.1128/JVI.00222-07
88 Pawliczek, T. and Crump, C.M. (2009) Herpes simplex virus type 1 production requires a functional ESCRT-III complex but is independent of TSG101 and ALIX expression. *J. Virol.* **83**, 11254–11264 doi:10.1128/JVI.00574-09
89 Glotzer, M. (2009) The 3Ms of central spindle assembly: microtubules, motors and MAPs. *Nat. Rev. Mol. Cell Biol.* **10**, 9–20 doi:10.1038/nrm2609
90 Glotzer, M. (2005) The molecular requirements for cytokinesis. *Science* **307**, 1735–1739 doi:10.1126/science.1096896
91 Pavicic-kaltenbrunner, V., Mishima, M. and Glotzer, M. (2007) Cooperative assembly of CYK-4/MgcRacGAP and ZEN-4/MKLP1 to form the centralspindlin complex. *Mol. Biol. Cell* **18**, 4992–5003 doi:10.1091/mbc.E07-05-0468
92 Carmena, M., Wheelock, M., Funabiki, H. and Earnshaw, W.C. (2012) The chromosomal passenger complex (CPC): from easy rider to the godfather of mitosis. *Nat. Rev. Mol. Cell Biol.* **13**, 789–803 doi:10.1038/nrm3474
93 Mishima, M., Pavicic, V., Grüneberg, U., Nigg, E.A. and Glotzer, M. (2004) Cell cycle regulation of central spindle assembly. *Nature* **430**, 908–913 doi:10.1038/nature02767
94 Hümmer, S. and Mayer, T.U. (2009) Cdk1 negatively regulates midzone localization of the mitotic kinesin Mklp2 and the chromosomal passenger complex. *Curr. Biol.* **19**, 607–612 doi:10.1016/j.cub.2009.02.046
95 Guse, A., Mishima, M. and Glotzer, M. (2005) Phosphorylation of ZEN-4/MKLP1 by Aurora B regulates completion of cytokinesis. *Curr. Biol.* **15**, 778–786 doi:10.1016/j.cub.2005.03.041
96 Su, K.-C., Takaki, T. and Petronczki, M. (2011) Targeting of the RhoGEF Ect2 to the equatorial membrane controls cleavage furrow formation during cytokinesis. *Dev. Cell* **21**, 1104–1115 doi:10.1016/j.devcel.2011.11.003
97 Pollard, T.D. (2010) Mechanics of cytokinesis in eukaryotes. *Curr. Opin. Cell Biol.* **22**, 50–56 doi:10.1016/j.ceb.2009.11.010
98 Matsumura, F. (2005) Regulation of myosin II during cytokinesis in higher eukaryotes. *Trends Cell Biol.* **15**, 371–377 doi:10.1016/j.tcb.2005.05.004
99 Mullins, J.M. and Biesele, J.J. (1977) Terminal phase of cytokinesis in D-98s cells. *J. Cell Biol.* **73**, 672–684 doi:10.1083/jcb.73.3.672
100 Euteneuer, U. and McIntosh, J.R. (1980) Polarity of midbody and phragmoplast microtubules. *J. Cell Biol.* **87**, 509–515 doi:10.1083/jcb.87.2.509
101 Saurin, A.T., Durgan, J., Cameron, A.J., Faisal, A., Marber, M.S. and Parker, P.J. (2008) The regulated assembly of a PKCε complex controls the completion of cytokinesis. *Nat. Cell Biol.* **10**, 891–901 doi:10.1038/ncb1749
102 Dambournet, D., Machicoane, M., Chesneau, L., Sachse, M., Rocancourt, M., El Marjou, A. et al. (2011) Rab35 GTPase and OCRL phosphatase remodel lipids and F-actin for successful cytokinesis. *Nat. Cell Biol.* **13**, 981–988 doi:10.1038/ncb2279
103 Schiel, J.A., Simon, G.C., Zaharris, C., Weisz, J., Castle, D., Wu, C.C. et al. (2012) FIP3-endosome-dependent formation of the secondary ingression mediates ESCRT-III recruitment during cytokinesis. *Nat. Cell Biol.* **14**, 1068–1078 doi:10.1038/ncb2577
104 Mierzwa, B. and Gerlich, D.W. (2014) Cytokinetic abscission: molecular mechanisms and temporal control. *Dev. Cell* **31**, 525–538 doi:10.1016/j.devcel.2014.11.006
105 Caballe, A. and Martin-Serrano, J. (2011) ESCRT machinery and cytokinesis: the road to daughter cell separation. *Traffic* **12**, 1318–1326 doi:10.1111/j.1600-0854.2011.01244.x
106 Zhao, W.-m., Seki, A. and Fang, G. (2006) Cep55, a microtubule-bundling protein, associates with centralspindlin to control the midbody integrity and cell abscission during cytokinesis. *Mol. Biol. Cell* **17**, 3881–3896 doi:10.1091/mbc.E06-01-0015
107 Fabbro, M., Zhou, B.-B., Takahashi, M., Sarcevic, B., Lal, P., Graham, M.E. et al. (2005) Cdk1/Erk2- and Plk1-dependent phosphorylation of a centrosome protein, Cep55, is required for its recruitment to midbody and cytokinesis. *Dev. Cell* **9**, 477–488 doi:10.1016/j.devcel.2005.09.003
108 Bastos, R.N. and Barr, F.A. (2010) Plk1 negatively regulates Cep55 recruitment to the midbody to ensure orderly abscission. *J. Cell Biol.* **191**, 751–760 doi:10.1083/jcb.201008108
109 Carlton, J.G., Agromayor, M. and Martin-Serrano, J. (2008) Differential requirements for Alix and ESCRT-III in cytokinesis and HIV-1 release. *Proc. Natl Acad. Sci. U.S.A.* **105**, 10541–10546 doi:10.1073/pnas.0802008105
110 Lee, H.H., Elia, N., Ghirlando, R., Lippincott-Schwartz, J. and Hurley, J.H. (2008) Midbody targeting of the ESCRT machinery by a noncanonical coiled coil in CEP55. *Science* **322**, 576–580 doi:10.1126/science.1162042
111 Christ, L., Wenzel, E.M., Liestøl, K., Raiborg, C., Campsteijn, C. and Stenmark, H. (2016) ALIX and ESCRT-I/II function as parallel ESCRT-III recruiters in cytokinetic abscission. *J. Cell Biol.* **212**, 499–513 doi:10.1083/jcb.201507009
112 Guizetti, J., Schermelleh, L., Mäntler, J., Maar, S., Poser, I., Leonhardt, H. et al. (2011) Cortical constriction during abscission involves helices of ESCRT-III-dependent filaments. *Science* **331**, 1616–1620 doi:10.1126/science.1201847
113 Elia, N., Sougrat, R., Spurlin, T.A., Hurley, J.H. and Lippincott-schwartz, J. (2011) Dynamics of endosomal sorting complex required for transport (ESCRT) machinery during cytokinesis and its role in abscission. *Proc. Natl Acad. Sci. U.S.A.* **108**, 4846–4851 doi:10.1073/pnas.1102714108
114 Wilson, G.M., Fielding, A.B., Simon, G.C., Yu, X., Andrews, P.D., Hames, R.S. et al. (2005) The FIP3-Rab11 protein complex regulates recycling endosome targeting to the cleavage furrow during late cytokinesis. *Mol. Biol. Cell* **16**, 849–860 doi:10.1091/mbc.E04-10-0927
115 Goss, J.W. and Toomre, D.K. (2008) Both daughter cells traffic and exocytose membrane at the cleavage furrow during mammalian cytokinesis. *J. Cell Biol.* **181**, 1047–1054 doi:10.1083/jcb.200712137
116 Gromley, A., Yeaman, C., Rosa, J., Redick, S., Chen, C.-T., Mirabelle, S. et al. (2005) Centriolin anchoring of exocyst and SNARE complexes at the midbody is required for secretory-vesicle-mediated abscission. *Cell* **123**, 75–87 doi:10.1016/j.cell.2005.07.027
117 Guizetti, J. and Gerlich, D.W. (2012) ESCRT-III polymers in membrane neck constriction. *Trends Cell Biol.* **22**, 133–140 doi: 10.1016/j.tcb.2011.11.007
118 Agromayor, M., Carlton, J.G., Phelan, J.P., Matthews, D.R., Carlin, L.M., Ameer-Beg, S. et al. (2009) Essential role of hIST1 in cytokinesis. *Mol. Biol. Cell* **20**, 1374–1387 doi:10.1091/mbc.E08-05-0474
119 Bajorek, M., Morita, E., Skalicky, J.J., Morham, S.G., Babst, M. and Sundquist, W.I. (2009) Biochemical analyses of human IST1 and its function in cytokinesis. *Mol. Biol. Cell* **20**, 1360–1373 doi:10.1091/mbc.E08-05-0475
120 Bajorek, M., Schubert, H.L., McCullough, J., Langelier, C., Eckert, D.M., Stubblefield, W.-M.B. et al. (2009) Structural basis for ESCRT-III protein autoinhibition. *Nat. Struct. Mol. Biol.* **16**, 754–762 doi:10.1038/nsmb.1621
121 Elia, N., Fabrikant, G., Kozlov, M.M. and Lippincott-Schwartz, J. (2012) Computational model of cytokinetic abscission driven by ESCRT-III polymerization and remodeling. *Biophys. J.* **102**, 2309–2320 doi:10.1016/j.bpj.2012.04.007

122 Fielding, A.B., Schonteich, E., Matheson, J., Wilson, G., Yu, X., Hickson, G.R.X. et al. (2005) Rab11-FIP3 and FIP4 interact with Arf6 and the exocyst to control membrane traffic in cytokinesis. *EMBO J.* **24**, 3389–3399 doi:10.1038/sj.emboj.7600803
123 Morita, E., Colf, L.A., Karren, M.A., Sandrin, V., Rodesch, C.K. and Sundquist, W.I. (2010) Human ESCRT-III and VPS4 proteins are required for centrosome and spindle maintenance. *Proc. Natl Acad. Sci. U.S.A.* **107**, 12889–12894 doi:10.1073/pnas.1005938107
124 Connell, J.W., Lindon, C., Luzio, J.P. and Reid, E. (2009) Spastin couples microtubule severing to membrane traffic in completion of cytokinesis and secretion. *Traffic* **10**, 42–56 doi:10.1111/j.1600-0854.2008.00847.x
125 Obita, T., Saksena, S., Ghazi-Tabatabai, S., Gill, D.J., Perisic, O., Emr, S.D. et al. (2007) Structural basis for selective recognition of ESCRT-III by the AAA ATPase Vps4. *Nature* **449**, 735–739 doi:10.1038/nature06171
126 Scott, A., Gaspar, J., Stuchell-Brereton, M.D., Alam, S.L., Skalicky, J.J. and Sundquist, W.I. (2005) Structure and ESCRT-III protein interactions of the MIT domain of human VPS4A. *Proc. Natl Acad. Sci. U.S.A.* **102**, 13813–13818 doi:10.1073/pnas.0502165102
127 Yang, D., Rismanchi, N., Renvoisé, B., Lippincott-Schwartz, J., Blackstone, C. and Hurley, J.H. (2008) Structural basis for midbody targeting of spastin by the ESCRT-III protein CHMP1B. *Nat. Struct. Mol. Biol.* **15**, 1278–1286 doi: 10.1038/nsmb.1512
128 Schiel, J.A., Park, K., Morphew, M.K., Reid, E., Hoenger, A. and Prekeris, R. (2011) Endocytic membrane fusion and buckling-induced microtubule severing mediate cell abscission. *J. Cell Sci.* **124**, 1411–1424 doi:10.1242/jcs.081448
129 Hadders, M.A., Agromayor, M., Obita, T., Perisic, O., Caballe, A., Kloc, M. et al. (2012) ESCRT-III binding protein MITD1 is involved in cytokinesis and has an unanticipated PLD fold that binds membranes. *Proc. Natl Acad. Sci. U.S.A.* **109**, 17424–17429. doi: 10.1073/pnas.1206839109
130 Lee, S., Chang, J., Renvoise, B., Tipirneni, A., Yang, S. and Blackstone, C. (2012) MITD1 is recruited to midbodies by ESCRT-III and participates in cytokinesis. *Mol. Biol. Cell* **23**, 4347–4361 doi:10.1091/mbc.E12-04-0292
131 Agromayor, M. and Martin-Serrano, J. (2013) Knowing when to cut and run: mechanisms that control cytokinetic abscission. *Trends Cell Biol.* **23**, 433–441 doi:10.1016/j.tcb.2013.04.006
132 Lafaurie-Janvore, J., Maiuri, P., Wang, I., Pinot, M., Manneville, J.-B., Betz, T. et al. (2013) ESCRT-III assembly and cytokinetic abscission are induced by tension release in the intercellular bridge. *Science* **339**, 1625–1629 doi:10.1126/science.1233866
133 Norden, C., Mendoza, M., Dobbelaere, J., Kotwaliwale, C.V., Biggins, S. and Barral, Y. (2006) The NoCut pathway links completion of cytokinesis to spindle midzone function to prevent chromosome breakage. *Cell* **125**, 85–98 doi:10.1016/j.cell.2006.01.045
134 Mendoza, M., Norden, C., Durrer, K., Rauter, H., Uhlmann, F. and Barral, Y. (2009) A mechanism for chromosome segregation sensing by the NoCut checkpoint. *Nat. Cell Biol.* **11**, 477–483 doi:10.1038/ncb1855
135 Steigemann, P., Wurzenberger, C., Schmitz, M.H.A., Held, M., Guizetti, J., Maar, S. et al. (2009) Aurora B-mediated abscission checkpoint protects against tetraploidization. *Cell* **136**, 473–484 doi:10.1016/j.cell.2008.12.020
136 Janssen, A., van der Burg, M., Szuhai, K., Kops, G.J.P.L. and Medema, R.H. (2011) Chromosome segregation errors as a cause of DNA damage and structural chromosome aberrations. *Science* **333**, 1895–1898 doi:10.1126/science.1210214
137 Gascoigne, K.E. and Cheeseman, I.M. (2013) Induced dicentric chromosome formation promotes genomic rearrangements and tumorigenesis. *Chromosom. Res.* **21**, 407–418 doi:10.1007/s10577-013-9368-6
138 Germann, S.M., Schramke, V., Pedersen, R.T., Gallina, I., Eckert-Boulet, N., Oestergaard, V.H. et al. (2014) TopBP1/Dpb11 binds DNA anaphase bridges to prevent genome instability. *J. Cell Biol.* **204**, 45–59 doi:10.1083/jcb.201305157
139 Mackay, D.R., Makise, M. and Ullman, K.S. (2010) Defects in nuclear pore assembly lead to activation of an Aurora B-mediated abscission checkpoint. *J. Cell Biol.* **191**, 923–931 doi:10.1083/jcb.201007124
140 Caballe, A., Wenzel, D.M., Agromayor, M., Alam, S.L., Skalicky, J.J., Kloc, M. et al. (2015) ULK3 regulates cytokinetic abscission by phosphorylating ESCRT-III proteins. *eLife* **4**, e06547 doi:10.7554/eLife.06547
141 Carlton, J.G., Caballe, A., Agromayor, M., Kloc, M. and Martin-Serrano, J. (2012) ESCRT-III governs the Aurora B-mediated abscission checkpoint through CHMP4C. *Science* **336**, 220–225 doi:10.1126/science.1217180
142 Amaral, N., Vendrell, A., Funaya, C., Idrissi, F.-Z., Maier, M., Kumar, A. et al. (2016) The Aurora-B-dependent NoCut checkpoint prevents damage of anaphase bridges after DNA replication stress. *Nat. Cell Biol.* **18**, 516–526 doi:10.1038/ncb3343
143 Capalbo, L., Montembault, E., Takeda, T., Bassi, Z.I., Glover, D.M. and D'Avino, P.P. (2012) The chromosomal passenger complex controls the function of endosomal sorting complex required for transport-III Snf7 proteins during cytokinesis. *Open Biol.* **2**, 120070 doi:10.1098/rsob.120070
144 Pharoah, P.D.P., Tsai, Y.-Y., Ramus, S.J., Phelan, C.M., Goode, E.L., Lawrenson, K. et al. (2013) GWAS meta-analysis and replication identifies three new susceptibility loci for ovarian cancer. *Nat. Genet.* **45**, 362–370, 370–372 doi:10.1038/ng.2564
145 Thoresen, S.B., Campsteijn, C., Vietri, M., Schink, K.O., Liestøl, K., Andersen, J.S. et al. (2014) ANCHR mediates Aurora-B-dependent abscission checkpoint control through retention of VPS4. *Nat. Cell Biol.* **16**, 550–560 doi: 10.1038/ncb2959
146 Azmi, I., Davies, B., Dimaano, C., Payne, J., Eckert, D., Babst, M. et al. (2006) Recycling of ESCRTs by the AAA-ATPase Vps4 is regulated by a conserved VSL region in Vta1. *J. Cell Biol.* **172**, 705–717 doi:10.1083/jcb.200508166
147 Merrill, S.A. and Hanson, P.I. (2010) Activation of human VPS4A by ESCRT-III proteins reveals ability of substrates to relieve enzyme autoinhibition. *J. Biol. Chem.* **285**, 35428–35438 doi:10.1074/jbc.M110.126318
148 Vild, C.J., Li, Y., Guo, E.Z., Liu, Y. and Xu, Z. (2015) A novel mechanism of regulating the ATPase VPS4 by its cofactor LIP5 and the endosomal sorting complex required for transport (ESCRT)-III protein CHMP5. *J. Biol. Chem.* **290**, 7291–7303 doi:10.1074/jbc.M114.616730
149 Capalbo, L., Mela, I., Abad, M.A., Jeyaprakash, A.A., Edwardson, J.M., Avino, P.P.D. et al. (2016) Coordinated regulation of the ESCRT-III component CHMP4C by the chromosomal passenger complex and centralspindlin during cytokinesis. *Open Biol.* **6**, 160248 doi:10.1098/rsob.160248
150 Hetzer, M.W. (2010) The nuclear envelope. *Cold Spring Harb. Perspect. Biol.* **2**, a000539 doi:10.1101/cshperspect.a000539
151 Wandke, C. and Kutay, U. (2013) Enclosing chromatin: reassembly of the nucleus after open mitosis. *Cell* **152**, 1222–1225 doi:10.1016/j.cell.2013.02.046
152 Güttinger, S., Laurell, E. and Kutay, U. (2009) Orchestrating nuclear envelope disassembly and reassembly during mitosis. *Nat. Rev. Mol. Cell Biol.* **10**, 178–191 doi:10.1038/nrm2641
153 Kutay, U. and Hetzer, M.W. (2008) Reorganization of the nuclear envelope during open mitosis. *Curr. Opin. Cell Biol.* **20**, 669–677 doi:10.1016/j.ceb.2008.09.010

Biochemical Society Transactions (2017) **45** 613–634
DOI: 10.1042/BST20160479

154 Schlaitz, A.-L., Thompson, J., Wong, C.C.L., Yates, J.R. and Heald, R. (2013) REEP3/4 ensure endoplasmic reticulum clearance from metaphase chromatin and proper nuclear envelope architecture. *Dev. Cell* **26**, 315–323 doi:10.1016/j.devcel.2013.06.016
155 Smyth, J.T., Beg, A.M., Wu, S., Putney, J.W. and Rusan, N.M. (2012) Phosphoregulation of STIM1 leads to exclusion of the endoplasmic reticulum from the mitotic spindle. *Curr. Biol.* **22**, 1487–1493 doi:10.1016/j.cub.2012.05.057
156 Vedrenne, C., Klopfenstein, D.R. and Hauri, H.-P. (2005) Phosphorylation controls CLIMP-63–mediated anchoring of the endoplasmic reticulum to microtubules. *Mol. Biol. Cell* **16**, 1928–1937 doi:10.1091/mbc.E04-07-0554
157 Anderson, D.J. and Hetzer, M.W. (2007) Nuclear envelope formation by chromatin-mediated reorganization of the endoplasmic reticulum. *Nat. Cell Biol.* **9**, 1160–1166 doi:10.1038/ncb1636
158 Mühlhäusser, P. and Kutay, U. (2007) An in vitro nuclear disassembly system reveals a role for the RanGTPase system and microtubule-dependent steps in nuclear envelope breakdown. *J. Cell Biol.* **178**, 595–610 doi:10.1083/jcb.200703002
159 Puhka, M., Vihinen, H., Joensuu, M. and Jokitalo, E. (2007) Endoplasmic reticulum remains continuous and undergoes sheet-to-tubule transformation during cell division in mammalian cells. *J. Cell Biol.* **179**, 895–909 doi:10.1083/jcb.200705112
160 Schellhaus, A.K., De Magistris, P. and Antonin, W. (2016) Nuclear reformation at the end of mitosis. *J. Mol. Biol.* **428**, 1962–1985 doi:10.1016/j.jmb.2015.09.016
161 Anderson, D.J. and Hetzer, M.W. (2008) Reshaping of the endoplasmic reticulum limits the rate for nuclear envelope formation. *J. Cell Biol.* **182**, 911–924 doi:10.1083/jcb.200805140
162 Lu, L., Ladinsky, M.S. and Kirchhausen, T. (2011) Formation of the postmitotic nuclear envelope from extended ER cisternae precedes nuclear pore assembly. *J. Cell Biol.* **194**, 425–440 doi:10.1083/jcb.201012063
163 Hetzer, M., Meyer, H.H., Walther, T.C., Bilbao-Cortes, D., Warren, G. and Mattaj, I.W. (2001) Distinct AAA-ATPase p97 complexes function in discrete steps of nuclear assembly. *Nat Cell Biol.* **3**, 1086–1091 doi:10.1038/ncb1201-1086
164 Ramadan, K., Bruderer, R., Spiga, F.M., Popp, O., Baur, T., Gotta, M. et al. (2007) Cdc48/p97 promotes reformation of the nucleus by extracting the kinase Aurora B from chromatin. *Nature* **450**, 1258–1262 doi:10.1038/nature06388
165 Bauer, I., Brune, T., Preiss, R. and Kölling, R. (2015) Evidence for a nonendosomal function of the saccharomyces cerevisiae ESCRT-III-Like protein Chm7. *Genetics* **201**, 1439–1452 doi:10.1534/genetics.115.178939
166 Olmos, Y., Perdrix-rosell, A., Carlton, J.G., Olmos, Y., Perdrix-rosell, A. and Carlton, J.G. (2016) The ESCRT machinery: new roles at new holes. *Curr. Opin. Cell Biol.* **38**, 1–11 doi:10.1016/j.ceb.2015.12.001
167 Ventimiglia, L.N. and Martin-Serrano, J. (2016) ESCRT machinery: damage control at the nuclear membrane. *Cell Res.* **26**, 641–642 doi:10.1038/cr.2016.52
168 Raab, M., Gentili, M., de Belly, H., Thiam, H.-R., Vargas, P., Jimenez, A.J. et al. (2016) ESCRT III repairs nuclear envelope ruptures during cell migration to limit DNA damage and cell death. *Science* **352**, 359–362 doi: 10.1126/science.aad7611
169 Denais, C.M., Gilbert, R.M., Isermann, P., McGregor, A.L., te Lindert, M., Weigelin, B. et al. (2016) Nuclear envelope rupture and repair during cancer cell migration. *Science* **352**, 353–358 doi:10.1126/science.aad7297
170 Webster, B.M. and Lusk, C.P. (2016) Border safety: quality control at the nuclear envelope. *Trends Cell Biol.* **26**, 29–39 doi:10.1016/j.tcb.2015.08.002
171 Hurt, E. and Beck, M. (2015) Towards understanding nuclear pore complex architecture and dynamics in the age of integrative structural analysis. *Curr. Opin. Cell Biol.* **34**, 31–38 doi:10.1016/j.ceb.2015.04.009
172 Alber, F., Dokudovskaya, S., Veenhoff, L.M., Zhang, W., Kipper, J., Devos, D. et al. (2007) The molecular architecture of the nuclear pore complex. *Nature* **450**, 695–701 doi:10.1038/nature06405
173 Bui, K.H.H., von Appen, A., DiGuilio, A.L., Ori, A., Sparks, L., Mackmull, M.-T. et al. (2013) Integrated structural analysis of the human nuclear pore complex scaffold. *Cell* **155**, 1233–1243 doi:10.1016/j.cell.2013.10.055
174 Frost, A., Elgort, M.G., Brandman, O., Ives, C., Collins, S.R., Miller-Vedam, L. et al. (2012) Functional repurposing revealed by comparing *S. pombe* and *S. cerevisiae* genetic interactions. *Cell* **149**, 1339–1352. doi:10.1016/j.cell.2012.04.028
175 Webster, B.M. and Lusk, C.P. (2015) ESCRTs breach the nuclear border. *Nucleus* **6**, 197–202 doi:10.1080/19491034.2015.1035844
176 Webster, B.M., Thaller, D.J., Jäger, J., Ochmann, S.E., Borah, S. and Lusk, C.P. (2016) Chm7 and Heh1 collaborate to link nuclear pore complex quality control with nuclear envelope sealing. *EMBO J.* **35**, 2447–2467 doi:10.15252/embj.201694574
177 Yewdell, W.T., Colombi, P., Makhnevych, T. and Lusk, C.P. (2011) Lumenal interactions in nuclear pore complex assembly and stability. *Mol. Biol. Cell* **22**, 1375–1388 doi:10.1091/mbc.E10-06-0554
178 Yang, B., Stjepanovic, G., Shen, Q., Martin, A. and Hurley, J.H. (2015) The noncoding explosion. *Nat. Struct. Mol. Biol.* **22**, 1 doi:10.1038/nsmb.2952
179 Nabhan, J.F., Hu, R., Oh, R.S., Cohen, S.N. and Lu, Q. (2012) Formation and release of arrestin domain-containing protein 1-mediated microvesicles (ARMMs) at plasma membrane by recruitment of TSG101 protein. *Proc. Natl Acad. Sci. U.S.A.* **109**, 4146–4151 doi:10.1073/pnas.1200448109
180 Kuo, L. and Freed, E.O. (2012) ARRDC1 as a mediator of microvesicle budding. *Proc. Natl Acad. Sci.* **109**, 4025–4026 doi:10.1073/pnas.1201441109
181 Choudhuri, K., Llodrá, J., Roth, E.W., Tsai, J., Gordo, S., Wucherpfennig, K.W. et al. (2014) Polarized release of T-cell-receptor-enriched microvesicles at the immunological synapse. *Nature* **507**, 118–123 doi:10.1038/nature12951
182 Wehman, A.M., Poggioli, C., Schweinsberg, P., Grant, B.D. and Nance, J. (2011) The P4-ATPase TAT-5 inhibits the budding of extracellular vesicles in *C. elegans* embryos. *Curr. Biol.* **21**, 1951–1959 doi:10.1016/j.cub.2011.10.040
183 Keyel, P.A., Loultcheva, L., Roth, R., Salter, R.D., Watkins, S.C., Yokoyama, W.M. et al. (2011) Streptolysin O clearance through sequestration into blebs that bud passively from the plasma membrane. *J. Cell Sci.* **124**, 2414–2423 doi:10.1242/jcs.076182
184 Babiychuk, E.B., Monastyrskaya, K., Potez, S. and Draeger, A. (2009) Intracellular Ca(2+) operates a switch between repair and lysis of streptolysin O-perforated cells. *Cell Death Differ.* **16**, 1126–1134 doi:10.1038/cdd.2009.30
185 McNeil, P.L. and Khakee, R. (1992) Disruptions of muscle fiber plasma membranes. Role in exercise-induced damage. *Am. J. Pathol.* **140**, 1097–1109 PMID:1374591
186 McNeil, P.L. and Steinhardt, R.A. (2003) Plasma membrane disruption: repair, prevention, adaptation. *Annu. Rev. Cell Dev. Biol.* **19**, 697–731 doi:10.1146/annurev.cellbio.19.111301.140101
187 Bi, G.-Q., Alderton, J.M. and Steinhardt, R.A. (1995) Calcium-regulated exocytosis is required for cell membrane resealing. *J. Cell Biol.* **131**, 1747–1758 doi:10.1083/jcb.131.6.1747

188 Sharma, N., Medikayala, S., Defour, A., Rayavarapu, S., Brown, K.J., Hathout, Y. et al. (2012) Use of quantitative membrane proteomics identifies a novel role of mitochondria in healing injured muscles. *J. Biol. Chem.* **287**, 30455–30467 doi:10.1074/jbc.M112.354415
189 Corrotte, M., Fernandes, M.C., Tam, C. and Andrews, N.W. (2012) Toxin pores endocytosed during plasma membrane repair traffic into the lumen of MVBs for degradation. *Traffic* **13**, 483–494 doi:10.1111/j.1600-0854.2011.01323.x
190 McNeil, P.L., Vogel, S.S., Miyake, K. and Terasaki, M. (2000) Patching plasma membrane disruptions with cytoplasmic membrane. *J. Cell Sci.* **113**(Pt 1), 1891–1902 PMID:10806100
191 Idone, V., Tam, C., Goss, J.W., Toomre, D., Pypaert, M. and Andrews, N.W. (2008) Repair of injured plasma membrane by rapid Ca^{2+} dependent endocytosis. *J. Cell Biol.* **180**, 905–914 doi:10.1083/jcb.200708010
192 Cocucci, E. and Meldolesi, J. (2015) Ectosomes and exosomes: shedding the confusion between extracellular vesicles. *Trends Cell Biol.* **25**, 364–372 doi:10.1016/j.tcb.2015.01.004
193 Baietti, M.F., Zhang, Z., Mortier, E., Melchior, A., Degeest, G., Geeraerts, A. et al. (2012) Syndecan–syntenin–ALIX regulates the biogenesis of exosomes. *Nat. Cell Biol.* **14**, 677–685 doi:10.1038/ncb2502
194 Hurley, J.H. and Odorizzi, G. (2012) Get on the exosome bus with ALIX. *Nat. Cell Biol.* **14**, 654–655 doi:10.1038/ncb2530
195 Teis, D., Saksena, S. and Emr, S.D. (2008) Ordered assembly of the ESCRT-III complex on endosomes is required to sequester cargo during MVB formation. *Dev. Cell* **15**, 578–589 doi:10.1016/j.devcel.2008.08.013
196 Muzioł, T., Pineda-Molina, E., Ravelli, R.B., Zamborlini, A., Usami, Y., Göttlinger, H. et al. (2006) Structural basis for budding by the ESCRT-III factor CHMP3. *Dev. Cell* **10**, 821–830 doi:10.1016/j.devcel.2006.03.013
197 McCullough, J., Colf, L.A. and Sundquist, W.I. (2013) Membrane fission reactions of the mammalian ESCRT pathway. *Annu. Rev. Biochem.* **82**, 663–692 doi: 10.1146/annurev-biochem-072909-101058
198 Tang, S., Henne, W.M., Borbat, P.P., Buchkovich, N.J., Freed, J.H., Mao, Y. et al. (2015) Structural basis for activation, assembly and membrane binding of ESCRT-III Snf7 filaments. *eLife* **4**, e12548 doi:10.7554/eLife.12548
199 Xiao, J., Chen, X.-W., Davies, B.A., Saltiel, A.R., Katzmann, D.J. and Xu, Z. (2009) Structural basis of Ist1 function and Ist1-Did2 interaction in the multivesicular body pathway and cytokinesis. *Mol. Biol. Cell* **20**, 3514–3524 doi:10.1091/mbc.E09-05-0403
200 McCullough, J., Clippinger, A.K., Talledge, N., Skowyra, M.L., Saunders, M.G., Naismith, T.V. et al. (2015) Structure and membrane remodeling activity of ESCRT-III helical polymers. *Science* **350**, 1548–1551 doi:10.1126/science.aad8305
201 Zamborlini, A., Usami, Y., Radoshitzky, S.R., Popova, E., Palu, G. and Göttlinger, H. (2006) Release of autoinhibition converts ESCRT-III components into potent inhibitors of HIV-1 budding. *Proc. Natl Acad. Sci. U.S.A.* **103**, 19140–19145 doi:10.1073/pnas.0603788103
202 Shim, S., Kimpler, L.A. and Hanson, P.I. (2007) Structure/function analysis of four core ESCRT-III proteins reveals common regulatory role for extreme C-terminal domain. *Traffic* **8**, 1068–1079 doi:10.1111/j.1600-0854.2007.00584.x
203 Hanson, P.I., Roth, R., Lin, Y. and Heuser, J.E. (2008) Plasma membrane deformation by circular arrays of ESCRT-III protein filaments. *J. Cell Biol.* **180**, 389–402 doi:10.1083/jcb.200707031
204 Henne, W.M., Buchkovich, N.J., Zhao, Y. and Emr, S.D. (2012) The endosomal sorting complex ESCRT-II mediates the assembly and architecture of ESCRT-III helices. *Cell* **151**, 356–371 doi:10.1016/j.cell.2012.08.039
205 Ghazi-Tabatabai, S., Saksena, S., Short, J.M., Pobbati, A.V., Veprintsev, D.B., Crowther, R.A. et al. (2008) Structure and disassembly of filaments formed by the ESCRT-III subunit Vps24. *Structure* **16**, 1345–1356 doi:10.1016/j.str.2008.06.010
206 Lata, S., Schoehn, G., Solomons, J., Pires, R., Göttlinger, H.G. and Weissenhorn, W. (2009) Structure and function of ESCRT-III. *Biochem. Soc. Trans.* **37**, 156–160 doi:10.1042/BST0370156
207 Teis, D., Saksena, S., Judson, B.L. and Emr, S.D. (2010) ESCRT-II coordinates the assembly of ESCRT-III filaments for cargo sorting and multivesicular body vesicle formation. *EMBO J.* **29**, 871–883 doi:10.1038/emboj.2009.408
208 Lata, S., Schoehn, G., Jain, A., Pires, R., Piehler, J., Gottlinger, H.G. et al. (2008) Helical structures of ESCRT-III are disassembled by VPS4. *Science* **321**, 1354–1357 doi:10.1126/science.1161070
209 Leung, K.F., Dacks, J.B. and Field, M.C. (2008) Evolution of the multivesicular body ESCRT machinery; retention across the eukaryotic lineage. *Traffic* **9**, 1698–1716 doi:10.1111/j.1600-0854.2008.00797.x
210 Yorikawa, C., Shibata, H., Waguri, S., Hatta, K., Horii, M., Katoh, K. et al. (2005) Human CHMP6, a myristoylated ESCRT-III protein, interacts directly with an ESCRT-II component EAP20 and regulates endosomal cargo sorting. *Biochem. J.* **387**, 17–26 doi:10.1042/BJ20041227
211 Pires, R., Hartlieb, B., Signor, L., Schoehn, G., Lata, S., Roessle, M. et al. (2009) A crescent-shaped ALIX dimer targets ESCRT-III CHMP4 filaments. *Structure* **17**, 843–856 doi:10.1016/j.str.2009.04.007
212 Teo, H., Perisic, O., González, B. and Williams, R.L. (2004) ESCRT-II, an endosome-associated complex required for protein sorting: crystal structure and interactions with ESCRT-III and membranes. *Dev. Cell* **7**, 559–569 doi:10.1016/j.devcel.2004.09.003
213 Fyfe, I., Schuh, A.L., Edwardson, J.M. and Audhya, A. (2011) Association of the endosomal sorting complex ESCRT-II with the Vps20 subunit of ESCRT-III generates a curvature-sensitive complex capable of nucleating ESCRT-III filaments. *J. Biol. Chem.* **286**, 34262–34270 doi:10.1074/jbc.M111.266411
214 Im, Y.J., Wollert, T., Boura, E. and Hurley, J.H. (2009) Structure and function of the ESCRT-II-III interface in multivesicular body biogenesis. *Dev. Cell* **17**, 234–243 doi:10.1016/j.devcel.2009.07.008
215 Lee, I.-H., Kai, H., Carlson, L.-A., Groves, J.T. and Hurley, J.H. (2015) Negative membrane curvature catalyzes nucleation of endosomal sorting complex required for transport (ESCRT)-III assembly. *Proc. Natl Acad. Sci. U.S.A.* **112**, 15892–15897 doi:10.1073/pnas.1518765113
216 Hierro, A., Sun, J., Rusnak, A.S., Kim, J., Prag, G., Emr, S.D. et al. (2004) Structure of the ESCRT-II endosomal trafficking complex. *Nature* **431**, 221–225 doi:10.1038/nature02914
217 Im, Y.J. and Hurley, J.H. (2008) Integrated structural model and membrane targeting mechanism of the human ESCRT-II complex. *Dev. Cell* **14**, 902–913 doi:10.1016/j.devcel.2008.04.004
218 Shen, Q.-T., Schuh, A.L., Zheng, Y., Quinney, K., Wang, L., Hanna, M. et al. (2014) Structural analysis and modeling reveals new mechanisms governing ESCRT-III spiral filament assembly. *J. Cell Biol.* **206**, 763–777 doi:10.1083/jcb.201403108
219 Effantin, G., Dordor, A., Sandrin, V., Martinelli, N., Sundquist, W.I., Schoehn, G. et al. (2013) ESCRT-III CHMP2A and CHMP3 form variable helical polymers *in vitro* and act synergistically during HIV-1 budding. *Cell. Microbiol.* **15**, 213–226 doi:10.1111/cmi.12041

Biochemical Society Transactions (2017) **45** 613–634
DOI: 10.1042/BST20160479

220 Cashikar, A.G., Shim, S., Roth, R., Maldazys, M.R., Heuser, J.E. and Hanson, P.I. (2014) Structure of cellular ESCRT-III spirals and their relationship to HIV budding. *eLife* **3**, e02184 doi:10.7554/eLife.02184
221 Chiaruttini, N., Redondo-Morata, L., Colom, A., Humbert, F., Lenz, M., Scheuring, S. et al. (2015) Relaxation of loaded ESCRT-III spiral springs drives membrane deformation. *Cell* **163**, 866–879 doi:10.1016/j.cell.2015.10.017
222 Bodon, G., Chassefeyre, R., Pernet-Gallay, K., Martinelli, N., Effantin, G., Hulsik, D.L. et al. (2011) Charged multivesicular body protein 2B (CHMP2B) of the endosomal sorting complex required for transport-III (ESCRT-III) polymerizes into helical structures deforming the plasma membrane. *J. Biol. Chem.* **286**, 40276–40286 doi:10.1074/jbc.M111.283671
223 Dobro, M.J., Samson, R.Y., Yu, Z., McCullough, J., Ding, H.J., Chong, P.L.-G. et al. (2013) Electron cryotomography of ESCRT assemblies and dividing *Sulfolobus* cells suggests that spiraling filaments are involved in membrane scission. *Mol. Biol. Cell* **24**, 2319–2327 doi:10.1091/mbc.E12-11-0785
224 Allison, R., Lumb, J.H., Fassier, C., Connell, J.W., Martin, D.T., Seaman, M.N.J. et al. (2013) An ESCRT–spastin interaction promotes fission of recycling tubules from the endosome. *J. Cell Biol.* **202**, 527–543 doi:10.1083/jcb.201211045
225 Schöneberg, J., Lee, I.-H., Iwasa, J.H. and Hurley, J.H. (2016) Reverse-topology membrane scission by the ESCRT proteins. *Nat. Rev. Mol. Cell Biol.* **18**, 5–17 doi:10.1038/nrm.2016.121
226 Boura, E., Rózycki, B., Chung, H.S., Herrick, D.Z., Canagarajah, B., Cafiso, D.S. et al. (2012) Solution structure of the ESCRT-I and -II supercomplex: Implications for membrane budding and scission. *Structure* **20**, 874–886 doi:10.1016/j.str.2012.03.008
227 Fabrikant, G., Lata, S., Riches, J.D., Briggs, J.A.G., Weissenhorn, W. and Kozlov, M.M. (2009) Computational model of membrane fission catalyzed by ESCRT-III. *PLoS Comput. Biol.* **5**, e1000575 doi: 10.1371/journal.pcbi.1000575
228 Henne, W.M., Buchkovich, N.J. and Emr, S.D. (2011) The ESCRT pathway. *Dev. Cell* **21**, 77–91 doi:10.1016/j.devcel.2011.05.015
229 Wollert, T., Wunder, C., Lippincott-Schwartz, J. and Hurley, J.H. (2009) Membrane scission by the ESCRT-III complex. *Nature* **458**, 172–177 doi:10.1038/nature07836
230 Lenz, M., Crow, D.J.G. and Joanny, J.-F. (2009) Membrane buckling induced by curved filaments. *Phys. Rev. Lett.* **103**, 038101 doi:10.1103/PhysRevLett.103.038101
231 Nickerson, D.P., Russell, M.R.G. and Odorizzi, G. (2007) A concentric circle model of multivesicular body cargo sorting. *EMBO Rep.* **8**, 644–650 doi:10.1038/sj.embor.7401004
232 Wollert, T. and Hurley, J.H. (2010) Molecular mechanism of multivesicular body biogenesis by ESCRT complexes. *Nature* **464**, 864–869 doi:10.1038/nature08849
233 Baumgärtel, V., Ivanchenko, S., Dupont, A., Sergeev, M., Wiseman, P.W., Kräusslich, H.-G. et al. (2011) Live-cell visualization of dynamics of HIV budding site interactions with an ESCRT component. *Nat. Cell Biol.* **13**, 469–474 doi:10.1038/ncb2215
234 Jouvenet, N., Zhadina, M., Bieniasz, P.D. and Simon, S.M. (2011) Dynamics of ESCRT protein recruitment during retroviral assembly. *Nat. Cell Biol.* **13**, 394–401 doi:10.1038/ncb2207
235 Saksena, S., Wahlman, J., Teis, D., Johnson, A.E. and Emr, S.D. (2009) Functional reconstitution of ESCRT-III assembly and disassembly. *Cell* **136**, 97–109 doi:10.1016/j.cell.2008.11.013
236 Skibinski, G., Parkinson, N.J., Brown, J.M., Chakrabarti, L., Lloyd, S.L., Hummerich, H. et al. (2005) Mutations in the endosomal ESCRTIII-complex subunit CHMP2B in frontotemporal dementia. *Nat. Genet.* **37**, 806–808 doi:10.1038/ng1609
237 van der Zee, J., Urwin, H., Engelborghs, S., Bruyland, M., Vandenberghe, R., Dermaut, B. et al. (2008) CHMP2B C-truncating mutations in frontotemporal lobar degeneration are associated with an aberrant endosomal phenotype in vitro. *Hum. Mol. Genet.* **17**, 313–322 doi:10.1093/hmg/ddm309
238 Yamazaki, Y., Takahashi, T., Hiji, M., Kurashige, T., Izumi, Y., Yamawaki, T. et al. (2010) Immunopositivity for ESCRT-III subunit CHMP2B in granulovacuolar degeneration of neurons in the Alzheimer's disease hippocampus. *Neurosci. Lett.* **477**, 86–90 doi:10.1016/j.neulet.2010.04.038